1973 SMITHSONIAN STANDARD EARTH (III)

Edited by E. M. GAPOSCHKIN

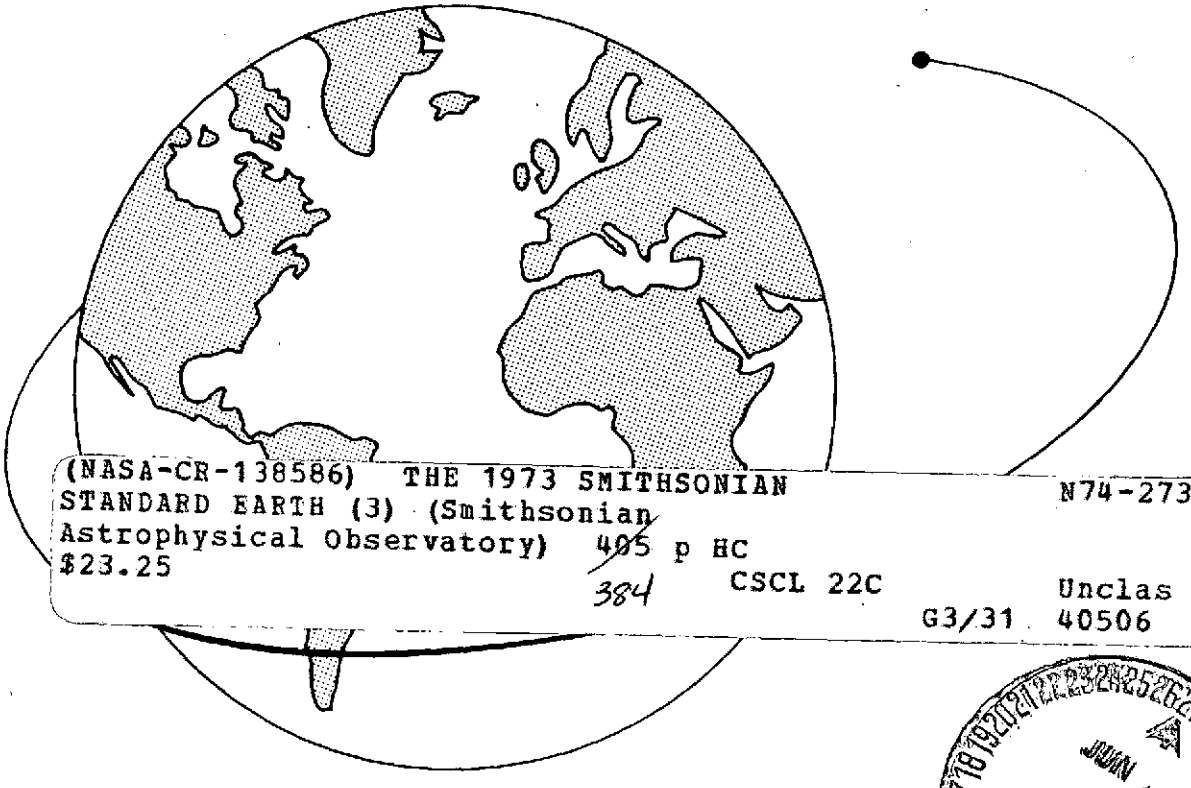

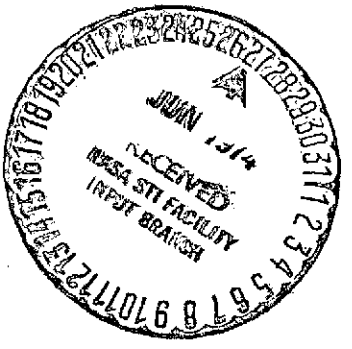

Smithsonian Astrophysical Observatory
SPECIAL REPORT 353

Research in Space Science
SAO Special Report No. 353

1973 SMITHSONIAN STANDARD EARTH (III)

Edited by E. M. Gaposchkin

November 28, 1973

Smithsonian Institution
Astrophysical Observatory
Cambridge, Massachusetts 02138

311-002

TABLE OF CONTENTS

TABLE OF CONTENTS (Cont.)

TABLE OF CONTENTS (Cont.)

TABLE OF CONTENTS (Cont.)

TABLE OF CONTENTS (Cont.)

FOREWORD

Almost 20 years ago, F. L. Whipple announced the broad scientific goals that comprise the subject of this publication. These goals encompassed the use of artificial earth satellites for geodesy, that is, the study of both the earth's figure (its geopotential) and its shape (its geometric surface). Although an astronomer rather than a geodesist, Whipple had the vision to see that these scientific opportunities would flow naturally from the Baker-Nunn camera network, then under construction. Approximately 10 years later, Whipple's ambitious geodetic goals were crystallized into the National Geodetic Satellite Program (NGSP). The NGSP focused on the determination of the gravity field of the earth represented by spherical harmonics to degree and order 15 and the determination of geocentric station coordinates to 10 m. Smithsonian Astrophysical Observatory's (SAO) pioneering work in satellite geodesy complemented the other main research efforts supporting the NGSP.

When the first artificial earth satellite was launched, geodesists had tentatively estimated only three or four coefficients of the gravity field, global geocentric coordinates were known to perhaps 500 m, and the earth was assumed to be in hydrostatic equilibrium. The subject of physical geodesy at that time was concerned with obtaining the earth's flattening or principal-oblateness term from a limited sample of local measurements. With the launch of numerous satellites dedicated to research, geodesy as a study has become completely changed. Now, from satellite measurements, the principal parts of the gravity field are known far more accurately than previously imagined. The nonhydrostatic figure of the earth, deduced from satellite observations, was a revelation to geodesist and geophysicist alike. Intercontinental distances have been determined to 5 or 10 m, and terrestrial geodesy now fits into a more comprehensive framework. Global properties of the earth are obtained from satellite data; local properties, from terrestrial data. This report presents a blending of both satellite and terrestrial methods.

Through the last decade, several groups have been pursuing studies in satellite geodesy, using many different methods and types of data. SAO has employed analytical solutions for the equations of motion, as described in Lundquist and Veis (1966) and

Kaula (1966a) (see also Part III of this Report). Alternatively, numerical methods have been used (Anderle, 1966; Martin, 1972). Both geometrical and dynamical methods have been employed in studying data obtained from satellites. From simultaneous satellite observations, we can determine site coordinates without precise knowledge of the satellite's orbit, while with knowledge of satellite motion, we can determine the geopotential in addition to site coordinates.

Satellite observations have been made by many agencies with different camera systems. SAO has obtained both Baker-Nunn camera and laser observations. Others include observations by the National Ocean Survey BC-4 cameras, the National Aeronautics and Space Administration's (NASA) MOTs cameras, PC-1000 cameras, and a number of individual systems. Laser range data have been obtained by NASA/Goddard Space Flight Center (GSFC) and by Centre National d'Etudes Spatiales, and doppler data have been taken in abundance by the TRANSIT system. Additional ranging systems, such as SECOR, have also been employed. Survey data and surface-gravity data are examples of ground-based data that have been added to the solutions.

Comprehensive gravity-field solutions using numerical-integration methods with doppler data have been undertaken at the Applied Physics Laboratory (Yionoulis, Heuring, and Guier, 1972; Guier and Newton, 1965). Similar analyses at the Naval Weapons Laboratory have led to global gravity-field determinations (Anderle, 1965a, b, 1967a, b; Anderle and Smith, 1967). A combination of doppler and camera data with analytical techniques has been employed by Kaula (see especially Kaula, 1966c). Kaula (1966b) also used surface-gravity data to verify satellite-determined gravity fields and attempted a combination of surface-gravity and satellite data. At NASA/GSFC, numerical methods combining camera and laser data with surface-gravity data have resulted in geopotential models (Smith, Lerch, and Wagner, 1973).

These studies express the geopotential in spherical harmonics. Alternative representations that use numerical methods and doppler tracking data have also been explored (see, e.g., Koch, 1968; Koch and Morrison, 1970; Koch and Witte, 1971). A number of these methods have combined surface-gravity data with satellite data. At Ohio State University, Rapp (1968, 1971, 1973) has obtained comprehensive solutions from surface-gravity data, while Arnold (1965, 1966, 1972) has determined gravity anomalies directly from satellite data.

Resonance between the satellite orbit and the gravity field allows selected spherical-harmonics coefficients to be established. Zonal harmonics are a specific example of such resonance, and a number of determinations have been made (Cazenave and Forestier, 1971; King-Hele, Cook, and Scott, 1969; King-Hele and Cook, 1973a, b). Resonance with selected tesseral and sectorial harmonics has been considered in all comprehensive gravity-field determinations. In addition, other selected resonances have been studied (Anderle, 1965b; Anderle and Smith, 1968; Hiller and King-Hele, 1972; King-Hele, 1973a, b; Pieplu and Lefebvre, 1973; Wagner, 1968a, b; Yionoulis, 1963; Douglas and Marsh, 1970).

The methods employed in the determination of station coordinates have been as diverse as those for studying the geopotential. Geometrical methods have been utilized at the National Oceanic and Atmospheric Administration. Analyzing the BC-4 data, Mueller (1974) has combined geometrical camera data from the BC-4 and the SAO networks with simultaneous range observations from the SECOR system. Semi-dynamical methods, using satellite orbits as an intermediary, have been successful (Cazenave and Dargnies, 1971; Holland, 1973; Krakiwsky, Wells, and Kirkham, 1972; Smith, Kolenkiewicz, and Dunn, 1972). Dynamical determinations of site coordinates have been made by Anderle (1965a, 1974), Anderle and Smith (1967), Marsh, Douglas, and Martin (1971), Marsh, Douglas, and Klosko (1973), and Smith et al. (1973). In another approach, station coordinates have been determined by the Jet Propulsion Laboratory (JPL) from deep-space-probe data (Mottinger, 1969). More recently, lunar laser range data have begun to provide station coordinates (Williams, Mulholland, and Bender, 1972).

With such a diversity of approaches and data, a comparison of all these results and contributions is far beyond the scope of the present publication. Our specific objective here is to describe the process used to obtain the 1973 Smithsonian Standard Earth (III) (SE III). With similar documentation from other groups, a careful comparison of all the results can be made; such a comparison is in preparation.

The geodetic parameters for SE III were first presented at the spring meeting of the American Geophysical Union (Gaposchkin, 1973) and at the First International Symposium on the Use of Artificial Satellites for Geodesy and Geodynamics (see Parts

V and VI). These results are the continuation of work at SAO on the determination of fundamental geodetic parameters. Major calculations were published in 1966 (SE I) (Lundquist and Veis, 1966) and again in 1969 (SE II) (Gaposchkin and Lambeck, 1970). These, in turn, were sequels to earlier results (Izsak, 1963a, 1964, 1966; Kozai, 1963a, b, 1964; Köhnlein, 1965; Veis, 1961, 1965).

The parameters that define a Standard Earth consist of 1) a set of cartesian coordinates for satellite-tracking stations and 2) a set of spherical-harmonic coefficients representing the earth's gravitational potential. Both sets of data are expressed in an orthogonal geocentric coordinate system defined by the Conventional International Origin (CIO) and by the Mean Greenwich Observatory, which determines the zero-degree meridian. The CIO is intended to be the mean pole of 1900 to 1905 as established by the International Association of Geodesy in 1967. The practical realization of this reference system is the use of pole-position data provided by the International Polar Motion Service and of Universal Time (UT1) as defined by the International Bureau de l'Heure. These data provide the transformation between terrestrial and celestial reference frames. Camera observations are expressed in the celestial system with precession and nutation through the Smithsonian Astrophysical Observatory Star Catalog (Staff, Smithsonian Astrophysical Observatory, 1966).

The calculation of a Standard Earth begins with five data types:

A. Individual satellites observations.
B. Simultaneous satellite observations.
C. Observations of deep-space probes.
D. Surface-gravity data.
E. Surface-triangulation data.

The individual and the simultaneous satellite observations from the SAO Baker-Nunn and laser network, described in Part II of this Report, serve as the foundation of SAO's analysis. The deep-space-probe data were provided by JPL in the form of normal equations. A compilation of surface-gravity data was obtained and statistical methods developed to transform these data into a form suitable for combination with satellite data (Part IV). Surface-triangulation data, expressed as geodetic coordinates,

are used as observations. The calculation begins with a determination of zonal harmonics from the long-period and secular perturbations, and these values are employed throughout the remaining analysis.

Individual satellite observations are combined with surface-gravity data to determine the gravity field, while individual observations, simultaneous observations, deep-space-probe observations, and surface-triangulation data all contribute to the determination of station coordinates. The solution for potential coefficients depends on the accuracy of station coordinates, and vice versa. If imperfections exist in the modeling of the gravity field, inaccurate orbits will result; and, of course, orbital errors limit the usefulness of individual observations in the determination of station coordinates in the dynamical mode. Conversely, inaccuracies in station position limit the determination of gravity-field parameters. This interdependency has led SAO to seek both station coordinates and gravity-field coefficients in the same calculation.

In previous work (Lundquist and Veis, 1966; Gaposchkin and Lambeck, 1970, 1971), solutions have been obtained for both coordinates and gravity-field coefficients in the same process. In this volume, however, these calculations are separated. Such a separation allows an optimum selection of orbits for each method. For example, orbits corrupted by large gravity-field errors – e.g., resonances, which must be included in the determination of potential coefficients – are eliminated from the determination of coordinates.

For SE III, computations are performed in parallel for each iteration, and the separate solutions are used as the initial values for the subsequent iteration. Each iteration starts with an adopted set of coordinates and potential coefficients. Reference orbits are calculated for each arc of an individual observation that was used. Then, in parallel, the system of normal equations is calculated for both potential coefficients and station coordinates. Each normal system is then combined with the other relevant ones. The combination of normal equations allows the use of different relative weights for each type of data. Since the absolute a priori weights for each set of data may be incorrect for a number of reasons, we have determined the optimum relative weight for each set of normal equations. It is reassuring that the relative weights determined in this way are reasonably close to the a priori values.

Establishing absolute uncertainties is very difficult since we have poor estimates of the systematic errors involved. Therefore, we do not rely on formal statistical quantities to establish errors but use intercomparison of several estimates (e.g., comparing the observed direction between two stations with the solution). The estimates arrived at in this way have proved quite reliable. The formal statistics are used to propagate the uncertainties once the overall uncertainty is known.

The details of each solution and the comparisons made are given here. A number of other computations are becoming available, and further comparisons are certainly of interest. New techniques and data are also going to supersede these results. The continued comparison of these results with the latest information will allow further assessment of the methods and tests used here.

E. M. Gaposchkin

ACKNOWLEDGMENTS

The publication of this 1973 Smithsonian Standard Earth (III) is the result of the combined efforts of many people in addition to the several authors. It has truly been a team effort, and an exciting and challenging one.

The methodology presented herein has been developing for more than 15 years. Contributions have been made by too many colleagues to acknowledge each individually. Three, however, require special mention: F. L. Whipple had the foresight to initiate this program and form the team of scientists, technologists, and administrators necessary for its execution. His continual interest and encouragement have been appreciated. C. A. Lundquist devoted his energy and enthusiasm without reserve. He encouraged ambitious goals and achievements and helped accomplish them. Finally, I. G. Izsak, who died prematurely in 1965, provided many of the scientific ideas for the program. We have tried to maintain the standards of originality and excellence that he set.

We gratefully acknowledge the National Aeronautics and Space Administration, which has supported our work over the course of this program under Grant NGR 09-015-002.

The results obtained have been significantly enhanced by the contribution of data from a number of cooperating agencies, who all gave data freely. These are listed below, alphabetically.

14th Aerospace Force, United States Air Force, Colorado Springs, Colorado
Australian Department of Supply, American Projects Division, Woomera, Australia
British Ministry of Technology, Royal Radar Establishment, Ordnance Survey, Malvern, England
California Institute of Technology, Jet Propulsion Laboratory, California
Comisión Nacional de Investigaciones Espaciales, Buenos Aires, Argentina
Comissão Nacional de Atividades Espaciais, São Paulo, Brazil

Council for Scientific and Industrial Research, Pretoria, South Africa
Curaçao Welfare Bureau, Williamstadt, Netherlands Antilles
French Centre National d'Etudes Spatiales, Paris, France
Haile Selassie I University, Addis Ababa, Ethiopia
Institute for Astronomy, Honolulu, Hawaii
Institute of Geophysics, Honolulu, Hawaii
Instituto Geofisico del Peru, Lima, Peru
Instituto y Observatorio de Marina, Cadiz, Spain
NASA Goddard Space Flight Center MOTS System and NASA National Geodetic Satellite Program Data Bank, Maryland
National Technical University, Athens, Greece
Observatoire de Paris, Section d'Astrophysique, Meudon, France
Observatorio Astronomico, Universidad Nacional de Cordoba, Cordoba, Argentina
Technische Hogeschool, Laboratorium voor Geodesie, Delft, The Netherlands
Tokyo Astronomical Observatory, Mitaka, Japan
Universidad Nacional de San Agustin, Arequipa, Peru
Universität Bern Astronomisches Institut, Bern, Switzerland
Université de Teheran, Institute Géophysique, Teheran, Iran
University of Hawaii, Honolulu, Hawaii
USSR Academy of Sciences, Astronomical Council, Moscow, USSR
Uttar Pradesh State Observatory, Naini Tal, India

PART I

HISTORICAL INTRODUCTION

ABSTRACT

The origins of the satellite geodesy program at the Smithsonian Astrophysical Observatory are described, starting with the International Geophysical Year, continuing through a number of international programs, and culminating with the National Geodetic Satellite Program and the results described in this publication. The philosophical basis for the Baker-Nunn camera and the laser ranging system, the evolution of international scientific cooperation, and the significance of the results are discussed.

RESUME

Description des origines du programme de géodésie par satellite du "Smithsonian Astrophysical Observatory," de l'Année Géophysique Internationale a l'apogée que représente le Programme National de Satellites Géodésiques, en passant par un certain nombre de programmes internationaux; les résultats en sont décrits dans cette publication. Egalement discutés: le fondement philosophique de l'appareil photographique Baker-Nunn et du système laser de repérage, l'évolution de la coopération scientifique internationale et la signification des résultats.

КОНСПЕКТ

Описываются происхождения программы геодезии спутников в Смитсониан Астрофизической Обсерватории, начиная с Международного Геофизического Года, продолжаясь в течение числа международных программ и достигли высшей точки при Государственной Геодезической Спутниковой программе и результатах описываемых в этой статье. Обсуждаются философская основа камеры Бэкер-Нунн и лазерной расстояние измеряющей системы, эволюции международного научного сотрудничества и значения результатов.

PART I

HISTORICAL INTRODUCTION

C. A. Lundquist and F. L. Whipple

1. INITIAL OBJECTIVES OF THE SAO SATELLITE-TRACKING PROGRAM

As the principal objective of its participation in the International Geophysical Year (IGY), the Smithsonian Astrophysical Observatory (SAO) conceived of and established a systematic program to observe positions of artificial satellites and to derive geophysical information from these observations (Whipple and Hynek, 1956, 1958a, b). The fundamental concepts for this program existed in the minds and studies of SAO Director Fred L. Whipple and his colleagues (see Ryan, 1952) well before President Eisenhower announced in 1955 that the United States would launch a scientific satellite during the IGY. These plans originated with Project Orbiter, followed by Project Vanguard, which in turn was superseded by the Army program that launched Explorer 1 (5800101), the first United States satellite (Hayes, 1968). When this satellite attained its orbit on January 30, 1958, the SAO observation network and analytical apparatus were ready with partial operational status.

As stated in 1957, the principal objectives of this early SAO activity were as follows: 1) "to tie together the observing stations and the center of the geoid to a precision of the order of 10 m," 2) "to add appreciably to our knowledge of the density distribution of the earth, particularly in crustal volumes," and 3) to provide "the value of the [atmospheric] density a few kilometers above the initial perigee distance, and periodic effects or predictable cyclic effects that may occur in the earth's high atmosphere" (Whipple and Hynek, 1958a). The first two objectives evolved into similar, but more demanding, ones for subsequent programs, such as the National Geodetic Satellite Program (NGSP) (Rosenberg, 1968).

2. ESTABLISHMENT OF THE BAKER-NUNN NETWORK

To establish the required satellite-observation capability, SAO initially developed a photographic system (Whipple and Hynek, 1958b). The basic tracking camera, named Baker-Nunn after its optical and mechanical designers, has f/1 Schmidt optics. During the first several years of field operation, a Normann time standard, also named for its designer, provided epoch measurements. The Baker-Nunn tracking system has accuracies in the arcsecond and millisecond range. Twelve stations with this equipment went into operation as a global network during the IGY.

With the passage of time, the Baker-Nunn network continued operation with only small changes (Whipple and Lundquist, 1967). The modes of camera operation required slight modification to accommodate a variety of satellite characteristics. A few stations were moved to higher latitudes because many satellites were launched into high-inclination orbits. A new, more accurate, time standard replaced the Normann standard.

It is a tribute to the designers of the Baker-Nunn system that for nearly a decade, the accuracy of the Baker-Nunn data exceeded those of the analytical treatment of these data and of the geodetic parameters derived from them. Indeed, Baker-Nunn observations contributed appreciably to the NGSP results reported here. By about 1966, however, the accuracy of the derived geodetic parameters began to approach that of the observations, thus motivating significant moves toward deployment of new tracking systems of superior accuracy.

3. INTRODUCTION OF LASER SYSTEMS

When the accuracy of photographic methods began to pose a serious limit on future geodetic investigations, laser systems to measure earth-to-satellite ranges offered the best prospect for substantial reduction of measurement uncertainties. Range measurements with pulsed laser systems became possible in 1964 after the BE-B satellite (6406401), which carried an array of optical retroreflectors, was launched (Plotkin, 1964). In 1965, SAO and the General Electric Company began laser ranging experiments in conjunction with the Baker-Nunn system at Organ Pass, New Mexico (Anderson, Lehr, Maestre, Halsey, and Snyder, 1966).

Experience with the equipment at Organ Pass led to the specification and development of a greatly improved instrument, and the prototype model of this ruby-laser system began operating in late 1967 at Mt. Hopkins Observatory, Arizona (Lehr, Maestre, and Downer, 1968). After appropriate tests of this prototype and after identification of design modifications indicated by them, SAO procured three additional laser ranging systems. In late 1970, these three units began operating at the SAO sites in Arequipa, Peru; Natal, Brazil; and Olifantsfontein, South Africa. The prototype remained at Mt. Hopkins.

These SAO instruments, and similar laser systems deployed by other groups, contributed the major data base used in the final NGSP results presented here. It is the improved accuracy of these data, relative to earlier observations, that allows further refinements of geodetic parameters.

4. EVOLUTION OF INTERNATIONAL COOPERATION

The network of Baker-Nunn satellite-tracking stations was conceived by SAO as a cooperative international enterprise under the aegis of the IGY. Its implementation depended crucially on agreements between SAO and appropriate scientific organizations in the nations hosting the stations. Many of these agreements have continued to the present, with occasional renewals and modifications as needed. The viability and success of such a network stem from a recognition that little can be accomplished on global problems by a single station working in isolation, whereas a well-coordinated global network can achieve much.

The cooperative aspects of the efforts coordinated by SAO naturally extend to the analysis and interpretation of the data. First, it has been a policy that data generated by the network are available to all network participants. Also, SAO data are eventually published or otherwise made available to the general scientific community. Second, several visiting scientists from host countries have been deeply involved at SAO in geodetic investigations that employ the network data. In particular, G. Veis of the National Technical University in Athens and Y. Kozai of the Tokyo Astronomical Observatory have contributed to the success of the network; some of their principal works are given in the References and Bibliography, at the end of this Report. K. Lambeck, S. Hamid, L. Aardoom, and G. Giacaglia all made contributions to the program during their stay at the Observatory.

In recent years, cooperative efforts have increased further through various international observing campaigns. These campaigns involve a concerted effort among the several existing networks, as well as between individual stations. Such campaigns have been responsible for some of the most valuable data used in the analyses reported here. Thus, credit for the basic support behind these results must go to many nations, organizations, and individuals.

5. COOPERATIVE OBSERVING PROGRAMS

The first of the internetwork cooperative observing programs occurred in the spring of 1967 (Lundquist, 1967). The timing of this campaign followed the launch of Diademe 1 (D1C, 6701101) and Diademe 2 (D1D, 6701401), which carried retroreflectors for laser ranging. The major participants, Centre National d'Etudes Spatiales (CNES), Goddard Space Flight Center (GSFC), and SAO, arranged an observing schedule to be followed by the stations of these three organizations. The arrangements emphasized the need to coordinate observations taken by the small number of laser instruments in operation at that time. Lasers were located at three CNES stations, in Haute Provence, France; Colomb-Bechir, Algeria; and Stephanion, Greece; at a GSFC station in Greenbelt, Maryland; and at the SAO station in Organ Pass. The Baker-Nunn and other camera systems also participated.

For this observation campaign, intervals of favorable satellite visiblity lasting several weeks were selected for the five satellites with laser retroreflectors. During each selected interval, all participating stations were dedicated to obtaining maximum tracking coverage of the designated satellite. This became known as the saturation-tracking mode. Such periods of high-density data are particularly valuable in determinations of longitude-dependent coefficients in the gravity field of the earth.

SAO took the initiative in organizing a second international geodetic-satellite tracking effort in 1968, following the launch of Geos 2 (6800201). Geos 2 was the second satellite launched under the aegis of the NGSP equipped with retroreflectors. Again, intervals of several weeks were designated for saturation tracking of the six retroreflector satellites. By 1968, a few more laser instruments were operational, and they participated in this observation campaign. The two CNES lasers were located at Haute Provence and at the SAO station in San Fernando, Spain; two NASA lasers were at Greenbelt and at Rosmund, North Carolina; and an SAO laser was located at Organ Pass.

A two-laser collocation experiment was conducted at the SAO Mt. Hopkins Observatory in 1969. A GSFC mobile laser system and the SAO prototype obtained simultaneous observations on Geos 2, enabling an evaluation of system performance to be made.

The next observation campaign in this series was the International Satellite Geodesy Experiment, organized by CNES in conjunction with the launch of Peole (7010901), a new retroreflector satellite in a low-inclination orbit (Brachet, 1970). This effort extended from January 5 to August 31, 1971.

6. EVOLUTION OF RESULTS

The results presented here by SAO, corresponding to the completion of the NGSP, are but the latest in a sequence of advances in the determination of geodetic parameters. This sequence started with the early works of Izsak (1963a, 1964, 1966), Kozai (1963a, b, 1964), and Veis (1965).

A major effort in 1966 resulted in the first Smithsonian Institution Standard Earth (Lundquist and Veis, 1966), the combined work of many authors. This was the first solution for geodetic parameters based on a combination of dynamical and geometrical data and analyses. The 1969 Smithsonian Standard Earth (II) (Gaposchkin and Lambeck, 1970) was the next milestone in the SAO series. This solution for geodetic parameters not only combined dynamical and geometric data, but also incorporated surface-gravity information and results from Jet Propulsion Laboratory's Deep Space Net. This was also the first solution to employ some laser range data, resulting from the 1967 and 1968 observation campaigns. Finally, the solution presented here is again a combination of all the varieties of data used in the 1969 solution, with laser range data playing a dominant role. The available surface-gravity data are more complete than they were in 1969 and, hence, bear strongly on the final results. Survey data are also included.

PART II

SAO NETWORK: INSTRUMENTATION AND DATA REDUCTION

ABSTRACT

The SAO optical satellite-tracking network that supported the National Geodetic Satellite Program is described. Particular attention is given to the instrumentation of the lasers, the Baker-Nunn cameras, and the station timing systems in use during the program. Network operations and data-reduction techniques are also discussed, along with a history of network site locations.

RESUME

Description du réseau optique de poursuite de satellite du SAO à la base du programme national de satellites géodésiques. Attention particulière donnée à l'instrumentation des lasers, des appareils photographiques Baker-Nunn et aux systèmes de synchronisation de la station utilisés au cours du programme. Egalement discutées: l'exploitation du réseau et les techniques de dépouillement des données, ainsi que l'historique des sites d'implantation du réseau.

КОНСПЕКТ

Описывается сеть оптического слежения за спутниками проводимого в Смитсониан Астрофизической Обсерватории, и которое оказало поддержку Государственной Геофизической Спутниковой Программе. Обращается особое внимание на оборудование лазеров, камер Бэкер-Нунн и систем синхронизирования станций в течение программы. Также обсуждаются работа сети и методы обработки данных совместно с историей местоположения станций входящих в сеть.

PART II

SAO NETWORK: INSTRUMENTATION AND DATA REDUCTION*

M. R. Pearlman, J. M. Thorp, C. R. H. Tsiang, D. A. Arnold,
C. G. Lehr, and J. Wohn

1. INSTRUMENTATION

1.1 Baker-Nunn Camera

1.1.1 Description of technique

The Baker-Nunn camera photographs satellites against a star background. It can photograph either passive sun-illuminated satellites or active satellite flashes under night-sky conditions. The Smithsonian Astrophysical Observatory Star Catalog (SAOC) has an average standard deviation in star position of 0".5 (epoch of 1963.5) (Staff, Smithsonian Astrophysical Observatory, 1966). The SAO field timing system is kept within 100 μsec or better of Universal Time Coordinated (UTC) as maintained by and referred to the United States Naval Observatory (USNO); hereafter, we shall express such time as UTC(USNO). With the use of the Catalog and the timing system, the reduction technique can provide an accuracy of 2". Observations are routinely reduced at the observing station to an accuracy of 40 to 60".

The camera was originally intended to photograph very small satellites in poorly known orbits without the aid of active systems on the satellites themselves. For this reason, it combines a fast optical system with a wide field of view. Pointing predictions need an accuracy of only several degrees.

*Also included in this Part is material originally prepared by G. Veis, K. Lambeck, and K. L. Haramundanis (see, in particular, Lambeck, 1968a; Haramundanis and Veis, 1971). We are grateful to them for their contributions.

1.1.2 Instrument description

The Baker-Nunn is a three-axis camera designed according to the specifications of SAO for satellite tracking – the optical system by James G. Baker, and the mounting and mechanical system by Joseph Nunn. The camera is approximately 2.5 m high and 3 m wide and weighs about 9000 kg. It combines an extremely fast f/1 optical system with a sophisticated film transport, and currently uses 55.6-mm Royal X extended red film (Kodak S0-338). It is best known for its light-gathering power and can photograph stars 3×10^4 fainter than those visible to the naked eye. The camera, which operates only at night, can photograph sun-illuminated satellites as well as satellites with flashing lights.

1.1.2.1 Camera operation

The Baker-Nunn camera (Figure 1) is basically a Schmidt telescope with refinements designed to improve its optical performance. The focal ratio of the system is f/1 with an aperture of 508 mm (20 inches). This focal length gives a film scale of $406'' \text{ mm}^{-1}$.

Light enters the camera through the three-element lens assembly (two positive and one negative), which corrects for spherical and chromatic aberrations, and is reflected from the 787-mm (31-inch) diameter spherical pyrex mirror onto the photographic film. During exposure, tension is applied to the film to force it to conform to the shape of the backup plate, which is configured to the required aspherical focal surface.

A clamshell-type focal-plane shutter begins and ends the exposure, which is preset for 0.2, 0.4, 0.8, 1.6, or 3.2 sec. A barrel-type shutter rotating in front of the focal surface chops the star trails or satellite trail (depending on the operating mode) and provides five reference breaks for measurement. The chopping shutter is coupled to a set of timing points that close at the third break and trigger a time presentation, readable to 0.1 msec, which is recorded on the film. When the exposure is completed, the film is advanced until the next frame is positioned against the backup plate. For a $15^\circ \times 5^\circ$ field, including time presentation, one frame is 152 mm of film.

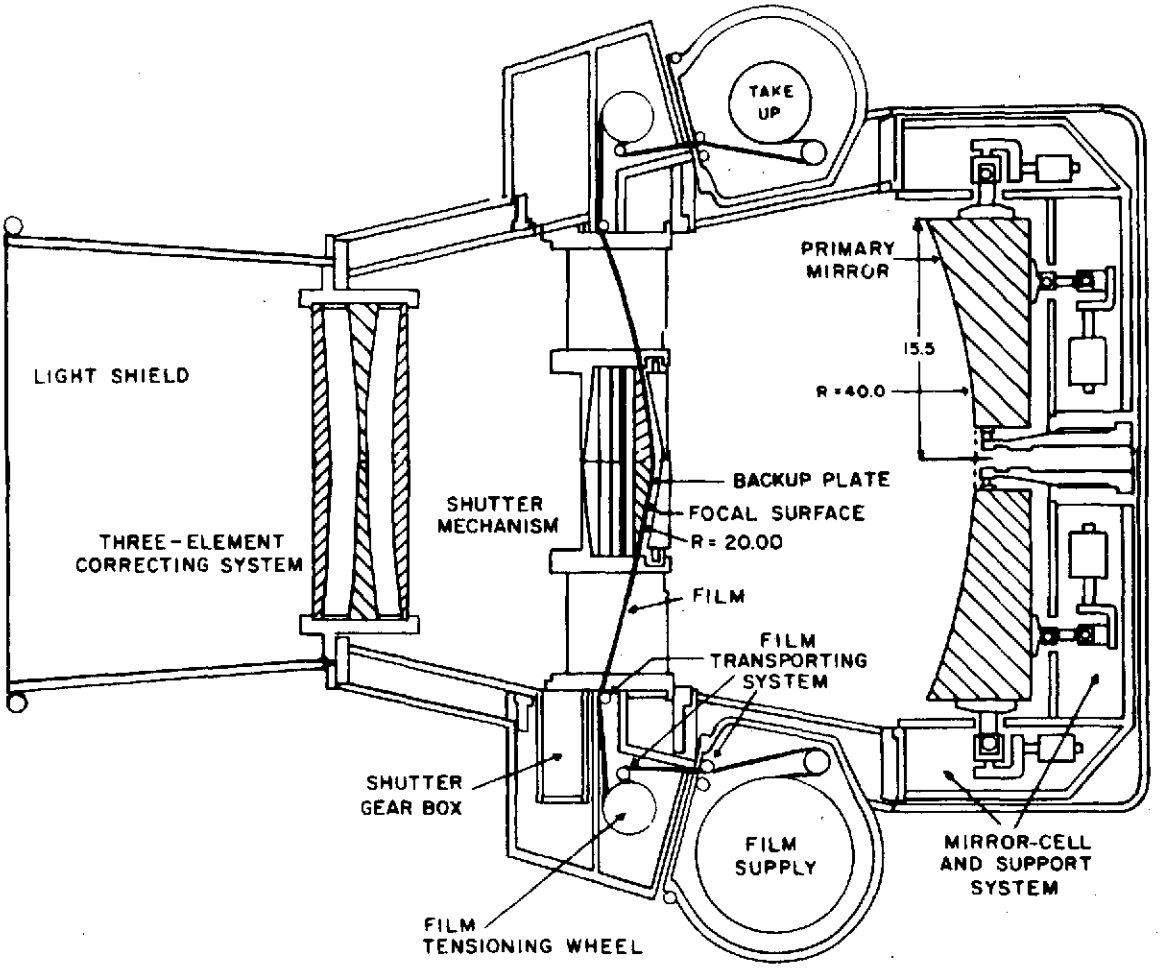

Figure 1. Cross section of the Baker-Nunn camera.

The film-transport mechanism, chopper shutter, and clamshell shutter are mechanically synchronized.

The camera is supported on a massive altitude-azimuth mount, with a third mechanized tracking axis normal to the altitude axis. Both altitude and azimuth are manually set, normally to ±0°.2, and clamped into position during photography. The camera then tracks along a great circle about the tracking axis at a prescribed rate. This motion approximates the apparent satellite motion over a short arc. Movement

about the azimuth axis (see Figure 2) is limited only by the length of the power and slave-clock cables, which permits approximately 400° of freedom. Altitude is limited by stops at 20° and 160°, and track angle is limited by microswitches at 27° and 153°. Continuously variable angular velocities of 0 to 7000" sec^{-1} are available.

1.1.2.2 Optics

The modified Schmidt optical system was chosen because it has a fast speed and a wide field of view and it yields good images over the entire field of view. To compensate for aberrations introduced by the spherical primary mirror, the camera has a three-element lens assembly, or corrector cell, mounted at the aperture stop. The cell has little focusing power but a strong spherical aberration approximately equal to and opposite that of the mirror. This permits large field, fast speed, and good images. In the Baker-Nunn, no attempt has been made to flatten the focal surface: Instead, the film is made to conform to the curved focal surface. Chromatic aberration is minimized in the corrector cell by the use of two types of glass: Schott K2FS-2 glass on the two outer elements and Schott SK-14 glass on the inner element. The outer glass is subject to etching in the presence of water, and care must be taken in the field to keep the outer surface dry.

The mirror is very accurately supported by 12 counterweights and a center collimating post to position the mirror at the correct distance from the film. This supporting system was designed to minimize image degradation due to temperature change and mechanical flexure.

1.1.2.3 Mechanics

The operation of the camera depends on the synchronous operation of a gross (clamshell) shutter and a fast (chopping) shutter. These shutters and the film transport are mechanically linked and driven by a synchronous motor and a cycle-speed-selector transmission. Speeds of 2, 4, 8, 16, or 32 sec per cycle can be selected. There are two exposures per cycle with an effective exposure time of one-tenth the cycle. The system was originally designed to have both a tracking and a stationary exposure on each frame. However, this complicated the problems of reduction, and the camera is

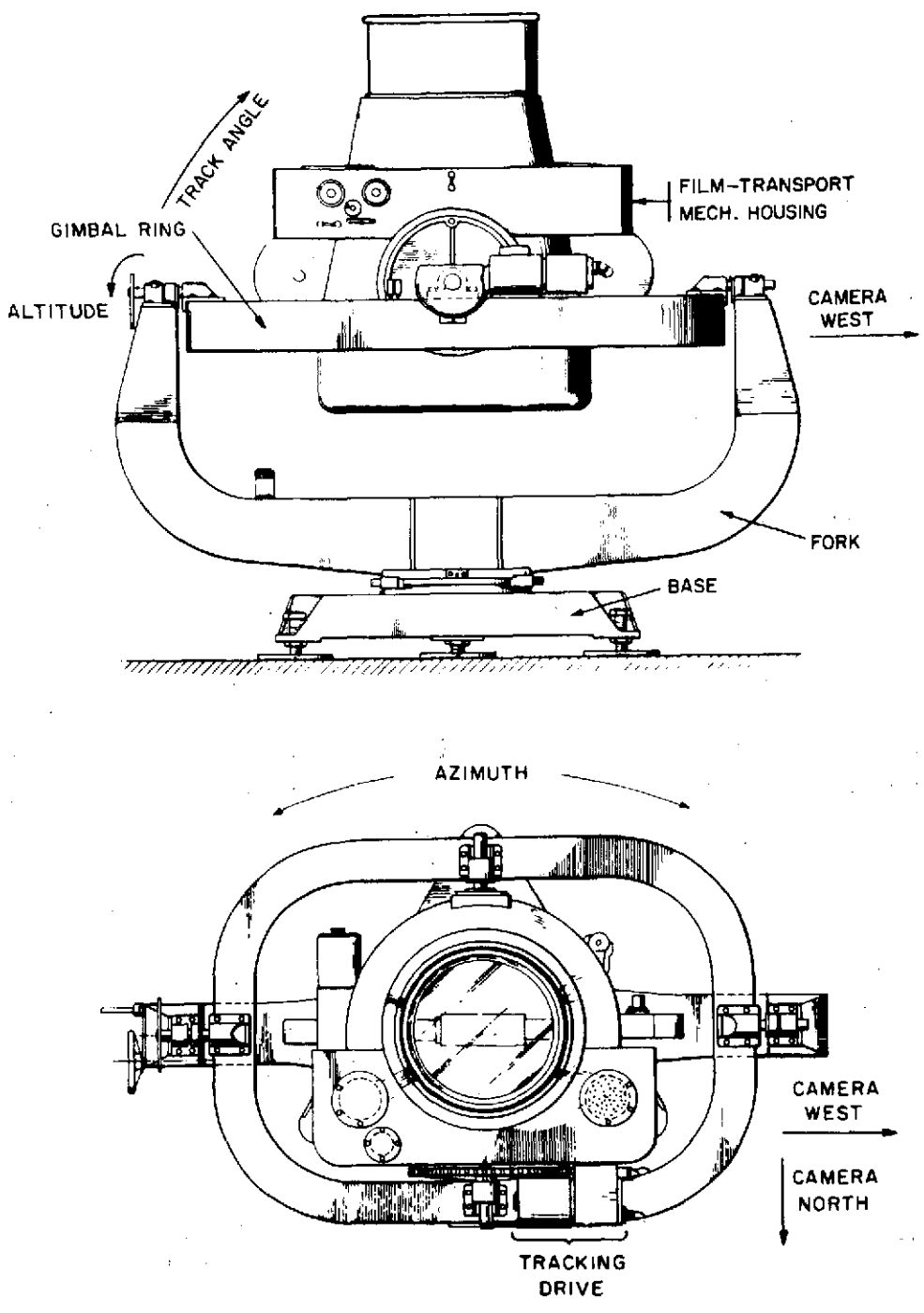

Figure 2. Top and side views of the Baker-Nunn camera, showing three axes of rotation.

now operated either in the stationary mode or in the tracking mode for the entire arc photographed. The latter is used for faint satellites, and the former, for the brighter (visual) satellites.

The film is transported from a supply reel to a takeup reel by means of two drums and a system of idler rollers. The drums are powered by a system that applies tension, transports, and holds to the film during the camera's operation cycle. The drive that operates the shutters also operates the film transport in such a way that as the cycle period is decreased, the speed of transport increases. For example, for a 2-sec cycle, the film is exposed and transported at 1 frame sec^{-1}.

Timing of an event on the Baker-Nunn camera requires exact knowledge of the position of the chopping shutter at the moment the time display is triggered. The camera timing points are adjusted so that an epoch corresponding to the third passage of the shutter through the field of view is recorded on the film. The break in the image caused by the passage of the shutter is called a "chop." Figure 3 is a Baker-Nunn photograph in which the satellite, shown by the arrow, is being tracked by the camera and the star trails are chopped five times. During the third passage of the shutter, a strobe lamp with a collimating lens, located in the body of the camera, illuminates the chopping shutter, whose shadow is recorded on the film. The length of this shadow on the film is measured and used in the reduction process to calculate the angular position of the chopper.

The track-angle axis of the Baker-Nunn camera mount is driven by a reversible synchronous motor, a Graham variable-speed drive, and a multiplier transmission. The Graham drive allows a variation in speed from 0 to 70" sec^{-1}. The transmission has three gearing ranges of 1, 10, and 100, allowing a total variation of 0 to 7000" sec^{-1}. The lower the gear range, the more accurately the angular velocity can be set.

1.1.2.4 Electronics

For proper sequencing of events, accurate exposure times, and accurate angular velocity, the camera must operate on precise 60-Hz power. Since this frequency is not available in many countries, the camera is operated on an amplified 60-Hz

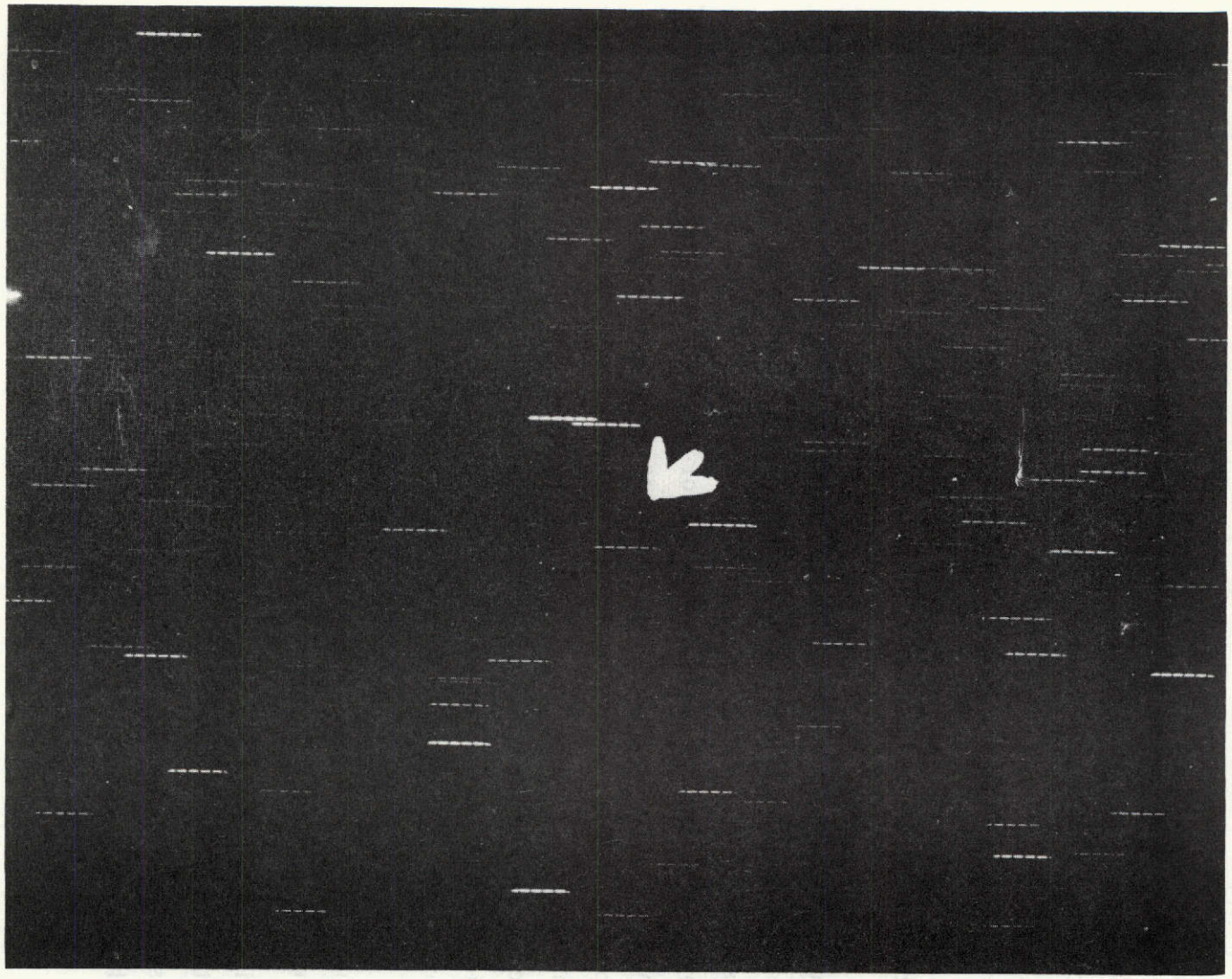

Figure 3. Baker-Nunn photograph of satellite 6506301 (EGRS-5). The satellite is indicated by the arrow, and the chopped star-image trails are in the background.

phase-shiftable reference signal from the station clock. By instantaneously increasing or decreasing the phase, the camera motors can be speeded up or slowed down. This allows the center (third) chop to occur at a preset firing time and the camera to be synchronized for satellite-flash photography.

A display of the station clock (see Section 1.3) is mounted on each camera at the point where film leaves the camera tube. On a demand pulse from the timing points, epoch is displayed and photographed by the camera. With the EECo clock, manufactured by the Electronic Engineering Company (EECo) of Santa Ana, California, time is displayed on the film in hours, minutes, seconds, and fractions to 0.0001 sec.

1.1.3 Accuracy and error budget

The accuracy of a satellite-position measurement with the Baker-Nunn camera is dictated primarily by 1) the film measurement and reduction procedure, 2) the accuracy of star positions, 3) atmospheric influences, and 4) the accuracy of timing maintained by the station clocks (see Section 1.3 for details on the station clocks). In those cases where the great-circle approximation is an accurate representation of the satellite's apparent motion, the instrumentation introduces very minor errors in measurement. In those cases where the great-circle approximation may no longer be accurate, the accuracy of the observation is degraded because the satellite image may be spread. This condition may occur when long exposure times are required to obtain images of very faint satellites, or when the satellite angular velocity is very large.

A summary of the principal error sources in the determination of star positions and an estimate of the total influence are given below (Lambeck, 1968b):

Measuring errors	1".2 (6 measurements)
Calibration of comparator	0".2
Film distortion and emulsion	0".8
Atmospheric refraction	1".1 (image motion for tracking camera) 0".8 (differential refraction) 0".3 (wandering)

Approximations in reduction method	0".2
Star positions from SAO Catalog	0".5 (random) 0".2 (systematic)
Total standard deviation of each star position	1".8 (stationary mode) 2".1 (tracking mode)

The principal error sources in the determination of satellite position and an estimate of the total influence are summarized below (Lambeck, 1968b):

Measuring errors	0".8 (12 measurements)
Calibration of comparator	0".2
Film distortion and emulsion shifts	0".8
Atmospheric refraction	1".1 (image motion along track, or flash images) 0".5 (image motion across track) 0".3 (wandering) 0".1 (parallactic refraction)
Contribution of standard deviation of 8 stars	0".8 (stationary) 0".9 (tracking)
Total standard deviation of satellite position	1".8 (stationary – along track) 1".5 (stationary – across track) 1".6 (tracking)

Before 1965, time was maintained at the stations by the Norrman clock and by the monitoring of WWV broadcasts at HF and VHF. The root-mean-square (rms) accuracy of an observation epoch was about 1 msec, with excursions of several milliseconds in some cases.

Installation of the EECo clock system in 1964 and use of frequency broadcasts on VLF and of portable clocks improved the timing situation. All the stations had ±100-μsec clock accuracies by 1967.

A summary of the overall accuracy of a single Baker-Nunn observation for different topocentric velocities of a satellite is given in Table 1.

Table 1. Accuracy of an observation as a function of topocentric velocity.

Cycle rate (sec)	Associated topocentric velocity of object (arcsec sec^{-1})	With VLF and portable clocks		With VHF	
		Along track	Across track	Along track	Across track
32	0– 250	1".8	1".8	1".8	1".8
16	250– 500	1.8	1.8	2.1	1.8
8	500–1000	1.9	1.8	2.3	1.8
4	1000–2000	1.9	1.8	2.7	1.8
2	>2000	2.0	1.8	3.7	1.8

Before the installation of the EECo clocks, the average accuracy of the synthetic observations was about 1".1 in each component. Now, with the improved timekeeping procedures, the average accuracy of the synthetic observation is about 0".9 along track and 0".7 across track.

1.2 Laser Ranging System

1.2.1 Description of technique

A laser ranging system is an optical radar used to measure the distance from a ground station to a satellite. When accurate timing and appropriate corrections for range bias caused by the atmosphere are incorporated, this is one of the most accurate satellite-tracking techniques available.

The technique is made possible by the availability of Q-switched lasers that produce sharply defined pulses of nearly monochromatic high energy in a beam with a very low angle of divergence. Equally important is the availability of nanosecond-risetime

electronics instrumentation to handle these optical signals. The fast-risetime, short-width pulses make time-interval measurements at nanosecond resolution possible on the basis of a single observation. The high degree of collimation enables the laser system to hit the satellite with a significant amount of radiant energy. Finally, the technique requires optical retroreflectors on the satellite to ensure measurable return signals. The monochromatic nature of the laser output allows for efficient filtering to improve the signal-to-noise ratio.

The basic ranging system consists of a laser transmitter, a photoreceiver, a mount for the transmitter and receiver, and a time-interval counter. The observed range time is the two-way time of flight of the laser pulse, measured by the time-interval counter.

In operation, the laser system is pointed to the predicted satellite position and is pulsed at specified times. During a normal satellite pass, the laser makes many range measurements in order to take advantage of the satellite geometry and to permit accumulation of data for analysis.

1.2.2 Instrument description

1.2.2.1 Smithsonian Astrophysical Observatory laser system

The SAO laser system (see Figures 4 and 5) was designed for the particular requirements and needs of the Observatory's program in satellite geodesy. The system has a static-pointing mount (or pedestal) that is aimed by means of computed predictions of satellite azimuth and altitude. This method of steering permits the system to operate when the station is in daylight or the satellite is in the earth's shadow, i.e., 24 hours per day. The static-pointing mount was selected because it is economical and operationally simple. The system operates routinely at 4 pulses min^{-1} and is capable of operating at rates as high as 10 pulses min^{-1}.

The laser, built in an oscillator-amplifier configuration, generates an output of 5 to 7 joules in a 20-nsec pulse (half-power, full width). The laser transmitter system was produced by Spacerays, Inc., of Englewood, Colorado. The system uses a

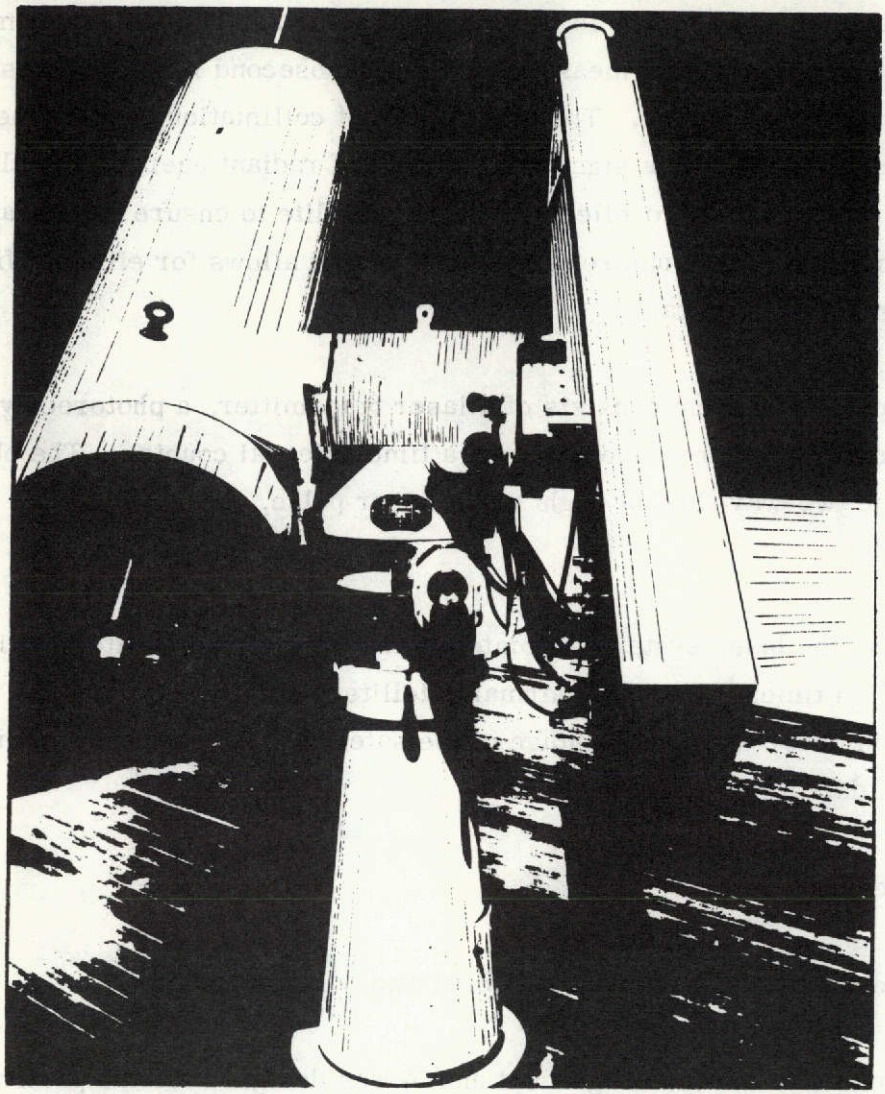

Figure 4. Stylized view of SAO laser tracking system.

Pockels cell and a Brewster stack for a Q-switch and can maintain a pulse repetition rate of 10 ppm. Both the 0.95-cm (3/8-inch) diameter oscillator ruby rod and the 1.59-cm (5/8-inch) diameter amplifier rod are mounted in 15.24-cm (6-inch) double elliptical cavities, each containing two linear flashlamps. The optical cavity of the oscillator is formed by a flat rear mirror, with a reflectivity of 99.9%, and the uncoated front of the oscillator rod.

The oscillator output of 1 to 2 joules is coupled into the amplifier through a small beam-expanding telescope. The amplifier has a single-pass gain of about 4. Both ends of the amplifier rod are antireflective-coated.

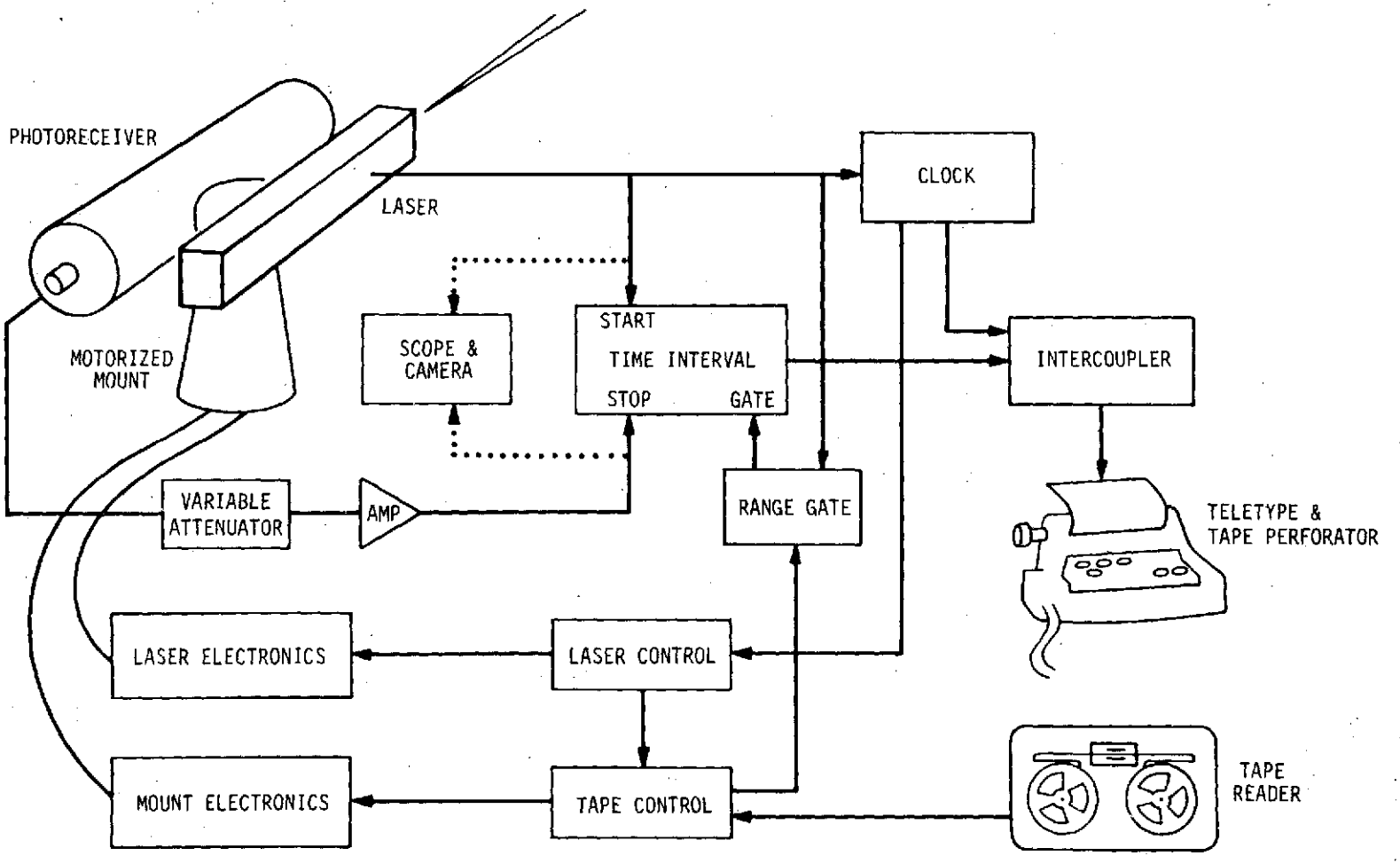

Figure 5. Block diagram of the laser system.

The amplifier output is expanded to fill the 12.7-cm (5-inch) objective lens of a Galilean telescope. The telescope optics allows adjustment of the output beam divergence from a diameter of 0.5 to 5.0 mrad. Mounted at the output of the laser, ITT FW128 photodiodes pick up atmospherically scattered light from the outgoing pulse and send an electrical start signal to the time-interval counter.

The optical elements of the laser are mounted on the machined upper surface of an aluminum I-beam so that dimensional stability between the optical components will be maintained for all pointing orientations. Separate water-cooling systems are provided for the ruby rods and for the flashlamps. The coolant for the ruby rods is maintained at a temperature of 10° ± 1° by thermostatically controlled cooling or heating elements. The lamp coolant is maintained within 10°C of the ambient air temperature. There is provision for applying nitrogen under pressure to the cavities, but experience has shown that this is not necessary. A cover over the I-beam is sealed, and desiccated air under slight pressure is circulated through the system.

The electronics of the laser transmitter are basically power supplies and pulse trigger circuits. The 1875-μf capacitor bank for the oscillator and amplifier lamps can be operated from 2000 to 4000 volts DC. Serial triggering of the lamps begins the discharge, which lasts slightly over 1 msec. Approximately 800 μsec after the lamp pulse begins, the system is Q-switched by quickly switching to ground the high-voltage input to the Pockels cell.

The ranging-system electronics consists of a clock, a firing control, a range-gate control, and a time-interval counter. The clock is synchronized to within ±1 μsec of the station master clock, controls the firing time of the laser, and provides the epoch of observation. The firing rate and the time of the laser firing are controlled by the laser control unit. The laser firing time can be shifted by a multiple of 0.001 sec, with a maximum of ±10 sec, to account for the early or late arrival of a satellite at a predicted point in its orbit. The range-gate control unit sends a delayed pulse of adjustable width to the counter so that the counter can be stopped only during a small interval of time about the predicted range time. The range gate provides protection against triggering by sky-background noise. The Eldorado 796 range counter is a time-interval counter with 1-nsec resolution. It uses leading-edge voltage threshold

discriminators on the start- and stop-signal lines. A start signal ranging from 5 to 20 volts is produced by the photodiode at the laser output. This signal is not processed nor amplified before it reaches the start channel of the counter. The photomultiplier tube (PMT) output passes through a 0- to 50-db variable-step attenuator and a 32-db fixed-gain pulse amplifier before it reaches the stop-channel discriminator.

Stepping motors that point the mount are driven by position-control electronics manufactured by Zehntel, Inc., Berkeley, California. Position information is maintained in the control units, which generate the appropriate number of drive pulses for the motors once a new azimuth or altitude position is demanded of the system.

The laser ranging system has a data subsystem that reads predicted satellite positions from punched paper tape and sends the information to the mount and laser control electronics and to the range gate. Azimuth and altitude pointing angles are given in thousandths of a degree; the range-gate setting is specified in microseconds. The epoch for a predicted observation is displayed. Once the predictions start, operation continues automatically until the satellite pass is completed. Operation of the punched paper-tape reader is synchronized with the rest of the system by the laser control unit. Output data are also handled automatically by the data subsystem. The binary-coded-decimal (BCD) form of the epoch of firing and the range-time interval in nanoseconds is serialized, converted to Baudot code, and printed by an ASR32 teletype machine. ASR32 punched tape can be fed directly into the radio communications system once a heading is put on each data pass. The input/output, clock, and control systems were designed and constructed by SAO.

The receiving telescope, made by Tinsley Laboratories, Inc., Berkeley, California, is a 50.8-cm (20-inch) Cassegrain system with additional optics designed to focus an image of the primary mirror on the photocathode of the PMT. The optics following the flat secondary mirror pass the collimated return signal through a 7 Å filter that is both tilt- and temperature-dependent. A micrometer tilt adjustment tunes the filter to compensate for effects of age and temperature. Adjustable field stops and a provision to insert combinations of neutral-density filters are available.

The photodetector, an RCA 7265, was chosen for its quantum efficiency of 4% or greater at 6943 Å. This PMT has a gain of 5×10^7 and a risetime of approximately 3 nsec as operated in the SAO system.

The azimuth-altitude static-pointing mount, also built by Tinsley, has a pointing accuracy of better than ±30". Verification of the mount position is made by viewing a goniometer in the mount; but under normal operations, the system is driven in a open-loop fashion from the electronic control unit. The stepping-motor drive-system gearing allows for slewing speeds of 2° sec^{-1} and positioning increments of 0°.001. The unit can be hand-cranked, but this limits the pulse repetition rate to 2 ppm, whereas the laser and the data subsystem have the capability to go to 10 ppm.

1.2.2.2 Athens laser system

The laser system in Athens was built as a cooperative project between the National Technical University (NTU) and SAO and began operation in 1968.

The laser transmitter is a Q-switched ruby laser, manufactured by the TRG Company, now Hadron, Inc., Westbury, Long Island. The laser transmitter has a 1-joule, 24-nsec (half-power, full width) output pulse. The Q-switch is a rotating roof prism with a bleachable dye. The roof prism is driven by a synchronous motor at a speed of 30,000 rpm (500 rps). The bleachable dye is Kodak Cryptocyanine, a metal pthalocyanine, in an alcohol solution. The laser beam divergence of 5 mrad is reduced to 1 to 2 mrad with a 5-cm-diameter Galilean telescope.

The flashlamp power supply has a 900-μf capacitor bank with a maximum charging voltage of 975 volts (960 joules). A typical threshold is 560 joules when all optical components are in good condition and accurately aligned.

Photosensitive monitors are used both to start the ranging counter when the laser beam leaves the transmitter and to monitor the output power. An RCA 931 PMT senses the light reflected from a glass plate oriented 45° to the beam. Its output is used to start the range counter. The power monitor is an EG&G SGD-100 semiconductor photodiode that senses the laser light scattered from the back of the rotating-prism Q-switch. The output of the photodiode is monitored on a high-speed oscilloscope.

The receiver of the system is a Cassegrain telescope with a 40.6-cm (16-inch) parabolic primary and a hyperbolic secondary. The system has a focal length of 6.55 m and a focal ratio of 16. Incoming light first passes through a 10' field stop at the focal plane and through a 20 Å interference filter and then falls directly on the PMT (RCA 7265), which is uncooled and operates at an anode voltage of 2400 volts.

The laser and photoreceiver are mounted on a modified surplus 3-inch gun mount, which is hand-cranked in altitude and azimuth by two observers. One observer tracks in azimuth and the other in altitude by observing the sun-illuminated satellite in the illuminated reticle of a 2.7-cm (5-inch) elbow telescope. Both observers sit directly on the mount and move with it as a system. This method of aiming the laser limits operations to times when the satellite is in sunlight and the station in darkness. Pulse detection is by leading-edge fixed-threshold discriminators.

The outgoing laser pulse starts a counter with 1-nsec resolution. The light pulse reflected from the satellite enters the receiving telescope and goes through the optical chain to the PMT, whose output is amplified and used to stop the counter. A range gate between the pulse amplifier and the ranging counter reduces the possibility of erroneous range measurements due to sky-background noise.

During operation, the laser fires every 30 sec – on the even minute and at 30 sec after the minute. Both the exact firing time of the laser and the range measurement are recorded with a camera system that automatically photographs the counter readings.

1.2.3 Accuracy and error budget

The accuracy of the laser systems can be discussed in terms of random and systematic error components. The former are those that are uncorrelated and appear as range scatter on a point-to-point basis, while systematic errors are correlated and vary regularly over a single pass or longer.

The random noise level of the systems has been computed from data on short-arc analyses taken during the International Satellite Geodesy Experiment (1971) and the Earth Physics Satellite Observation Campaign (1971 to 1973). This type of analysis generally detects only random errors, because systematic errors tend to be absorbed into the orbit parameters when they are adjusted in the least-squares-fitting procedures. The best-fitting curves for single transits were obtained by varying the mean anomaly, its first derivative, and the right ascension of the node. The standard deviation of the data varied from 30 to 120 cm, with a median of less than 60 cm. The dominant random-error component is due to the variation in size and shape of the return signals. The fixed-threshold, leading-edge pulse-detection system we are now using is very susceptible to such irregularities in return pulses. The return signals from the PMT may contain as few as 1 to 10 photoelectrons. They also may vary widely in size and shape during a single transit, owing primarily to scintillation from the satellite retroreflector array, irregularities in the laser beam pattern, and the statistical nature of the PMT detector. The expected random variation in the triggering times of the leading-edge threshold is a few nanoseconds (50 cm) for our transmitted pulse width of 20 nsec. Other random influences in the data, such as the least-count error in the counter and the random variability of the atmosphere, have smaller effects.

Systematic errors are considerably more difficult to grasp. However, the size of the systematic errors, per pass, has been estimated from performance and field tests. The ±50-μsec uncertainty in epoch timing could be responsible for a systematic error of as much as 35 cm for some satellite-pass geometries. The models used by SAO and others compute the optical range correction due to tropospheric refraction from ground-based data. These models have an estimated systematic error of a few centimeters at zenith, with an approximate secant dependence for zenith angles down to about 70°. The residual error in current tropospheric-propagation-correction models is, on the average, probably about 4 cm per pass. The geometry of the satellite and the placement of the retroreflectors relative to the satellite's center of mass are responsible for a systematic contribution of about 10 cm. This error is the result of the following uncertainties: 1) in satellite attitude, 2) in retroreflector optical properties and placement, and 3) in the resultant return-signal shape and size from the entire satellite retroreflector array. The fixed-threshold, leading-edge detection

system is probably responsible for systematic errors of about 3 nsec (50 cm) for a 20-nsec pulse width. This is in addition to the random variations and arises from systematic differences in the triggering point on the outgoing and the return pulses. Calibration on a fixed target is also an area where systematic influences are introduced through survey error and inaccuracies in the time-interval measurement. It is estimated that systematic errors of about 10 cm may be introduced during calibration. If the sources of these errors are assumed to be independent, the total estimated influence, or root sum squared, is about 57 cm.

A two-laser collocation test was performed on satellite 6800201 (Geos 2) at SAO's Mt. Hopkins Observatory, Arizona, from October 1969 to January 1970. SAO's laser there and a mobile laser system operated by National Aeronautics and Space Administration (NASA) participated. The objective was to determine the relative accuracy of two laser systems that were being used in the routine collection of satellite geodetic data. Since the two systems were built, calibrated, and operated by independent groups and since the instrumentation designs were different, the experiment gave a good estimate of the system-induced bias errors that can be expected. During the experiment, the two systems demonstrated a relative ranging accuracy of 1 to 2 m. In half the satellite passes, the difference in the range measurements of the two systems had a bias of less than 1.2 m (see Figure 6). The sign of the bias changed several times during the 4-month experiment. At the time, it was felt that these bias components were primarily introduced into one or both of the systems during the calibration procedure, which involved a determination of the system delay by ranging on a target at a known distance from each laser. Both systems have undergone significant modifications since the time of the collocation, and the systematic error in each has been substantially reduced.

1.3 Timing System

1.3.1 Station clock

Each station has a timekeeping system to provide precise epoch data for each observation. The station clock is basically a crystal oscillator, a time accumulator, and a system of time and frequency monitoring aids. The clock has a dual-channel redundancy and a battery-backed power system to guard against loss of time continuity.

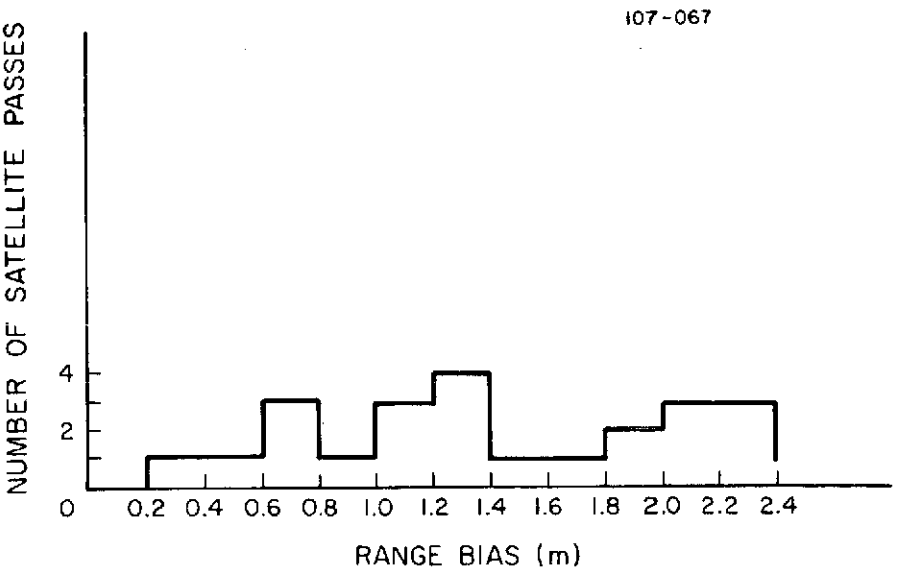

Figure 6. Distribution of relative system biases.

The Norrman clocks, which were used in the Baker-Nunn network until the mid-1960s, relied on a WWV-emitted time pulse and tone reference for both time and frequency settings. The active electronic components were vacuum tubes, and the time readout was in the form of rotating mechanical indicators and a rotating spot on an oscilloscope. Limitations on the stability and reading accuracy of the oscilloscope display led to the use of a fully electronic system featuring solid-state digital circuitry and a high-stability frequency standard.

The present clock has a Sulzer 5-MHz crystal oscillator stable to 1×10^{-10} day^{-1} and is generally kept within 5×10^{-10} of UTC(USNO). It can be adjusted to 1×10^{-10}. The frequency of the oscillator is maintained through frequency and phase comparisons with stable VLF transmissions from stations such as NAA and NLF.

A locally generated 100-kHz signal is phase-locked to the VLF signal and then compared in phase to a 100-kHz reference signal from the clock. A relative phase position record is kept, which helps maintain station time to greater accuracies than is possible with the HF timing pulses.

The components of the EECo timing system are the clock's accumulator, the Sulzer oscillator, a VLF tracking receiver, a WWV receiver, a chart recorder to display the VLF/clock phase relationship, an oscilloscope (Tektronix 561A), and an AC-DC-AC battery-backed power system. Some stations have a secondary timing system, made up by duplicating most of these same chassis. Other stations have a backup clock, consisting simply of an oscillator and a miniaturized digital counter.

The accumulator of the master clock system is a 100-kHz digital counter that offers a visual display of time in hours, minutes, seconds, and fractions of seconds to 10-μsec resolution, as well as a BCD digital presentation of time. A digital phase-shifting circuit allows the clock to be adjusted in 0.1-μsec steps for precise timing control.

Timing at the stations is checked primarily by means of portable-clock trips (see Section 1.3.2). Although the VLF tracking receiver does not give epoch information, it does provide an accurate method of maintaining a record of time position relative to the setting obtained from the portable-clock comparison. Maintenance of accurate time between trips is facilitated in some locations by using the time tick of WWV and time sources of other agencies. The HF time signals offer the station a convenient time reference, but accuracies are limited to ±0.5 msec at best, owing to variations occurring over the long propagation paths to the stations.

At the laser stations, clocks routinely provide epoch to ±50 μsec (UTC) by means of portable-clock trips, which are conducted once a year on the average. During specific experimental periods, time has been corrected to ±25 μsec through extra care in VLF monitoring, more frequent checks by portable clocks, or other means of reference. The less stringent timing requirements at the camera stations (±100 μsec) are achieved through less frequent portable-clock trips.

1.3.2 Station-clock synchronization

Synchronization of the station clocks throughout the network is achieved by relating all the time and frequency references to UTC as maintained by USNO. The field stations steer their clock frequencies with VLF transmissions from stations NAA and

NLK, and in some cases, WWVL or WWVB. Crude epoch checks are made at many of the stations by monitoring HF/VHF time signals. The USNO and the National Bureau of Standards (NBS) timing bulletins, which give the relative phase values of VLF stations and time intercomparisons with other timing services, are used to relate all field timing values to UTC(USNO).

Use of a portable clock is the principal method of epoch synchronizing with a source of reliable timing. The comparison of the portable clock with the clock at the station gives a correction relating the station time to the source time, and published comparison values relate the source time to UTC(USNO). Therefore, each field-station clock is referred to a common time scale with an accuracy dependent on the reliability of the portable-clock comparison and on the accuracy of the published comparison value.

The clock trips to the field stations have been conducted with a Sulzer A5 portable crystal clock that carries time related to UTC(USNO). These trips have been run by SAO or, in some instances, by other agencies (such as NASA, USNO, Naval Research Laboratory, and NBS) who have either carried an SAO clock or been in the vicinity of an SAO field station with a clock of their own. Portable-clock comparisons are made with each station on a biennial basis. However, to maintain higher levels of accuracy and reliability, a portable-clock comparison is made at least once a year at the laser stations. Time corrections, determined to be necessary by portable-clock comparisons or intercomparison between station-clock and VLF-monitor readings, are documented and applied directly to the station clocks. Corrections for the difference between the VLF stations and USNO are applied in Cambridge during data preprocessing.

1.3.3 Accuracy and error budget

The accuracy of station timing depends on 1) the success of the portable-clock trips, 2) the ability to trace the relationship of the time references back to USNO, 3) the ability of the station to maintain the time setting with the aid of the VLF tracking receiver, and 4) the uncontrollable variations in propagation path of the VLF signal. The requirements for system timing originally called for the station clocks to be within ±1 msec of WWV-emitted (rms of net deviation from UTC(NBS) over a

month). This requirement was tightened to ±100 μsec UTC(USNO) for the camera stations and ±50 μsec for the laser stations. This improvement was made possible by the installation of the EECo timing systems in the mid-1960s and was realized by 1967. In practice, many of the camera stations have been operating within ±50 μsec of UTC(USNO).

The synchronization accuracy by use of a portable clock depends on the amount of unpredictable time drift experienced during the period spent traveling to and from the field station. Most of the clock trips to the field stations use a crystal clock and provide an epoch time set accurately to within 5 to 25 μsec of USNO. The least reliable results have been in India and South America, where the stations are fairly remote and long travel times are involved.

USNO publishes a weekly bulletin, "Daily Phase Values, Series 4," giving the emitted phase values of the major VLF transmitting stations to 1 μsec. The time differences between UTC as maintained by USNO, NBS, and the Bureau International de l'Heure (BIH) are well documented by each agency to microsecond accuracy. The relationships between the HF time broadcasts of foreign countries and UTC(USNO) are generally less precisely known.

Timing accuracy at the field station is maintained by controlling the clock drift with the aid of VLF monitoring equipment. In cases of minor clock failures, time has often been recovered with fair accuracy by referring to backup clocks and to VLF and HF monitor references. The clock time drift is a product of oscillator frequency offset and is generally controlled to keep the station epoch within 50 μsec of the VLF reference position.

The accuracy of VLF-derived time is a function of receiver and propagation-path stability. The uncertainties of the day-to-day and seasonal path variations added to the error contribution of the receiver amount to less than 5 μsec in epoch uncertainty. The system timing accuracy is a composite figure encompassing setting accuracy, uncorrected drift of the clock, and inaccuracy of the VLF monitor.

The degree of accuracy in setting a portable clock gives the initial accuracy of the station epoch, and VLF monitoring permits the clock to maintain time. When subsequent incidents of minor clock failure that affect time and frequency increase the epoch's uncertainty to ±50 μsec, another portable-clock comparison is considered. When requirements are stringent, additional efforts are made to obtain more accurate time comparisons, to reduce the oscillator's drift, and to minimize the accrual of uncertainty due to repeated clock resets. This extra effort is the key to maintaining station epochs at the ±50-μsec level with a minimum of clock trips.

2. DATA REDUCTION

2.1 Baker-Nunn Data Reduction

2.1.1 SAO Star Catalog

The Smithsonian Astrophysical Observatory Star Catalog was compiled in the early 1960s to meet the needs of computer-oriented reduction of photographic plates of artificial earth satellites. The Catalog covers the entire sky uniformly, contains proper motions for all the stars given, and provides an average density of four stars per square degree. All the catalogs used were reduced to a homogeneous reference frame, that of the FK4. The final Catalog contains close to 260,000 stars. The SAOC contains the following data:

Right ascension and declination for equator, equinox, and epoch 1950.0 and for epoch of observation.

Standard deviation of the position at epoch 1950.0.

Mean epochs of the original observations, given separately for each coordinate.

Standard deviation of each coordinate at epoch of observation.

Annual proper motion in right ascension and declination.

Standard deviation for each proper motion.

Visual magnitude (for 99% of the entries).

Photographic magnitude (for 50% of the stars).

Spectral type (for 83% of the stars).

Durchmusterung number (BD, CD, CPD).

Reference to the source catalog.

Star number from the source catalog.

Special notes.

The SAOC is available in three forms: magnetic tapes, a printed version, and a set of star charts.

A. All the Catalog data have been stored in a blocked binary format on magnetic tapes compatible with IBM 729 II tape units. The data have been sorted at epoch 1950.0 by right ascension in 10° bands of declination. A description of the tape format and the means for obtaining copies are available from

Star Catalog
Smithsonian Astrophysical Observatory
60 Garden Street
Cambridge, Massachusetts 02138

B. A four-volume printed version contains virtually all the data available on the magnetic tapes. Owing to space limitations, some of the magnitudes have been rounded to one less significant digit than is given on the magnetic tapes. The book is organized in the same way as the magnetic tapes (by right ascension in 10° bands of declination at epoch 1950.0). Its introduction describes in detail the preparation of the Catalog. The set of four volumes can be obtained from

Superintendent of Documents
U.S. Government Printing Office
Washington, D.C. 20402

C. A set of 152 star charts has been reproduced at a scale of 6!95 mm^{-1} (the scale of the films of the Baker-Nunn cameras). In addition to the stars of the SAOC, the charts contain special symbols for galaxies brighter than 13th magnitude, globular clusters, planetary nebulae, all objects listed in the New General Catalogue (NGC) and Index Catalog (IC) of Dreyer, and a small number of stars close to the south celestial pole for which the proper motions were not known. The introduction to the boxed set of charts describes their preparation and the projections used; it also includes several useful indices and complete lists of the constellations and of the 198 stars with names. The star charts can be obtained from

The MIT Press
28 Carleton Street
Cambridge, Massachusetts 02139

Table 2 lists the catalogs used in the compilation of the SAOC, along with the original system of each and the zone it covers. Since the FK4 was not originally available, a catalog not in the FK3 system (except the FK4) was initially reduced to the FK3 system before its data were combined with those from the other catalogs. When data from all the catalogs were combined, duplicate entries for the same star were eliminated.

Table 2. Catalogs used in the SAO Star Catalog.

Declination*	Catalog	Original system
+85 to +90	Yale	Instrumental system
+60 to +85	AGK2†	FK3
+50 to +60	Yale	Instrumental system
+30 to +50	AGK2†	FK3
+20 to +30	Yale	FK3
-30 to +20	Yale	Instrumental system
-40 to -30	Cape Annals	FK3
-52 to -40	Cape Zone	Instrumental system
-64 to -52	Cape Annals	FK3
-90 to -64	Melbourne	Instrumental system

*Positions from the GC, FK3, and FK4 occur in all sky areas.

†For this catalog, proper motions have been computed by SAO.

The order of preference in the choice of data from the catalogs was the following: 1) FK4, 2) FK3, 3) GC, and 4) Cape, Yale, AGK2, Cape Zone, Me 4, and Me 3, according to epoch of observation. Each catalog in the last group covers only a segment of the sky and therefore overlaps only marginally with another; where overlaps do occur, the more modern position has been taken. The GC is older than the three fundamental source catalogs (Cape, Yale, AGK2), but because its positions and motions were derived by the combination of many sources, it appears to represent the positions and motions for the stars better than do the zone catalogs. With respect to the standard deviations of the positions when dated to a modern epoch (say, 1965.0), this proved to be the case in only about one-third of the GC positions. A small number of stars missing from the SAOC in the range of visual magnitude m_v,

$$6.5 < m_v < 7.5 \quad \text{(where } < \text{ stands for fainter than)} \quad ,$$

were apparently too faint to be included in the GC and too bright to be in the zone catalogs. Figure 7 illustrates the number of stars of each visual magnitude retained in the final SAOC.

After all the catalogs were combined into a unified list at epoch, equator, and equinox 1950.0, the positions and motions were reduced to the FK4 system.

The positional accuracies of the SAOC can be divided into either random errors (standard deviations) or systematic errors.

The first has been evaluated in three ways in the Catalog itself: 1) by tabulation of σ_{1950}, the standard deviation of the position at epoch 1950.0, for every entry in the Catalog, with errors in both position and proper motion taken into account; 2) by calculation of the average standard deviation for the entire Catalog at epoch 1963.5 $\langle \sigma_{1963.5} \rangle = \pm 0\overset{''}{.}49$; and 3) by a histogram of $\sigma_{1963.5}$ and $\sigma_{1975.0}$, in which the number of stars within each $0\overset{''}{.}1$ of standard deviation are given (Figure 8).

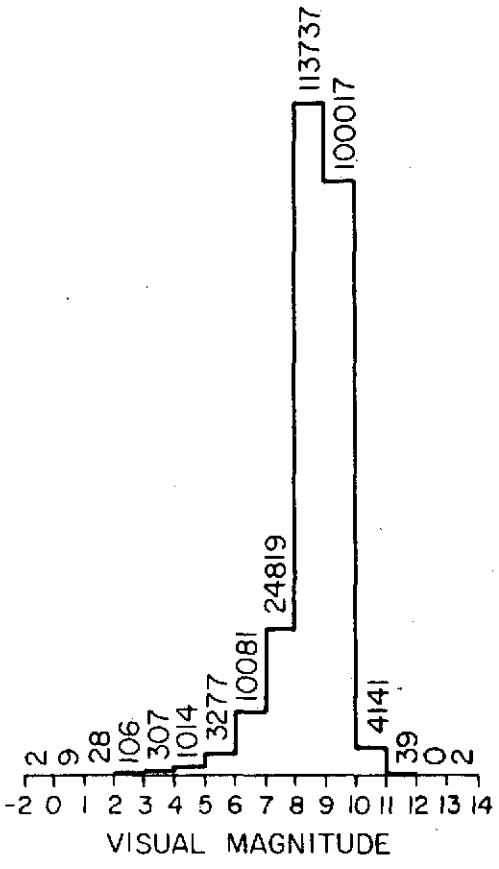

Figure 7. Number of stars of each m_v in SAOC.

All computations were performed with the simplified formula given in the Catalog. It has been criticized (Eichhorn and Googe, 1968) as giving standard errors that are somewhat too large. Another evaluation of the Catalog standard deviation (Haramundanis, 1967), comparing the standard deviation at 1964.5 with the epoch of observation (see Figure 9), illustrates that a large part of the cumulative error is a direct result of errors in the proper motions.

Any evaluation of the random errors of the SAOC by means of the data given in it depends naturally on the fact that the original errors have been correctly assigned; it should be realized that, in general, the errors in the SAOC were assigned en bloc.

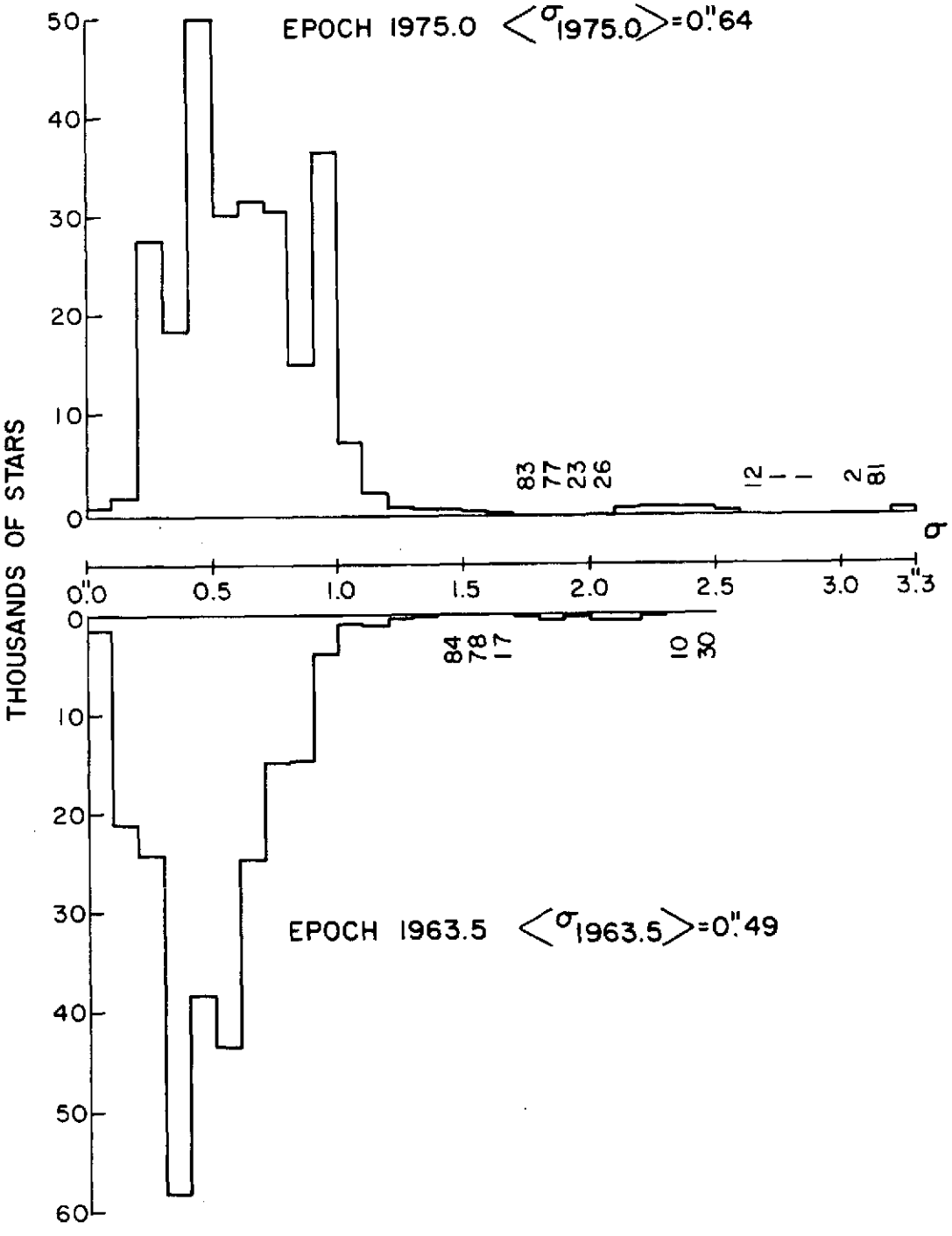

Figure 8. Histogram of standard deviation of position at epoch 1963.5 and 1975.0. Abscissa = σ (arcsec); ordinate = number of stars per 0".1 standard deviation.

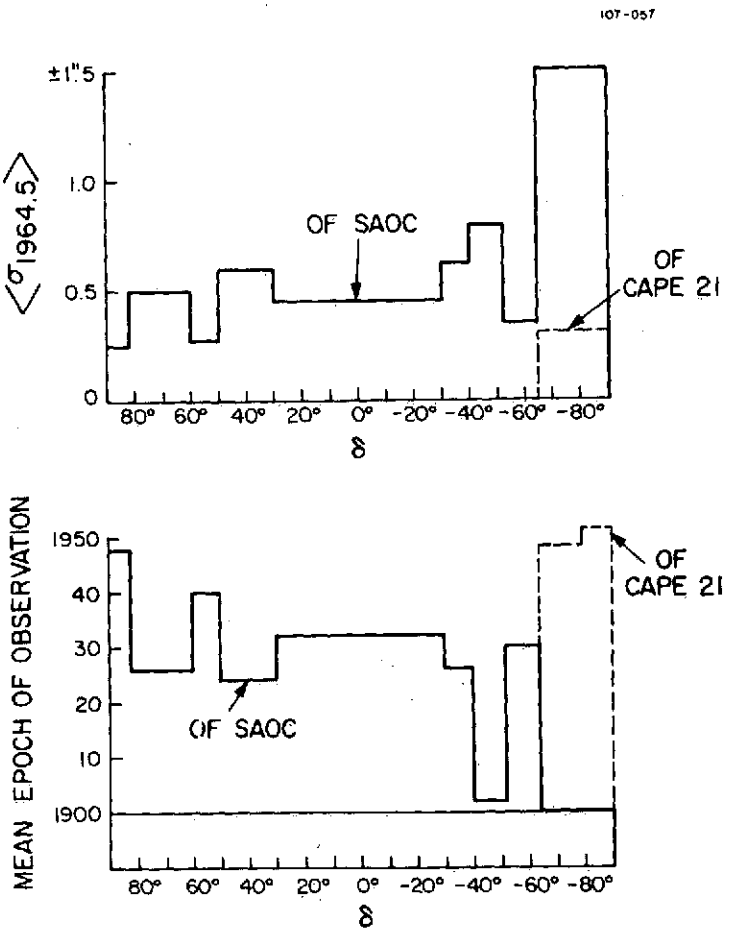

Figure 9. Mean standard deviation at epoch 1964.5 and mean epoch of source-catalog positions as a function of declination δ.

The graph for 1964.5 shows that in the far southern hemisphere, there are some serious deficiencies in the existing SAOC positions and motions.

Evaluation of the systematic errors of the SAOC requires an independent check of the positions and motions by comparison with a catalog not used in the SAOC compilation. Two such studies have been carried out: one (Scott and Smith, 1967) north of +60°, the other (Haramundanis, 1970) south of -63°. These studies attempted to determine the deviation of the SAOC system from that of the newer observations, both sets of data purporting to be in the FK4 system. Both studies indicated that a source-dependent systematic error exists in the SAOC at certain declinations. In the northern

sector under comparison, the systematic error was not more than 0".2 on the average. In the southern hemisphere, the errors were similar when the comparison was made with the GC stars, but they were substantially larger (1 to 2") when compared with stars in the Melbourne catalogs (see Figure 10). In the preparation of the SAOC, no systematic corrections were applied to the Melbourne motions, because none were available. Further, the Melbourne catalogs were the only ones at that time that contained accurate positions and proper motions in that zone.

Both comparisons are of positions in the FK4 system and are affected not only by the intrinsic errors of each catalog but also, possibly, by the errors of the FK4 system itself.

The SAOC has been extensively used in plate reductions over the past 11 years. For reduction purposes, a single tape is prepared for the appropriate year, and the data are recorded in an order and form most efficient for computerized random-access searching. In the thousands of plate reductions obtained using the SAOC, no significant errors have been encountered. By taking the rms average of the residuals of the star positions (observed - computed) in a sample of plate reductions, an upper bound can be obtained for the error in the positions. This value is close to 2".0. With the available films and equipment, this is as good as can be expected, although it cannot be used for testing the star positions themselves, since their intrinsic accuracy is better than 2".0.

2.1.2 Precise reductions

2.1.2.1 Methods and rationale

The reduction procedure of SAO's Baker-Nunn observations has been discussed by Haefner (1967) and Haefner and Martin (1966); the latter presents, with some minor modifications, the standard reduction procedures now in use at SAO. Our reduction procedure is based on astrometric principles, which differ significantly from the photogrammetric methods, widely used in conjunction with ballistic cameras.

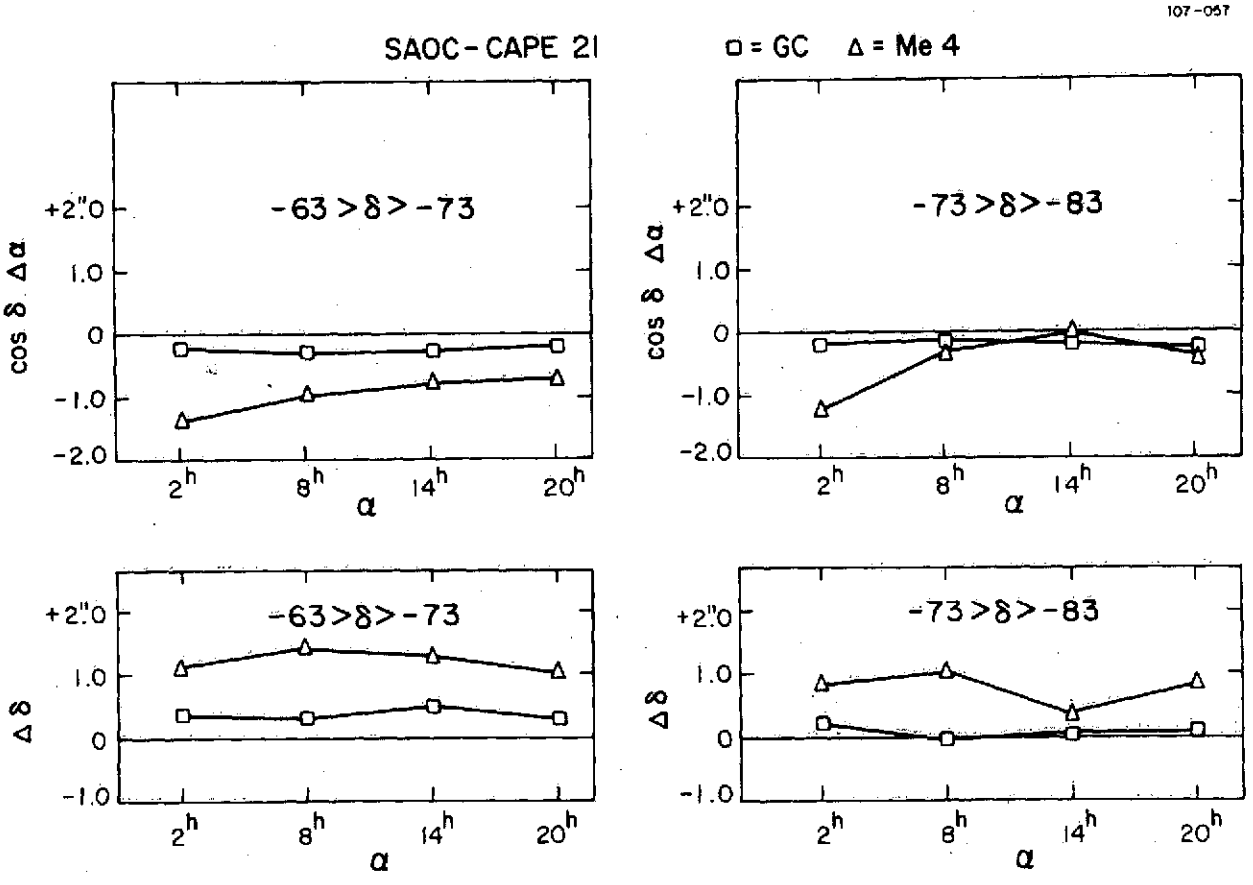

Figure 10. Systematic errors SAOC - Cape 21 at 1950.0. □ = SAOC stars from GC; △ = SAOC stars from Me 4.

Because of the differences in the data-acquisition and reduction techniques, a direct comparison of the astrometric and photogrammetric methods is not valid. A brief generalization, however, can be made: Astrometric methods are most suitable where narrow fields (< 5°) are used; the photogrammetric methods are most applicable to wide fields (20° to 30°); and in the intervening range, a compromise between the two methods will often provide the most practical solution. The reduction procedure to be employed is the one that is most economical yet commensurate with the physical characteristics of the camera and with the external phenomena affecting the observations. This economic requirement is particularly important because a total of over 200,000 Baker-Nunn observations have been reduced during the program.

The chief advantage of the astrometric, or Turner's, method is that a variety of phenomena affecting the relative positions of the satellite and the star images need not be corrected for explicitly. The method describes an affine transformation between the standard coordinates and the plate coordinates. It assumes that 1) the two coordinate planes are parallel and 2) a small field is used. This first requirement is adequately satisfied by the design of the camera, the principal ray at any point being normal to the backup plate. The second requirement is met by using only those reference stars that lie within 2° to 2.5 of the satellite image. The reductions are valid for any small area away from the physical film center, although residual distortions at the outer parts of the field mean that the satellite image should lie within about 10° of the center.

2.1.2.2 Transformations

The relationship between the stellar coordinates and the standard coordinates is expressed by the azimuthal equidistant projection. Let D_0 and A_0, respectively, denote the declination and right ascension of the adopted film center, and δ and α, the declination and right ascension of the satellite position. Then

$$\begin{pmatrix} v_1 \\ v_2 \\ v_3 \end{pmatrix} = \begin{pmatrix} 1 & 0 & 0 \\ 0 & \sin D_0 & \cos D_0 \\ 0 & -\cos D_0 & \sin D_0 \end{pmatrix} \begin{pmatrix} -\sin A_0 & \cos A_0 & 0 \\ -\cos A_0 & -\sin A_0 & 0 \\ 0 & 0 & 1 \end{pmatrix} \begin{pmatrix} \cos \alpha \cos \delta \\ \sin \alpha \cos \delta \\ \sin \delta \end{pmatrix},$$

and the standard coordinates (ξ, η) of a reference point become

$$\xi = \frac{v_1}{v_2} \cdot \frac{\theta}{D} \cdot f$$

and

$$\eta = \frac{v_2}{v_3} \cdot \frac{\theta}{D} \cdot f \quad ,$$

where f is the camera focal length and θ is the angle between the plate center and the star; that is,

$$\theta = \tan^{-1} \left(\frac{\sqrt{v_1^2 + v_2^2}}{v_3} \right)$$

and

$$D = \tan \theta \quad .$$

Such a projection is valid for any region of the film. The adopted choice for the film "center" is the geometric center of the selected images of reference stars. With well-distributed reference points, the separation between this center and the satellite image is less than 0°.5. The projection preserves the azimuth and scale in the radial direction from the adopted film center, but distortions in other directions will occur. These distortions, however, are small, and the average distortion over the small field used is less than 0.5 μ, which is equivalent to 0".2.

2.1.2.3 Corrections

In the process of precise reductions, a number of corrections must be applied to the data.

A. Shutter corrections. During the exposure of the Baker-Nunn film, the satellite image and the star images trail along the film. These trails are periodically

broken into six segments by the two diametrically opposite staves of a rotating barrel shutter. The third break corresponds to the satellite position to be measured, and its time is not directly recorded; the other breaks are not currently used. At some instant during the stave passage, its position and time are recorded on the film. The time of the image and the time of the stave passage are related by the shutter-sweep correction. Thus, if β is the angle of rotation of the shutter about its axis between the two events, the sweep correction Δt is given in the first instance by

$$\Delta t = \frac{\beta}{\omega} \quad ,$$

ω being the angular velocity of the shutter.

The situation is somewhat complicated because the time is not necessarily displayed when the stave passes over the film center. However, if the stave displacement $\Delta\beta$ is not excessive, the camera has a device for measuring $\Delta\beta$, and the total sweep correction becomes

$$\Delta t = \frac{\beta - \Delta\beta}{\omega} \quad .$$

Zadunaisky (1960) gives the equations necessary to compute the angles β and $\Delta\beta$. These formulations are based on a number of simplifying assumptions whose effects on the accuracy of the time determination can be investigated.

B. Aberration corrections. The film reduction is carried out in the epoch of 1950.0, and the only aberration correction applied at this stage is for annual aberration. Owing to the small field, the correction is applied to the satellite position, rather than to each star position individually. The formulas used are the closed expressions:

$$\Delta\alpha = - \frac{20''.47 \sin\alpha \sin\odot + 18''.87 \cos\alpha \cos\odot}{\cos\delta} \quad ,$$

$$\Delta\delta = - [20''.47 \sin\delta \cos\alpha \sin\odot + 18''.87 (0.4336661 \cos\delta - \sin\delta \sin\alpha) \cos\odot] \quad ,$$

where $\odot$ is the geocentric longitude of the sun. Though not rigorous, these expressions will always be correct to better than 0".1 (Scott, 1964).

C. Atmospheric-refraction corrections. In the film-reduction process, atmospheric-refraction corrections are not applied to individual star positions, since it is assumed that the atmospheric-refraction correction varies linearly over the 4° to 5° field used in the reduction. This condition is nearly always satisfied because observations are seldom made at zenith distances of greater than 70°. At this zenith distance, the average departure of the differential refraction from linearity is about 1", and with eight well-distributed stars, the uncertainty in the satellite position (all other factors being ignored) will be at most 0".4.

A parallactic-refraction correction is applied to the satellite position during analysis. The value for the refractivity constant in this correction is based not on the atmospheric conditions at the time of observation, but rather on the average year-round, nighttime conditions for the station from which the observations are made. For the present Baker-Nunn camera locations, the error in the refraction correction is less than 20% of the value of the correction itself. As this correction is already small, the error is minimal.

Of greater importance than uncertainties in the parallactic-refraction correction is the random-image displacement caused by microturbulence in the atmosphere. When the Baker-Nunn camera is used in the stationary mode, this image motion will exist in both the along-track and the across-track directions, with the greater deviations occurring in the former because of the different time-integration effects. The satellite position will not be seriously affected when the camera is used in the tracking mode, but each star image may be displaced. The average one-dimensional deviation from the mean, σ_{ψ}, can be approximately formulated (Lambeck, 1968b) as follows:

$$\sigma_{\psi} = \left\{ (0.03)^2 + \left[4.5 \frac{\sec^{1/2} \zeta}{\sqrt{D}} (1 - 0.35 \log \Delta t) \right]^2 \right\}^{1/2} , \qquad \Delta t < 1000 \text{ msec} ,$$

where D is the aperture in centimeters and Δt, the exposure time in milliseconds.

D. Geos flash corrections. The star and satellite images of Baker-Nunn films of passive objects refer to the same instant of time. This is not the case for observations of flashing satellites, so a correction must be applied to the observed position to ensure that both the star images and the satellite image refer to the same time instant. For operational reasons, the star-trail exposure is offset by ≈0.1 sec from the flash time. The correction is computed by precessing the satellite position to the date of observation, adding the correction

$$\Delta\alpha = 1.0027 \times \text{(time difference between satellite and star exposure)} \quad ,$$

and precessing the corrected position back to the epoch of 1950.0. Because of the small time interval between the star exposures and the flash observation, nutation need not be considered.

2.1.3 Synthetic observations

The arcs formed by several successive observations can be used to create synthetic observations at some intermediate time by interpolation. Simultaneous observations used in the geometrical satellite solution rely almost entirely on such synthetic observations, and they are also used in the dynamical solution whenever four or more successive frames are available.

Since it is virtually impossible to observe a passive satellite at exactly the same time instant from two or more distant stations, the only practical way of obtaining simultaneous observations is to observe the satellite from the participating stations for approximately the same time interval and to interpolate for a fictitious simultaneous instant. In orbital analysis, use of synthetic observations reduces the amount of data to be handled without any significant loss of accuracy and resolution. But probably the most cogent reason for using synthetic observations is that a better accuracy or reliability estimate can be associated with the synthetic observation than with a single observation. Only average values can be assigned to the errors in a single observation. Some of these errors vary more or less randomly from exposure to exposure and will be reflected in the residuals resulting from a least-squares interpolation procedure for a synthetic observation.

A second-degree polynomial is adequate for the majority of observations. Since a seven-frame arc generally subtends less than 10° of arc, the object's orbit can be adequately approximated by quadratic functions. When there are more than seven or eight frames in a sequence, a third-degree polynomial may be required, but proper constraints must be placed on the coefficients to ensure that the curve approximates the orbit and does not reflect characteristics of the image-forming process for the points in the sequence. If higher degree polynomials are used without such constraints, the accuracy estimates of the interpolated positions become optimistic, although the mean position of the satellite is not seriously affected.

The interpolation procedure is based on several assumptions: 1) that the errors in successive positions in the arc are uncorrelated, 2) that the along- and across-track errors for each position are uncorrelated, 3) that the along-track uncertainties are equal for all frames, and 4) that the across-track uncertainties are equal for all frames. Since systematic errors in timing would destroy the first assumption, timing uncertainties are not included in the uncertainty of each position. Other correlations between successive Baker-Nunn images are much smaller than with ballistic cameras, where images lie on a single frame. For the Baker-Nunn, plate constants are derived independently for each frame, so that the influence of such factors as measuring uncertainties, nonlinear lens and film distortions, and short-period atmospheric effects (on each satellite position) will be random from frame to frame. Since the same reference stars may be used in two or even three successive frames, errors in stellar coordinates could introduce some correlated errors between successive frames.

Synthetic simultaneous directions are corrected for parallactic refraction, diurnal aberration, and light travel time between the station and the satellite (see Haefner and Martin (1966) for the corrections used) and refer to the terrestrial system defined by the mean pole of 1900–1905 and by the meridian plane at 75°03'55!'94 east of the mean meridian of the USNO. The time of the observations is expressed in Smithsonian Atomic Time (see Appendix A). The directions are given as direction cosines, and their standard deviations are given in the along- and across-track components. Timing uncertainties have been introduced in the former. The angle the satellite trail makes with the right-ascension axis is also computed so that the accuracy of the direction in the right-ascension and declination components can be determined.

2.2 Laser Data Reduction

2.2.1 Calibration

The laser systems are calibrated by ranging on a fixed land-based target situated at a known distance from the laser. The system delay or system-calibration constant is the difference between the raw target range time measured by the laser, τ_m, and the range time to the target, τ_s, computed from the surveyed distance between the laser and the target and corrected for local atmospheric refraction. The targets, which are 8 ft × 8 ft wooden surfaces painted flat white, are 0.5 to 2.0 km distant from the laser. The exact placement is usually dictated by local terrain.

The routine calibration of the system is performed nightly and consists of 20 measurements on the target. For these measurements, the return-pulse intensity is controlled by use of neutral-density filters to produce signal levels similar to satellite echoes.

Computation of a calibration correction factor τ_c, which must be added (algebraically) to all satellite range-time observations, is obtained from

$$\tau_c = \tau_s - \tau_m \quad ,$$

where τ_m is the average of the 20 range-time measurements. The computed range time to the target is given by

$$\tau_s = \frac{d_s}{0.15} \left[1 + (N \times 10^{-6}) + (6.917 \times 10^{-4})\right] \quad ,$$

where d_s is the surveyed distance to the target and N is the local atmospheric refractivity

$$N = 80.29 \frac{P}{T} - 11.9 \frac{e}{T} \quad ,$$

in which P is the measured barometric pressure in millibars, e is the partial pressure of water vapor, and T is the temperature in degrees Kelvin.

The effect of local variations in barometric pressure on the value of τ_s for distances of less than 1 km was found to be small enough so that a constant value of the atmospheric refractivity could be defined for each station. This value was taken from a chart prepared to give a direct conversion from station altitude in kilometers to values of N (Gaposchkin, 1972a, Figure 1, p. 26).

During individual nightly (or daily) calibration sequences, the range scatter from one measurement to the next is seldom more than a few nanoseconds. The variation in the target-range averages is rarely more than a few tenths of a nanosecond from calibration to calibration, giving a stability of better than 10 cm. The target surveys at the stations currently have an estimated accuracy of about 10 cm.

2.2.2 Atmospheric corrections

Laser ranges determined by using the vacuum velocity of light must be corrected for the fact that the laser pulse travels at a lower velocity in the earth's atmosphere. We used the following correction during this program (G. Thayer, 1967, private communication):

$$r_m = r_v - \frac{2.238 + 0.0414\ PT^{-1} - 0.238\ h_s}{\sin a + 10^{-3} \cot a} \quad ,$$

where r_v is the uncorrected range in meters, r_m is the corrected range in meters, P is the atmospheric pressure at the laser station, T is the temperature at the laser station, h_s is the laser's height above mean sea level in kilometers, and a is the elevation angle of the satellite. The formula holds for a ruby laser, which operates at 694 nm.

The formula was derived from a regression analysis based on a large sample of radiosonde balloon flights from a number of locations that were chosen to give a reasonable sampling of anticipated atmospheric conditions. The error in range correction is estimated to be about 2 to 3 cm at zenith.

2.2.3 Satellite–retroreflector-array transfer functions

Range errors now present in routine laser tracking are actually smaller than the satellite's dimensions. Since we must relate all observations to the satellite's center of mass (both for dynamic and for purely geometric analyses), it is necessary to derive some means for reducing each range observation to the distance from the ground-based laser to the satellite's center of mass, which, in all cases, is displaced from the reflecting elements. For this purpose, we have developed and applied in our geodetic analyses a set of retroreflector-array transfer functions for each of the United States satellites with laser cube corners now in orbit. These transfer functions are computed from the geometric and optical parameters of each retroreflector array and take into account the satellite geometry and position. The functions for 6508901 (Geos 1), Geos 2, 6406401 (BE-B), 6503201 (BE-C), 6701101 (D1C), 6701401 (D1D), and 7010901 (Peole) are given in Appendix B.

The computer model includes both incoherent and coherent return signals for arrays of retroreflectors whose faces are cut in the form of a circle, triangle, or even-sided polygon (such as a hexagon). Diffraction, including changes in amplitude and polarization of the reflected laser beam, and influences of dihedral-angle errors can also be accounted for. The model accommodates obscuration of retroreflectors by satellite and subsystem structure, a particular problem with the two Geos spacecraft and with Peole. When the position of each reflector is being computed, the model accounts for the dielectric properties of the retroreflectors in terms of ray bending and propagation velocity. Once the return signal has been constructed, the relationship of the centroid of the signal to the satellite's center of mass is determined and then applied as a range correction to the laser data used in the geodetic analyses.

The major limitation on the accuracy with which transfer functions can be determined for the existing laser satellites is the lack of precise information on the beam patterns of the cube corners in relation to the large size of the arrays. With the existing uncertainties in retroreflector optical characteristics, geometric placement, and satellite attitude, we estimate that the range corrections for these satellites have an accuracy of about 10 cm. It should be noted that this error is quite systematic.

2.3 Timing-System Data Reduction

During data reduction, observation epochs are corrected for 1) phase drift in the transmitted VLF signal and 2) clock jumps, which can be recovered by the redundant hardware at the station. Epochs are then converted to Smithsonian Atomic Time (see Appendix A) for use in analysis.

Initial phase relationships between station clocks and the received VLF signals are established during routine portable-clock trips. The station-clock oscillators are subsequently steered to maintain phase with VLF transmissions. The epoch corrections due to drift in the phase of the transmitted signal are determined from the values published in USNO's "Daily Phase Values, Series 4." Even with clock steering, the phase relationship with VLF has periodic variations, which are reported monthly and used to estimate the timing uncertainty at each station.

Before September 20, 1967, the station clocks were referred to WWV-emitted and were steered to track WWV. The propagation times to the stations were computed and published (Haefner and Martin, 1966). Any deviations were reported and applied as a correction to observation epochs.

3. SAO SATELLITE-TRACKING NETWORK

3.1 Sites

The first Baker-Nunn camera was sent to Organ Pass, New Mexico, at the observing site of the Harvard Meteor Program. The first successful observation was made November 26, 1957, just a month and a half after the launch of the first artificial earth satellite. The network had expanded by the following August to 12 operating Baker-Nunn stations. Table 3 shows the history of the Baker-Nunn sites to date.

After 8 years, it became apparent that higher accuracies were needed for future scientific projects. By March 1966, SAO had assembled, tested, and operated its first laser tracking system. It consisted of a rented General Electric laser mounted on a 3-inch gun mount with a searchlight receiver. This system operated successfully for over a year at the New Mexico site, during which time plans were formulated for a prototype laser tracking system with components designed and built specifically for that purpose.

The prototype system was operating at Mt. Hopkins in December 1967. Three production laser systems, based on the design and experience gained with the prototype, were fielded in late 1970. In 1972, the Mt. Hopkins prototype was reworked to make it similar to the three production systems. Table 4 shows the history of the lasers to date. Figure 11 shows the present global distribution of Smithsonian stations, including the laser sites.

The present SAO sites that contain both a laser and a Baker-Nunn camera are Mt. Hopkins, South Africa, Peru, and Brazil. The last three stations are staffed and operated by SAO personnel with logistic support provided by cooperating agencies in each country: the Council for Scientific and Industrial Research in South Africa, the Instituto Geofisico del Peru and the Universidad Nacional de San Agustin in Peru, and the Instituto Nacional de Pesquisas Espaciais in Brazil.

Table 3. History of the SAO Baker-Nunn satellite-tracking cameras.

Satellite camera number	COSPAR number and station location	First successful observation	Last successful observation	Transferred to number and station	First successful observation	Last successful observation	Transferred to number and station	First successful observation	Last successful observation
SC-1	9001 Organ Pass, New Mexico	November 28, 1957	March 18, 1968	9021 Mt. Hopkins, Arizona	March 31, 1968	–			
SC-2	9002 Olifantsfontein, South Africa	March 18, 1958	December 17, 1970	9022 Olifantsfontein, South Africa (new building)	January 5, 1971	–			
SC-3	9003 Woomera, Australia	March 11, 1968	June 1964	9023 Island Lagoon, Australia	July 1964	April 13, 1973	9043 Orroral Valley, Australia	January 1974 (est)	–
SC-4	9004 San Fernando, Spain	March 18, 1958	–						
SC-5	9005 Tokyo, Japan	April 5, 1958	May 24, 1968	9025 Dodaira, Japan	May 24, 1968	–			
SC-6	9006 Naini Tal, India	August 29, 1958	–						
SC-7	9007 Arequipa, Peru	July 4, 1958	May 30, 1970	9027 Arequipa, Peru (new building)	June 1, 1970	–			
SC-8	9008 Shiraz, Iran	May 20, 1958	July 15, 1966	9088 Addis Ababa, Ethiopia	August 15, 1968	–			
SC-9	9009 Curaçao, Netherlands Antilles	June 22, 1958	July 10, 1966	9029 Natal, Brazil	September 27, 1966	May 5, 1970	9039 Natal, Brazil (new building)	May 7, 1970	–
SC-10	9010 Jupiter, Florida	June 10, 1958	October 12, 1967	9091 Dionysos, Greece	December 7, 1967	June 25, 1969	9030 Dionysos, Greece (new building)	July 3, 1969	–
SC-11	9011 Villa Dolores, Argentina	July 10, 1958	October 28, 1966	9031 Comodoro Rivadavia, Argentina	November 14, 1966	January 1970	See SC-11a		
SC-11a	9040 Dakar, Senegal	December 1970	September 1971	9040 Ouagadougou, Upper Volta	May 1972	–			
SC-12	9012 Maui, Hawaii	July 4, 1958	–						

On loan to CNES.

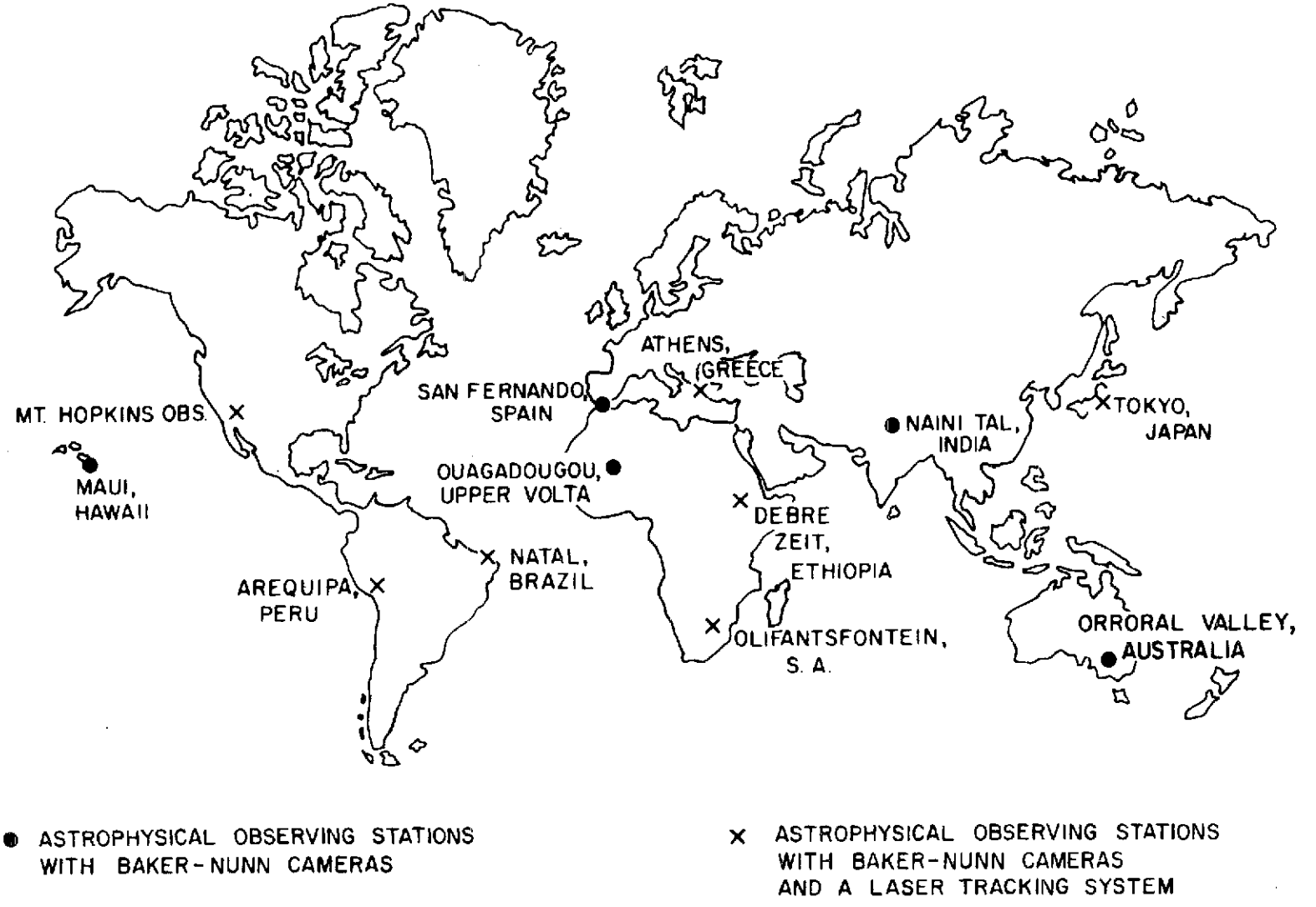

Figure 11. SAO field stations.

Table 4. Laser sites.

Station number	Station location	Period of operation
7901	Organ Pass, New Mexico	March 1966 to July 1967
7912	Maui, Hawaii	May 24, 1968, to March 27, 1969
7902	Olifantsfontein, South Africa	February 1971 to present
7907	Arequipa, Peru	December 1970 to present
7921	Mt. Hopkins, Arizona (prototype)	December 1967 to June 20, 1972
7921	Mt. Hopkins, Arizona (rebuilt system)	November 1972 to present
7929	Natal, Brazil	November 1970 to present
7991	Athens, Greece	September 1968 to June 1969
7930	Dionysos, Greece	July 1969 to present
7925	Tokyo, Japan	November 1972 to present

The Baker-Nunn site in Maui, Hawaii, is staffed and operated by SAO personnel in conjunction with the University of Hawaii. The camera in Australia is operated by the Department of Supply of the Australian government. The stations in Spain, Ethiopia, and Greece are supported and operated jointly by the Smithsonian and cooperating agencies: the Spanish Naval Observatory in Spain, the Haile Selassie I University in Ethiopia, and the NTU in Greece. NTU also operates a laser system. A laser system belonging to the Centre National d'Etudes Spatiales (CNES) is currently located at Addis Ababa, Ethiopia.

The tracking station in Japan is operated by the Tokyo Astronomical Observatory and has, in addition to the Baker-Nunn camera, a laser system designed and built in Japan. The Baker-Nunn camera in India is operated by the Uttar Pradesh State Observatory.

A Baker-Nunn camera on loan to CNES has been used at several locations in Africa; it is currently in operation in Ouagadougou, Upper Volta.

Beginning in 1964, several Baker-Nunn cameras operated by the 7th Aerospace Squadron at ENT Air Force Base have participated in SAO satellite-tracking programs. The sites are listed in Table 5. SAO scheduled observing times and provided predictions for simultaneous observations. These data have been included in the SAO analysis and are incorporated in the SAO data file.

Table 5. Air Force Baker-Nunn sites.

Station number	Station location	Period of operation
9113	Edwards AFB, California (Rosamund)	December 1960 to present
9114	Cold Lake, Canada (I)	January 1963 to June 1971
9115	Harestua, Norway	December 1959 to July 1967
9116	Santiago, Chile	September 1960 to May 1964
9117	Sand Island (Johnston Island), Pacific	September 1963 to present
9118	Kwajalein Island	Not operational for satellite photography
9119	Mt. John, New Zealand	October 1969 to present
9120	San Vito, Italy	March 1971 to present
9124	Cold Lake, Canada (II)	July 1971 to present
9010*	Jupiter, Florida (AF)	June 1968 to July 1971

*Site previously occupied by SAO Baker-Nunn camera (see Figure 11).

3.2 Operations

The SAO Baker-Nunn cameras and laser systems receive new satellite predictions each week. The predictions are computed from up-to-date observations provided by the SAO network and by camera, minitrack, and laser observations made by other agencies (see Table 6).

The predictions for the Baker-Nunn camera consist of azimuth- and altitude-pointing angles, which need be accurate to only a few degrees, and tracking-angle rates to simulate the satellite motion (Cherniack and Gaposchkin, 1963). These predictions are generated from orbits computed with a simple model of the earth's gravity field. The short-periodic terms due to J_2 and the long-period terms due to the odd

Table 6. Sources of data used in the orbit-generation program.

Agency	Instrument
SAO	Baker-Nunn cameras Lasers Moonwatch
NASA/GSFC	Prime Minitrack Lasers
U.S. Air Force	Baker-Nunn cameras
CNES	CNES cameras Lasers

zonal harmonics are included. The secular rate of the apsidal line and the argument of perigee are determined from the data for each orbit. The orbits are generated with the Smithsonian's Differential Orbit Improvement (DOI) program (Gaposchkin, 1964) from observations covering a period of about 2 weeks.

The laser, on the other hand, requires azimuth- and altitude-predicted pointing angles accurate to within several minutes of arc and a predicted range propagation time accurate to within 20 μsec for a given epoch. Orbits for laser tracking predictions are also generated with the DOI program by using a gravity field with most of the tesseral harmonics through degree and order 16 and with a number of higher resonance terms. Lunar perturbations are also included. Again, orbits are computed from data covering a period of about 2 weeks. Predictions for satellites equipped with retro-reflectors are made for passes that reach altitudes greater than 25°.

The success of the network has depended on the timely flow of data from the field, the development of pointing predictions from up-to-date data, and the use of these fresh predictions at the field stations. The rapid data-prediction cycle is most critical for the laser, which has stringent pointing requirements; however, it is also an important factor in the Baker-Nunn operation, especially for simultaneous observations between stations for geometric geodesy.

Until 1968, direct links by teletype between the field stations and Cambridge provided real-time communications. Since then, a combination of means has been used to give real-time or near real-time communications at each site. Peru and Brazil receive predictions and send their camera and laser data by direct radio-teletype link operated by SAO personnel. These stations have prearranged contact times for data transmission. Atmospheric disturbances severe enough to affect the link are infrequent. The tracking sites in Hawaii, Japan, Spain, Greece, and Arizona use facilities of the United States military communications network for transmission and receipt of data. The first three stations have direct access to this network, while those in Greece and Arizona must pick up and deliver messages at local military bases. The stations in Australia and South Africa use the NASA data network (teletype). Predictions for the Ethiopia station are sent via NASA teletype link to CNES in France and are retransmitted on their lines to Ethiopia. CNES generates and sends predictions for their laser, located in Ethiopia, as well as predictions for the 12th Baker-Nunn camera, now in Upper Volta. Data are currently returned to Cambridge by Embassy mail. The site in India receives predictions from SAO via the United States Embassy in New Delhi and sends its data back by way of commercial cable.

For the Baker-Nunn camera, predictions cover a period of 1 week, with an extra day in case of transmission delays. At present, an average of 10 arcs is predicted per station per night. In the past, as many as 50 arcs were predicted for each station. Observations are reduced in the field to an accuracy of 40 to 60" and sent to Cambridge immediately for use in the prediction cycle. The camera film is sent by commercial mail for subsequent precise reduction (photoreduction).

Predictions for the laser system are in the form of punched paper tape, which is used directly to point the laser mount. Each predicted arc contains from 10 to 90 separate points (4 min^{-1}), depending on the geometry of the pass. Stations receive 40 to 100 predicted arcs per week for three satellites currently being tracked – Geos 1, Geos 2, and BE-C. All seven retroreflector-equipped satellites have been tracked. Satellite ranging data, system calibration data, and ground-based meteorological data are sent to SAO.

4. INFORMATION FLOW

In the analysis described here, satellite-tracking data are combined with other types of data to determine geodetic parameters. Camera tracking data are given in the system of right ascension and declination. The transformation of directions in right ascension to the terrestrial system, and vice versa, requires observation of pole position and sidereal angle. These observed quantities are published by BIH, USNO, and the International Polar Motion Service. The conversion formulas are given in Volume 1, Part III. The numerical values used in converting from one system to another, together with the formulas, constitute the definition of the terrestrial reference system. The values for pole position and UT1 are given in Appendices C and D.

Surface-gravity measurements supplement satellite data in the determination of the geopotential. Surface triangulation data, in the form of geodetic coordinates, provide useful information about stations separated by less than 100 km.

Observations of deep-space probes by the five globally distributed radio antennas of the Jet Propulsion Laboratory's Deep Space Net provide additional data relating the relative longitudes and spin-axis distances of these antennas.

Figure 12 indicates how these data types are used. Subsequent parts of this report discuss the analysis and results.

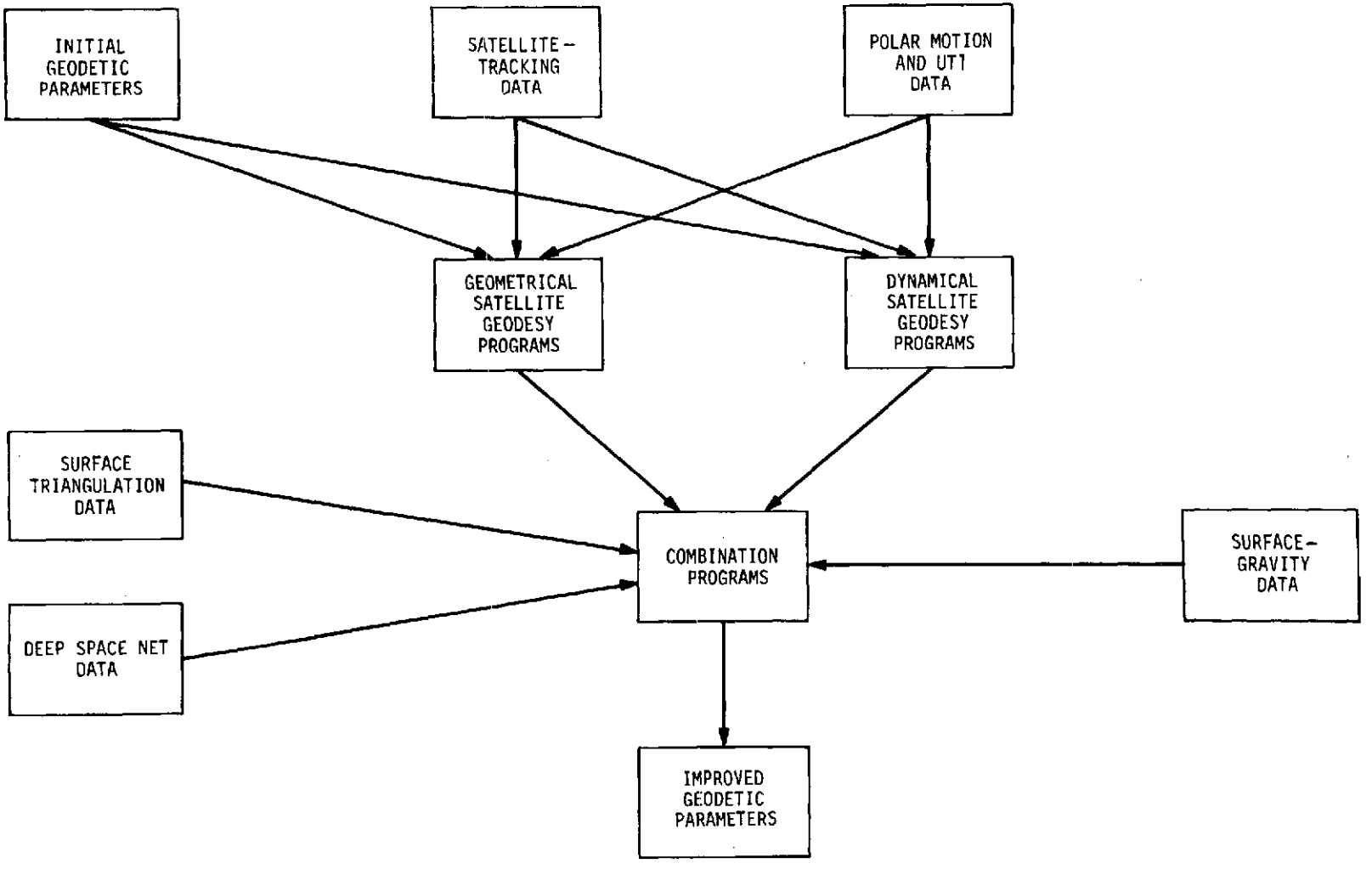

Figure 12. Data flow for the determination of geodetic parameters.

APPENDIX A

SMITHSONIAN ATOMIC TIME

Since September 20, 1967, SAO's satellite observations have been referred to UTC(USNO). Before that date, observations were referred to time of emission of WWV signals (WWV-emitted). Both timing systems are readily available for use in the field, yet both have occasional discontinuities, which make them inappropriate for analysis.

When the satellite-tracking program began in the late 1950s, uniform time standards such as A1 and their differences from WWV-emitted (and later UTC) were not available in a timely fashion. However, the intended relations between WWV (and later UTC) and the uniform time standard A1 were published regularly. SAO has used these intended relations to generate a facsimile of A1 from WWV and UTC data.

Smithsonian Atomic Time (A.S) is defined with respect to WWV-emitted before September 20, 1967, and with respect to UTC(USNO) after that date. Tables A-1 and A-2 list the coefficients of the linear expression used for defining the difference between A.S and the reference time system.

Table A-1. $(A.S - WWV) = A + B\,(T - T_0)$, where A is in seconds, B is in seconds per day, and T and T_0 are in Modified Julian Days.

Interval		A	B	T_0
1961 Jan. 01.0	1961 Jul. 01.0	$1^s.458\,858$	$0^s.001\,296\,000$	(T - 37300.0)
1961 Jul. 01.0	1961 Jul. 13.0	1.693 434	0.001 292 000	(T - 37480.0)
1961 Jul. 13.0	1961 Aug. 01.0	1.694 215	0.001 245 000	(T - 37480.0)
1961 Aug. 01.0	1961 Sep. 21.0	1.643 160	0.001 280 000	(T - 37480.0)
1961 Sep. 21.0	1961 Oct. 01.0	1.641 500	0.001 300 000	(T - 37480.0)
1961 Oct. 01.0	1961 Nov. 01.0	1.642 184	0.001 290 764	(T - 37480.0)
1961 Nov. 01.0	1962 Jan. 01.0	1.643 272	0.001 289 444	(T - 37480.0)
1962 Jan. 01.0	1962 Apr. 01.0	1.865 000	0.001 123 200	(T - 37650.0)
1962 Apr. 01.0	1962 Jul. 01.0	1.864 620	0.001 126 800	(T - 37650.0)
1962 Jul. 01.0	1963 Jan. 01.0	1.864 704	0.001 126 370	(T - 37650.0)
1963 Jan. 01.0	1963 Nov. 01.0	2.292 725	0.001 118 458	(T - 38030.0)
1963 Nov. 01.0	1964 Jan. 01.0	2.392 725	0.001 118 458	(T - 38030.0)
1964 Jan. 01.0	1964 Apr. 01.0	2.800 962	0.001 293 560	(T - 38395.0)
1964 Apr. 01.0	1964 Jul. 01.0	2.900 766	0.001 295 716	(T - 38395.0)
1964 Jul. 01.0	1964 Sep. 01.0	2.901 518	0.001 292 659	(T - 38395.0)
1964 Sep. 01.0	1964 Oct. 01.0	3.001 518	0.001 292 659	(T - 38395.0)
1964 Oct. 01.0	1965 Jan. 01.0	3.001 589	0.001 296 048	(T - 38395.0)
1965 Jan. 01.0	1965 Mar. 01.0	3.575 732	0.001 296 000	(T - 38761.0)
1965 Mar. 01.0	1965 Jul. 01.0	3.675 732	0.001 296 000	(T - 38761.0)
1965 Jul. 01.0	1965 Sep. 01.0	3.775 732	0.001 296 000	(T - 38761.0)
1965 Sep. 01.0	1966 Jan. 01.0	3.875 732	0.001 296 000	(T - 38761.0)
1966 Jan. 01.0	1967 Jan. 01.0	4.348 772	0.002 592 000	(T - 39126.0)
1967 Jan. 01.0	1967 Sep. 20.0	5.294 852	0.002 592 000	(T - 39491.0)

Table A-2. [A.S - UTC(USNO)] = A + B (T - T_0), where A is in seconds, B is in seconds per day, and T and T_0 are in Modified Julian Days.

Interval	A	B	T_0
1967 Sep. 20.0–1968 Jan. 01.0	$5^s.294\ 688$	$+ 0^s.002\ 592\ 000$	(T - 39491.0)
1968 Jan. 01.0–1968 Feb. 01.0	6.240 768	+ 0.002 592 000	(T - 39856.0)
1968 Feb. 01.0–1969 Jan. 01.0	6.140 768	+ 0.002 592 000	(T - 39856.0)
1969 Jan. 01.0–1970 Jan. 01.0	7.089 440	+ 0.002 592 000	(T - 40222.0)
1970 Jan. 01.0–1971 Jan. 01.0	8.035 520	+ 0.002 592 000	(T - 40587.0)
1971 Jan. 01.0–1972 Jan. 01.0	8.981 600	+ 0.002 592 000	(T - 40952.0)
1972 Jan. 01.0–1972 Jul. 01.0	10.035 280	+ 0.000 000 000	(T - 41317.0)

APPENDIX B

SATELLITE CENTER OF MASS

Laser range measurements are extrapolated to the satellite's center of mass by means of the following formulas. These formulas relate the range correction Δ in meters to ϕ, the angle in degrees between the satellite's axis of symmetry and the line of sight to the observing station.

BE-B and BE-C

$$\Delta = 0.3493 - 1.09183 \times 10^{-3} \times \phi + 2.9222 \times 10^{-6} \times \phi^2 - 1.5338 \times 10^{-7} \times \phi^3$$

($\Delta = 0$ for $\phi > 120°$)

D1C and D1D

$$\Delta = 0.164612 - 2.824 \times 10^{-3} \times \phi + 2.0639 \times 10^{-5} \times \phi^2 + 8.1214 \times 10^{-7} \times \phi^3 - 5.81302 \times 10^{-9} \times \phi^4$$

($\Delta = 0$ for $\phi > 120°$)

Geos 1

$$\Delta = 0.3972 \cos \phi$$

Geos 2

$$\Delta = 0.4298 \cos \phi$$

Peole

$$\Delta = 0.48 - 1.108 \times 10^{-2} \times \phi + 4.19267 \times 10^{-4} \times \phi^2 - 3.619 \times 10^{-6} \times \phi^3 + 8.12555 \times 10^{-9} \times \phi^4$$

($\Delta = 0.768$ for $\phi > 96°$)

APPENDIX C

POLAR MOTION

Polar-motion data for dates before January 1, 1962, were obtained from the Bureau Central des Telegrammes Astronomiques Circulaire No. 1804, of August 15, 1962 (coordinates supplied by G. Cecchini Torino), and were compiled and distributed by the International Latitude Service (ILS).

Data for 1962 through 1971 were taken from the Annual Reports of the IPMS, and since 1972, from their Monthly Notes, published by the Central Bureau of the International Polar Motion Service, Mizusawa-shi, Japan. All data are referred to the mean pole of 1900 to 1905 (Conventional International Origin, CIO). Since December 1, 1967, the BIH has published polar-motion data referred to the same origin (Circular D monthly and annual reports). The rms difference between BIH and IPMS pole positions is 1.5 m.

Table C-1 gives the instantaneous pole coordinates referred to the CIO. The sources of the data are listed in the last column. Those labeled ILS 180462 have been taken from Bureau Central des Telegrammes Astronomiques Circulaire No. 1804 of 1962. Data from IPMS are from their Annual Reports, labeled IPMS ARPT64 through ARPT73, where the last two digits indicate the year of the Report, or from their Monthly Notes, IPMS MN0272 through MN0873, where the last four digits represent the month and the year.

Table C-1. Instantaneous pole coordinates.

Date	MJD	x (arcsec)	y (arcsec)	Source
1960 01 01	36934.	.135	.043	ILS 180462
1960 01 19	36952.	.073	.007	ILS 180462
1960 02 07	36971.	.046	-.012	ILS 180462
1960 02 25	36989.	.035	-.007	ILS 180462
1960 03 14	37007.	.013	.025	ILS 180462
1960 04 01	37025.	-.027	.059	ILS 180462
1960 04 20	37044.	-.074	.094	ILS 180462
1960 05 08	37062.	-.097	.124	ILS 180462
1960 05 26	37080.	-.107	.153	ILS 180462
1960 06 13	37098.	-.104	.183	ILS 180462
1960 07 02	37117.	-.088	.209	ILS 180462
1960 07 20	37135.	-.040	.238	ILS 180462
1960 08 07	37153.	.003	.263	ILS 180462
1960 08 25	37171.	.041	.288	ILS 180462
1960 09 13	37190.	.070	.300	ILS 180462
1960 10 01	37208.	.091	.305	ILS 180462
1960 10 19	37226.	.107	.301	ILS 180462
1960 11 06	37244.	.116	.288	ILS 180462
1960 11 25	37263.	.116	.270	ILS 180462
1960 12 13	37281.	.109	.248	ILS 180462
1961 01 01	37300.	.092	.220	ILS 180462
1961 01 19	37318.	.074	.188	ILS 180462
1961 02 07	37337.	.065	.161	ILS 180462
1961 02 25	37355.	.064	.149	ILS 180462
1961 03 15	37373.	.063	.150	ILS 180462
1961 04 02	37391.	.056	.157	ILS 180462
1961 04 21	37410.	.045	.161	ILS 180462
1961 05 09	37428.	.035	.159	ILS 180462
1961 05 27	37446.	.030	.154	ILS 180462
1961 06 14	37464.	.032	.151	ILS 180462
1961 07 03	37483.	.040	.149	ILS 180462
1961 07 21	37501.	.044	.150	ILS 180462
1961 08 08	37519.	.044	.152	ILS 180462
1961 08 26	37537.	.042	.157	ILS 180462
1961 09 14	37556.	.038	.165	ILS 180462
1961 10 02	37574.	.028	.173	ILS 180462
1961 10 20	37592.	.019	.191	ILS 180462
1961 11 07	37610.	-.011	.212	ILS 180462
1961 11 26	37629.	-.028	.243	ILS 180462
1961 12 14	37647.	-.023	.275	ILS 180462

Table C-1. (Cont.)

Date	MJD	x (arcsec)	y (arcsec)	Source
1962 01 01	37665.	-.009	.297	IPMS ARPT64
1962 01 19	37683.	.008	.309	IPMS ARPT64
1962 02 07	37702.	.027	.314	IPMS ARPT64
1962 02 25	37720.	.047	.312	IPMS ARPT64
1962 03 15	37738.	.071	.304	IPMS ARPT64
1962 04 02	37756.	.095	.290	IPMS ARPT64
1962 04 21	37775.	.120	.271	IPMS ARPT64
1962 05 09	37793.	.142	.246	IPMS ARPT64
1962 05 27	37811.	.162	.214	IPMS ARPT64
1962 06 14	37829.	.173	.175	IPMS ARPT64
1962 07 03	37848.	.171	.132	IPMS ARPT64
1962 07 21	37866.	.157	.092	IPMS ARPT64
1962 08 08	37884.	.128	.068	IPMS ARPT64
1962 08 26	37902.	.094	.060	IPMS ARPT64
1962 09 14	37921.	.056	.067	IPMS ARPT64
1962 10 02	37939.	.017	.083	IPMS ARPT64
1962 10 20	37957.	-.019	.104	IPMS ARPT64
1962 11 07	37975.	-.054	.128	IPMS ARPT64
1962 11 26	37994.	-.086	.160	IPMS ARPT64
1962 12 14	38012.	-.110	.200	IPMS ARPT64
1963 01 01	38030.	-.121	.248	IPMS ARPT65
1963 01 19	38048.	-.119	.295	IPMS ARPT65
1963 02 07	38067.	-.105	.329	IPMS ARPT65
1963 02 25	38085.	-.076	.356	IPMS ARPT65
1963 03 15	38103.	-.038	.376	IPMS ARPT65
1963 04 02	38121.	.009	.388	IPMS ARPT65
1963 04 21	38140.	.070	.387	IPMS ARPT65
1963 05 09	38158.	.134	.375	IPMS ARPT65
1963 05 27	38176.	.191	.349	IPMS ARPT65
1963 06 14	38194.	.239	.307	IPMS ARPT65
1963 07 03	38213.	.274	.251	IPMS ARPT65
1963 07 21	38231.	.301	.193	IPMS ARPT65
1963 08 08	38249.	.281	.139	IPMS ARPT65
1963 08 26	38267.	.237	.091	IPMS ARPT65
1963 09 14	38286.	.176	.046	IPMS ARPT65
1963 10 02	38304.	.112	.008	IPMS ARPT65
1963 10 20	38322.	.048	-.020	IPMS ARPT65
1963 11 07	38340.	-.011	.005	IPMS ARPT65
1963 11 26	38359.	-.069	.041	IPMS ARPT65
1963 12 14	38377.	-.122	.078	IPMS ARPT65

Table C-1. (Cont.)

Date	MJD	x (arcsec)	y (arcsec)	Source
1964 01 01	38395.	-.171	.120	IPMS ARPT66
1964 01 19	38413.	-.206	.168	IPMS ARPT66
1964 02 07	38432.	-.194	.230	IPMS ARPT66
1964 02 25	38450.	-.169	.294	IPMS ARPT66
1964 03 14	38468.	-.139	.353	IPMS ARPT66
1964 04 01	38486.	-.101	.412	IPMS ARPT66
1964 04 20	38505.	-.055	.455	IPMS ARPT66
1964 05 08	38523.	.004	.467	IPMS ARPT66
1964 05 26	38541.	.074	.459	IPMS ARPT66
1964 06 13	38559.	.164	.436	IPMS ARPT66
1964 07 02	38578.	.214	.394	IPMS ARPT66
1964 07 20	38596.	.240	.339	IPMS ARPT66
1964 08 07	38614.	.241	.275	IPMS ARPT66
1964 08 25	38632.	.239	.219	IPMS ARPT66
1964 09 13	38651.	.255	.168	IPMS ARPT66
1964 10 01	38669.	.250	.123	IPMS ARPT66
1964 10 19	38687.	.219	.085	IPMS ARPT66
1964 11 06	38705.	.161	.060	IPMS ARPT66
1964 11 25	38724.	.099	.046	IPMS ARPT66
1964 12 13	38742.	.042	.043	IPMS ARPT66
1965 01 01	38761.	-.012	.049	IPMS ARPT67
1965 01 19	38779.	-.067	.069	IPMS ARPT67
1965 02 07	38798.	-.120	.103	IPMS ARPT67
1965 02 25	38816.	-.160	.153	IPMS ARPT67
1965 03 15	38834.	-.185	.226	IPMS ARPT67
1965 04 02	38852.	-.196	.286	IPMS ARPT67
1965 04 21	38871.	-.194	.334	IPMS ARPT67
1965 05 09	38889.	-.174	.374	IPMS ARPT67
1965 05 27	38907.	-.130	.408	IPMS ARPT67
1965 06 14	38925.	-.072	.434	IPMS ARPT67
1965 07 03	38944.	-.003	.444	IPMS ARPT67
1965 07 21	38962.	.071	.433	IPMS ARPT67
1965 08 08	38980.	.127	.399	IPMS ARPT67
1965 08 26	38998.	.168	.349	IPMS ARPT67
1965 09 14	39017.	.201	.303	IPMS ARPT67
1965 10 02	39035.	.221	.259	IPMS ARPT67
1965 10 20	39053.	.227	.221	IPMS ARPT67
1965 11 07	39071.	.220	.186	IPMS ARPT67
1965 11 26	39090.	.194	.156	IPMS ARPT67
1965 12 14	39108.	.138	.131	IPMS ARPT67

Table C-1. (Cont.)

Date	MJD	x (arcsec)	y (arcsec)	Source
1966 01 01	39126.	.075	.114	IPMS ARPT68
1966 01 19	39144.	.033	.103	IPMS ARPT68
1966 02 07	39163.	.000	.098	IPMS ARPT68
1966 02 25	39181.	-.029	.100	IPMS ARPT68
1966 03 15	39199.	-.058	.108	IPMS ARPT68
1966 04 02	39217.	-.086	.124	IPMS ARPT68
1966 04 21	39236.	-.105	.149	IPMS ARPT68
1966 05 09	39254.	-.116	.181	IPMS ARPT68
1966 05 27	39272.	-.119	.215	IPMS ARPT68
1966 06 14	39290.	-.115	.255	IPMS ARPT68
1966 07 03	39309.	-.104	.298	IPMS ARPT68
1966 07 21	39327.	-.086	.330	IPMS ARPT68
1966 08 08	39345.	-.057	.344	IPMS ARPT68
1966 08 26	39363.	-.010	.345	IPMS ARPT68
1966 09 14	39382.	.052	.337	IPMS ARPT68
1966 10 02	39400.	.096	.324	IPMS ARPT68
1966 10 20	39418.	.117	.308	IPMS ARPT68
1966 11 07	39436.	.125	.291	IPMS ARPT68
1966 11 26	39455.	.123	.273	IPMS ARPT68
1966 12 14	39473.	.115	.253	IPMS ARPT68
1967 01 01	39491.	.098	.234	IPMS ARPT69
1967 01 19	39509.	.075	.214	IPMS ARPT69
1967 02 07	39528.	.053	.193	IPMS ARPT69
1967 02 25	39546.	.032	.176	IPMS ARPT69
1967 03 15	39564.	.013	.164	IPMS ARPT69
1967 04 02	39582.	.000	.156	IPMS ARPT69
1967 04 21	39601.	-.006	.153	IPMS ARPT69
1967 05 09	39619.	-.007	.153	IPMS ARPT69
1967 05 27	39637.	-.002	.155	IPMS ARPT69
1967 06 14	39655.	.011	.159	IPMS ARPT69
1967 07 03	39674.	.037	.166	IPMS ARPT69
1967 07 21	39692.	.055	.174	IPMS ARPT69
1967 08 08	39710.	.047	.184	IPMS ARPT69
1967 08 26	39728.	.026	.195	IPMS ARPT69
1967 09 14	39747.	.006	.207	IPMS ARPT69
1967 10 02	39765.	-.013	.221	IPMS ARPT69
1967 10 20	39783.	-.031	.237	IPMS ARPT69
1967 11 07	39801.	-.049	.253	IPMS ARPT69
1967 11 26	39820.	-.062	.273	IPMS ARPT69
1967 12 24	39838.	-.064	.292	IPMS ARPT69

Table C-1. (Cont.)

Date	MJD	x (arcsec)	y (arcsec)	Source
1968 01 01	39856.	-.055	.305	IPMS ARPT70
1968 01 19	39874.	-.037	.310	IPMS ARPT70
1968 02 07	39893.	-.014	.309	IPMS ARPT70
1968 02 25	39911.	.009	.302	IPMS ARPT70
1968 03 14	39929.	.030	.290	IPMS ARPT70
1968 04 01	39947.	.048	.274	IPMS ARPT70
1968 04 20	39966.	.057	.259	IPMS ARPT70
1968 05 08	39984.	.059	.244	IPMS ARPT70
1968 05 26	40002.	.061	.229	IPMS ARPT70
1968 06 13	40020.	.067	.214	IPMS ARPT70
1968 07 02	40039.	.089	.198	IPMS ARPT70
1968 07 20	40057.	.104	.183	IPMS ARPT70
1968 08 07	40075.	.095	.169	IPMS ARPT70
1968 08 25	40093.	.060	.160	IPMS ARPT70
1968 09 13	40112.	.016	.158	IPMS ARPT70
1968 10 01	40130.	-.022	.162	IPMS ARPT70
1968 10 19	40148.	-.053	.175	IPMS ARPT70
1968 11 06	40166.	-.084	.201	IPMS ARPT70
1968 11 25	40185.	-.111	.236	IPMS ARPT70
1968 12 13	40203.	-.127	.268	IPMS ARPT70
1969 01 01	40222.	-.123	.290	IPMS ARPT71
1969 01 19	40240.	-.106	.306	IPMS ARPT71
1969 02 07	40259.	-.099	.323	IPMS ARPT71
1969 02 25	40277.	-.085	.344	IPMS ARPT71
1969 03 15	40295.	-.036	.372	IPMS ARPT71
1969 04 02	40313.	.015	.392	IPMS ARPT71
1969 04 21	40332.	.052	.396	IPMS ARPT71
1969 05 09	40350.	.090	.387	IPMS ARPT71
1969 05 27	40368.	.126	.366	IPMS ARPT71
1969 06 14	40386.	.158	.337	IPMS ARPT71
1969 07 03	40405.	.180	.302	IPMS ARPT71
1969 07 21	40423.	.188	.257	IPMS ARPT71
1969 08 08	40441.	.184	.211	IPMS ARPT71
1969 08 26	40459.	.165	.167	IPMS ARPT71
1969 09 14	40478.	.125	.135	IPMS ARPT71
1969 10 02	40496.	.079	.114	IPMS ARPT71
1969 10 20	40514.	.036	.106	IPMS ARPT71
1969 11 07	40532.	-.014	.106	IPMS ARPT71
1969 11 26	40551.	-.069	.113	IPMS ARPT71
1969 12 14	40569.	-.116	.133	IPMS ARPT71

Table C-1. (Cont.)

Date	MJD	x (arcsec)	y (arcsec)	Source
1970 01 01	40587.	-.157	.169	IPMS ARPT72
1970 01 19	40605.	-.180	.219	IPMS ARPT72
1970 02 07	40624.	-.180	.276	IPMS ARPT72
1970 02 25	40642.	-.161	.332	IPMS ARPT72
1970 03 15	40660.	-.131	.382	IPMS ARPT72
1970 04 02	40678.	-.098	.422	IPMS ARPT72
1970 04 21	40697.	-.063	.450	IPMS ARPT72
1970 05 09	40715.	-.026	.467	IPMS ARPT72
1970 05 27	40733.	.021	.463	IPMS ARPT72
1970 06 14	40751.	.092	.436	IPMS ARPT72
1970 07 03	40770.	.159	.395	IPMS ARPT72
1970 07 21	40788.	.209	.350	IPMS ARPT72
1970 08 08	40806.	.241	.302	IPMS ARPT72
1970 08 26	40824.	.249	.252	IPMS ARPT72
1970 09 14	40843.	.234	.198	IPMS ARPT72
1970 10 02	40861.	.204	.150	IPMS ARPT72
1970 10 20	40879.	.166	.113	IPMS ARPT72
1970 11 07	40897.	.121	.079	IPMS ARPT72
1970 11 26	40916.	.072	.045	IPMS ARPT72
1970 12 14	40934.	.024	.014	IPMS ARPT72
1971 01 01	40952.	-.045	.019	IPMS ARPT73
1971 01 19	40970.	-.128	.051	IPMS ARPT73
1971 02 07	40989.	-.203	.092	IPMS ARPT73
1971 02 25	41007.	-.243	.143	IPMS ARPT73
1971 03 15	41025.	-.228	.204	IPMS ARPT73
1971 04 02	41043.	-.189	.272	IPMS ARPT73
1971 04 21	41062.	-.136	.340	IPMS ARPT73
1971 05 09	41080.	-.075	.399	IPMS ARPT73
1971 05 27	41098.	-.018	.447	IPMS ARPT73
1971 06 14	41116.	.024	.479	IPMS ARPT73
1971 07 03	41135.	.077	.485	IPMS ARPT73
1971 07 21	41153.	.142	.468	IPMS ARPT73
1971 08 08	41171.	.214	.445	IPMS ARPT73
1971 08 26	41189.	.266	.404	IPMS ARPT73
1971 09 14	41208.	.277	.337	IPMS ARPT73
1971 10 02	41226.	.255	.278	IPMS ARPT73
1971 10 20	41244.	.212	.235	IPMS ARPT73
1971 11 07	41262.	.174	.203	IPMS ARPT73
1971 11 26	41281.	.139	.167	IPMS ARPT73
1971 12 14	41299.	.110	.120	IPMS ARPT73

Table C-1. (Cont.)

Date	MJD	x (arcsec)	y (arcsec)	Source
1972 01 01	41317.	.071	.070	IPMS MN0272
1972 01 19	41335.	.015	.033	IPMS MN0472
1972 02 06	41353.	-.015	.030	IPMS MN0472
1972 02 25	41372.	-.042	.053	IPMS MN0472
1972 03 14	41390.	-.081	.109	IPMS MN0572
1972 04 02	41409.	-.125	.174	IPMS MN0572
1972 04 20	41427.	-.139	.242	IPMS MN0772
1972 05 09	41446.	-.120	.308	IPMS MN0772
1972 05 27	41464.	-.073	.358	IPMS MN0772
1972 06 14	41482.	-.017	.384	IPMS MN0772
1972 07 02	41500.	.033	.398	IPMS MN0872
1972 07 21	41519.	.065	.404	IPMS MN0972
1972 08 08	41537.	.084	.404	IPMS MN0972
1972 08 26	41555.	.105	.398	IPMS MN1072
1972 09 13	41573.	.142	.383	IPMS MN1072
1972 10 02	41592.	.180	.360	IPMS MN1172
1972 10 20	41610.	.206	.334	IPMS MN1272
1972 11 07	41628.	.219	.310	IPMS MN1272
1972 11 25	41646.	.223	.278	IPMS MN0173
1972 12 14	41665.	.220	.212	IPMS MN0273
1973 01 01	41683.	.205	.137	IPMS MN0373
1973 01 19	41701.	.177	.116	IPMS MN0373
1973 02 07	41720.	.149	.123	IPMS MN0473
1973 02 25	41738.	.120	.134	IPMS MN0473
1973 03 15	41756.	.079	.123	IPMS MN0573
1973 04 02	41774.	.045	.120	IPMS MN0573
1973 04 21	41793.	.019	.138	IPMS MN0573
1973 05 09	41811.	-.005	.176	IPMS MN0573
1973 05 27	41829.	-.029	.228	IPMS MN0773
1973 06 14	41847.	-.043	.265	IPMS MN0773
1973 07 03	41866.	-.037	.288	IPMS MN0873
1973 07 21	41884.	-.019	.306	IPMS MN0873
1973 08 08	41902.	.006	.325	IPMS MN0873

APPENDIX D

UNIVERSAL TIME (UT1)

Before January 5, 1962, SAO used UT1 values referred to UTC(USNO) as published by USNO. Since that date, SAO has used UT1 values from Circular D provided by BIH, referred to International Atomic Time (IAT). IAT and Smithsonian Atomic Time (A.S) (see Appendix A) are related through published differences with A1(USNO).

The differences between A.S and UT1, tabulated in Table D-1, are expressed in 25- or 50-day intervals as a second-degree polynomial of the form

$$A.S - UT1 = A_0 + A_1 (T - T_0) + A_2 (T - T_0)^2 \quad ,$$

where A.S - UT1 is in seconds, T is in Modified Julian Days, and T_0 is the beginning of the interval in MJD. Table D-1 gives T_0 in MJD, year, month, and day; the interval (25 or 50 days); and the coefficients A_0, A_1, and A_2.

The polynomial fit determined for the last interval (August 2, 1970) was used to extrapolate UT1 values for subsequent observations.

Table D-1. $(A.S-UT1) = A_0 + A_1(T-T_0) + A_2(T-T_0)^2$, where A_0 is in seconds, A_1 is in seconds per day, A_2 is in seconds per day squared, and T and T_0 are in Modified Julian Days.

MJD	Interval	Year	M	D	A_0	A_1	A_2
36204	50	1958	1	1	3.3419436E-02	1.7413966E-03	-1.9653803E-06
36254	50	1958	2	20	1.1579783E-01	1.6564313E-03	2.3026866E-06
36304	50	1958	4	11	2.0376647E-01	1.9724053E-03	-6.4075849E-06
36354	50	1958	5	31	2.8634967E-01	1.1769024E-03	-6.7556608E-06
36404	50	1958	7	20	3.2915559E-01	4.7403947E-04	3.9854468E-06
36454	50	1958	9	8	3.6300644E-01	9.8815046E-04	7.5413763E-06
36504	50	1958	10	28	4.3150837E-01	1.6881441E-03	-7.0276712E-07
36554	50	1958	12	17	5.1412208E-01	1.6352886E-03	-1.4187507E-06
36604	50	1959	2	5	5.9269873E-01	1.3369852E-03	5.3305095E-07
36654	50	1959	3	27	6.6077901E-01	1.4851055E-03	-1.4231052E-06
36704	50	1959	5	16	7.3101019E-01	1.2950031E-03	-5.4199867E-06
36754	50	1959	7	5	7.8254341E-01	6.5357649E-04	9.7018371E-07
36804	50	1959	8	24	8.1781323E-01	8.9608601E-04	7.8326401E-06
36854	50	1959	10	13	8.8181973E-01	1.7266513E-03	5.4035308E-07
36904	50	1959	12	2	9.6965913E-01	1.6164842E-03	-4.2088497E-06
36954	50	1960	1	21	1.0403734E+00	1.2334624E-03	3.6669612E-06
37004	50	1960	3	11	1.1111673E+00	1.6275209E-03	-2.2991768E-07
37054	50	1960	4	30	1.1915729E+00	1.5900046E-03	-7.8592544E-06
37104	25	1960	6	19	1.2514738E+00	7.5151427E-04	-9.0206712E-06
37129	25	1960	7	14	1.2647636E+00	3.1729027E-04	1.7171124E-06
37154	50	1960	8	8	1.2739287E+00	3.9334216E-04	8.8466494E-06
37204	50	1960	9	27	1.3157101E+00	1.2979207E-03	2.2318567E-06
37254	50	1960	11	16	1.3859456E+00	1.5040488E-03	-2.3808790E-06
37304	25	1961	1	5	1.4545978E+00	1.3634637E-03	-1.1360556E-05
37329	25	1961	1	30	1.4816626E+00	7.1469680E-04	8.6378757E-06
37354	25	1961	2	24	1.5049539E+00	1.2979237E-03	1.1227052E-05
37379	25	1961	3	21	1.5441614E+00	1.8519622E-03	-1.2927014E-05
37404	50	1961	4	15	1.5811533E+00	1.2896141E-03	-2.5516547E-06
37454	50	1961	6	4	1.6391211E+00	1.0192945E-03	-5.1144989E-06
37504	50	1961	7	24	1.6766858E+00	4.0909512E-04	4.7788142E-06
37554	50	1961	9	12	1.7091307E+00	9.7682976E-04	5.6015027E-06
37604	50	1961	11	1	1.7717014E+00	1.5238953E-03	-1.9881058E-06
37654	50	1961	12	21	1.8430139E+00	1.2295078E-03	-2.8505878E-07
37704	50	1962	2	9	1.9044770E+00	1.3384595E-03	2.7442956E-06
37754	50	1962	3	31	1.9780244E+00	1.6742467E-03	-1.8004766E-06
37804	25	1962	5	20	2.0582739E+00	1.3325185E-03	-1.1249769E-05
37829	25	1962	6	14	2.0846350E+00	7.6860070E-04	-5.1197803E-06
37854	50	1962	7	9	2.1010537E+00	4.1305649E-04	4.9204879E-06
37904	50	1962	8	28	2.1354427E+00	1.0523506E-03	6.1131265E-06
37954	50	1962	10	17	2.2031024E+00	1.7030925E-03	1.4501712E-06
38004	26	1962	12	6	2.2916445E+00	1.7995139E-03	-5.4912033E-06
38030	50	1963	1	1	2.3269576E+00	1.5368569E-03	-7.5189051E-06
38080	50	1963	2	20	2.3858924E+00	7.9361884E-04	9.5144150E-06
38130	50	1963	4	11	2.4505509E+00	1.9460152E-03	-1.2050727E-06
38180	50	1963	5	31	2.5443493E+00	1.7242581E-03	-1.0561687E-05
38230	50	1963	7	20	2.6043955E+00	2.3185199E-04	1.1552844E-05
38280	50	1963	9	8	2.6446542E+00	1.8522630E-03	7.3695482E-06
38330	50	1963	10	28	2.7531461E+00	2.2768322E-03	-2.6890519E-06
38380	15	1963	12	17	2.8602283E+00	1.9983618E-03	-5.2916922E-06
38395	50	1964	1	1	2.8866372E+00	1.9522648E-03	2.9715617E-06
38445	50	1964	2	20	2.9915075E+00	2.1117754E-03	-3.3204747E-07
38495	50	1964	4	10	3.0981172E+00	2.2064573E-03	-3.0462964E-06
38545	50	1964	5	30	3.2005684E+00	1.9919421E-03	-8.0343568E-06
38595	50	1964	7	19	3.2802299E+00	5.2400395E-04	1.2772361E-05
38645	50	1964	9	7	3.3387022E+00	1.6493401E-03	1.0265087E-05
38695	50	1964	10	27	3.4491442E+00	2.7563918E-03	-8.5611800E-06

Table D-1. (Cont.)

MJD	Interval	Year	M	D	A_0	A_1	A_2
38745	50	1964	12	16	3.5655665E+00	2.1287401E-03	5.8758603E-07
38795	50	1965	2	4	3.6718494E+00	1.8453748E-03	4.7325927E-06
38845	50	1965	3	26	3.7750795E+00	3.0476974E-03	-6.2714711E-06
38895	50	1965	5	15	3.9102900E+00	2.2125419E-03	-3.2115184E-06
38945	50	1965	7	4	4.0125784E+00	1.0852979E-03	8.8935871E-06
38995	50	1965	8	23	4.0885572E+00	1.7553996E-03	1.1832432E-05
39045	50	1965	10	12	4.2072461E+00	2.9223026E-03	-3.6010971E-06
39095	50	1965	12	1	4.3441718E+00	2.7888667E-03	-1.1682098E-05
39145	25	1966	1	20	4.4535446E+00	1.8992217E-03	1.7107806E-05
39170	25	1966	2	14	4.5114650E+00	2.7014006E-03	-6.6244354E-06
39195	50	1966	3	11	4.5742014E+00	2.2465772E-03	7.3111285E-06
39245	50	1966	4	30	4.7039857E+00	2.7923520E-03	-3.2345506E-06
39295	30	1966	6	19	4.8351114E+00	2.3118914E-03	-1.7869077E-05
39325	25	1966	7	19	4.8889083E+00	1.2467044E-03	6.0010529E-06
39350	25	1966	8	13	4.9236500E+00	1.7664349E-03	1.6217865E-05
39375	25	1966	9	7	4.9778342E+00	2.5195217E-03	5.7495114E-06
39400	25	1966	10	2	5.0440874E+00	2.8623178E-03	7.4753583E-06
39425	25	1966	10	27	5.1203506E+00	3.1954189E-03	-8.5663248E-06
39450	25	1966	11	21	5.1947787E+00	2.6966650E-03	2.8393821E-06
39475	25	1966	12	16	5.2637328E+00	2.9598943E-03	-2.0632503E-05
39500	25	1967	1	10	5.3257218E+00	1.2855956E-03	1.4117794E-05
39525	25	1967	2	4	5.3664227E+00	2.0286361E-03	1.5512874E-05
39550	50	1967	3	1	5.4258436E+00	2.8546333E-03	-9.4031774E-07
39600	50	1967	4	20	5.5664568E+00	2.7318431E-03	-1.6141669E-06
39650	25	1967	6	9	5.6990115E+00	2.6875036E-03	-2.2352390E-05
39675	25	1967	7	4	5.7524250E+00	1.3222263E-03	-5.5641305E-06
39700	50	1967	7	29	5.7823178E+00	1.4590736E-03	1.0329558E-05
39750	50	1967	9	17	5.8817508E+00	2.3572726E-03	3.5880216E-06
39800	25	1967	11	6	6.0095601E+00	2.8367568E-03	-1.0950763E-06
39825	31	1967	12	1	6.0794995E+00	3.0157712E-03	-1.6686241E-05
39856	44	1968	1	1	6.1421671E+00	2.5326990E-03	1.3150000E-06
39900	50	1968	2	14	6.2556448E+00	2.8169932E-03	-4.8698554E-06
39950	25	1968	4	4	6.3836121E+00	3.4455413E-03	-1.6231575E-05
39975	25	1968	4	29	6.4593955E+00	2.4756578E-03	-1.6887416E-07
40000	50	1968	5	24	6.5211747E+00	2.6430618E-03	-1.0778385E-05
40050	50	1968	7	13	6.6276017E+00	1.8369700E-03	5.4185294E-06
40100	50	1968	9	1	6.7330783E+00	2.4313746E-03	2.7533980E-06
40150	50	1968	10	21	6.8608866E+00	2.6823980E-03	1.6945720E-06
40200	50	1968	12	10	6.9992317E+00	2.5587021E-03	-1.2562317E-06
40250	50	1969	1	29	7.1241715E+00	2.6096955E-03	6.4258524E-06
40300	50	1969	3	20	7.2698598E+00	3.1022034E-03	1.1934881E-08
40350	50	1969	5	9	7.4240364E+00	2.8990167E-03	-6.6505806E-06
40400	50	1969	6	28	7.5522970E+00	1.9273908E-03	5.7887906E-07
40450	50	1969	8	17	7.6501718E+00	2.1390599E-03	9.7481887E-06
40500	50	1969	10	6	7.7805765E+00	2.8622157E-03	6.6903742E-07
40550	50	1969	11	25	7.9247163E+00	2.9445376E-03	-3.5282170E-07
40600	50	1970	1	14	8.0711926E+00	2.7371500E-03	4.1451478E-06
40650	50	1970	3	5	8.2187073E+00	3.2240917E-03	-7.2612965E-07
40700	50	1970	4	24	8.3779081E+00	3.2458833E-03	-9.2363808E-06
40750	50	1970	6	13	8.5171191E+00	2.3386116E-03	-5.8353263E-06
40800	50	1970	8	2	8.6197877E+00	1.7498399E-03	7.6171554E-06
40850	50	1970	9	21	8.7261389E+00	2.7079800E-03	4.6054737E-06
40900	50	1970	11	10	8.8726687E+00	3.0954253E-03	-4.5499449E-06
40950	50	1970	12	30	9.0159238E+00	2.5853853E-03	-3.9493257E-07
41000	25	1971	2	18	9.1441356E+00	2.5118515E-03	7.9534503E-06
41025	25	1971	3	15	9.2112657E+00	3.5479501E-03	-9.1074737E-06

Table D-1. (Cont.)

MJD	Interval	Year	M	D	A_0	A_1	A_2
41050	50	1971	4	9	9.2932740E+00	3.1713471E-03	3.9504943E-07
41100	25	1971	5	29	9.4517811E+00	3.0035859E-03	-1.2618819E-05
41125	25	1971	6	23	9.5190744E+00	2.2190693E-03	5.2932524E-06
41150	25	1971	7	18	9.5778642E+00	2.5574090E-03	-5.4158487E-06
41175	25	1971	8	12	9.6385396E+00	2.1791598E-03	1.3574835E-05
41200	50	1971	9	6	9.7018485E+00	2.7342531E-03	9.0682717E-06
41250	50	1971	10	26	9.8605108E+00	3.8720920E-03	-8.4939023E-06
41300	50	1971	12	15	1.0032261E+01	2.6273203E-03	7.1118106E-06
41350	50	1972	2	3	1.0181630E+01	3.3520633E-03	1.0581663E-06
41400	50	1972	3	24	1.0351935E+01	3.5608308E-03	-1.1697178E-06
41450	50	1972	5	13	1.0526966E+01	3.5474932E-03	-1.0218236E-05
41500	50	1972	7	2	1.0679247E+01	2.3685534E-03	3.7023648E-06
41550	50	1972	8	21	1.0806706E+01	2.3625545E-03	1.1719805E-05
41600	50	1972	10	10	1.0953845E+01	3.1689969E-03	1.6692998E-06
41650	50	1972	11	29	1.1116856E+01	3.2993442E-03	-1.8889984E-06
41700	50	1973	1	18	1.1277005E+01	3.1569184E-03	2.7673671E-06
41750	50	1973	3	9	1.1441101E+01	3.5979081E-03	-1.5604452E-06
41800	50	1973	4	28	1.1616809E+01	3.4529641E-03	-6.2582473E-06
41850	50	1973	6	17	1.1774713E+01	2.4511068E-03	-1.0821043E-06
41900	50	1973	8	6	1.1895333E+01	2.3851799E-03	6.6039045E-06
41950	25	1973	9	25	1.2031231E+01	2.9611480E-03	8.8689681E-06

PART III

SATELLITE DYNAMICS

ABSTRACT

The perturbations of an artificial close-earth satellite are developed in analytical form. Gravitational perturbations due to the geopotential, the sun, the moon, the body tide, and the ocean tides are treated; and nongravitational perturbations due to atmospheric drag and radiation pressure are developed. Also discussed are applications of the development for orbit determination and computation.

RESUME

Les pertubations d'un satellite artificiel proche de la terre sont développées sous forme analytique. Les perturbations de gravitation dûes au géopotentiel, au soleil, à la lune, à la marée du corps et aux marées océaniques sont traitées; et les perturbations ne tenant pas à la gravitation mais à la résistance atmosphérique et à la pression des radiations sont développées. Sont également discutées les applications du développement pour la détermination et le calcul de l'orbite.

КОНСПЕКТ

Разработаны в аналитической форме возмущения искуственного близь-земного спутника. Рассматриваются гравитационные возмущения вызываемые геопотенциалом, солнцем, луной, приливом тела и океанскими приливами; разрабатываются негравитационные возмущения вызываемые атмосферным драгом и давлением излучения. Также обсуждаются применения развития определения и вычисления орбит.

PART III

SATELLITE DYNAMICS

E. M. Gaposchkin

1. INTRODUCTION

The general results of analytical mechanics are deceptively simple to state. They have been refined for over 250 years and are presented with a clarity and a directness that are captivating. Celestial mechanics, as a part of analytical mechanics, has received considerable attention, and many of the general results came from topics in celestial mechanics. There are a number of excellent modern treatments of mechanics (see, e.g., Lanczos, 1966; Goldstein, 1959): This article will draw the necessary background from these sources and attempt to present a coherent view of the tools necessary for dealing with the problem of the close-earth satellites. A number of general treatments of celestial mechanics already exist (see, e.g., Plummer, 1918; Smart, 1953; Brouwer and Clemence, 1961; Kaula, 1966a; Hagihara, 1970, 1972).

For any one problem, the more general view may not be necessary. For example, the original papers on satellite geodesy did not use the full power of analytical mechanics. There are three reasons for the following overall view. First, a unified treatment allows comparison and blending of results, with consequent efficiency. Second, future work requiring essentially more accurate analysis will need the greater capability offered by this approach. Third, there is benefit in the greater insight provided when these results are applied.

The subject to be discussed is formally quite mathematical. However, to make any practical headway, one must make use of the physical realities of the earth. For example, its dominant anomalous potential feature is its oblateness, which is 1000 times the size of the remaining anomalous field and 1/1000 the central-force part. We are

led to consider the physics of the solid earth, of the atmosphere, and of the ocean. There are sizable effects from all these. In order to proceed, we must have a model, even though, for example, the radiation-pressure effect is difficult to take into account because of our imperfect knowledge of the solar constant, the earth's albedo, the satellite's reflectivity, and the satellite's orientation.

There is the question of approach. With modern computers, direct numerical integration of the equations of motion is feasible. Numerical-integration techniques have advanced considerably, in both accuracy and efficiency: What is lost in insight is compensated for by the simpler mathematics. After all, we are interested in the numbers to compare with observations. The question of efficiency hinges on technique, the particular computer, and the particular problem. A subsequent study will contrast numerical, semianalytical, and formal developments. Here we consider analytical techniques only, although some of the results can be used in purely numerical treatments.

Exact solutions of the equations of motion, except for the two-body problem, have eluded analysts. We are thus led to approximate solutions by use of a perturbation method: A reference orbit is obtained by some means, and corrections or perturbations are determined that include an effect absent from the reference orbit. This process can be iterated so long as the corrected orbit does not change enough to invalidate its use as a reference. We therefore wish to include the largest effects first, and then proceed to smaller ones. Table 1 gives the orbital effects considered, in decreasing importance for geodetic satellites, i.e., satellites with mean heights between 700 and 4000 km.

Table 1. Size and character of orbital perturbations.*

Force	Short period, < 1 day	Intermediate period, 1 to 30 days	Long period, > 30 days	Secular
J_2	2.5 km		10^{-6}	yes
J_{2n+1}	50 m		10^{-3}	no
J_{2n}	50 m			yes
Solar	~1 m		800 m	yes
Lunar	~1 m	120 m		yes
Tesseral harmonics	200 m	2-km resonances	>2-km resonances	no
Air drag	< 1 m			yes†
Radiation pressure	< 1 m		10^{-2}	no‡
Body tides		15 m	90 m	no
Ocean tides		5 m?	?	no
Atmospheric tides				no

*These orbital sizes are meant to be characteristic.

†For air drag, we have a monotonic decrease in the energy. The distinction between periodic and secular effects is not clear, as it is in the case for gravitational perturbations.

‡The radiation-pressure effects, in principle, can have no true secular effects. In fact, however, one would have to wait very long for that to be true.

2. DYNAMICAL SYSTEMS

We are concerned with a system of differential equations resulting from Newton's law: Mass times acceleration equals force; that is,

$$m\ddot{\bar{x}} = \bar{F} \quad . \tag{1}$$

For n particles, 3n coordinates and 3n velocities need to be determined. A solution is found when we can determine these 6n quantities for some arbitrary time. A set of formulas is said to be a theory. In satellite geodesy, we are concerned with determining the orbit of a single point, and thus the number of equations or independent variables is reduced to 6.

The classical form of (1) in cartesian coordinates is not particularly tractable. We obtain alternate, and completely equivalent, coordinates or variables. To show how this is done, a review of some fundamental ideas from analytical dynamics is given. Elaborate proofs can be found in Goldstein (1959) or Whittaker (1964).

The use of generalized coordinates is very important. The first step is to realize that velocities and coordinates are on an equal footing. Hamilton's canonical equations (Goldstein, 1959, p. 217) illustrate this. Following the customary practice of labeling the coordinates $q_i = x_i$ and the momenta $p_i = m\dot{q}_i$, we can write the equivalent of (1) in terms of the Hamiltonian, where

$$\mathcal{H} = \mathcal{T} + \mathcal{U} = \mathcal{H}(q_i, p_i) \quad . \tag{2}$$

Here $\mathcal{T}$ is the kinetic energy, and $\mathcal{U}$ is the potential energy. The differential equations equivalent to (1) are

$$\begin{aligned} \dot{q}_i &= \partial \mathcal{H} / \partial p_i \quad , \\ \dot{p}_i &= -\partial \mathcal{H} / \partial q_i \quad ; \end{aligned} \tag{3}$$

these are known as the canonical equations of Hamilton. All variables appear in pairs – a coordinate q_i and a conjugate momenta p_i – and have equal importance in the system of differential equations.

We observe immediately that if a q_i or a p_i does not occur explicitly in $\mathcal{H}$, then the conjugate variable is a constant of the motion. A missing coordinate is called ignorable. This leads to our searching for coordinate systems with ignorable coordinates. For example, in the two-body problem, the Hamiltonian is

$$\mathcal{H} = \frac{1}{2m}(\dot{x}^2 + \dot{y}^2) - \frac{1}{(x^2+y^2)^{1/2}} \quad ,$$

$$= \frac{1}{2m}(P_x^2 + P_y^2) - \frac{1}{(x^2+y^2)^{1/2}} \quad ,$$

expressed in cartesian coordinates; whereas in polar coordinates, it is

$$\mathcal{H} = \frac{1}{2m}\left(p_r^2 + \frac{p_v^2}{r^2}\right) - \frac{1}{r} \quad ,$$

where $p_r = m\dot{r}$ and $p_v = mr^2\dot{v}$. In polar coordinates, v is an ignorable coordinate leading immediately to $p_v = mr^2\dot{v} = N$, a constant (see Section 4 for a complete discussion). In general, coordinate systems are suggested by the problem rather than resulting from analysis.

The transformation from one set of variables to another is done through a canonical transformation, which leaves the transformed equations in the form (3). The vehicle used for the transformation is a generating function F. In order for this to be a transformation between 2n old variables and 2n new variables, F must be a function of the 4n variables. However, only 2n of these variables are independent. Therefore, the generating function can be written in only four forms:

$$F_1(q, Q, t) \quad , \qquad F_2(q, P, t) \quad , \qquad F_3(p, Q, t) \quad , \qquad F_4(p, P, t) \quad ,$$

where, following Whittaker (1964), we use capital letters for the new variables. Depending on the transformation chosen, the 2n variables are

$$p_i = \partial F_1(q, Q, t)/\partial q_i \quad ,$$

$$P_i = -\partial F_1/\partial Q_i \quad , \tag{4a}$$

or

$$p_i = \partial F_2(q, P, t)/\partial q_i \quad ,$$

$$Q_i = \partial F_2/\partial P_i \quad , \tag{4b}$$

or

$$q_i = -\partial F_3(p, Q, t)/\partial p_i \quad ,$$

$$P_i = -\partial F_3/\partial Q_i \quad , \tag{4c}$$

or

$$q_i = -\partial F_4(p, P, t)/\partial p_i \quad ,$$

$$Q_i = \partial F_4/\partial P_i \quad ; \tag{4d}$$

and the new Hamiltonian is always

$$\mathcal{H}^* = \mathcal{H} + (\partial F_i/\partial t) \quad . \tag{5}$$

From equations (4), we can obtain

$$q_i = q_i(Q_j, P_j, t) \quad ,$$

$$p_i = p_i(Q_i, P_i, t) \quad , \tag{6}$$

which can be substituted in (5) to obtain the equations in new variables.

The success of canonical transformation hinges on our finding a determining function F, and the usefulness of the formal development may therefore not be so great. However, Poincaré (1893) considered other expressions that would be invariant under a canonical transformation. He showed that in the 2n-dimensional space, the n surface integrals

$$
\begin{aligned}
J_1 &= \iint \sum_i dq_i \, dp_i \quad , \\
J_2 &= \iiiint \sum_{ik} dq_i \, dp_i \, dq_k \, dp_k \quad , \\
&\vdots \\
J_n &= \iint \cdots \iint \sum_{i,j,\ldots,k} dq_i \, dp_i \cdots dq_k \, dp_k
\end{aligned}
\tag{7}
$$

are invariant. These are very powerful in determining invariants, as well as the constants of motion. They play a vital role in the discussion of action and angle variables in the theory of Hamilton and Jacobi, although that topic is beyond the scope of this article. These J_n are equivalent to saying that the volume in phase space is invariant under a canonical transformation.

The main interest here is an alternate statement of invariance in terms of Lagrange and Poisson brackets. Consider the relations

$$
\begin{aligned}
q_i &= q_i(u, v) \quad , \\
p_i &= p_i(u, v) \quad .
\end{aligned}
$$

The Lagrange bracket is defined as

$$
\sum_i \left(\frac{\partial q_i}{\partial u} \frac{\partial p_i}{\partial v} - \frac{\partial p_i}{\partial u} \frac{\partial q_i}{\partial v} \right) = \{u, v\}_{q,p} \quad ; \tag{8}
$$

obviously,

$$\{u, v\}_{q,p} = -\{v, u\}_{q,p} \quad . \tag{9}$$

The invariance of J_1 means that the Jacobian

$$\frac{\partial(q_i, p_i)}{\partial(u, v)} = \begin{vmatrix} \partial q_i/\partial u & \partial p_i/\partial u \\ \partial q_i/\partial v & \partial p_i/\partial v \end{vmatrix} \tag{10}$$

must also be invariant. Therefore,

$$\sum_i \frac{\partial(q_i, p_i)}{\partial(u, v)} = \sum_k \frac{\partial(Q_k, P_k)}{\partial(u, v)} \tag{11}$$

or

$$\{u, v\}_{q,p} = \{u, v\}_{Q,P} \quad . \tag{12}$$

Accordingly, we can use any set of canonical variables to evaluate the Lagrange brackets and we can drop the subscripts. With the use of some algebra, we can also show that

$$\begin{aligned} \{q_i, q_j\} &= 0 \quad , \\ \{p_i, p_j\} &= 0 \quad , \\ \{q_i, p_j\} &= \delta_{ij} \quad ; \end{aligned} \tag{13}$$

these are sometimes known as the fundamental Lagrange brackets.

We are led to consider another quantity, the Poisson bracket, which is defined as

$$[u, v]_{q,p} = \sum_i \left(\frac{\partial u}{\partial q_i} \frac{\partial v}{\partial p_i} - \frac{\partial u}{\partial p_i} \frac{\partial v}{\partial q_i} \right) , \tag{14}$$

where we have

$$[u, v]_{q,p} = - [v, u]_{q,p} \quad . \tag{15}$$

Considering the Lagrange and Poisson brackets as purely mathematical objects, we can show that

$$\sum_{\ell=1}^{2n} \{u_\ell, u_i\}_{q,p} [u_\ell, u_j]_{q,p} = \delta_{ij} \quad .$$

In fact, for the matrices $[L] = \{u_i, u_j\}_{q,p}$ and $[P] = [u_i, u_j]_{q,p}$, we can show that

$$P = L^{-1} \quad . \tag{16}$$

Therefore, we can compute the set of Poisson brackets from the set of Lagrange brackets, and vice versa. Relation (16) holds even if the coordinates are not canonical. Since the Lagrange brackets are invariant, so are the Poisson brackets. Further, we can write the fundamental Poisson brackets as

$$\begin{aligned} [p_i, p_j] &= 0 \quad , \\ [q_i, q_j] &= 0 \quad , \\ [q_i, p_j] &= \delta_{ij} \quad . \end{aligned} \tag{17}$$

Since the fundamental Lagrange and Poisson brackets must hold for canonical variables, (13) or (17) provides a test for canonical variables.

Consider the canonical equations

$$\begin{aligned} \dot{x}_i &= p_i \quad , \\ \dot{p}_i &= - \partial \mathcal{U} / \partial x_i \quad , \end{aligned} \tag{18}$$

and a transformation to the variables $\mathcal{E}_i$; that is,

$$\begin{aligned} x_i &= x_i(\mathcal{E}_j) \quad , \\ p_i &= p_i(\mathcal{E}_j) \quad . \end{aligned} \tag{19}$$

Now

$$\begin{aligned} \dot{x}_i &= \sum_j \frac{\partial x_i}{\partial \mathcal{E}_j} \frac{d\mathcal{E}_j}{dt} \quad , \\ \dot{p}_i &= \sum_j \frac{\partial p_i}{\partial \mathcal{E}_j} \frac{d\mathcal{E}_j}{dt} \quad . \end{aligned} \tag{20}$$

Multiplying the first part of (20) by $\partial \dot{x}_i / \partial \mathcal{E}_k$ and the second by $\partial x_i / \partial \mathcal{E}_k$ and then subtracting, we have

$$\sum_j \left(\frac{\partial \dot{x}_i}{\partial \mathcal{E}_k} \frac{\partial x_i}{\partial \mathcal{E}_j} - \frac{\partial x_i}{\partial \mathcal{E}_k} \frac{\partial p_i}{\partial \mathcal{E}_j} \right) \frac{d\mathcal{E}_i}{dt} = \frac{\partial}{\partial \mathcal{E}_k} (-\mathcal{K}) \quad , \tag{21}$$

where the Hamiltonian is

$$\mathcal{K} = \tfrac{1}{2} v^2 + \mathcal{U} \quad .$$

Now (21) can be written with Lagrange brackets

$$\sum_j \{\mathcal{E}_k, \mathcal{E}_j\} \, d\mathcal{E}_j/dt = - \partial \mathcal{K} / \partial \mathcal{E}_k \quad , \tag{22a}$$

or

$$[L_{kj}] \, d\mathcal{E}_j/dt = - \partial \mathcal{K} / \partial \mathcal{E}_k \tag{22b}$$

in the notation of (16). By inverting the matrix of Lagrange brackets, we can write the equations of motion

$$d\mathcal{E}_j/dt = - [P_{jk}] \, \partial \mathcal{H}/\partial \mathcal{E}_k \quad . \tag{23}$$

Equation (23) is equivalent to (18). This development uses only the mathematical properties of the Poisson and Lagrange brackets; it does not depend on the new variables being canonical. Therefore, we have reduced obtaining equations of motion in any variables to obtaining Poisson brackets and expressing the Hamiltonian in the chosen variables.

If we have succeeded in finding a set of variables $\mathcal{E}_i$ that are constants of the motion, and if we can write

$$\begin{aligned} x_i &= x_i(\mathcal{E}_j, t) \quad , \\ \dot{x}_i &= \dot{x}_i(\mathcal{E}_j, t) \quad , \end{aligned} \tag{24}$$

then the Poisson and Lagrange brackets must be constants; that is,

$$\frac{\partial}{\partial t} \{\mathcal{E}_i, \mathcal{E}_j\} = \frac{d}{dt} \{\mathcal{E}_i, \mathcal{E}_j\} = 0 \quad . \tag{25}$$

For canonical variables, this of course follows from (13) and (17). This can be true for any variables – for example, Kepler elements in a potential field. This can be shown by our taking

$$\ddot{x}_i = - \partial \mathcal{U}/\partial x_i \quad ;$$

now

$$\frac{\partial}{\partial t}\{p,q\} = \frac{\partial}{\partial t}\sum_i\left(\frac{\partial x_i}{\partial p}\frac{\partial \dot{x}_i}{\partial q} - \frac{\partial \dot{x}_i}{\partial p}\frac{\partial x_i}{\partial q}\right) ,$$

$$= \sum\left(\frac{\partial x_i}{\partial p}\frac{\partial^2 \mathcal{U}}{\partial q\,\partial x_i} - \frac{\partial x_i}{\partial q}\frac{\partial^2 \mathcal{U}}{\partial p\,\partial x_i}\right) ,$$

$$= \sum \frac{\partial}{\partial q}\left(\frac{\partial \mathcal{U}}{\partial x_i}\frac{\partial x_i}{\partial p}\right) - \frac{\partial}{\partial p}\left(\frac{\partial \mathcal{U}}{\partial x_i}\frac{\partial x_i}{\partial q}\right) . \tag{26}$$

Using

$$\frac{\partial \mathcal{U}}{\partial p} = \sum \frac{\partial \mathcal{U}}{\partial x_i}\frac{\partial x_i}{\partial p}$$

and

$$\frac{\partial \mathcal{U}}{\partial q} = \sum \frac{\partial \mathcal{U}}{\partial x_i}\frac{\partial x_i}{\partial q} ,$$

we have the desired result:

$$\frac{\partial}{\partial t}\{\mathcal{E}_i, \mathcal{E}_j\} = 0 . \tag{27}$$

In fact, (27) is true for any potential for which a solution of the form (24) can be found. Expression (27) says that once expressions (24), which involve time, are used in the Lagrange brackets, the result is independent of time and must be a constant of the motion. This property facilitates our obtaining Lagrange brackets, since they can be evaluated at any convenient time. Proving (27) for Lagrange brackets immediately proves the same for Poisson brackets from (16), giving

$$\frac{\partial}{\partial t}[\mathcal{E}_i, \mathcal{E}_j] = 0 . \tag{28}$$

Consider the problem

$$\dot{q}_i = \partial \mathcal{H} / \partial p_i \quad ,$$
$$\dot{p}_i = - \partial \mathcal{H} / \partial q_i \quad , \tag{29}$$

with

$$\mathcal{H} = \mathcal{H}_0 + \mathcal{H}_1 \quad ,$$

and assume that we can solve (27) with $\mathcal{H} = \mathcal{H}_0$ and obtain the 2n constants α_i. We can write the solution

$$q_i^0 = q_i^0(t, \alpha_j) \quad ,$$
$$p_i^0 = p_i^0(t, \alpha_j) \quad . \tag{30}$$

We hope to write the complete solution,

$$q_i = q_i^0 \ [t, \alpha_j(t)] \quad ,$$
$$p_i = p_i^0 \ [t, \alpha_j(t)] \quad , \tag{31}$$

and look for an expression for $\alpha_j(t)$. We proceed by writing

$$\dot{q}_i = \frac{d}{dt} q_i^0 \ [t, \alpha_j(t)] \quad ,$$
$$= \sum_j \frac{\partial q_i^0}{\partial \alpha_j} \dot{\alpha}_j + \frac{\partial q_i^0}{\partial t} = \frac{\partial \mathcal{H}_0}{\partial p_i} + \frac{\partial \mathcal{H}_1}{\partial p_i}$$

and

$$\dot{p}_i = \sum_j \frac{\partial p_i^0}{\partial \alpha_j} \dot{\alpha}_j + \frac{\partial p_i^0}{\partial t} = - \frac{\partial \mathcal{H}_0}{\partial q_i} - \frac{\partial \mathcal{H}_1}{\partial q_i} \quad .$$

Now

$$dq_i^0/dt = \partial q_i^0/\partial t \quad , \qquad \text{from (30)} \quad ,$$

$$= \partial \mathcal{K}_0/\partial p_i \quad , \qquad \text{from (29)} \quad .$$

Therefore, we have

$$\sum_j \frac{\partial q_i^0}{\partial a_j} \dot{a}_j = \frac{\partial \mathcal{K}_1}{\partial p_i} \quad , \tag{32}$$

and similarly

$$-\sum_j \frac{\partial p_i^0}{\partial a_j} \dot{a}_j = \frac{\partial \mathcal{K}_1}{\partial q_i} \quad . \tag{33}$$

If we multiply (32) by $\partial p_i/\partial a_\ell$ and let

$$\frac{\partial \mathcal{K}_1}{\partial p_i} = \sum_k \frac{\partial \mathcal{K}_1}{\partial a_k} \frac{\partial a_k}{\partial p_i} \quad ,$$

then multiply (33) by $\partial q_i/\partial a_\ell$ and let

$$\frac{\partial \mathcal{K}_1}{\partial q_i} = \sum_k \frac{\partial \mathcal{K}_1}{\partial a_k} \frac{\partial a_i}{\partial q_i} \quad ,$$

where

$$\frac{\partial q_i}{\partial a_\ell} = \left.\frac{\partial q_i^0}{\partial a_\ell}\right|_{a=a(t)} \quad ,$$

and finally sum over all variables, we obtain

$$\sum_j \{a_\ell, a_j\}_{q^0, p^0} \dot{a}_j = - \partial \mathcal{H}_1 / \partial a_\ell \quad . \tag{34}$$

We have explicitly written the subscripts q^0, p^0 on the Lagrange bracket to emphasize that the variables to be used are those of the solved problem (with $\mathcal{H}_0$). Since for the solved problem, the a_i's are constant, the Lagrange brackets are constant from (27) and are much easier to obtain. Equation (34) and its inverse in terms of Poisson brackets are the basis for the method of variation of parameters and will be used to derive the Lagrange Planetary Equations (LPE).

We will make some use of elements of the Hamilton-Jacobi theory. The basic idea is as follows. Say we have a dynamical system

$$\begin{aligned} \dot{q}_i &= \partial \mathcal{H} / \partial p_i \quad , \\ \dot{p}_i &= - \partial \mathcal{H} / \partial q_i \quad , \end{aligned} \tag{35}$$

and suppose we look for a new set of variables Q_i, P_i so that the new Hamiltonian does not depend on some of the new variables. In general, one tries to remove all the variables, which would be the case if the new Hamiltonian was identically zero. That is,

$$\begin{aligned} \dot{Q}_i &= \partial \mathcal{H}^* / \partial P_i \equiv 0 \quad , \qquad \therefore \quad Q_i = \text{constant} \quad , \\ \dot{P}_i &= - \partial \mathcal{H}^* / \partial Q_i \equiv 0 \quad , \qquad \therefore \quad P_i = \text{constant} \quad . \end{aligned} \tag{36}$$

For example, let the generating function be $S = F_2(q, P, t)$. Then we have

$$p_i = \partial S(q, P, t) / \partial q_i \quad . \tag{37}$$

Putting this into $\mathcal{H}$ gives

$$\mathcal{H}(q_i, p_i, t) = \mathcal{H}^* \left(q_i, \frac{\partial S}{\partial q_i}, t \right) + \frac{\partial S}{dt} = 0 \quad . \tag{38}$$

Known as the Hamilton-Jacobi equation, (38) is a partial differential equation in n + 1 variables for the generating function S. In general, it is not possible to find S. The method of Von Zeipel, to be introduced in Section 10, assumes that $\mathcal{E}_i$ and S can be written in convergent series and that each term of S can be found under rather general conditions.

3. TRANSFORMATIONS AND COORDINATE SYSTEMS

Consider the coordinate system x_1, y_1, z_1, a point

$$[P] = \begin{bmatrix} p_x \\ p_y \\ p_z \end{bmatrix} ,$$

and a second coordinate system rotated about the z axis by an angle Ω, as shown in Figure 1.

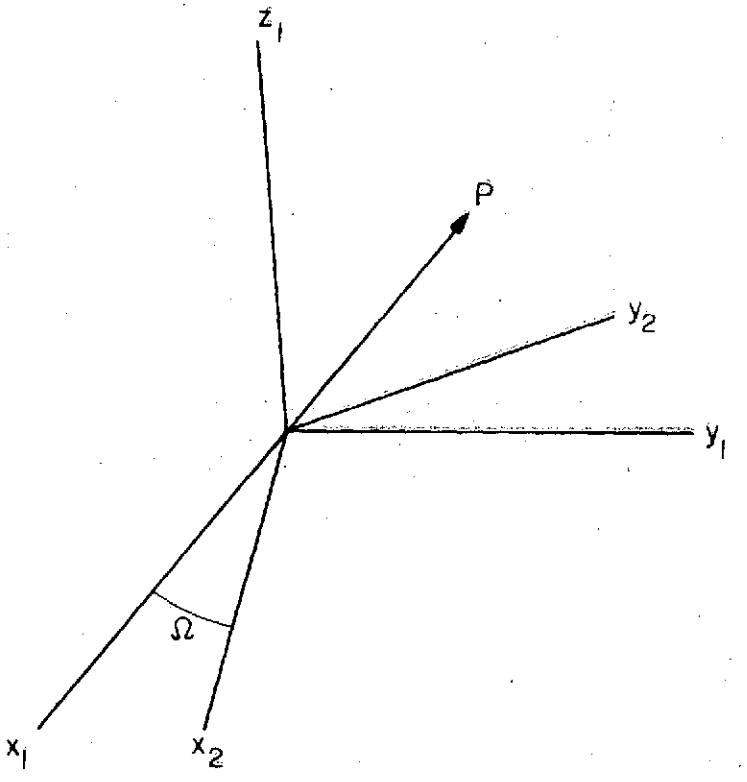

Figure 1. Geometry of rotation transformation.

The coordinates of p in the x_2, y_2, z_2 system can be expressed with the matrix operation

$$[P_2] = R_3(\Omega)\ [P_1] \quad ,$$

where

$$R_3 = \begin{bmatrix} \cos\Omega & \sin\Omega & 0 \\ -\sin\Omega & \cos\Omega & 0 \\ 0 & 0 & 1 \end{bmatrix} \quad . \tag{39}$$

In an analogous way, we can define rotation around any axis with

$$R_1 = \begin{bmatrix} 1 & 0 & 0 \\ 0 & \cos I & -\sin I \\ 0 & \sin I & \cos I \end{bmatrix} \qquad \text{about the x axis} \quad , \tag{40}$$

and

$$R_2 = \begin{bmatrix} \cos\phi & 0 & -\sin\phi \\ 0 & 1 & 0 \\ \sin\phi & 0 & \cos\phi \end{bmatrix} \qquad \text{about the y axis} \quad . \tag{41}$$

Here, R_1, R_2, and R_3 are matrices, and their mathematical properties are the subject of linear algebra. We need know only that these quantities have the following properties:

A. The length of a vector is unchanged by rotation.

B. Multiplication of matrices does not commute; that is,

$$R_i(\phi)\, R_j(\lambda) \neq R_j(\lambda)\, R_i(\phi) \quad .$$

C. Multiplication does satisfy the associative rule; that is,

$$R_i(R_j R_k) = (R_i R_j)\, R_k \quad .$$

D. Rotation about the same axis is additive; that is,

$$R_i(\phi)\, R_i(\lambda) = R_i(\phi + \lambda) \quad .$$

E. For rotation matrices, the inverse and transpose are related by

$$R_i^{-1}(\phi) = R_i^T(\phi) = R_i(-\phi) \quad .$$

F. We also have

$$(R_i R_j)^{-1} = R_j^{-1} R_i^{-1} \quad .$$

G. Differentiation and integration are performed on each element.

Although multiplication does not commute, for small rotations around the x, y, and z axes – that is, ϵ_x, ϵ_y, ϵ_z – we can define the infinitesimal rotation matrix

$$R(\epsilon_x, \epsilon_y, \epsilon_z) = \begin{bmatrix} 1 & \epsilon_z & -\epsilon_y \\ -\epsilon_z & 1 & \epsilon_x \\ \epsilon_y & -\epsilon_x & 1 \end{bmatrix} \quad . \tag{42}$$

In satellite geodesy, dynamical astronomy, and astrometry, we are concerned with four reference frames:

A. The terrestrial system.

B. The inertial system.

C. The celestial (sidereal) system.

D. The orbital system.

Since a systematic account of these systems and of their relationships to one another can be found in Veis (1960a, 1963a), we confine ourselves to a descriptive summary. A number of texts are present classical geodesy (e.g., Bomford, 1962; Heiskanen and Vening-Meinesz, 1958).

The terrestrial system is fixed to the earth. Positions on the surface can be considered invariant in time if we ignore tides and crustal motions for the moment. The materialization of the terrestrial system can be in terms of geocentric coordinates or datum coordinates. The datum can be defined in a geocentric system with the following seven parameters: the three datum origin coordinates, the three orientation parameters, and a scale factor. Datum coordinates can be determined from precise knowledge of the geocentric coordinates. One of the objectives of satellite geodesy is to determine coordinates in a geocentric system. Through coordinates common to geocentric and datum systems, the relation of the datum to the geocentric system is determined.

The inertial system is fundamental to dynamics, and all orbit theory is ultimately developed in this system. We hope to materialize the inertial through the celestial system. The latter is defined by the stars and, it is hoped, with respect to the distant galaxies. By Mach's principle, the distant galaxies define an inertial reference frame.

The celestial system is materialized with coordinates of stars insofar as we can treat proper motion accurately. Individual star catalogs are similar to geodetic datums in that the positions are relative. Positions can be combined into a uniform system by use of common stars to any two catalogs. This technique was used to compile the SAO Star Catalog (Staff, Smithsonian Astrophysical Observatory, 1966), which is in computer-accessible form, covers the whole sky, and contains about 250,000 stars with their positions and proper motions reduced to the FK4 system.

The equations of motion are most easily given in an inertial reference frame. However, in this system, the earth is moving in an irregular manner, and the gravity field, assumed static in an earth-fixed system, has an irregular time dependence. This irregular temporal variation will give rise to perturbations.

For this reason, we have adopted an intermediate, quasi-inertial reference frame. This orbital system has a fixed epoch (the mean equinox of 1950.0) and a moving equator (the instantaneous equator of date), and the gravity field is rotating about the z axis at a constant rate. This orbital system has been shown by Kozai (1960) and Kozai and Kinoshita (1973) to be optimum for our work. That is to say, short-period terms are unaffected by the change, and the effects of being noninertial and those of variations of the gravity field are minimized. We can then proceed with the theory for periodic perturbations as if we had an inertial reference frame and make some corrections (see Section 9). A further result of this choice is that the earth is rotating uniformly in this system, thus giving a particularly simple expression for the sidereal angle.

The relation between the celestial system and the terrestrial is established in two steps. A general theory of precession and nutation deals with the secular and periodic parts, respectively, of the forced motion due to the gravitational attraction of the sun and moon. A general reference for these effects is Chapter 2 of the Explanatory Supplement to the Astronomical Ephemeris and the American Ephemeris and Nautical

Almanac (1961) (hereafter called ESAENA). The instantaneous position (orientation) of the earth is described to 2×10^{-6} rad with these formulas. The irregular fluctuations of the earth's position with respect to this computed position are routinely measured as three angles and published by the Bureau International de l'Heure. The free nutation of the earth is the motion of the adopted reference point of the z axis about the spin axis in the terrestrial system. The spin axis, of course, moves owing to precession and nutation, and that axis defines the astronomical equator. The rotation rate has small fluctuations, resulting in irregular fluctuations in the true sidereal angle. The coordinates of the reference pole (x, y) and the change in the sidereal angle (ΔUT1) are observed quantities and provide the relationship between the celestial and the terrestrial systems.

The variations of pole position are not strictly periodic. There is considerable uncertainty about the actual properties of the polar motion. As a result, an arbitrary reference point was adopted by the International Union of Geodesy in 1967. This point was the mean pole for the time 1900.0 to 1905.0, and all pole coordinates are now given with respect to it. The mean pole today is about 10 m west of the adopted pole.

In summary, we now give the relations between the orbital system and the others. If X_0 is the position of a station in an earth-fixed system, then X is the position in the orbital system:

$$X = R_3(-\theta)\, R(y, x, 0)\, X_0 \quad , \tag{43}$$

where θ is the sidereal angle computed from

$$\theta = 0.277987616 + 1.00273781191\,(T - 33282.0) + \Delta UT1\,(rev) \quad , \tag{44}$$

and x and y are the observed coordinates of the pole.

In general, camera observations provide directions in a celestial system at some epoch T_0. To express this direction in the adopted orbital system, we must apply precession κ, ω, ν from T_0 to 1950.0, and then apply κ, ω, ν to the motion of the equator, thus preserving the origin of 1950.0. If κ(b, a) is the amount of precession in right ascension from dates a to b, and if similar expressions are given for ω and ν, then

$$[\hat{\ell}] = R(-\Delta\epsilon, \psi \sin \epsilon, 0)\ R_3[\kappa(T, 1950)]\, R_2[\nu(T, 1950)]\ R_3[-\kappa(T, 1950)]$$

$$\times R_3[-\omega(1950, T_0)]\ R_2[-\nu(1950, T_0)]\ R_3[-\kappa(1950, T_0)]\ [\hat{\ell}_0] \qquad (45)$$

expresses the direction in the orbital system. The nutation ($\Delta\epsilon$, $\psi \sin \epsilon$) must also be applied to the original direction if the true coordinates are given. The reader is referred to the ESAENA for numerical values. It has been found satisfactory to use the quadratic expressions for precession and to retain all terms in nutation such that the total neglected part is less than 0.5 m.

4. TWO-BODY MOTION

The first approximation for satellite motion is two-body motion, which forms the reference for all subsequent analysis. Two-body motion can be completely solved. We start in the context of Hamilton's canonical equations (3).

We have to determine the coordinates and momenta of both bodies. We can write the equations for M_2 with respect to the center of gravity of M_1. By using the reduced mass $M'[(1/m') = (1/m_1) + (1/m_2)]$ in the kinetic energy (Goldstein, 1959, p. 59), we obtain the same equations for M_2 that would result from holding M_1 fixed. The Hamiltonian becomes

$$\mathcal{H} = \frac{m'}{2} [\dot{r}^2 + (r\dot{v})^2] + \mathcal{U} \quad . \tag{46}$$

Two-body motion occurs, with $\mathcal{U}(r) = -GM_1 M_2/r$. The force derived from this potential is toward the center of gravity and is known as a central force. Since no torque is applied, the angular momentum

$$\overline{L} = \overline{r} \times \overline{p} \tag{47}$$

is conserved, and $\overline{r}$ must always be perpendicular to $\overline{L}$ and lie in a plane. Therefore, we can limit the discussion to two dimensions in a plane. The Hamiltonian becomes

$$\mathcal{H} = \frac{m'}{2} (\dot{r}^2 + r^2 \dot{v}^2) - \frac{GM_1 M_2}{r} \quad . \tag{48}$$

For an earth satellite, $m' \approx M_2$; and (48) can be written for a unit-mass test particle. Hereafter, we will drop the prime and subscript and consider the Hamiltonian per unit mass, which now becomes

$$\mathcal{H} = \frac{1}{2} \left\{ p_r^2 + \frac{p_v^2}{r^2} \right\} - \frac{GM}{r} \quad , \tag{49}$$

with the momenta conjugate to r and v

$$p_v = r^2 \dot{v} \quad ,$$
$$p_r = \dot{r} \quad ; \tag{50}$$

and Hamilton's canonical equations are

$$\dot{p}_v = -\frac{\partial \mathcal{H}}{\partial v} \quad , \qquad \dot{v} = \frac{\partial \mathcal{H}}{\partial p_v} \quad ,$$
$$\dot{p}_r = -\frac{\partial \mathcal{H}}{\partial r} \quad , \qquad \dot{r} = \frac{\partial \mathcal{H}}{\partial p_r} \quad . \tag{51}$$

Since v does not appear in the Hamiltonian, it is an ignorable coordinate. Therefore,

$$\dot{p}_v = 0 \tag{52a}$$

and

$$p_v = N \quad \text{(a constant)}$$
$$= r^2 \dot{v} \quad . \tag{52b}$$

We immediately have one constant of integration. We can obtain an equation for r from the Hamiltonian itself by substituting (52) into (49) to give

$$\dot{r} = \frac{dr}{dt} = \left(2\mathcal{H} + \frac{2\mu}{r} - \frac{N^2}{r^2} \right)^{1/2} \quad , \tag{53}$$

where $\mu = GM$.

Formula (53) can be integrated, but only with difficulty. We proceed instead to obtain an equation for r in terms of v by assuming

$$r(t) = r[v(t)] \quad , \tag{54}$$

and we find

$$\dot{r} = \frac{dr}{dv}\frac{dv}{dt} = \frac{dr}{dv}\dot{v} = \frac{dr}{dv}\frac{N}{r^2} = -\frac{d}{dv}\left(\frac{N}{r}\right) \quad .$$

Equation (53) becomes

$$-N\frac{d}{dv}\left(\frac{1}{r}\right) = \left(2\mathcal{H} + \frac{2\mu}{r} - \frac{N^2}{r^2}\right)^{1/2} \quad , \tag{55}$$

which suggests the substitution $x = 1/r$. Equation (55) can be integrated; the result is of the form

$$x = \frac{1}{r} = A + B\cos(v - v_0) \quad . \tag{56}$$

By substituting (56) into (55), we find that

$$A = \frac{\mu}{N^2} \quad ,$$

$$NB = \left(2\mathcal{H} + \frac{\mu^2}{N^2}\right)^{1/2} \quad .$$

We see that (56) is the equation of an ellipse centered at a focus, which is equivalent to Kepler's first law. The general form for the equation of an ellipse is

$$r = \frac{a(1-e^2)}{1 + e\cos(v - v_0)} = a(1 - e\cos E - E_0) \quad , \tag{57}$$

with

$$r\sin v = a(1-e^2)^{1/2}\sin E \quad , \qquad r\cos v = a(\cos E - e) \quad ;$$

the angles are defined in Figure 2. By comparing the constants, we find that

$$e = \left(1 + 2\mathcal{H}\frac{N^2}{\mu^2}\right)^{1/2} \quad ,$$

$$a = -\frac{\mu}{2\mathcal{H}} = \frac{N^2}{\mu(1-e^2)} \quad . \tag{58}$$

Hyperbolic orbits occur when $\mathcal{H} > 0$, giving $a < 0$.

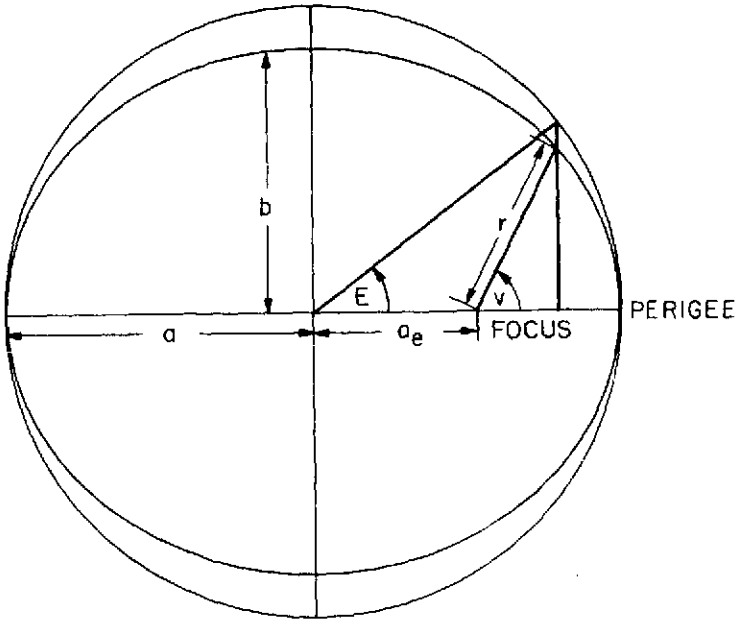

Figure 2. Geometry of an ellipse.

Returning to (52), we see that $\frac{1}{2}r[r(dv/dt)]$ is an element of area. Equation (52b) says that it takes equal time to sweep out equal areas, which is Kepler's second law. If we integrate (52) with respect to time for one full revolution, we have

$$\int_0^T r^2 \frac{dv}{dt}\, dt = \int_0^T N\, dt \quad , \tag{59a}$$

or

$$\int_0^{2\pi} r^2\, dv = NT \quad . \tag{59b}$$

The left side of (59b) is twice the area of the ellipse ($2\pi ab$), giving

$$NT = 2\pi a^2 (1 - e^2)^{1/2} \quad . \tag{60}$$

Now the average rate of mean motion n will be $2\pi/T$. By using $N = [\mu a(1-e^2)]^{1/2}$ from (58) and (60), we have

$$n^2 a^3 = \mu \quad , \tag{61}$$

which is equivalent to Kepler's third law.

We proceed to find v(t) by differentiating (57):

$$\frac{dr}{dt} = ae \sin E \frac{dE}{dt} = \frac{a(1-e^2)\, e \sin v}{1+e \cos v} \frac{dv}{dt} \quad . \tag{62}$$

By using (52) for dv/dt and (57), this equation reduces to

$$\frac{dE}{dt} = \left(\frac{\mu}{a}\right)^{1/2} \frac{1}{r} = \frac{\mu^{1/2}}{a^{3/2}(1-e \cos E)} \quad , \tag{63}$$

which integrates to

$$E - e \sin E = n(t-t_0) \equiv M \quad , \tag{64}$$

which is Kepler's equation.

We have formally solved the two-body problem and obtained the conserved quantities. Given a time, (64) must be solved by iteration. Using (57), we obtain the true anomaly v and the radius vector r. The position is calculated from

$$\begin{bmatrix} x \\ y \\ z \end{bmatrix} = r \begin{bmatrix} \cos v \\ \sin v \\ 0 \end{bmatrix} = a \begin{bmatrix} \cos E - e \\ (1-e^2)^{1/2} \sin E \\ 0 \end{bmatrix} \quad . \tag{65}$$

The velocity is obtained directly by differentiation and by use of (52), (58), and (61):

$$\begin{bmatrix} \dot{x} \\ \dot{y} \\ \dot{z} \end{bmatrix} = \frac{na}{(1-e^2)^{1/2}} \begin{bmatrix} -\sin v \\ e+\cos v \\ 0 \end{bmatrix} = \frac{na}{1-e \cos E} \begin{bmatrix} -\sin E \\ (1-e^2)^{1/2} \cos E \\ 0 \end{bmatrix} \quad . \tag{66}$$

To reverse the process, we compute the Kepler elements a, e, and $M=n(t-t_0)$, given $\overline{x}$, $\dot{\overline{x}}$. First, we derive the vis viva integral obtained from the Hamiltonian (50) with (58):

$$\mathcal{H} = -\frac{\mu}{2a} = \frac{1}{2}V^2 - \frac{\mu}{r} \quad . \tag{67}$$

The total velocity squared is

$$V^2 = \dot{x}^2 + \dot{y}^2 + \dot{z}^2 \quad ,$$

and the radius vector squared is

$$r^2 = x^2 + y^2 + z^2 \quad .$$

We compute a from

$$V^2 = \mu\left(\frac{2}{r} - \frac{1}{a}\right) \quad , \tag{68}$$

known as the vis viva integral. Then we compute $\mathcal{H}$ from (67) and determine N from (52b) by using

$$\dot{v} = \frac{x\dot{y} - y\dot{x}}{r^2} \quad . \tag{69}$$

With N, $\mathcal{H}$, and, of course, μ, we compute e from (58). With a, r, e, x, and y, either E or v can be obtained from (57), giving M from (64). Use can also be made of

$$\cos E = \frac{\cos v + e}{1 + e\cos v} \quad , \qquad \sin E = \frac{(1-e^2)^{1/2}\sin v}{1 + e\sin v} \quad ,$$

$$\cos v = \frac{\cos E - e}{1 - e\cos E} \quad , \qquad \sin v = \frac{(1-e^2)^{1/2}\sin E}{1 - e\cos E} \quad , \tag{70}$$

$$\tan\frac{v}{2} = \left(\frac{1+e}{1-e}\right)^{1/2}\tan\frac{E}{2} \quad , \qquad V^2 = \frac{\mu^2(1 + 2e\cos v + e^2)}{N^2} = \frac{\mu(1 + e\cos E)}{r} \quad .$$

We have given the analysis of two-body Keplerian motion in a plane. To refer the position $\begin{bmatrix} x \\ y \\ 0 \end{bmatrix}$ to the orbital system, we perform the coordinate transformation

$$[X] = R_3(-\Omega)\, R_1(-I)\, R_3(-\omega) \begin{bmatrix} x \\ y \\ 0 \end{bmatrix} \quad . \tag{71}$$

The angle ω corresponds to v_0 in (56). The angles Ω and I specify the orientation of the orbital plane, as indicated in Figure 2.

Given the position and velocity, we use the constancy of the angular momentum to determine the angles Ω, I, ω. The direction of the angular momentum is computed from

$$[\hat{L}] = [\bar{X}] \times [\dot{\bar{X}}] / |\bar{X}|\, |\dot{\bar{X}}| \quad , \tag{72}$$

and the inclination is obtained from

$$\cos I = \left| [\hat{L}] \times \begin{bmatrix} 0 \\ 0 \\ 1 \end{bmatrix} \right| \quad . \tag{73}$$

If $\hat{L}_z$ is negative, the convention is to take $\pi - I$ for the inclination. The node is defined by a unit vector in the direction of the node:

$$\hat{e}_\Omega = \begin{bmatrix} \cos \Omega \\ \sin \Omega \\ 0 \end{bmatrix} = \begin{bmatrix} 0 \\ 0 \\ 1 \end{bmatrix} \times [\hat{L}] \quad . \tag{74}$$

To find ω, we must determine the satellite's position in the orbital plane referred to the node. Using

$$[X'] = R_1(I)\, R_3(\Omega)\, [X] \quad ,$$

we have

$$\cos (v + \omega) = X'_x/r \quad ,$$

$$\sin (v + \omega) = X'_y/r \quad ,$$

which determine $v + \omega$. With v from (57), we immediately have ω.

We give here the equations for a hyperbolic orbit. The position is

$$x = r \cos v = -a(e - \cosh F) \quad ,$$

$$y = r \sin v = -a(e^2 - 1)^{1/2} \sinh F \quad ,$$

$$r = \frac{-a(e^2 - 1)}{1 + e \cos v} = a(e \cosh F - 1) \quad ,$$

where $a < 0$. We still have

$$n^2 (-a)^3 = \mu \quad ;$$

Kepler's equation becomes

$$n(t - t_0) = e \sinh F - F \quad ;$$

$r^2\dot{v} = N$ is still a constant of the motion; and (48) and (58) still hold.

The final question in the discussion of two-body motion concerns the development of (57) and its generalization in series. Kepler's equation, (64), is transcendental, and closed expressions are not possible. However, rapidly converging series are available. They are needed for the development of perturbations, a topic that will be treated by itself in Section 8.

5. EQUATIONS OF MOTION

We noted in equation (18) that for conservative forces, rectangular coordinates are canonical, and that the Poisson brackets have the values

$$\begin{aligned} [\dot{x}_i, \dot{x}_j] &= 0 \quad , \\ [x_i, x_j] &= 0 \quad , \\ [x_i, \dot{x}_j] &= \delta_{ij} \quad . \end{aligned} \tag{75}$$

Further, we noted that the equations of motion can be written in any set of variables by using Poisson brackets (21):

$$d\mathcal{E}_i/dt = -\sum_k [\mathcal{E}_i, \mathcal{E}_k]\, \partial\mathcal{H}/\partial\mathcal{E}_k \quad . \tag{76}$$

In addition, if $\mathcal{H} = \mathcal{H}_0 + \mathcal{H}_1$ and if we can obtain a solution

$$\begin{aligned} x_i^0 &= x_i^0(a_i, t) \quad , \\ \dot{x}_i^0 &= \dot{x}_i^0(a_i, t) \end{aligned}$$

(a_i being constant for $\mathcal{H}_0$), then by selecting $\mathcal{E}_i$ to be a_i, we can write

$$d\mathcal{E}_i/dt = -\sum_k [\mathcal{E}_i, \mathcal{E}_k]_{x^0, \dot{x}^0}\, \partial\mathcal{H}_1/\partial\mathcal{E}_k \quad , \tag{77}$$

where $[\mathcal{E}_i, \mathcal{E}_k]_{x^0, \dot{x}^0}$ are evaluated for the solvable problem. In what follows, we will use only variables that are the solution of the two-body problem (Section 4). This choice is not unique, for one could select any combination of $\mathcal{H}$ that had a solution.

For example, there is a separable solution for a potential:

$$\mathcal{U} = -\frac{\mu}{r}\left[1 + \sum_{n=1}^{\infty}\left(\frac{a_e}{r}\right)^n (-J_2)^n P_{2n}(\sin\phi)\right] \quad , \tag{78}$$

which is due to Vinti (1959) and has been explored by Izsak (1963b).

The Kepler elements a, e, I, M, ω, Ω developed in Section 4 are the most commonly used. Directly using (71) in (8) and employing the time independence of $\{\mathcal{E}_i, \mathcal{E}_j\}_{x^0, \dot{x}^0}$, we obtain for the Lagrange brackets

$$\begin{aligned}
\{\Omega, I\} &= -\{I, \Omega\} = -(\mu a)^{1/2}(1-e^2)^{1/2}\sin I \quad , \\
\{\Omega, a\} &= -\{a, \Omega\} = (1-e^2)^{1/2}[\cos(I/2)](\mu/a)^{1/2} \quad , \\
\{\Omega, e\} &= -\{e, \Omega\} = [-(\mu a)^{1/2}\cos I]/(1-e^2)^{1/2} \quad , \\
\{\omega, a\} &= -\{a, \omega\} = [(1-e^2)^{1/2}/2](\mu/a)^{1/2} \quad , \\
\{\omega, e\} &= -\{e, \omega\} = -(\mu a)^{1/2} e/(1-e^2)^{1/2} \quad , \\
\{a, M\} &= -\{M, a\} = -\frac{1}{2}(\mu/a)^{1/2} \quad ,
\end{aligned} \tag{79}$$

the other combinations being zero. By inverting the matrix implied by (16), we obtain for the Poisson brackets

$$\begin{aligned}
[a, M] &= -[M, a] = 2(a/\mu)^{1/2} \quad , \\
[e, \omega] &= -[\omega, e] = -(1-e^2)^{1/2}/(\mu a)^{1/2} e \quad , \\
[I, \Omega] &= -[\Omega, I] = -1/[(\mu a)^{1/2}(1-e^2)^{1/2}\sin I] \quad , \\
[e, M] &= -[M, e] = (1-e^2)/(\mu a)^{1/2} e \quad , \\
[I, \omega] &= -[\omega, I] = (\cos I)/(\mu a)^{1/2}(1-e^2)^{1/2}\sin I \quad .
\end{aligned} \tag{80}$$

Equations (80) inserted into (77) can be integrated numerically. They remain a set of coupled differential equations. Analytical solutions are obtained by approximate methods. A particular difficulty arises if these equations are used in a straightforward manner.

It is customary to express the Hamiltonian

$$\mathcal{H} = \frac{1}{2} V^2 + u = \frac{1}{2} V^2 - \frac{\mu}{r} - R \quad , \tag{81}$$

where $R < \mu/a$ and is called the disturbing function. Then R is expressed in a trigonometric series of the form

$$\sum A(a, e, I) \begin{matrix} \sin \\ \cos \end{matrix} [\alpha M + \beta\omega + \gamma\Omega + \phi(t)] \quad ,$$

with $M = M_0 + nt$ from the two-body motion. Straightforward use of (80) introduces

$$\frac{\partial}{\partial a} A(a, e, I) \begin{matrix} \sin \\ \cos \end{matrix} [\alpha M + \beta\omega + \gamma\Omega + \phi(t)] \quad ,$$

giving

$$\frac{\partial A}{\partial a} \begin{matrix} \sin \\ \cos \end{matrix} [\alpha M + \beta\omega + \gamma\Omega + \phi(t)] + A \begin{matrix} \cos \\ \sin \end{matrix} [\alpha M + \beta\omega + \gamma\Omega + \phi(t)] \, \alpha \frac{\partial n}{\partial a} t \quad ,$$

since $n^2 a^3 = \text{const}$. The occurrence of t outside a trigonometric argument leads to terms that are not strictly periodic.

If we consider all occurrences of a in coefficients of trigonometric terms and all occurrences of n in the trigonometric argument, then the differential equation for M becomes

$$\dot{M} = 2\left(\frac{a}{\mu}\right)^{1/2} \left\{ \frac{\partial \mathcal{H}}{\partial a}\bigg|_{n=\text{const}} + \frac{\partial \mathcal{H}}{\partial M} \frac{dM}{dn} \frac{dn}{da} \right\} + \frac{1 - e^2}{(\mu a)^{1/2} e} \frac{\partial \mathcal{H}}{\partial e} \quad .$$

Now

$$\frac{da}{dt} = -2\left(\frac{a}{\mu}\right)^{1/2} \frac{\partial \mathcal{H}}{\partial M}$$

and

$$\frac{dM}{dn} = t \quad ,$$

giving

$$\frac{\partial \mathcal{H}}{\partial a} = \frac{\mu}{2a} - \left.\frac{\partial R}{\partial a}\right|_{n=const} \quad ,$$

$$\frac{\partial \mathcal{H}}{\partial e} = -\frac{\partial R}{\partial e} \quad ,$$

$$\frac{\partial \mathcal{H}}{\partial M} = -\frac{\partial R}{\partial M} \quad ;$$

that is,

$$\dot{M} = n - t\frac{dn}{dt} - 2\left(\frac{a}{\mu}\right)^{1/2} \left.\frac{\partial R}{\partial a}\right|_{n=const} - \frac{1-e^2}{(\mu a)^{1/2} e} \frac{\partial R}{\partial e} \quad ,$$

which formally integrates to

$$M = nt - nt + \int n\,dt - 2\int \left(\frac{a}{\mu}\right)^{1/2} \left.\frac{\partial R}{\partial a}\right|_{n=const} dt - \int \frac{1-e^2}{(\mu a)^{1/2} e} \frac{\partial R}{\partial e} \quad ,$$

where $n = (\mu)^{1/2}/a^{3/2}$ and is not constant.

With the previously described separation of a and n, we can write the Lagrange planetary equations in their usual form:

$$\frac{da}{dt} = \frac{2}{na}\frac{\partial R}{\partial M} \quad ,$$

$$\frac{de}{dt} = \frac{1-e^2}{na^2e}\frac{\partial R}{\partial M} - \frac{(1-e^2)^{1/2}}{na^2e}\frac{\partial R}{\partial \omega} \quad ,$$

$$\frac{d\omega}{dt} = -\frac{\cos I}{na^2(1-e^2)^{1/2}\sin I}\frac{\partial R}{\partial I} - \frac{(1-e^2)^{1/2}}{na^2e}\frac{\partial R}{\partial e} \quad ,$$

$$\frac{dI}{dt} = \frac{\cos I}{na^2(1-e^2)^{1/2}\sin I}\frac{\partial R}{\partial \omega} - \frac{1}{na^2(1-e^2)^{1/2}\sin I}\frac{\partial R}{\partial \Omega} \quad , \tag{82}$$

$$\frac{d\Omega}{dt} = \frac{1}{na^2(1-e^2)^{1/2}\sin I}\frac{\partial R}{\partial I} \quad ,$$

$$\frac{dM}{dt} = n - \frac{1-e^2}{na^2e}\frac{\partial R}{\partial e} - \frac{2}{na}\frac{\partial R}{\partial a} \quad ,$$

$$n^2a^3 = \mu \quad .$$

Kepler elements are used extensively. They have the advantage over cartesian coordinates in that five of the elements are constant for two-body motion and the sixth (M) increases linearly with time. In addition, each element has a geometrical interpretation. However, any five constants could be chosen, as long as they lead to a unique calculation of position and velocity.

As $e \to 0$, the element ω ceases to have any geometrical meaning. Since the position of the satellite depends on $v + \omega$, we can consider the new variables

$$\begin{aligned} \lambda &= M + \tilde{\omega} \quad , & e &= e \quad , \\ \tilde{\omega} &= \omega + \Omega \quad , & \Omega &= \Omega \quad , \\ a &= a \quad , & I &= I \quad , \end{aligned} \tag{83}$$

with the Poisson brackets

$$
\begin{aligned}
[a,\lambda] &= -[\lambda,a] = \frac{2}{na} \quad , \\
[\lambda,e] &= -[e,\lambda] = \frac{(1-e^2)^{1/2}\,[1-(1-e^2)^{1/2}]}{na^2e} \quad , \\
[\lambda,I] &= -[I,\lambda] = \frac{\tan(I/2)}{na^2(1-e^2)^{1/2}} \quad , \\
[e,\tilde{\omega}] &= -[\tilde{\omega},e] = -\frac{(1-e^2)^{1/2}}{na^2e} \quad , \\
[\Omega,I] &= -[I,\Omega] = \frac{1}{na^2(1-e^2)^{1/2}\sin I} \quad , \\
[I,\tilde{\omega}] &= -[\tilde{\omega},I] = [I,\lambda] \quad .
\end{aligned}
\tag{84}
$$

It has also been found useful to eliminate e and $\tilde{\omega}$ by use of the variables

$$
\begin{aligned}
h &= e\sin\tilde{\omega} \quad , \\
k &= e\cos\tilde{\omega} \quad , \\
\lambda &= \lambda \quad , \\
a &= a \quad , \\
\Omega &= \Omega \quad , \\
I &= I \quad .
\end{aligned}
\tag{85}
$$

These variables have the following Poisson brackets, written for convenience in terms of e:

$$
\begin{aligned}
[h,k] &= -[k,h] = \frac{(1-e^2)^{1/2}}{na^2} \quad , \\
[h,\lambda] &= -[\lambda,h] = \frac{-h(1-e^2)^{1/2}}{na^2[1+(1-e^2)^{1/2}]} \quad , \\
[h,I] &= -[I,h] = \frac{k \tan(I/2)}{na^2(1-e^2)^{1/2}} \quad , \\
[k,\lambda] &= -[\lambda,k] = \frac{-k(1-e^2)^{1/2}}{na^2[1+(1-e^2)^{1/2}]} \quad , \\
[k,I] &= -[I,k] = \frac{-h \tan(I/2)}{na^2(1-e^2)^{1/2}} \quad ,
\end{aligned}
\tag{86}
$$

with $[a,\lambda]$, $[\lambda,I]$, $[\Omega,I]$ as given in (84). Of course, these equations hold for all eccentricities.

A further modification would be to use the variables

$$
\begin{aligned}
p &= \tan I \sin \Omega \quad , \\
q &= \tan I \cos \Omega \quad , \\
h &= h \quad , \\
k &= k \quad , \\
\lambda &= \lambda \quad , \\
a &= a \quad .
\end{aligned}
\tag{87}
$$

These have the following Poisson brackets, written for convenience in terms of e and I:

$$
\begin{aligned}
[p, q] &= -[q, p] = \frac{\cos I}{na^2(1 - e^2)^{1/2}} \quad , \\
[p, \lambda] &= -[\lambda, p] = \frac{1}{k}[p, h] = -\frac{1}{k}[h, p] = -\frac{1}{h}[p, k] = \frac{1}{h}[k, p] \quad , \\
&= -\frac{p \cos I}{2na^2(1 - e^2)^{1/2} \cos^2(I/2)} \quad , \\
[q, \lambda] &= -[\lambda, q] = \frac{1}{k}[q, h] = -\frac{1}{k}[h, q] = -\frac{1}{h}[q, k] = \frac{1}{h}[k, q] \quad , \\
&= -\frac{q \cos I}{2na^2(1 - e^2)^{1/2} \cos^2(I/2)} \quad , \\
[q, p] &= -\frac{\cos I}{na^2(1 - e^2)^{1/2}} \quad ,
\end{aligned}
\tag{88}
$$

where $[h, k]$, $[h, \lambda]$, $[k, \lambda]$ are the same as (86) and where we take $[a, \lambda]$ from (84). The variables p and q should not be confused with generalized coordinates. These expressions are valid for all e and I but are especially valuable for small e and I – for example, in the planetary theory.

It is possible to construct other combinations. For example, one could use

$$
\begin{aligned}
\chi &= M + \omega \quad , \\
\xi &= e \sin \omega \quad , \\
\eta &= e \cos \omega \quad , \\
a &= a \quad , \\
\Omega &= \Omega \quad , \\
I &= I \quad .
\end{aligned}
\tag{89}
$$

We now turn to sets of canonical variables that have the simplest form of Poisson brackets. We have observed that cartesian coordinates are canonical. We give two other sets, the Delaunay and the Hill.

The combination of coordinates and conjugate momenta for Delaunay variables are the following:

Coordinates	Momenta
$\ell = M$	$L = (\mu a)^{1/2}$
$g = \omega$	$G = [\mu a(1-e^2)]^{1/2}$
$h = \Omega$	$H = [\mu a(1-e^2)]^{1/2} \cos I$.

(90)

Now, ℓ, g, h are new labels for three familiar Kepler elements, in order to provide a symmetric notation. We see that G is the angular-momentum constant N in the two-body motion given by (58) and that H is the projection of the angular momentum on the z axis.

Another set of canonical variables introduced into satellite theory by Izsak (1962) and used to great advantage by Aksnes (1970) consists of the Hill variables, as follows:

Coordinates	Momenta
$r = a(1 - e \sin E)$	$\dot{r} = (e/r)\, L \sin E$
$u = v + \omega$	$G = G$
$h = \Omega$	$H = H$.

(91)

These are natural coordinates, with the important advantage that there is no singularity for small eccentricity – in contrast to the situation with Delaunay variables, which complicates their use.

Finally, we consider the equations of LPE type, which contain the forces explicitly. Consider the forces with components S, T, and W, which are, respectively, along the

radius vector, in the orbital plane normal to the radius vector (along track), and perpendicular to the orbital plane (cross track). The direction cosines of the satellite position are

$$\hat{\ell}_S = R_3(-\Omega)\, R_1(-I)\, R_3(-u) \begin{bmatrix} 1 \\ 0 \\ 0 \end{bmatrix} \quad . \tag{92}$$

We can define the direction cosines along track and cross track with

$$\hat{\ell}_T = R_3(-\Omega)\, R_1(-I)\, R_3(-\Omega) \begin{bmatrix} \dot{x} \\ \dot{y} \\ 0 \end{bmatrix} \Big/ (\dot{x}^2 + \dot{y}^2)^{1/2} \quad , \tag{93}$$

$$\hat{\ell}_W = \hat{\ell}_T \times \hat{\ell}_S \quad , \tag{94}$$

where $\dot{x}$, $\dot{y}$ are obtained from (66). If we let $\mathcal{E}_i$ be any variable, then

$$\frac{\partial R}{\partial \mathcal{E}_i} = \frac{\partial R}{\partial x}\frac{\partial x}{\partial \mathcal{E}_i} + \frac{\partial R}{\partial y}\frac{\partial y}{\partial \mathcal{E}_i} + \frac{\partial R}{\partial z}\frac{\partial z}{\partial \mathcal{E}_i} \quad .$$

But $\frac{\partial R}{\partial x}$, $\frac{\partial R}{\partial y}$, $\frac{\partial R}{\partial z}$ are the components of force along x, y, z given by

$$\begin{bmatrix} \frac{\partial R}{\partial x} \\ \frac{\partial R}{\partial y} \\ \frac{\partial R}{\partial z} \end{bmatrix} = \begin{bmatrix} & & \\ \hat{e}_S & \hat{e}_T & \hat{e}_W \\ & & \end{bmatrix} \begin{matrix} S \\ T \\ W \end{matrix} \quad . \tag{95}$$

With expressions $\bar{x} = \bar{x}(\mathcal{E}_i)$, say (71), we can form $\partial x/\partial \mathcal{E}$ and substitute the result in (77). This could be done for any set of variables. We give here the results for the Kepler elements, since they are widely used. We have

$$\frac{da}{dt} = \frac{2}{n(1-e^2)^{1/2}} \left[S\, e \sin v + T \frac{p}{r} \right] ,$$

$$\frac{de}{dt} = \frac{(1-e^2)^{1/2}}{na} \left\{ S \sin v + T \left[\cos v + \frac{1}{e} \left(1 - \frac{r}{a} \right) \right] \right\} ,$$

$$\frac{dI}{dt} = \frac{1}{na\,(1-e^2)^{1/2}} W \frac{r}{a} \cos (v + \omega) ,$$

$$\frac{d\Omega}{dt} = \frac{1}{na\,(1-e^2)^{1/2} \sin I} W \frac{r}{a} \sin (v + \omega) , \qquad (96)$$

$$\frac{d\omega}{dt} = - \cos I \frac{d\Omega}{dt} + \frac{1}{na} \frac{(1-e^2)^{1/2}}{e} \left[- S \cos v + T \left(1 + \frac{r}{p} \right) \sin v \right] ,$$

$$\frac{dM}{dt} = n - \frac{2}{na} S \frac{r}{a} - (1-e^2)^{1/2} \left(\frac{d\omega}{dt} + \cos I \frac{d\Omega}{dt} \right) ,$$

$$p = a(1-e^2) .$$

These expressions are known as the LPE in gaussian form. They have been calculated by using a force derived from a potential. However, the equations would have the same form for any force, and they can be so used. These expressions are especially useful in numerical integration and with nonconservative forces such as air drag and radiation pressure.

6. SPHERICAL HARMONICS

Legendre functions and associated Legendre functions arise naturally in the solution of Laplace's equations in spherical coordinates. They also constitute a set of orthogonal base functions for mapping arbitrary functions in spherical coordinates. In dynamical astronomy and satellite geodesy, spherical coordinates are the natural ones. We find that much of the subsequent analysis is facilitated by use of these functions, and we give here a short summary of their properties. Hobson (1955) is an excellent reference for mathematical proofs, and texts on mathematical physics (e.g., Jeffreys and Jeffreys, 1956; Morse and Feshback, 1953) provide many useful formulas. Legendre functions are extensively used in quantum mechanics, and its literature is recommended for the transformation properties.

First, we consider the conventional Legendre polynomials, which can be defined as

$$P_{\ell m}(z) = (1/2^{\ell}\, \ell!)\, (1 - z^2)^{m/2}\, (d^{\ell+m}/dz^{\ell+m})\, (z^2 - 1)^{\ell} \quad . \tag{97}$$

For computational and analytical purposes, we can use

$$P_{\ell m}(z) = \frac{(1-z^2)^{m/2}}{2^{\ell}} \sum_{k=0}^{\{(\ell-m)/2\}} \frac{(-1)^k\, (2\ell - 2k)!}{k!(\ell-k)!\, (\ell-m-2k)!}\, z^{\ell-m-2k} \quad , \tag{98}$$

where we take $\{x\}$ to be the greatest integer in x.

These polynomials are orthogonal such that

$$\int_{\text{sphere}} P_{\ell m}(z)\, P_{\ell' m'}(z) \begin{bmatrix}\sin\\ \cos\end{bmatrix} m\lambda \begin{bmatrix}\sin\\ \cos\end{bmatrix} m'\lambda \cos\phi\, d\phi\, d\lambda = \begin{cases} \dfrac{2\pi\,(\ell+m)!}{\epsilon_m (2\ell+1)\,(\ell-m)!} \quad , & \ell = \ell',\ m = m' \\ 0 \quad , & \ell \neq \ell',\ m \neq m',\ \text{or both,} \end{cases} \tag{99}$$

where

$$\epsilon_m = \begin{cases} 1 & m = 0 \\ 2 & m \neq 0 \end{cases} .$$

Each $P_{\ell m}(z)$ can have a scale factor, called the normalization. We can choose this scale factor such that

$$\int_{\text{sphere}} \left[\overline{P}_{\ell m}(z)\right]^2 \begin{bmatrix} \sin \\ \cos \end{bmatrix}^2 m\lambda \cos \phi \, d\phi \, d\lambda = 4\pi \quad ; \tag{100}$$

that is,

$$\overline{P}_{\ell m}(z) = [\epsilon_m (2\ell + 1) \, (\ell - m)!/(\ell + m)!]^{1/2} \, P_{\ell m}(z) \quad ; \tag{101}$$

these are called fully normalized Legendre polynomials. For statistical analysis, this normalization has the advantage that the mean square of the spherical harmonic is unity and the degree variance is just the sum of the fully normalized spherical-harmonic coefficients squared. We note that the Jeffreys and Jeffreys text uses

$$p_\ell^m(z) = [(\ell - m)!/\ell!] \, P_{\ell m}(z) \quad . \tag{102}$$

For numerical computation, (98) can be used. This expression can have large roundoff errors, and direct use of (98) may require multiple-precision computation. One alternative device is to employ the recurrence relationship

$$P_{\ell, m+2}(z) + 2(m+1) \, [z/(1 - z^2)^{1/2}] \, P_{\ell, m+1}(z) + (\ell - m)(\ell + m + 1) \, P_{\ell m}(z) = 0 \quad , \tag{103}$$

where $z = \sin \phi$, and use

$$P_{\ell\ell}(z) = [(2\ell)!/2^\ell \ell!] \, \cos^\ell \phi, \qquad P_{\ell, \ell-1}(z) = z \, P_{\ell\ell}(z) \quad .$$

For each degree ℓ, we compute all the $P_{\ell m}(z)$ from (103). In general, we require all the $P_{\ell m}(z)$, and this device will be efficient as well as accurate.

Because of the orthogonality and completeness of the Legendre functions, we can express any function on the surface of a sphere by

$$F(\phi,\lambda) = \sum_{\ell=0}^{\infty} \sum_{m=0}^{\ell} \overline{P}_{\ell m}(\sin\phi)\,(\overline{C}_{\ell m}\cos m\lambda + \overline{S}_{\ell m}\sin m\lambda) \quad , \tag{104}$$

or by a similar expression in terms of conventional harmonics.

As a solution of Laplace's equation for the potential outside a sphere of radius a_e containing all the mass, we have

$$\mathcal{U}(r,\phi,\lambda) = \sum_{\ell=0}^{\infty} \sum_{m=0}^{\ell} \left(\frac{a_e^{\ell}}{r^{\ell+1}}\right) \overline{P}_{\ell m}(\sin\phi)\,(\overline{C}_{\ell m}\cos m\lambda + \overline{S}_{\ell m}\sin m\lambda) \quad , \tag{105}$$

or a similar expression in terms of conventional harmonics.

We can write (105) in the equivalent complex notation:

$$\mathcal{U}(r,\phi,\lambda) = \mathcal{R}e \sum_{\ell=0}^{\infty} \sum_{m=0}^{\ell} \left(\frac{a_e^{\ell}}{r^{\ell+1}}\right) \overline{\mathcal{C}}_{\ell m}\, \overline{P}_{\ell m}(\sin\phi)\, e^{im\lambda} \quad , \tag{106}$$

where

$$\overline{\mathcal{C}}_{\ell m} = \overline{C}_{\ell m} - i\,\overline{S}_{\ell m} \tag{107}$$

and $\mathcal{R}e\{\ \}$ designates the real part of $\{\ \}$; this has some theoretical advantages. If the coefficients $\mathcal{C}_{\ell m} = C_{\ell m} - i\,S_{\ell m}$ are given, we can compute $\overline{\mathcal{C}}_{\ell m}$ from

$$\overline{\mathcal{C}}_{\ell m} = \left[\frac{\epsilon_m (2\ell+1)\,(\ell-m)!}{(\ell+m)!}\right]^{1/2} \mathcal{C}_{\ell m} \quad . \tag{108}$$

Fully normalized spherical harmonics are particularly useful for expressing the reciprocal distance between two points. Consider points x, x′ as in Figure 3, with $r < r'$:

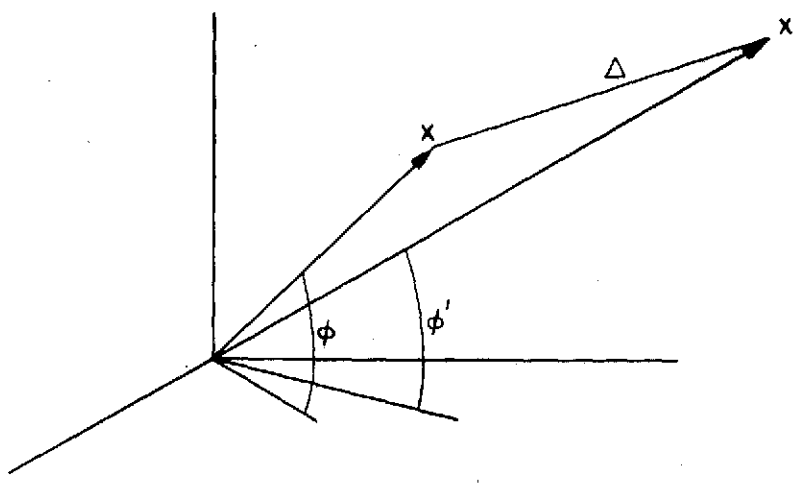

Figure 3. Geometry of the third-body potential function.

Then we can write

$$\frac{1}{\Delta} = \mathcal{R}e \sum_{\ell=0}^{\infty} \sum_{m=0}^{\ell} \frac{1}{2\ell+1} \frac{r^{\ell}}{r'^{\ell+1}} \overline{P}_{\ell m}(\sin\phi)\, \overline{P}_{\ell m}(\sin\phi')\, e^{im(\lambda-\lambda')} \quad . \quad (109)$$

We will need to find the expression for $\overline{P}_{\ell m}(z)\, e^{im\lambda}$ in a coordinate system rotated by the Euler angles I, Ω, ω. The rotation formula is used in quantum mechanics. It was introduced into satellite geodesy by Izsak (1964). The results given here are taken from Jeffreys (1965). We can write

$$\overline{P}_{\ell m}(\sin\phi)\, e^{im\lambda} = \sum_{s=-\ell}^{\ell} (i)^{s-m}\, E_{\ell ms}(I)\, \overline{P}_{\ell s}(\sin\phi')\, e^{i[s(\lambda'+\omega') + m\Omega]} \quad , \quad (110)$$

with

$$E_{\ell ms}(I) = N_{\ell ms} \sum_{r=\max\left|\begin{matrix}0\\-(m+s)\end{matrix}\right.}^{\min\left|\begin{matrix}\ell-s\\\ell-m\end{matrix}\right.} (-1)^{\ell-m-r} \binom{\ell+m}{m+s+r} \binom{\ell-m}{r} \gamma^{2r+m+s}\, \sigma^{2(\ell-r)-m-s} \quad , \quad (111)$$

where

$$\gamma = \cos(I/2) \quad , \qquad \sigma = \sin(I/2) \quad ,$$

$$N^2_{\ell ms} = \frac{(\ell-s)!\ (\ell+s)!\ \epsilon_m}{(\ell-m)!\ (\ell+m)!\ \epsilon_s} \quad .$$

Further, if $\phi' = 0$, we can write this in a more compact form as

$$\overline{P}_{\ell m}(\sin\phi)\, e^{im\lambda} = \sum_{p=0}^{\ell} (i)^{\ell-m} D_{\ell mp}(I)\, e^{i[(\ell-2p)(\lambda'+\omega') + m\Omega]} \quad , \quad -\ell \geq m \geq \ell \quad , \tag{112}$$

where

$$D_{\ell mp}(I) = \frac{1}{N_{\ell m}} \frac{(\ell+m)!}{2^\ell\ \ell!} \sum_{r=\max\left|\begin{smallmatrix}0\\2p-\ell-m\end{smallmatrix}\right.}^{\min\left|\begin{smallmatrix}\ell-m\\2p\end{smallmatrix}\right.} (-1)^{\ell-m-r} \binom{\ell}{p}\binom{2p}{r}\binom{2\ell-2p}{\ell-m-r} \gamma^{\ell+m+2r-2p}\, \sigma^{\ell-m-2r+2p} \quad , \tag{113}$$

where

$$r = \cos(I/2) \quad , \qquad \sigma = \sin(I/2) \quad ,$$

$$N^2_{\ell m} = \frac{(\ell+m)!}{\epsilon_m (2\ell+1)\ (\ell-m)!} \quad .$$

We note that

$$\overline{P}_{\ell,-m}(z) = (-1)^m\, \overline{P}_{\ell,|m|}(z) \quad . \tag{114}$$

If we make the association $v = \lambda$, we see that (112) is a natural expression of spherical harmonics in Kepler elements. The development has been carried out by Kaula (1966a) on other considerations for conventional harmonics. The $D_{\ell mp}(I)$ here are related to the inclination functions of Kaula by

$$D_{\ell mp}(I) = \left[(-1)^{\{(\ell-m)/2\}} / N_{\ell m}\right] F_{\ell mp}(I) \quad . \tag{115}$$

The two developments are equivalent. We give here the expressions for calculating $F_{\ell mp}(I)$ as derived by Kaula, since they are extensively used:

$$F_{\ell mp}(I) = \sum_{t=0}^{\min\left|\{(\ell-m)/2\}, p\right.} \frac{(2\ell-2t)!}{t!\,(\ell-t)!\,(\ell-m-2t)!\,2^{2\ell-2t}} S^{\ell-m-2t}$$

$$\times \sum_{s=0}^{m} \binom{m}{s} C^s \sum_{c} \binom{\ell-m-2t+s}{c} \binom{m-s}{p-t-c} (-1)^{c-k} \quad , \tag{116}$$

where $S = \sin I$ and $C = \cos I$. Kaula gives tables of $F_{\ell mp}(I)$ through 4, 4, 4. Since (116) has three summations, whereas (113) has only one, the latter is somewhat more economical for computing numerical values.

7. ELLIPTIC EXPANSIONS

In Section 4, we found the relation between the mean anomaly M, the eccentric anomaly E, and the true anomaly v. Whereas E and v have geometric significance and are related by

$$\tan (v/2) = [(1+e)/(1-e)]^{1/2} \tan (E/2) \quad , \tag{117}$$

the mean anomaly has dynamical significance, increasing proportionally with time; that is,

$$M = M_0 + nt \quad . \tag{118}$$

The connection between M and E and hence v is made through Kepler's equation (64):

$$M = n(t - t_0) = E - e \sin E \quad . \tag{119}$$

Equations (117) to (119) are sufficient for all computations in two-body motion. Equation (119) is transcendental for E in terms of M and can easily be solved numerically by iteration. The obvious iteration is

$$\begin{aligned} E_0 &= M \quad , \\ E_{n+1} &= M + e \sin E_n \quad , \end{aligned} \tag{120}$$

which converges very quickly for small eccentricity. Typical geodetic satellites have $e < 0.1$, for which (120) is quite sufficient. There are numerical methods to speed convergence, and in cases where efficiency is important, methods like Newton's have been successful.

In developing complete solutions by use of, for example, LPE, we are faced with integrals of the form

$$\int f(v)\, dt \qquad \text{or} \qquad \int f(E)\, dt \quad . \tag{121}$$

It is therefore useful to be able to express functions of v and E in terms of t or M. These expressions generally involve infinite series in powers of eccentricity.

A particularly useful device for transforming (121) is to use (52) with (58) and with (61) or (63). We have in the first case

$$dv = (a/r)^2 (1-e^2)^{1/2} dM = (a/r)^2 (1-e^2)^{1/2} n\, dt \quad , \tag{122}$$

and in the second

$$dE = (a/r)\, dM = (a/r)\, n\, dt \quad .$$

By use of (122), integrals in t can be converted to integrals in v or E. Where necessary, a/r can be expressed in v or E by (57), repeated here for convenience:

$$a/r = (1+e\cos v)/a(1-e^2) = 1/(1-e\cos E) \quad . \tag{123}$$

Transformation (122) is useful when M is absent from the integral. Generally, this is not the case, and we must explicitly make the conversion. More general expressions are used, complete developments being carried out on computers either numerically or algebraically. In the following, we develop some of these formulas.

If, following many authors (e.g., Plummer, 1918), we define the variable $\beta(e)$ by

$$(1+\beta)/(1-\beta) = [(1+e)/(1-e)]^{1/2} \quad , \tag{124}$$

we have

$$e = 2\beta/(1+\beta^2) \tag{125}$$

or

$$\beta = e/[1 + (1-e^2)^{1/2}] \quad . \tag{126}$$

We see that $\beta \approx e/2$.

By using the Bessel function $J_n(x)$, we can write

$$E - M = 2 \sum_{s=1}^{\infty} \frac{1}{s} J_s(se) \sin sM \tag{127}$$

and

$$v - M = 2 \sum_{s=1}^{\infty} \frac{1}{s} \left\{ J_s(se) + \sum_{p=1}^{\infty} \beta^p \left[J_{s-p}(se) + J_{s+p}(se) \right] \right\} \sin sM \quad . \tag{128}$$

The first few terms of (127) and (128) are

$$\begin{aligned} E - M = & \left(e - \frac{1}{8} e^3 + \ldots \right) \sin M \\ & + \left(\frac{e^2}{2} + \ldots \right) \sin 2M \\ & + \left(\frac{3}{8} e^3 + \ldots \right) \sin 3M \end{aligned} \tag{129}$$

and

$$\begin{aligned} v - M = & \left(2e - \frac{1}{4} e^3 + \ldots \right) \sin M \\ & + \left(\frac{5}{4} e^2 + \ldots \right) \sin 2M \\ & + \left(\frac{13}{12} e^3 + \ldots \right) \sin 3M \quad . \end{aligned} \tag{130}$$

Brouwer and Clemence (1961) give these expressions to 7th order in eccentricity.

We have need of similar expressions when v or E occurs in the argument of a trigonometric function. There are several methods to obtain such expressions. We give two here. The first is due to Kaula (1966a) and taken from Tisserand (1960). Kaula investigates the conversion of

$$\left(\frac{a}{r} \right)^{\ell+1} \begin{pmatrix} \cos \\ \sin \end{pmatrix} [(\ell - 2p) v + \psi] \quad ,$$

where ψ does not depend on v, and gives it in the form

$$\left(\frac{a}{r}\right)^{\ell+1}\begin{pmatrix}\cos\\ \sin\end{pmatrix}\left[(\ell-2p)v+\psi\right]=\sum_{q=-\infty}^{\infty}G_{\ell pq}(e)\begin{pmatrix}\cos\\ \sin\end{pmatrix}\left[(\ell-2p+q)m+\psi\right] \quad . \tag{131}$$

This form is natural for the computation of perturbations due to tesseral harmonics. The formulas have two forms. The first is for "long-period" terms, i.e., those terms in (131) independent of M – that is, $q = 2p-\ell$. These can be obtained by integrating (131) with respect to M from 0 to 2π. Using the transformation (122), we obtain

$$G_{\ell p,\,2p-\ell}(e)=\frac{1}{(1-e^2)^{\ell-(1/2)}}\sum_{d=0}^{p'-1}\binom{\ell-1}{2d+\ell-2p'}\binom{2d+\ell-2p'}{d}\left(\frac{e}{2}\right)^{2d+\ell-2p'} \quad , \tag{132}$$

in which

$$p' = p \qquad \text{for} \qquad p \le \ell/2 \quad ,$$

$$p' = \ell - p \qquad \text{for} \qquad p \ge \ell/2 \quad .$$

For the short-period terms, $\ell - 2p + q \neq 0$, we have

$$G_{\ell pq}(e) = (-1)^{|q|}\,(1+\beta^2)^{\ell}\,\beta^{|q|}\sum_{k=0}^{\infty}P_{\ell pqk}\,Q_{\ell pqk}\,\beta^{2k} \quad , \tag{133}$$

where

$$\beta = e/[1+(1-e^2)^{1/2}] \quad ;$$

$$P_{\ell pqk}=\sum_{r=0}^{h}\binom{2p'-2\ell}{h-r}\frac{(-1)^r}{r!}\left[\frac{(\ell-2p'+q')e}{2\beta}\right]^r \quad , \tag{134}$$

$$h = k + q' \quad , \quad q' > 0 \quad ; \qquad h = k \quad , \quad q' < 0 \quad ;$$

and

$$Q_{\ell pqk} = \sum_{r=0}^{h} \binom{-2p'}{h-r} \frac{1}{r!} \left[\frac{(\ell - 2p' + q')e}{2\beta}\right]^r \quad , \tag{135}$$

$$h = k \quad , \quad q' > 0 \quad ; \quad h = k - q' \quad , \quad q' < 0 \quad ;$$

$$p' = p \quad , \quad q' = q \text{ for } p \le \ell/2 \quad ; \quad p' = \ell - p \quad , \quad q' = -q \text{ for } p > \ell/2 \quad .$$

The transformation (131) is a doubly infinite sum over q. However, it is important to note that

$$G_{\ell pq}(e) \propto \beta^{|q|} \approx (e/2)^{|q|} \quad .$$

We can choose a desired accuracy and select a finite number of terms. For small e, the number can be very limited. This selection can be made numerically or analytically.

A second and more general method for this development, given in Plummer (1918, p. 44), involves the Hansen coefficients X_q^{nm}, defined by

$$(r/a)^n e^{imv} = \sum_{q=-\infty}^{\infty} X_q^{nm}(e)\, e^{iqM} \quad , \tag{136}$$

where the $X_q^{nm}(e)$ are polynomials in eccentricity. We have

$$X_q^{nm}(e) = (1+\beta^2)^{-(n+1)} \sum_p J_p(qe)\, X_{qp}^{nm} \quad , \tag{137}$$

and

$$X_{qp}^{nm} = (-\beta)^{q-p-m} \binom{n+1-m}{q-p-m} F(q-p-n-1,\ -m-n-1,\ q-p-m+1, \beta^2) \quad ,$$

$$\text{for } q-p-m > 0 \quad ,$$

$$X_{qp}^{nm} = (-\beta)^{-q+p+m} \binom{n+1+m}{-q+p+m} F(-q+p-n-1,\ m-n-1,\ -q+p+m+1, \beta^2) \quad , \tag{138}$$

$$\text{for } q-p-m < 0 \quad ,$$

$$X_{qp}^{nm} = F(m-n-1,\ -m-n-1,\ 1,\ \beta^2) \quad , \qquad \text{for } q-p-m = 0 \quad .$$

We have the Bessel function

$$J_n(z) = (z/2)^n \sum_{k=0}^{\infty} \left(-\frac{1}{4} z^2\right)^k \Big/ [k!\ (n+k)!] \tag{139}$$

and the hypergeometric function

$$F(a, b, c, z) = \sum_{n=0}^{\infty} [(a)_n\ (b)_n/(c)_n]\ (z^n/n!) \quad , \tag{140}$$

where Pochhammer's symbol is

$$(a)_n = a(a+1)\ (a+2)\ \ldots\ (a+n-1) \tag{141a}$$

and

$$(a)_0 = 1 \quad . \tag{141b}$$

We see by comparing coefficients that

$$G_{\ell pq}(e) = X_{\ell-2p+q}^{-(\ell+1),\ \ell-2p}(e) \quad . \tag{142}$$

However, formulas (133) to (135) are valid only for $\ell + 1 > 0$, whereas (136) to (142) are valid for any $n = -(\ell + 1)$. Both forms have been used. With recent developments in the computing of elementary functions, the latter seems more economical for numerical calculation. For use with computer algebra, one would prefer to obtain polynomials in eccentricity with rational fractions as coefficients. This has been done through a recurrence relation originated by Andoyer (1903) and introduced into satellite work by Izsak, Gerard, Efimba, and Barnett (1964). The method starts with the observation that

$$(r/a)^{\pm n} e^{i(\pm m v)} = X^{\pm n, \pm m} = (X^{\pm 1, 0})^n (X^{0, \pm 1})^m \quad .$$

We compute $X^{\pm 1, 0}$, $X^{0, \pm 1}$ by any method, and all other combinations are determined by simple polynomial multiplication. Cherniack (1972) gives these polynomials to 12th order in e. Kaula (1966a) gives a table through 4, 4, 2. Cayley (1961) gives more extensive tables.

8. FIRST-ORDER PERTURBATIONS DUE TO THE GEOPOTENTIAL

We have seen that the geopotential, an arbitrary function, can be expressed in terms of associated Legendre functions (Section 6) and a set of numerical constants,

$$\mathcal{U} = \mathcal{R}e \left(\frac{GM}{r}\right) \left[1 + \sum_{\ell=2}^{\infty} \sum_{m=0}^{\ell} \overline{C}_{\ell m} \left(\frac{a_e}{r}\right)^{\ell} \overline{P}_{\ell m}(\sin\phi)\, e^{im\lambda}\right] , \qquad (143)$$

where ϕ, λ, r are the coordinates of a point in the terrestrial or earth-fixed system. The terms $\overline{C}_{1,0}$, $\overline{C}_{1,1}$, $\overline{C}_{2,1}$ are missing owing to the orientation and origin of the system chosen. In fact, the elastic earth introduces the terms $\overline{C}_{2,1}$, which will be discussed along with other questions relating to the earth's elasticity in Section 9. Selecting Kepler elements, we now use (143) in (82) for the disturbing function r, omitting, of course, GM/r.

The conversion of $R(r, \phi, \lambda)$ to $R(a, e, I, v, \omega, \Omega-\theta)$ is accomplished as follows. We express $R(r, \phi, \lambda)$ in the orbital system by rotating by $-\theta$. This introduces $\lambda-\theta$ in place of λ in (143). From the rotation theorem (112), we have

$$R = \mathcal{R}e \left(\frac{GM}{r}\right) \sum_{\ell=2}^{\infty} \sum_{m=0}^{\ell} \overline{C}_{\ell m} \left(\frac{a_e}{r}\right)^{\ell} (i)^{\ell-m} \sum_{p=0}^{\ell} D_{\ell mp}(I)\, e^{i[(\ell-2p)(v+\omega)+m(\Omega-\theta)]} , \qquad (144)$$

where $i = \sqrt{-1}$ and $D_{\ell mp}(I)$ are polynomials in cos (I/2), sin (I/2). This is further converted to the mean anomaly with (133) or (136), giving

$$R = \mathcal{R}e\, GM \sum_{\ell=2}^{\infty} \sum_{m=0}^{\ell} \sum_{p=0}^{\ell} \sum_{q=-\infty}^{\infty} \left(\frac{1}{a}\right) \left(\frac{a_e}{a}\right)^{\ell} (i)^{\ell-m} D_{\ell mp}(I)\, G_{\ell pq}(e)\, e^{i\psi} , \qquad (145)$$

where

$$\psi = (\ell - 2p)\omega + (\ell - 2p + q)M + m(\Omega - \theta) \quad ;$$

equation (145) can also be written in terms of Hansen coefficients with (142).

The first-order secular rates can be determined by selecting terms in R independent of ω, Ω, M, θ. These arise for $m = 0$ – that is, only zonal harmonics and $\ell - 2p = q = 0$. By use of algebra, we find secular terms only in ω, Ω, M. A corollary is that the size a of the orbit, its shape e, and its orientation can have only periodic perturbations. We have shown it to first order only, but it is true for any order (Kozai, 1959a). We obtain for the first-order secular rates

$$\begin{aligned}
\dot{\omega} &= n(3\sqrt{5}/4)\,[\overline{C}_{2,0}/(1-e^2)^2]\;(a_e/a)^2\;(1-5\cos^2 I) \quad , \\
\dot{\Omega} &= n(3\sqrt{5}/2)\,[\overline{C}_{2,0}/(1-e^2)^2]\;(a_e/a)^2\;\cos I \quad , \\
\dot{M} &= n\left\{1 - (3\sqrt{5}/4)\,[\overline{C}_{2,0}/(1-e^2)^{3/2}]\;(a_e/a)^2\;(3\cos^2 I - 1)\right\} \quad .
\end{aligned} \tag{146}$$

First-order periodic perturbations are easily obtained by assuming that a, e, I are relatively constant on the right-hand side of (82) and that ω, Ω, M, θ have linear rates; that is,

$$\begin{aligned}
\omega &= \omega_0 + \dot{\omega}t \quad , \\
\Omega &= \Omega_0 + \dot{\Omega}t \quad , \\
M &= M_0 + nt \quad , \\
\theta &= \theta_0 + \dot{\theta}t \quad .
\end{aligned} \tag{147}$$

The equations are integrated as a linear harmonic oscillator for those terms containing any of the variables in (147). In actual computation, we would use the observed values of $\dot{\omega}$, $\dot{\Omega}$, n, $\dot{\theta}$.

Letting $\mathcal{E}_i$ be a generic element, we have the following:

$$\Delta\mathcal{E}_i = \sum_{\ell=2}^{\infty} \sum_{m=0}^{\ell} \sum_{p=0}^{\ell} \sum_{q=-\infty}^{\infty} \Delta\mathcal{E}_{\ell mpq} \,,$$

$$\Delta a_{\ell mpq} = \mathcal{R}e \frac{GM\, a_e^{\ell}\, (i)^{\ell-m}}{n a^{\ell+2}} \frac{2}{\dot{\psi}_{\ell mpq}} D_{\ell mp}(I)\, G_{\ell pq}(e)\, (\ell - 2p + q)\, \overline{\mathcal{C}}_{\ell m}\, e^{i\psi_{\ell mpq}} \,,$$

$$\Delta e_{\ell mpq} = \mathcal{R}e \frac{GM\, a_e^{\ell}\, (i)^{\ell-m}}{n a^{\ell+3}\, e\, \dot{\psi}_{\ell mpq}} D_{\ell mp}\, G_{\ell pq}\, (1-e^2)^{1/2}$$

$$\times \left[(1-e^2)^{1/2}\, (\ell - 2p + q) - (\ell - 2p)\right] \overline{\mathcal{C}}_{\ell m}\, e^{i\psi_{\ell mpq}} \,,$$

$$\Delta I_{\ell mpq} = \mathcal{R}e \frac{GM\, a_e^{\ell}\, (i)^{\ell-m}}{n a^{\ell+3}\, (1-e^2)^{1/2}\, \dot{\psi}_{\ell mpq}} D_{\ell mp}\, G_{\ell pq} \left[(\ell - 2p)\cos I - m\right] \overline{\mathcal{C}}_{\ell m}\, e^{i\psi_{\ell mpq}} \,, \tag{148}$$

$$\Delta\omega_{\ell mpq} = \mathcal{R}e \frac{GM\, a_e^{\ell}\, (i)^{\ell-m-1}}{n a^{\ell+3}\, (1-e^2)^{1/2} \sin I\, \dot{\psi}_{\ell mpq}}$$

$$\times \left[\frac{(1-e^2)^{1/2}}{e} D_{\ell mp} \frac{\partial G_{\ell m}}{\partial e} - \frac{\cos I}{\sin I} \frac{G_{\ell mp}}{(1-e^2)^{1/2}} \frac{\partial D_{\ell mp}}{\partial I}\right] \overline{\mathcal{C}}_{\ell m}\, e^{i\psi_{\ell mpq}} \,,$$

$$\Delta\Omega_{\ell mpq} = \mathcal{R}e \frac{GM\, a_e^{\ell}\, (i)^{\ell-m-1}\, G_{\ell pq}}{n a^{\ell+3}\, (1-e^2)^{1/2} \sin I\, \dot{\psi}_{\ell mpq}} \frac{\partial D_{\ell mp}}{\partial I} \overline{\mathcal{C}}_{\ell m}\, e^{i\psi_{\ell mpq}} \,,$$

$$\Delta M_{\ell mpq} = \mathcal{R}e \frac{GM\, a_e^{\ell}\, (i)^{\ell-m-1}}{n a^{\ell+3}\, \dot{\psi}_{\ell mpq}}$$

$$\times \left[-\frac{(1-e^2)^{1/2}}{e} \frac{\partial G_{\ell pq}}{\partial e} + 2(\ell+1)\, G_{\ell pq}\right] D_{\ell mp}\, \overline{\mathcal{C}}_{\ell m}\, e^{i\psi_{\ell mpq}} \,,$$

where

$$\dot{\psi}_{\ell mpq} = (\ell - 2p)\,\dot{\omega} + (\ell - 2p + q)\,n + m(\dot{\Omega} - \dot{\theta}) \quad .$$

After the substitution of (110), these formulas agree with those of Kaula (1966a).

The final calculation necessary is to determine $\int n\,dt$ for the perturbation in M according to (82). We see that for $\ell - 2p + q \neq 0$, we have a perturbation in $\underline{a}$ from the first equation of (148). From $n^2 a^3 = GM$, we have

$$\Delta n_{\ell mpq} = -\,(3/2)\,(n/a)\,\Delta a_{\ell mpq} \quad . \tag{149}$$

Therefore, to the last equation of (148), we must add the term

$$\Delta M^2_{\ell mpq} = \int \Delta n_{\ell mpq}\,dt = \mathcal{R}e\left[-3\,GM\,a_e^{\ell}\,(i)^{\ell-m-1}/a^{\ell+3}\,(\dot{\psi}_{\ell mpq})^2\right]$$

$$\times D_{\ell mp}\,G_{\ell pq}(\ell - 2p + q)\,\overline{\mathcal{C}}_{\ell m}\,e^{i\psi_{\ell mpq}} \quad . \tag{150}$$

We can combine both parts and obtain

$$\Delta M_{\ell mpq} = \mathcal{R}e\,\frac{GM\,a_e^{\ell}\,D_{\ell mp}}{a^{\ell+3}}\left[-\frac{(1-e^2)^{1/2}}{ne\,\dot{\psi}_{\ell mpq}}\,\frac{\partial G_{\ell pq}}{\partial e} + \frac{2(\ell+1)}{n\dot{\psi}_{\ell mpq}}\,G_{\ell pq} - \frac{3\,G_{\ell pq}(\ell - 2p + q)}{(\dot{\psi}_{\ell mpq})^2}\right]$$

$$\times i^{\ell-m+1}\,\overline{\mathcal{C}}_{\ell m}\,e^{i\psi_{\ell mpq}} \quad .$$

This completes the first-order theory. If we take as our goal an accuracy of 10^{-7}, then it is quite satisfactory unless $|\overline{\mathcal{C}}_{\ell m}|$ is larger than 10^{-4} or $\dot{\psi}_{\ell mpq}$ is very small. From observations, we find that $\overline{C}_{2,0} \approx 10^{-3}$ and that all the remaining $|\overline{\mathcal{C}}_{\ell m}| \approx 10^{-6}$. Therefore, this theory is inadequate for the effects of $\overline{C}_{2,0} = -J_2/\sqrt{5}$, and so other methods are used, as described in Section 10. The discussion of small $\dot{\psi}_{\ell mpq}$ goes by the name of resonance, which will be dealt with shortly.

This completes the first-order theory. If we take as our goal an accuracy of 10^{-7}, then it is quite satisfactory unless $|\overline{\mathcal{C}}_{\ell m}|$ is larger than 10^{-4} or $\dot{\psi}_{\ell mpq}$ is very small. From observations, we find that $\overline{C}_{2,0} \approx 10^{-3}$ and that all the remaining $|\overline{\mathcal{C}}_{\ell m}| \approx 10^{-6}$. Therefore, this theory is inadequate for the effects of $\overline{C}_{2,0} = -J_2/\sqrt{5}$, and so other methods are used, as described in Section 10. The discussion of small $\dot{\psi}_{\ell mpq}$ goes by the name of resonance, which will be dealt with shortly.

If we consider the rate

$$\dot{\psi}_{\ell mpq} = (\ell - 2p)\,\dot{\omega} + (\ell - 2p + q)\,n + m\,(\dot{\Omega} - \dot{\theta}) \tag{151}$$

and $\dot{\omega}$, $\dot{\Omega}$ from (146), we see that $(\dot{\omega}, \dot{\Omega}) \propto 10^{-3}$ n. The rotation rate of the earth $\dot{\theta}$ is once per day, and n for geodetic satellites is 12 ± 2 revolutions per day. Therefore, the period of a perturbation is primarily determined by

$$2\pi/P = (\ell - 2p + q)n - m\dot{\theta} \quad . \tag{152}$$

We see that in general the largest perturbations – that is, the smallest divisors – are for $\ell - 2p + q = 0$, and we have periodic terms with frequency $m\dot{\theta}$. Resonance occurs with the near-commensurability of $(\ell - 2p + q)n$ and $m\dot{\theta}$. That means that when the mean motion of the satellite is approximately equal to the order of the tesseral harmonics, we can have arbitrary long periods and large amplitudes. When analyzing terms with small divisors, we must include the effects of $\dot{\omega}$ and $\dot{\Omega}$ to obtain meaningful results. Resonance has yet to be treated completely. For a single resonant term, a solution in terms of elliptic functions can be obtained, and these have played an important role in the study of synchronous satellites. For close-earth satellites, the problems are more difficult, since the satellite will be resonant with the whole set of harmonics of order m. In addition, if the drag changes n appreciably during one resonant oscillation, the theory is not even approximately correct. Fortunately, geodetic satellites have had relatively short resonant periods ($\approx$ 10 days), and the linear theory seems to work well enough.

A second class of long-period perturbations is due to the zonal harmonics ($m = 0$, $\ell - 2p + q = 0$). These have the principal period of the rotation of perigee, as given by (146). The period of these terms can go to zero for the so-called critical inclination – that is, when $(1 - 5\cos^2 I) = 0$ or $I \cong 63^\circ.4$. The theory given here is not valid near that region of inclination. It has variously been viewed as a resonant phenomenon and as a physically important effect. Izsak (1963c), Garfinkle (1963), and others have discussed this question.

Table 2 gives here for a typical geodetic satellite a short table of amplitudes of the perturbations due to the earth's gravity field.

Table 2. Sensitivity coefficients for satellite 6701401 (in units of meters, with $|\overline{C}_{\ell m}| \times 10^6$).

e = 0.0843130 A = 7614 km
I = 39.45459 perigee = 594 km
n = 13.064356 apogee = 1878 km

m \ ℓ	11	12	13	14	15	16	17	18	19	20
1	154	229	121	75	139	160	66	69	118	67
2	113	43	61	94	58	35	59	46	0	33
3	52	78	65	25	54	43	12	18	39	26
4	66	34	19	39	38	14	10	27	0	0
5	38	28	51	29	0	23	10	0	0	18
6	65	48	42	14	27	19	0	17	0	0
7	68	62	61	45	10	0	18	16	0	0
8	46	62	45	37	18	12	0	0	18	0
9	21	30	46	64	55	53	23	0	0	0
10	0	0	29	44	43	58	37	32	0	0
11	0	0	8	16	27	48	47	57	48	44
12		0	0	21	44	64	89	101	75	99
13			425	1203	2987	4758	8014	9531	12277	11613
14				0	0	20	47	77	111	145
15					0	0	0	0	16	20
16						0	0	0	0	0
17							0	0	0	0
18								0	0	0
19									0	0
20										0

9. THIRD-BODY PERTURBATIONS, ELASTICITY, AND TIDES

There is an extensive literature on third-body perturbations. The principal effect of the moon is a perturbation ≈ 120 m, and that of the sun, about 6 times that amount. Continuous analysis has been necessary because of three factors:

A. The moon's motion is itself complicated, making integration of the equations of motion difficult. The inclination of the moon's orbit is not constant in the adopted orbital system. There is a rich spectrum of periodic terms in the lunar longitude.

B. The moon and sun deform the elastic earth. This variation in mass distribution has significant orbital effects. Improved geophysical information is needed in order to account for them.

C. The sun and moon cause precession and nutation. These motions are the reason for our adopting a quasi-inertial reference system. We must include in the theory terms to compensate for the noninertialness. These terms can be viewed as an indirect effect of the lunisolar perturbations.

There are two avenues to be taken. The first is to eliminate periodic perturbations with periods commensurate with the length of orbit we wish to determine – that is, periods < 20 days. We take an analytical approach by assuming linear variation of the orbital elements of the disturbing body. The second avenue is for long-period analysis, in which we obtain averaged equations – that is, ones not depending on the mean anomaly of the satellite. These can be integrated numerically and are used for study of all long-period effects.

In the following, we develop the disturbing function for the moon; that for the sun has the same form. We assume that the semimajor axis of the satellite is small with respect to that of the sun or the moon. This disturbing function can be averaged and then numerically integrated with (82), or if a', e', I' of the moon are assumed constant, it can be integrated approximately.

We introduce the elastic deformation of the earth at this point, as it is most easily incorporated into the theory from the beginning. Following A. E. H. Love (Munk and MacDonald, 1960, Chap. 5), the additional potential due to the deformation from a potential of degree n, $\mathcal{U}_n$, is

$$\mathcal{U}'_n = k_n (a_e/r)^{2n+1} \mathcal{U}_n \quad , \tag{153}$$

where k_n are numerical constants depending on the elastic properties of the earth. The total potential acting on the satellite is then

$$\left[1 + k_n (a_e/r)^{2n+1}\right] \mathcal{U}_n \quad . \tag{154}$$

Now the direct potential acting on the satellite due to the moon (or sun) can be written

$$\mathcal{U} = GM' \left[(1/\Delta) - (\bar{r} \cdot \bar{r}'/|r'|^3)\right] \quad , \tag{155}$$

where $\bar{r}$ and $\bar{r}'$ are the positions of the satellite and of the disturbing body, respectively, M′ is the mass of the disturbing body, and Δ is the distance between r and r′. From (109), we can write $1/\Delta$ in spherical harmonics. To calculate orbital perturbations, we use the gradient of $\mathcal{U}$ with respect to the satellite position, and we can drop the $\ell = 0$ term in $1/\Delta$. The $\ell = 1$ term just cancels $\bar{r} \cdot \bar{r}'/|r'|^3$. Thus, we have for the third-body potential, including the tidal deformation,

$$\mathcal{U} = GM' \mathcal{R}e \sum_{\ell=2}^{\infty} \sum_{m=0}^{\ell} \frac{1}{2\ell+1} \left[\frac{r^\ell}{r'^{\ell+1}} + \frac{k_\ell a_e^{2\ell+1}}{(r'r)^{\ell+1}}\right] \bar{P}_{\ell m}(\sin\phi)\, \bar{P}_{\ell m}(\sin\phi')\, e^{im(\lambda-\lambda')} \quad . \tag{156}$$

To include the effects of tidal phase lag, we introduce a fictitious moon lagging the real moon by Δt and separate (156) into two parts. In this case, the disturbing potential cannot be written in such a compact form. We proceed by assuming $\Delta t = 0$, the revision of the theory being straightforward if the effect of lag is desired.

By introducing the rotation operation (111) and Hansen coefficients (136), we can write the disturbing function as

$$R = \mathcal{R}e \sum_{\ell=2}^{\infty} \sum_{m=0}^{\ell} \sum_{p=0}^{\ell} \sum_{p'=0}^{\ell} \sum_{q=-\infty}^{\infty} \sum_{q'=-\infty}^{\infty} R_{\ell mpp'qq'} \quad , \tag{157}$$

where

$$R_{\ell mpp'qq'} = \frac{GM' (-1)^{\ell+m}}{2\ell+1} D_{\ell mp}(I)\, D_{\ell,-m,p'}(I')$$

$$\times \left[\frac{a^{\ell}}{a'^{\ell+1}} X_q^{\ell m}(e)\, X_{q'}^{-\ell-1,m}(e') + \frac{k_{\ell}\, a_e^{2\ell+1}}{(a'a)^{\ell+1}} X_q^{-\ell-1,m}(e)\, X_{q'}^{-\ell-1,m}(e') \right] e^{i\psi} \tag{158}$$

in which

$$\psi = qM + q'M' + (\ell - 2p)\omega + (\ell - 2p')\omega' + m(\Omega - \Omega') \quad .$$

We can integrate the LPE (82) by utilizing the disturbing function (157) and the same techniques used for the tesseral harmonics. Considerable simplification is achieved by the following steps:

A. We delete all terms containing M — that is, q=0. These short-period effects are about 1 m and can be ignored for some problems. A consequence is that $\Delta a = 0$.

B. For the second-degree terms, we can use, for the moon,

$$GM_{\oplus} = n_{\leftmoon}^2 a_{\leftmoon}^3 \tag{159a}$$

and

$$GM' = GM_{\oplus} (M_{\leftmoon}/M_{\oplus}) = (M_{\leftmoon}/M_{\oplus})\, n_{\leftmoon}^2 a_{\leftmoon}^3 \quad , \qquad M_{\leftmoon}/M_{\oplus} = 1/81.53 \quad ; \tag{159b}$$

and for the sun,

$$GM' = n_{\odot}^2 a_{\odot}^3 \quad . \tag{159c}$$

C. The third-degree terms from the sun are negligible, and those from the moon are ≈ 1 m and can be ignored for some problems. However, the third-degree terms and the short-period terms in the second-degree development must be included

for future work. The interaction between J_2 and the lunar perturbations is the same size and must also be added, that is, the contributions to $\dot{\omega}$ and $\dot{\Omega}$ from

$$\frac{d\dot{\omega}}{de}\Delta e + \frac{\partial\dot{\omega}}{\partial I}\Delta I \quad , \qquad \frac{d\dot{\Omega}}{de}\Delta e + \frac{d\dot{\Omega}}{dI}\Delta I \quad ,$$

$$\frac{d\dot{M}}{de}\Delta e + \frac{d\dot{M}}{dI}\Delta I \quad , \tag{160}$$

where $\dot{\omega}$, $\dot{\Omega}$, and $\dot{M}$ are given by (146).

A number of formulas have been used (e.g., Kozai, 1973; Gaposchkin, 1966). We give here just the secular rates in ω, Ω, and M and a representative periodic term. The complete expressions for lunar perturbations are developed by computer algebra and are described in Section 13. We have

$$\dot{\omega}_{L-S} = \frac{3}{4}\frac{n'^2}{n} m' \frac{1}{(1-e^2)^{1/2}} \left(2 - \frac{5}{2}\sin^2 I + \frac{1}{2}e^2\right)\left(1 - \frac{3}{2}\sin^2 I'\right)\left(1 + \frac{3}{2}e'^2\right)\left[1 + k_2\left(\frac{a_e}{a}\right)^2\right] \quad ,$$

$$\dot{\Omega}_{L-S} = -\frac{3}{4}\frac{n'^2}{n} m' \frac{\cos I}{(1-e^2)^{1/2}} \left(1 + \frac{3}{2}e^2\right)\left(1 - \frac{3}{2}\sin^2 I'\right)\left(1 + \frac{3}{2}e'^2\right)\left[1 + k_2\left(\frac{a_e}{a}\right)^2\right] \quad , \tag{161}$$

$$\dot{M}_{L-S} = -\frac{1}{4}\frac{n'^2}{n} m' \left(1 - \frac{3}{2}\sin^2 I'\right)\left(1 - \frac{3}{2}\sin^2 I\right)\left(1 + \frac{3}{2}e'^2\right)\left[7 + 3e^2 - 3(1+4e^2)k_2\left(\frac{a_e}{a}\right)^2\right] \quad ,$$

where for the moon

$$m' = M_{\leftmoon}/M_{\oplus} = 1/81.53 \quad ,$$

and for the sun,

$$m' = 1 \quad ,$$

and where

$$\sin^2 I' = \frac{1}{2}\sin^2 J\,(1+\cos^2\epsilon) + \sin^2\epsilon\,\cos^2 J + \frac{1}{2}\sin 2\epsilon\,\sin 2J\cos N - \frac{1}{2}\sin^2 J\,\sin^2\epsilon\,\cos 2N \tag{162}$$

here, J is the lunar inclination, N is the lunar longitude referred to the ecliptic, and ϵ is the obliquity. Although I' is not constant, it is a reasonable approximation for a year or so. We note that $J = 5.^{\circ}145396$. The other elements can be taken from the ESAENA. For the sun, of course, $m' = J = 0$. For the periodic perturbation, we give as an example, for the second degree,

$$\Delta I_{2,m,p,p',q,q'} = \frac{n'^2\,(-1)^m}{5\dot{\psi}}\,D_{2,m,p}(I)\,D_{2,-m,p'}(I')$$
$$\times\left[X_q^{2,m}(e)\,X_{q'}^{-3,m}(e') + k_2\left(\frac{a_e}{a}\right)^5 X_q^{-3,m}(e)\,X_{q'}^{-3,m}(e')\right]$$
$$\times\left[2(1-p)\cos I - m\right]\cos\psi \quad , \tag{163}$$

where

$$\dot{\psi} = 2(1-p)\dot{\omega} + 2(1-p')\dot{\omega}' + qn + q'n' + m(\dot{\Omega} - \dot{\Omega}') \quad .$$

We note that the secular rates depend on k_2, which corresponds to that part of the oblateness resulting from the permanent tidal deformation. Conventionally, this term is omitted from the lunar theory and is effectively included in the numerical value of J_2. A slight error will arise since, in the lunar theory, k_2 occurs multiplied by $(a_e/a)^5$, whereas J_2 is multiplied by $(a_e/a)^3$. Furthermore, the secular term in M must be included in the definition of the semimajor axis.

The adopted reference system for orbit computation is the equinox of 1950.0 and the equator of date. The equations of motion must be modified to include the motion of the reference system. There is no need to modify the short-period perturbations in the linear theory described above. However, the complete set of LPE for long-period

perturbations should include the following factors (Kozai and Kinoshita, 1973):

$$\left.\begin{aligned} di/dt &= \ldots + \partial i/\partial t \\ d\omega/dt &= \ldots + \partial \omega/\partial t \\ d\Omega/dt &= \ldots + \partial \Omega/\partial t \end{aligned}\right\} ,$$

where

$$\left.\begin{aligned} \frac{\partial i}{\partial t} &= -\frac{d(\theta \cos a)}{dt} \cos \Omega - \frac{d(\theta \sin a)}{dt} \sin \Omega \\ \frac{\partial \omega}{\partial t} &= \operatorname{cosec} i \left[\frac{d(\theta \sin a)}{dt} \cos \Omega - \frac{d(\theta \cos a)}{dt} \sin \Omega\right] \\ \frac{\partial \Omega}{\partial t} &= -\cot i \left[\frac{d(\theta \sin a)}{dt} \cos \Omega - \frac{d(\theta \cos a)}{dt} \sin \Omega\right] \\ &\quad + \frac{1}{2}\left[\frac{d(\theta \sin a)}{dt} \theta \cos a - \frac{d(\theta \cos a)}{dt} \theta \sin a\right] \end{aligned}\right\} , \qquad (164)$$

$$\left.\begin{aligned} \theta \sin a &= (0.3979 + \epsilon_1 - \epsilon_0) \sin \psi \\ \theta \cos a &= 0.3651\ (1 - \cos \psi) - \epsilon_1 + \epsilon_0 \end{aligned}\right\} , \qquad (165)$$

$$\psi = -17''.24 \sin N + 0''.21 \sin 2N - 1''.27 \sin 2L_\odot + 0''.13 \sin \ell_\odot$$
$$-0''.20 \sin 2L_\mathbb{C} + 0''.07 \sin \ell_\mathbb{C} + 0''.1379146\, t \ ,$$

and

$$\epsilon_1 - \epsilon_0 = 9''.21 \cos N - 0''.09 \cos 2N + 0''.55 \cos 2L_\odot + 0''.09 \cos 2L_\mathbb{C} - 0''.001281\, t \ .$$

Here, $\ell_\odot$, $\ell_\mathbb{C}$, $L_\odot$, and $L_\mathbb{C}$ are the mean anomalies and mean longitudes of the sun and the moon, respectively; t is the number of days from 1950.0; and N is the lunar ascending node referred to the ecliptic. We have

$$\left.\begin{aligned}
\frac{d(\theta \sin a)}{dt} &= 0.9175 \sin \psi \frac{d(\epsilon_1 - \epsilon_0)}{dt} + 0.3979 \cos \psi \frac{d\psi}{dt} \\
\frac{d(\theta \cos a)}{dt} &= -(0.1583 + 0.8418 \cos \psi) \frac{d(\epsilon_1 - \epsilon_0)}{dt} + 0.3651 \sin \psi \frac{d\psi}{dt}
\end{aligned}\right\} \quad (166)$$

and

$$\left.\begin{aligned}
\frac{d\psi}{dt} &= -17''.24\, \dot{N} \cos N + 0''.42\, \dot{N} \cos 2N - 2''.54\, n_\odot \cos 2L_\odot + 0''.13\, n_\odot \cos \ell_\odot \\
&\quad - 0''.40\, n_\leftmoon \cos 2L_\leftmoon + 0''.07\, n_\leftmoon \cos \ell_\leftmoon + 0''.1379146 \\
\frac{d(\epsilon_1 - \epsilon_0)}{dt} &= -9''.21\, \dot{N} \sin N + 0''.18\, \dot{N} \sin 2N - 1''.10\, n_\odot \sin 2L_\odot \\
&\quad - 0''.18\, n_\leftmoon \sin 2L_\leftmoon - 0''.001281
\end{aligned}\right\}, \quad (167)$$

where $\dot{N} = dN/dt$, $n_\odot$ is the mean motion of the sun, and $n_\leftmoon$ is the mean motion of the moon.

The effects of body tides on satellite motion have been developed. There remain to be included ocean and atmospheric tides. The former, expressed in spherical harmonics, are not yet very well known and so we give only a qualitative analysis. The M_2 tide has been studied by Pekeris and Accad (1969) and by Hendershott (1972). If we develop the tide in an earth-fixed system as

$$\zeta = \mathcal{R}e \sum_{\ell m} \mathcal{C}_{\ell m} \overline{P}_{\ell m} (\sin \phi)\, e^{i(m\lambda + \theta t)} , \quad (168)$$

then the tide will appear static in the inertial reference frame of the satellite. The external potential due to this tide, including the loading effect, is

$$\mathcal{U} = \mathcal{R}e \sum_{\ell m} \frac{(1 + k'_\ell)\, 4\pi G \rho_w a_e^{\ell + 2}}{(2\ell + 1)\, r^{\ell + 1}} \mathcal{C}_{\ell m} \overline{P}_{\ell m} (\sin \phi)\, e^{im\lambda} , \quad (169)$$

where k'_ℓ is the loading Love number (Munk and MacDonald, 1960) and ρ_w is the density of ocean water. This can be developed in terms of orbital elements along the lines of the tesseral harmonics; we have

$$\mathcal{U} = \sum_{\ell mp} \mathcal{U}_{\ell mp} \quad ,$$

in which

$$\mathcal{U}_{\ell mp} = \Gamma_{\ell m} \, (a_e^{\ell+2}/r^{\ell+1}) \, D_{\ell mp}(I) \, e^{i[(\ell-2p)(v+\omega) + m(\Omega - v' - \omega' - \Omega')]} \quad , \tag{170}$$

where

$$\Gamma_{\ell m} = 4\pi \, G \, \rho_w (1+k'_\ell) \, \overline{C}_{\ell m} / (2\ell+1) \quad . \tag{171}$$

We can develop equation (170) into perturbations, giving, for example,

$$\Delta\omega_{\ell mpqq'} = \mathcal{R}_e \, (i)^{\ell - m - 1} \, \Gamma_{\ell m} \, (a_e^{\ell+2}/n a^{\ell+3}) \, [D_{\ell mp}(I)/\dot{\psi}] \, X_q^{-\ell-1}(e)^{\ell-2p} \, X_{q'}^{0,m}(e')$$

$$\times [(\ell - 2p)\cos I - m] \, e^{i\psi} \quad , \tag{172}$$

where

$$\psi = qM + q'M' + (\ell - 2p)\omega + m(\Omega - \Omega' - \omega') \quad ,$$

$$\dot{\psi} = qn + q'n' + (\ell - 2p)\dot{\omega}' + m(\dot{\Omega} - \dot{\Omega}' - \dot{\omega}') \quad .$$

It is useful to note characteristics of lunar and solar perturbations in addition to the secular terms given in (161). The principal periodic terms from the moon have a 14-day period and an amplitude of about 120 m. The principal solar term is of 6-month period and about 800 m. The tidal effects are of the order of 10% of the direct effect, or about 15 m for the lunar tides. Therefore, it is essential to compute lunar effects when orbits are being determined for more than a few days. The solar effects can be absorbed in the orbital elements. There are also very

important long-period perturbations from the moon. Of greater difficulty in the treatment of long-period perturbations is the solar radiation pressure, which is yet to be satisfactorily computed (Section 11).

It is instructive to determine the ocean-tide equivalent of the body tide. We can do this only approximately. The correspondence is made by comparing the potentials in (158) and (172) for a particular ℓmp combination. We have

$$\mathcal{U}^{\text{body}}_{\ell mp} = \frac{GM'(-1)^{\ell+m}}{2\ell+1} \frac{k_\ell \, a_e^{\ell+1}}{r'^{\ell+1} \, r^{\ell+1}} D_{\ell mp}(I) \sum_{p'=0}^{\ell} D_{\ell(-m)p'}(I') \, e^{i\phi} \quad , \tag{173}$$

where

$$\phi = (\ell - 2p)(v+\omega) + (\ell - 2p')(v'+\omega') + m(\Omega - \Omega') \quad ;$$

and

$$\mathcal{U}^{M_2}_{\ell mp} = \frac{4\pi G \rho_\omega (1+k'_\ell)}{2\ell+1} \frac{a_e^{\ell+2}}{r^{\ell+1}} \overline{\mathcal{C}}_{\ell m} (i)^{\ell-m} D_{\ell mp}(I') \, e^{i\psi} \quad ,$$

where

$$\psi = (\ell - 2p)(v+\omega) - m(v'+\omega'+\Omega'-\Omega) \quad . \tag{174}$$

We note that the lunar inclination is $I' = 23° \pm 5°$ and that $D_{2,-2,0} \cong 0.925$, $D_{2,-2,1} \cong 0.160$, and $D_{2,-2,2} \cong 0.0036$. So for the principal semidiurnal term, we can take $\ell = 2$, $m = 2$, $\ell - 2p = 2$, $p = 0$, and $p' = 0$, giving

$$\frac{k_2}{1+k'_2} = \frac{4\pi G \rho_\omega \overline{\mathcal{C}}_{2,2}}{\mu n'^2 a_e \, D_{2,-2,0}(I')} \quad , \tag{175}$$

or

$$\overline{\mathcal{C}}_{2,2} = \frac{k_2}{1+k'_2} \frac{\mu n'^2 a_e \, D_{2,-2,0}(I')}{4\pi G \rho_\omega} \quad , \tag{176}$$

where k_2 would have a complex value. Using nominal values, we have

$$k_2 = 0.0114\, \overline{C}_{\ell m} / D_{2,-2,0}(I') \quad . \tag{177}$$

From K. Lambeck (1972, private communication), the Pekeris and Accad (1969) solution with dissipation gives

$$\overline{C}_{2,2} = 4.4\, e^{-i330\pi/180} = -2.19 - 3.81\, i \qquad \text{(cm)} \quad .$$

We then have $k_2^{ocean} = -0.026 - 0.047\, i$. Adding this to the body tide, we obtain the effective Love number that a satellite would sense. Choosing $k_2^{body} = 0.29$ with no dissipation, we have

$$k_2^{effective} = k_2^{body} + k_2^{ocean} = 0.264 - 0.047\, i \quad .$$

Therefore, a satellite would sense a Love number of 0.268 with a phase lag of 10.09 or 40 m. Conversely, by adopting a value for k_2^{body} and determining $k_2^{effective}$ from satellite observations, the height of the ocean tide could be calculated.

We have analyzed perturbations due to the $\overline{P}_{2,2}$ component of the ocean tide and note that they have the same dependence on the satellite inclination as does the body tide. Therefore, it is not possible to separate the second-degree body and ocean tide with satellite perturbation analysis. The ocean tides have a much richer spectrum in spherical harmonics than do the body tides (Hendershott, 1973). Selected terms of equation (168) are important, principally, $\overline{P}_{4,2}$ and $\overline{P}_{6,2}$. Although they result in orbital perturbations with the same frequency spectrum as does $\overline{P}_{2,2}$, the inclination dependence allows the determination of these coefficients by use of several satellites, in an analogous way to the geopotential.

Finally, we consider another effect of the earth's elasticity. The orbital system we have adopted is not precisely a system of the principal axis of inertia. Rather, we

use a mean pole. There is a free nutation of the earth called polar motion, which introduces the tesseral harmonics $\overline{C}_{\ell m} = \overline{C}_{\ell m} - i\,\overline{S}_{\ell m}$. There are two effects that to some extent cancel each other: The first is the motion of the axis of the principal moment of inertia; the second, the deformation due to the rotation about a moving axis. If we let ξ, η be the coordinates of the principal moments with respect to the mean pole and let ℓ_1, ℓ_2 be the coordinates of the instantaneous rotation axis, then we can write

$$\overline{C}_{2,1} = -\overline{C}_{2,0}\,\sqrt{3}\,(\xi - i\eta) - k_2\left(\omega_e^2\, a_e^3/\sqrt{15}\,GM\right)(\ell_1 - i\ell_2) \quad ,$$

where $\omega_e = \dot{\theta}$. This harmonic is a slowly varying function of time with a 14-month period. If we assume $\xi = \ell_1$, $\eta = \ell_2$ – that is, that we know where the principal axes are – then we have

$$\overline{C}_{2,1} = \left[-\overline{C}_{2,0}\,\sqrt{3} - k_2\left(\omega_e^2\, a_e^3/\sqrt{15}\,GM\right)\right](\xi - i\eta) \quad .$$

Using these values, we know

$$\overline{C}_{2,1} = (0.838 - k_2 \times 0.893)\,(\xi - i\eta) \quad ,$$

the elasticity reducing the effect by about 1/3. The perturbations for the seven retro-reflector satellites are all about 1 m.

10. HIGHER ORDER PERTURBATIONS DUE TO OBLATENESS; THE METHODS OF VON ZEIPEL AND LIE-HORI

Although a linear first-order approximation to the equations of motion proved adequate to obtain 1-m accuracy for the tesseral harmonics and the zonal harmonics excluding J_2 and J_3, we must have a more thorough treatment for the oblateness perturbations. Various solutions and formulas have been used (Brouwer, 1959; Kozai, 1959a, 1962a, 1966a; Gaposchkin, Cherniack, Briggs, and Benima, 1971; Izsak, 1963b; Aksnes, 1970), but only the last has proved completely satisfactory. Except for Kozai's (1959a), the methods depend on a canonical transformation. We sketch the basic ideas here. There are two equivalent approaches. The first, based on a device employed by Von Zeipel (1916) and known by his name, utilizes expansions in the form of Taylor series. It was introduced into the satellite problem by Brouwer (1959). The second, from a transformation due to Hori (1966), is based on expansions in Lie series and is known as the Lie-Hori method.

In both developments, we use canonical variables,

$$\begin{aligned} \ell &= M \quad , & L &= (\mu a)^{1/2} \quad , \\ g &= \omega \quad , & G &= L(1-e^2)^{1/2} \quad , \\ h &= \Omega \quad , & H &= G \cos I \quad . \end{aligned} \tag{178}$$

In the Aksnes theory, use is also made of the Hill variables introduced into satellite theory by Izsak (1963d):

$$r,\ v+\omega,\ h,\ \dot{r},\ G,\ H \quad . \tag{179}$$

In the mathematical problem we are discussing, the Hamiltonian is

$$\mathcal{H} = \frac{\mu^2}{2L^2} - \frac{\mu^4 J_2 a^2 e}{L^6} \left\{ \left[-\frac{1}{2} + \frac{3}{2}\left(\frac{H}{G}\right)^2 \right] \left(\frac{a}{r}\right)^3 + \left[\frac{3}{2} - \frac{3}{2}\left(\frac{H}{G}\right)^2 \right] \left(\frac{a}{r}\right)^3 \cos(2g + 2v) \right\} \quad . \tag{180}$$

Since t and h are both absent from $\mathcal{H}$, we therefore have immediately

$$H = G \cos I = \text{const} \quad , \tag{181}$$

and $\mathcal{H}$ = const from (5). We have limited this discussion to J_2, and all the developments mentioned above have carried the analysis to higher orders.

The method of Von Zeipel (1916) was proposed by Poincaré (1893). The latter showed that a transformation was always possible, but he was not convinced that the expansion would converge; Barrar (1970) has discussed this question further. The basic idea of the Von Zeipel method comes from (25). We look for a determining function $S(L', G', H', \ell, g, h) = F_2$ relating the new momenta and old coordinates, such that the new Hamiltonian $\mathcal{H}^*$ does not depend on ℓ; that is,

$$\mathcal{H}(L, G, H, \ell, g) = \mathcal{H}^*(L', G', H', g) \quad . \tag{182}$$

From (4), we then have

$$\begin{aligned} \ell' &= \partial S/\partial L' \quad , & L &= \partial S/\partial \ell \quad , \\ g' &= \partial S/\partial G' \quad , & G &= \partial S/\partial g \quad , \\ h' &= \partial S/\partial H' \quad , & H &= \partial S/\partial h \quad . \end{aligned} \tag{183}$$

Since this is a canonical transformation, we have

$$dL'/dt = \partial \mathcal{H}^*/\partial \ell' \quad , \qquad d\ell'/dt = -\partial \mathcal{H}^*/\partial L' \quad , \tag{184}$$

and four similar equations. Having solved this problem, we can perform a second transformation to eliminate g′ and obtain a third set of variables, L″, G″, H″, ℓ″, g″, h″, where the Hamiltonian is

$$\mathcal{H}^{**}(L'', G'', H'') = \mathcal{H}^*(L', G', H', g) \quad .$$

We proceed by expressing $\mathcal{H}$ and S in a Taylor series in terms of a small parameter α, which will be proportional to J_2:

$$\begin{aligned}
\mathcal{H} &= \mathcal{H}_0 + \alpha \mathcal{H}_1 \quad , \\
S &= S_0 + \alpha S_1 + \alpha^2 S_2 + \ldots \quad , \\
\mathcal{H}^* &= \mathcal{H}^*_2 + \alpha \mathcal{H}^*_1 + \alpha^2 \mathcal{H}^*_2 + \ldots \quad .
\end{aligned} \tag{185}$$

We want an identity transformation for $\alpha = 0$; therefore,

$$S_0 = L'\ell + G'g + H'h \quad . \tag{186}$$

We proceed by using expression (183) in (182) to give

$$\mathcal{H}_0\left(\frac{\partial S}{\partial L}\right) + \mathcal{H}_1\left(\frac{\partial S}{\partial \ell}, \frac{\partial S}{\partial g}, \frac{\partial S}{\partial h}, \ell, g\right) \equiv \mathcal{H}^*_0 + \mathcal{H}^*_1\left(L', G', H', \frac{\partial S}{\partial G'}\right) \quad . \tag{187}$$

If we expand (187) into a Taylor series and equate equal powers of α, we have

$$\begin{aligned}
&\mathcal{H}_0(L') = \mathcal{H}^*_0(L') = \frac{\mu^2}{2L'^2} \quad , \\
&\frac{\partial \mathcal{H}_0}{\partial L'}\frac{\partial S_1}{\partial \ell} + \mathcal{H}_1 = \mathcal{H}^*_1 \quad , \\
&\frac{\partial \mathcal{H}_0}{\partial L'}\frac{\partial S_2}{\partial \ell} + \frac{1}{2}\frac{\partial^2 \mathcal{H}_0}{\partial L'^2}\left(\frac{\partial S_1}{\partial \ell}\right)^2 + \frac{\partial \mathcal{H}_1}{\partial L'}\frac{\partial S_1}{\partial \ell} + \frac{\partial \mathcal{H}_1}{\partial G'}\frac{\partial S_1}{\partial g} = \mathcal{H}^*_2 + \frac{\partial \mathcal{H}^*_1}{\partial g}\frac{\partial S_1}{\partial G} \quad .
\end{aligned} \tag{188}$$

Kozai (1962a) correctly gives the third-order expression.

We now separate $\mathcal{H}_1$ into a part independent of ℓ (called $\mathcal{H}_{1\,\mathrm{sec}}$) and a part dependent on ℓ (called $\mathcal{H}_{1\,\mathrm{p}}$) and then make the association

$$\frac{\partial \mathcal{H}_0}{\partial L'} \frac{\partial S_1}{\partial \ell} + \mathcal{H}_{1p} = 0 \quad ,$$

$$\mathcal{H}_{1\,sec} = \mathcal{H}_1^* \quad . \tag{189}$$

The expression for S_1 obtained from (189) can be used in the last line of equation (188), again separating parts dependent on ℓ or not. We obtain a solution for S_2, and so on. Through equations (183), we obtain

$$\ell' = \ell'(L', G', H', \ell, g) \quad , \qquad L = L(L', G', H', \ell, g) \quad ,$$

and four similar expressions for g', h', L, H. These expressions must be inverted to obtain

$$\ell = \ell(L', G', H', \ell', g') \quad , \qquad L = L(L', G', H', \ell', g') \quad , \tag{190}$$

which is accomplished by Taylor expansion to the desired order and is very tedious.

The Lie-Hori method is developed along somewhat different lines. Hori (1966) considered a transformation from p, q to P, Q given by

$$p_i = P_i + \frac{\partial S}{\partial Q_i} + \frac{1}{2}\left[\frac{\partial S}{\partial Q_i}, S\right] + \cdots \quad ,$$

$$q_i = Q_i - \frac{\partial S}{\partial P_i} - \frac{1}{2}\left[\frac{\partial S}{\partial P_i}, S\right] + \cdots \quad , \tag{191}$$

where $[a, b]$ are Poisson brackets. In this notation, any function can be written

$$f(p, q) = f(P, Q) + [f, S] + \frac{1}{2}\left[[f, S], S\right] + \cdots \quad . \tag{192}$$

The canonical equations are

$$dP/dt = \partial \mathcal{H}^*/\partial Q_i \quad , \qquad dQ_i/dt = -\partial \mathcal{H}^*/\partial P_i \quad . \tag{193}$$

We further assume that S and $\mathcal{H}$ can be written in terms of a small parameter

$$S = S_1 + S_2 + \cdots ,$$
$$\mathcal{H}^* = \mathcal{H}_2^* + \mathcal{H}_1^* + \cdots . \tag{194}$$

If a parameter τ defined by

$$dP/d\tau = \partial \mathcal{H}_0/\partial Q_i , \qquad dQ_i/d\tau = -\partial \mathcal{H}_0/\partial P_i \tag{195}$$

is eliminated from $\mathcal{H}^*$, we have

$$\mathcal{H}_0^* = \text{const} ,$$
$$\mathcal{H} = \text{const} . \tag{196}$$

This development led Hori to the following formulas:

$$\mathcal{H}_0^* = \mathcal{H}_0 ,$$
$$\mathcal{H}_1^* = \mathcal{H}_{1\,\text{sec}} ,$$
$$S_1 = \int \mathcal{H}_{1\,p}\, d\tau , \tag{197}$$
$$\mathcal{H}_2^* = \mathcal{H}_{2\,\text{sec}} + \frac{1}{2}\left[\mathcal{H}_1 + \mathcal{H}_1^*, S_1\right]_{\text{sec}} ,$$
$$S_2 = \int \left(\mathcal{H}_{2\,p} + \frac{1}{2}\left[\mathcal{H}_1 + \mathcal{H}_1^*, S_1\right]_p\right) d\tau .$$

Here we designate the subscripts sec and p to mean the parts independent of and dependent on ℓ, respectively, as in the Von Zeipel method. These formulas are given by Aksnes (1970).

The Lie-Hori method has a number of advantages. The transformation is completely in terms of the new variables, and no inversion of series is necessary. The formulas are all canonically invariant, so they hold for any canonical variables. Aksnes could then make two fundamental advances in the treatment of oblateness perturbations. First, he chose as an intermediate orbit a precessing ellipse that incorporated all the first-order secular terms and most of the periodic terms. That is to say, in the analogous process of finding (32), he discovered another solution, q^0, p^0, that included a part of the disturbing function instead of a Kepler ellipse. Second, with a canonically invariant formulation, he employed appropriate variables. For long-period and secular effects, Delaunay variables were used. The results agree with the Von Zeipel method. For short-period perturbations, Hill variables were used, a procedure that eliminates the difficulty with small eccentricities.

The first-order determining functions for the Lie-Hori and the Von Zeipel methods are the same, as can be seen by comparing the defining equations or the results (Kozai, 1962a; Aksnes, 1970). In fact, this must be so because both formulations work for Delaunay variables and have been shown to be equivalent. Therefore, the first-order perturbations are the same.

Space does not permit us to give a more detailed account of this beautiful theory or the detailed formulas, for which we refer the reader to Aksnes (1970).

We summarize the status of oblateness perturbations:

A. Two complete second-order developments, one by the Von Zeipel method (Kozai, 1962a; verified by Gaposchkin et al., 1971) and the other by the Lie-Hori method, have been compared. For short-periodic perturbations, the agreement is 10 cm. The secular rates predicted by the two theories can be reconciled to within their given accuracy (Aksnes, 1972).

B. The second-order development of Aksnes has the advantages of compactness and efficiency of computation, and no singularity for small eccentricity. The small-eccentricity problem is avoided by the use of Hill variables.

C. For long-period and secular perturbations to 10 cm, further work is necessary. Terms in $J_2 J_3$, $J_2 J_4$, etc. must be included, as well as interaction with all other forces – lunar and solar effects, tesseral harmonics, drag, and radiation pressure.

We cannot give the complete set of formulas, but we present the first-order periodic and second-order secular perturbations as developed by Aksnes (1970), although we have dropped the primes:

$$\Delta\dot{r} = (-\gamma G^3/2\mu r^2)\left[s^2 \sin 2u - \frac{1}{8} D\, s^2\, e \sin(2u - v)\right] ,$$

$$\Delta r = (\gamma G^2/4\mu)\left[1 - 3c^2 + s^2 \cos 2u - \frac{1}{4} D\, s^2\, e \cos(2u - v)\right] ,$$

$$\Delta G = (\gamma G/4)\left[3s^2\, e \cos(2u - v) + s^2\, e \cos(2u + v) - \frac{1}{4} D\, s^2\, e^2 \cos(2u - 2v)\right] ,$$

$$\Delta u = (-\gamma/4)\left\{(2 - 12c^2)\, e \sin v - \frac{1}{8}(4 + De^2)\, s^2 \sin 2u - (2 - 5c^2 + \frac{1}{2} D s^2) \times e \sin(2u - v) + c^2\, e \sin(2u + v) - \frac{1}{4}\,[D - D^{(1)} s^2]\; c^2 e^2 \sin(2u - 2v)\right\} ,$$

$$\Delta h = (-\gamma c/4)\left\{6e \sin v - 3e \sin(2u - v) - e \sin(2u + v) + \frac{1}{4}[D - D^{(1)} s^2] e^2 \sin(2u - v)\right\} ,$$

where

$$D = (1 - 15\, c^2)/(1 - 5c^2) ,$$

$$D^{(1)} = \partial D/\partial c^2 ,$$

and

$$c = \cos I , \qquad s = \sin I , \qquad \gamma = J_2/a^2 \eta^4 , \qquad \eta^2 = 1 - e^2 .$$

The secular rates can be obtained from letting

$$g_{21} = -\frac{3}{4}\,\gamma\,(1 - 5c^2) - \frac{1}{64}\,\gamma^2\,(41 + 30c^2 - 135c^4) ,$$

$$g_{32} = -\frac{3}{16}\, c\, [8\gamma + \gamma^2 (7 - 33c^2)] ,$$

with

$$\gamma_4 = J_4/J_2^2 \quad ,$$

$$\dot{M} = n + \frac{3}{128} n \gamma^2 \eta \left[8(1 - 6c^2 + 5c^4) - 5(5 - 18c^2 + 5c^4)e^2 \right.$$
$$\left. - 15 \gamma_4 (3 - 30c^2 + 35c^4)e^2\right] \quad ,$$

$$\dot{\omega} = \dot{g} + g_{21}(\dot{g} + \dot{M})$$

$$= -\frac{1}{128} n \gamma^2 \left[44 - 300c^4 + (75 - 378c^2 + 135c^4)e^2 + 60 \gamma_4 (3 - 36c^2 + 49c^4) \right.$$
$$\left. + 135 \gamma_4 (1 - 14c^2 + 21c^4)e^2\right] \quad ,$$

$$\dot{\Omega} = \dot{h} + g_{32}(\dot{\omega} + \dot{M}) \quad ,$$

$$\dot{h} = \frac{3}{32} nc\gamma^2 \left[2 - 10c^2 - (9 - 5c^2)e^2 - 5\gamma_4 (3 - 7c^2)(2 + 3e^2)\right] \quad .$$

As discussed in Section 7, periodic perturbations for J_2 were developed by using computer algebra. The expressions were employed in orbit computation, and the orbital fits were identical. This agreement validates both sets of formulas since they are based on quite different methods. The mean elements in the two developments are different by factors of order J_2. Aksnes (1970) has given the formulas relating the two theories and a numerical verification. If we let a subscript 0 designate the Von Zeipel element, then the elements of a, e, I are related by

$$1/a = (1/a_0)\left\{1 - \frac{1}{2}\eta_0 \gamma_0 (1 - 3\cos^2 I_0) + \frac{1}{32}\eta_0 \gamma_0^2 \left[1 + 6\eta_0 - (6 + 36\eta_0)\cos^2 I_0 \right.\right.$$
$$\left.\left. + (45 + 54\eta_0)\cos^4 I_0\right] + \ldots\right\} ,$$

$$G = G_0 \left[1 + \frac{1}{4}\gamma_0 (1 - 3\cos^2 I_0)\right] + \ldots \quad ,$$

$$\cos I = \cos I_0 = \left[1 + \frac{3}{4}\gamma_0 (1 - \cos^2 I_0)\right] + \ldots \quad ,$$

$$\eta^2 = 1 - e^2 \quad , \qquad G^2 = \eta^2 \mu a \quad , \qquad \gamma = J_2/a^2\eta^4 \quad .$$

11. ATMOSPHERIC DRAG AND RADIATION PRESSURE

For several reasons, atmospheric drag and radiation pressure are treated by different methods than are gravitational perturbations. First, they are not conservative forces derivable from a potential function. Second, they involve considerably more unknowns. Whereas the geopotential may be considered unknown and require improvement, we can assume that the main field is constant in time, that tidal variations are known, and that the geopotential has a known mathematical and physical form. Similarly, for lunar and solar perturbations, we assume sufficient knowledge of the mass and position of the moon and the sun. With drag and radiation pressure, we are in a much less favorable position. In drag perturbations, the atmospheric density is critical; it has been studied extensively from its orbital effects. The parameters controlling density variations are becoming known, and one can probably predict a posteriori the mean-density structure to within a factor of 2. However, the satellite aspect and the drag coefficient must also be known. Radiation-pressure effects involve similar problems: What is the value of the solar constant and is it constant? How much is diffuse and how much specular reflection? How do the reflective properties change with time? How variable is the albedo radiation? How does the satellite aspect change? And how is the boundary of the earth's shadow defined? For some satellites, this information is available, though difficult to obtain. Some of these questions are subjects of current research.

The following treatment of radiation pressure developed by Kozai (1963c) and extended by Lála (1968, 1971) and Lála and Sehnal (1969) assumes, for one revolution, the following:

A. The satellite is spherical, with constant reflective properties.
B. The solar parallax can be neglected.
C. The solar flux is constant.
D. There is no albedo radiation.

The natural vehicle for treating forces directly is the Lagrange planetary equations in gaussian form (96). The forces are expressed as

$$\begin{aligned} S &= n^2 a^3 \, F \, S(v) \quad , \\ T &= n^2 a^3 \, F \, T(v) \quad , \\ W &= n^2 a^3 \, F \, W \quad , \end{aligned} \tag{198}$$

where

$$F = (A/M)\,(K/GM) \approx 0.5 \times 10^{-4}\,(A/M) \quad ,$$

with A/M in $cm^2\, g^{-1}$. We have

$$\begin{aligned} S(v) = &- \cos^2(I/2)\cos^2(\epsilon/2)\cos(\lambda_\odot - L - \Omega) - \sin^2(I/2)\sin^2(\epsilon/2)\cos(\lambda_\odot + \Omega - L) \\ &- \tfrac{1}{2}\sin I \sin\epsilon\left[\cos(\lambda_\odot - L) - \cos(-\lambda_\odot - L)\right] - \sin^2(I/2)\cos^2(\epsilon/2)\cos(\Omega - \lambda_\odot - L) \\ &- \cos^2(I/2)\sin^2(\epsilon/2)\cos(-\lambda_\odot - L - \Omega) \quad , \end{aligned} \tag{199}$$

$$\begin{aligned} T(v) = &- \cos^2(I/2)\cos^2(\epsilon/2)\sin(\lambda_\odot - L - \Omega) - \sin^2(I/2)\cos^2(\epsilon/2)\sin(\lambda_\odot + \Omega - L) \\ &- \tfrac{1}{2}\sin I \sin\epsilon\left[\sin(\lambda_\odot - L) - \sin(-\lambda_\odot - L)\right] - \sin^2(I/2)\cos^2(\epsilon/2)\sin(\Omega - \lambda_\odot - L) \\ &- \cos^2(I/2)\sin^2(\epsilon/2)\sin(-\lambda_\odot - L - \Omega) \quad , \end{aligned} \tag{200}$$

$$W = \sin I \cos^2(\epsilon/2)\sin(\lambda_\odot - \Omega) - \sin I \sin^2(\epsilon/2)\sin(\lambda_\odot + \Omega) - \cos I \sin\epsilon \sin\lambda_\odot \quad , \tag{201}$$

where

$$L = v + \omega \quad ,$$

$\lambda_{\odot}$ = the longitude of the sun ,

ϵ = the obliquity .

We have the LPE

$$\frac{da}{dt} = \frac{2na^3}{(1-e^2)^{1/2}} F \left[S(v)\, e \sin v + T(v) \frac{p}{r}\right] ,$$

$$\frac{de}{dt} = na^2 (1-e^2)^{1/2} F \left\{S(v) \sin v + T(v) \left[\cos v + \frac{1}{e}\left(1 - \frac{r}{a}\right)\right]\right\} ,$$

$$\frac{dI}{dt} = \frac{na^2}{(1-e^2)^{1/2}} W F \frac{a}{r} \cos L ,$$

(202)

$$\sin I \frac{d\Omega}{dt} = \frac{na^2}{(1-e^2)^{1/2}} W F \frac{r}{a} \sin L ,$$

$$\frac{d\omega}{dt} = -\cos I \frac{d\Omega}{dt} + na^2 \frac{(1-e^2)^{1/2}}{e} F \left[-S(v) \cos v + T(v) \left(1 + \frac{r}{p}\right) \sin v\right] ,$$

$$\frac{dM}{dt} = n - 2a^2 F S(v) \frac{r}{a} n - (1-e^2)^{1/2} \left(\frac{d\omega}{dt} + \cos I \frac{d\Omega}{dt}\right) ,$$

$$p = a(1-e^2) .$$

Since radiation pressure is a discontinuous force, it is difficult to obtain analytical solutions for it. Two approaches have been used successfully. The first, by Kozai (1963c), is to determine numerically the time of shadow exit E_1 and shadow entry E_2 in terms of the eccentric anomaly. Then, by assuming everything else constant for one revolution, Kozai obtains the following first-order perturbations after one revolution, where $S = S(0)$, $T = T(0)$ are written for their values at $L = \omega$:

$$\delta a = 2a^3 F \left[S \cos E - T (1-e^2)^{1/2} \sin E \right]_{E_1}^{E_2} ,$$

$$\delta e = a^2 F (1-e^2)^{1/2} \left[\frac{1}{4} S (1-e^2)^{1/2} \cos 2E + T \left(-2e \sin E + \frac{1}{4} \sin 2E \right) \Big|_{E_1}^{E_2} + \frac{3}{2} \int T \, dE \right] ,$$

$$\delta I = a^2 F \frac{W}{(1-e^2)^{1/2}} \left\{ \left[(1+e^2) \sin E - \frac{e}{4} \sin 2E \right] \cos \omega \right.$$

$$\left. + (1-e^2)^{1/2} \left(\cos E - \frac{e}{4} \cos 2E \right) \sin \omega \Big|_{E_1}^{E_2} - \frac{3}{2} e \int \cos \omega \, dE \right\} ,$$

$$\sin I \, \delta\Omega = a^2 F \frac{W}{(1-e^2)^{1/2}} \left\{ \left[(1+e^2) \sin E - \frac{e}{4} \sin 2E \right] \sin \omega \right.$$

$$\left. - (1-e^2)^{1/2} \left(\cos E - \frac{e}{4} \cos 2E \right) \cos \omega \Big|_{E_1}^{E_2} - \frac{3}{2} e \int \sin \omega \, dE \right\} , \qquad (203)$$

$$\delta\omega = - \cos I \, \delta\Omega + a^2 F \frac{(1-e^2)^{1/2}}{e} \left[S \left(e \sin E + \frac{1}{4} \sin 2E \right) \right.$$

$$\left. + \frac{T}{(1-e^2)^{1/2}} \left(e \cos E - \frac{1}{4} \cos 2E \right) \Big|_{E_1}^{E_2} - \frac{3}{2} \int S \, dE \right] ,$$

$$\delta M = - \frac{3}{2} \int_0^{2\pi} \frac{\delta a}{a} \, dM - (1-e^2)^{1/2} \delta\omega - (1-e^2)^{1/2} \cos I \, \delta\Omega$$

$$- 2a^2 F \left\{ S \left[(1+e^2) \sin E - \frac{e}{4} \sin 2E \right] - T (1-e^2)^{1/2} \left(\cos E - \frac{e}{4} \cos 2E \right) \Big|_{E_1}^{E_2} \right.$$

$$\left. - \frac{3}{2} e \int S \, dE \right\} .$$

If the satellite does not enter the shadow, then the terms evaluated at E_1 and E_2 vanish. How the perturbations after part of a revolution can be computed is obvious. These expressions provide the differential equations to be integrated for mean elements – that is, $d\bar{a}/dt = \delta a/\delta t = n \, \delta a$, and so on. This is the method used to calculate the long-term effects due to radiation pressure in the determination of zonal harmonics and tidal

parameters. In addition, one can determine quite reasonable mean reflectivities for the satellites.

An alternative approach was taken by Lála (1968, 1971) and Lála and Sehnal (1969). They developed the shadow function in Fourier series in E and found solutions for the periodic perturbations. They required 36 terms in the development to obtain agreement with the above special perturbation formulas. These periodic perturbations were formally integrated. For further details, the reader is referred to the Lala and Sehnal papers.

The development of drag perturbations by Sterne (1959) follows the same lines. Assuming a rotating atmosphere with an oblate planet, he considers the drag force per unit mass

$$\frac{1}{2} C_D \frac{A}{M} \rho V^2 \quad , \tag{204}$$

where C_D is a drag coefficient, A/M is the area-to-mass ratio, ρ is the atmospheric density, and V is the satellite velocity with respect to the atmosphere. Now, C_D, A/M, and ρ are all difficult to know. Sterne adopts $C_D \approx 2.2$. If precise values of A/M are not known, then the average A is taken as one-fourth the total surface area. He then gives the forces acting on the satellite as

$$\begin{bmatrix} S \\ T \\ W \end{bmatrix} = \begin{bmatrix} \ddot{r} \\ r\dot{v} - \dot{\theta} r \cos I \\ \dot{\theta} r \sin I \cos (v + \omega) \end{bmatrix} \quad . \tag{205}$$

After some calculations, the velocity is given by

$$V = \left(\frac{\mu}{a}\right)^{1/2} \left(\frac{1+e \cos E}{1-e \cos E}\right)^{1/2} \left(1 - d \frac{1-e \cos E}{1+e \cos E}\right) \quad , \tag{206}$$

where

$$d = \frac{\dot{\theta}}{n} (1-e^2)^{1/2} \cos I \quad , \tag{207}$$

and the forces per unit mass are

$$\begin{bmatrix} S \\ T \\ W \end{bmatrix} = \frac{1}{2} C_D \frac{A}{M} \rho a V \begin{Bmatrix} e \sin E \, \dot{E} \\ -(1-e^2)^{1/2} \left[1 - d \frac{(1-e\cos E)^2}{1-e^2}\right] \dot{E} \\ -\frac{\dot{\theta}}{n} (1-e\cos E)^2 \sin I \cos(v+\omega) \dot{E} \end{Bmatrix} . \qquad (208)$$

With these equations, the LPE can be integrated numerically. Alternatively, if we can specify how C_D, A/M, and ρ vary, we could attempt a formal solution. We make the analogous solution to that for radiation pressure, assuming C_D and A/M constant, and obtain formal quadrature formulas for the perturbations after one revolution. We have

$$\delta a = - C_D \frac{A}{M} a^2 \int_0^{2\pi} \rho(E) \frac{(1+e\cos E)^{3/2}}{(1-e\cos E)^{1/2}} \left(1 - d \frac{1-e\cos E}{1+e\cos E}\right)^2 dE \quad ,$$

$$\delta e = - C_D \frac{A}{M} \frac{(1-e^2)^{1/2} a}{2\pi} \int_0^{2\pi} \rho(E) \left(\frac{1+e\cos E}{1-e\cos E}\right)^{1/2} \left(1 - d \frac{1-e\cos E}{1+e\cos E}\right)$$

$$\times \left[\cos E - \frac{d}{2(1-e^2)} (1-e\cos E)(2\cos E - e - e\cos^2 E)\right] dE \quad ,$$

$$\delta I = - \frac{1}{8\pi} C_D \frac{A}{M} \frac{a}{n} \dot{\theta} \sin I \frac{1}{(1-e^2)^{1/2}} \int_0^{2\pi} \rho(E) (1-e\cos E)^{1/2} (1+e\cos E)^{1/2}$$

$$\times \left(1 - d \frac{1-e\cos E}{1+e\cos E}\right) \left[1 + \cos 2\omega \frac{(2-e^2)\cos^2 E - 1 + 2e^2 - 2e\cos E}{(1-e\cos E)^2}\right] dE \quad , \qquad (209)$$

$$\delta\Omega = - \frac{1}{8\pi} C_D \frac{A}{M} \frac{a}{n} \frac{\dot{\theta} \sin 2\omega}{(1-e^2)^{1/2}} \int_0^{2\pi} \rho(E) (1-e^2\cos^2 E)^{1/2} \left(1 - d \frac{1-e\cos E}{1+e\cos E}\right)$$

$$\times \left[2e^2 - 1 - 2e\cos E + (2-e^2)\cos^2 E\right] dE \quad ,$$

$$\delta\omega = - \cos I \, \delta\Omega \quad ,$$

$$\delta M = - (1-e^2)^{1/2} d\omega + \int \delta n \, dt \quad .$$

We see from the last two expressions of (209) that the direct perturbation in $M + \omega$ is quite small, the major change in M coming from

$$\delta n = (-3n/2a)\ \delta a \quad .$$

These expressions are used with numerical quadrature to obtain the evolution of mean elements. The implementation is done by Slowey (1973) for studying drag. Alternatively, taking Jacchia's (1960, 1964) density model, Sehnal and Mills (1966) have developed ρ in harmonic functions and obtained formulas for the periodic terms. These are sometimes used in analyses of satellite orbits. However, since for geodetic satellites the short-period drag terms are always less than 1 m, we can ignore them. The secular part is more conveniently absorbed in some constants of our orbital model. Therefore, the principal use of these formulas is in the analysis of long-period effects by numerical integration of these mean elements, along the same lines as those used for radiation pressure. In this case, we are able to make a reliable determination of drag factors, which could be systematic errors in the density model, or an estimate of C_D or A/M. These factors are generally between 0.5 and 1.5, which is less than the uncertainty of these parameters.

12. COMPUTER ALGEBRA

A great deal of the analysis used for satellite-perturbation theory involves considerable tedious algebra. One is led to do some of this work on a computer. A major support of the development of analytical theories has been the computer program Smithsonian Package for Algebra and Symbolic Manipulation (SPASM), described by Hall and Cherniack (1969), and Cherniack (1973) has contrasted it with other algebra systems. Since the subject of computer algebra is beyond the scope of this article, we confine ourselves to a few remarks and the description of two problems in satellite theory.

Algebra programs perform the elementary operations of addition, multiplication, subtraction, division, differentiation, and integration of a certain class of functions. We can define functions, make substitutions, and truncate on powers of designated parameters. We can traverse expressions term by term and parenthesize and expand them. Numerical coefficients are kept as rational numbers where possible. One can read expressions in, print them out, or punch them as FORTRAN cards for subsequent numerical computation. We have two forms of internal representation – expressions and Poisson series. Each has its advantages. An expression may be

```
(ETA**2 - R)/E   .
```

The Poisson series are of the form

$$\sum A_i \begin{pmatrix} \sin \\ \cos \end{pmatrix} B_i \quad ,$$

where A_i and B_i are any expressions. All the operations described apply to both expressions and Poisson series.

Poisson series have three advantages:

A. All trigonometric identities are automatically applied.

B. Because of the highly structured nature of Poisson series, multiplication and addition can be optimized. Further, we can use secondary computer storage for long Poisson series.

C. The bulk of problems in celestial mechanics is solved by developing the disturbing function in Poisson series and integrating term by term.

In addition to the operations described above, we can convert from expressions to Poisson series, and then back. Great efficiency is gained by judiciously choosing the form. Consider

$$(\cos^{20} x)^{30} - (\cos^{30} x)^{20} \quad .$$

As a trigonometric polynomial, this operation is trivial; as a Poisson series, it is not. We have here two very important features of computer algebra: the non-commutativity of operations with respect to time, and intermediate swell. The above expression is obviously zero, but one has two 50-term Poisson series along the way. Neither of these problems occurs in numerical work.

SPASM is 99% in FORTRAN; storage management is accomplished with SLIP, which is accessible from FORTRAN programs. We are concerned with the efficiency of SPASM and with the size and speed of the FORTRAN code generated. These are part of the more general problem of expression simplification.

Although general simplification seems to be very difficult, we have had some success with the following approach. We assume that the coefficients of Poisson series can be factored as the product of polynomials. Further, we want to consider the choice of variables. In developing perturbation theories, we convert to Poisson series all angle variables except the inclination. Therefore, we have the side relations

$$\eta^2 + e^2 = 1 \quad ,$$
$$SI^2 + CI^2 = SIP^2 + CIP^2 = 1 \quad ,$$

where we have substituted SI for sin (I), CI for cos (I), SIP for sin (IP), and CIP for cos (IP). The P designates the primed variables – in this case, the elements of the disturbing body (see Section 9). We try each substitution, as indicated. It would be more direct to convert each coefficient of the Poisson series to a Poisson series, using $e = \sin \phi$, $\eta = \cos \phi$, in order to obtain all simplifications, and then to convert

back to an expression. However, the substitution and the test for length of expression are easily done. We retain the expression that has the fewest terms and remove all common factors. Next, we assume that the remaining expression can be written

$$f\binom{e\ \ SI\ \ eP\ \ SIP}{\eta,\ CI,\ \eta P,\ CIP} = P_e\binom{e}{\eta}\, P_I\binom{SI}{CI}\, P_{e'}\binom{eP}{\eta P}\, P_{I'}\binom{SIP}{CIP} \quad ,$$

where P_i is just a polynomial. In turn, by setting all the variables but one equal to zero, we obtain each polynomial. The results of factorization are then verified by expanding and subtracting. We have found that in this way we obtain all the simplifications that would have been obtained by hand.

SPASM has been used for a wide variety of problems. We describe here two of particular relevance to satellite theory: development of oblateness perturbations in Delaunay variables by the method of Von Zeipel, and third-body perturbations in Kepler elements by use of LPE.

Von Zeipel's method is described in Section 10. Two features can be pointed out. First, once the determining function S is known, the perturbations are obtained by differentiation. Second, the first- and second-order determining functions can be obtained in closed form, as was done by Kozai (1962a) by a change of variable using

$$dv = (1/\eta^3)\,(a/r)^3\, d\ell \quad .$$

Both these operations are within the scope of SPASM, and the problem proved tractable.

The necessity of an accurate theory for J_2 was discussed in Section 10. The development by Kozai (1962a) had been used, but with such complication that further verification was necessary. The details of the work are recounted in Gaposchkin et al. (1971). The important results are the following:

A. The problem proved tractable with an algebra program.

B. The determining function of Kozai (1962a) has been verified, and the problem solved to second order.

C. The accuracy of the theory and the inversion have been verified against numerical integration. The inversion was checked by use of the numerical inverse from (190).

D. The difficulty with the small eccentricity remains. The third-order periodic perturbations were developed and were shown to contain 1/e terms. Numerical tests indicate $1/e^2$ terms in the fourth order. We conclude that this is due to the Delaunay variables we had selected.

E. The development of computer algebra enabled us to obtain the third-order perturbations in 3 weeks; we would probably not have attempted it by hand.

F. The perturbation theory was used in the orbit-computation program. The theory of Aksnes (1970) (see Section 10) was also used; it gave identical results for orbital position, thus verifying both developments.

The second problem attempted is the perturbation due to a third body. In this case, we start with equation (155) (Section 9 analytically develops that expression). Using the algebra program, we now determine $1/\Delta$ by analytical inversion. The basic idea, due to Broucke (1971), allows the inversion of invertible expressions; that is,

$$(E)^{-a/b} = Z \quad .$$

An iterative scheme is developed, with each iterant

$$Z_{n+1} - Z_n = \Delta Z_n = -\frac{a}{b}\left(E\, Z_n^{b/a} - 1\right) Z_n \quad .$$

This is enormously powerful. Since we can invert any expression without division, it is applicable to computers without a divide instruction. In the case of lunar perturbations, we have a/b = 1/2, where

$$E = (\overline{X} - \overline{Y}) \cdot (\overline{X} - \overline{Y}) \quad .$$

Here, $\overline{X}$ is the position of the satellite, and $\overline{Y}$ is the position of the moon. We have

$$\overline{X} = r \begin{bmatrix} \cos u \cos \Omega - \sin u \sin \Omega \cos I \\ \cos u \sin \Omega + \sin u \cos \Omega \cos I \\ \sin u \sin I \end{bmatrix} \quad .$$

A similar expression for Y uses r′, u′, Ω′, I′. With this expression, we perform the analytical inversion, starting with $Z_0 = 1/r'$ and truncating on r^3. We have a simple check: The r/r'^2 are all canceled by the $(X \cdot Y)/|Y|^3$ term. The effects of body tides are easily introduced at this point by the substitution

$$r^n \rightarrow r^n + k_n \frac{a_e^{2n+1}}{r^{n+1}} \quad .$$

Next, the expressions are expanded with use of Hansen coefficients as described in Section 7. The resulting expressions are then put in the LPE and integrated on the assumption that the angular variables, except the inclinations, have a linear change with time. The resulting expressions are simplified as described above. Figures 4a and 4b give the first part of the SPASM printed output and the FORTRAN program for calculating the perturbation in I.

In conclusion, we can say that computer algebra has been a successful tool for satellite-dynamics problems. It balances efficiency and expediency. The lunar perturbations were being used in the orbit computation program a month after the work started with SPASM, and we developed the third-order perturbation due to J_2 in 3 weeks. We can develop even more efficient programs by careful analysis (cf. formulas of Kozai (1962a) and Aksnes (1970)).

```
(45/32*CI*E**2/ETA*SI*SIP**2)/(-2*WPD+2*WD-2*MPD)                                   COS  (2*WP-2*W+2*MP)

845/48*EP**3*(15/16*CI/ETA*SIP*(1+KAPA)-9/16*CI*ETA*SIP*(1+KAPA)+15/16*CI*CIP       COS  (2*WP+OP-O+5*MP)
/ETA*SIP*(1+KAPA)-9/16*CI*CIP*ETA*SIP*(1+KAPA))/(-2*WPD-OPD+OD-5*MPD)

845/48*EP**3*(15/32/ETA*SI*(1+KAPA)-9/32*ETA*SI*(1+KAPA)-15/16*CIP/ETA*SI*(1       COS  (2*WP-2*OP+2*O+5*MP)
+KAPA)+9/16*CIP*ETA*SI*(1+KAPA)+15/32*CIP**2/ETA*SI*(1+KAPA)-9/32*CIP**2*ETA*SI
*(1+KAPA))/(-2*WPD+2*OPD-2*OD-5*MPD)

-15/32*E**2/ETA*SI*SIP**2*(1-CI)/(-2*WD-2*OPD+2*OD)                                 COS  (2*W+2*OP-2*O)

-15/16*CIP*E**4/ETA*SIP*(1-CI-2*CI**2)/(-2*WD+OPD-OD)                               COS  (2*W-OP+O)

1/(-2*WP+2*W-MP)*(-45/64*CI*E**2*EP/ETA*SI*SIP**2)                                  COS  (2*WP-2*W+MP)

845/48*EP**3*(-15/32/ETA*SI*(1+KAPA)+9/32*ETA*SI*(1+KAPA)-15/16*CIP/ETA*SI*(1       COS  (2*WP+2*OP-2*O+5*MP)
+KAPA)+9/16*CIP*ETA*SI*(1+KAPA)-15/32*CIP**2/ETA*SI*(1+KAPA)+9/32*CIP**2*ETA*SI
*(1+KAPA))/(-2*WPD-2*OPD+2*OD-5*MPD)

845/48*EP**3*(15/16*CI/ETA*SIP*(1+KAPA)-9/16*CI*ETA*SIP*(1+KAPA)-15/16*CI*CIP      COS  (2*WP-OP+O+5*MP)
/ETA*SIP*(1+KAPA)+9/16*CI*CIP*ETA*SIP*(1+KAPA))/(-2*WPD+OPD-OD-5*MPD)

17/2*EP**4*(15/16*CI/ETA*SIP*(1+KAPA)-9/16*CI*ETA*SIP*(1+KAPA)+15/16*CI*CIP        COS  (2*WP+OP-O+4*MP)
/ETA*SIP*(1+KAPA)-9/16*CI*CIP*ETA*SIP*(1+KAPA))/(-2*WPD-OPD+OD-4*MPD)
```

Figure 4a. Part of SPASM output for the perturbation in I.

```
      T(  1) = 1.-CIP
      T(  2) = 1.+CI
      C1     = 2.
      C2     = 2.
      C3     = -2.
      C4     = 2.
      DI     = 15./128.*E**2/ETA*SI*T(1)**2*T(2)*(2.*C(2.)-EP*C(1.)
     C         +7.*EP*C(3.))
      T(  3) = 1.+CI-2.*CI**2
      T(  4) = 1.+CIP
      C1     = 2.
      C2     = 2.
      C3     = 1.
      C4     = -1.
      DI     = 15./64.*E**2/ETA*SIP*T(3)*T(4)*(2.*C(2.)-EP*C(1.)+7.
     C         *EP*C(3.))+DI
      T(  5) = 1.+KAPA
      T(  6) = 12.*EP-EP**3
      T(  7) = -5./ETA+3.*ETA
      T(  8) = 2.-5.*EP**2
      T(  9) = -56.*EP+123.*EP**3
      C1     = 2.
      C2     = 0
      C3     = 1.
      C4     = -1.
      DI     = DI+1./256.*CI*SIP*T(4)*T(5)*T(7)*(2.*T(6)*C(1.)-24.
     C         *T(8)*C(2.)+3.*T(9)*C(3.)-408.*EP**2*C(4.)-845.*EP**3
     C         *C(5.))
      T( 10) = 1.-CI
      C1     = 2.
      C2     = -2.
      C3     = -2.
      C4     = 2.
      DI     = 15./128.*E**2/ETA*SI*T(1)**2*T(10)*(2.*C(2.)-EP*C(1.)
     C         +7.*EP*C(3.))+DI
      T( 11) = 1.-CI-2.*CI**2
      C1     = 2.
      C2     = -2.
      C3     = 1.
      C4     = -1.
      DI     = -15./64.*E**2/ETA*SIP*T(11)*T(4)*(2.*C(2.)-EP*C(1.)+7.
     C         *EP*C(3.))+DI
      C1     = 2.
      C2     = 0
      C3     = -2.
      C4     = 2.
      DI     = 1./512.*SI*T(1)**2*T(5)*T(7)*(2.*T(6)*C(1.)-24.*T(8)*C
     C         (2.)+3.*T(9)*C(3.)-408.*EP**2*C(4.)-845.*EP**3*C(5.))
     C         +DI
      C1     = 2.
      C2     = 2.
      C3     = -1.
      C4     = 1.
      DI     = -15./64.*E**2/ETA*SIP*T(1)*T(11)*(2.*C(2.)+7.*EP*C(3.)
     C         -EP*C(1.))+DI
```

Figure 4b. Part of the FORTRAN program produced by SPASM for calculating the perturbation in I.

13. ORBIT COMPUTATION AND PARAMETER ESTIMATION

The elaboration of an orbital theory, the main objective of the preceding sections, is but one of the four aspects of using satellite-tracking data to obtain ephemerides and other information. We also have the data reduction, the relation between the observations and the parameters sought, and the estimation procedure.

We adopt Kepler elements as the orbital parameters to be determined. However, we choose to determine n, the mean motion, rather than a, as n is the best known of the orbital parameters. In addition, we recognize that the coefficients of the gravity field and the nongravitational forces are imperfectly known, thus introducing model errors. We can mitigate these errors to some extent by determining secular rates for each of the elements. Therefore, the uncertainty in the orbital model will be limited to the short-period perturbations.

The polynomial representations of the elements account for the bulk of the nongravitational forces, including the long-period effect of gravitational perturbations. The polynomials (mean elements) can be analyzed to obtain the zonal harmonics of the gravity field, some long-term resonant terms, and the reflective and drag properties of the satellites.

The basic relation used here is

$$\begin{aligned} \bar{\rho} &= \bar{r} - \bar{R} \quad , \\ \dot{\bar{\rho}} &= \frac{d}{dt}\bar{\rho} = \dot{\bar{r}} - \dot{\bar{R}} \quad , \end{aligned} \tag{210}$$

where $\bar{\rho}$ is the topocentric station-to-satellite vector, $\bar{r}$ is the satellite position, and $\bar{R}$ is the station position. It is convenient to use this equation in the orbital system; therefore, $\bar{R}$ is given by (44) and $\bar{r}$ by (71). We generally observe $A\bar{\rho}$, where A is a transformation matrix. So we have

$$\mathcal{O} = \text{observation} = A\bar{\rho} = A\bar{r} - A\bar{R} \quad . \tag{211}$$

In principle, any parameter that enters (211) can be determined from the observations, but they may not be unique.

There are basically four distinct types of observation to be considered:

A. Optical directions given in a celestial reference frame (e.g., Baker-Nunn data).

B. Direction observations in a topocentric reference frame (e.g., minitrack).

C. Range observations (e.g., laser).

D. Range-rate observations (e.g., TRANET doppler).

The transformations for each type are as follows:

A. Right ascension and declination:

$$\begin{bmatrix} \Delta\delta \\ \cos\delta\,\Delta\alpha \end{bmatrix} = \begin{bmatrix} -\cos\alpha\sin\delta & -\sin\alpha\sin\delta & \cos\delta \\ -\sin\alpha & \cos\alpha & 0 \end{bmatrix} \overline{\Delta\rho} \quad .$$

B. Altitude (a), azimuth (Az), range (ρ):

$$\begin{bmatrix} da \\ -\cos a\, d(Az) \\ \frac{d\rho}{\rho} \end{bmatrix} = \left\{ \begin{pmatrix} -\sin Az\sin a & -\cos Az\sin a & \cos a \\ \cos Az & \sin Az & 0 \end{pmatrix} \begin{bmatrix} -\sin(\lambda+\theta) & \cos(\lambda+\theta) & 0 \\ -\cos(\lambda+\theta)\sin\phi & -\sin(\lambda+\theta)\sin\phi & \cos\phi \\ \sin(\lambda+\theta)\cos\phi & \sin(\lambda+\theta)\cos\phi & \sin\phi \end{bmatrix} \right\} \overline{\Delta\rho} \quad ,$$

$\rho_x/\rho \qquad \rho_y/\rho \qquad \rho_z/\rho$

where ϕ, λ are the latitude and longitude of the observer, and ρ_x, ρ_y, ρ_z are the components of $\overline{\rho}$.

C. Range:

$$\Delta\rho = \hat{\rho} \cdot \overline{\Delta\rho} = (\overline{\rho}/|\overline{\rho}|)\,\overline{\Delta\rho} \quad .$$

D. Range rate:

$$\Delta\dot{\rho} = \hat{\rho} \cdot \dot{\overline{\Delta\rho}} \quad .$$

The domain of parameters to be determined can be expanded to include gravity-field coefficients, station coordinates, GM, a scale factor for all stations, and the position of the earth's pole of rotation. For unique and meaningful results to be

obtained, several orbits may have to be combined. This is most conveniently done by dealing with normal equations, which will be discussed later.

If we wish to determine any parameter p_i from observations, we use our elaborated theory for $\bar{r}$ and our initial estimate for p_i^0 and compute

$$\mathcal{C} = A\bar{\rho} \quad . \tag{212}$$

In general, the dependence of $\mathcal{C}$ on p_i is nonlinear and we must linearize. We want to find a correction to p_i that will reduce the difference between $\mathcal{O}$ and $\mathcal{C}$; that is,

$$\mathcal{O} - \mathcal{C} = (\partial/\partial p_i)\, A\bar{\rho}\, \Delta p_i \quad . \tag{213}$$

Now if A can be determined from the observation, we need obtain only $\partial\bar{\rho}/\partial p_i$. For range rate, A depends on p_i, and the expressions are more involved. For those parameters influencing $\mathcal{C}$ through the orbit, we obtain

$$\frac{\partial\bar{r}}{\partial p_i} = \frac{\partial\bar{r}}{\partial\omega}\frac{\partial\omega}{\partial p_i} + \frac{\partial\bar{r}}{\partial\Omega}\frac{\partial\Omega}{\partial p_i} + \frac{\partial\bar{r}}{\partial I}\frac{\partial I}{\partial p_i} + \frac{\partial\bar{r}}{\partial e}\frac{\partial e}{\partial p_i} + \frac{\partial\bar{r}}{\partial M}\frac{\partial M}{\partial p_i} - \frac{2}{3}\frac{a}{n}\frac{\partial\bar{r}}{\partial a}\frac{\partial n}{\partial p_i} \quad .$$

Now, from Izsak (1962) and Gaposchkin (1966, p. 107), we have

$$\partial\bar{r}/\partial\omega = \hat{e}_n \times \bar{r} \quad ,$$

$$\partial\bar{r}/\partial\Omega = \hat{e}_z \times \bar{r} \quad ,$$

$$\partial\bar{r}/\partial I = r \sin u\, \hat{e}_n \quad ,$$

$$\partial\bar{r}/\partial e = (\hat{e}_n \times \bar{r})\,(a/r)\,[\sin E/(1-e^2)^{1/2}] - \bar{a} \quad ,$$

$$\partial\bar{r}/\partial M = 2\pi\,\dot{\bar{r}}/n \quad ,$$

$$\partial\bar{r}/\partial a = \bar{r}/a \quad ,$$

where

$$u = v + \omega \quad ,$$

$$\hat{e}_n = \begin{bmatrix} \sin I \sin \Omega \\ -\sin I \cos \Omega \\ \cos I \end{bmatrix} \quad ,$$

$$\hat{e}_z = \begin{bmatrix} 0 \\ 0 \\ 1 \end{bmatrix} \quad ,$$

expressed in the orbital system. For example, if $p_i = \omega_0$, the constant of perigee is then

$$\partial\omega/\partial p_i = 1 \quad ,$$

the others being zero. If $p_i = \overline{C}_{\ell m}$, then, with $\overline{\mathcal{C}}_{\ell m} = 1$,

$$\partial\omega/\partial C_{\ell m} = \sum_p \sum_q \Delta\omega_{\ell mpq} \quad ,$$

$$\partial\Omega/\partial C_{\ell m} = \sum_p \sum_q \Delta\Omega_{\ell mpq} \quad ,$$

and so on. If $p_i = GM$, then

$$\partial\bar{r}/\partial(GM) = \frac{1}{3}\,\bar{r}/GM \quad .$$

If we want to determine station coordinates, we have

$$\bar{R} = R_3(-\theta)\, R(y, x, 0)\, \bar{X}_0 \quad ,$$

giving

$$\left[\frac{\partial\bar{\rho}}{\partial X}\right]\left[\frac{\partial\bar{\rho}}{\partial Y}\right]\left[\frac{\partial\bar{\rho}}{\partial Z}\right] = -\,R_3(-\theta)\, R(y, x, 0) \begin{bmatrix} 1 & 0 & 0 \\ 0 & 1 & 0 \\ 0 & 0 & 1 \end{bmatrix} \quad .$$

If we want a scale factor α for all stations – that is, $\overline{\Delta R} = \alpha \overline{R}_0$ – we have

$$\partial\overline{\rho}/\partial\alpha = - R_3(-\theta)\, R(y, x, 0)\, \overline{X}_0 \quad .$$

To determine the polar motion, we have

$$\frac{\partial\overline{\rho}}{\partial x} = \begin{bmatrix} \cos\theta\, Z_0 \\ \sin\theta\, Z_0 \\ -X_0 \end{bmatrix} \quad ,$$

$$\frac{\partial\overline{\rho}}{\partial y} = \begin{bmatrix} \sin\theta\, Z_0 \\ -\cos\theta\, Z_0 \\ Y_0 \end{bmatrix} \quad .$$

If we have the instantaneous coordinate $\overline{R} = \begin{bmatrix} X \\ Y \\ Z \end{bmatrix}$ of the station, then

$$X_0 = X \cos\theta + Y \sin\theta \quad ,$$

$$Y_0 = -X \sin\theta + Y \cos\theta \quad ,$$

$$Z_0 \approx Z \quad .$$

The data reduction falls into two parts: those reductions necessary for all data, and those related to particular data types.

All data must be expressed in the same time system. For orbital computation, we need a uniform time system, and so we have chosen AS, an atomic time system, as a standard. The differences between AS and A3 and between AS and A1 are

$$AS - A1 = 0.8983 \text{ msec} \quad ,$$

$$AS - A3 = 35.4 \text{ msec} \quad .$$

Although these values change slowly, the adopted constants are sufficient for data taken between 1965 and 1971. Numerical values of AS – UTC are given in the form of polynomials and are published (e.g., Gaposchkin, 1972b; see also Part II of this Report).

We must also know the physical point to be associated with each time. For optical data, the time detected is that of receiving the light. The orbital position corresponds to an earlier time, the difference being the travel time of light. For a flashing-light satellite, the flash times are given at the satellite. Nominal values of range are sufficient for correcting the time associated with the satellite position. With ranging data, we often have the time of firing of the laser – that is, the time of transmission – and therefore the satellite time is later by the travel time. In all cases, we must know precisely what the satellite time is.

We have a similar situation with the station position. The position of the earth is a measured quantity given in terms of UT1. We must use the actual value of UT1 to compute the sidereal angle in (44). The time associated with the station is the received time for optical observations, but it is the satellite time for range observations. The satellite time corresponds to the average position of the station during the round trip of the signal.

Optical data must be reduced to the adopted reference system by use of (45). In addition, we must apply annual aberration and parallactic refraction. The first is usually applied during film reduction, and parallactic refraction is computed from

$$\Delta R = [(0.435 \times 0.484813 \times 10^{-5})/\rho] \, (\tan z/\cos z) \, [1 - \exp(-138.5 \, \rho \cos z)] \quad ,$$

where ρ is the topocentric range in megameters, z is the zenith angle, and ΔR is the correction in radians. Now we have

$$\Delta\delta = -\Delta R \cos q \quad ,$$

$$\Delta\alpha = -\Delta R \sin q/\cos \delta \quad ,$$

where q is the parallactic angle measured in a positive clockwise direction from the object to the pole great circle (Veis, 1960a, p. 119). This correction is based on standard pressure and temperature. If measured values are available, a better value can be obtained by taking mean nighttime data. A table of corrections is given in Gaposchkin (1972b).

For laser range observations, we make a correction for the tropospheric refraction and for the geometry of the satellite. The refraction correction becomes (Lehr, 1972)

$$\Delta r = - \frac{2.238 + 0.0414\ (P/T) - 0.238\ h_s}{\sin \alpha + 10^{-3} \cot \alpha} \quad ,$$

where P is the atmospheric pressure (mb) at the laser station, T is the temperature (K), h_s is the elevation above mean sea level (km), and α is the elevation angle of the satellite. This formula holds true for a ruby laser at 694 nm when the apparent elevation angle is greater than 5°.

The accuracy of laser data is commensurate with the physical size of the satellite equipped with corner reflectors. Arnold (1972) gives in tabular form a correction to reduce the observed range to the center of mass of the satellite as a function of angle of incidence. By use of these data, all laser observations can be reduced to the center of mass.

Equation (213) will, in general, be overdetermined, and so we use the method of least squares to obtain an estimate of the unknowns. The general references are Arley and Buch (1950) and Linnik (1961). By collecting normal equations, we can merge the observations from many orbital arcs.

In the least-squares estimate, the weight or accuracy of each observation must be established a priori. For the estimation process, only the relative accuracy is important; however, one can have greater confidence if the standard error of unit weight comes to be unity.

For the weighting, we assume that the errors are uncorrelated, probably not a bad assumption with data taken over several years. We have given each observation an individual weight, as described in Table 3.

In addition, where there were more than 30 points in a pass of laser data, 30 points were chosen, evenly distributed through the pass. Some numerical tests indicate this was no worse than if we had averaged the points.

Table 3. Assumed accuracy for Standard Earth III.

Data	Weight	Remarks
Baker-Nunn	4 "	
Smoothed Baker-Nunn	2"	
SAO laser	5 m	Taken before 1970, observed before 1970
CNES laser	10 m	Taken before 1970, observed before 1970
GSFC laser	5 m	Taken before 1970, observed before 1970
ISAGEX laser	2 m	1971 International Campaign

Finally, the process of parameter estimation must be iterative, for two reasons: The model is nonlinear, and gross observation errors must be discarded. On each iteration, the computation discards data on a 3σ criterion; that is, a point is discarded if

$$(O-C)/w > 3\sigma \quad ,$$

where w is the weight, and σ is the standard deviation of the last iteration. Every observation is reconsidered on each iteration. The process is said to converge or stabilize when

$$|(\sigma_n - \sigma_{n-1})/\sigma_n| < 0.01 \quad .$$

14. THE SYSTEM OF CONSTANTS AND UNITS

We measure days from Julian Day (JD) 2400000.5, called the Modified Julian Day (MJD); that is,

$$\text{MJD} = \text{JD} - 2400000.5 \quad .$$

The day changes at midnight in this system.

The natural length scale and the time scale for dynamics come from GM, which has units length^3 time^{-2}. The preferred value seems to be

$$GM = 3.986013 \times 10^{20} \text{ cm}^3 \text{ sec}^{-2} \quad .$$

If we were to choose the length scale and the time scale appropriately, then GM could be unity. A natural length scale is the mean radius of the earth,

$$a_e = 6.378140 \times 10^8 \text{ cm} \quad .$$

If the time unit is chosen to be

$$806.8108 \text{ sec} \quad ,$$

then GM = 1. With these units, all subprograms for orbit computation can be written uniformly and do not require revision as these constants change. For the velocity of light, we have adopted

$$\begin{aligned} c &= 2.997925 \times 10^{10} \text{ cm sec}^{-1} \quad , \\ &= 2.590207 \times 10^7 \text{ Mm day}^{-1} \quad . \end{aligned}$$

Some other constants are given here for easy reference:

$G = 6.67 \times 10^{-6}\ cm^3 g^{-1} sec^{-2}$,	the universal constant of gravitation,
$C_D = 2.2$,	the drag coefficient,
$f = 1/298.256$,	the earth's flattening,
$\dot{\theta} = 0.7292115085 \times 10^{-4}\ sec^{-1}$,	the rotation rate of the earth.

15. ACKNOWLEDGMENTS

I have been fortunate over the last 12 years to know and work with some of the individuals whose research has been reviewed here. In particular, Y. Kozai, W. M. Kaula, L. Sehnal, and I. Izsak were very helpful. I have had occasion to use most of these theoretical developments in the course of analyzing satellite-tracking data in pursuit of "the orbit." I also thank C. A. Lundquist for continuous encouragement and support. I am also very grateful to the numerous programers who have made possible the realization of these theories. Finally, I want to thank the Groupe de Recherches Géodesie Spatiale at the Observatoire de Meudon, Université de Paris, for their hospitality during the time I prepared this manuscript.

PART IV

ESTIMATE OF GRAVITY ANOMALIES

ABSTRACT

The method of obtaining 5° × 5° mean gravity anomalies from 1° × 1° mean free-air gravimetry data is discussed, and various estimate procedures are considered. The assumption of the stationarity of the gravity data is also investigated. We conclude that a simplified estimate procedure is the best one for obtaining the 5° × 5° mean anomalies.

RESUME

On discute la méthode destinée à obtenir les anomalies moyennes de gravité de 5° X 5° à partir de la gravimétrie moyenne en air libre de 1° X 1° et l'on considère les diverses procédures d'évaluation. On examine également la supposition selon laquelle les données de gravité seraient stationnaires. On en conclut qu'une procédure d'évaluation simplifiée est la meilleure façon d'obtenir les anomalies moyennes de 5° X 5°.

КОНСПЕКТ

Обсуждаются метод получения средних аномалий притяжения 5° x 5°, исходя из данных средней гравиметрии свободного воздуха 1° x 1°, и рассматриваются различные методики определения. Также исследуется предположение о стационарности данных притяжения. Мы заключаем что упрощенная методика определения является найлучшей для получения средних аномалий 5° x 5°.

PART I

ESTIMATE OF GRAVITY ANOMALIES

M. R. Williamson and E. M. Gaposchkin

1. ESTIMATE OF GRAVITY BY COVARIANCE METHODS. BACKGROUND

The approach used here is based on covariance analysis, following the ideas of Wiener (1966) and Kolmogoroff. It is sometimes known as filtering theory owing to its extensive use in communications engineering. Many of the terms come from that discipline, e.g., power spectrum and lag. The ideas given here are the extension by Kaula (1967) of a one-dimensional time series to the two-dimensional surface of a sphere.

The primary objective of this analysis is to obtain mean anomalies for regions 550 km × 550 km. These data are to be combined with satellite-perturbation analysis to determine a spherical-harmonic representation of the geopotential. A set of gravity data with known, and preferably simple, statistical properties is needed. A second objective is to find the geophysical information contained in those average properties of gravity represented by the covariance function.

To obtain these mean anomalies, an estimate of each 1° × 1° free-air gravity anomaly in the 550 km × 550 km region is necessary. For the unobserved 1° × 1° units, an estimate is made by using the neighboring observed data. A linear estimate that depends only on the covariance can be derived when stationarity and isotropy are assumed. That is, the expected value of the gravity anomaly g can be expressed as the linear transformation of the measurements f_i,

$$\langle g_i \rangle = \bar{g}_i = \sum_{j=1}^{N} a_{ij} f_j \quad .$$

When the coefficients of the estimate a_{ij} are chosen so as to minimize the mean-square error $\langle (g_i - \bar{g}_i)^2 \rangle$, we obtain

$$a_{ij} = \sum_k \langle g_i f_k \rangle K^{-1}_{jk} \quad .$$

Here, K_{jk} is the covariance matrix with elements $\langle f_j f_k \rangle$. We assume that $\langle f_j f_k \rangle$ depends only on the distance τ_{jk} between the two points; we then write

$$K_{jk} = \langle f_j f_k \rangle = K(f, \tau_{jk}) \quad ,$$

where $K(f, \tau)$ is the covariance function. Further, we assume that f and g have the same statistical properties, so that

$$\bar{g}_i = \sum_{j=1}^{N} \sum_{k=1}^{N} K(f, \tau_{ik}) [K_{jk}]^{-1} f_j \quad , \tag{1}$$

and the standard error is

$$\sigma(\bar{g}_i) = \left[\langle (g_i - \bar{g}_i)^2 \rangle \right]^{1/2}$$

$$= \left[K(f, 0) - \sum_{j=1}^{N} \sum_{k=1}^{N} K(f, \tau_{ik}) [K_{jk}]^{-1} K(f, \tau_{ij}) \right]^{1/2} \quad . \tag{2}$$

In addition, the accuracy of the estimate depends on those of the observed gravity and of the covariance function.

To calculate an estimate of the covariance function from observations, τ becomes a discrete variable. The estimate is

$$\hat{K}(f, \tau) = \sum_{j,k} A_j A_k f_i f_k \Big/ \sum_{j,k} A_j A_k \tag{3}$$

The measurements f_i represent mean values over an area A_i. The sums include all measurements with

$$\tau - \frac{\Delta x}{2} < \tau_{jk} < \tau + \frac{\Delta x}{2} \quad .$$

The estimation of gravity by covariance methods hinges on the stationarity of gravity data. Stationarity means that the statistical properties of the data are the same no matter where the data are taken. There is some evidence that gravity data are not stationary. However, if there are subsets of the total gravity population that are stationary, then intergravity and intragravity covariance functions can be defined. Equation (1) needs the covariance between each pair of points. These covariances can be derived from different functions.

2. THE 1° × 1° DATA AVAILABLE

We obtained a set of 1° × 1° mean free-air anomalies compiled by the Aeronautical Chart and Information Center (ACIC, 1971). These data contained 19,115 measured means. In addition, a set of 1454 1° × 1° means for Australia was obtained from Mather (1970). The two sets of data were combined, the Mather data being used for regions where they were available. The combined data set contained 19,328 points, out of the 64,800 1° × 1° areas. A complete set of 1° × 1° mean topographic height data was obtained from Kaula (Kaula and Lee, 1967). Topographic height was used to define oceanic and continental areas. A 0-km depth and a 1-km depth were used to define the ocean–continent boundary. The distribution of 1° × 1° mean gravity data is summarized in Table 1. Figure 1 is a map showing the distribution of the data.

Table 1. Distribution of 1° × 1° mean surface-gravity anomalies.

Boundary (km)	Ocean		Continent	
	Measured	Total	Measured	Total
0	9213	42918	10115	21882
-1	7015	36199	12313	28601

The estimated uncertainty is given for each gravity anomaly. The uncertainties of 99.9% of the anomalies are less than 25 mgal. Comparison of the Mather data with the ACIC data at the 1241 common points indicates that the average difference is 1.7 mgal and that the root-mean-square (rms) difference is 20 mgal.

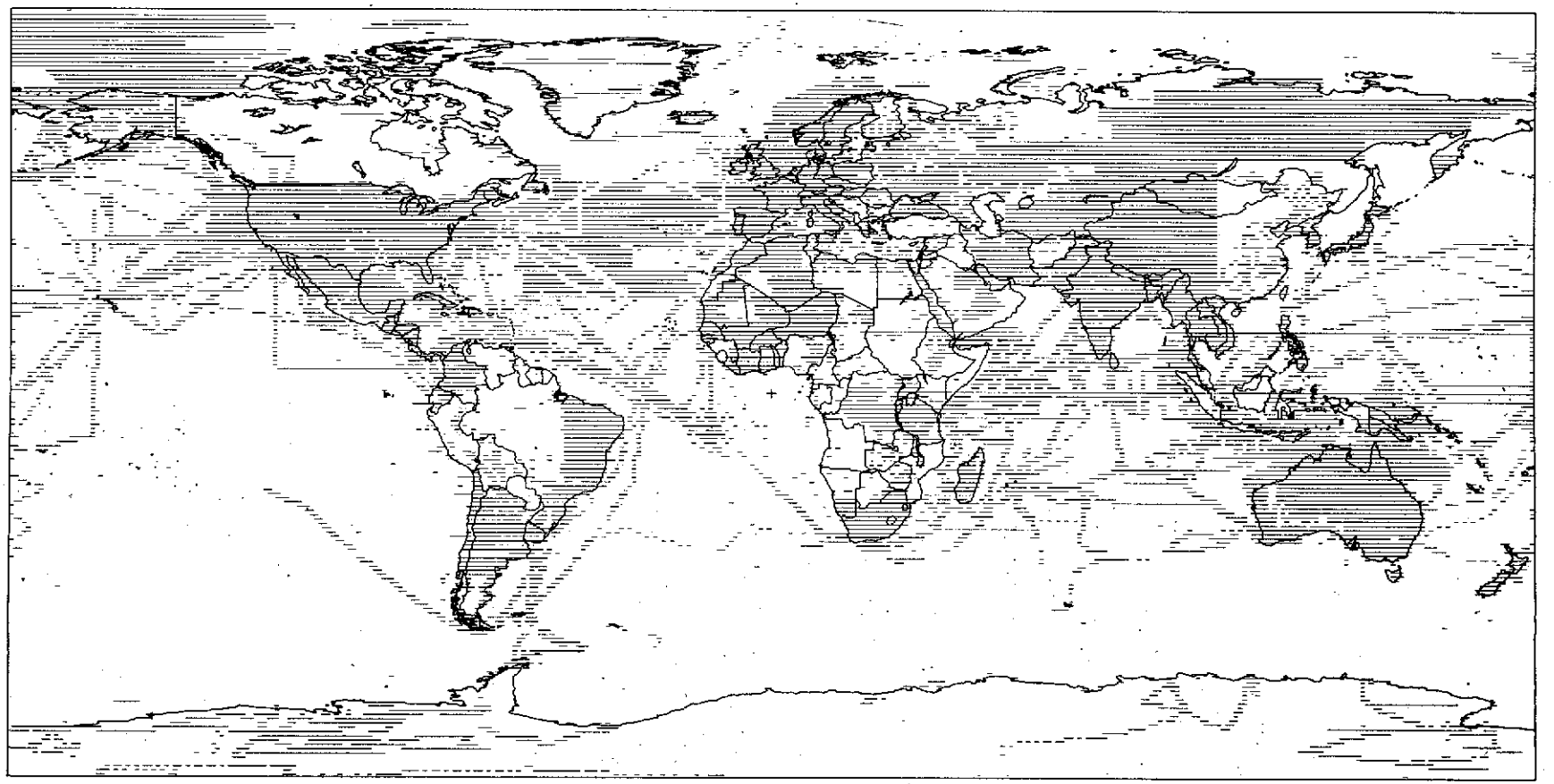

Figure 1. Distribution of 1° × 1° mean surface-gravity data.

3. USE OF BLOCK COVARIANCE

Kaula has developed a modified procedure that greatly simplifies the calculation of the covariance function and the gravity estimates. The earth is divided into blocks of approximately equal area. Their boundaries are adjusted to lie on integral degrees of latitude and longitude. Each block is subdivided into 25 units, the boundaries of which are also adjusted to lie on integral degrees of latitude and longitude. There are 1654 blocks of approximately 550 km $\times$ 550 km. At the equator, a block is $5° \times 5°$ and a unit is $1° \times 1°$. The unit mean gravity anomalies are taken to be the average of the observed $1° \times 1°$ mean gravity anomalies within the unit. The data set used here has 14,640 observed unit anomalies. The estimate for the gravity anomaly of an unobserved unit is assumed to depend on only the observed unit anomalies within the same block. The block covariance function is calculated from equation (3) by using pairs of observed unit anomalies f_i and f_j from the same block. Then a block covariance matrix can be defined as the covariance between the ith and jth unit anomalies within a block, because the ith and jth units are approximately the same distance apart in all blocks. The elements of the block covariance matrix are obtained from linear estimates of the calculated block covariance function. The estimated gravity anomalies are calculated from equation (1), where the sums over j and k include only the measured anomalies in the same block and where the covariances K are the elements of the block covariance matrix.

This method has two disadvantages:

A. The estimate of gravity does not make use of all the gravity information; i.e., the estimates are not so good as possible.

B. The covariance function to be employed must be determined by using only the combinations of anomalies within blocks and therefore does not employ all possible combinations of the data.

The method has three advantages:

A. It greatly simplifies the calculation of the covariance function and the gravity estimates.

B. It produces 550 km × 550 km mean anomalies that have uncorrelated errors.

C. The statistical properties of data within a block may be closer to stationarity since the method involves primarily the short-distance covariance.

The block covariance function is given in Figure 2 and Table 2, and the block covariance matrix, in Table 3.

Table 2. The block covariance function of unit gravity anomalies.

Average angular distance	Covariance function ($mgal^2$)
0°	1078
0.29	604
0.93	662
1.21	505
1.78	420
2.18	329
2.80	278
3.17	251
3.70	246
4.19	211
4.75	179
5.22	168
5.69	200
6.20	- 2
6.69	575

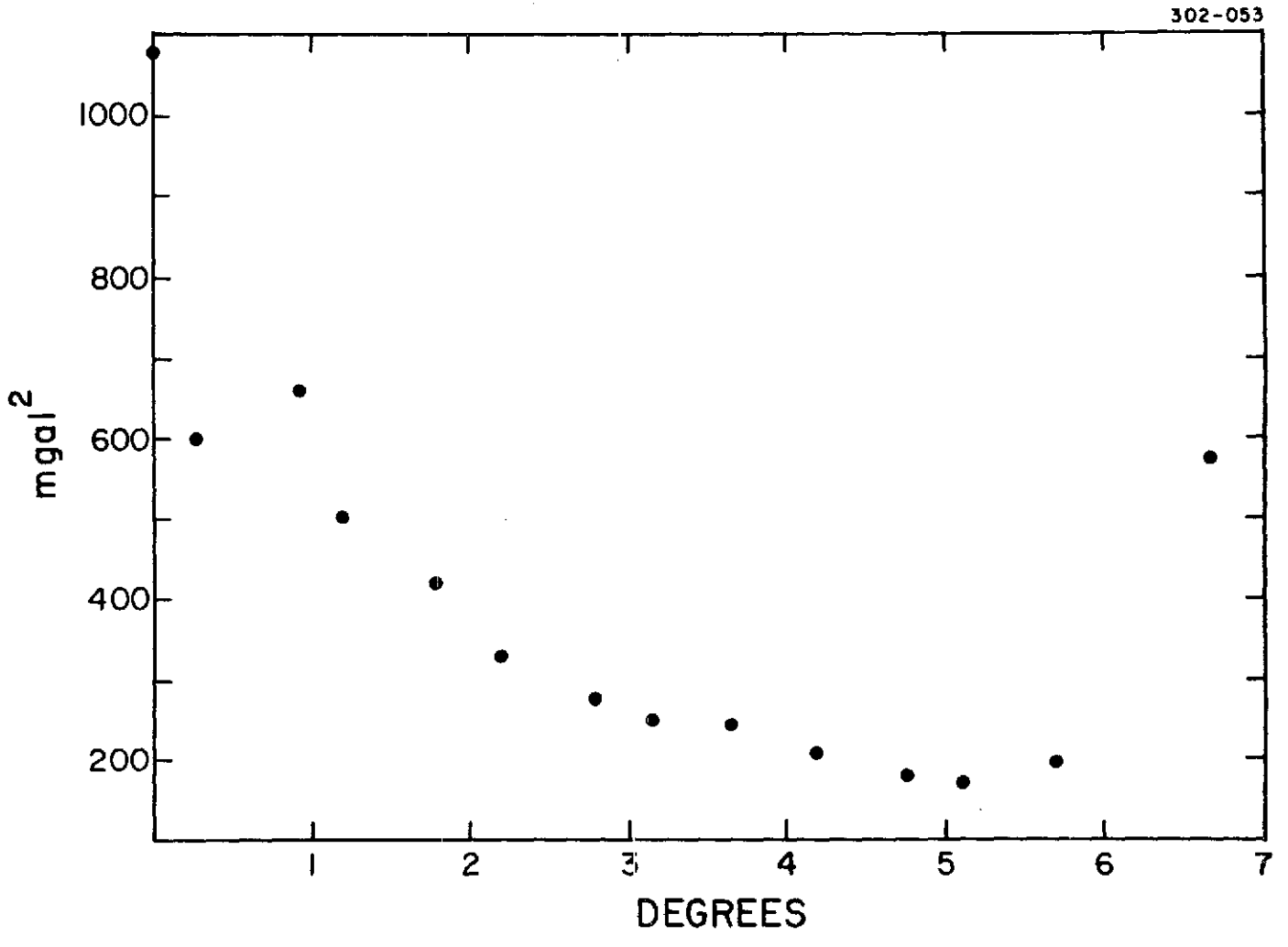

Figure 2. The block covariance function of unit gravity anomalies.

Table 3. The block covariance matrix.

	1	2	3	4	5	6	7	8	9	10	11	12	13
1	1.0785E+03	6.2104E+02	3.6983E+02	2.6329E+02	2.2470E+02	6.2104E+02	4.7352E+02	3.2475E+02	2.5139E+02	2.1619E+02	3.6983E+02	3.2475E+02	2.7587E+02
2	6.2104E+02	1.0785E+03	6.2104E+02	3.6983E+02	2.6329E+02	4.7352E+02	6.2104E+02	4.7352E+02	3.2475E+02	2.5139E+02	3.2475E+02	3.6983E+02	3.2475E+02
3	3.6983E+02	6.2104E+02	1.0785E+03	6.2104E+02	3.6983E+02	3.2475E+02	4.7352E+02	6.2104E+02	4.7352E+02	3.2475E+02	2.7587E+02	3.2475E+02	3.6983E+02
4	2.6329E+02	3.6983E+02	6.2104E+02	1.0785E+03	6.2104E+02	2.5139E+02	3.2475E+02	4.7352E+02	6.2104E+02	4.7352E+02	2.4660E+02	2.7587E+02	3.2475E+02
5	2.2470E+02	2.6329E+02	3.6983E+02	6.2104E+02	1.0785E+03	2.1619E+02	2.5139E+02	3.2475E+02	4.7352E+02	6.2104E+02	1.9535E+02	2.4660E+02	2.7587E+02
6	6.2104E+02	4.7352E+02	3.2475E+02	2.5139E+02	2.1619E+02	1.0785E+03	6.2104E+02	3.6983E+02	2.6329E+02	2.2470E+02	6.2104E+02	4.7352E+02	3.2475E+02
7	4.7352E+02	6.2104E+02	4.7352E+02	3.2475E+02	2.5139E+02	6.2104E+02	1.0785E+03	6.2104E+02	3.6983E+02	2.6329E+02	4.7352E+02	6.2104E+02	4.7352E+02
8	3.2475E+02	4.7352E+02	6.2104E+02	4.7352E+02	3.2475E+02	3.6983E+02	6.2104E+02	1.0785E+03	6.2104E+02	3.6983E+02	3.2475E+02	4.7352E+02	6.2104E+02
9	2.5139E+02	3.2475E+02	4.7352E+02	6.2104E+02	4.7352E+02	2.6329E+02	3.6983E+02	6.2104E+02	1.0785E+03	6.2104E+02	2.5139E+02	3.2475E+02	4.7352E+02
10	2.1619E+02	2.5139E+02	3.2475E+02	4.7352E+02	6.2104E+02	2.2470E+02	2.6329E+02	3.6983E+02	6.2104E+02	1.0785E+03	2.1619E+02	2.5139E+02	3.2475E+02
11	3.6983E+02	3.2475E+02	2.7587E+02	2.4660E+02	1.9535E+02	6.2104E+02	4.7352E+02	3.2475E+02	2.5139E+02	2.1619E+02	1.0785E+03	6.2104E+02	3.6983E+02
12	3.2475E+02	3.6983E+02	3.2475E+02	2.7587E+02	2.4660E+02	4.7352E+02	6.2104E+02	4.7352E+02	3.2475E+02	2.5139E+02	6.2104E+02	1.0785E+03	6.2104E+02
13	2.7587E+02	3.2475E+02	3.6983E+02	3.2475E+02	2.7587E+02	3.2475E+02	4.7352E+02	6.2104E+02	4.7352E+02	3.2475E+02	3.6983E+02	6.2104E+02	1.0785E+03
14	2.4660E+02	2.7587E+02	3.2475E+02	3.6983E+02	3.2475E+02	2.5139E+02	3.2475E+02	4.7352E+02	6.2104E+02	4.7352E+02	2.6329E+02	3.6983E+02	6.2104E+02
15	1.9535E+02	2.4660E+02	2.7587E+02	3.2475E+02	3.6983E+02	2.1619E+02	2.5139E+02	3.2475E+02	4.7352E+02	6.2104E+02	2.2470E+02	2.6329E+02	3.6983E+02
16	2.6329E+02	2.5139E+02	2.4660E+02	2.0849E+02	1.7319E+02	3.6983E+02	3.2475E+02	2.7587E+02	2.4660E+02	1.9535E+02	6.2104E+02	4.7352E+02	3.2475E+02
17	2.5139E+02	2.6329E+02	2.5139E+02	2.4660E+02	2.0849E+02	3.2475E+02	3.6983E+02	3.2475E+02	2.7587E+02	2.4660E+02	4.7352E+02	6.2104E+02	4.7352E+02
18	2.4660E+02	2.5139E+02	2.6329E+02	2.5139E+02	2.4660E+02	2.7587E+02	3.2475E+02	3.6983E+02	3.2475E+02	2.7587E+02	3.2475E+02	4.7352E+02	6.2104E+02
19	2.0849E+02	2.4660E+02	2.5139E+02	2.6329E+02	2.5139E+02	2.4660E+02	2.7587E+02	3.2475E+02	3.6983E+02	3.2475E+02	2.5139E+02	3.2475E+02	4.7352E+02
20	1.7319E+02	2.0849E+02	2.4660E+02	2.5139E+02	2.6329E+02	1.9535E+02	2.4660E+02	2.7587E+02	3.2475E+02	3.6983E+02	2.1619E+02	2.5139E+02	3.2475E+02
21	2.2470E+02	2.1619E+02	1.9535E+02	1.7319E+02	1.9839E+02	2.6329E+02	2.5139E+02	2.4660E+02	2.0849E+02	1.7319E+02	3.6983E+02	3.2475E+02	2.7587E+02
22	2.1619E+02	2.2470E+02	2.1619E+02	1.9535E+02	1.7319E+02	2.5139E+02	2.6329E+02	2.5139E+02	2.4660E+02	2.0849E+02	3.2475E+02	3.6983E+02	3.2475E+02
23	1.9535E+02	2.1619E+02	2.2470E+02	2.1619E+02	1.9535E+02	2.4660E+02	2.5139E+02	2.6329E+02	2.5139E+02	2.4660E+02	2.7587E+02	3.2475E+02	3.6983E+02
24	1.7319E+02	1.9535E+02	2.1619E+02	2.2470E+02	2.1619E+02	2.0849E+02	2.4660E+02	2.5139E+02	2.6329E+02	2.5139E+02	2.4660E+02	2.7587E+02	3.2475E+02
25	1.9839E+02	1.7319E+02	1.9535E+02	2.1619E+02	2.2470E+02	1.7319E+02	2.0849E+02	2.4660E+02	2.5139E+02	2.6329E+02	1.9535E+02	2.4660E+02	2.7587E+02

	14	15	16	17	18	19	20	21	22	23	24	25
1	2.4660E+02	1.9535E+02	2.6329E+02	2.5139E+02	2.4660E+02	2.0849E+02	1.7319E+02	2.2470E+02	2.1619E+02	1.9535E+02	1.7319E+02	1.9839E+02
2	2.7587E+02	2.4660E+02	2.5139E+02	2.6329E+02	2.5139E+02	2.4660E+02	2.0849E+02	2.1619E+02	2.2470E+02	2.1619E+02	1.9535E+02	1.7319E+02
3	3.2475E+02	2.7587E+02	2.4660E+02	2.5139E+02	2.6329E+02	2.5139E+02	2.4660E+02	1.9535E+02	2.1619E+02	2.2470E+02	2.1619E+02	1.9535E+02
4	3.6983E+02	3.2475E+02	2.0849E+02	2.4660E+02	2.5139E+02	2.6329E+02	2.5139E+02	1.7319E+02	1.9535E+02	2.1619E+02	2.2470E+02	2.1619E+02
5	3.2475E+02	3.6983E+02	1.7319E+02	2.0849E+02	2.4660E+02	2.5139E+02	2.6329E+02	1.9839E+02	1.7319E+02	1.9535E+02	2.1619E+02	2.2470E+02
6	2.5139E+02	2.1619E+02	3.6983E+02	3.2475E+02	2.7587E+02	2.4660E+02	1.9535E+02	2.6329E+02	2.5139E+02	2.4660E+02	2.0849E+02	1.7319E+02
7	3.2475E+02	2.5139E+02	3.2475E+02	3.6983E+02	3.2475E+02	2.7587E+02	2.4660E+02	2.5139E+02	2.6329E+02	2.5139E+02	2.4660E+02	2.0849E+02
8	4.7352E+02	3.2475E+02	2.7587E+02	3.2475E+02	3.6983E+02	3.2475E+02	2.7587E+02	2.4660E+02	2.5139E+02	2.6329E+02	2.5139E+02	2.4660E+02
9	6.2104E+02	4.7352E+02	2.4660E+02	2.7587E+02	3.2475E+02	3.6983E+02	3.2475E+02	2.0849E+02	2.4660E+02	2.5139E+02	2.6329E+02	2.5139E+02
10	4.7352E+02	6.2104E+02	1.9535E+02	2.4660E+02	2.7587E+02	3.2475E+02	3.6983E+02	1.7319E+02	2.0849E+02	2.4660E+02	2.5139E+02	2.6329E+02
11	2.6329E+02	2.2470E+02	6.2104E+02	4.7352E+02	3.2475E+02	2.5139E+02	2.1619E+02	3.6983E+02	3.2475E+02	2.7587E+02	2.4660E+02	1.9535E+02
12	3.6983E+02	2.6329E+02	4.7352E+02	6.2104E+02	4.7352E+02	3.2475E+02	2.5139E+02	3.2475E+02	3.6983E+02	3.2475E+02	2.7587E+02	2.4660E+02
13	6.2104E+02	3.6983E+02	3.2475E+02	4.7352E+02	6.2104E+02	4.7352E+02	3.2475E+02	2.7587E+02	3.2475E+02	3.6983E+02	3.2475E+02	2.7587E+02
14	1.0785E+03	6.2104E+02	2.5139E+02	3.2475E+02	4.7352E+02	6.2104E+02	4.7352E+02	2.4660E+02	2.7587E+02	3.2475E+02	3.6983E+02	3.2475E+02
15	6.2104E+02	1.0785E+03	2.1619E+02	2.5139E+02	3.2475E+02	4.7352E+02	6.2104E+02	1.9535E+02	2.4660E+02	2.7587E+02	3.2475E+02	3.6983E+02
16	2.5139E+02	2.1619E+02	1.0785E+03	6.2104E+02	3.6983E+02	2.6329E+02	2.2470E+02	6.2104E+02	4.7352E+02	3.2475E+02	2.5139E+02	2.1619E+02
17	3.2475E+02	2.5139E+02	6.2104E+02	1.0785E+03	6.2104E+02	3.6983E+02	2.6329E+02	4.7352E+02	6.2104E+02	4.7352E+02	3.2475E+02	2.5139E+02
18	4.7352E+02	3.2475E+02	3.6983E+02	6.2104E+02	1.0785E+03	6.2104E+02	3.6983E+02	3.2475E+02	4.7352E+02	6.2104E+02	4.7352E+02	3.2475E+02
19	6.2104E+02	4.7352E+02	2.6329E+02	3.6983E+02	6.2104E+02	1.0785E+03	6.2104E+02	2.5139E+02	3.2475E+02	4.7352E+02	6.2104E+02	4.7352E+02
20	4.7352E+02	6.2104E+02	2.2470E+02	2.6329E+02	3.6983E+02	6.2104E+02	1.0785E+03	2.1619E+02	2.5139E+02	3.2475E+02	4.7352E+02	6.2104E+02
21	2.4660E+02	1.9535E+02	6.2104E+02	4.7352E+02	3.2475E+02	2.5139E+02	2.1619E+02	1.0785E+03	6.2104E+02	3.6983E+02	2.6329E+02	2.2470E+02
22	2.7587E+02	2.4660E+02	4.7352E+02	6.2104E+02	4.7352E+02	3.2475E+02	2.5139E+02	6.2104E+02	1.0785E+03	6.2104E+02	3.6983E+02	2.6329E+02
23	3.2475E+02	2.7587E+02	3.2475E+02	4.7352E+02	6.2104E+02	4.7352E+02	3.2475E+02	3.6983E+02	6.2104E+02	1.0785E+03	6.2104E+02	3.6983E+02
24	3.6983E+02	3.2475E+02	2.5139E+02	3.2475E+02	4.7352E+02	6.2104E+02	4.7352E+02	2.6329E+02	3.6983E+02	6.2104E+02	1.0785E+03	6.2104E+02
25	3.2475E+02	3.6983E+02	2.1619E+02	2.5139E+02	3.2475E+02	4.7352E+02	6.2104E+02	2.2470E+02	2.6329E+02	3.6983E+02	6.2104E+02	1.0785E+03

4. THE COVARIANCE FUNCTION

The global covariance function, calculated from equation (3) by using the 1°× 1° mean gravity anomalies, is given in Figure 3 and Table 4.

Table 4. The covariance function of 1° × 1° mean gravity anomalies.

Average angular distance	Covariance function ($mgal^2$)
0°	1150
0.92	656
1.62	431
2.52	326
3.50	266
4.50	234
5.49	208
6.47	185
7.47	180
8.48	163
9.48	145
10.48	131
11.47	124
12.48	124
13.48	111
14.48	105
15.47	92
16.48	95
17.48	86
18.48	84
19.48	78

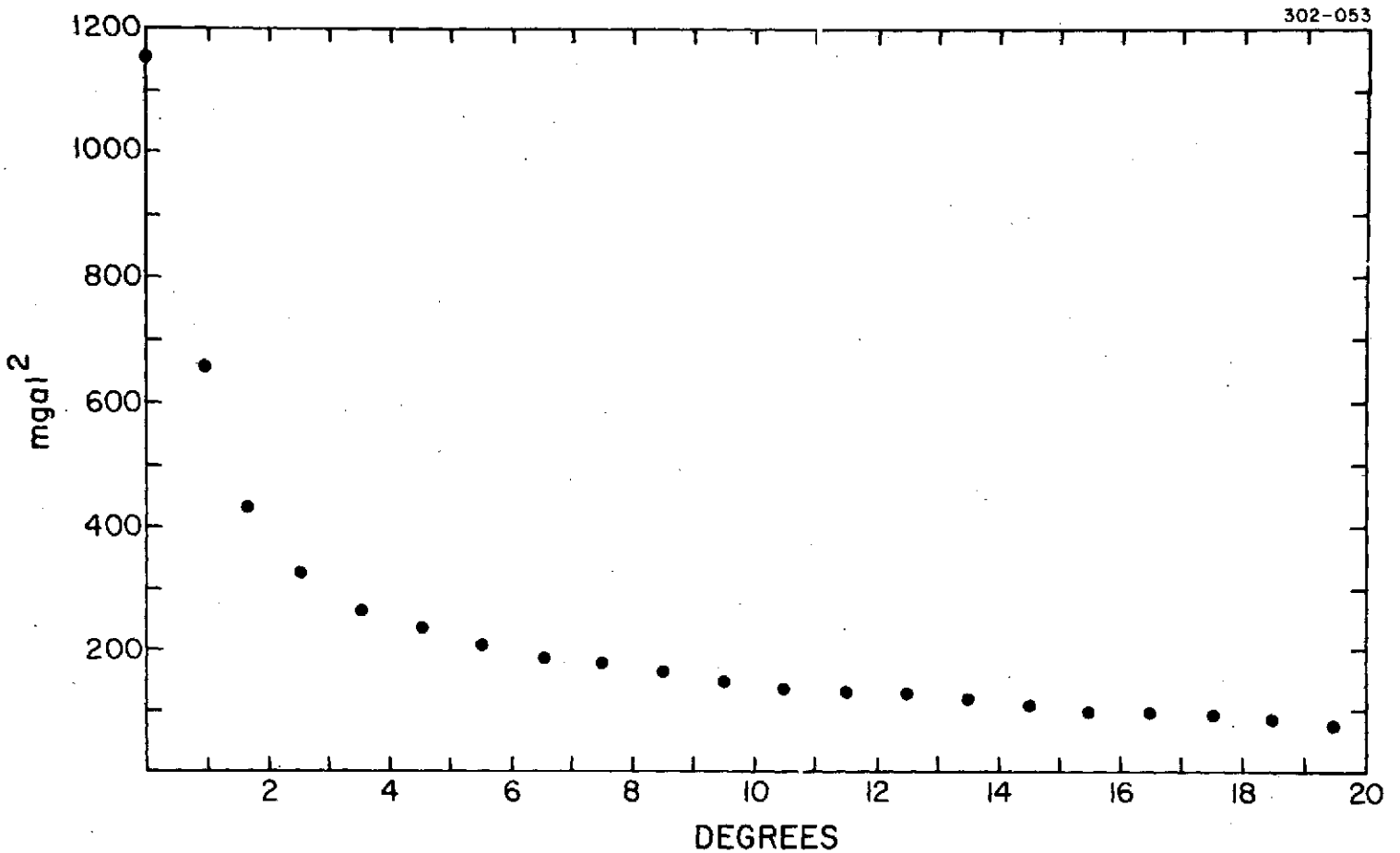

Figure 3. The covariance function of 1° × 1° mean gravity anomalies.

If gravity were a stationary process, then it would have the same statistical properties everywhere. Possible nonstationarity was investigated by determining the covariance function for subsets of the gravity data. A separation of oceanic and continental gravity was used. The ocean–continent boundary was determined from topographic data by using a zero depth in one case and a depth of 1 km in a second. In such an analysis, one also obtains the covariance of oceanic gravity with continental gravity. The results are given in Figures 4 and 5 and in Tables 5 and 6.

Isotropy has been assumed; that is, the covariance between two gravity anomalies is independent of azimuth. Two anomalies on an ocean–continent boundary separated by τ will not necessarily be characteristically oceanic or continental. Therefore, the boundary between ocean and continent was expanded to a width of 400 km. The covariance functions were computed without the gravity data in that region; the results are displayed in Figure 6 and Table 7.

Another separation was made that was arbitrary. The gravity data were divided into an equatorial set with latitudes $|\phi| < 45°$ and a polar set with latitudes $|\phi| > 45°$. These covariances are displayed in Figures 7 and 8 and Tables 8 and 9.

The differences between the covariances are significant, and one must conclude that gravity is not stationary. Any estimation procedure that assumes stationarity must be carefully examined.

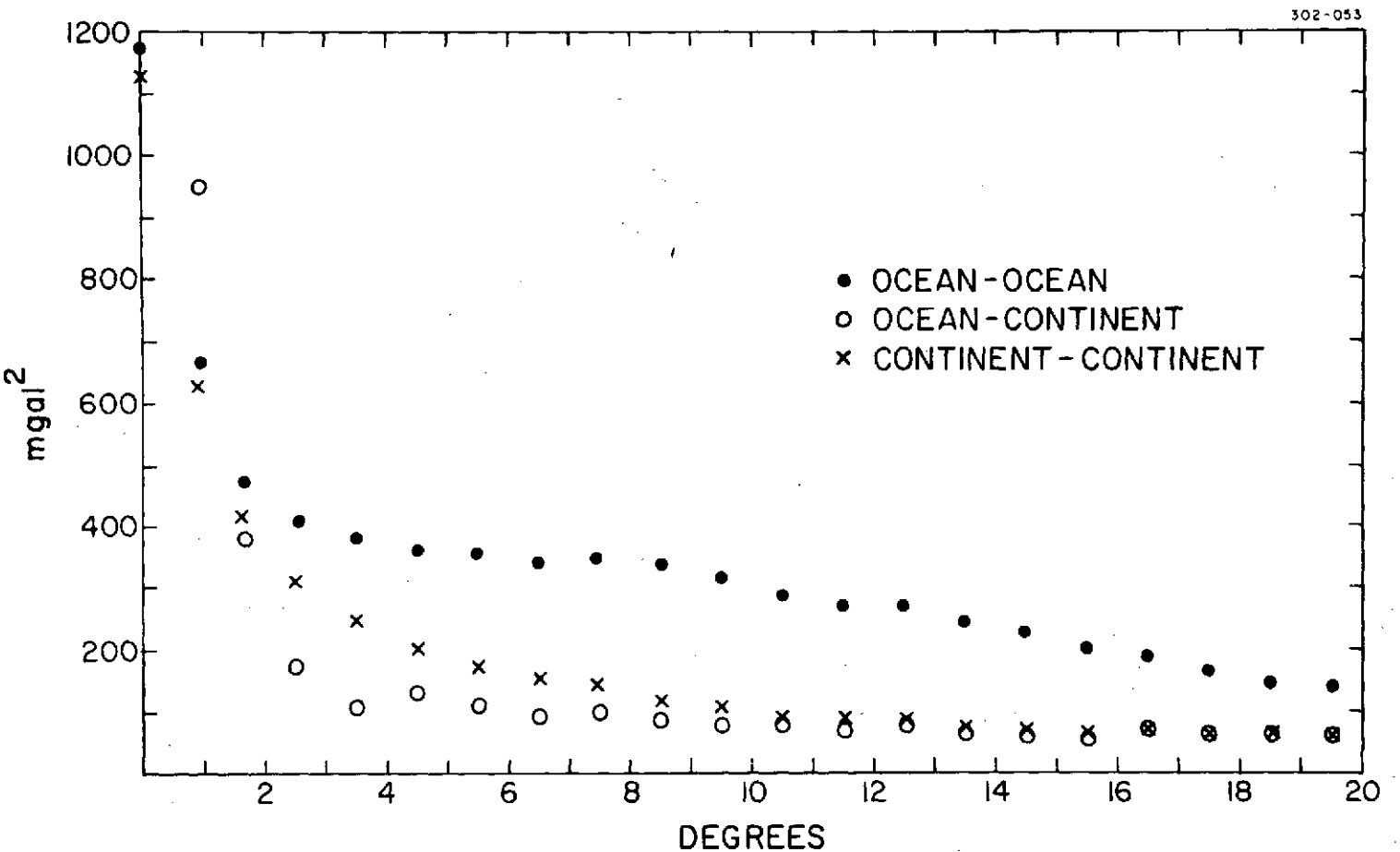

Figure 4. The covariance functions of 1° × 1° mean gravity anomalies for a -1-km ocean–continent boundary.

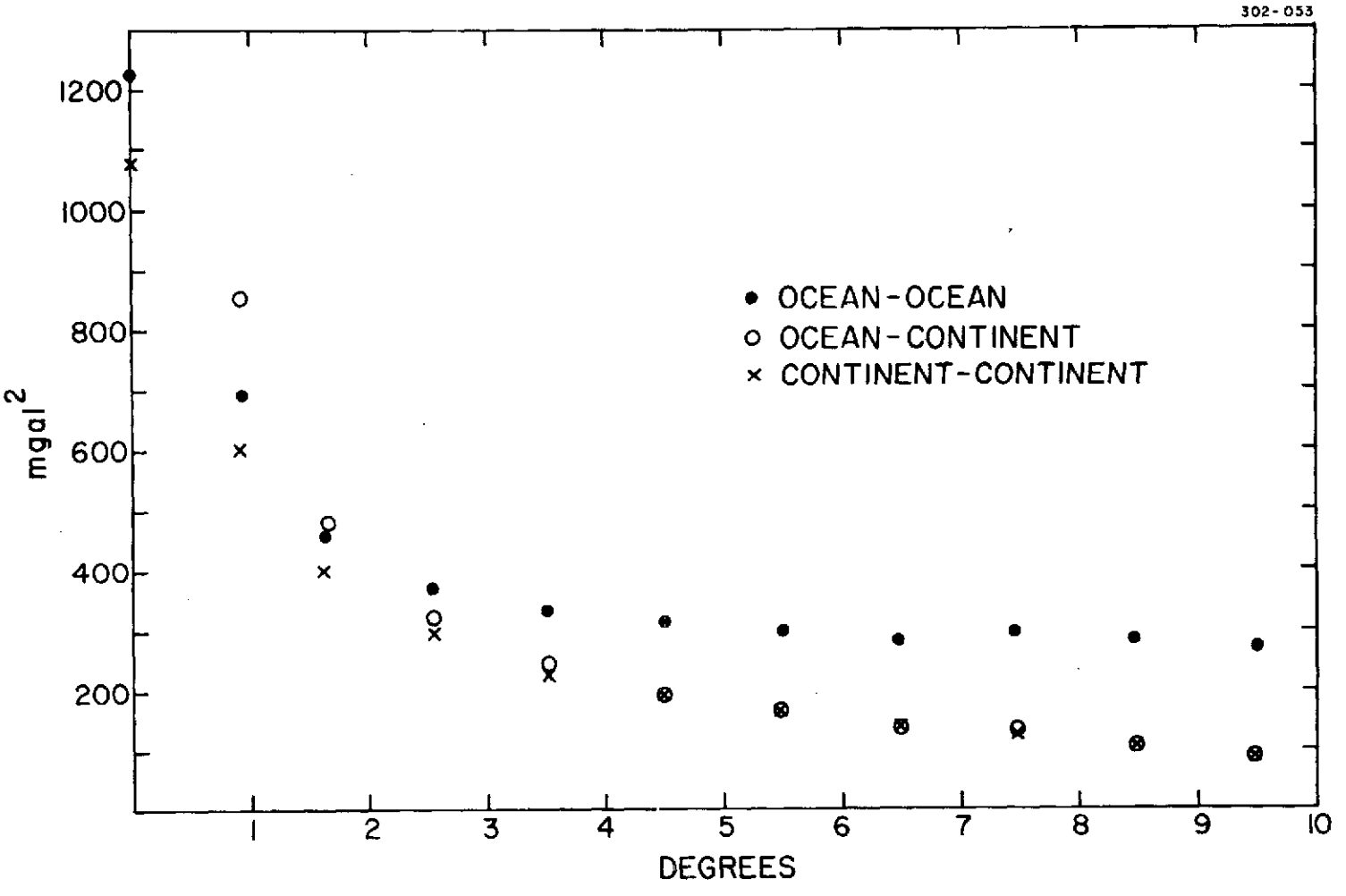

Figure 5. The covariance functions of 1° × 1° mean gravity anomalies for a 0-km ocean–continent boundary.

Table 5. The covariance functions of 1° × 1° mean gravity anomalies for a -1-km ocean–continent boundary.

Ocean–ocean		Ocean–continent		Continent–continent	
Average angular distance	Covariance function ($mgal^2$)	Average angular distance	Covariance function ($mgal^2$)	Average angular distance	Covariance function ($mgal^2$)
0°	1174			0°	1133
0.94	667	0.96	948	0.91	629
1.64	473	1.68	382	1.61	418
2.53	408	2.56	176	2.52	314
3.49	384	3.51	106	3.50	247
4.51	360	4.53	131	4.49	206
5.50	356	5.52	112	5.49	176
6.47	337	6.48	94	6.47	155
7.46	350	7.48	98	7.47	143
8.47	335	8.49	91	8.47	124
9.49	315	9.50	82	9.48	105
10.48	288	10.49	81	10.47	95
11.46	273	11.48	74	11.47	91
12.48	268	12.48	78	12.47	89
13.48	244	13.49	71	13.47	80
14.48	231	14.48	65	14.47	78
15.48	204	15.48	59	15.47	68
16.48	193	16.48	74	16.47	69
17.48	171	17.48	68	17.48	64
18.48	155	18.48	65	18.47	69
19.48	143	19.48	64	19.47	63

Table 6. The covariance functions of 1° × 1° mean gravity anomalies for a 0-km ocean–continent boundary.

Ocean–ocean		Ocean–continent		Continent–continent	
Average angular distance	Covariance function ($mgal^2$)	Average angular distance	Covariance function ($mgal^2$)	Average angular distance	Covariance function ($mgal^2$)
0°	1225			0°	1068
0.94	696	0.93	858	0.91	602
1.63	461	1.66	483	1.61	403
2.53	373	2.56	318	2.52	296
3.49	334	3.51	237	3.50	228
4.51	316	4.52	194	4.49	190
5.50	299	5.51	163	5.48	164
6.47	284	6.49	134	6.47	142
7.46	293	7.48	131	7.47	127
8.47	288	8.48	107	8.47	107
9.49	272	9.49	94	9.47	86

Table 7. The covariance functions of 1° × 1° mean gravity anomalies for a -1-km ocean–continent boundary of width 400 km.

Ocean–ocean		Ocean–continent		Continent–continent	
Average angular distance	Covariance function ($mgal^2$)	Average angular distance	Covariance function ($mgal^2$)	Average angular distance	Covariance function ($mgal^2$)
0°	756			0°	888
0.94	494			0.91	510
1.64	413			1.61	345
2.53	373	3.00	-534	2.52	250
3.50	361	3.69	-359	3.49	188
4.51	354	4.64	-102	4.49	157
5.50	351	5.56	21	5.48	131
6.47	313	6.52	63	6.47	111
7.46	301	7.51	78	7.47	96
8.47	284	8.51	76	8.47	77
9.49	269	9.51	68	9.47	58

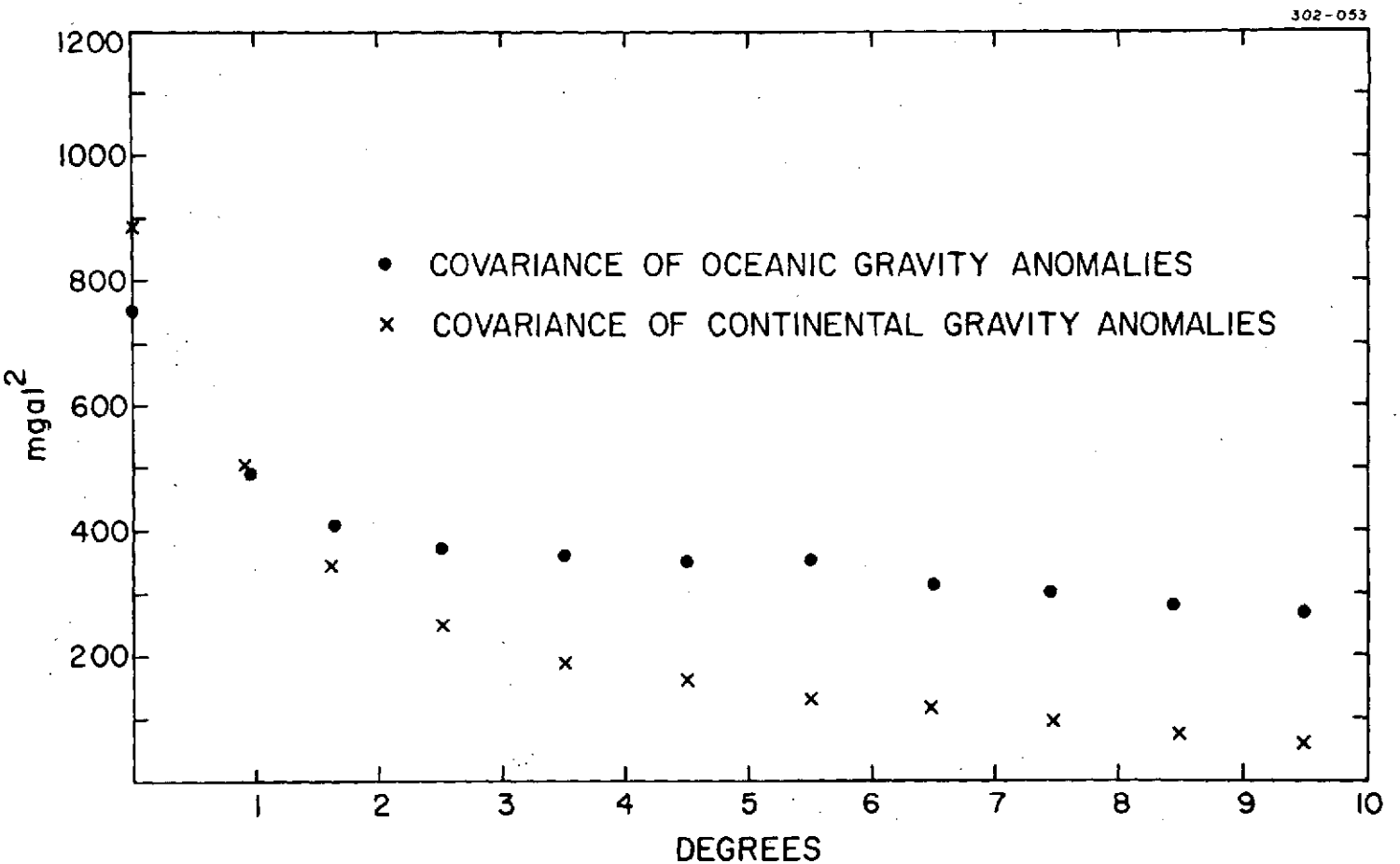

Figure 6. The covariance functions of 1° × 1° mean gravity anomalies for a -1-km ocean–continent boundary of width 400 km.

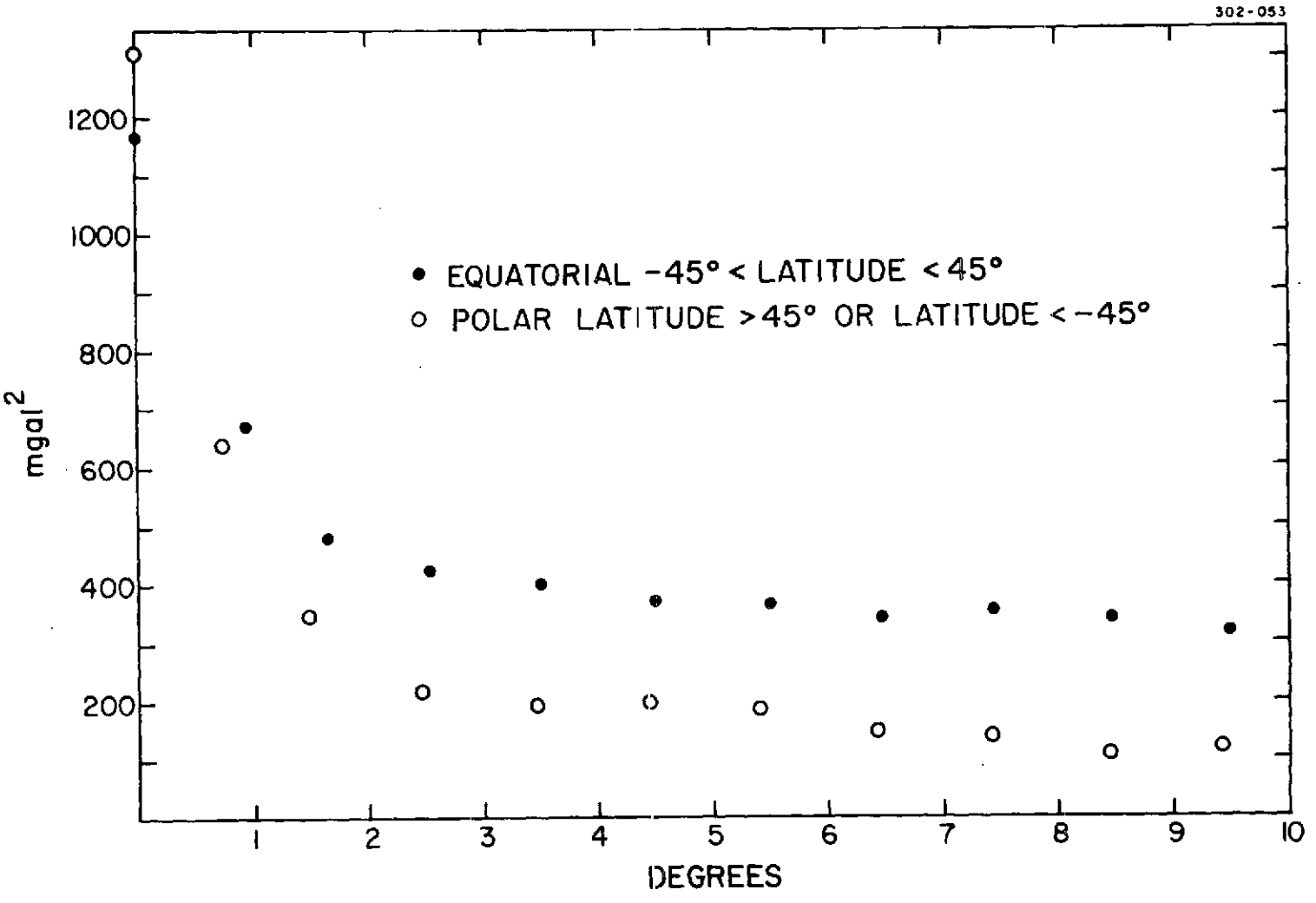

Figure 7. The covariance functions of 1° × 1° mean oceanic gravity anomalies for polar and equatorial regions.

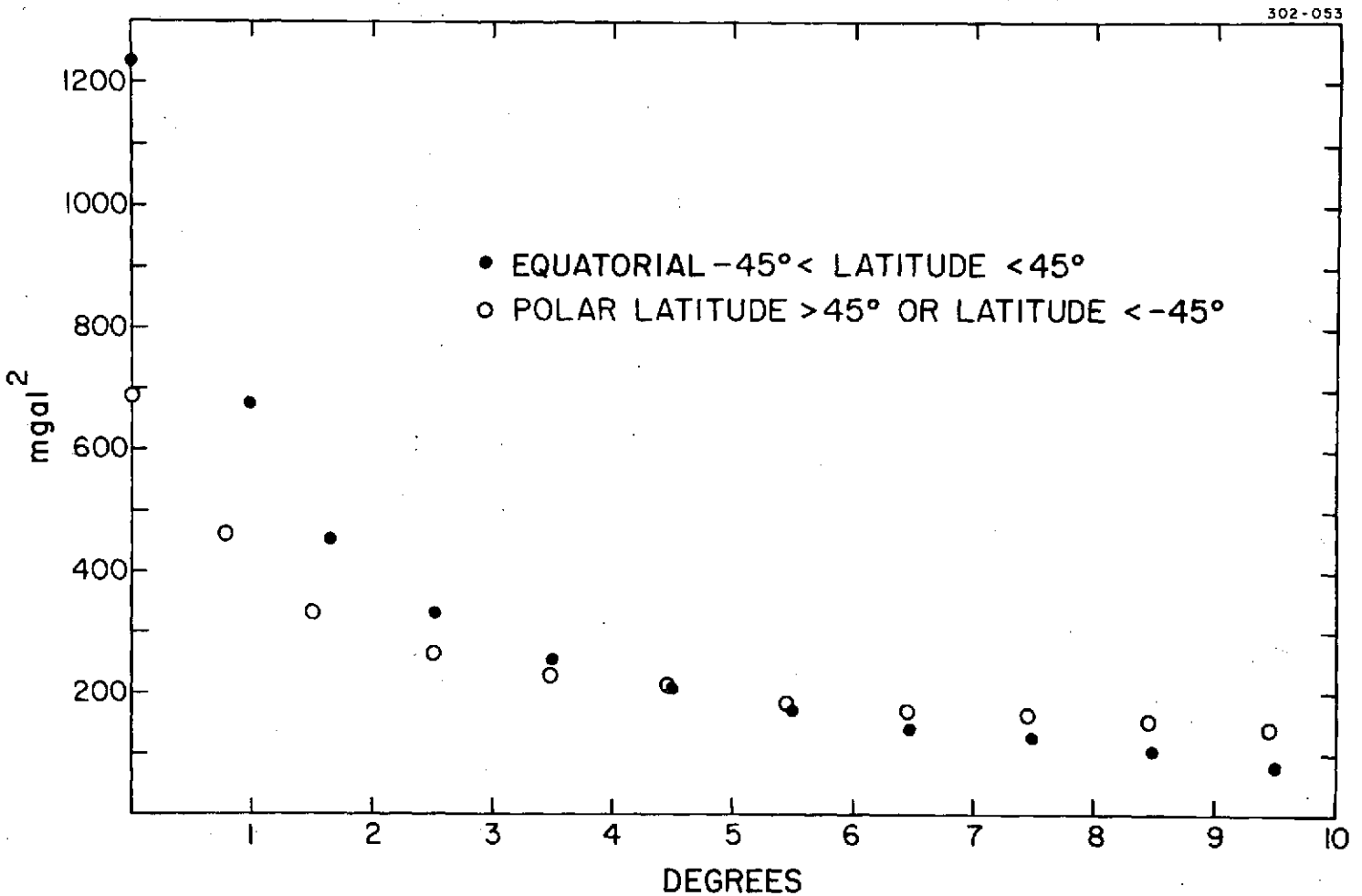

Figure 8. The covariance functions of 1° × 1° mean continental gravity anomalies for polar and equatorial regions.

Table 8. The covariance functions of 1° × 1° mean gravity anomalies for a -1-km ocean–continent boundary in the polar region |latitude| > 45°.

Ocean–ocean		Ocean–continent		Continent–continent	
Average angular distance	Covariance function ($mgal^2$)	Average angular distance	Covariance function ($mgal^2$)	Average angular distance	Covariance function ($mgal^2$)
0°	1308			0°	689
0.73	637	0.83	278	0.77	458
1.47	343	1.55	-34	1.51	329
2.46	218	2.50	27	2.48	265
3.46	193	3.48	94	3.48	231
4.44	195	4.47	97	4.47	211
5.44	184	5.46	102	5.47	185
6.44	146	6.46	111	6.47	173
7.44	141	7.45	105	7.47	164
8.44	106	8.45	96	8.47	157
9.43	115	9.45	121	9.47	148

Table 9. The covariance functions of 1° × 1° mean gravity anomalies for a -1-km ocean–continent boundary in the equatorial region |latitude| < 45°.

Ocean–ocean		Ocean–continent		Continent–continent	
Average angular distance	Covariance function ($mgal^2$)	Average angular distance	Covariance function ($mgal^2$)	Average angular distance	Covariance function ($mgal^2$)
0°	1167			0°	1234
0.95	670	0.97	1001	0.95	676
1.66	486	1.70	449	1.65	455
2.54	423	2.57	204	2.53	333
3.50	400	3.52	115	3.50	254
4.52	369	4.54	146	4.50	207
5.51	365	5.52	122	5.49	172
6.47	345	6.49	99	6.47	145
7.46	357	7.48	105	7.47	130
8.47	340	8.49	99	8.48	104
9.49	316	9.50	82	9.48	82

5. ESTIMATION OF GRAVITY

For this analysis, we want to know how much variation in the estimates of gravity is due to the lack of stationarity and to the use of the block covariance estimator.

Estimates of $1° \times 1°$ mean gravity anomalies were obtained from equation (1) by using: 1) the global covariance function, 2) the covariance functions with a 0-km boundary, and 3) the covariance functions with a -1-km boundary. A linear estimate was used to obtain values of the covariance functions between the calculated points. To reduce the computer time involved, the five closest data points were used whenever the error of the estimate given by equation (2) was less than 30 mgal. If the covariance matrix was singular or ill conditioned, the number of points was reduced. The three estimates of gravity were the same except at a few points. Estimates of unit mean gravity anomalies were also obtained by using the block covariance estimator. Some unit means do differ significantly from the $1° \times 1°$ means.

At the equator, units coincide with $1° \times 1°$ boundaries so that the four estimates can be compared directly. Figure 9 shows a few blocks at the equator. The large differences are in blocks with few observed points. In the combination with satellite data, these points will have a small effect due to the weighting, which is proportional to the number of units contributing to the average.

Therefore, by means of the block covariance estimator, a statistically independent set of $5° \times 5°$ mean gravity anomalies can be obtained with no loss of accuracy. We conclude that the block covariance estimator provides the optimum set of gravity anomalies to be used for combination with satellite observations. Of course, for detailed gravity predictions of $1° \times 1°$ means, the other covariance estimators may be preferable.

In Table 10, the computed $5° \times 5°$ mean anomalies and the number of observed units contributing to each mean are given. Finally, we calculate the covariance functions of the $5° \times 5°$ means. These are shown in Figures 10 and 11 and Tables 11 and 12.

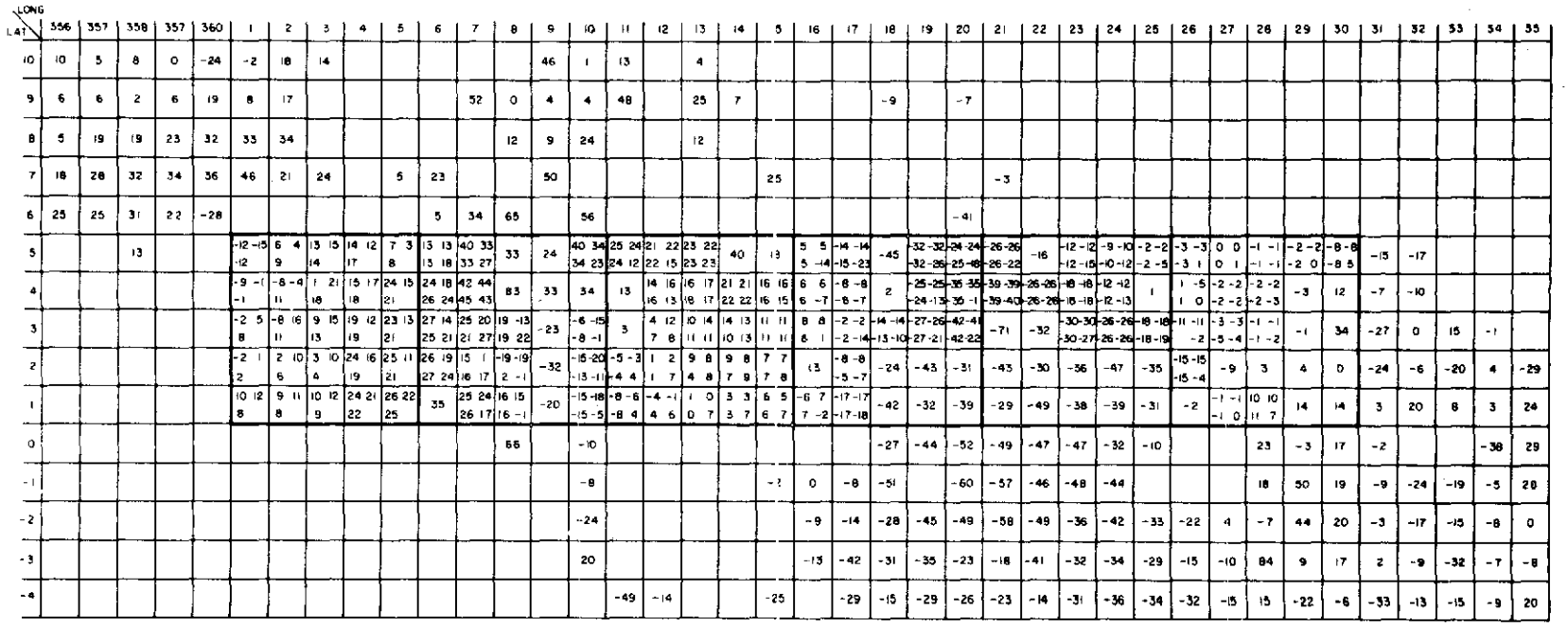

Figure 9. Comparison of the four estimate procedures. $1° \times 1°$ squares with single numbers represent the measured mean free-air gravity anomalies. $1° \times 1°$ squares with four numbers represent estimates as follows. Upper left: the split covariance estimator with a 0-km ocean–continent boundary. Lower left: the global covariance estimator. Upper right: the split covariance estimator with a -1-km ocean–continent boundary. Lower right: the Kaula estimator.

Table 10. Estimated block gravity anomaly.

Lat. (deg.)	Long. (deg.)	Area (deg. sq.)	Gravity anomaly (mgal)	No.	Lat. (deg.)	Long. (deg.)	Area (deg. sq.)	Gravity anomaly (mgal)	No.	Lat. (deg.)	Long. (deg.)	Area (deg. sq.)	Gravity anomaly (mgal)	No.
87.5	61.0	26.163	8.012	3	67.5	148.5	24.867	18.800	25	57.5	153.5	24.171	22.103	3
87.5	181.0	26.163	16.393	13	67.5	161.5	24.867	22.933	25	57.5	162.5	24.171	18.139	5
87.5	301.0	26.163	14.452	8	67.5	174.5	24.867	20.756	21	57.5	181.0	26.856	8.153	4
					67.5	187.5	24.867	7.380	21	57.5	190.5	24.171	21.262	16
82.5	21.0	26.097	20.629	7	67.5	200.5	24.867	8.670	22	57.5	199.5	24.171	38.137	14
82.5	61.0	26.097	41.744	1	67.5	213.5	24.867	27.575	23	57.5	208.5	24.171	14.196	23
82.5	181.0	26.097	8.532	16	67.5	226.0	22.954	4.847	9	57.5	218.0	26.856	14.394	15
82.5	221.0	26.097	16.527	20	67.5	251.5	24.867	-10.187	1	57.5	227.5	24.171	20.274	13
82.5	261.0	26.097	8.552	3	67.5	264.5	24.867	-18.355	4	57.5	236.5	24.171	8.120	8
82.5	301.0	26.097	4.212	3	67.5	277.5	24.867	-14.170	1	57.5	245.5	24.171	1.467	4
82.5	341.0	26.097	26.732	5	67.5	290.5	24.867	-3.792	2	57.5	273.5	24.171	-22.465	4
					67.5	303.5	24.867	.150	11	57.5	282.5	24.171	-38.381	7
77.5	12.5	24.883	4.270	9	67.5	316.0	22.954	6.753	2	57.5	291.5	24.171	-2.433	8
77.5	35.0	23.801	3.771	2	67.5	328.5	24.867	36.607	3	57.5	301.0	26.856	11.550	4
77.5	57.5	24.883	-1.911	7	67.5	341.5	24.867	38.350	11	57.5	310.5	24.171	-4.725	2
77.5	80.0	23.801	-5.477	4	67.5	354.5	24.867	14.388	3	57.5	319.5	24.171	12.098	5
77.5	125.0	23.801	-14.552	1						57.5	338.0	26.856	3.880	2
77.5	147.5	24.883	-33.856	1	62.5	6.5	25.388	17.560	25	57.5	347.5	24.171	18.492	11
77.5	170.0	23.801	2.617	7	62.5	17.5	25.388	-1.376	23	57.5	356.5	24.171	19.382	24
77.5	192.5	24.883	15.380	24	62.5	28.5	25.388	2.296	21					
77.5	215.0	23.801	-1.744	25	62.5	39.5	25.388	10.852	19	52.5	5.0	24.343	3.580	25
77.5	237.5	24.883	6.811	16	62.5	50.5	25.388	9.998	20	52.5	13.0	24.343	15.060	25
77.5	260.0	23.801	5.258	6	62.5	61.0	23.080	3.379	3	52.5	21.5	27.386	5.909	23
77.5	282.5	24.883	-5.510	4	62.5	71.5	25.388	-12.621	2	52.5	30.0	24.343	8.604	24
77.5	305.0	23.801	23.289	10	62.5	82.5	25.388	-9.886	22	52.5	38.0	24.343	6.902	22
77.5	327.5	24.883	-6.287	7	62.5	93.5	25.388	-24.680	25	52.5	46.0	24.343	3.057	22
77.5	350.0	23.801	34.593	5	62.5	104.5	25.388	-27.447	25	52.5	54.0	24.343	-1.020	25
					62.5	115.5	25.388	-18.073	25	52.5	62.0	24.343	8.600	25
72.5	9.0	24.049	29.005	12	62.5	126.5	25.388	-13.700	25	52.5	70.5	27.386	4.072	16
72.5	25.5	25.552	7.806	18	62.5	137.5	25.388	9.687	25	52.5	79.0	24.343	-15.320	25
72.5	42.0	24.049	4.590	2	62.5	148.5	25.388	29.247	25	52.5	87.0	24.343	-1.880	25
72.5	58.0	24.049	1.781	14	62.5	159.5	25.388	26.905	20	52.5	95.0	24.343	-19.080	25
72.5	74.5	25.552	.268	4	62.5	191.5	25.388	8.670	20	52.5	103.0	24.343	-20.954	20
72.5	91.0	24.049	-.187	8	62.5	202.5	25.388	26.432	18	52.5	111.5	27.386	-6.287	8
72.5	107.5	25.552	.391	22	62.5	213.5	25.388	30.940	25	52.5	120.0	24.343	10.619	3
72.5	124.0	24.049	17.327	25	62.5	224.5	25.388	28.811	10	52.5	128.0	24.343	11.895	7
72.5	173.0	24.049	1.633	1	62.5	235.5	25.388	3.267	1	52.5	160.5	27.386	26.809	9
72.5	189.0	24.049	5.518	18	62.5	290.5	25.388	-1.915	1	52.5	177.0	24.343	30.145	3
72.5	205.5	25.552	-5.650	25	62.5	311.5	25.388	-23.013	9	52.5	185.0	24.343	-16.471	18
72.5	222.0	24.049	4.533	25	62.5	322.5	25.388	13.641	3	52.5	193.0	24.343	11.977	17
72.5	238.0	24.049	-.984	8	62.5	333.5	25.388	39.325	9	52.5	201.5	27.386	-16.402	11
72.5	254.5	25.552	1.188	1	62.5	344.5	25.388	31.628	12	52.5	210.0	24.343	14.884	4
72.5	271.0	24.049	12.110	5	62.5	355.5	25.388	19.935	13	52.5	218.0	24.343	9.595	10
72.5	287.5	25.552	.989	1						52.5	226.0	24.343	-12.411	13
72.5	304.0	24.049	.578	9	57.5	5.5	24.171	10.100	25	52.5	234.0	24.343	11.205	6
72.5	320.0	24.049	29.975	8	57.5	14.5	24.171	3.680	25	52.5	242.0	24.343	8.498	5
72.5	336.5	25.552	18.946	7	57.5	24.0	26.856	-4.188	20	52.5	250.5	27.386	-3.977	4
72.5	353.0	24.049	24.010	2	57.5	33.5	24.171	9.177	22	52.5	275.0	24.343	-5.643	1
					57.5	42.5	24.171	9.314	17	52.5	291.5	27.386	-2.966	1
67.5	7.5	24.867	21.220	25	57.5	51.5	24.171	12.996	22	52.5	300.0	24.343	10.528	3
67.5	20.5	24.867	7.250	22	57.5	61.0	26.856	14.100	25	52.5	308.0	24.343	5.073	16
67.5	33.5	24.867	7.368	8	57.5	70.5	24.171	-10.300	25	52.5	324.0	24.343	11.582	1
67.5	46.0	22.954	-.222	6	57.5	79.5	24.171	-9.340	25	52.5	332.0	24.343	20.611	5
67.5	58.5	24.867	-2.787	7	57.5	88.5	24.171	-13.300	25	52.5	340.5	27.386	7.251	1
67.5	71.5	24.867	-8.329	3	57.5	98.0	26.856	-20.500	25	52.5	349.0	24.343	21.426	17
67.5	84.5	24.867	-2.752	19	57.5	107.5	24.171	-11.280	25	52.5	357.0	24.343	16.307	22
67.5	97.5	24.867	-4.847	25	57.5	116.5	24.171	-30.740	25					
67.5	110.5	24.867	-12.880	25	57.5	125.5	24.171	-22.940	25	47.5	4.5	23.638	16.320	25
67.5	123.5	24.867	-7.607	25	57.5	134.5	24.171	.280	25	47.5	12.0	27.015	18.940	25
67.5	136.0	22.954	13.067	25	57.5	144.0	26.856	9.761	5	47.5	19.5	23.638	26.464	23

Table 10. (Cont.)

Lat. (deg.)	Long. (deg.)	Area (deg. sq.)	Gravity anomaly (mgal)	No.	Lat. (deg.)	Long. (deg.)	Area (deg. sq.)	Gravity anomaly (mgal)	No.	Lat. (deg.)	Long. (deg.)	Area (deg. sq.)	Gravity anomaly (mgal)	No.
47.5	26.5	23.638	18.192	19	42.5	119.5	25.797	7.232	8	37.5	206.0	23.793	.564	13
47.5	34.0	27.015	10.680	25	42.5	126.5	25.797	27.285	18	37.5	212.5	27.759	-.023	11
47.5	41.5	23.638	.255	22	42.5	133.5	25.797	18.679	2	37.5	219.0	23.793	-17.343	21
47.5	48.5	23.638	-12.144	17	42.5	140.5	25.797	48.137	13	37.5	225.0	23.793	-15.869	17
47.5	56.0	27.015	-14.214	15	42.5	147.0	22.111	-15.626	9	37.5	231.5	27.759	-22.540	25
47.5	63.5	23.638	-7.186	18	42.5	187.5	25.797	-7.714	3	37.5	238.0	23.793	-10.940	25
47.5	70.5	23.638	-9.080	25	42.5	201.5	25.797	.677	11	37.5	244.0	23.793	2.985	24
47.5	78.0	27.015	-23.460	25	42.5	208.5	25.797	-.228	5	37.5	250.5	27.759	16.360	25
47.5	85.5	23.638	-26.340	25	42.5	215.0	22.111	3.893	2	37.5	257.0	23.793	6.731	24
47.5	93.0	27.015	-11.440	25	42.5	221.5	25.797	-9.996	11	37.5	263.0	23.793	-8.860	25
47.5	100.5	23.638	-12.000	25	42.5	228.5	25.797	-2.956	23	37.5	269.5	27.759	-1.232	24
47.5	107.5	23.638	3.732	5	42.5	235.5	25.797	.580	25	37.5	276.0	23.793	-5.480	25
47.5	115.0	27.015	.402	5	42.5	242.5	25.797	16.400	25	37.5	282.0	23.793	3.620	25
47.5	122.5	23.638	17.238	14	42.5	249.0	22.111	20.580	25	37.5	288.5	27.759	-18.920	25
47.5	129.5	23.638	14.685	12	42.5	255.5	25.797	21.020	25	37.5	295.0	23.793	-19.095	19
47.5	137.0	27.015	16.098	2	42.5	262.5	25.797	1.560	25	37.5	301.0	23.793	-11.935	15
47.5	144.5	23.638	14.652	2	42.5	269.5	25.797	-8.660	25	37.5	307.0	23.793	-7.971	20
47.5	181.0	27.015	18.042	3	42.5	276.0	22.111	-4.540	25	37.5	313.5	27.759	4.810	21
47.5	188.5	23.638	23.216	8	42.5	282.5	25.797	-6.805	24	37.5	320.0	23.793	21.740	25
47.5	195.5	23.638	17.917	5	42.5	289.5	25.797	7.120	25	37.5	326.0	23.793	39.420	25
47.5	203.0	27.015	11.657	8	42.5	296.5	25.797	-2.538	16	37.5	332.5	27.759	39.540	25
47.5	210.5	23.638	.325	3	42.5	303.5	25.797	-16.723	22	37.5	339.0	23.793	11.447	21
47.5	217.5	23.638	-4.101	2	42.5	310.0	22.111	23.679	18	37.5	345.0	23.793	14.005	14
47.5	225.0	27.015	-.082	11	42.5	316.5	25.797	6.864	24	37.5	351.5	27.759	12.933	19
47.5	232.5	23.638	-8.338	23	42.5	323.5	25.797	19.840	25	37.5	358.0	23.793	15.174	22
47.5	239.5	23.638	1.558	21	42.5	330.5	25.797	33.840	25					
47.5	247.0	27.015	15.432	23	42.5	337.5	25.797	25.980	25	32.5	4.0	25.294	-1.760	25
47.5	254.5	23.638	17.862	19	42.5	344.0	22.111	8.020	24	32.5	10.0	25.294	-.880	16
47.5	261.5	23.638	10.711	22	42.5	350.5	25.797	12.989	18	32.5	16.0	25.294	3.822	16
47.5	269.0	27.015	5.376	21	42.5	357.5	25.797	11.300	25	32.5	22.0	25.294	3.116	15
47.5	276.5	23.638	-9.277	8						32.5	28.0	25.294	-32.065	17
47.5	284.0	27.015	-5.625	7	37.5	4.0	23.793	24.337	19	32.5	33.5	21.078	.852	14
47.5	291.5	23.638	-5.400	17	37.5	10.5	27.759	21.369	21	32.5	39.0	25.294	27.318	15
47.5	298.5	23.638	1.352	4	37.5	17.0	23.793	9.843	20	32.5	45.0	25.294	-5.310	7
47.5	306.0	27.015	25.753	15	37.5	23.0	23.793	4.559	11	32.5	51.0	25.294	16.660	25
47.5	313.5	23.638	17.716	20	37.5	29.5	27.759	6.805	7	32.5	57.0	25.294	22.340	25
47.5	320.5	23.638	12.349	22	37.5	36.0	23.793	21.488	6	32.5	63.0	25.294	31.193	11
47.5	328.0	27.015	31.351	22	37.5	42.0	23.793	13.583	8	32.5	69.0	25.294	-6.827	17
47.5	335.5	23.638	38.421	17	37.5	48.5	27.759	52.137	14	32.5	75.0	25.294	-8.536	24
47.5	342.5	23.638	18.663	19	37.5	55.0	23.793	1.635	20	32.5	81.0	25.294	36.740	25
47.5	350.0	27.015	4.428	20	37.5	61.0	23.793	-16.040	25	32.5	87.0	25.294	23.100	25
47.5	357.5	23.638	6.160	25	37.5	67.0	23.793	-29.370	23	32.5	92.5	21.078	11.200	25
					37.5	73.5	27.759	6.200	25	32.5	98.0	25.294	11.280	25
42.5	4.5	25.797	17.424	22	37.5	80.0	23.793	-4.220	25	32.5	104.0	25.294	-8.424	15
42.5	11.5	25.797	15.249	22	37.5	86.0	23.793	.240	25	32.5	110.0	25.294	-29.849	11
42.5	18.0	22.111	33.907	16	37.5	92.5	27.759	12.640	25	32.5	116.0	25.294	-15.304	15
42.5	24.5	25.797	28.354	12	37.5	99.0	23.793	14.320	25	32.5	122.0	25.294	1.734	7
42.5	31.5	25.797	-11.706	17	37.5	105.0	23.793	9.249	15	32.5	128.0	25.294	26.259	13
42.5	38.5	25.797	-17.176	17	37.5	111.5	27.759	-18.962	7	32.5	134.0	25.294	21.732	12
42.5	45.5	25.797	7.513	19	37.5	118.0	23.793	-8.571	10	32.5	140.0	25.294	37.237	14
42.5	52.0	22.111	-5.581	2	37.5	124.0	23.793	14.602	11	32.5	146.0	25.294	7.471	9
42.5	58.5	25.797	-4.200	25	37.5	130.5	27.759	28.931	12	32.5	151.5	21.078	-6.093	9
42.5	65.5	25.797	-19.800	25	37.5	137.0	23.793	43.596	14	32.5	157.0	25.294	-6.987	9
42.5	72.5	25.797	-21.220	25	37.5	143.0	23.793	44.774	11	32.5	163.0	25.294	-13.019	5
42.5	79.5	25.797	-10.480	25	37.5	162.0	23.793	-11.876	3	32.5	169.0	25.294	-18.827	7
42.5	86.0	22.111	-19.100	25	37.5	168.5	27.759	7.953	5	32.5	175.0	25.294	-10.740	4
42.5	92.5	25.797	-25.700	25	37.5	175.0	23.793	-6.853	7	32.5	181.0	25.294	-18.247	3
42.5	99.5	25.797	3.720	25	37.5	181.0	23.793	-3.200	3	32.5	193.0	25.294	-14.493	4
42.5	106.5	25.797	7.766	10	37.5	193.5	27.759	-10.234	5	32.5	199.0	25.294	1.438	6
42.5	113.0	22.111	-2.253	2	37.5	200.0	23.793	-4.725	9	32.5	205.0	25.294	-1.714	7

Table 10. (Cont.)

Lat. (deg.)	Long. (deg.)	Area (deg. sq.)	Gravity anomaly (mgal)	No.	Lat. (deg.)	Long. (deg.)	Area (deg. sq.)	Gravity anomaly (mgal)	No.	Lat. (deg.)	Long. (deg.)	Area (deg. sq.)	Gravity anomaly (mgal)	No.
32.5	210.5	21.078	-4.129	12	27.5	189.5	22.168	6.534	5	22.5	170.5	23.090	.330	1
32.5	216.0	25.294	-11.941	8	27.5	195.0	26.602	6.759	8	22.5	175.5	23.090	-9.547	6
32.5	222.0	25.294	-7.428	18	27.5	201.0	26.602	11.870	5	22.5	181.0	27.708	-7.099	12
32.5	228.0	25.294	-16.136	22	27.5	206.5	22.168	-2.376	9	22.5	186.5	23.090	2.744	11
32.5	234.0	25.294	-22.527	17	27.5	212.0	26.602	-3.406	16	22.5	191.5	23.090	20.087	9
32.5	240.0	25.294	-19.175	23	27.5	217.5	22.168	-.200	15	22.5	197.0	27.708	12.114	14
32.5	246.0	25.294	-8.080	25	27.5	223.0	26.602	-13.130	8	22.5	202.5	23.090	28.256	19
32.5	252.0	25.294	4.700	25	27.5	229.0	26.602	-17.445	8	22.5	208.0	27.708	-.410	16
32.5	258.0	25.294	-3.232	23	27.5	234.5	22.168	-21.641	8	22.5	213.5	23.090	-7.222	10
32.5	264.0	25.294	-5.579	23	27.5	240.0	26.602	-24.254	16	22.5	218.5	23.090	-5.783	11
32.5	269.5	21.078	1.455	23	27.5	246.0	26.602	-17.416	20	22.5	224.0	27.708	-10.465	11
32.5	275.0	25.294	1.840	25	27.5	251.5	22.168	4.105	24	22.5	229.5	23.090	-12.001	12
32.5	281.0	25.294	-4.541	21	27.5	257.0	26.602	12.440	25	22.5	234.5	23.090	-10.317	4
32.5	287.0	25.294	-38.961	15	27.5	262.5	22.168	-10.680	25	22.5	240.0	27.708	-12.501	5
32.5	293.0	25.294	-18.609	15	27.5	268.0	26.602	-1.979	22	22.5	245.5	23.090	2.079	1
32.5	299.0	25.294	-10.942	11	27.5	274.0	26.602	-3.740	15	22.5	251.0	27.708	-7.997	17
32.5	305.0	25.294	-13.469	18	27.5	279.5	22.168	6.468	24	22.5	256.5	23.090	18.122	23
32.5	311.0	25.294	-.505	16	27.5	285.0	26.602	-27.445	14	22.5	261.5	23.090	11.412	23
32.5	317.0	25.294	17.217	21	27.5	291.0	26.602	-25.254	7	22.5	267.0	27.708	2.660	25
32.5	323.0	25.294	28.654	23	27.5	296.5	22.168	-2.681	1	22.5	272.5	23.090	17.865	21
32.5	328.5	21.078	20.253	9	27.5	302.0	26.602	-24.495	19	22.5	277.5	23.090	.701	24
32.5	334.0	25.294	4.532	6	27.5	307.5	22.168	-16.313	21	22.5	283.0	27.708	7.338	21
32.5	340.0	25.294	9.545	9	27.5	313.0	26.602	1.498	17	22.5	288.5	23.090	-10.849	6
32.5	346.0	25.294	8.015	14	27.5	319.0	26.602	3.523	13	22.5	294.0	27.708	-16.652	9
32.5	352.0	25.294	42.795	20	27.5	324.5	22.168	.618	24	22.5	299.5	23.090	-16.494	10
32.5	358.0	25.294	35.700	25	27.5	330.0	26.602	-.058	20	22.5	304.5	23.090	-23.594	21
					27.5	336.0	26.602	-9.968	20	22.5	310.0	27.708	-23.233	18
27.5	4.0	26.602	-3.900	25	27.5	341.5	22.168	20.733	13	22.5	315.5	23.090	4.431	9
27.5	9.5	22.168	2.745	19	27.5	347.0	26.602	6.655	11	22.5	320.5	23.090	-.751	14
27.5	15.0	26.602	10.779	6	27.5	352.5	22.168	8.775	19	22.5	326.0	27.708	.597	13
27.5	21.0	26.602	8.068	7	27.5	358.0	26.602	-4.785	14	22.5	331.5	23.090	3.579	15
27.5	26.5	22.168	.631	7						22.5	337.0	27.708	-.745	17
27.5	32.0	26.602	7.804	13	22.5	3.5	23.090	24.720	25	22.5	342.5	23.090	1.768	13
27.5	37.5	22.168	1.917	7	22.5	9.0	27.708	21.400	25	22.5	347.5	23.090	-4.726	20
27.5	43.0	26.602	8.222	15	22.5	14.5	23.090	3.930	24	22.5	353.0	27.708	-13.986	15
27.5	49.0	26.602	-17.550	23	22.5	19.5	23.090	-8.569	1	22.5	358.5	23.090	2.287	17
27.5	54.5	22.168	-8.080	25	22.5	30.5	23.090	8.581	3					
27.5	60.0	26.602	15.640	25	22.5	36.0	27.708	2.646	10	17.5	3.5	23.835	5.800	25
27.5	66.0	26.602	2.358	24	22.5	41.5	23.090	23.047	7	17.5	8.5	23.835	7.120	25
27.5	71.5	22.168	-8.560	25	22.5	46.5	23.090	-12.120	10	17.5	14.0	28.602	-7.151	21
27.5	77.0	26.602	-24.983	24	22.5	52.0	27.708	-31.853	19	17.5	19.5	23.835	-10.951	13
27.5	82.5	22.168	-69.261	24	22.5	57.5	23.090	-15.820	1	17.5	24.5	23.835	5.682	8
27.5	88.0	26.602	-11.540	25	22.5	68.0	27.708	-.944	15	17.5	35.0	28.602	11.865	8
27.5	94.0	26.602	-32.480	25	22.5	73.5	23.090	1.698	24	17.5	40.5	23.835	9.647	15
27.5	99.5	22.168	-6.320	25	22.5	79.0	27.708	.500	25	17.5	45.5	23.835	1.338	11
27.5	105.0	26.602	-25.814	21	22.5	84.5	23.090	.854	24	17.5	50.5	23.835	-18.320	11
27.5	111.0	26.602	-19.230	12	22.5	89.5	23.090	-11.798	20	17.5	55.5	23.835	8.335	5
27.5	116.5	22.168	-3.088	11	22.5	95.0	27.708	-24.000	25	17.5	61.0	28.602	-8.343	2
27.5	122.0	26.602	6.931	7	22.5	100.5	23.090	-21.920	25	17.5	66.5	23.835	-10.439	7
27.5	127.5	22.168	20.764	10	22.5	105.5	23.090	-14.763	16	17.5	71.5	23.835	-24.118	13
27.5	133.0	26.602	-8.830	3	22.5	111.0	27.708	-12.675	14	17.5	76.5	23.835	-21.835	21
27.5	139.0	26.602	27.968	7	22.5	116.5	23.090	-3.431	8	17.5	81.5	23.835	-1.698	21
27.5	144.5	22.168	-10.762	6	22.5	122.0	27.708	-1.704	12	17.5	87.0	28.602	-16.689	10
27.5	150.0	26.602	.594	1	22.5	127.5	23.090	.030	10	17.5	92.5	23.835	-21.873	11
27.5	156.0	26.602	-2.079	1	22.5	132.5	23.090	-2.219	5	17.5	97.5	23.835	-11.847	22
27.5	161.5	22.168	-7.876	3	22.5	143.5	23.090	2.016	4	17.5	102.5	23.835	-15.411	24
27.5	167.0	26.602	-13.724	3	22.5	148.5	23.090	20.492	1	17.5	108.0	28.602	-8.346	11
27.5	172.5	22.168	-13.008	5	22.5	154.0	27.708	-2.571	5	17.5	113.5	23.835	-2.673	1
27.5	178.0	26.602	-9.635	5	22.5	159.5	23.090	-15.757	6	17.5	118.5	23.835	38.841	5
27.5	184.0	26.602	-4.614	1	22.5	165.0	27.708	-10.984	4	17.5	123.5	23.835	26.661	10

Table 10. (Cont.)

Lat. (deg.)	Long. (deg.)	Area (deg. sq.)	Gravity anomaly (mgal)	No.	Lat. (deg.)	Long. (deg.)	Area (deg. sq.)	Gravity anomaly (mgal)	No.	Lat. (deg.)	Long. (deg.)	Area (deg. sq.)	Gravity anomaly (mgal)	No.
17.5	128.5	23.835	1.321	2	12.5	75.5	24.400	-32.596	19	7.5	74.5	24.778	-43.102	17
17.5	134.0	28.602	6.831	6	12.5	80.5	24.400	-26.509	11	7.5	79.5	24.778	-24.526	22
17.5	139.5	23.835	12.330	7	12.5	91.0	29.280	-23.737	7	7.5	84.5	24.778	-48.402	15
17.5	144.5	23.835	23.339	8	12.5	96.5	24.400	-2.787	21	7.5	89.5	24.778	-8.197	15
17.5	149.5	23.835	21.259	4	12.5	101.5	24.400	-10.314	19	7.5	94.5	24.778	-24.249	24
17.5	155.0	28.602	-16.680	2	12.5	106.5	24.400	-.440	25	7.5	99.5	24.778	9.033	22
17.5	160.5	23.835	-11.444	5	12.5	111.5	24.400	-4.382	9	7.5	104.5	24.778	-1.144	4
17.5	165.5	23.835	-3.574	6	12.5	116.5	24.400	8.448	12	7.5	110.0	29.734	4.180	11
17.5	170.5	23.835	-14.614	12	12.5	121.5	24.400	38.081	17	7.5	115.5	24.778	8.621	16
17.5	175.5	23.835	-10.051	10	12.5	127.0	29.280	33.149	13	7.5	120.5	24.778	53.542	4
17.5	181.0	28.602	1.291	11	12.5	132.5	24.400	.891	1	7.5	125.5	24.778	34.820	13
17.5	186.5	23.835	2.664	5	12.5	137.5	24.400	7.089	2	7.5	130.5	24.778	20.759	8
17.5	191.5	23.835	-3.076	4	12.5	142.5	24.400	23.264	10	7.5	135.5	24.778	22.346	10
17.5	196.5	23.835	-1.179	6	12.5	147.5	24.400	-6.104	9	7.5	140.5	24.778	15.922	4
17.5	201.5	23.835	7.899	10	12.5	152.5	24.400	-1.968	10	7.5	145.5	24.778	4.707	13
17.5	207.0	28.602	25.874	9	12.5	157.5	24.400	-5.099	6	7.5	150.5	24.778	.336	12
17.5	212.5	23.835	5.880	6	12.5	163.0	29.280	-10.044	5	7.5	155.5	24.778	7.425	1
17.5	217.5	23.835	-8.161	3	12.5	168.5	24.400	-8.190	2	7.5	170.5	24.778	74.369	1
17.5	222.5	23.835	-11.922	8	12.5	178.5	24.400	26.378	7	7.5	181.0	29.734	6.409	7
17.5	228.0	28.602	-12.474	2	12.5	188.5	24.400	1.782	1	7.5	186.5	24.778	-13.212	6
17.5	233.5	23.835	-14.532	4	12.5	193.5	24.400	-.740	7	7.5	191.5	24.778	-3.122	10
17.5	238.5	23.835	-18.863	3	12.5	199.0	29.280	5.451	12	7.5	196.5	24.778	-2.970	1
17.5	243.5	23.835	-19.618	9	12.5	209.5	24.400	-.891	1	7.5	201.5	24.778	23.280	7
17.5	248.5	23.835	-15.457	10	12.5	214.5	24.400	1.293	7	7.5	241.5	24.778	-9.624	5
17.5	254.0	28.602	-15.074	22	12.5	219.5	24.400	-.481	2	7.5	246.5	24.778	-7.118	5
17.5	259.5	23.835	-8.370	15	12.5	240.5	24.400	-12.434	5	7.5	252.0	29.734	-4.460	5
17.5	264.5	23.835	16.954	15	12.5	255.5	24.400	-2.858	5	7.5	257.5	24.778	-.205	6
17.5	269.5	23.835	22.787	23	12.5	260.5	24.400	1.478	6	7.5	262.5	24.778	2.903	5
17.5	275.0	28.602	19.296	12	12.5	265.5	24.400	2.979	12	7.5	267.5	24.778	3.012	7
17.5	280.5	23.835	4.214	17	12.5	271.0	29.280	10.933	19	7.5	272.5	24.778	14.875	15
17.5	285.5	23.835	18.139	12	12.5	276.5	24.400	28.110	13	7.5	277.5	24.778	18.089	23
17.5	290.5	23.835	22.254	18	12.5	281.5	24.400	-14.649	12	7.5	282.5	24.778	34.310	19
17.5	295.5	23.835	-27.373	19	12.5	286.5	24.400	-13.152	18	7.5	287.5	24.778	16.117	20
17.5	301.0	28.602	-51.823	9	12.5	291.5	24.400	-38.809	16	7.5	292.5	24.778	-5.648	6
17.5	306.5	23.835	-16.073	3	12.5	296.5	24.400	-28.872	17	7.5	297.5	24.778	-18.865	5
17.5	311.5	23.835	-14.523	7	12.5	301.5	24.400	-51.337	20	7.5	302.5	24.778	-24.645	5
17.5	316.5	23.835	-16.527	5	12.5	307.0	29.280	-30.641	17	7.5	307.5	24.778	-25.476	10
17.5	321.5	23.835	-22.278	4	12.5	312.5	24.400	-26.131	9	7.5	312.5	24.778	-35.382	15
17.5	327.0	28.602	-5.346	1	12.5	317.5	24.400	-17.224	16	7.5	317.5	24.778	-19.054	13
17.5	332.5	23.835	3.642	2	12.5	322.5	24.400	9.316	2	7.5	323.0	29.734	-14.654	12
17.5	337.5	23.835	19.459	5	12.5	327.5	24.400	-14.729	4	7.5	328.5	24.778	7.260	9
17.5	342.5	23.835	4.871	15	12.5	332.5	24.400	-5.311	9	7.5	333.5	24.778	-.446	10
17.5	348.0	28.602	13.180	19	12.5	337.5	24.400	-12.754	10	7.5	343.5	24.778	12.547	12
17.5	353.5	23.835	3.334	11	12.5	343.0	29.280	12.717	13	7.5	348.5	24.778	34.832	13
17.5	358.5	23.835	7.011	24	12.5	348.5	24.400	10.234	15	7.5	353.5	24.778	20.520	25
					12.5	353.5	24.400	8.520	25	7.5	358.5	24.778	14.360	25
12.5	3.5	24.400	-1.404	19	12.5	358.5	24.400	-.400	25					
12.5	8.5	24.400	10.796	17						2.5	8.5	24.968	16.366	9
12.5	13.5	24.400	7.106	15	7.5	3.5	24.778	16.281	11	2.5	13.5	24.968	11.947	4
12.5	19.0	29.280	.795	4	7.5	8.5	24.778	29.811	15	2.5	18.5	24.968	-17.784	9
12.5	24.5	24.400	-8.612	2	7.5	13.5	24.778	15.582	8	2.5	23.5	24.968	-28.735	14
12.5	29.5	24.400	4.239	5	7.5	18.5	24.778	-11.503	3	2.5	28.5	24.968	2.524	11
12.5	34.5	24.400	-16.513	3	7.5	23.5	24.778	-.989	1	2.5	33.5	24.968	-1.824	18
12.5	39.5	24.400	23.836	18	7.5	39.0	29.734	26.724	13	2.5	38.5	24.968	-1.909	2
12.5	44.5	24.400	1.695	16	7.5	44.5	24.778	3.669	2	2.5	43.5	24.968	-14.520	4
12.5	49.5	24.400	-1.885	17	7.5	49.5	24.778	-37.806	4	2.5	48.5	24.968	-37.729	15
12.5	55.0	29.280	-2.774	20	7.5	54.5	24.778	-25.621	19	2.5	53.5	24.968	-28.233	19
12.5	60.5	24.400	-13.282	14	7.5	59.5	24.778	-14.626	14	2.5	58.5	24.968	-23.980	19
12.5	65.5	24.400	-15.675	3	7.5	64.5	24.778	-31.264	17	2.5	63.5	24.968	-22.755	19
12.5	70.5	24.400	-36.628	16	7.5	69.5	24.778	-45.421	17	2.5	68.5	24.968	-38.951	9

Table 10. (Cont.)

Lat. (deg.)	Long. (deg.)	Area (deg. sq.)	Gravity anomaly (mgal)	No.	Lat. (deg.)	Long. (deg.)	Area (deg. sq.)	Gravity anomaly (mgal)	No.	Lat. (deg.)	Long. (deg.)	Area (deg. sq.)	Gravity anomaly (mgal)	No.
2.5	73.5	24.968	-43.730	15	-2.5	118.5	24.968	15.853	16	-7.5	160.5	24.778	38.830	12
2.5	78.5	24.968	-51.962	14	-2.5	123.5	24.968	-6.425	17	-7.5	170.5	24.778	-12.902	6
2.5	83.5	24.968	-39.937	8	-2.5	128.5	24.968	5.539	22	-7.5	175.5	24.778	-1.307	8
2.5	88.5	24.968	-20.365	9	-2.5	133.5	24.968	12.320	14	-7.5	181.0	29.734	-.524	9
2.5	93.5	24.968	-16.169	23	-2.5	138.5	24.968	6.852	12	-7.5	186.5	24.778	-8.019	1
2.5	98.5	24.968	-4.216	16	-2.5	143.5	24.968	24.280	25	-7.5	201.5	24.778	21.180	6
2.5	103.5	24.968	14.914	9	-2.5	148.5	24.968	39.795	23	-7.5	221.5	24.778	14.502	1
2.5	108.5	24.968	16.834	13	-2.5	153.5	24.968	22.087	14	-7.5	277.5	24.778	-6.911	5
2.5	113.5	24.968	13.864	4	-2.5	158.5	24.968	14.876	5	-7.5	282.5	24.778	-20.434	4
2.5	118.5	24.968	9.692	3	-2.5	173.5	24.968	-13.661	1	-7.5	287.5	24.778	-11.808	7
2.5	123.5	24.968	15.716	11	-2.5	178.5	24.968	1.834	12	-7.5	292.5	24.778	6.500	2
2.5	128.5	24.968	20.713	11	-2.5	183.5	24.968	-10.306	2	-7.5	297.5	24.778	2.226	1
2.5	133.5	24.968	15.161	1	-2.5	188.5	24.968	-3.894	2	-7.5	312.5	24.778	-31.498	22
2.5	143.5	24.968	10.360	16	-2.5	198.5	24.968	22.451	6	-7.5	317.5	24.778	-27.720	25
2.5	148.5	24.968	3.894	9	-2.5	273.5	24.968	-2.037	1	-7.5	323.0	29.734	.675	21
2.5	153.5	24.968	1.505	8	-2.5	278.5	24.968	-.677	8	-7.5	328.5	24.778	-24.126	11
2.5	158.5	24.968	.862	4	-2.5	283.5	24.968	18.736	10	-7.5	333.5	24.778	-4.959	3
2.5	178.5	24.968	2.909	6	-2.5	288.5	24.968	36.665	7	-7.5	338.5	24.778	-8.228	11
2.5	183.5	24.968	5.252	13	-2.5	298.5	24.968	-8.350	2	-7.5	343.5	24.778	-1.202	19
2.5	188.5	24.968	-5.817	9	-2.5	303.5	24.968	-7.244	2	-7.5	348.5	24.778	1.915	14
2.5	198.5	24.968	20.046	5	-2.5	308.5	24.968	-13.784	7	-7.5	353.5	24.778	-11.186	2
2.5	268.5	24.968	2.717	1	-2.5	313.5	24.968	-36.604	22	-7.5	358.5	24.778	-3.364	2
2.5	273.5	24.968	.954	3	-2.5	318.5	24.968	-17.034	15					
2.5	278.5	24.968	-.066	14	-2.5	323.5	24.968	-.221	4	-12.5	13.5	24.400	12.036	3
2.5	283.5	24.968	32.640	25	-2.5	328.5	24.968	-7.542	15	-12.5	24.5	24.400	1.072	6
2.5	288.5	24.968	18.844	21	-2.5	333.5	24.968	-5.591	18	-12.5	29.5	24.400	-14.394	12
2.5	303.5	24.968	-22.399	3	-2.5	338.5	24.968	-11.656	14	-12.5	34.5	24.400	-10.281	12
2.5	308.5	24.968	-3.098	3	-2.5	343.5	24.968	-9.872	9	-12.5	39.5	24.400	-22.606	6
2.5	313.5	24.968	-11.648	2	-2.5	348.5	24.968	4.045	3	-12.5	44.5	24.400	-27.116	12
2.5	318.5	24.968	-9.196	8	-2.5	353.5	24.968	3.462	3	-12.5	49.5	24.400	9.853	12
2.5	323.5	24.968	-4.127	14						-12.5	55.0	29.280	-6.300	11
2.5	328.5	24.968	9.909	18	-7.5	8.5	24.778	-9.439	4	-12.5	60.5	24.400	-33.435	5
2.5	333.5	24.968	2.486	8	-7.5	13.5	24.778	21.014	3	-12.5	65.5	24.400	6.266	10
2.5	343.5	24.968	-9.763	9	-7.5	18.5	24.778	-7.426	3	-12.5	70.5	24.400	-2.645	3
2.5	348.5	24.968	-18.940	2	-7.5	23.5	24.778	-15.282	16	-12.5	80.5	24.400	-21.535	6
2.5	353.5	24.968	13.537	3	-7.5	28.5	24.778	-9.624	20	-12.5	91.0	29.280	-24.265	5
2.5	358.5	24.968	4.415	1	-7.5	33.5	24.778	2.922	24	-12.5	96.5	24.400	-12.736	14
					-7.5	39.0	29.734	-9.979	19	-12.5	101.5	24.400	-4.876	16
-2.5	8.5	24.968	13.370	5	-7.5	44.5	24.778	-34.675	18	-12.5	106.5	24.400	8.505	13
-2.5	13.5	24.968	-13.306	4	-7.5	49.5	24.778	-11.957	13	-12.5	111.5	24.400	-10.129	22
-2.5	18.5	24.968	-28.943	21	-7.5	54.5	24.778	-3.941	10	-12.5	116.5	24.400	-20.489	20
-2.5	23.5	24.968	-36.689	24	-7.5	59.5	24.778	-10.570	6	-12.5	121.5	24.400	6.849	24
-2.5	28.5	24.968	8.202	21	-7.5	64.5	24.778	-4.842	7	-12.5	127.0	29.280	17.720	25
-2.5	33.5	24.968	-9.115	23	-7.5	69.5	24.778	-9.777	10	-12.5	132.5	24.400	25.930	23
-2.5	38.5	24.968	15.188	14	-7.5	74.5	24.778	-3.710	5	-12.5	137.5	24.400	17.015	22
-2.5	43.5	24.968	-40.196	20	-7.5	79.5	24.778	-28.105	7	-12.5	142.5	24.400	22.560	25
-2.5	48.5	24.968	-13.733	10	-7.5	89.5	24.778	-14.255	1	-12.5	147.5	24.400	12.120	25
-2.5	53.5	24.968	-11.514	22	-7.5	94.5	24.778	-10.598	5	-12.5	152.5	24.400	24.650	21
-2.5	58.5	24.968	-21.095	23	-7.5	99.5	24.778	-1.145	13	-12.5	157.5	24.400	24.160	9
-2.5	63.5	24.968	-21.198	13	-7.5	104.5	24.778	-5.725	24	-12.5	163.0	29.280	50.406	14
-2.5	68.5	24.968	-31.126	9	-7.5	110.0	29.734	16.111	22	-12.5	168.5	24.400	14.160	15
-2.5	73.5	24.968	-44.473	13	-7.5	115.5	24.778	19.249	20	-12.5	178.5	24.400	-.820	7
-2.5	78.5	24.968	-55.063	13	-7.5	120.5	24.778	.295	22	-12.5	183.5	24.400	15.270	5
-2.5	83.5	24.968	-51.399	20	-7.5	125.5	24.778	-18.224	24	-12.5	188.5	24.400	31.729	8
-2.5	88.5	24.968	-22.670	13	-7.5	130.5	24.778	-26.800	25	-12.5	193.5	24.400	3.856	8
-2.5	93.5	24.968	-14.404	10	-7.5	135.5	24.778	13.330	13	-12.5	199.0	29.280	13.372	3
-2.5	98.5	24.968	-4.687	19	-7.5	140.5	24.778	20.482	24	-12.5	281.5	24.400	-14.079	7
-2.5	103.5	24.968	40.694	7	-7.5	145.5	24.778	33.440	25	-12.5	286.5	24.400	3.681	6
-2.5	108.5	24.968	25.538	17	-7.5	150.5	24.778	16.440	25	-12.5	291.5	24.400	16.763	5
-2.5	113.5	24.968	9.633	2	-7.5	155.5	24.778	43.493	23	-12.5	296.5	24.400	35.801	5

Table 10. (Cont.)

Lat. (deg.)	Long. (deg.)	Area (deg. sq.)	Gravity anomaly (mgal)	No.	Lat. (deg.)	Long. (deg.)	Area (deg. sq.)	Gravity anomaly (mgal)	No.	Lat. (deg.)	Long. (deg.)	Area (deg. sq.)	Gravity anomaly (mgal)	No.
-12.5	307.0	29.280	-31.921	1	-17.5	353.5	23.835	-.330	1	-27.5	54.5	22.168	11.861	3
-12.5	312.5	24.400	4.914	20	-17.5	358.5	23.835	.391	4	-27.5	60.0	26.602	-1.154	10
-12.5	317.5	24.400	-7.800	25						-27.5	66.0	26.602	16.978	5
-12.5	322.5	24.400	-5.204	16	-22.5	3.5	23.090	2.979	6	-27.5	71.5	22.168	37.801	8
-12.5	327.5	24.400	-10.802	8	-22.5	9.0	27.708	-7.821	2	-27.5	77.0	26.602	9.062	2
-12.5	343.0	29.280	-4.075	8	-22.5	14.5	23.090	15.062	4	-27.5	82.5	22.168	-8.809	5
-12.5	348.5	24.400	-7.906	10	-22.5	19.5	23.090	1.146	6	-27.5	88.0	26.602	-2.474	5
-12.5	353.5	24.400	-4.770	2	-22.5	25.0	27.708	8.290	10	-27.5	94.0	26.602	-11.078	5
-12.5	358.5	24.400	-3.653	2	-22.5	30.5	23.090	2.687	18	-27.5	99.5	22.168	-11.218	5
					-22.5	36.0	27.708	-5.662	6	-27.5	105.0	26.602	-21.909	9
-17.5	3.5	23.835	13.958	1	-22.5	41.5	23.090	-8.375	21	-27.5	111.0	26.602	-17.837	10
-17.5	8.5	23.835	-7.422	1	-22.5	46.5	23.090	29.488	19	-27.5	116.5	22.168	1.299	23
-17.5	14.0	28.602	6.796	2	-22.5	52.0	27.708	2.990	10	-27.5	122.0	26.602	-7.391	17
-17.5	19.5	23.835	6.534	1	-22.5	57.5	23.090	7.109	22	-27.5	127.5	22.168	-10.660	22
-17.5	24.5	23.835	-1.555	7	-22.5	62.5	23.090	24.575	15	-27.5	133.0	26.602	-16.484	23
-17.5	29.5	23.835	8.143	12	-22.5	68.0	27.708	26.512	15	-27.5	139.0	26.602	-7.600	25
-17.5	35.0	28.602	-11.134	9	-22.5	73.5	23.090	12.843	16	-27.5	144.5	22.168	-1.640	25
-17.5	40.5	23.835	-15.263	12	-22.5	79.0	27.708	1.788	5	-27.5	150.0	26.602	17.580	25
-17.5	45.5	23.835	8.262	20	-22.5	84.5	23.090	-11.814	4	-27.5	156.0	26.602	26.062	8
-17.5	50.5	23.835	13.040	9	-22.5	89.5	23.090	-15.716	5	-27.5	161.5	22.168	10.026	5
-17.5	55.5	23.835	-3.940	14	-22.5	95.0	27.708	-22.964	6	-27.5	167.0	26.602	20.928	3
-17.5	61.0	28.602	16.267	15	-22.5	100.5	23.090	-29.388	8	-27.5	172.5	22.168	8.569	1
-17.5	66.5	23.835	-1.092	7	-22.5	105.5	23.090	-5.182	2	-27.5	178.0	26.602	8.322	5
-17.5	71.5	23.835	-1.188	1	-22.5	111.0	27.708	6.657	11	-27.5	184.0	26.602	34.426	4
-17.5	76.5	23.835	8.516	6	-22.5	116.5	23.090	2.465	17	-27.5	246.0	26.602	.769	4
-17.5	81.5	23.835	-14.863	12	-22.5	122.0	27.708	-2.560	25	-27.5	251.5	22.168	-.856	8
-17.5	87.0	28.602	-20.553	11	-22.5	127.5	23.090	-7.640	25	-27.5	291.0	26.602	54.388	23
-17.5	92.5	23.835	-31.077	13	-22.5	132.5	23.090	-7.400	25	-27.5	296.5	22.168	6.735	24
-17.5	97.5	23.835	-19.937	12	-22.5	138.0	27.708	14.620	25	-27.5	302.0	26.602	10.505	16
-17.5	102.5	23.835	-13.004	8	-22.5	143.5	23.090	3.560	25	-27.5	307.5	22.168	-1.413	20
-17.5	108.0	28.602	-14.904	7	-22.5	148.5	23.090	25.161	23	-27.5	313.0	26.602	-19.275	17
-17.5	113.5	23.835	-21.595	15	-22.5	154.0	27.708	9.715	9	-27.5	319.0	26.602	-10.402	3
-17.5	118.5	23.835	2.726	22	-22.5	159.5	23.090	5.248	3	-27.5	324.5	22.168	-7.075	4
-17.5	123.5	23.835	10.200	25	-22.5	165.0	27.708	46.006	9	-27.5	352.5	22.168	-5.643	1
-17.5	128.5	23.835	12.720	25	-22.5	170.5	23.090	18.574	6					
-17.5	134.0	28.602	4.660	25	-22.5	175.5	23.090	27.652	3	-32.5	4.0	25.294	8.285	1
-17.5	139.5	23.835	7.440	25	-22.5	181.0	27.708	41.331	3	-32.5	10.0	25.294	7.421	9
-17.5	144.5	23.835	23.880	25	-22.5	186.5	23.090	-1.998	6	-32.5	16.0	25.294	2.616	17
-17.5	149.5	23.835	14.640	25	-22.5	240.0	27.708	4.707	4	-32.5	22.0	25.294	24.920	25
-17.5	155.0	28.602	9.080	25	-22.5	245.5	23.090	4.897	4	-32.5	28.0	25.294	11.290	21
-17.5	160.5	23.835	-.108	13	-22.5	283.0	27.708	1.978	1	-32.5	33.5	21.078	29.045	10
-17.5	165.5	23.835	14.419	3	-22.5	288.5	23.090	11.143	12	-32.5	39.0	25.294	-12.681	7
-17.5	170.5	23.835	26.919	6	-22.5	294.0	27.708	50.681	16	-32.5	45.0	25.294	40.892	7
-17.5	175.5	23.835	33.870	8	-22.5	299.5	23.090	10.104	5	-32.5	51.0	25.294	9.488	3
-17.5	181.0	28.602	10.188	7	-22.5	304.5	23.090	-7.737	8	-32.5	63.0	25.294	-6.376	6
-17.5	201.5	23.835	16.979	1	-22.5	310.0	27.708	-16.743	22	-32.5	75.0	25.294	23.630	5
-17.5	207.0	28.602	37.108	1	-22.5	315.5	23.090	-4.580	19	-32.5	92.5	21.078	11.293	2
-17.5	212.5	23.835	28.865	1	-22.5	320.5	23.090	-9.694	7	-32.5	98.0	25.294	-13.817	8
-17.5	217.5	23.835	1.184	1	-22.5	326.0	27.708	-18.491	6	-32.5	104.0	25.294	-19.971	9
-17.5	269.5	23.835	1.113	1	-22.5	358.5	23.090	2.047	3	-32.5	110.0	25.294	-21.511	11
-17.5	280.5	23.835	-21.446	1						-32.5	116.0	25.294	-.900	24
-17.5	285.5	23.835	8.016	4	-27.5	4.0	26.602	2.170	5	-32.5	122.0	25.294	-13.688	24
-17.5	290.5	23.835	61.835	13	-27.5	9.5	22.168	2.199	5	-32.5	128.0	25.294	-14.334	12
-17.5	295.5	23.835	32.567	15	-27.5	15.0	26.602	13.646	15	-32.5	134.0	25.294	-8.299	20
-17.5	301.0	28.602	17.191	10	-27.5	21.0	26.602	17.090	23	-32.5	140.0	25.294	4.620	25
-17.5	306.5	23.835	-6.592	1	-27.5	26.5	22.168	27.600	25	-32.5	146.0	25.294	4.696	24
-17.5	311.5	23.835	-21.122	18	-27.5	32.0	26.602	25.801	17	-32.5	151.5	21.078	26.407	22
-17.5	316.5	23.835	-25.200	25	-27.5	37.5	22.168	-16.830	12	-32.5	157.0	25.294	2.367	4
-17.5	321.5	23.835	-17.521	17	-27.5	43.0	26.602	15.210	12	-32.5	175.0	25.294	32.424	2
-17.5	327.0	28.602	-17.618	7	-27.5	49.0	26.602	9.626	18	-32.5	181.0	25.294	-21.087	5

Table 10. (Cont.)

Lat. (deg.)	Long. (deg.)	Area (deg. sq.)	Gravity anomaly (mgal)	No.	Lat. (deg.)	Long. (deg.)	Area (deg. sq.)	Gravity anomaly (mgal)	No.	Lat. (deg.)	Long. (deg.)	Area (deg. sq.)	Gravity anomaly (mgal)	No.
-32.5	187.0	25.294	9.826	2	-47.5	70.5	23.638	24.069	5	-77.5	170.0	23.801	2.559	12
-32.5	252.0	25.294	-3.354	3	-47.5	166.5	23.638	49.171	6	-77.5	192.5	24.883	-7.921	10
-32.5	258.0	25.294	-6.059	6	-47.5	173.5	23.638	16.816	3	-77.5	215.0	23.801	-7.606	9
-32.5	264.0	25.294	-28.340	1	-47.5	186.5	23.638	1.782	1	-77.5	237.5	24.883	5.369	21
-32.5	287.0	25.294	33.359	10	-47.5	269.0	27.015	9.129	2	-77.5	260.0	23.801	-1.197	22
-32.5	293.0	25.294	14.200	25	-47.5	276.5	23.638	13.083	6	-77.5	282.5	24.883	15.695	9
-32.5	299.0	25.294	10.840	25	-47.5	284.0	27.015	-11.696	3	-77.5	305.0	23.801	9.217	2
-32.5	305.0	25.294	21.636	19	-47.5	291.5	23.638	-3.243	13	-77.5	327.5	24.883	-4.844	8
-32.5	311.0	25.294	9.453	7	-47.5	298.5	23.638	-8.655	7					
-32.5	317.0	25.294	8.160	4	-47.5	306.0	27.015	-4.645	15	-82.5	61.0	26.097	43.711	6
-32.5	323.0	25.294	2.743	4						-82.5	141.0	26.097	-25.305	11
-32.5	328.5	21.078	-14.174	3	-52.5	70.5	27.386	22.384	3	-82.5	181.0	26.097	-17.748	14
-32.5	334.0	25.294	12.040	3	-52.5	160.5	27.386	24.719	1	-82.5	221.0	26.097	-6.052	10
-32.5	352.0	25.294	-2.793	3	-52.5	169.0	24.343	18.802	2	-82.5	261.0	26.097	7.337	24
-32.5	358.0	25.294	16.348	3	-52.5	275.0	24.343	7.128	1	-82.5	301.0	26.097	-2.389	13
					-52.5	283.0	24.343	5.317	9					
-37.5	10.5	27.759	-.912	4	-52.5	291.5	27.386	10.538	11	-87.5	181.0	26.163	-11.254	13
-37.5	23.0	23.793	9.760	9	-52.5	300.0	24.343	10.639	17	-87.5	301.0	26.163	-5.175	10
-37.5	29.5	27.759	10.872	12	-52.5	308.0	24.343	-15.984	2					
-37.5	36.0	23.793	9.708	4	-52.5	324.0	24.343	35.131	2					
-37.5	42.0	23.793	20.979	3										
-37.5	61.0	23.793	.758	3	-57.5	282.5	24.171	-12.770	1					
-37.5	73.5	27.759	-3.986	7	-57.5	291.5	24.171	18.871	7					
-37.5	80.0	23.793	-3.384	7	-57.5	301.0	26.856	29.660	8					
-37.5	86.0	23.793	8.137	3	-57.5	310.5	24.171	17.135	13					
-37.5	92.5	27.759	-6.915	4	-57.5	319.5	24.171	5.049	1					
-37.5	99.0	23.793	-15.164	6	-57.5	328.5	24.171	32.736	3					
-37.5	105.0	23.793	-24.974	4	-57.5	338.0	26.856	16.979	1					
-37.5	137.0	23.793	3.940	8										
-37.5	143.0	23.793	6.314	20	-62.5	301.0	23.080	46.673	19					
-37.5	149.5	27.759	17.581	14	-62.5	311.5	25.388	35.603	5					
-37.5	156.0	23.793	-4.093	5										
-37.5	162.0	23.793	1.597	2	-67.5	33.5	24.867	36.547	6					
-37.5	168.5	27.759	7.819	5	-67.5	46.0	22.954	38.894	2					
-37.5	175.0	23.793	22.308	14	-67.5	58.5	24.867	35.643	5					
-37.5	181.0	23.793	-.403	7	-67.5	71.5	24.867	21.231	3					
-37.5	257.0	23.793	-2.376	1	-67.5	84.5	24.867	19.622	4					
-37.5	263.0	23.793	-2.120	7	-67.5	97.5	24.867	31.134	12					
-37.5	286.5	27.759	31.916	16	-67.5	110.5	24.867	21.734	11					
-37.5	295.0	23.793	1.630	20	-67.5	123.5	24.867	12.617	1					
-37.5	301.0	23.793	16.278	21	-67.5	136.0	22.954	28.097	7					
-37.5	307.0	23.793	5.925	10	-67.5	264.5	24.867	7.581	1					
-37.5	313.5	27.759	-12.828	6	-67.5	290.5	24.867	27.971	7					
-37.5	339.0	23.793	10.132	2										
-37.5	345.0	23.793	13.843	1	-72.5	25.5	25.552	17.115	4					
-37.5	351.5	27.759	4.123	2	-72.5	91.0	24.049	18.121	12					
					-72.5	107.5	25.552	-27.781	6					
-42.5	72.5	25.797	-1.028	5	-72.5	140.0	24.049	-8.875	8					
-42.5	147.0	22.111	17.171	5	-72.5	156.5	25.552	-9.218	4					
-42.5	167.5	25.797	3.057	6	-72.5	173.0	24.049	-13.404	1					
-42.5	174.5	25.797	15.599	16	-72.5	205.5	25.552	-13.372	2					
-42.5	262.5	25.797	1.782	1	-72.5	238.0	24.049	-19.105	2					
-42.5	269.5	25.797	-4.229	8	-72.5	254.5	25.552	-1.188	1					
-42.5	282.5	25.797	2.816	3	-72.5	271.0	24.049	17.750	6					
-42.5	289.5	25.797	37.122	19	-72.5	287.5	25.552	38.943	8					
-42.5	296.5	25.797	2.044	12										
-42.5	303.5	25.797	-7.730	15	-77.5	80.0	23.601	24.472	5					
-42.5	310.0	22.111	-13.162	8	-77.5	102.5	24.883	-5.698	11					
-42.5	357.5	25.797	-12.524	1	-77.5	125.0	23.801	-.455	2					
					-77.5	147.5	24.883	-23.413	14					

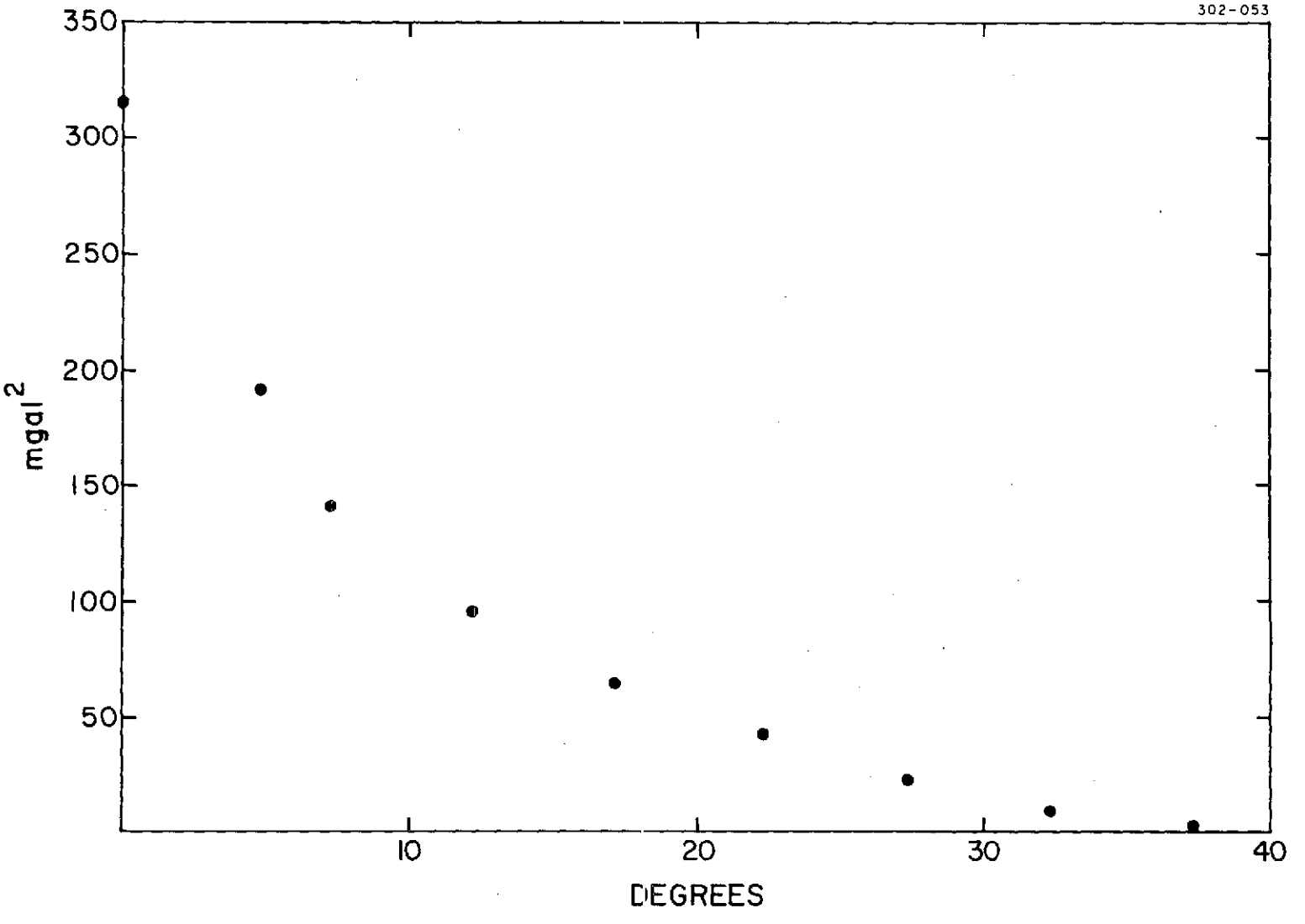

Figure 10. The covariance function of 5° × 5° mean block gravity anomalies.

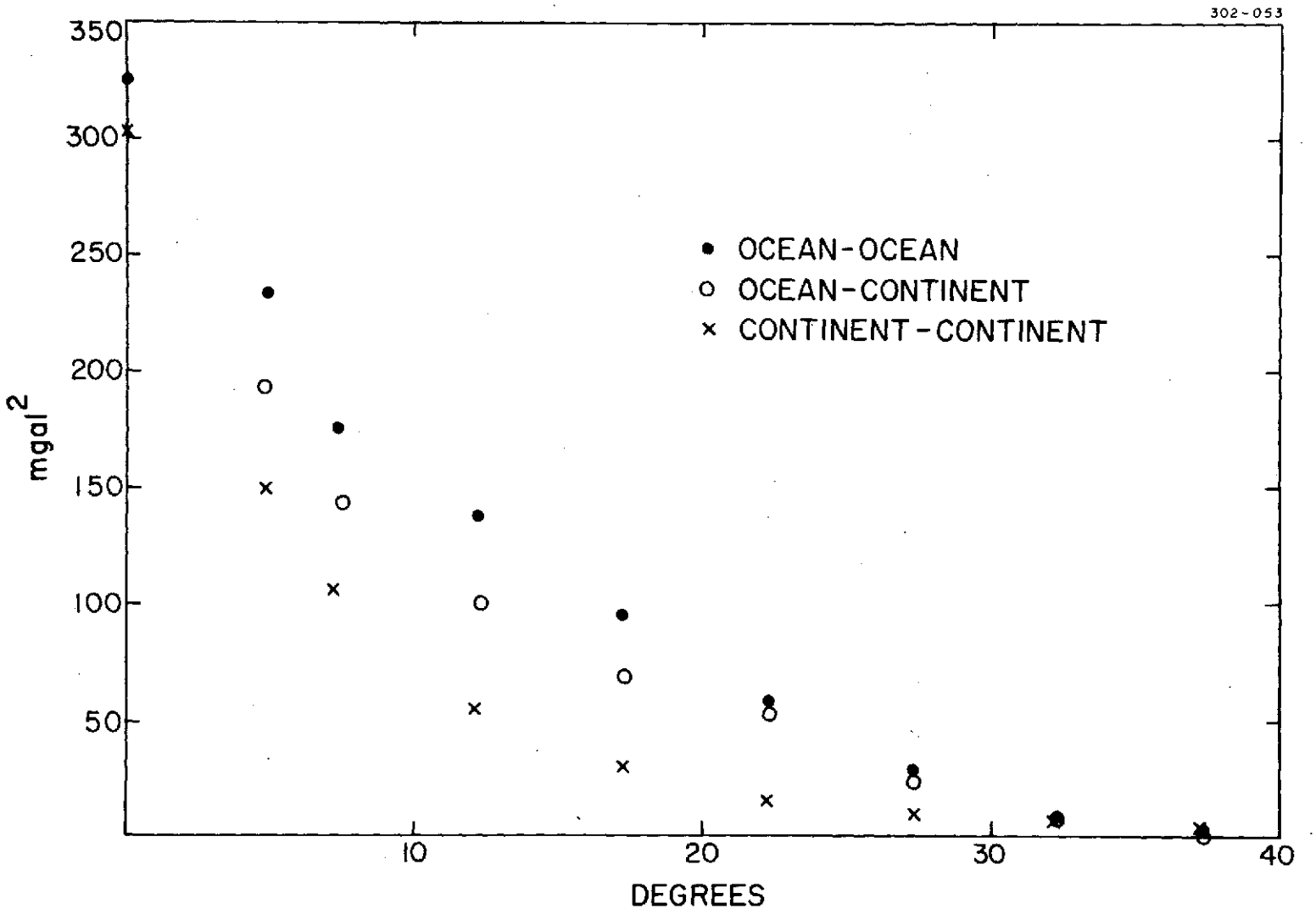

Figure 11. The covariance functions of 5° × 5° mean block gravity anomalies for a -1-km ocean–continent boundary.

Table 11. The covariance function of 5° × 5° mean block gravity anomalies.

Average angular distance	Covariance function ($mgal^2$)
0°	314
4.85	192
7.32	141
12.23	97
17.25	65
22.32	43
27.33	22
32.29	8
37.33	2

Table 12. The covariance functions of 5° × 5° mean block gravity anomalies for a -1-km ocean–continent boundary.

Ocean–ocean		Ocean–continent		Continent–continent	
Average angular distance	Covariance function ($mgal^2$)	Average angular distance	Covariance function ($mgal^2$)	Average angular distance	Covariance function ($mgal^2$)
0°	325			0°	302
4.84	233	4.87	192	4.85	150
7.31	175	7.55	143	7.22	107
12.27	141	12.36	100	12.18	50
17.25	94	17.32	72	17.19	29
22.31	59	22.38	52	22.25	16
27.32	32	27.36	25	27.29	9
32.28	9	32.30	8	32.30	7
37.34	4	37.34	0	37.31	5

PART V

DETERMINATION OF THE GEOPOTENTIAL

ABSTRACT

Laser and optical satellite-tracking data are combined with surface-gravity data to determine spherical harmonics representing the geopotential to 18th degree and order. The resulting generalized gravity field has an accuracy of 64 $mgal^2$, i.e., a generalized geoid with an accuracy of 2.5 m. Satellite orbits are computed to an accuracy of 5 to 10 m.

RESUME

Les données laser et optiques de poursuite de satellites sont combinées à celles de gravité de surface, de manière à déterminer les harmoniques sphériques représentant le géopotentiel au 18 ème degré. Le champ de gravité généralisé qui en résulte a une précision de 64 $mgal^2$, c'est-à-dire un géoïde généralisé ayant une précision de 2,5m. Les orbites de satellites sont calculées avec une précision de 5 à 10 m.

КОНСПЕКТ

Совмещаются данные лазерного и оптического слежений за спутниками с данными площади-гравитации для определения сферических гармоник представляющих геопотенциал, до 18-ой степени и порядка. Исходное общее поле гравитации имеет точность в 64 $мгал^2$, т.е. обобщенный геоид с точностью в 2,5 м. Орбиты спутников вычисляются с точностью от 5 до 10 м.

SMITHSONIAN INSTITUTION STANDARD EARTH III (GEOPOTENTIAL)

E. M. Gaposchkin, M. R. Williamson, Y. Kozai, and G. Mendes

1. INTRODUCTION

The Smithsonian Astrophysical Observatory (SAO) has published a series of Standard Earth models based on satellite-tracking and other data (Kozai, 1964, 1969; Gaposchkin, 1967, 1970a; Köhnlein, 1967; Veis, 1967a, b; Whipple, 1967; Lundquist and Veis, 1966; Lambeck, 1969, 1970; Gaposchkin and Lambeck, 1970). There has been a steady advance in the accuracy of the analytical treatment, the accuracy and completeness of the data, and the significance of the results.

Each Standard Earth model consists of 1) a set of geocentric coordinates for stations observing satellites and 2) a set of spherical harmonics representing the geopotential. These two sets of unknowns can be correlated, and both sets of parameters have been determined in the same computation. This led, for example in Gaposchkin and Lambeck (1970), to solving a system with 428 unknowns – i.e., for 39 stations and gravity-field coefficients complete through degree and order 16. Evaluation of the Gaposchkin and Lambeck (1970) results indicated that the remaining errors in these parameters were small; that is, the corrections to the parameters would be small. Therefore, the effect of errors in the adopted station coordinates on the determination of the gravity field, and vice versa, would be small, and the two sets of parameters could be computed separately.

A general revision of the parameters for Standard Earth III (SE III) was undertaken because of new and improved data for almost all types of observations. Optical satellite observations have been augmented by a large body of laser data with global coverage from the International Satellite Geodesy Experiment (ISAGEX). Two satellites with inclinations significantly lower (5° and 15°) than previously available have been launched

since 1970. Available surface-gravity data have been significantly improved by the distribution of a compilation of gravity anomalies by the Aeronautical Chart and Information Center (ACIC). Determinations of station coordinates have been improved by data from the worldwide BC-4 geometrical network. Finally, information on site locations from the Deep Space Net (DSN) of the Jet Propulsion Laboratory (JPL) has been revised with the addition of new data and improved processing techniques.

The analysis was divided into two parts because of the initial high accuracy of the geodetic parameters, the good coverage of all types of observational material, and the result from Gaposchkin and Lambeck (1970) indicating that the interaction between the gravity field and the station coordinates is relatively small. The determinations of the gravity field and of station coordinates were carried out in parallel; the latter is described in Gaposchkin, Latimer, and Veis (1973). In an iterative process, the improved coordinates were used in the next iteration for the gravity field, and then the improved gravity field was used in the subsequent iteration for the station coordinates. This process, known as the block Gauss-Seidel iteration, will rigorously converge.

Gaposchkin (1970a) has shown that, except for isolated harmonics, the gravity field beyond 18th or 20th degree has a negligible effect on a satellite. The only exceptions are some zonal harmonics that give rise to secular and long-period effects, and the resonant harmonics. Therefore, one cannot hope to obtain from analysis of satellite perturbations much more detail beyond 16th degree and order than is already available. Greater detail will have to come from other methods, such as terrestrial gravimetry (see Section 7). The purpose here is to improve those harmonics to which satellite orbits are sensitive. Many of the harmonics between 10th and 18th degree are not very well determined from satellite-perturbation analysis, but terrestrial gravimetry, when combined with satellite data, provides a good determination of these coefficients. So, the objectives are to improve the low-degree and low-order harmonics from satellite data and the higher degree and order harmonics from terrestrial data.

Since the gravity field beyond 18th degree does not give rise to an observable change in satellite position, the satellite observations could be modeled with the use of a gravity field complete through degree and order 18, including, of course, some additional resonant and zonal harmonics. Therefore, there is no model error due to neglected higher harmonics. However, the surface-gravity data are given in area means of 550 km × 550 km squares. This surface distribution of gravity would require a spherical harmonic development to $\ell = m = 36$. Therefore, using a gravity field through degree and order 18 will have a significant model error that must be taken into account in establishing weights and making comparisons with surface-gravity data.

2. TERRESTRIAL GRAVITY DATA

The primary objective of the analysis of terrestrial gravity data is to obtain mean anomalies for regions 550 km × 550 km. When these data are combined with the satellite-perturbation analysis, the spherical harmonics representing the geopotential can be determined. A set of gravity data with known (and preferably simple) statistical properties is needed. Our approach is based on covariance analysis, following the ideas of Wiener (1966) and Kolmogoroff. When this technique is used in communications engineering, it is sometimes known as filtering theory. The ideas here are an extension of a one-dimensional time series to the two-dimensional surface of a sphere (Kaula, 1967).

Estimation of gravity by covariance methods hinges on the stationarity of gravity data; that is, the statistical properties of the data are the same no matter where the data are taken. There is some evidence that gravity data are not stationary; however, if some subsets of the total gravity population are stationary, then gravity covariance functions between sets and within each set can be defined.

2.1 The 1° × 1° Data Available

A set of 1° × 1° mean free-air anomalies, containing 19,115 measured means, was obtained from ACIC (1971), and another set, of 1454 1° × 1° means for Australia, from Mather (1970). The two sets were combined, with the Mather data being used for all areas they covered. Figure 1 shows the geographical coverage of all the data. The combined data set contained 19,328 means. A complete set of 1° × 1° mean topographic heights, used to define oceanic and continental areas, was obtained from Kaula (Kaula and Lee, 1967). The distribution of 1° × 1° mean gravity data is summarized in Table 1.

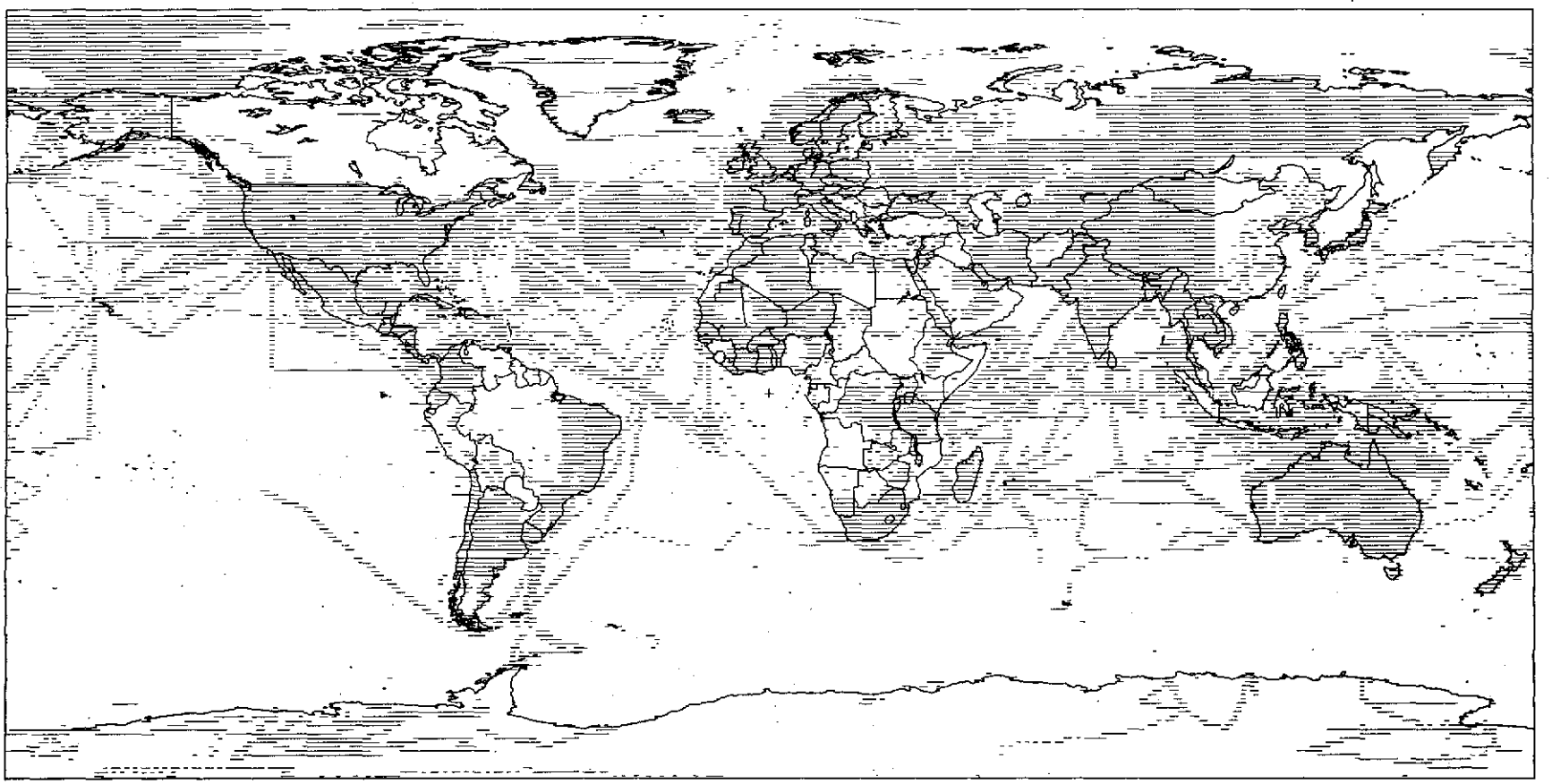

Figure 1. Distribution of 1° × 1° mean surface-gravity data.

Table 1. Distribution of 1° × 1° mean gravity anomalies.

Boundary (km)	Ocean		Continent	
	Measured	Total	Measured	Total
0	9213	42918	10115	21882
-1	7015	36199	12313	28601

The estimated uncertainty given with each gravity anomaly for 99.9% of the data is less than 25 mgal. Comparing the Mather data with the ACIC data at the 1241 common points, we find that the average difference is 1.7 mgal and the root-mean-square difference is 20 mgal. At a number of points, the discrepancy between the two sets exceeds 100 mgal.

2.2 The Estimate Procedure

Kaula (1967) has developed a procedure that greatly simplies the calculation of the covariance function, which is called the block covariance function, and the gravity estimates. This method has both advantages and disadvantages. The disadvantages follow:

A. The estimate of gravity does not make use of all the gravity information; i.e., the estimates are not so good as possible.

B. The covariance function must be determined by using only the combinations of anomalies within blocks and therefore does not employ all possible combinations of the data.

The advantages of Kaula's method are as follows:

A. It greatly simplifies calculation of the covariance function and the gravity estimates.

B. It produces mean anomalies 550 km × 550 km with uncorrelated errors.

C. The statistical properties of data within a block may be closer to stationarity since the method involves primarily the short-distance covariance.

If the gravity signal were a stationary process, then it would have the same statistical properties everywhere. Possible nonstationarity was investigated by determining the covariance function for subsets of gravity data. A separation of oceanic from continental gravity was used. A 0- and a 1-km depth were used to define the ocean–continent boundary, which was determined from topographic data. The boundary was also expanded to a width of 400 km for the 1-km depth, and the covariance functions were computed without the gravity data in that region. Finally, gravity data were divided into an equatorial set, $|\phi| < \pi/4$, and a polar set, $|\phi| > \pi/4$. The covariance functions for all the gravity data and for the four sets of split data and the block covariance function are plotted in Figures 2a to 2g. Detailed numerical values are given in Part IV of this Report. Since the differences between the covariance functions are significant, we conclude that gravity is not stationary. Any estimation procedure that makes that assumption must be carefully examined.

The different estimates of gravity from the global covariance estimator, from the split covariance estimators with a 0- and a -1-km ocean–continent boundary, and from the Kaula estimator were obtained and compared. At the equator, the Kaula-type units and the $1° \times 1°$ areas coincide, so that the four estimates can be compared directly. Figure 3 shows a few blocks at the equator. Large differences are in blocks with few observed points. In the combination with satellite data, these points will have a small effect due to the weighting, which is proportional to the number of units contributing to the average. Therefore, by using the block covariance estimator of Kaula, we obtained a statistically independent set of 550 km × 550 km averages with no loss of accuracy. Block covariance provides the optimum set of gravity anomalies to be used in combination with satellite observations. Of course, of all the methods used here, a split covariance estimator is preferable for the prediction of $1° \times 1°$ mean gravity anomalies.

The gravity anomalies are given with respect to the international gravity formula (Heiskanen and Moritz, 1967, p. 79) and must be corrected to refer to the best-fitting ellipsoid defined by J_2 and the adopted values of a_e, GM, and ω_e. We must also include the Potsdam correction of -14 mgal. Using the following initial values:

$$J_2 = 1082.637 \quad ,$$

$$a_e = 6.378140 \times 10^8 \text{ cm} \quad ,$$

$$GM = 3.986013 \times 10^{20} \text{ cm}^3 \text{ sec}^{-2} \quad ,$$

and

$$\omega_e = 7.292115085 \times 10^{-5} \text{ sec}^{-1} \quad ,$$

we have

$$1/f = 298.256 \quad ,$$

and the correction

$$\delta g_{SAO} - \delta g_{int} = 1.3 - 13.8 \sin^2 \phi \text{ mgal} \quad .$$

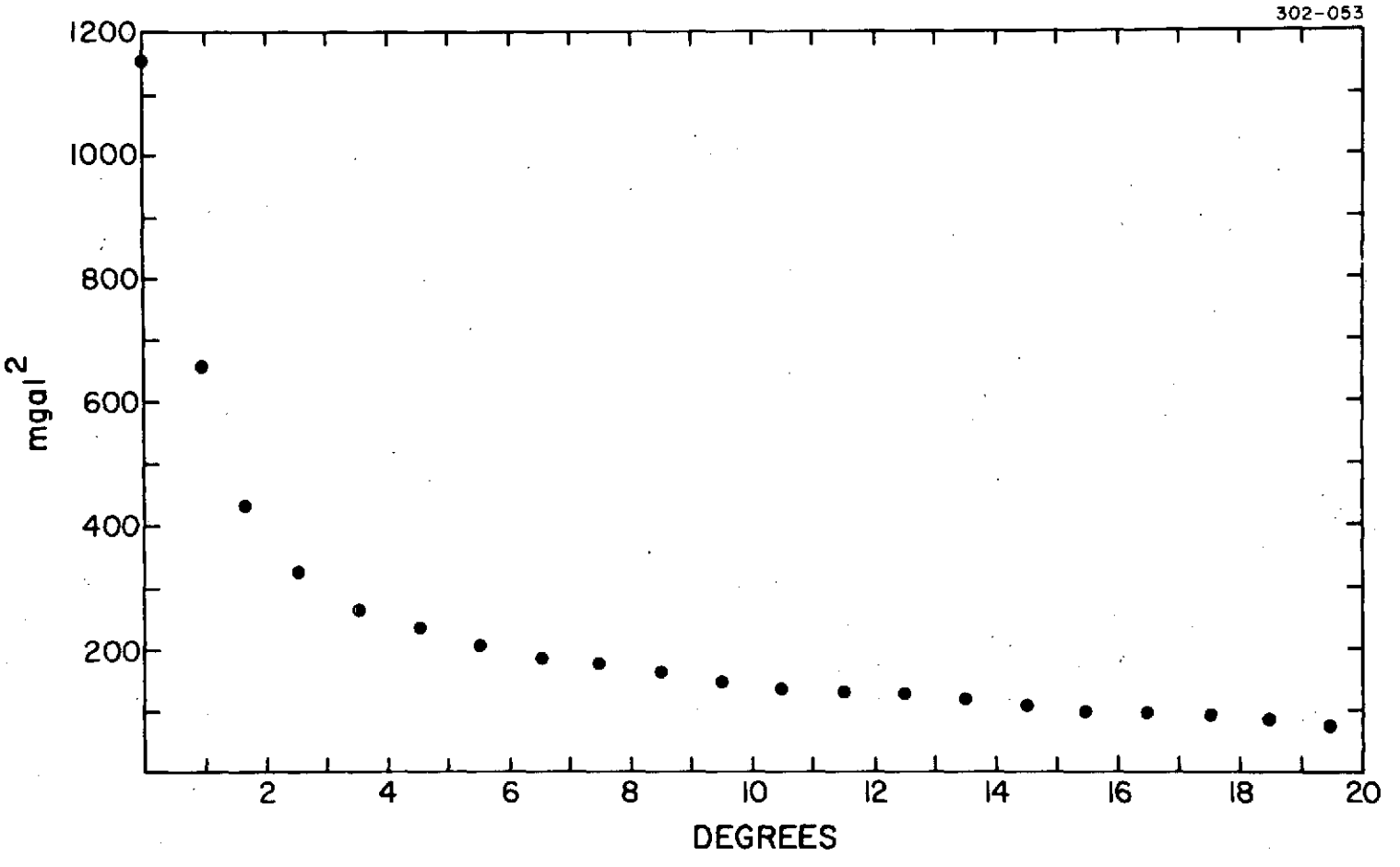

Figure 2a. The covariance function of 1° × 1° mean gravity anomalies.

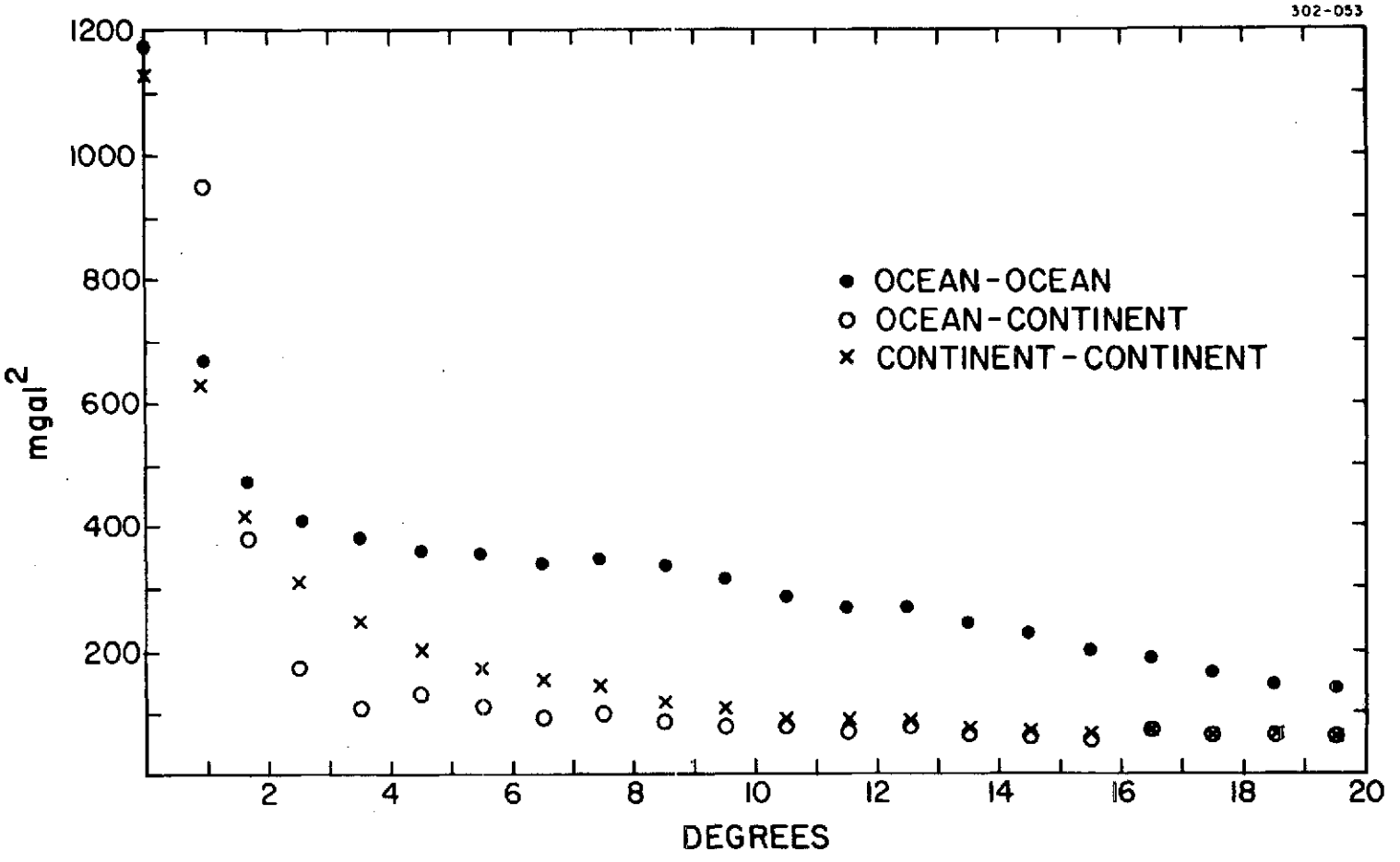

Figure 2b. The covariance functions of 1° × 1° mean gravity anomalies for a -1-km ocean–continent boundary.

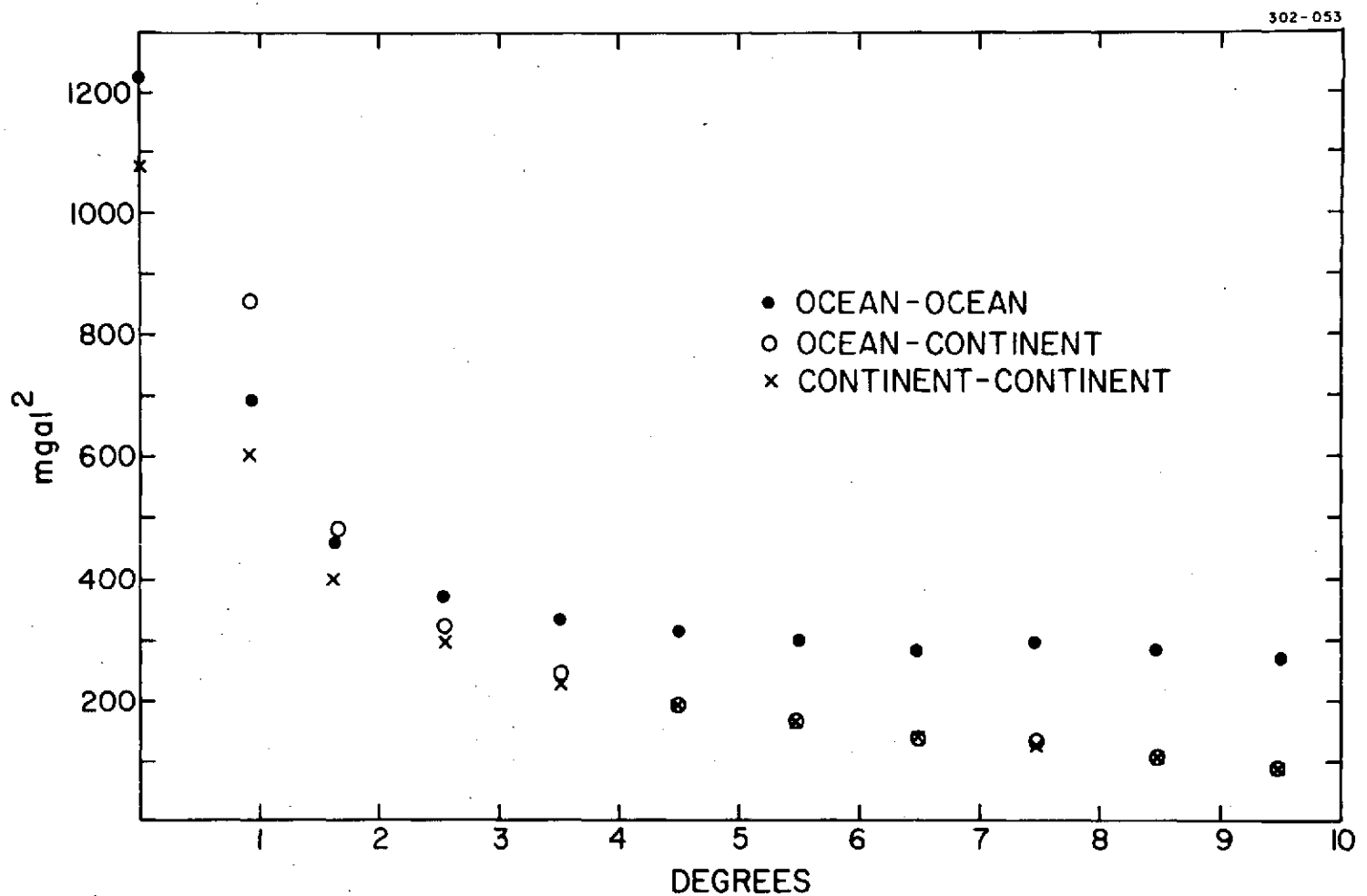

Figure 2c. The covariance functions of 1° × 1° mean gravity anomalies for a 0-km ocean–continent boundary.

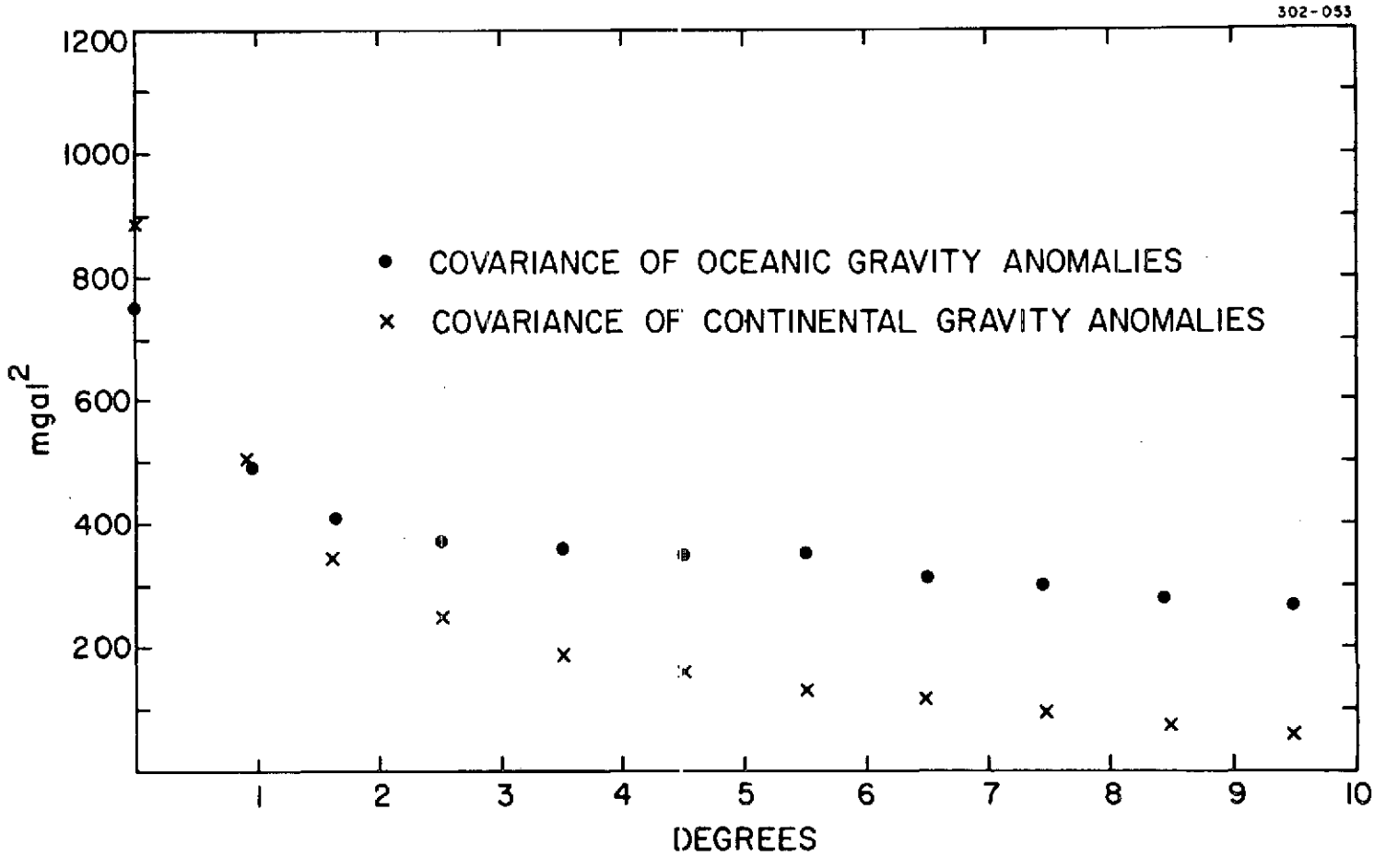

Figure 2d. The covariance functions of 1° × 1° mean gravity anomalies for a -1-km ocean–continent boundary of 400-km width.

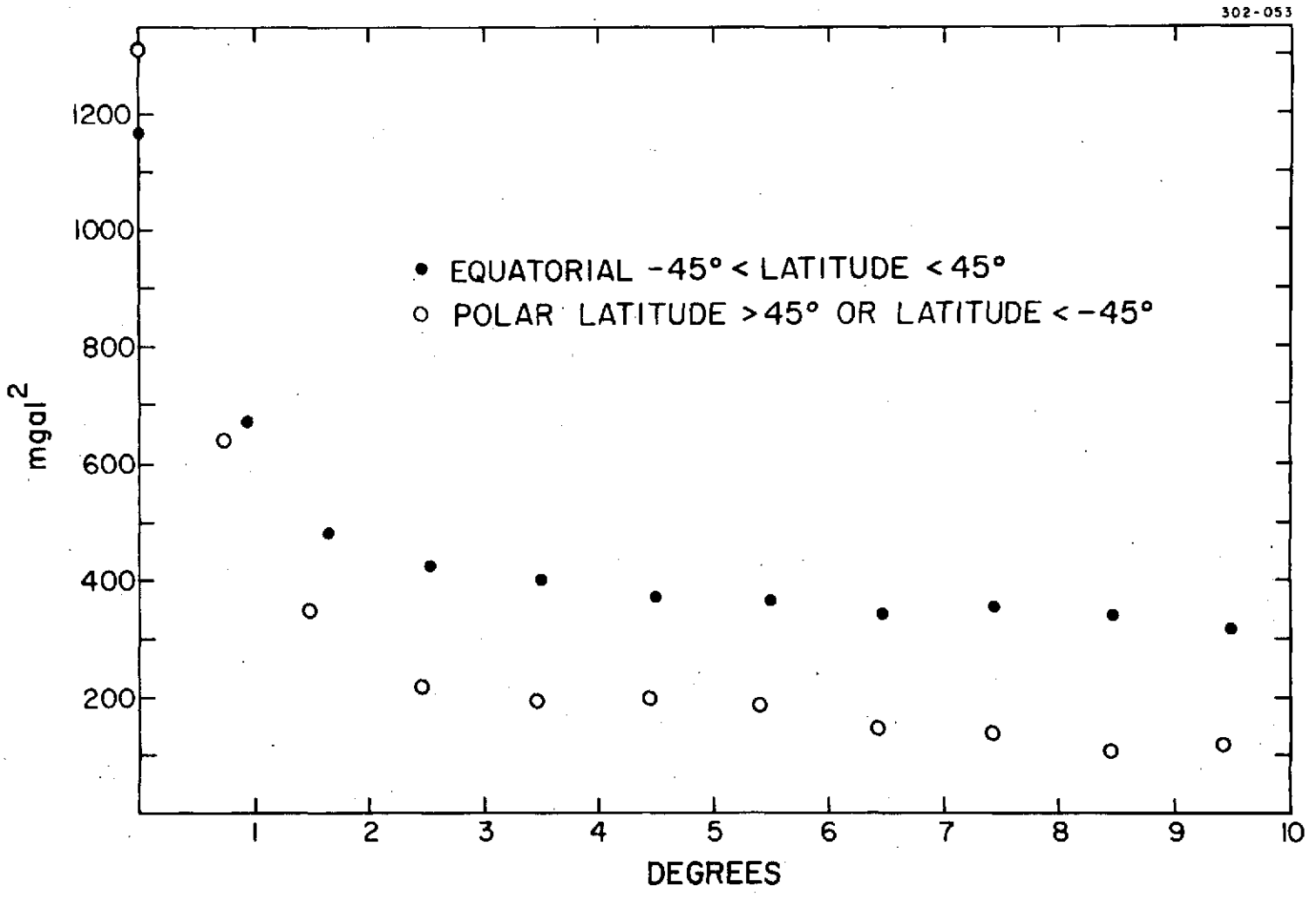

Figure 2e. The covariance functions of 1° × 1° mean oceanic gravity anomalies for polar and equatorial regions.

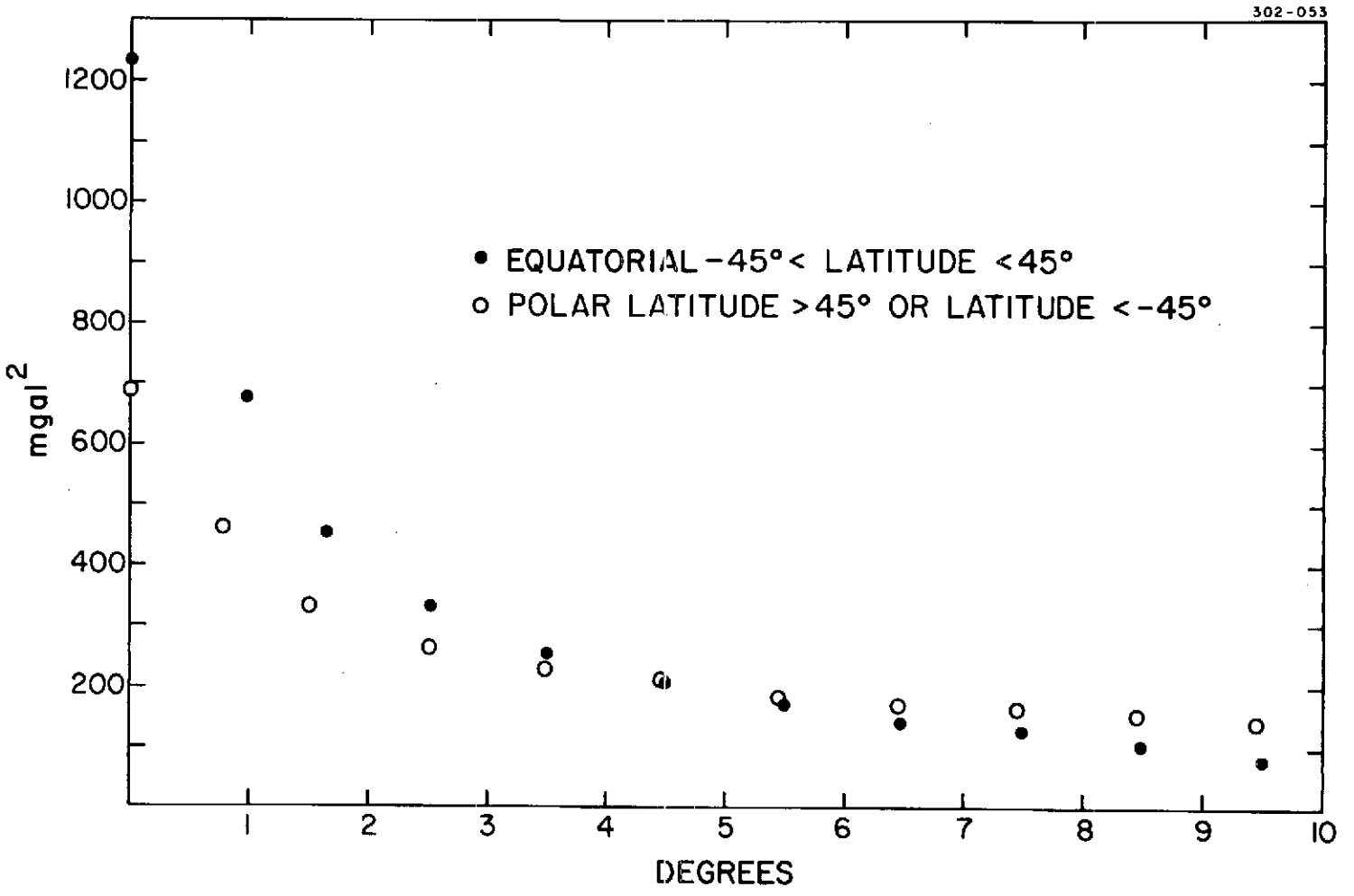

Figure 2f. The covariance functions of 1° × 1° mean continental gravity anomalies for polar and equatorial regions.

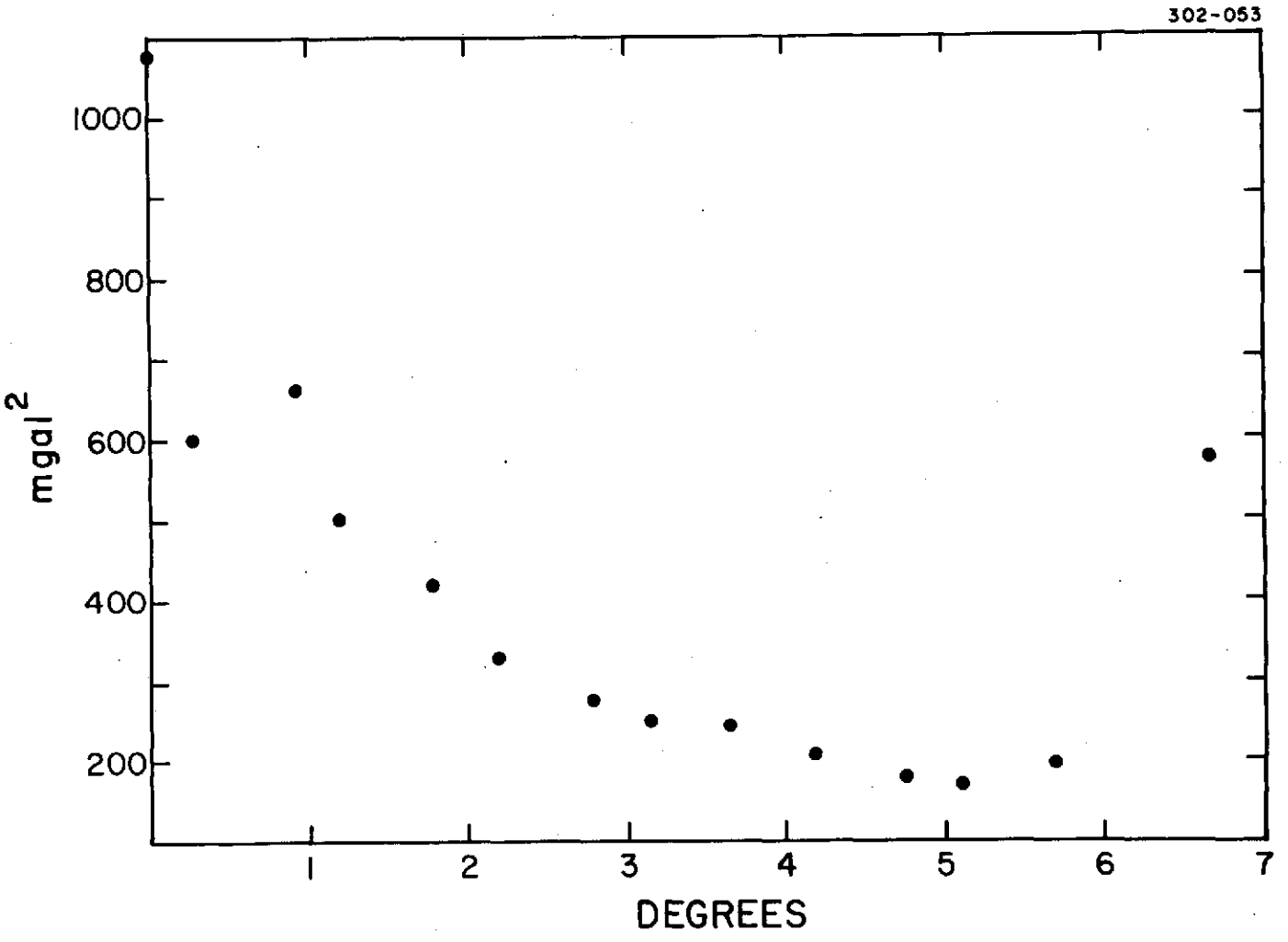

Figure 2g. The block covariance function of unit gravity anomalies.

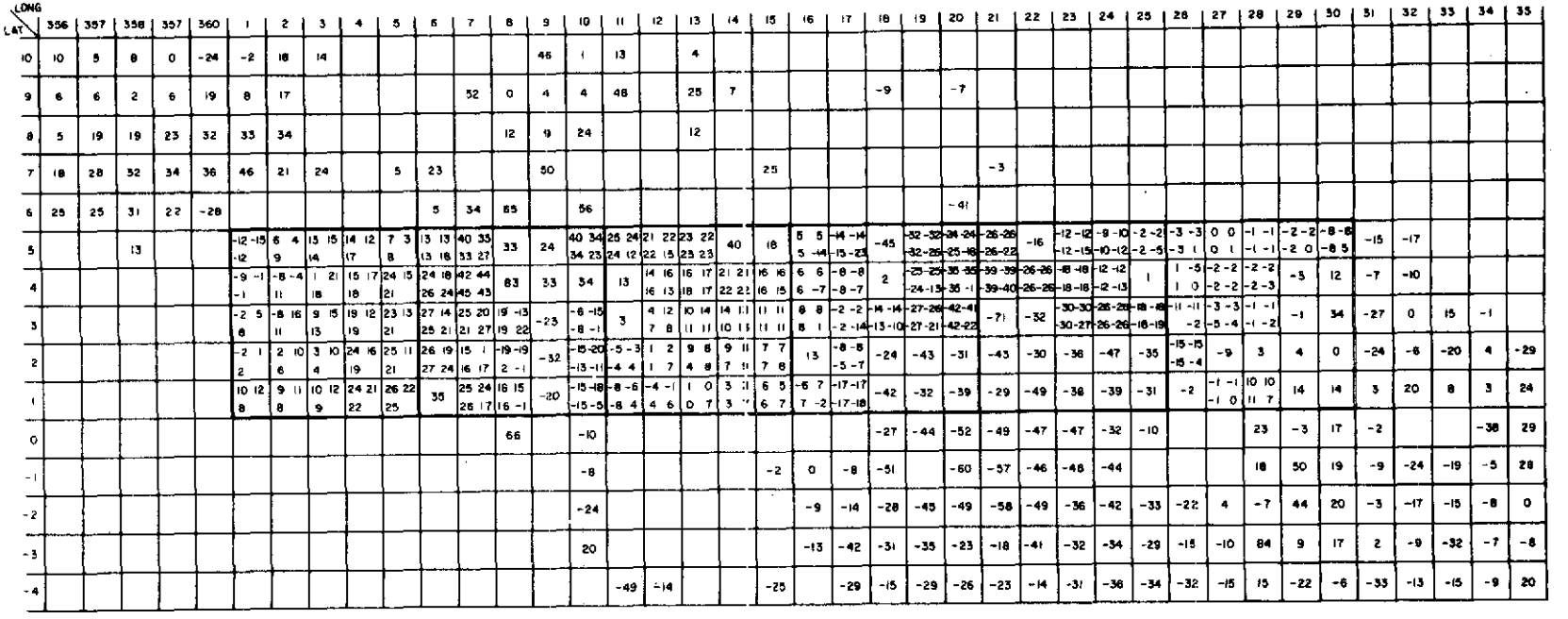

Figure 3. Comparison of the four estimate procedures. 1° × 1° squares with single numbers represent the measured mean free-air gravity anomalies. 1° × 1° squares with four numbers represent estimates as follows. Upper left: the split covariance estimator with a 0-km ocean–continent boundary. Lower left: the global covariance estimator. Upper right: the split covariance estimator with a -1-km ocean–continent boundary. Lower right: the Kaula estimator.

3. SATELLITE DATA

3.1 Analysis of Satellite Orbital Data

The external potential of the earth is represented by a set of orthogonal functions:

$$\mathcal{U} = \mathcal{R}e \frac{GM}{r} \sum_{\ell=0}^{\infty} \sum_{m=0}^{\ell} \left(\frac{a_e}{r}\right)^{\ell} \overline{\mathcal{C}}_{\ell m} \overline{P}_{\ell m}(\sin\phi)\, e^{im\lambda} \quad , \tag{1}$$

where M is the mass of the earth, including the atmosphere; G is the universal constant of gravity; $\overline{\mathcal{C}}_{\ell m} = \overline{C}_{\ell m} - i\overline{S}_{\ell m}$; $\overline{C}_{\ell 0} = -J_{\ell}/\sqrt{2\ell+1}$; $\mathcal{R}e\{\ \}$ designates the real part of $\{\ \}$; $\overline{P}_{\ell m}(\sin\phi)$ are fully normalized associated Legendre polynomials; and r, ϕ, λ are the coordinates of the test particle. It is possible to choose a coordinate system such that

$$\overline{\mathcal{C}}_{2,0} = \overline{\mathcal{C}}_{1,1} = \overline{\mathcal{C}}_{2,1} = 0 + i\,0 \quad ,$$

and we assume that the instantaneous spin axis as defined by the International Polar Motion Service and the center of gravity of the earth are that system. This assumption is not strictly true, but the departures are small and are ignored in this analysis (see Part III of this Report).

It is observed that for the earth the amplitude of $E\left(|\overline{\mathcal{C}}_{\ell m}|\right)$ decreases uniformly according to

$$E\left(|\overline{\mathcal{C}}_{\ell m}|\right) = \frac{10^5}{\ell^2} \quad . \tag{2}$$

Although for theoretical reasons $E\left(|\overline{\mathcal{C}}_{\ell m}|\right)$ must decrease more rapidly than equation (2) at some point, and individual coefficients can be arbitrarily large, this rule seems valid throughout the range of ℓ used in this investigation.

We use two types of data on the earth's gravity field: those derived from gravimeters and those obtained from the motion of artificial satellites. The gravity calculated from the gradient of equation (1) is

$$\Delta g = \gamma \mathcal{R}e \sum_{\ell=2}^{\infty} \sum_{m=0}^{\ell} (\ell - 1) \left(\frac{a_e}{r}\right)^{\ell} \overline{C}'_{\ell m} \overline{P}_{\ell m}(\sin \phi)\, e^{im\lambda} \quad , \tag{3}$$

where $\gamma = GM/r^2$ and $\overline{C}'_{\ell m}$ are $\overline{C}_{\ell m}$ modified to accommodate those effects of the reference ellipsoid (or gravity formula) that change the definition of $\overline{C}_{2,0}$, $\overline{C}_{4,0}$, and $\overline{C}_{6,0}$. By comparing equations (1) and (3), it is apparent that Δg is relatively more influenced by $\overline{C}_{\ell m}$ of high degree and order than is $\mathcal{U}$ because of the $\ell - 1$ multiplier and that measurements of Δg are more useful for determining these high-degree and high-order coefficients.

Determination of $\overline{C}_{\ell m}$ from analysis of satellite observations requires a theory for satellite motion. General solutions for the motion in an arbitrary potential field have not yet been found. We must therefore restrict ourselves to approximate solutions, which are quite sufficient for the following reasons. It is observed that for the earth, the second-degree zonal harmonic $\overline{C}_{2,0}$ makes the largest contribution to the anomalous potential and is 10^{-3} of the main term. The remaining anomalous potential is 10^{-3} of $\overline{C}_{2,0}$, or 10^{-6} of the main term. Therefore, to calculate the trajectory to 10^{-6} (our objective), we require at least a second-order theory for $\overline{C}_{2,0}$ (i.e., one including $\overline{C}^2_{2,0}$), but only a first-order linear theory for the remaining $\overline{C}_{\ell m}$. Although there are notable exceptions – resonances and some zonal harmonics – these considerations provide a workable base.

The earth's motion is complicated because of precession, nutation, polar motion, and rotation. A convenient reference frame is defined by the stars and, in practice, is defined (imperfectly) in terms of a star catalog at some epoch. On the other hand, in an inertial frame, the earth's gravity field has a temporal variation that significantly complicates the construction of an analytical theory. For this reason, a compromise quasi-inertial reference frame referred to an equinox (epoch 1950.0) and an equator (epoch of date) has been adopted. Veis (1960a) knew, Kozai (1960) proved, and we have used the fact that this coordinate system minimizes the additional effects required to account for the temporal variations of the gravity field and the noninertial property of the coordinate system.

Accordingly, the determination of $\overline{C}_{\ell m}$ from analysis of satellite observations uses the elaboration of a satellite perturbation theory. This elaboration is too lengthy to detail here, so we confine ourselves to a few remarks. The perturbation theory is developed by expressing equation (1) in terms of satellite coordinates (a, the semi-major axis; e, the eccentricity; I, the inclination; ω, the argument of perigee; Ω, the right ascension of the ascending node; and M, the mean anomaly). If we express equation (1) as

$$\mathcal{U} = \sum_{\ell=0}^{\infty} \sum_{m=0}^{\ell} \mathcal{U}_{\ell m} \quad , \tag{4}$$

we can write

$$\mathcal{U}_{\ell m} = \mathcal{R}e \sum_{p=0}^{\ell} \sum_{q=-\infty}^{\infty} \overline{C}_{\ell m} A_{\ell mpq}(a, e, I)\, e^{i\psi} \quad , \tag{5a}$$

where

$$A_{\ell mpq}(a, e, I) = \frac{GM}{a} \left(\frac{a_e}{a}\right)^{\ell} D_{\ell mp}(I)\, G_{\ell pq}(e) \tag{5b}$$

and

$$\psi = (\ell - 2p)\omega + (\ell - 2p + q)M + m(\Omega - \theta) + (\ell - m)\frac{\pi}{2} \quad . \tag{5c}$$

These four equations are the exact equivalent of equation (1). Expressed in this way, the variables with large secular changes (ω, Ω, M) are separated from those with only periodic changes (a, e, I). Therefore, the functions $A_{\ell mpq}(a, e, I)$ can, with sufficient accuracy, be considered constant. In addition, $G_{\ell pq}(e) \approx O(e^{|q|})$. Since satellites of interest have small or modest eccentricity, only a few terms in the sum over q are necessary. The number of terms is selected automatically for each satellite by means of a numerical test; typically, $|q| < 5$ is sufficient.

The differential equations relating the disturbing potential and the changes in orbital elements are known as the Lagrange Planetary Equations, a set of simultaneous ordinary differential equations of the form

$$\frac{d}{dt}\mathcal{E}^k = \mathcal{L}^k(a,e,I)\,\mathcal{U} \quad , \tag{6}$$

where $\mathcal{E}^k$ is a generic element, $\mathcal{L}^k(a,e,I)$ is a linear differential operator, and $\mathcal{U}$ is the disturbing potential. If we assume that the interaction of perturbations can be ignored, then we can write

$$\mathcal{E}^k = \mathcal{E}_0^k + \sum_{\ell=2}^{\infty}\sum_{m=0}^{\ell} \delta\mathcal{E}_{\ell m}^k \quad , \tag{7}$$

where $\mathcal{E}_0^k$ is the unperturbed element. This is an excellent assumption except for $\overline{\mathcal{C}}_{2,0}$. The secular changes in ω, Ω, and M due to $\overline{\mathcal{C}}_{2,0}$ interact significantly with all the perturbations, and so for these angles variables, we use

$$\mathcal{E}^k = \mathcal{E}_0^k + \dot{\mathcal{E}}^k t + \sum_{\ell=2}^{\infty}\sum_{m=0}^{\ell} \delta\mathcal{E}_{\ell m}^k \quad . \tag{8}$$

Substituting equations (4), (5), (7), and (8) into equation (6), formally expanding the resulting equation, and discarding all interactions on the right-hand side, we obtain

$$\frac{d}{dt}\delta\mathcal{E}_{\ell m}^k = \mathcal{R}e\,\mathcal{L}^k(a_0,e_0,I_0)\sum_{p=0}^{\ell}\sum_{q=-\infty}^{\infty}\overline{\mathcal{C}}_{\ell m}\,A_{\ell mpq}(a_0,e_0,I_0)\,e^{i\psi_0} \quad , \tag{9a}$$

where

$$\psi_0 = (\ell-2p)(\omega_0+\dot{\omega}t) + (\ell-2p+q)(M_0+nt) + m(\Omega_0+\dot{\Omega}t-\theta) + (\ell-m)\frac{\pi}{2} \quad . \tag{9b}$$

Here, $\dot{\omega}$, n, and $\dot{\Omega}$ are the secular rates of ω, M, and Ω. The rotation of the earth is sufficiently uniform so that we can write

$$\theta = \theta_0 + \dot{\theta}t \quad . \tag{10}$$

Finally, $\delta\mathcal{E}^k_{\ell m}$ is the perturbation in element $\mathcal{E}^k$ due to the potential coefficient $\overline{C}_{\ell m}$. Equations (9) are now uncoupled differential equations, which can be integrated immediately to

$$\delta\mathcal{E}^k_{\ell m} = \mathcal{R}e\,\mathcal{L}^k(a_0, e_0, I_0) \sum_{p=0}^{\ell} \sum_{q=-\infty}^{\infty} \overline{C}_{\ell m} A_{\ell mpq}(a_0, e_0, I_0) \frac{e^{i[\psi_0 - (\pi/2)]}}{\dot{\psi}_0} \quad , \tag{11a}$$

$$\dot{\psi}_0 = (\ell - 2p)\dot{\omega} + (\ell - 2p + q)n + m(\dot{\Omega} - \dot{\theta}) \quad . \tag{11b}$$

The general properties of the solution are now apparent. We see that $\dot{\psi}$ can be exactly zero only when m=0. Therefore, only even zonal harmonics $\overline{C}_{\ell 0}$ can cause secular perturbations. The period of the periodic terms is given by equation (11b), and we see from equation (11a) that the longer the period is, the larger the perturbation. Thus, when m=0, long-period terms with argument ω, 2ω, 3ω, ... occur when $q = -1, -2, -3, \ldots$. For nonzonal harmonics, long-period, large-amplitude perturbations arise when $\dot{\psi} \approx 0$. Since $n(\approx 13 \text{ rev day}^{-1}) > \dot{\theta}(\approx 1 \text{ rev day}^{-1}) \gg \dot{\omega}, \dot{\Omega} \propto \overline{C}_{2,0} n = 10^{-3} n$, this resonance condition occurs when $n \approx m\dot{\theta}$ – that is, when the mean motion n is approximately an integral number (the order m) of revolutions per day. In fact, resonant conditions always exist to some extent. Resonant terms occur in both satellite theory and planetary theory, and there is extensive literature on the subject (e.g., Kaula, 1966a; Hagihara, 1961), but as yet there is no completely satisfactory treatment. It is true, for example, that a solution such as that employed here by using linearized equations can be invalid for some cases, since the series are not uniformly convergent; fortunately, this does not occur here. The occurrence of resonances between the gravity field of the earth and a satellite has been viewed as an opportunity to determine particular harmonics to high precision. In fact, some of the low-degree harmonics have been studied extensively with synchronous satellites, and many harmonics of orders 12, 13, and 14 have been determined by SAO and others. Long-period terms in ω, 2ω, 3ω, ... from the zonal harmonics are resonant perturbations in the sense of the term as discussed here. Satellites with strong resonances interact with the gravity field to $\ell = 35$ and higher. Finally, we have seen that the largest perturbations result when equation (11b) is smallest. With m = 0, the largest terms

are for $\ell - 2p + q = 0$ – that is, there is no dependence on M. Therefore, long-period terms can be analyzed. For $m \neq 0$, the largest effects are also without M. In this case, the frequency is m oscillations per day, and the first-order term will be the largest. Terms for $m = 8$ – that is, eight oscillations per day – become very difficult to determine, and reliable values for $m \geq 10$ can be obtained only by the study of resonances or from terrestrial gravimetry.

The formal theory, equation (11), accounts for both resonances and short-period terms. For example, the resonant perturbation in mean anomaly for satellite 5900701 is

$$\delta M = \overline{C}_{11,11} \left\{ -1.387 \times 10^{2} \cos\left[\frac{2\pi}{35.8}(t - t_0)\right] - 1.798 \times 10^{5} \cos\left[\frac{2\pi}{1124.8}(t - t_0)\right] + \ldots \right\} , \tag{12}$$

with similar terms for $\overline{S}_{11,11}$, $\overline{C}_{12,11}$, ... The 1124-day term is much longer than any span of data for one orbit. Because we have imperfect knowledge of the coefficient $\overline{C}_{11,11}$, the empirically determined orbit will absorb the residual 1124-day term into the mean elements. The mean elements can be analyzed for improvements to the gravity field in the same way as is done for zonal harmonics.

Because most of the zonal harmonics give rise to short-period perturbations, the residuals of individual observations are analyzed to determine these gravity-field coefficients. Since we are dealing with instantaneous observations of position, the observation equation is of the form

$$\Delta\overline{X} = \left(\frac{\partial \overline{r}}{\partial M} \frac{\partial \delta M}{\partial \overline{C}_{\ell m}} + \frac{\partial \overline{r}}{\partial \omega} \frac{\partial \delta \omega}{\partial \overline{C}_{\ell m}} + \ldots \right) \Delta\overline{C}_{\ell m} , \tag{13}$$

where δM would be computed from equation (12). Therefore, when we use equation (13), terms in δM and $\delta\omega$ with periods longer than the span of data must be detected.

With the theory developed in harmonic functions, the deleting of specific perturbations is quite trivial. The analogous operation with a numerical-integration technique would be much more difficult.

As an example, the perturbations in M for satellite D1D (6701401) are given below for only the principal terms, with $m = 1, 2$; $\ell = 3, 4, 5, 6, 7, 8$. For this satellite, $a = 7614$ km, $e = 0.0843$, and $I = 39.^{\circ}455$.

$$\begin{aligned}
\delta M = {} & \bar{C}_{3,1}[-7.1 \sin(\omega + \Omega - \theta) + 0.8 \sin(\omega + 2M + \Omega - \theta) - 63.3 \sin(-\omega + \Omega - \theta) + \ldots] \\
& + \bar{C}_{3,2}\{-42.5 \cos[\omega + 2(\Omega - \theta)] + 10.5 \cos[\omega + 2M + 2(\Omega - \theta)] - 13.6 \cos[-\omega + 2(\Omega - \theta)] + \ldots\} \\
& + \bar{C}_{4,1}[7.0 \cos(-M + \Omega - \theta) - 8.2 \cos(M + \Omega - \theta) + 5.1 \cos(-2\omega + \Omega - \theta) + \ldots] \\
& + \bar{C}_{4,2}\{-10.3 \sin[-M + 2(\Omega - \theta)] + 14.2 \sin[M + 2(\Omega - \theta)] + \ldots\} \\
& + \bar{C}_{5,1}[-87.4 \sin(\omega + \Omega - \theta) + 6.9 \sin(\omega + 2M + \Omega - \theta) + 87.9 \sin(-\omega + \Omega - \theta) + \ldots] \\
& + \bar{C}_{5,2}\{8.6 \cos[\omega + 2(\Omega - \theta)] - 1.4 \cos[\omega + 2M + 2(\Omega - \theta)] + 43.9 \cos[-\omega + 2(\Omega - \theta)] + \ldots\} \\
& + \bar{C}_{6,1}[5.1 \cos(-M + \Omega - \theta) - 6.0 \cos(M + \Omega - \theta) - 16.2 \cos(-2\omega + \Omega - \theta) + \ldots] \\
& + \bar{C}_{6,2}\{5.4 \sin[-M + 2(\Omega - \theta)] - 7.4 \sin[M + 2(\Omega - \theta)] + \ldots\} \\
& + \bar{C}_{7,1}[33.1 \sin(\omega + \Omega - \theta) + 0.0 \sin(\omega + 2M + \Omega - \theta) + 1.4 \sin(-\omega + \Omega - \theta) + \ldots] \\
& + \bar{C}_{7,2}\{40.0 \cos[\omega + 2(\Omega - \theta)] - 5.5 \cos[\omega + 2M + 2(\Omega - \theta)] - 40.3 \cos[-\omega + 2(\Omega - \theta)] + \ldots\} \\
& + \bar{C}_{8,1}[-6.8 \cos(-M + \Omega - \theta) + 7.9 \cos(M + \Omega - \theta) + 19.1 \cos(-2\omega + \Omega - \theta) + \ldots] \\
& + \bar{C}_{8,2}\{4.1 \sin[-M + 2(\Omega - \theta)] - 5.7 \sin[M + 2(\Omega - \theta)] + \ldots\} \quad . \qquad (14)
\end{aligned}$$

We can rearrange this expression in terms of the same frequency (with the period P of each term in days given in parentheses):

$$\begin{aligned}
\delta M = {} & (-7.1 \bar{C}_{3,1} - 87.4 \bar{C}_{5,1} + 33.1 \bar{C}_{7,1} + \ldots) \sin(\omega + \Omega - \theta) && (-1.001 \text{ days}) \\
& + (0.8 \bar{C}_{3,1} + 6.9 \bar{C}_{5,1} + 0.0 \bar{C}_{7,1} + \ldots) \sin(\omega + 2M + \Omega - \theta) && (0.040) \\
& + (-63.3 \bar{C}_{3,1} + 87.9 \bar{C}_{5,1} + 1.4 \bar{C}_{7,1} + \ldots) \sin(-\omega + \Omega - \theta) && (-0.971) \\
& + (7.0 \bar{C}_{4,1} + 5.1 \bar{C}_{6,1} - 6.8 \bar{C}_{8,1} + \ldots) \cos(-M + \Omega - \theta) && (-0.071) \\
& + (-8.2 \bar{C}_{4,1} - 6.0 \bar{C}_{6,1} + 7.9 \bar{C}_{8,1} + \ldots) \cos(M + \Omega - \theta) && (0.083)
\end{aligned}$$

$$+ (5.1\,\overline{C}_{4,1} - 16.2\,\overline{C}_{6,1} + 19.1\,\overline{C}_{8,1} + \ldots) \cos(-2\omega + \Omega - \theta) \qquad (-0.958 \text{ day})$$

$$+ (-42.5\,\overline{C}_{3,2} + 8.6\,\overline{C}_{5,2} + 40.0\,\overline{C}_{7,2} + \ldots) \cos[\omega + 2(\Omega - \theta)] \qquad (-0.497)$$

$$+ (10.5\,\overline{C}_{3,2} - 1.4\,\overline{C}_{5,2} - 5.5\,\overline{C}_{7,2} + \ldots) \cos[\omega + 2M + 2(\Omega - \theta)] \qquad (0.041)$$

$$+ (-13.6\,\overline{C}_{3,2} + 43.9\,\overline{C}_{5,2} - 40.3\,\overline{C}_{7,2} + \ldots) \cos[-\omega + 2(\Omega - \theta)] \qquad (-0.327)$$

$$+ (-10.3\,\overline{C}_{4,2} + 5.4\,\overline{C}_{6,2} + 4.1\,\overline{C}_{8,2} + \ldots) \sin[-M + 2(\Omega - \theta)] \qquad (-0.066)$$

$$+ (14.2\,\overline{C}_{4,2} - 7.4\,\overline{C}_{6,2} - 5.7\,\overline{C}_{8,2} + \ldots) \sin[M + 2(\Omega - \theta)] \qquad (0.091)$$

$$+ \ldots \quad . \qquad (15)$$

Even if we assume the satellite to be a perfect filter, uncontaminated by other model errors, and the tracking data and analysis process to be perfect, we see that with one satellite, we can determine only spectral components that are linear combinations of the gravity field ($\overline{C}_{\ell m}$) and functions of orbital elements [$A_{\ell mpq}(a, e, I)$]. From each satellite, we obtain one or two linear combinations of harmonics for ℓ odd and for ℓ even. With additional data, we can only refine the numerical value of these linear combinations. The coefficients of the relations will depend on the orbital elements, so that other linear combinations can be determined only from additional distinct orbits. Generally, this is achieved by selecting satellites with different inclinations, but independent linear relations can also be obtained with changes in eccentricity or semimajor axis.

As the degree increases, the perturbations become negligible, and so the linear relation does not involve an infinite number of parameters. Of course, the spectrum analysis gives both amplitude and phase, or, as generally written, $\overline{C}_{\ell m}$.

From equation (15), we see that one linear combination of $\overline{C}_{3,1}$, $\overline{C}_{5,1}$, $\overline{C}_{7,1}$, ... can be determined from the -1.001-day period term and another of equal size from the -0.971-day term. The third term is a factor of 10 smaller and will not contribute

significantly as an observation equation; there are also many smaller terms. The linear combination of $\bar{C}_{3,2}$, $\bar{C}_{5,2}$, $\bar{C}_{7,2}$, ... has only one significant spectral component for the -0.327-day period.

The linear relations are not determined with equal accuracy; for example, the resonant harmonics have a very large effect and the spectral component is strongly determined. However, the resonant period is commensurate with the arc length, which will cover only a small number of cycles. This makes it difficult to separate nearly commensurate periods.

If we consider equations (11) as expressing the spectral decomposition of the perturbation, we see that each harmonic $\bar{C}_{\ell m}$ of order m causes the same spectrum of perturbations. Further, the spectrum has several lines close together. With a short span of data, these spectral components are difficult to separate.

The large number of harmonics affecting a satellite is related by a linear equation similar to equation (15). For one satellite, only a linear combination of coefficients can be determined. In those cases where an insufficient number of satellites is observed, additional assumptions are necessary in order to obtain independent equations. The usual assumption is to set some of the higher degree terms to zero, leading to lumped coefficients that are useful for orbit determination but that may be unrelated to the actual gravity field.

In summary, the process of gravity-field determination begins with the evaluation of the secular and long-period perturbations to determine the J_n. The perturbations accumulate for weeks and months, and the effects are very large. The mean orbital elements, determined from overlapping 4-day arcs, constitute the basic data used in the analysis. Data and reference orbits of moderate accuracy are adequate for the J_n determination. The unbiased recovery of the J_n requires painstaking evaluation of the long-period and secular perturbations from other sources, principally solar radiation pressure, atmospheric drag, and lunar and solar attraction. This phase of the analysis is accomplished first. The tesseral harmonics are determined from the short-period (1-revolution to 1-day) changes in the orbit. The detailed structure of the orbit must be observed, and each observation provides an observation equation.

Data of the highest possible precision are needed. The unbiased recovery of $\overline{C}_{\ell m}$ requires the evaluation of the periodic terms from other sources that have periods similar to those arising from the gravity-field coefficients. The most important are the short-period terms due to J_n and the lunar attraction. Because they are smaller than 1 m for the satellites used in this analysis, the periodic effects of air drag and radiation pressure can be ignored. The nonperiodic terms are empirically determined and hence accounted for. The short-period terms due to J_2 must be carried to second order.

3.2 Satellite Data Used

Laser data from ISAGEX provide global coverage with 2-m accuracy for the first time. Table 2 lists all the satellites used in the analysis, and Figure 4 shows their distribution in inclination and height. Separation of the station-coordinate and the gravity-field determinations allowed a better selection of satellite data. For the former, high satellites less affected by the anomalous gravity field were emphasized, while for the latter, lower satellites, with a better distribution, were stressed. Certain satellites with unmanageable long-period resonances (e.g., 5900701) were used only for the determination of station coordinates; they have such a rich body of data that relatively short-arc orbits (4 days) could be derived for this purpose.

Each observation was given an a priori weight (detailed in Table 3), so that when the normal equations were combined, each type of data could be scaled. The scale factor for surface-gravity data (see Section 2) was arrived at by experiment. The scale factors for the 550 km × 550 km anomalies and for the zero anomalies were chosen so that the resulting solution improved the satellite orbit, the surface-gravity residuals, and the errors in the surface-gravity comparison (see Table 19 of Section 6.1), and did not introduce spurious short-wavelength detail where no surface-gravity data were available.

All available optical data were used for the orbital arcs chosen. For each pass of laser data containing more than 30 points, approximately 30 uniformly distributed observations were selected.

Table 2. Dynamical data used in SE III.

Satellite Number	Satellite Name	Inclination	Eccentricity	a (km)	Perigee (km)	Laser observations	Station coordinates	Zonal harmonics	Tesseral harmonics	Number of files
7001701	Dial	5°	0.088	7344	301			x		
7010901	Peole	15	0.017	7070	635	x		x	x	4
6001301	Courier 1B 1960 ν1	28	0.016	7465	965		x	x	x	7
5900101	Vanguard 2 1959 α1	33	0.165	8300	557		x	x	x	7
5900701	1959 η1	33	0.188	8483	515		x			18
6100401	1961 δ1	39	0.119	7960	700				x	4
6701401	D1D	39	0.053	7337	569	x	x		x	10
6701101	D1C	40	0.052	7336	579	x	x		x	9
6503201	Explorer 24 BE-C	41	0.026	7311	941	x	x		x	13
6202901	Telstar 1 1962 $\alpha\epsilon$1	44	0.241	9672	962			x		4
6000902	1960 ι2	47	0.011	7971	1512		x	x	x	10
6206001	Anna 1B 1962 $\beta\mu$1	50	0.007	7508	1077		x	x	x	12
6302601	Geophysical Research	50	0.062	7237	424			x		6
6508901	Explorer 29 Geos 1	59	0.073	8074	1121	x	x	x	x	56
6101501	Transit 4A 6101	67	0.008	7318	885			x	x	10
6101502	Injun 1 6102	67	0.008	7316	896				x	9
6506301	Secor 5	69	0.079	8159	1137		x		x	2
6400101		70	0.002	7301	921			x	x	4
6406401	Explorer 22 BE-B	80	0.012	7362	912	x	x	x	x	6
6508101	OGO 2	87	0.075	7344	420			x	x	5
6600501	Oscar 07	89	0.023	7417	868		x		x	1
6304902	5BN-2	90	0.005	7473	1070		x		x	5
6102801	Midas 4 1961 $\alpha\delta$1	96	0.013	10005	3503		x	x	x	6
6800201	Explorer 36 Geos 2	106	0.031	7709	1101	x	x		x	13
6507801	OV1-2	144	0.182	8306	416		x		x	4

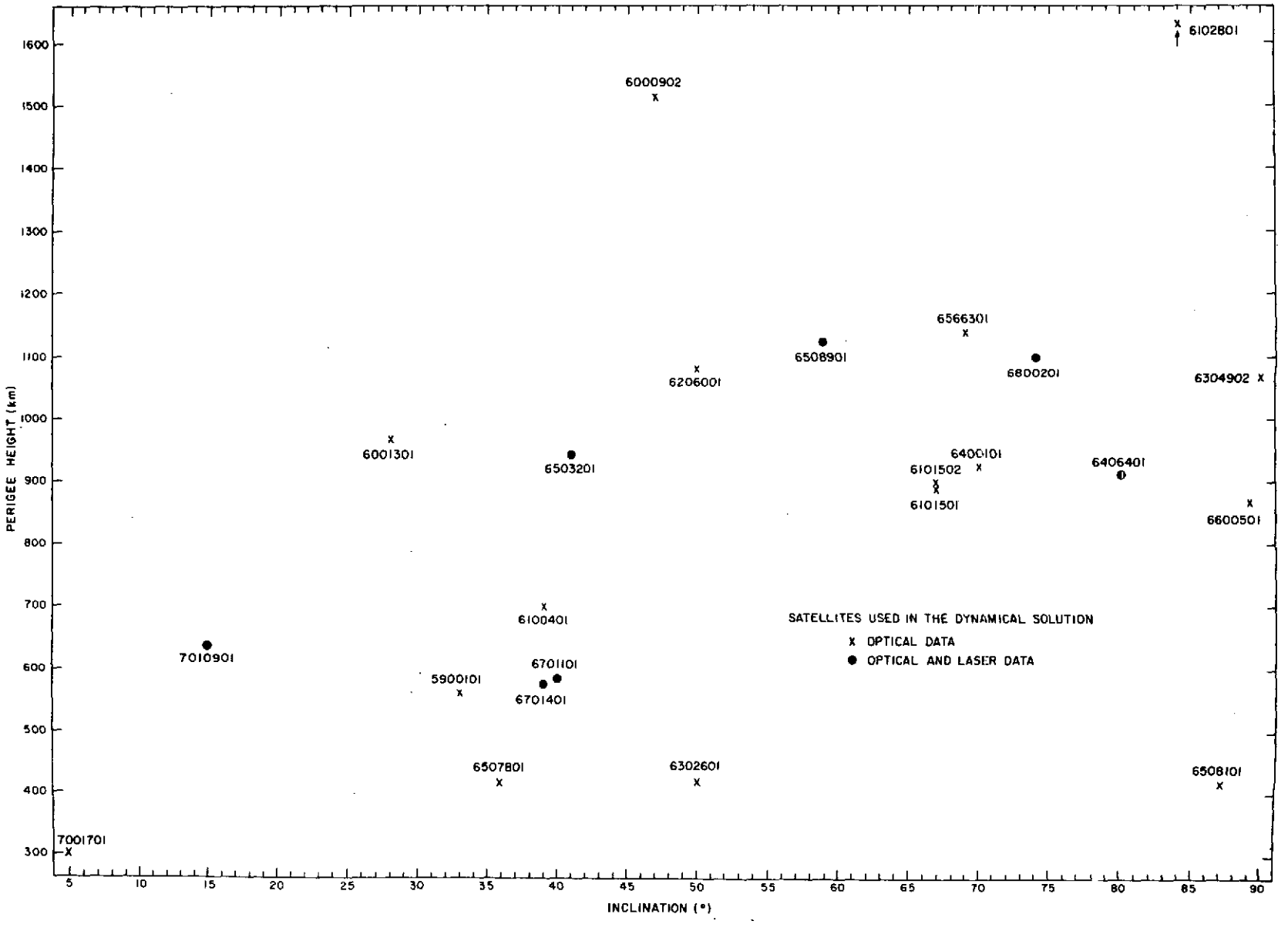

Figure 4. Distribution of perigee heights and inclinations of the satellites used in SE III.

Table 3. Assumed accuracy for SE III.

Data	Weight	Remarks
Baker-Nunn	4''	
Smoothed Baker-Nunn	2''	
SAO laser	5 m	Taken before 1970, observed before 1970
CNES laser	10 m	Taken before 1970, observed before 1970
GSFC laser	5 m	Taken before 1970, observed before 1970
ISAGEX laser	2 m	1971 International Campaign
Gravity anomalies	$\langle A \rangle \frac{13.5}{nA}$ mgal	n is the number of $1° \times 1°$ squares in each $5° \times 5°$ mean
Model (zero) anomalies	$\langle A \rangle \frac{27}{A}$ mgal	A is the area

4. COEFFICIENTS OF ZONAL SPHERICAL HARMONICS IN THE GEOPOTENTIAL

4.1 Introduction

Coefficients of zonal spherical harmonics in the geopotential determined from secular motions of angular variables and from amplitudes of long-periodic terms with the argument of perigee ω in the orbits of artificial satellites are more accurate than are coefficients derived by classical terrestrial methods. The reason is that the component of geoid height represented by the zonal harmonics is amplified by a factor of 1000 when they appear as secular and long-periodic perturbations of satellites. However, because these perturbations are averaged effects, contributions from the harmonics in each are not very different from one satellite to another unless their orbital elements are quite different. Also, few satellites with inclinations below 30° have been employed in the determination of the coefficients, since accurate observations of such satellites have been scarce. It was also found that many more terms than expected were necessary to represent the geopotential. Therefore, it has usually been very difficult to separate the contributions from each harmonic in the observed values of the secular motions and of the amplitudes of the long-periodic terms. In other words, different sets of coefficients could represent these observations within observed accuracies for satellites with inclinations larger than 30°.

Now, however, data for two low-inclination satellites – Dial (7001701; $I = 5.^{\circ}4$, $e = 0.09$, $a = 1.15$) and Peole (7010901; $I = 15.^{\circ}0$, $e = 0.02$, $a = 1.10$) – have become available since our last determination of zonal harmonics (Kozai, 1969). We expect the data from them will significantly improve the coefficients of the zonal harmonics in the geopotential.

The values of (O - C) for the secular motions and the amplitudes of $\begin{matrix}\sin\\ \cos\end{matrix}\ \omega$ terms based on 1964 values (Kozai, 1964) follow:

	$\dot{\omega}$ day^{-1}	$\dot{\Omega}$ day^{-1}	A_ω	A_Ω	A_I	A_e
Dial	-0.°01806 ±9	0.°01012 ±7	-0.°070 ±5	-0.°019 ±3	0.°0043 ±3	-9.1×10^{-5} ±6
Peole	-0.0022 ±8	0.00516 ±10	0.045 ±30	-0.002 ±5	-0.0017 ±30	2.8×10^{-5} ±2.0

The large values of (O - C) for these two satellites show that the previous sets of zonal-harmonic coefficients were inadequate.

The data for Dial were derived from orbital elements from March 18 to July 16, 1970; during that period, the argument of perigee made four revolutions. The orbital elements for Peole were obtained for January 9 to March 13, 1971, and for March 28 to August 30, 1971. These data are not so accurate as those for Dial, since there were not enough observations and there was a period during which no orbital elements were available.

In this new determination, the (O - C) values for satellite 6000902 are a revision by Gaposchkin for February 10, 1961, to April 21, 1963.

The other satellites included in this determination are 6001301, 5900101, 6202901, 6302601, 6206001, 6508901, 6101501, 6400101, 6406401, 6508101, and 6102801. The data for these satellites are the same as those given by Kozai (1964). The (O - C) values were computed from the 1964 values of coefficients as given in Table 4. Corrections to the values in Table 4 are solved in Section 4.3.

Table 4. Coefficients of J_n based on Kozai's (1964) values (in units of 10^{-6}).

$J_2 = 1082.639$	$J_3 = -2.546$
$J_4 = -1.649$	$J_5 = -0.210$
$J_6 = 0.646$	$J_7 = -0.333$
$J_8 = -0.270$	$J_9 = -0.053$
$J_{10} = -0.054$	$J_{11} = 0.302$
$J_{12} = -0.357$	$J_{13} = -0.114$
$J_{14} = 0.179$	

The following values have been used for the geocentric gravitational constant and the equatorial radius of the earth:

$$GM = 3.98601 \times 10^{20} \text{ cm}^2 \text{ sec}^{-2} \quad ,$$
$$a_e = 6.37816 \times 10^{8} \text{ cm} \quad . \tag{16}$$

4.2 Equations of Condition

A computer program has been developed to calculate coefficients of J_n ($n \leqq 55$) in expressions of secular motion and of the amplitudes of $\underset{\sin}{\cos}\, 2\omega$ and $\underset{\sin}{\cos}\, \omega$ terms. Numerical values for $n \leqq 37$ are given in Tables 5 to 7 for the 14 satellites. Since secondary effects due to the interaction with the J_2 secular terms were not included, the values here for the coefficients of the amplitudes of the long-periodic terms in the argument of perigee and the longitude of the ascending node are slightly different from those we gave previously.

For the two angular variables ω and Ω, the secular and long-periodic perturbations have been derived from

$$\frac{d(\omega, \Omega)}{dt} = (\dot{\omega}, \dot{\Omega}) + A \sin \omega + B \cos 2\omega \quad , \tag{17}$$

where $\dot{\omega}$ and $\dot{\Omega}$, the secular parts, are functions of the semimajor axis, inclination, and eccentricity, which are not constant and, except for the semimajor axis, have long-periodic terms. The inclination and the eccentricity cannot be assumed constant in expressions for $\dot{\omega}$, $\dot{\Omega}$ in equation (17) but must include long-period terms. The effects of these long-period terms are of the same order as A and B and produce secondary effects. Therefore, if constant values for secular motions are adopted in order to analyze the data, the secondary effects in expressions for the long-period terms must be included in equation (17). In earlier papers by Kozai, the secular motions were determined from observation by assuming they were constant. Corrections to the secular motions and the amplitudes of the long-periodic terms were derived in recent papers by fitting the observed orbital elements with the integrated results of equation (17) by using assumed values of J_n and the instaneous observed mean values

Table 5. Coefficients of J_n in expressions of secular motion (in degrees per day).

Satellite		J_2	J_4	J_6	J_8	J_{10}	J_{12}	J_{14}	J_{16}	J_{18}	J_{20}	J_{22}	J_{24}	J_{26}	J_{28}	J_{30}	J_{32}	J_{34}	J_{36}
7001701	$\dot{\omega}$	11306	-21362	28183	-31767	32678	-31593	29139	-25835	22092	-18218	14437	-10903	7717	-4936	2585	-665	-842	1968
	$\dot{\Omega}$	-5691	10807	-14617	16932	-18043	18215	-17685	16649	-15268	13667	-11950	10197	-8473	6828	-5299	3913	-2688	1632
7010901	$\dot{\omega}$	12165	-20770	21325	-14509	3882	6305	-12812	14276	-11222	5463	756	-5539	7823	-7500	5223	-2046	-967	3043
	$\dot{\Omega}$	-6414	11751	-13867	12620	-8995	4414	-194	-2781	4171	-4117	3065	-1574	144	891	-1393	1397	-1052	547
6001301	$\dot{\omega}$	7625	-5479	-2224	6043	-3260	-1675	3731	-2045	-744	1979	-1213	-223	952	-671	-17	424	-348	38
	$\dot{\Omega}$	-4671	5169	-2137	-945	1924	-1071	-157	703	-487	17	249	-211	37	84	-88	26	27	-36
5900101	$\dot{\omega}$	4868	-1560	-2711	2473	409	-1902	926	665	-1045	244	535	-517	-14	357	-230	-87	214	-85
	$\dot{\Omega}$	-3236	2540	-200	-1095	787	106	-522	274	141	-264	85	114	-131	13	78	-61	-11	48
6202901	$\dot{\omega}$	1836	1040	-823	-645	400	342	-204	-179	107	94	-57	-50	31	27	-17	-14	9	8
	$\dot{\Omega}$	-1717	301	512	-127	-208	60	97	-31	-48	16	24	-9	-13	5	7	-3	-4	1
6000902	$\dot{\omega}$	2753	2685	-1224	-2302	317	1425	39	-763	-121	373	106	-171	-71	73	42	-30	-23	11
	$\dot{\Omega}$	-2864	261	1168	-16	-480	-37	194	34	-76	-21	29	12	-11	-6	4	3	-1	-1
6302601	$\dot{\omega}$	3245	5104	-765	-6141	-1782	4990	3273	-3127	-3678	1374	3334	-72	-2612	-717	1794	1073	-1055	-1122
	$\dot{\Omega}$	-3855	-145	2333	645	-1331	-761	677	685	-272	-540	41	385	77	-250	-124	144	128	-68
6206001	$\dot{\omega}$	2741	4130	-334	-4065	-1359	2597	1845	-1190	-1593	289	1095	139	-632	-264	305	243	-112	-173
	$\dot{\Omega}$	-3334	-187	1667	489	-747	-441	278	301	-69	-174	-9	89	27	-39	-24	14	16	-3
6508901	$\dot{\omega}$	605	2454	2144	39	-1392	-1096	-10	604	438	-12	-240	-161	12	92	57	-7	-34	-20
	$\dot{\Omega}$	-2076	-976	260	562	239	-92	-163	-64	32	50	18	-12	-16	-5	4	3	2	-2
6101501	$\dot{\omega}$	-641	1893	4419	4327	1628	-1619	-3300	-2743	-816	1016	1750	1305	295	-544	-809	-548	-82	264
	$\dot{\Omega}$	-2240	-2037	-809	331	811	657	219	-150	-284	-211	-57	62	98	67	14	-25	-34	-21
6400101	$\dot{\omega}$	-1176	774	3506	4737	3659	1074	-1486	-2816	-2596	-1330	132	1095	1294	884	237	-292	-518	-449
	$\dot{\Omega}$	-1971	-2044	-1205	-210	457	653	495	196	-60	-184	-179	-102	-14	43	58	43	16	-6
6406401	$\dot{\omega}$	-2341	-2483	-1458	12	1376	2310	2708	2622	2189	1576	931	363	-68	-342	-471	-487	-427	-326
	$\dot{\Omega}$	-996	-1298	-1252	-1026	-735	-455	-224	-59	44	96	110	101	79	55	33	15	2	-5
6508101	$\dot{\omega}$	-2814	-3984	-4371	-4299	-3969	-3508	-2998	-2491	-2016	-1588	-1213	-893	-626	-406	-229	-90	18	-99
	$\dot{\Omega}$	-261	-375	-422	-431	-417	-392	-360	-327	-293	-260	-230	-201	-175	-152	-131	-112	-96	-81
6102801	$\dot{\omega}$	-903	-637	-331	-144	-53	-15	-2	2	2	1	1	0	0	0	0	0	0	0
	$\dot{\Omega}$	194.2	144.5	82.4	41.7	19.6	8.7	3.7	1.5	0.6	0.2	0.1	0.0	0.0	0.0	0.0	0.0	0.0	0.0

Table 6. Coefficients of J_n in expressions of amplitudes of $\begin{matrix}\cos\\ \sin\end{matrix}$ 2ω terms (in units of 10^3 degrees for ω, 10^2 degrees for Ω, 10 degrees for I, and 10^6 for e, per day).

Satellites		J_2	J_4	J_6	J_8	J_{10}	J_{12}	J_{14}	J_{16}	J_{18}	J_{20}	J_{22}	J_{24}	J_{26}	J_{28}	J_{30}	J_{32}	J_{34}	J_{36}
7001701	ω	0	0	0	0	1	-2	3	-4	6	-7	9	-11	12	-13	14	-15	15	-15
	Ω	0	-1	6	-15	25	-37	46	-54	57	-57	53	-46	36	-24	12	1	-13	23
	I	0	-1	6	-15	26	-39	52	-64	74	-81	85	-87	86	-82	77	-70	63	-55
	e	0	0	-1	3	-5	7	-10	12	-14	15	-16	16	-16	15	-14	13	-12	10
7010901	ω	0	-1	6	-13	20	-23	22	-15	6	4	-12	16	-15	11	-5	-1	6	-8
	Ω	0	0	0	0	0	0	-1	1	-2	2	-1	1	0	-1	2	-2	1	-1
	I	0	0	1	-1	2	-2	2	-2	1	0	-1	2	-2	1	0	0	1	-1
	e	0	0	-2	4	-6	7	-6	4	-2	-1	3	-4	4	-3	1	0	-2	2
6001301	ω	0	-4	10	-9	0	9	-9	2	4	-6	2	2	-3	2	1	-1	1	0
	Ω	0	0	0	0	0	0	0	0	0	0	0	0	0	0	0	0	0	0
	I	0	0	1	0	0	0	0	0	0	0	0	0	0	0	0	0	0	0
	e	0	1	-3	3	0	-3	3	-1	-1	2	-1	0	1	0	0	0	0	0
5900101	ω	0	-5	9	-4	-6	9	-2	-5	6	0	-4	3	1	-3	1	1	-2	1
	Ω	0	-2	-5	15	-11	-7	17	-8	-8	12	-3	-7	7	0	-5	4	1	-3
	I	0	-20	33	-9	-21	24	-2	-14	11	1	-8	4	2	-4	1	2	-2	0
	e	0	13	-22	6	14	-16	2	9	-7	-1	5	-3	-1	3	-1	-1	1	0
6202901	ω	0	-8	2	8	-3	-5	2	3	-2	-2	1	1	-1	-1	0	0	0	0
	Ω	0	2	-18	3	18	-4	-12	3	8	-2	-4	1	2	-1	-1	0	1	0
	I	0	-40	5	34	-6	-16	4	8	-2	-4	1	2	-1	-1	0	0	0	0
	e	0	27	-4	-23	4	12	-3	-6	1	3	-1	-1	0	1	0	0	0	0
6000902	ω	0	-10	-2	13	2	-9	-2	5	2	-3	-1	1	1	-1	0	0	0	0
	Ω	0	0	0	0	0	0	0	0	0	0	0	0	0	0	0	0	0	0
	I	0	0	0	0	0	0	0	0	0	0	0	0	0	0	0	0	0	0
	e	0	2	0	-3	0	2	0	-1	0	1	0	0	0	0	0	0	0	0
6302601	ω	0	-14	-9	27	19	-25	-26	16	27	-6	-25	-2	20	7	-14	-10	8	10
	Ω	0	1	-3	-3	6	7	-6	-10	4	11	0	-11	-3	9	5	-6	-6	3
	I	0	-4	-3	8	6	-7	-7	4	6	-1	-6	-1	5	2	-3	-2	2	2
	e	0	14	9	-27	-19	24	25	-14	-26	5	22	3	-17	-7	11	8	-6	-8
6206001	ω	0	-13	-9	20	15	-14	-16	6	13	-1	-9	-2	5	3	-2	-2	1	2
	Ω	0	0	0	0	0	0	0	0	0	0	0	0	0	0	0	0	0	0
	I	0	0	0	0	0	0	0	0	0	0	0	0	0	0	0	0	0	0
	e	0	2	1	-2	-2	2	2	-1	-2	0	1	0	-1	0	0	0	0	0
6508901	ω	0	-22	-53	-16	35	38	5	-20	-18	-1	9	7	0	-4	-3	0	2	1
	Ω	0	4	-1	-12	-10	4	12	7	-3	-7	-3	2	4	1	-1	-2	-1	1
	I	0	-6	-16	-5	10	11	2	-6	-5	0	2	2	0	-1	-1	0	0	0
	e	0	26	65	19	-41	-44	-7	22	19	1	-9	-7	0	3	2	0	-1	-1
6101501	ω	0	4	78	114	62	-33	-97	-92	-34	29	59	47	13	-18	-29	-21	-4	9
	Ω	0	0	0	0	0	0	0	0	0	0	0	0	0	0	0	0	0	0
	I	0	0	0	0	0	0	0	0	0	0	0	0	0	0	0	0	0	0
	e	0	-1	-11	-16	-9	5	14	13	5	-4	-8	-7	-2	2	4	3	1	-1
6400101	ω	0	-5	30	62	60	24	-19	-47	-47	-27	0	20	25	18	5	-5	-10	-9
	Ω	0	0	0	0	0	0	0	0	0	0	0	0	0	0	0	0	0	0
	I	0	0	0	0	0	0	0	0	0	0	0	0	0	0	0	0	0	0
	e	0	0	-1	-2	-2	-1	1	1	1	1	0	-1	-1	0	0	0	0	0
6406401	ω	0	-11	-11	-2	8	17	22	23	20	15	9	4	0	-3	-5	-5	-4	-3
	Ω	0	0	0	0	0	0	0	0	0	0	0	0	0	0	0	0	0	0
	I	0	0	0	0	0	0	0	0	0	0	0	0	0	0	0	0	0	0
	e	0	2	2	1	-2	-4	-5	-5	-4	-3	-2	-1	0	1	1	1	1	1
6508101	ω	0	-13	-21	-25	-26	-25	-23	-20	-17	-14	-11	-8	-6	-4	-2	-1	0	1
	Ω	0	0	-1	-2	-4	-5	-6	-7	-8	-9	-9	-9	-9	-8	-8	-7	-7	-6
	I	0	0	-1	-1	-1	-1	-1	0	0	0	0	0	0	0	0	0	0	0
	e	0	16	26	31	31	29	26	22	18	14	11	8	6	4	2	1	0	-1
6102801	ω	0	-7	-5	-3	-1	0	0	0	0	0	0	0	0	0	0	0	0	0
	Ω	0	0	0	0	0	0	0	0	0	0	0	0	0	0	0	0	0	0
	I	0	0	0	0	0	0	0	0	0	0	0	0	0	0	0	0	0	0
	e	0	1	1	1	0	0	0	0	0	0	0	0	0	0	0	0	0	0

Table 7. Coefficients of J_n in expressions of amplitudes of $\begin{matrix}\cos\\ \sin\end{matrix}$ ω terms (in units of 10^3 degrees for ω, 10^2 degrees for Ω, 10 degrees for I, and 10^6 for e, per day).

Satellite		J_3	J_5	J_7	J_9	J_{11}	J_{13}	J_{15}	J_{17}	J_{19}	J_{21}	J_{23}	J_{25}	J_{27}	J_{29}	J_{31}	J_{33}	J_{35}	J_{37}
7001701	ω	-5	12	-23	36	-50	63	-75	84	-90	93	-93	90	-85	77	-69	60	-50	40
	Ω	-211	381	-471	484	-436	347	-235	116	-1	-103	190	-258	307	-337	350	-348	334	-310
	I	203	-384	507	-573	592	-576	537	-484	423	-360	299	-241	190	-144	105	-72	45	-24
	e	-38	72	-95	107	-110	107	-100	90	-79	67	-56	45	-35	27	-20	13	-8	4
7010901	ω	-378	668	-753	644	-410	141	87	-229	275	-241	157	-59	-25	79	-97	86	-57	22
	Ω	-12	12	5	-31	54	-66	60	-40	12	16	-35	43	-38	25	-8	-7	18	-21
	I	38	-68	76	-64	41	-13	-9	23	-27	23	-15	5	3	-8	9	-8	5	-2
	e	-109	192	-216	183	-115	38	26	-66	77	-67	42	-15	-8	22	-26	23	-15	5
6001301	ω	-647	589	-67	-290	286	-76	-97	122	-47	-29	49	-25	-7	19	-12	-1	7	-5
	Ω	-2	-12	22	-12	-6	16	-11	-1	9	-7	1	4	-4	1	2	-2	1	1
	I	33	-29	3	15	-14	4	5	-6	2	1	-2	1	0	-1	1	0	0	0
	e	-187	164	-19	-84	82	-21	-28	35	-13	-8	14	-7	-2	5	-3	0	2	-1
5900101	ω	-77	53	14	-47	24	15	-26	8	12	-14	1	9	-7	-1	6	-3	-2	3
	Ω	9	-128	122	13	-103	65	25	-62	25	24	-34	7	18	-17	-1	12	-8	-3
	I	290	-143	-71	114	-33	-38	39	-4	-19	14	2	-9	5	2	-4	1	2	-2
	e	-193	95	48	-76	22	25	-26	3	12	-9	-1	6	-3	-2	3	-1	-1	1
6202901	ω	-74	-15	45	6	-25	-3	13	1	-7	-1	4	0	-2	0	1	0	-1	0
	Ω	103	-150	-66	96	33	-52	-16	28	8	-15	-4	8	2	-4	-1	2	1	-1
	I	319	98	-124	-31	45	11	-18	-4	8	2	-3	-1	2	0	-1	0	0	0
	e	-215	-66	83	21	-30	-7	12	3	-5	-1	2	1	-1	0	0	0	0	0
6000902	ω	-1365	-828	698	451	-269	-221	94	103	-29	-46	8	20	-1	-9	0	4	0	-1
	Ω	7	-9	-9	7	7	-4	-4	2	2	-1	-1	0	1	0	0	0	0	0
	I	16	10	-8	-5	3	3	-1	-1	0	1	0	0	0	0	0	0	0	0
	e	-271	-165	138	89	-53	-44	16	20	-6	-9	2	4	0	-2	0	1	0	0
6302601	ω	-305	-325	189	293	-61	-227	-17	159	55	-100	-68	55	66	-22	-55	1	42	11
	Ω	52	-57	-109	40	126	-1	-112	-32	84	50	-52	-54	25	49	-5	-39	-7	28
	I	91	97	-52	-82	14	58	6	-37	-14	21	15	-10	-12	3	9	0	-6	-2
	e	-311	-332	179	282	-49	-200	-20	126	47	-71	-50	34	42	-11	-31	-1	21	6
6206001	ω	-2466	-2550	1113	1803	-168	-1033	-175	509	224	-213	-174	68	109	-8	-59	-11	28	13
	Ω	6	-6	-11	3	10	1	-7	-3	4	3	-2	-2	0	2	0	-1	0	0
	I	10	10	-5	-7	1	4	1	-2	-1	1	1	0	0	0	0	0	0	0
	e	-301	-311	136	220	-20	-126	-21	62	27	-26	-21	8	13	-1	-7	-1	3	2
6508901	ω	-268	-862	-417	160	309	126	-66	-106	-39	26	37	12	-10	-13	-4	4	5	1
	Ω	213	80	-186	-212	-32	108	97	8	-47	-37	-1	18	14	0	-7	-5	0	3
	I	77	249	119	-40	-78	-32	14	23	8	-5	-7	-2	2	2	1	-1	-1	0
	e	-314	-1019	-489	164	320	130	-57	-93	-34	19	27	9	-6	-8	-2	2	2	1
8101501	ω^*	-265	744	1046	652	48	-345	-396	-215	6	134	137	67	-10	-50	-46	-20	6	18
	Ω	-30	-40	-9	34	52	36	2	-26	-32	-18	1	14	15	7	-2	-7	-7	-3
	I	7	-20	-29	-16	-1	9	11	6	0	-4	-4	-2	0	1	1	1	0	0
	e	-370	1037	1459	909	68	-480	-551	-299	9	185	190	92	-14	-68	-64	-27	8	25
6400101	ω^*	-1447	1211	2666	2438	1244	-17	-771	-899	-598	-170	154	280	238	114	-6	-74	-83	-54
	Ω	-3	-5	-3	1	4	5	3	1	-2	-3	-2	-1	0	1	1	1	0	0
	I	1	-1	-2	-2	-1	0	1	1	0	0	0	0	0	0	0	0	0	0
	e	-378	317	698	638	326	-4	-202	-235	-157	-45	40	73	62	30	-2	-19	-22	-14
6406401	ω	-1750	-1123	-378	169	477	585	557	454	323	197	94	20	-26	-48	-54	-48	-38	-26
	Ω	-7	-15	-20	-21	-17	-12	-6	0	4	6	7	6	5	3	2	1	0	-1
	I	5	3	1	-1	-1	-2	-2	-1	-1	-1	0	0	0	0	0	0	0	0
	e	-394	-252	-85	38	107	130	124	101	71	43	21	4	-6	-10	-12	-10	-8	-6
6508101	ω	-318	-307	-261	-214	-173	-138	-109	-85	-65	-49	-36	-26	-17	-11	-5	-1	2	4
	Ω	-9	-22	-35	-45	-53	-57	-59	-59	-57	-54	-50	-46	-42	-37	-33	-29	-25	-22
	I	8	7	6	5	4	3	2	1	1	1	1	0	0	0	0	0	0	0
	e	-401	-377	-309	-242	-185	-139	-104	-76	-55	-39	-27	-18	-11	-7	-3	-1	1	2
6102801	ω	-1388	-638	-242	-81	-23	-5	0	1	1	0	0	0	0	0	0	0	0	0
	Ω	2	3	3	2	1	0	0	0	0	0	0	0	0	0	0	0	0	0
	I	-2	-1	0	0	0	0	0	0	0	0	0	0	0	0	0	0	0	0
	e	-293	-135	-51	-17	-5	-1	0	0	0	0	0	0	0	0	0	0	0	0

*For these satellites, ω is in units of 10^2 degrees.

of the semimajor axis, inclination, and eccentricity. Thus, it is not necessary to incorporate the interaction terms, as they have already been included numerically and subtracted from the observed data.

As Tables 5 to 7 show, the convergence of the coefficients with orders of the harmonics is slow, particularly for low-altitude and for low-inclination satellites. For Dial and Peole, the coefficients of the secular motions for lower harmonics are not independent, as $\dot{\omega}$ is almost twice as large as $-\dot{\Omega}$.

For low-inclination satellites, the signs of the coefficients change continually as the order of the harmonics is increased, while for high-inclination satellites, they change only rarely. Therefore, to reduce correlations between the coefficients in the determination of zonal spherical harmonics, it is necessary to use data for satellites with well-distributed orbital elements. However, such data are usually not available.

Table 8 gives the orbital elements for the 14 satellites of this analysis. Gaps still exist in inclinations around 20° and 40°. Table 9 lists the values of (O - C), based on the coefficients from Kozai (1964), for the secular motions of the 14 satellites and their standard deviations. The latter are used to compute weights assigned to the data. The columns headed I and II represent the residuals computed by 12 unknowns and 11 unknowns, respectively (discussed in Section 4.3), and the dates refer to previous Kozai solutions (see specifically Kozai, 1959b, 1961a, 1963a, 1969). Kozai (1969) intentionally increased some of the standard deviations, since he thought that neglect of higher order terms would cause errors larger than the standard deviations of the observed values. For the same reason, we have increased the standard deviation (10^{-6} degree per day) to 3×10^{-6} degree per day for $\dot{\omega}$ of satellite 5900101 and $\dot{\Omega}$ of satellites 5900101, 6000902, 6302601, 6206001, 6101501, and 6508101. The standard deviation assigned to the secular motions of 6508901 was erroneously given in the previous paper.

In the determination of even-order harmonic coefficients, we have used the secular motions and the amplitudes of $\begin{matrix}\cos \\ \sin\end{matrix}$ 2ω terms for selected orbital elements of those satellites for which the eccentricities are small. We could not use data from the other satellites, since the orbital elements available for them were not of sufficient

accuracy. The (O - C) values and their standard deviations for the amplitudes of the long-periodic terms are given in Tables 10 and 11. The longitude of the ascending node and the inclination have been omitted for some of the satellites in Tables 10 and 11 because their amplitudes are extremely small. The residuals for ω of 6508901 and 6101501 and for e of 6400101 computed after the determination were found to be much larger than their standard deviations computed from observations. Also, since the inclinations of these satellites are near the critical inclination, higher degree interaction terms neglected in the computations – such as J_3^2/J_2 and $J_2^2 J_3/J_4$ – might have affected the data reduction. For these reasons, we increased the standard deviations assigned to these data from 1.5, 2, and 1 to 4, 5, and 3, respectively; the increased values are given in Table 11. One misprint appeared in Table 2b of Kozai (1969): (O - C) for ω of 6508901 should be $(6 \pm 2) \times 10^{-3}$ instead of $(6 \pm 2) \times 10^{-4}$.

Table 8. Orbital elements of adopted satellites.

Satellite	n (rev day^{-1})	I	e
7001701	13.800	5°.410	0.0880
7010901	14.811	15.040	0.0165
6001301	13.454	28.330	0.0166
5900101	11.460	32.880	0.1650
6202901	9.126	44.800	0.2428
6000902	12.197	47.230	0.0114
6302601	14.108	49.740	0.0600
6206001	13.345	50.140	0.0070
6508901	11.968	59.380	0.0717
6101501	13.870	66.820	0.0080
6400101	13.920	69.910	0.0015
6406401	13.746	79.700	0.0129
6508101	13.805	87.370	0.0743
6102801	8.677	95.850	0.0121

4.3 Solutions

The equations of condition were solved by least squares for both the even-order and the odd-order harmonics. They were solved first with 11 unknowns, J_n ($n \leqq 23$),

and then with 12, the twelfth being J_n ($24 \leqq n \leqq 49$). Seven solutions were obtained. The solutions, given in Tables 12 and 13, include the sums of the squared residuals. The values for coefficients of degrees lower than 14 express corrections to those in Table 4.

Table 9. (O - C) for secular motion and their residuals (in units of 10^{-6} degrees per day).

Satellite		(O - C)	I	II	1969	1963	1961	1959
7001701	$\dot{\omega}$	-18060 ± 90	-57	271	29090	9540	18250	18840
	$\dot{\Omega}$	10120 ± 70	-51	258	-17400	-5390	-9950	-10240
7010901	$\dot{\omega}$	-2200 ± 800	-1530	-857	-4700	100	6200	6900
	$\dot{\Omega}$	5160 ± 100	-83	99	-2160	-1450	-5560	-5900
6001301	$\dot{\omega}$	170 ± 100	43	61	40	-300	-670	-90
	$\dot{\Omega}$	-125 ± 5	-4	-10	-1	59	-611	-928
5900101	$\dot{\omega}$	32 ± 3	1	3	1	18	-129	278
	$\dot{\Omega}$	-9 ± 3	2	7	0	10	-248	-488
6202901	$\dot{\omega}$	40 ± 6	11	10	2	300	827	1013
	$\dot{\Omega}$	7 ± 3	5	8	2	-39	-247	-395
6000902	$\dot{\omega}$	170 ± 50	0	21	47	-287	770	1070
	$\dot{\Omega}$	-1 ± 3	1	5	4	-43	-342	-594
6302601	$\dot{\omega}$	920 ± 10	-1	-6	-52	2650	4900	5290
	$\dot{\Omega}$	1 ± 3	0	-2	19	261	-2	-352
6206001	$\dot{\omega}$	600 ± 60	16	84	60	2230	4180	4500
	$\dot{\Omega}$	-42 ± 3	1	2	8	-56	-437	-740
6508901	$\dot{\omega}$	-110 ± 10	-1	-29	-26	1460	3180	3285
	$\dot{\Omega}$	-70 ± 3	0	-6	-7	-670	-1465	-1670
6101501	$\dot{\omega}$	-300 ± 80	14	97	65	-81	1900	2500
	$\dot{\Omega}$	22 ± 3	-1	-1	3	-1252	-2815	-3057
6400101	$\dot{\omega}$	600 ± 800	729	718	620	-600	580	-500
	$\dot{\Omega}$	56 ± 8	10	6	9	-1073	-2703	-2921
6406401	$\dot{\omega}$	-400 ± 100	-95	-231	-110	-2000	-4000	-4300
	$\dot{\Omega}$	90 ± 10	9	9	15	-220	-1351	-1467
6508101	$\dot{\omega}$	620 ± 30	15	100	-8	300	-3290	-3630
	$\dot{\Omega}$	50 ± 3	-2	-9	-27	35	-306	-337
6102801	$\dot{\omega}$	-35 ± 50	-47	-47	-47	-340	-915	-1008
	$\dot{\Omega}$	-2.9 ± 0.5	0.6	0.7	0.6	62.7	192.3	212.6

Tables 12 and 13 show that the solutions are quite stable, especially for lower order coefficients, and that the data can be expressed quite nicely by including J_{35} and J_{36}. The sum of the squared residuals drops from 114 to 39 when J_{36} is included for the even order and from 53.7 to 40.6 when J_{35} is incorporated for the odd order. Although there is some uncertainty as to whether J_{35} and J_{36} can have such large values, the 12-unknown solutions that include them are regarded as the best. The sum of squared residuals cannot be reduced much further even if the number of unknowns were increased beyond 12.

Table 10. (O - C) for amplitudes of $\frac{\cos}{\sin}$ 2ω terms and their residuals (in units of 10^3 degrees for ω, 10^4 degrees for Ω, 10^5 degrees for I, and 10^6 for e, per day).

Satellite		(O - C)	I	II	1969	1963	1961	1959
5900101	ω	0.3 ± 0.5	-0.2	-0.2	-0.3	-0.6	1.5	1.4
	Ω	-2 ± 2	-1	-2	-2	-1	-4	-4
	I	-3 ± 6	-4	-4	-5	-4	3	3
	e	0 ± 1	1	1	1	1	-4	-4
6202901	ω	-0.1 ± 0.3	-0.2	-0.2	-0.2	-0.8	-2.5	-2.7
	Ω	-1 ± 1	1	1	1	-8	-14	-14
	I	4 ± 4	5	4	4	-3	-14	-15
	e	0 ± 1	0	0	0	5	12	12
6000902	ω	-3 ± 4	-2	-2	-2	-6	-10	-10
	e	0 ± 1	0	0	0	0	1	1
6302601	ω	-6 ± 2	-1	0	0	-14	-23	-23
	Ω	2 ± 2	3	3	3	-2	-3	-3
	I	-1 ± 3	1	1	1	-4	-6	-6
	e	3 ± 2	-3	-3	-3	12	20	20
6206001	ω	3 ± 6	7	6	6	-5	-13	-13
	e	1 ± 1	1	1	0	2	3	3
6508901	ω	6 ± 2	1	2	2	-22	-49	-50
	Ω	4 ± 2	2	2	0	9	10	10
	I	5 ± 5	4	4	4	-3	-11	-11
	e	-4 ± 1	2	1	1	30	62	63
6101501	ω^*	-1 ± 2	-1	0	0	-3	0	0
	e	1 ± 2	0	0	-1	3	-1	-1
6406401	ω^*	0 ± 2	0	0	0	-1	-1	-1
	e	4 ± 4	3	4	3	5	7	7
6508101	ω	7 ± 3	3	4	3	12	0	0
	Ω	1 ± 1	1	0	0	2	2	2
	I	-2 ± 8	-2	-2	-2	-2	-2	-2
	e	-6 ± 2	-1	-2	-1	-11	3	3

*For these satellites, ω is in units of 10^2 degrees.

Table 11. (O - C) for amplitudes of $\overset{\cos}{\sin}\ \omega$ terms and their residuals (in units of 10^3 degrees for ω, 10^4 degrees for Ω, 10^5 degrees for I, and 10^6 for e, per day).

Satellite		(O - C)	I	II	1969	1963	1961	1959
7001701	ω	-70 ± 5	-2	0	-126	-104	-85	-87
	Ω	-190 ± 30	0	-28	-248	-570	-168	-237
	I	430 ± 30	-34	-31	740	900	480	550
	e	-91 ± 6	-5	-5	-149	-179	-99	-112
7010901	ω	45 ± 30	9	41	160	-411	232	112
	Ω	-18 ± 45	-44	-48	0	10	9	7
	I	-170 ± 300	-166	-170	-181	-120	-190	-177
	e	28 ± 20	18	27	61	-102	83	49
6001301	ω	4 ± 1	0	0	0	46	314	241
	Ω	0 ± 3	2	2	0	3	-10	-7
	I	0 ± 30	0	0	0	-2	-16	-12
	e	1.6± 1.0	0.5	0.5	0.6	13.5	90.7	69.8
5900101	ω	-1.7± 0.3	0.0	0.3	0.0	4.8	22.4	17.2
	Ω	-2 ± 2	2	1	2	-7	-87	-58
	I	1 ± 5	-3	-3	-4	-8	-64	-57
	e	-3.1± 0.5	-0.3	-0.7	-0.1	3.2	40.0	35.6
6202901	ω	-0.1± 0.2	0.0	0.0	-0.1	-1.2	-4.0	6.1
	Ω	2 ± 3	2	3	3	16	5	31
	I	-2 ± 3	-5	-4	-4	-11	-26	-78
	e	-1.5± 0.8	0.2	0.0	0.2	4.2	15.2	49.7
6000902	ω	-19 ± 3	-4	-4	-10	42	1	315
	Ω	1 ± 1	1	1	0	3	4	6
	I	-2 ± 6	-2	-2	-6	-3	-2	-6
	e	-2.0± 0.6	1.0	1.0	0.3	10.5	2.4	64.8
6302601	ω	-17 ± 2	0	-4	-1	9	-17	86
	Ω	-6 ± 1	0	0	1	20	52	60
	I	14 ± 15	10	11	10	6	12	-19
	e	-12 ± 1	0	-1	2	16	-6	99
6206001	ω	-59 ± 4	0	5	0	187	122	931
	Ω	-2 ± 2	-2	-2	-2	0	3	4
	I	0 ± 10	0	0	0	-1	0	-4
	e	-8 ± 1	-1	0	-1	22	14	113
6508901	ω	3 ± 4	7	7	0	119	264	486
	Ω	10 ± 2	3	3	2	-10	8	-29
	I	-8 ± 8	-9	-9	-7	-40	-80	-144
	e	-4 ± 1	0	0	-2	127	292	555

Table 11. (Cont.)

Satellite		(O - C)	I	II	1969	1963	1961	1959
6101501	ω^*	-19 ± 5	-11	-11	-8	-46	-265	-413
	Ω	-3 ± 4	2	2	0	7	17	29
	I	0 ± 5	0	0	0	1	7	11
	e	-11 ± 1	0	0	4	-48	-354	-560
6400101	ω^*	-200 ± 10	6	3	1	-72	-445	-593
	e	-58 ± 3	-4	-5	-9	-24	-122	-161
6406401	ω	-110 ± 20	23	36	30	23	510	930
	Ω	6 ± 3	1	1	1	5	11	16
	I	0 ± 8	0	0	0	0	-2	-3
	e	-34 ± 5	-4	-2	-2	-4	106	199
6508101	ω	60 ± 2	1	-1	3	64	197	296
	Ω	20 ± 1	0	2	2	16	26	32
	I	-10 ± 10	-9	-9	-10	-10	-13	-16
	e	60 ± 3	-4	-5	-2	67	231	354
6102801	ω	-30 ± 50	-48	-47	-40	15	390	663
	Ω	-2 ± 2	-2	-2	-2	-2	-3	-4
	I	-6 ± 7	-6	-6	-6	-6	-6	-5
	e	3.0± 1.5	-0.7	-0.6	0.0	12.5	91.8	149.2

*For these satellites, ω is in units of 10^2 degrees.

In Tables 9, 10, and 11, the residuals computed by the 12 unknowns and by the 11 unknowns are given under the headings I and II, respectively. Solution I for even orders can express the secular motions of all the satellites except 7010901 and 6202901. Since only in Table 9 is the difference between residual I and residual II much larger than the standard deviation for the data on 7001701, 6508901, and 6508101, it can be said that J_{36} is determined essentially from the data on these three satellites. If more accurate data become available for 7010901, so that the standard deviations for this satellite become smaller than the differences, a more definite conclusion regarding J_{36} can be obtained. In Table 11, there is no essential difference between residuals I and II. Thus, for odd orders, it is not yet definite that the 12-unknown solution is much better than the 11-unknown one.

For comparison, five previous solutions (Kozai, 1959b, 1961a, 1963a, 1964, 1969) are given in Table 14. These solutions were derived from the following numbers of satellites with inclinations ranging from 28° to 96°:

	1959	1961	1963	1964	1969
Number of satellites	1	3	13	9	12
Inclination range	34°	33°–50°	32°–65°	33°–96°	28°–96°

Except for some of the 1963 determination, the standard deviations in the first three determinations are more than 10 times larger than the present ones; therefore, the residuals computed by these solutions are very large even for satellites within the indicated inclination ranges. The residuals from the 1964 solution are listed as (O-C) in Tables 9, 10, and 11. Both the 1964 and the 1969 solutions give very large residuals for Peole and Dial. Table 14 also includes a solution by Cazenave, Forestier, Nouel, and Pieplu (1971), who incorporated data for Peole, Dial, and SAS (7010701; I = 3°) in addition to the satellites used by Kozai (1969). Their solution agrees quite well with ours except for the odd higher order coefficients.

Table 12. Solutions for even-order harmonics (in units of 10^{-9}). Corrections are given for n = 14.

J_2	J_4	J_6	J_8	J_{10}	J_{12}	J_{14}	J_{16}	J_{18}	J_{20}	J_{22}	J_n	n	Residual
-3	30	-94	66	-178	161	-78	43	-77	-108	75			114
±1	±2	±3	±4	±4	±3	±8	±7	±9	±9	±13			
-3	31	-97	68	-178	155	-74	30	-75	-104	72	31	24	106
±1	±2	±3	±4	±4	±5	±7	±10	±6	±9	±12	±17		
-3	30	-94	67	-177	161	-76	43	-74	-108	73	-9	26	113
±1	±2	±3	±4	±4	±3	±8	±7	±9	±9	±13	±20		
-2	30	-89	61	-181	162	-80	35	-83	-132	80	94	28	67
±1	±2	±3	±3	±3	±2	±6	±6	±5	±8	±9	±17		
-3	28	-92	61	-178	167	-80	44	-75	-104	97	-61	30	103
±1	±2	±3	±4	±4	±4	±7	±7	±6	±9	±15	±28		
-3	29	-94	67	-176	159	-82	41	-76	-111	75	33	32	110
±1	±2	±3	±4	±4	±3	±8	±7	±6	±9	±12	±25		
-3	30	-94	66	-178	162	-78	40	-78	-107	74	14	34	113
±1	±2	±3	±4	±4	±3	±7	±9	±7	±9	±12	±33		
-2	31	-94	65	-183	165	-74	34	-102	-119	92	199	36	39
±1	±1	±2	±2	±2	±2	±4	±4	±5	±5	±7	±22		

Table 13. Solutions for odd-order harmonics (in units of 10^{-9}). Corrections are given for n = 13.

J_3	J_5	J_7	J_9	J_{11}	J_{13}	J_{15}	J_{17}	J_{19}	J_{21}	J_{23}	J_n	n	Residual
6	-20	-12	-109	15	-222	104	-227	83	-70	111			53.7
±3	±5	±7	±8	±7	±7	±11	±11	±12	±14	±21			
8	-23	-8	-106	10	-210	88	-210	78	-83	137	-41	25	49.4
±3	±4	±7	±7	±7	±10	±13	±13	±11	±13	±18	±20		
3	-15	-18	-98	19	-226	121	-237	101	-78	101	-58	27	44.7
±3	±4	±7	±8	±6	±7	±11	±11	±12	±11	±13	±20		
5	-19	-12	-107	17	-222	107	-227	84	-64	103	-16	29	53.0
±3	±5	±7	±8	±7	±7	±11	±11	±12	±14	±17	±23		
6	-20	-11	-109	15	-220	106	-227	87	-72	115	-23	31	52.8
±3	±4	±7	±8	±7	±8	±10	±11	±12	±12	±14	±28		
7	-22	-11	-109	13	-219	102	-218	78	-69	124	-47	33	51.1
±3	±4	±7	±8	±7	±8	±10	±12	±12	±12	±16	±32		
5	-18	-19	-101	10	-225	105	-220	99	-83	145	-134	35	40.6
±3	±4	±7	±7	±6	±7	±9	±10	±11	±11	±15	±36		
6	-21	-11	-109	15	-222	102	-225	86	-66	110	-30	37	53.1
±3	±4	±7	±8	±7	±7	±11	±11	±13	±13	±13	±44		

Table 14. Comparison of results (in units of 10^{-6}).

Solution	J_2	J_4	J_6	J_8	J_{10}	J_{12}	J_{14}	J_{16}	J_{18}	J_{20}	J_{22}	J_{36}
1959	1082.1	-2.15										
1961	1082.19 ±3	-2.13 ±5										
1963	1082.48 ±4	-1.84 ±9	0.39 ±9	-0.02 ±7								
1964	1082.639 ±6	-1.649 ±16	0.646 ±30	-0.270 ±50	-0.054 ±50	-0.357 ±44	0.179 ±63					
1969	1082.628 ±2	-1.593 ±7	0.502 ±14	-0.118 ±20	-0.354 ±25	-0.042 ±27	-0.073 ±28	0.187 ±26	-0.231 ±22	-0.005 ±22		
1973 I	1082.637 ±1	-1.618 ±1	0.552 ±2	-0.205 ±2	-0.237 ±2	-0.192 ±2	0.105 ±4	0.034 ±4	-0.102 ±5	-0.119 ±5	0.092 ±7	0.199 ±22
1973 II	1082.636 ±1	-1.619 ±2	0.552 ±3	-0.204 ±4	-0.232 ±4	-0.196 ±3	0.101 ±8	0.043 ±7	-0.077 ±9	-0.108 ±9	0.075 ±13	
Cazenave et al. (1971)	1082.637 ±4	-1.619 ±10	0.558 ±17	-0.209 ±24	-0.233 ±26	-0.188 ±27	0.085 ±34	0.048 ±43	-0.137 ±44	-0.087 ±52		

Solution	J_3	J_5	J_7	J_9	J_{11}	J_{13}	J_{15}	J_{17}	J_{19}	J_{21}	J_{23}	J_{35}
1959	-2.20 ±8											
1961	-2.29 ±2	-0.23 ±2										
1963	-2.562 ±7	-0.064 ±7	-0.470 ±10	0.117 ±11								
1964	-2.546 ±20	-0.210 ±25	-0.333 ±39	-0.053 ±60	0.302 ±35	-0.114 ±84						
1969	-2.538 ±4	-0.230 ±7	-0.361 ±15	-0.100 ±23	0.202 ±35	-0.123 ±49	-0.174 ±61	0.085 ±65	-0.216 ±53	0.145 ±29		
1973 I	-2.541 ±3	-0.228 ±4	-0.352 ±7	-0.154 ±7	0.312 ±6	-0.339 ±7	0.105 ±9	-0.220 ±10	0.099 ±11	-0.083 ±11	0.145 ±15	-0.134 ±36
1973 II	-2.540 ±3	-0.230 ±3	-0.345 ±7	-0.162 ±8	0.317 ±7	-0.336 ±7	0.104 ±11	-0.227 ±11	0.083 ±12	-0.070 ±17	0.111 ±21	
Cazenave et al. (1971)	-2.543 ±5	-0.226 ±7	-0.365 ±12	-0.118 ±13	0.236 ±12	-0.202 ±14	-0.081 ±21	-0.027 ±23	-0.112 ±23	0.106 ±15		

5. DETERMINATION OF TESSERAL HARMONICS

Tesseral harmonics are computed by combining satellite perturbations and terrestrial gravimetry. In the computation of the normal system, terms with small contributions have been omitted. Therefore, the normal system determined from satellite analysis is complete through $\ell = m = 12$. In each higher order, terms have been omitted – for example, 13, 6 through 13, 9 and 14, 5 through 14, 11. Resonant harmonics through 23, 14 have been incorporated. Of course, all terms were included in the computation of the residuals. In the same way, for surface gravity all available geopotential coefficients have been used, but no partial derivatives for the zonal harmonics or tesseral harmonics less than 9th degree were computed, since they are negligibly small.

For each orbital arc, a set of six mean elements, $\mathcal{E}_i$, is determined. The linear rates are derived empirically, as is the mean anomaly. In addition, higher polynomials in the mean anomaly are employed, where appropriate, to account for the nonperiodic, yet nonsecular, effects of air drag and radiation pressure. Twelve or more orbital elements are determined for each arc, and the arcs range in length from 4 to 30 days. Therefore, with the more than 100 orbital arcs used in this solution, over 1500 additional parameters need to be determined. By use of a device described in Part IV of this Report for reducing the normal equations, this can be accomplished without dealing with 2000×2000 matrices. For systems of 2000 unknowns, the time required to compute reduced normal equations is much greater than that for the adopted method, which is a block Gauss-Seidel iteration. Reduced normal equations are used with more limited problems – e.g., in a solution for resonant harmonics – because they rigorously account for the interaction of the elements and unknowns.

The determination of orbital elements and that of geodetic parameters (gravity field and station coordinates) are separated and iterations are performed alternately; this method improves first one set and then the other. As the iterations proceed, the choice of unknowns is modified: Satellites are either deleted or augmented, depending on whether gravity-field coefficients (and station coordinates) appear to be ill determined or significant.

Equations (11) lead us to the method of selecting those gravity-field coefficients that affect the orbit and that therefore can be determined from observing the orbit. We know that $\overline{C}_{\ell m}$, a, e, and I determine the size of $\delta \mathcal{E}^{k}_{\ell mpq}$, which can be computed by using an estimate of $|\overline{C}_{\ell m}|$ and the value of the mean elements. We estimate $|\overline{C}_{\ell m}| = \alpha \ell^{-\beta}$ to test for significance, and only terms greater than $\alpha \ell^{-\beta}$ are retained. All the $\delta \mathcal{E}^{k}$ are calculated and combined into a shift of position $\sqrt{d\bar{\rho} \cdot d\bar{\rho}}$; they are given in Table 15 for satellite 6701401 with ℓ = 11, 12, ..., 20. The units are adjusted so that with $\overline{C}_{\ell m}$ expressed in units of 10^{-6} (e.g., $\overline{C}_{2,2} = 2.4$), the perturbation in position is in meters. Conservative values for α and β are used, and more terms are carried than are perhaps necessary. For example, for ℓ = 11, m = 5, and $C_{\ell m} = 10^{-5}/\ell^{2} = 0.083$, the perturbation is $0.083 \times 38 \approx 3$ m. From such tabulations for each satellite, we can choose the coefficients that affect the motion of the satellite and ascertain how many satellites contribute to the determination of a coefficient. In addition, the accuracy of the available data controls the size of the effect that can be detected. The choice of coefficients is made by balancing the amount and precision of the data available for a particular satellite against the sensitivity of that satellite to particular coefficients. Further, it is apparent that the surface-gravity data are stronger than the satellite information for some coefficients, and for that reason some higher coefficients have been dropped from the satellite solution.

Table 15 illustrates two points referred to earlier. The amplitudes for m = 13 are quite large because of the resonance; the large size of the effects continues well into the 20th-degree terms. The m = 12 and m = 14 harmonics also have sizable effects because they are adjacent to a resonant harmonic. Tables for the other satellites used are given in Gaposchkin (1970b).

Apart from the resonant harmonics, terms higher than ℓ = 12, m = 12 are weakly determined by the satellite data, but it had been demonstrated in earlier iterations that the surface gravity could determine these higher harmonics. The satellite solution was limited to those harmonics that have an effect greater than 3 to 4 m on the orbit. The resulting terms were complete through ℓ = 12, m = 12. The higher order terms selected were C/S(ℓ, 1) $13 \le \ell \le 16$; C/S(ℓ, 2) $13 \le \ell \le 15$; C/S(14, 3); C/S(ℓ, 12) $13 \le \ell \le 19$; C/S(ℓ, 13) $13 \le \ell \le 2$; and C/S(ℓ, 14) $14 \le \ell \le 24$.

Table 15. Sensitivity coefficients for satellite 6701401 (in units of meters, with $|\overline{C_{\ell m}}| \times 10^6$).

e = 0.0843130 A = 7614 km
I = 39.°45459 perigee = 594 km
n = 13.064356 apogee = 1878 km

m \ ℓ	11	12	13	14	15	16	17	18	19	20
1	154	229	121	75	139	160	66	69	118	67
2	113	43	61	94	58	35	59	46	0	33
3	52	78	65	25	54	43	12	18	39	26
4	66	34	19	39	38	14	10	27	0	0
5	38	28	51	29	0	23	10	0	0	18
6	65	48	42	14	27	19	0	17	0	0
7	68	62	61	45	10	0	18	16	0	0
8	46	62	45	37	18	12	0	0	18	0
9	21	30	46	64	55	53	23	0	0	0
10	0	0	29	44	43	58	37	32	0	0
11	0	0	8	16	27	48	47	57	48	44
12		0	0	21	44	64	89	101	75	99
13			425	1203	2987	4758	8014	9531	12277	11613
14				0	0	20	47	77	111	145
15					0	0	0	0	16	20
16						0	0	0	0	0
17							0	0	0	0
18								0	0	0
19									0	0
20										0

The m = 9, 12, 13, 14 terms are resonant with some satellites, which are listed in Table 16 along with their resonant periods. Several satellites are resonant with more than one order. For example, 6701101 has a 1.6-day period with the 13th order and a 2.6-day period with the 14th, the latter being the principal effect. Other resonances have several periods, as illustrated by equation (12) for 5900701 (which was not used in the final solution) and in Table 16 for 6701401. The multiple periods are due to the nonzero eccentricity, which causes the frequency splitting.

Table 16. Resonant periods.

Resonant with order (m)	Satellite	Inclination	Period (days)
9	6102801	95°	2.90
12	6100401	39	15.0
12	6000902	47	15.5
12	6508901	59	7.2
12	6506301	69	3.3
12	6507801	144	2.3
13	6701401	39	9.4, 10.9, 13.1, ...
13	6503201	41	5.6
13	6701101	40	1.6
13	6206001	50	5.3
13	6800201	105	6.3
13	6600501	89	1.8
13	6304901	90	2.5
14	6701101	40	2.6
14	6302601	50	12.2
14	6101501	67	3.84
14	6101502	67	3.76
14	6400101	70	4.9
14	6406401	80	2.9
14	6408101	87	3.8
14	6600501	89	2.2

The results of the dynamical solution must be discussed in the context of the combination solutions. A summary of the data is given in Table 2. The selection of data and unknowns evolved through the analysis. The number of satellites used ranged from 21 to 25, and the number of arcs in the largest solution was 203. Arcs were added or rejected on the basis of their contribution to the normal equations, the number of observations for a particular station, the improvement of distribution for a resonant harmonic, and the quality of the orbital fit.

Two iterations were performed for the gravity field. The first employed the gravity field and station coordinates determined by Gaposchkin and Lambeck (1970) as initial values; and the second used the results of the first iteration for the gravity field plus the station coordinates determined in Part VI of this Report. Other basic constants adopted are as follows:

$$GM = 3.986013 \times 10^{20} \text{ cm}^3 \text{ sec}^{-2}$$

$$c = 2.997925 \times 10^{10} \text{ cm sec}^{-1} \text{ (velocity of light)}$$

$$k_2 = 0.30 \text{ (Love number)}$$

$$a_e = 6.378140 \text{ Mm} \quad .$$

For each iteration, several solutions were obtained. Orbital arcs were added or deleted to improve the satellite distribution and the variance-covariance matrix.

Several weights for the surface gravity were used. For areas without surface-gravity data, we had four choices of treatment:

A. We could make no assumptions about unobserved areas.

B. We could use a zero anomaly with a very large variance; that is, the expected value of gravity would be zero.

C. We could use a reference gravity field with a very large variance; that is, only the higher harmonics would have an expected value of zero.

D. We could use a model anomaly, for example, one determined from topography.

Adoption of method A would introduce very large short-wavelength features into those regions where no gravity is measured. In addition, the statistical comparisons discussed later are very poor, although the (O - C) values and the satellite orbits are good.

Therefore, A had to be discarded. Gaposchkin and Lambeck tried methods B and D and found them equivalent. Choice C is an improvement over B because the low-degree and low-order terms are well determined by means of satellite data. Therefore, C was adopted, with the weight given in Table 3. Comparing the results of choices A and C, we found that satellite comparisons are identical, the (O - C) for the surface gravity is marginally improved, and the statistical comparisons of the surface gravity are quite acceptable.

The fully normalized spherical-harmonic coefficients for the zonal harmonics and the tesseral harmonics are given in Tables 17 and 18. Figure 5 shows the mean potential coefficient by degree and the $10^{-5}/\ell^2$ rule. The mean potential coefficient for degrees 2 through 36 is determined by numerical quadrature of surface-gravity data (see Section 7) and is also plotted in Figure 5. Figure 6 plots the geoid heights and gravity anomalies: Figures 6a and 6b are calculated from the coefficients in Tables 17 and 18 with respect to the best-fitting ellipsoid; Figures 6c and 6d, with respect to the hydrostatic ellipsoid; and Figures 6e and 6f, with respect to the 5th-degree and order reference surface defined by the 5th-degree and order coefficients from Tables 17 and 18.

Table 17. Zonal harmonics in fully normalized form. $\bar{C}_{\ell,0} = -J_\ell/\sqrt{2\ell+1}$; J_ℓ is from solution 1973 I, Table 14.

Harmonic	Value	Harmonic	Value
$\bar{C}_{2,0}$	-4.84170E-04	$\bar{C}_{14,0}$	-1.94980E-08
$\bar{C}_{3,0}$	9.60408E-07	$\bar{C}_{15,0}$	-1.88586E-08
$\bar{C}_{4,0}$	5.39333E-07	$\bar{C}_{16,0}$	-5.91864E-09
$\bar{C}_{5,0}$	6.87446E-08	$\bar{C}_{17,0}$	3.71868E-08
$\bar{C}_{6,0}$	-1.53097E-07	$\bar{C}_{18,0}$	1.67687E-08
$\bar{C}_{7,0}$	9.08860E-08	$\bar{C}_{19,0}$	-1.58527E-08
$\bar{C}_{8,0}$	4.97198E-08	$\bar{C}_{20,0}$	1.85847E-08
$\bar{C}_{9,0}$	3.53300E-08	$\bar{C}_{21,0}$	1.26574E-08
$\bar{C}_{10,0}$	5.17176E-08	$\bar{C}_{22,0}$	-1.37146E-08
$\bar{C}_{11,0}$	-6.50565E-08	$\bar{C}_{23,0}$	-2.11504E-08
$\bar{C}_{12,0}$	3.84000E-08	$\bar{C}_{35,0}$	1.59029E-08
$\bar{C}_{13,0}$	6.52406E-08	$\bar{C}_{36,0}$	-2.32912E-08

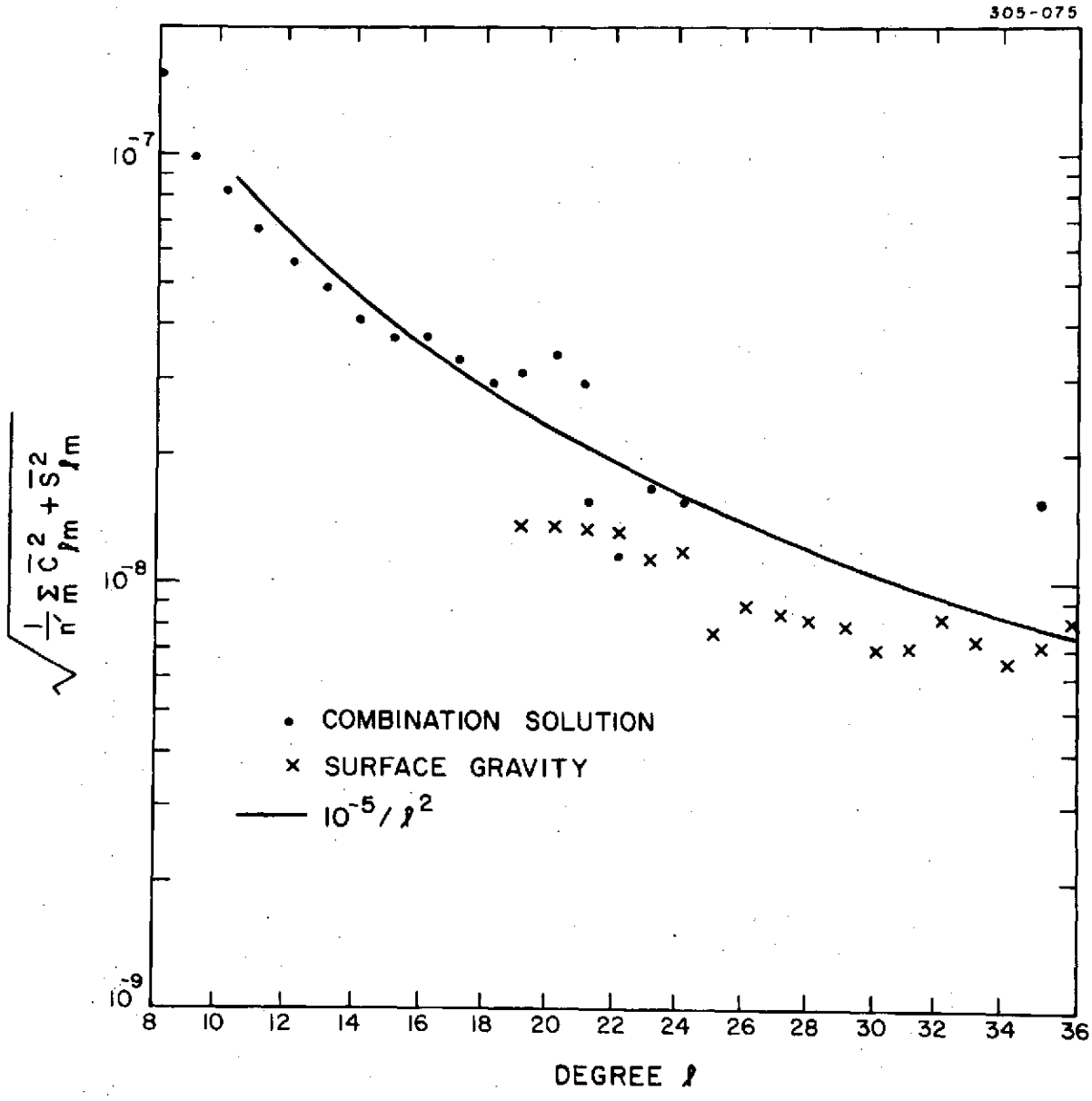

Figure 5. Mean potential coefficient by degree.

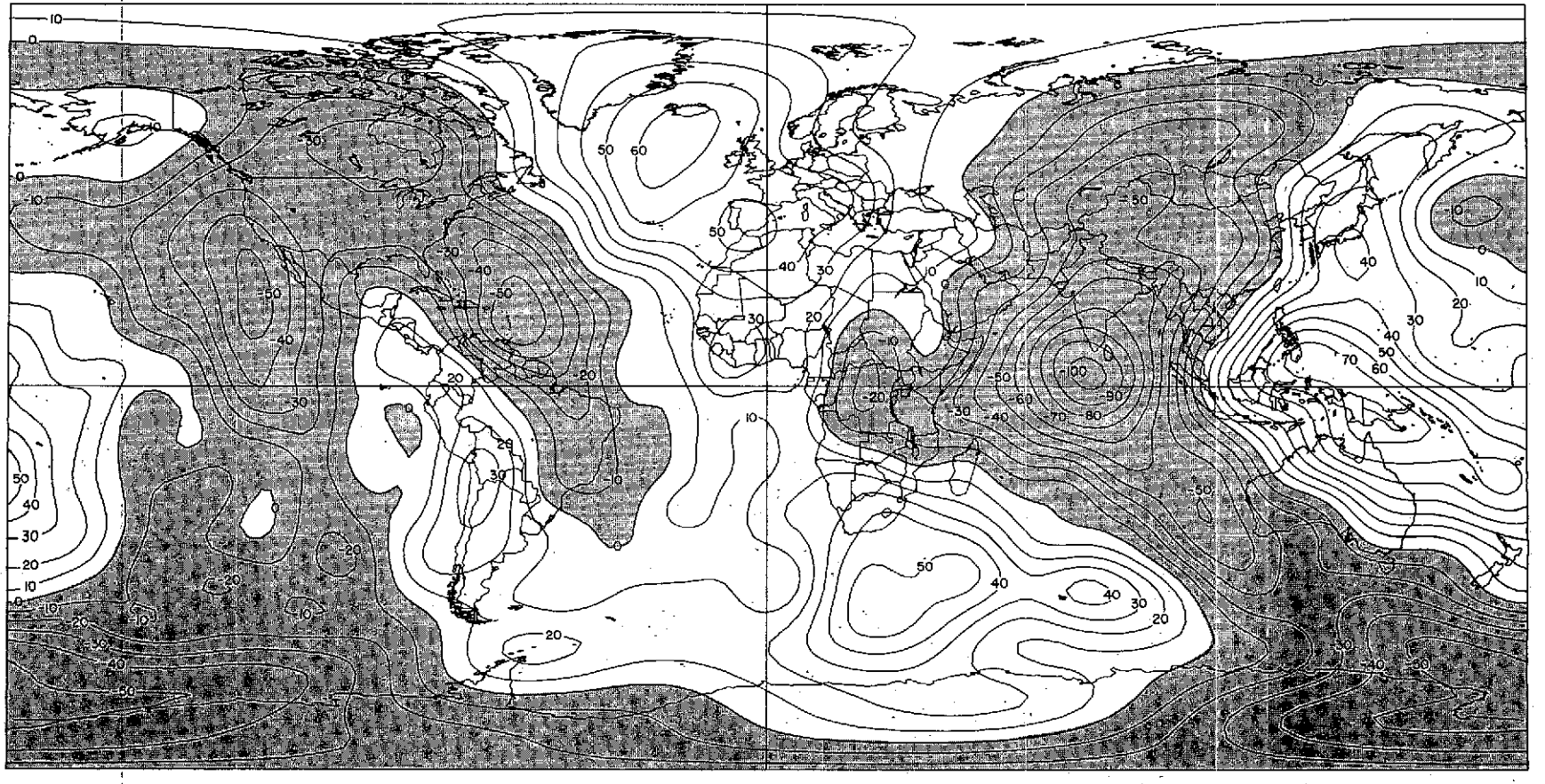

Figure 6a. SE III geoid heights in meters calculated with respect to the best-fitting ellipsoid, f = 1/298.256.

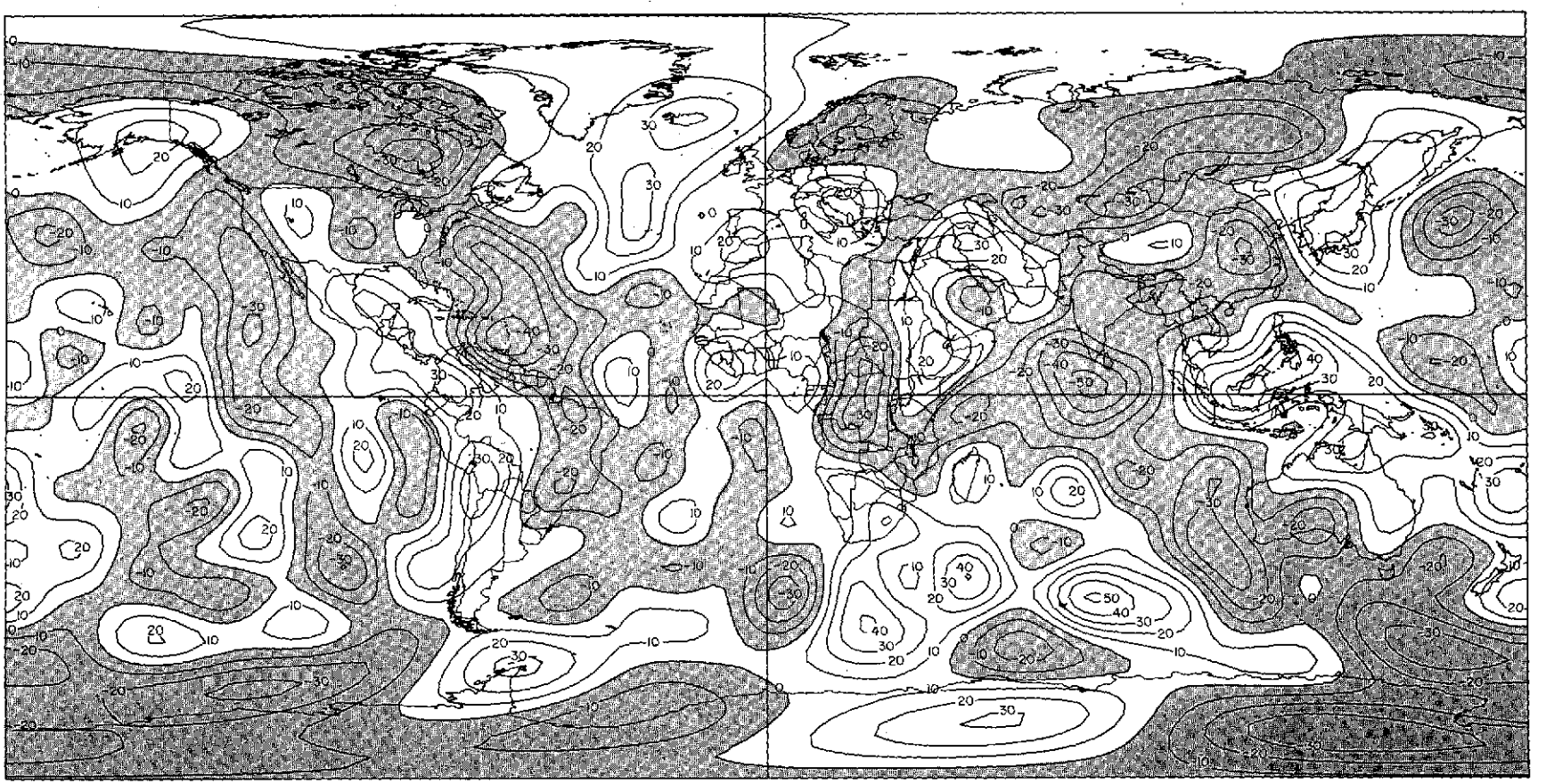

Figure 6b. SE III gravity anomalies in milligals calculated with respect to the best-fitting ellipsoid, f = 1/298.256.

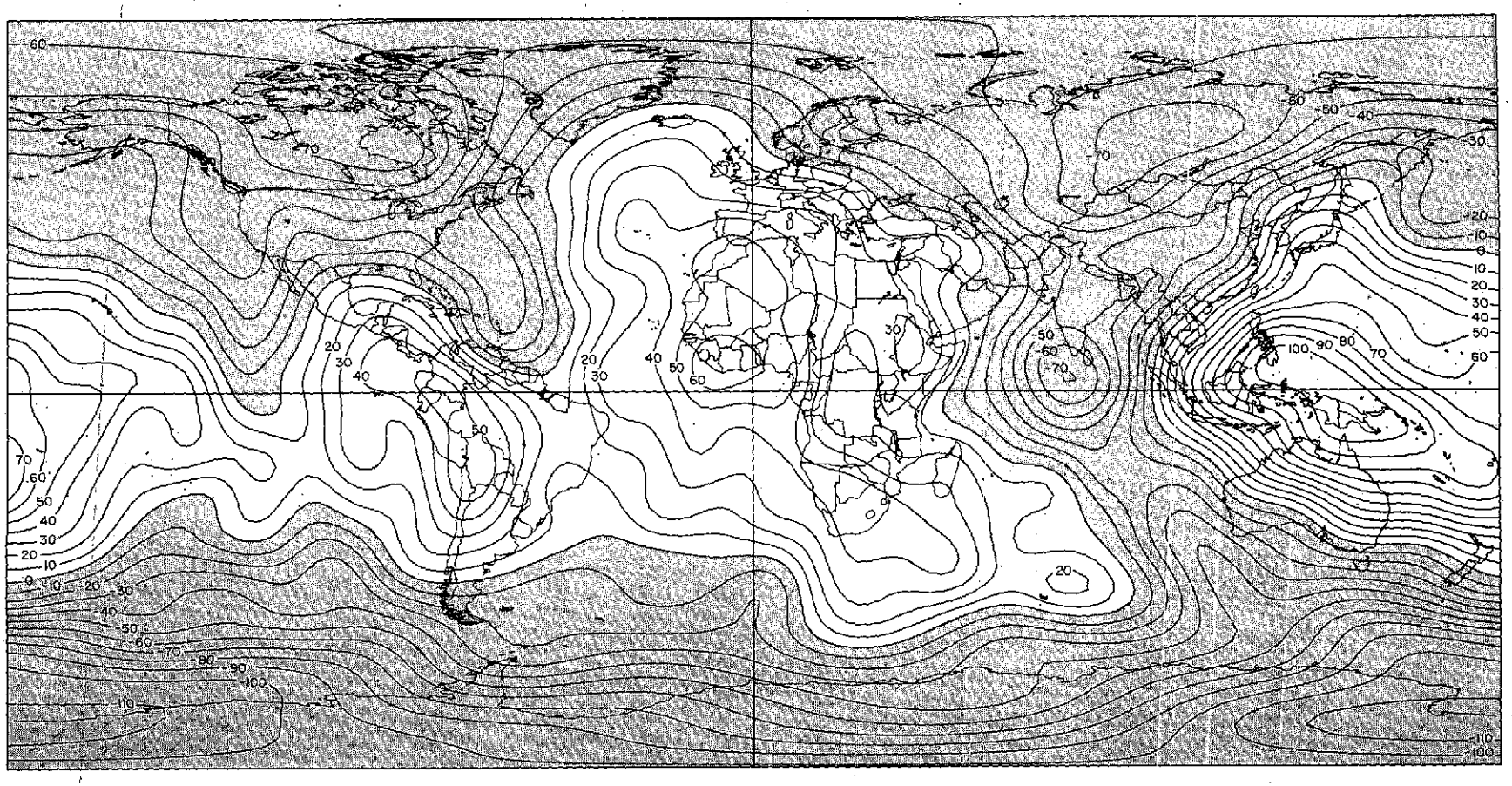

Figure 6c. SE III geoid heights in meters calculated with respect to the hydrostatic ellipsoid, f = 1/299.67.

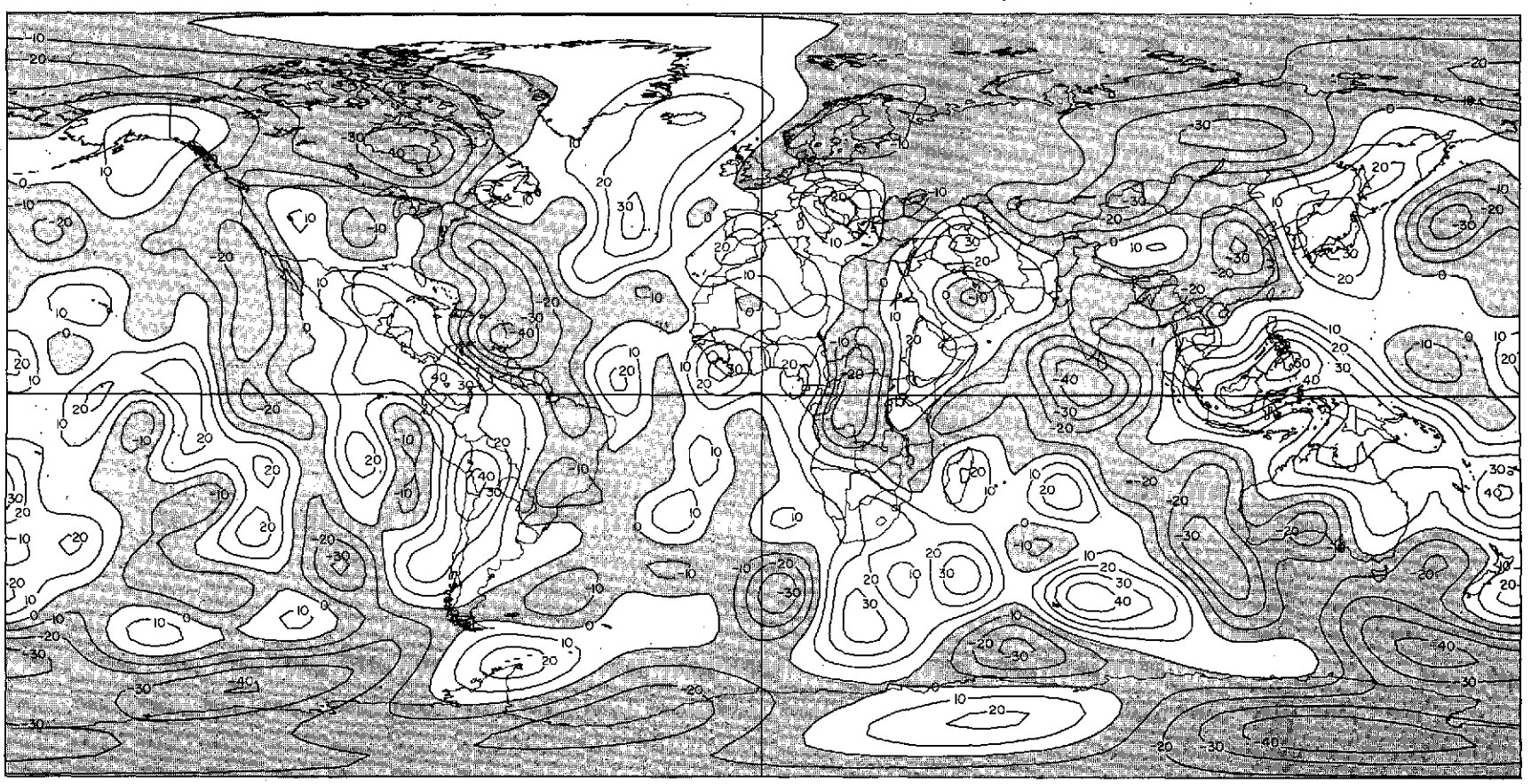

Figure 6d. SE III gravity anomalies in milligals calculated with respect to the hydrostatic ellipsoid, f = 1/299.67.

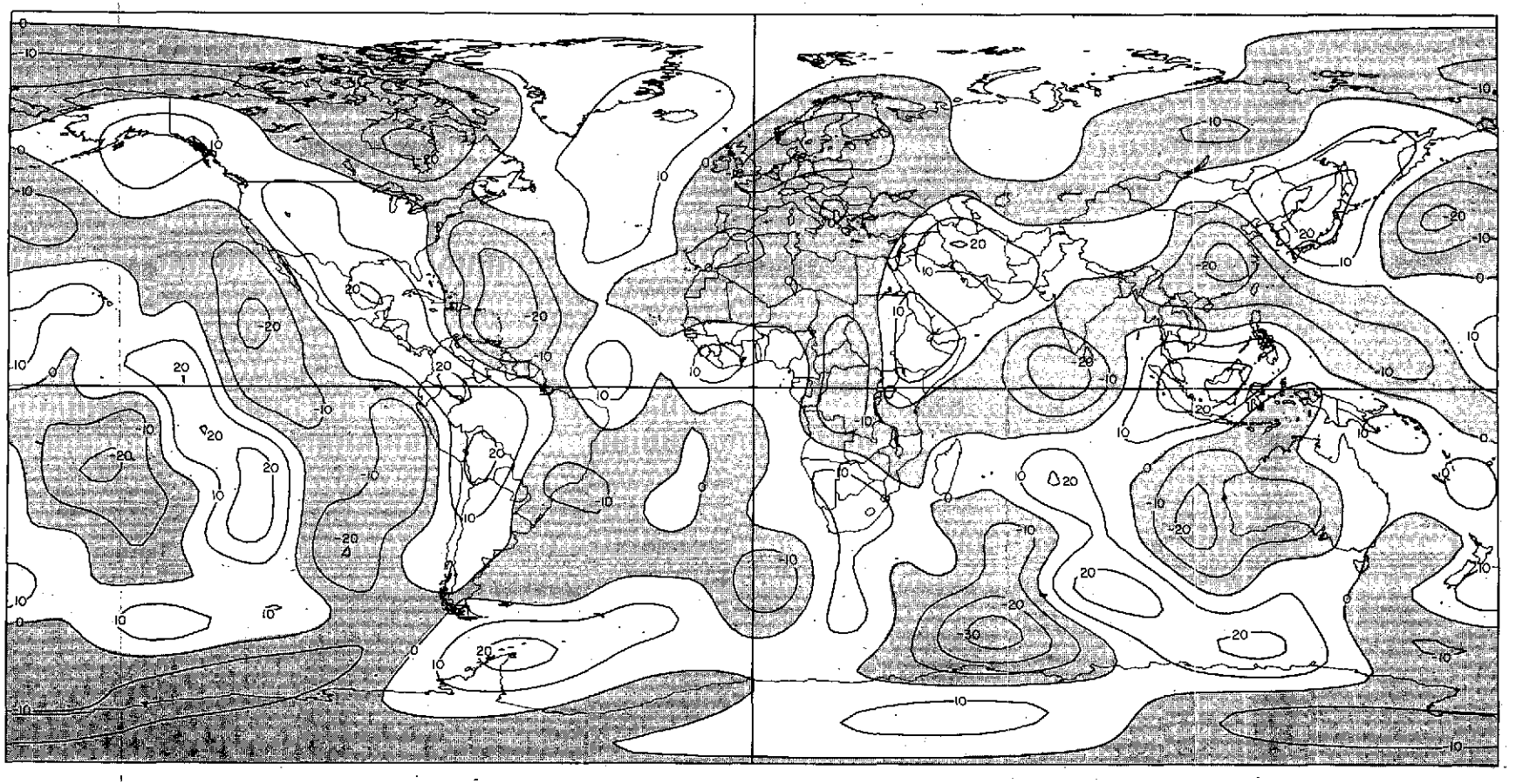

Figure 6e. SE III geoid heights in meters calculated with respect to the 5th-degree and order reference surface, $\bar{C}_{\ell m} = \bar{S}_{\ell m} = 0$ if $\ell \leq 5$ and $m \leq 5$.

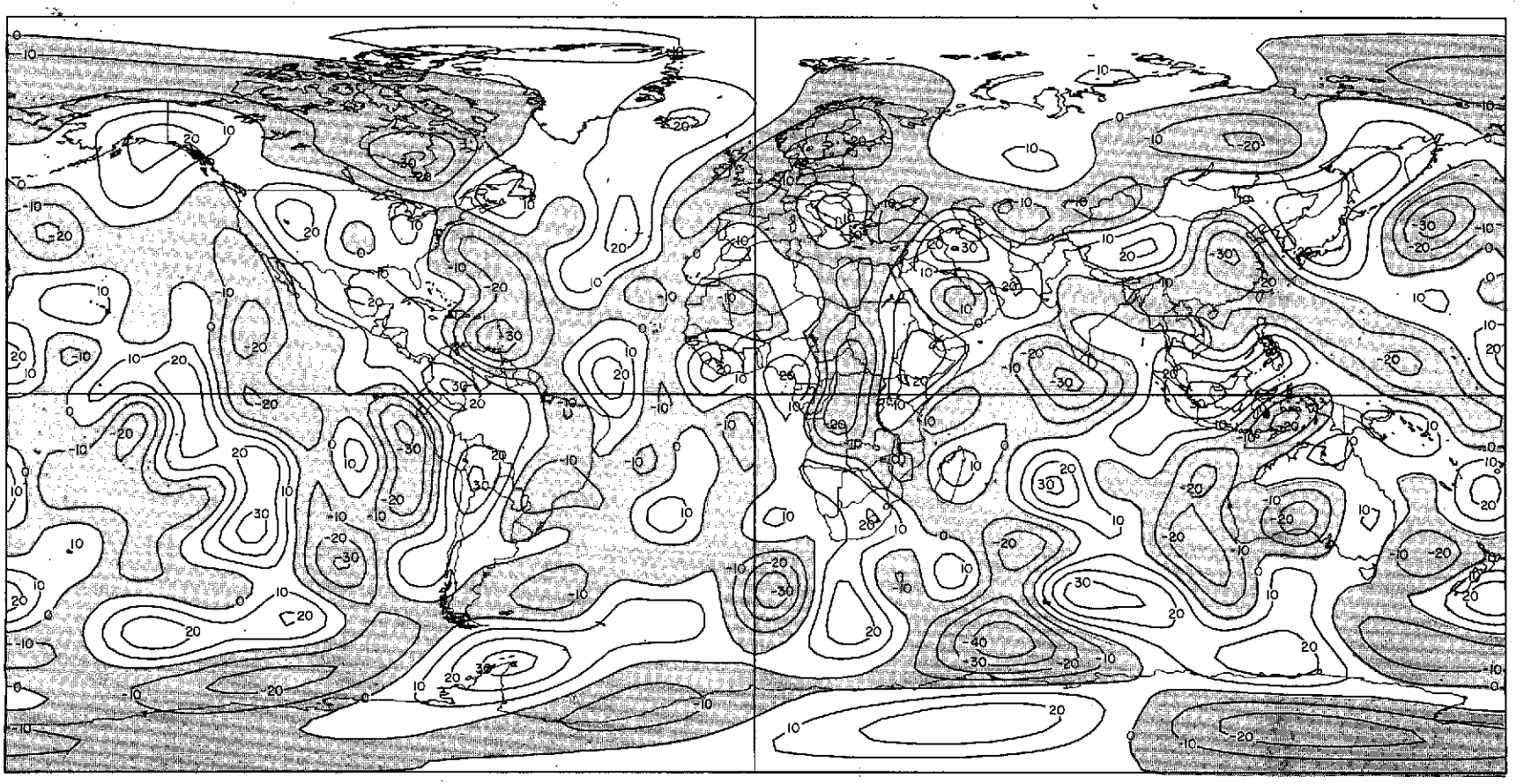

Figure 6f. SE III gravity anomalies in milligals calculated with respect to the 5th-degree and order reference surface, $\overline{C}_{\ell m} = \overline{S}_{\ell m} = 0$ if $\ell \leq 5$ and $m \leq 5$.

Table 18. Fully normalized tesseral-harmonic coefficients for the geopotential.

Harmonic	Value	Harmonic	Value	Harmonic	Value	Harmonic	Value
$\bar{C}_{2,2}$	2.3799E-06	$\bar{S}_{2,2}$	-1.3656E-06	$\bar{C}_{3,1}$	1.9977E-06	$\bar{S}_{3,1}$	2.2337E-07
$\bar{C}_{3,2}$	7.7830E-07	$\bar{S}_{3,2}$	-7.5519E-07	$\bar{C}_{3,3}$	4.9011E-07	$\bar{S}_{3,3}$	1.5283E-06
$\bar{C}_{4,1}$	-5.1748E-07	$\bar{S}_{4,1}$	-4.8140E-07	$\bar{C}_{4,2}$	3.4296E-07	$\bar{S}_{4,2}$	6.7174E-07
$\bar{C}_{4,3}$	1.0390E-06	$\bar{S}_{4,3}$	-1.1923E-07	$\bar{C}_{4,4}$	-1.0512E-07	$\bar{S}_{4,4}$	3.5661E-07
$\bar{C}_{5,1}$	-5.3667E-08	$\bar{S}_{5,1}$	-7.9973E-08	$\bar{C}_{5,2}$	5.9869E-07	$\bar{S}_{5,2}$	-3.9910E-07
$\bar{C}_{5,3}$	-5.8429E-07	$\bar{S}_{5,3}$	-1.6338E-07	$\bar{C}_{5,4}$	-1.1583E-07	$\bar{S}_{5,4}$	-4.5393E-08
$\bar{C}_{5,5}$	1.3956E-07	$\bar{S}_{5,5}$	-8.6841E-07	$\bar{C}_{6,1}$	-7.2166E-08	$\bar{S}_{6,1}$	1.7756E-08
$\bar{C}_{6,2}$	2.4670E-08	$\bar{S}_{6,2}$	-4.0654E-07	$\bar{C}_{6,3}$	4.4139E-09	$\bar{S}_{6,3}$	2.9055E-08
$\bar{C}_{6,4}$	-1.0003E-07	$\bar{S}_{6,4}$	-3.0297E-07	$\bar{C}_{6,5}$	-1.3504E-07	$\bar{S}_{6,5}$	-6.0964E-07
$\bar{C}_{6,6}$	-2.9136E-08	$\bar{S}_{6,6}$	-2.6327E-07	$\bar{C}_{7,1}$	2.3532E-07	$\bar{S}_{7,1}$	5.5634E-08
$\bar{C}_{7,2}$	2.0425E-07	$\bar{S}_{7,2}$	1.7321E-07	$\bar{C}_{7,3}$	2.1994E-07	$\bar{S}_{7,3}$	-3.4644E-07
$\bar{C}_{7,4}$	-2.8617E-07	$\bar{S}_{7,4}$	-2.7738E-07	$\bar{C}_{7,5}$	3.4727E-08	$\bar{S}_{7,5}$	8.7014E-08
$\bar{C}_{7,6}$	-2.7496E-07	$\bar{S}_{7,6}$	8.5865E-08	$\bar{C}_{7,7}$	-2.4856E-08	$\bar{S}_{7,7}$	-8.8968E-09
$\bar{C}_{8,1}$	1.0946E-08	$\bar{S}_{8,1}$	4.8429E-08	$\bar{C}_{8,2}$	1.1084E-07	$\bar{S}_{8,2}$	1.0359E-07
$\bar{C}_{8,3}$	-8.8578E-08	$\bar{S}_{8,3}$	-5.0715E-08	$\bar{C}_{8,4}$	-2.2315E-07	$\bar{S}_{8,4}$	2.6511E-07
$\bar{C}_{8,5}$	1.5318E-07	$\bar{S}_{8,5}$	8.1158E-08	$\bar{C}_{8,6}$	-9.7542E-08	$\bar{S}_{8,6}$	2.8082E-07
$\bar{C}_{8,7}$	2.0498E-07	$\bar{S}_{8,7}$	2.4592E-07	$\bar{C}_{8,8}$	1.6967E-07	$\bar{S}_{8,8}$	9.3261E-08
$\bar{C}_{9,1}$	1.8099E-07	$\bar{S}_{9,1}$	4.1091E-08	$\bar{C}_{9,2}$	-2.2013E-08	$\bar{S}_{9,2}$	2.4215E-08
$\bar{C}_{9,3}$	-9.9252E-08	$\bar{S}_{9,3}$	-2.3085E-08	$\bar{C}_{9,4}$	-4.0867E-08	$\bar{S}_{9,4}$	-3.8525E-08
$\bar{C}_{9,5}$	-5.8957E-08	$\bar{S}_{9,5}$	3.6834E-09	$\bar{C}_{9,6}$	4.8812E-08	$\bar{S}_{9,6}$	1.1115E-07
$\bar{C}_{9,7}$	-1.9880E-07	$\bar{S}_{9,7}$	-1.4978E-07	$\bar{C}_{9,8}$	2.3523E-07	$\bar{S}_{9,8}$	9.6355E-09
$\bar{C}_{9,9}$	-3.4533E-08	$\bar{S}_{9,9}$	5.9502E-08	$\bar{C}_{10,1}$	8.9008E-08	$\bar{S}_{10,1}$	-6.0157E-08
$\bar{C}_{10,2}$	-3.7256E-08	$\bar{S}_{10,2}$	-6.3676E-08	$\bar{C}_{10,3}$	-1.3307E-07	$\bar{S}_{10,3}$	-7.2728E-08

Table 18. (Cont.)

Harmonic	Value	Harmonic	Value	Harmonic	Value	Harmonic	Value
$\bar{C}_{10,4}$	-2.1887E-08	$\bar{S}_{10,4}$	-7.8408E-08	$\bar{C}_{10,5}$	-6.1509E-09	$\bar{S}_{10,5}$	-1.1904E-07
$\bar{C}_{10,6}$	-9.4142E-08	$\bar{S}_{10,6}$	-1.1728E-08	$\bar{C}_{10,7}$	1.8525E-07	$\bar{S}_{10,7}$	2.1656E-08
$\bar{C}_{10,8}$	1.0887E-09	$\bar{S}_{10,8}$	7.0781E-09	$\bar{C}_{10,9}$	7.8473E-08	$\bar{S}_{10,9}$	5.6381E-09
$\bar{C}_{10,10}$	1.3321E-07	$\bar{S}_{10,10}$	9.8839E-08	$\bar{C}_{11,1}$	-1.2194E-08	$\bar{S}_{11,1}$	7.5463E-08
$\bar{C}_{11,2}$	-2.0255E-08	$\bar{S}_{11,2}$	-6.2998E-08	$\bar{C}_{11,3}$	-1.0988E-09	$\bar{S}_{11,3}$	-3.8098E-08
$\bar{C}_{11,4}$	1.5676E-08	$\bar{S}_{11,4}$	-1.9551E-07	$\bar{C}_{11,5}$	-1.8591E-09	$\bar{S}_{11,5}$	6.1113E-08
$\bar{C}_{11,6}$	6.3601E-08	$\bar{S}_{11,6}$	-2.6457E-08	$\bar{C}_{11,7}$	-3.3761E-08	$\bar{S}_{11,7}$	-1.2825E-07
$\bar{C}_{11,8}$	-1.3634E-08	$\bar{S}_{11,8}$	4.5229E-08	$\bar{C}_{11,9}$	2.1256E-08	$\bar{S}_{11,9}$	6.6721E-08
$\bar{C}_{11,10}$	5.2555E-08	$\bar{S}_{11,10}$	-7.7401E-08	$\bar{C}_{11,11}$	8.6996E-08	$\bar{S}_{11,11}$	-2.5691E-08
$\bar{C}_{12,1}$	-5.6935E-08	$\bar{S}_{12,1}$	-6.6159E-08	$\bar{C}_{12,2}$	-9.7424E-08	$\bar{S}_{12,2}$	4.6341E-08
$\bar{C}_{12,3}$	1.1555E-07	$\bar{S}_{12,3}$	-4.8666E-08	$\bar{C}_{12,4}$	-5.0379E-08	$\bar{S}_{12,4}$	5.3568E-08
$\bar{C}_{12,5}$	8.1834E-08	$\bar{S}_{12,5}$	2.7932E-08	$\bar{C}_{12,6}$	-2.1177E-08	$\bar{S}_{12,6}$	3.5034E-08
$\bar{C}_{12,7}$	2.9751E-08	$\bar{S}_{12,7}$	3.1783E-08	$\bar{C}_{12,8}$	4.0190E-08	$\bar{S}_{12,8}$	5.6877E-08
$\bar{C}_{12,9}$	-1.1503E-07	$\bar{S}_{12,9}$	1.4508E-08	$\bar{C}_{12,10}$	-4.5921E-08	$\bar{S}_{12,10}$	-4.3264E-08
$\bar{C}_{12,11}$	-7.8443E-09	$\bar{S}_{12,11}$	-4.7858E-08	$\bar{C}_{12,12}$	-2.7617E-08	$\bar{S}_{12,12}$	-1.6808E-08
$\bar{C}_{13,1}$	8.6136E-09	$\bar{S}_{13,1}$	-3.2401E-08	$\bar{C}_{13,2}$	-1.0679E-08	$\bar{S}_{13,2}$	-9.0670E-08
$\bar{C}_{13,3}$	-3.2361E-08	$\bar{S}_{13,3}$	4.9286E-08	$\bar{C}_{13,4}$	3.9852E-08	$\bar{S}_{13,4}$	-1.0608E-07
$\bar{C}_{13,5}$	4.0047E-08	$\bar{S}_{13,5}$	3.8114E-08	$\bar{C}_{13,6}$	-2.1906E-08	$\bar{S}_{13,6}$	-1.1321E-08
$\bar{C}_{13,7}$	-7.6933E-08	$\bar{S}_{13,7}$	1.1140E-08	$\bar{C}_{13,8}$	-2.7448E-09	$\bar{S}_{13,8}$	1.4309E-08
$\bar{C}_{13,9}$	-1.1588E-08	$\bar{S}_{13,9}$	7.2989E-08	$\bar{C}_{13,10}$	4.1979E-09	$\bar{S}_{13,10}$	7.6769E-09
$\bar{C}_{13,11}$	-5.4381E-08	$\bar{S}_{13,11}$	1.3450E-08	$\bar{C}_{13,12}$	-4.6633E-08	$\bar{S}_{13,12}$	7.9963E-08
$\bar{C}_{13,13}$	-6.8944E-08	$\bar{S}_{13,13}$	7.1891E-08	$\bar{C}_{14,1}$	-1.4359E-08	$\bar{S}_{14,1}$	5.2390E-08

Table 18. (Cont.)

Harmonic	Value	Harmonic	Value	Harmonic	Value	Harmonic	Value
$\bar{C}_{14,2}$	-1.5908E-08	$\bar{S}_{14,2}$	2.7374E-08	$\bar{C}_{14,3}$	9.6915E-08	$\bar{S}_{14,3}$	-2.5631E-08
$\bar{C}_{14,4}$	-2.9864E-08	$\bar{S}_{14,4}$	-3.8189E-09	$\bar{C}_{14,5}$	-1.3828E-09	$\bar{S}_{14,5}$	-5.8680E-08
$\bar{C}_{14,6}$	-1.3872E-08	$\bar{S}_{14,6}$	-2.7976E-08	$\bar{C}_{14,7}$	7.1056E-08	$\bar{S}_{14,7}$	2.4043E-09
$\bar{C}_{14,8}$	-1.8779E-08	$\bar{S}_{14,8}$	-5.8750E-08	$\bar{C}_{14,9}$	-2.4322E-08	$\bar{S}_{14,9}$	6.0461E-08
$\bar{C}_{14,10}$	2.8985E-08	$\bar{S}_{14,10}$	-3.4224E-08	$\bar{C}_{14,11}$	8.2611E-08	$\bar{S}_{14,11}$	-1.9627E-09
$\bar{C}_{14,12}$	1.1751E-09	$\bar{S}_{14,12}$	-3.0967E-08	$\bar{C}_{14,13}$	3.0793E-08	$\bar{S}_{14,13}$	4.7620E-08
$\bar{C}_{14,14}$	-6.5969E-08	$\bar{S}_{14,14}$	3.3030E-09	$\bar{C}_{15,1}$	2.9358E-08	$\bar{S}_{15,1}$	-1.6691E-08
$\bar{C}_{15,2}$	-1.2291E-08	$\bar{S}_{15,2}$	-6.8963E-08	$\bar{C}_{15,3}$	-5.8921E-08	$\bar{S}_{15,3}$	4.4772E-08
$\bar{C}_{15,4}$	1.4876E-08	$\bar{S}_{15,4}$	7.0359E-09	$\bar{C}_{15,5}$	3.6806E-08	$\bar{S}_{15,5}$	-8.4051E-09
$\bar{C}_{15,6}$	1.0081E-08	$\bar{S}_{15,6}$	-3.0473E-08	$\bar{C}_{15,7}$	3.0439E-08	$\bar{S}_{15,7}$	1.5775E-08
$\bar{C}_{15,8}$	-6.8884E-08	$\bar{S}_{15,8}$	6.0808E-08	$\bar{C}_{15,9}$	-4.5169E-08	$\bar{S}_{15,9}$	5.5556E-08
$\bar{C}_{15,10}$	6.2126E-08	$\bar{S}_{15,10}$	-7.1799E-09	$\bar{C}_{15,11}$	-4.4724E-08	$\bar{S}_{15,11}$	-3.4391E-09
$\bar{C}_{15,12}$	-4.2025E-08	$\bar{S}_{15,12}$	5.9072E-09	$\bar{C}_{15,13}$	-4.1654E-08	$\bar{S}_{15,13}$	-5.5892E-09
$\bar{C}_{15,14}$	9.5654E-09	$\bar{S}_{15,14}$	-2.7145E-08	$\bar{C}_{15,15}$	-5.6358E-08	$\bar{S}_{15,15}$	3.4895E-08
$\bar{C}_{16,1}$	-9.9588E-09	$\bar{S}_{16,1}$	5.4160E-08	$\bar{C}_{16,2}$	5.5086E-09	$\bar{S}_{16,2}$	4.9455E-08
$\bar{C}_{16,3}$	5.4189E-08	$\bar{S}_{16,3}$	5.4887E-09	$\bar{C}_{16,4}$	4.6176E-08	$\bar{S}_{16,4}$	3.6270E-08
$\bar{C}_{16,5}$	-2.4432E-08	$\bar{S}_{16,5}$	2.9671E-08	$\bar{C}_{16,6}$	-3.7203E-09	$\bar{S}_{16,6}$	-2.0786E-08
$\bar{C}_{16,7}$	-2.2794E-09	$\bar{S}_{16,7}$	3.0609E-09	$\bar{C}_{16,8}$	-1.0459E-07	$\bar{S}_{16,8}$	-4.4731E-08
$\bar{C}_{16,9}$	2.4845E-08	$\bar{S}_{16,9}$	-8.6262E-08	$\bar{C}_{16,10}$	-3.9928E-08	$\bar{S}_{16,10}$	-4.5058E-09
$\bar{C}_{16,11}$	-2.0848E-08	$\bar{S}_{16,11}$	2.9738E-08	$\bar{C}_{16,12}$	1.5930E-08	$\bar{S}_{16,12}$	-1.2703E-08
$\bar{C}_{16,13}$	2.5280E-08	$\bar{S}_{16,13}$	6.6240E-09	$\bar{C}_{16,14}$	-1.4852E-08	$\bar{S}_{16,14}$	-8.1713E-09
$\bar{C}_{16,15}$	-7.7425E-08	$\bar{S}_{16,15}$	-2.6491E-08	$\bar{C}_{16,16}$	-1.8538E-08	$\bar{S}_{16,16}$	-2.2310E-08

Table 18. (Cont.)

Harmonic	Value	Harmonic	Value	Harmonic	Value	Harmonic	Value
$\bar{C}_{17,1}$	8.6593E-09	$\bar{S}_{17,1}$	-4.1093E-08	$\bar{C}_{17,2}$	-9.0769E-09	$\bar{S}_{17,2}$	-2.7205E-08
$\bar{C}_{17,3}$	-7.7864E-09	$\bar{S}_{17,3}$	-1.7913E-08	$\bar{C}_{17,4}$	-4.3231E-08	$\bar{S}_{17,4}$	6.8203E-08
$\bar{C}_{17,5}$	4.1513E-08	$\bar{S}_{17,5}$	-2.5453E-08	$\bar{C}_{17,6}$	-4.5453E-08	$\bar{S}_{17,6}$	-1.7273E-08
$\bar{C}_{17,7}$	1.6938E-08	$\bar{S}_{17,7}$	-3.3752E-08	$\bar{C}_{17,8}$	4.1231E-08	$\bar{S}_{17,8}$	5.8792E-09
$\bar{C}_{17,9}$	-4.3119E-08	$\bar{S}_{17,9}$	-1.5974E-08	$\bar{C}_{17,10}$	-1.0844E-08	$\bar{S}_{17,10}$	5.5628E-08
$\bar{C}_{17,11}$	-4.4136E-08	$\bar{S}_{17,11}$	-4.3123E-09	$\bar{C}_{17,12}$	3.1661E-08	$\bar{S}_{17,12}$	6.2982E-09
$\bar{C}_{17,13}$	2.5147E-08	$\bar{S}_{17,13}$	9.7728E-09	$\bar{C}_{17,14}$	-5.5945E-09	$\bar{S}_{17,14}$	7.2604E-09
$\bar{C}_{17,15}$	4.9113E-08	$\bar{S}_{17,15}$	3.1958E-08	$\bar{C}_{17,16}$	-2.3540E-08	$\bar{S}_{17,16}$	-1.5882E-08
$\bar{C}_{17,17}$	-9.0191E-08	$\bar{S}_{17,17}$	-9.4775E-09	$\bar{C}_{18,1}$	-2.3557E-08	$\bar{S}_{18,1}$	-7.4536E-08
$\bar{C}_{18,2}$	-9.4249E-09	$\bar{S}_{18,2}$	3.0353E-08	$\bar{C}_{18,3}$	-3.5003E-08	$\bar{S}_{18,3}$	-2.0464E-08
$\bar{C}_{18,4}$	2.9433E-08	$\bar{S}_{18,4}$	-4.4672E-08	$\bar{C}_{18,5}$	1.7511E-09	$\bar{S}_{18,5}$	-6.0367E-09
$\bar{C}_{18,6}$	2.3931E-08	$\bar{S}_{18,6}$	-4.4966E-09	$\bar{C}_{18,7}$	-7.8040E-10	$\bar{S}_{18,7}$	-8.2010E-09
$\bar{C}_{18,8}$	5.3819E-08	$\bar{S}_{18,8}$	-2.2106E-08	$\bar{C}_{18,9}$	-3.6120E-10	$\bar{S}_{18,9}$	-5.0562E-09
$\bar{C}_{18,10}$	4.2146E-08	$\bar{S}_{18,10}$	7.8924E-09	$\bar{C}_{18,11}$	2.4981E-08	$\bar{S}_{18,11}$	2.3183E-08
$\bar{C}_{18,12}$	-6.2242E-09	$\bar{S}_{18,12}$	6.6025E-09	$\bar{C}_{18,13}$	-2.6685E-08	$\bar{S}_{18,13}$	-4.2500E-08
$\bar{C}_{18,14}$	9.1191E-09	$\bar{S}_{18,14}$	-3.3129E-08	$\bar{C}_{18,15}$	-4.1521E-08	$\bar{S}_{18,15}$	-1.7610E-08
$\bar{C}_{18,16}$	2.4850E-08	$\bar{S}_{18,16}$	-4.8182E-09	$\bar{C}_{18,17}$	3.5357E-08	$\bar{S}_{18,17}$	-4.7166E-08
$\bar{C}_{18,18}$	-3.4701E-10	$\bar{S}_{18,18}$	5.0554E-08	$\bar{C}_{19,12}$	3.6058E-08	$\bar{S}_{19,12}$	-3.4421E-09
$\bar{C}_{19,13}$	9.6876E-09	$\bar{S}_{19,13}$	-6.6095E-08	$\bar{C}_{19,14}$	7.6389E-09	$\bar{S}_{19,14}$	-2.7649E-08
$\bar{C}_{20,13}$	2.7630E-08	$\bar{S}_{20,13}$	3.2389E-08	$\bar{C}_{20,14}$	3.3687E-08	$\bar{S}_{20,14}$	-6.5741E-08
$\bar{C}_{21,13}$	-1.9799E-08	$\bar{S}_{21,13}$	-3.0711E-08	$\bar{C}_{21,14}$	1.6623E-08	$\bar{S}_{21,14}$	8.7215E-09
$\bar{C}_{22,13}$	-7.9435E-09	$\bar{S}_{22,13}$	4.1452E-09	$\bar{C}_{22,14}$	2.8516E-09	$\bar{S}_{22,14}$	-4.2148E-08
$\bar{C}_{23,13}$	-1.3236E-08	$\bar{S}_{23,13}$	-4.8892E-09	$\bar{C}_{23,14}$	-2.1148E-08	$\bar{S}_{23,14}$	2.2010E-08
$\bar{C}_{24,14}$	3.4668E-09	$\bar{S}_{24,14}$	2.2983E-08				

6. EVALUATION OF RESULTS

6.1 Orbit Determination by Use of SE III

A detailed evaluation of SE III results with satellite orbits is difficult. Although other effects – such as lunar and solar perturbations, body tides, radiation pressure, and air drag – are all included in the orbit computation, none of these is known without error, and each, in itself, provides a number of problems. Also, the coordinates of the tracking stations are not known without error. Furthermore, incomplete orbital coverage can result in overoptimistic estimates of orbital accuracy from formal statistics. Finally, the tracking data contain errors. A few comparisons are given here to indicate approximately the accuracy of the total orbit-computation system. The gravity field is certainly one of the larger contributors to the error budget.

From ISAGEX data, consecutive orbits were computed every 2 days, by using 4 days of data (except for 6800201, where 6 days of data were employed). This type of analysis is especially valuable for

A. Detection of bad observations, since each observation is used in two orbits.

B. Evaluation of the reliability of the orbital elements by comparison of adjacent orbits.

Results for 6508901, 6800201, and 6701401 are given in Table 19, together with the number of observed points used in the final iteration. All calculations were performed by using the final station coordinates and the tidal parameter $k_2 = 0.30$; radiation-pressure perturbations were calculated with a fixed area-to-mass ratio.

We see that with good orbital coverage, we can expect to have root-mean-square (rms) residuals of between 4 and 10 m. Satellite 6701401 has a relatively low perigee, and the poorer orbits from MJD 41072 to 41078 coincide with an increase in solar activity that resulted in increased drag.

Table 19. Comparison of SE III with satellite observations.

Epoch (MJD)	σ(m)	n	Epoch (MJD)	σ(m)	n
	6508901 (Geos A), A/M = 0.05 cgs				
41000	4.1	289	41010	7.7	523
41002	5.5	367	41012	9.8	577
41004	3.2	314	41014	9.2	715
41006	8.9	601	14016	4.1	425
41008	10.6	696	41018	3.6	221
	6800201 (Geos B), A/M = 0.05 cgs				
41038	2.4	249	41046	2.7	441
41040	6.5	533	41048	3.8	304
41042	7.8	681	41052	2.8	388
41044	6.3	651	41054	6.6	602
	6701401 (D1D), A/M = 0.1 cgs				
41072	10.3	467	41080	7.4	621
41074	9.9	332	41082	6.9	764
41076	16.3	341	41084	4.9	427
41078	17.0	254	41086	3.6	519

Of the 4- to 10-m rms residuals, 2 to 3 m come from station coordinates and 1 to 4 m could be attributed to the orbital theory. Therefore, the accuracy of the gravity field for orbit computation may actually be somewhat better than indicated by Table 19.

6.2 Comparison with Surface Gravity

To compare a geopotential model (g_s) with observed values of surface gravity (g_t), the following quantities defined by Kaula (1966b) can be computed:

$\langle g_t^2 \rangle$	The mean value of g_t^2, where g_t is the mean free-air gravity anomaly based on surface gravity, indicating the amount of information contained in the surface-gravity anomalies.
$\langle g_s^2 \rangle$	The mean value of g_s^2, where g_s is the mean free-air gravity anomaly computed from the geopotential model, indicating the amount of information in the computed gravity anomalies.
$\langle g_t g_s \rangle$	An estimate of g_h – i.e., the true value of the contribution to the gravity anomaly of the geopotential model and the amount of information common to both g_t and g_s.
$\langle (g_t - g_s)^2 \rangle$	The mean-square difference of g_t and g_s.
$E(\epsilon_s^2)$	The mean-square error in the geopotential model.
$E(\epsilon_t^2)$	The mean-square error of the observed gravity.
$E(\delta g^2)$	The mean square of the error of omission – that is, the difference between true gravity and g_h; this term is then the model error.

If the geopotential model were perfect, then $\langle g_s^2 \rangle = \langle g_h^2 \rangle$, which in turn would equal $\langle g_t g_s \rangle$ if g_t were free from error and known everywhere. Then, ϵ_s^2 would be zero even though g_s would not contain all the information necessary to describe the total field. The information not contained in the model field – i.e., the error of omission, δg – then consists of the higher order coefficients. The quantity $\langle (g_t - g_s)^2 \rangle$ is a measure of the agreement between the two estimates g_t and g_s and is equal to

$$\langle (g_t - g_s)^2 \rangle = E(\epsilon_s^2) + E(\epsilon_t^2) + E(\delta g^2) \quad .$$

Another estimate of g_h can be obtained from the gravimetric estimates of degree variance σ_ℓ^2 (Kaula, 1966b):

$$E(g_h^2) = D = \sum_\ell \frac{n_\ell}{2\ell + 1} \sigma_\ell^2 \quad ,$$

where n_ℓ is the number of coefficients of degree ℓ included in g_h, and

$$\sigma_\ell^2 = \gamma^2 (\ell - 1)^2 \sum_m \left(\overline{C}_{\ell m}^2 + \overline{S}_{\ell m}^2 \right) .$$

We also have

$$E(\epsilon_s^2) = \langle g_s^2 \rangle - \langle g_s g_t \rangle$$

and

$$E(\epsilon_t^2) = \langle g_t^2 \rangle / \langle n \rangle .$$

Table 20 summarizes the above quantities for SE III. The improvement over SE II in the coverage of surface-gravity data is evident. The more limited gravity coverage used for SE II resulted in accuracy estimates that were consistently optimistic. The revised set of gravity anomalies has greater coverage and is more independent of the geopotential model. Even so, line 2 represents an estimate of the accuracy, $E(\epsilon_s^2) = 52$ mgal^2, that is more optimistic than that based on independent gravity data for SE II, which was 99 mgal^2 (Gaposchkin and Lambeck, 1970).

We used the 306 gravity anomalies with more than 19 observed units in each average for the comparison. There is very good agreement between $\langle g_t g_s \rangle$, $\langle g_s^2 \rangle$, and D, which would be equal for a perfect solution. In $E(\delta g^2)$, we have a measure of the information remaining in the higher harmonics. The formal statistics give an error in the combination reference field of $E(\epsilon_s^2) = 15$ mgal^2.

An alternative approach is to eliminate δg by use of

$$\begin{bmatrix} \Delta\overline{C}_{\ell m} \\ \Delta\overline{S}_{\ell m} \end{bmatrix} = \frac{1}{4\pi\gamma(\ell - 1)} \int_{\text{sphere}} (g_t - g_{\text{ref}}) \left\langle \overline{P}_{\ell m}(\sin\phi) \begin{bmatrix} \cos m\lambda \\ \sin m\lambda \end{bmatrix} \right\rangle d\sigma \quad ,$$

Table 20. Comparison of SE III combination solution with surface gravity (in $mgal^2$).

Solution	ℓ, m	$\langle(g_t-g_s)^2\rangle$	$\langle g_t g_s\rangle$	$\langle g_s^2\rangle$	D	$\langle g_t^2\rangle$	$E(\epsilon_s^2)$	$E(\epsilon_t^2)$	$E(\delta g^2)$	n*
SE II†	16	75	184	186	163	253	2	11	63	≥ 20
SE II	16	187	177	229	203	311	52	13	122	(306 anomalies)
SE III	18	105	221	236	237	311	15	13	77	
SE III	10	195	150	192	163	302	42	24	129	≥ 1
	14	174	174	220	198	302	47	24	103	(1183 anomalies)
	18	156	202	258	237	302	56	24	75	
SE III	10	184	183	205	163	345	22	19	143	≥ 10
	14	151	215	236	198	345	20	19	111	(659 anomalies)
	18	117	255	281	237	345	26	19	63	
SE III	10	186	151	176	163	311	25 (24)	13	148	≥ 20
	14	146	182	200	198	311	17 (21)	13	116	(306 anomalies)
	18	105	221	236	237	311	15 (18)	13	77	

*n is the number of 1° × 1° mean gravity anomalies used to obtain the 5° × 5° mean gravity anomalies.

†From the available data, there were 935, 369, and 136 gravity anomalies with n ≥ 1, 10, and 20 1° × 1° anomalies.

where

$$\left\langle \bar{P}_{\ell m}(\sin\phi) \begin{bmatrix} \cos m\lambda \\ \sin m\lambda \end{bmatrix} \right\rangle \quad \text{is the mean of} \quad \bar{P}_{\ell m}(\sin\phi) \begin{bmatrix} \cos m\lambda \\ \sin m\lambda \end{bmatrix}$$

over the area defined for the gravity anomaly. We can compute any harmonic with respect to a reference gravity field, but care must be used in treating areas where no observed gravity is available. A gravity field defined by g_{ref} and the $\Delta\bar{C}_{\ell m}$, $\Delta\bar{S}_{\ell m}$ will have an error of

$$\langle (g_t - g)^2 \rangle = E(\epsilon_s^2) + E(\epsilon_t^2) + E(\delta g^2) + E(\epsilon_{quad}^2) \quad ,$$

where $E(\epsilon_s^2)$ is the error in the composite field and $E(\epsilon_{quad}^2)$ is the error due to the inexact quadrature and imperfect distribution of the data.

Table 21 gives the results of this numerical quadrature with reference fields defined by the first ℓ degrees of SE III. Computing all the geopotential coefficients to $\ell = m = 36$, i.e., the null reference field, we get $E(\epsilon_s^2) \equiv 0$, and

$$E(\epsilon_t^2) + E(\delta g^2) + E(\epsilon_{quad}^2) = 29 \text{ mgal}^2 \quad .$$

Using an increasingly detailed reference field, we obtain an estimate of $E(\epsilon_s^2)$ as a function of degree. As expected, the mean-square error for the low-degree and low-order harmonics estimated from a comparison with terrestrial gravimetry is quite small. The satellite data provide accurate values, and the low harmonics have a smaller effect on gravity anomalies. The mean-square error for the 8th to 18th degrees is relatively constant, as expected, since these harmonics are determined largely by surface-gravity data. The mean-square error $E(\epsilon_s^2)$ estimated from the quadrature is in good agreement with that obtained from statistical analysis. For comparison, the values are given in Table 20.

The estimate of $E(\epsilon_s^2)$ assumes that g_s and g_t are independent; i.e., they have uncorrelated errors. Since the terrestrial gravity (g_t) was used to determine the combination solution (g_s), this assumption is certainly incorrect, and therefore, the estimate of $E(\epsilon_s^2) = 15 \text{ mgal}^2$ is definitely optimistic. A better test could be made with

independent data for g_t. Since the mean gravity anomalies used in the combination solution were computed, two compilations of 1° × 1° anomalies have been published: for North America and the North Atlantic (Talwani, Poppe, and Rabinowitz, 1972) and for the Indian Ocean (Kahle and Talwani, 1973). These compilations were published after the set of mean anomalies used here became available, but some basic data are probably common to both; furthermore, these two new compilations may not be completely independent of the data used in the SAO combination solution. The processing methods used by Talwani and his coworkers were different from those of ACIC, and additional data were included.

Table 21. Surface-gravity residuals for an $\ell = m = 36$ potential from numerical quadrature (in $mgal^2$).

Degree of reference field	$\langle (g_t - g_s)^2 \rangle$		$\langle (g_s - g_{ref})^2 \rangle$	$E(\epsilon_s^2)$
	$n \geq 1$	$n \geq 20$	$n = 0$	
0	28	29	12	
6	38	39	12	10
8	53	54	20	25
10	56	53	21	24
14	61	50	19	21
18	70	48	16	18
Anomalies used:	1183	306	471	

Two comparisons are nevertheless instructive. A simple 5° × 5° average was computed for these data since all 1° × 1° areas had values given in the region of interest. These 5° × 5° averages, with the mean of the whole region subtracted, were used to compute the same statistical quantities as in Table 20 and are given in Table 22. The number n is the number of points, centered in a 1° × 1° area, for which a 5° × 5° mean was computed. Therefore, we have a moving 5° × 5° mean calculated every 1°. Most of the gravity data in these ancillary compilations were taken at sea, and the estimate of their uncertainty $E(\epsilon_t^2)$ may be optimistic. The weighted mean of $E(\epsilon_s^2)$ is 65 $mgal^2$, equivalent to 3.1 m in geoid height. The remaining gravity information in the higher harmonics, ∂g, equals 68 $mgal^2$. We notice that ∂g for the

Table 22. Comparison with independent surface-gravity data (in $mgal^2$).

Comparison field, g_s	Maximum ℓ, m	n	$\langle (g_t - g_s)^2 \rangle$	$\langle g_t g_s \rangle$	$\langle g_s^2 \rangle$	D	$\langle g_t^2 \rangle$	$E(\epsilon_s^2)$	$E(\epsilon_t^2)$	$E(\delta_g^2)$	Region
SE III	18	3726	147	209	284	237	282	75	13	59	North Atlantic
SE III	18	1794	145	188	232	237	290	44	13	88	Indian Ocean
Averages								$64 \approx 3$ m		68	

Indian Ocean is larger than ∂g for North America and the Atlantic and is probably due to the very sharp low below the Indian subcontinent, which cannot be modeled very well by the generalized geoid. Further confidence in this comparison comes from $\langle (g_t - g_s)^2 \rangle$, $\langle g_s^2 \rangle$, $\langle g_t^2 \rangle$, and $\langle g_t g_s \rangle$, which are all in good agreement with the global values from Table 20. Therefore, we feel reasonably certain that for comparison purposes, both the North America and North Atlantic region and the Indian Ocean region are typical. Thus, we conclude that the generalized geoid has an accuracy of ± 3 m in geoid height and ± 8 mgal for the whole earth. Figures 7 to 11 give north–south and east–west profiles for both North America and the Indian Ocean.

Figure 11 was selected because of the large change in the values at the India Low from those given in SE II. However, the terrestrial gravity and the combination solution are in good agreement there. A further point is the disagreement, east of Borneo, between the observed gravity from the ACIC compilation and the anomalies used in 1969.

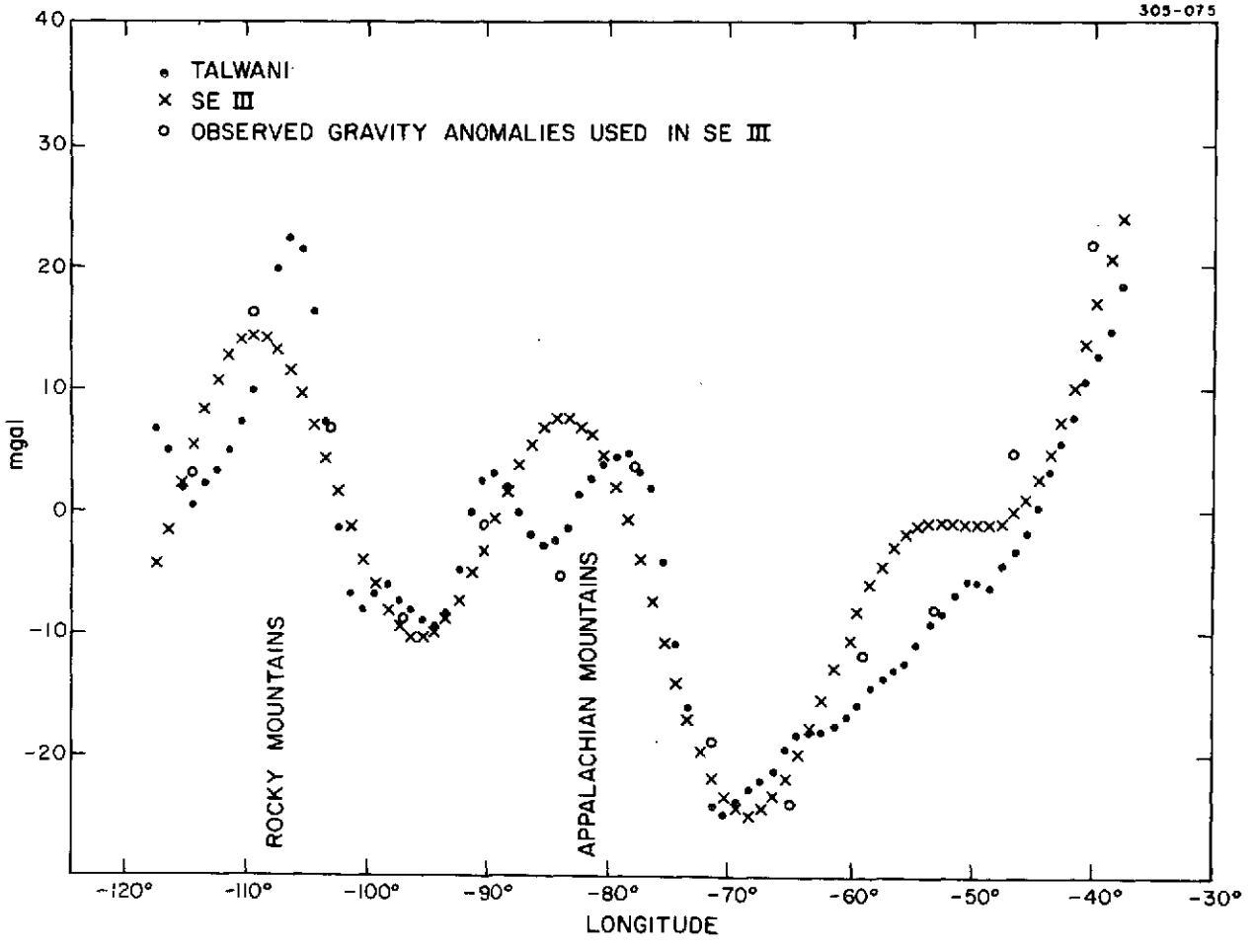

Figure 7. Free-air gravity anomalies for North America at latitude 37°.5.

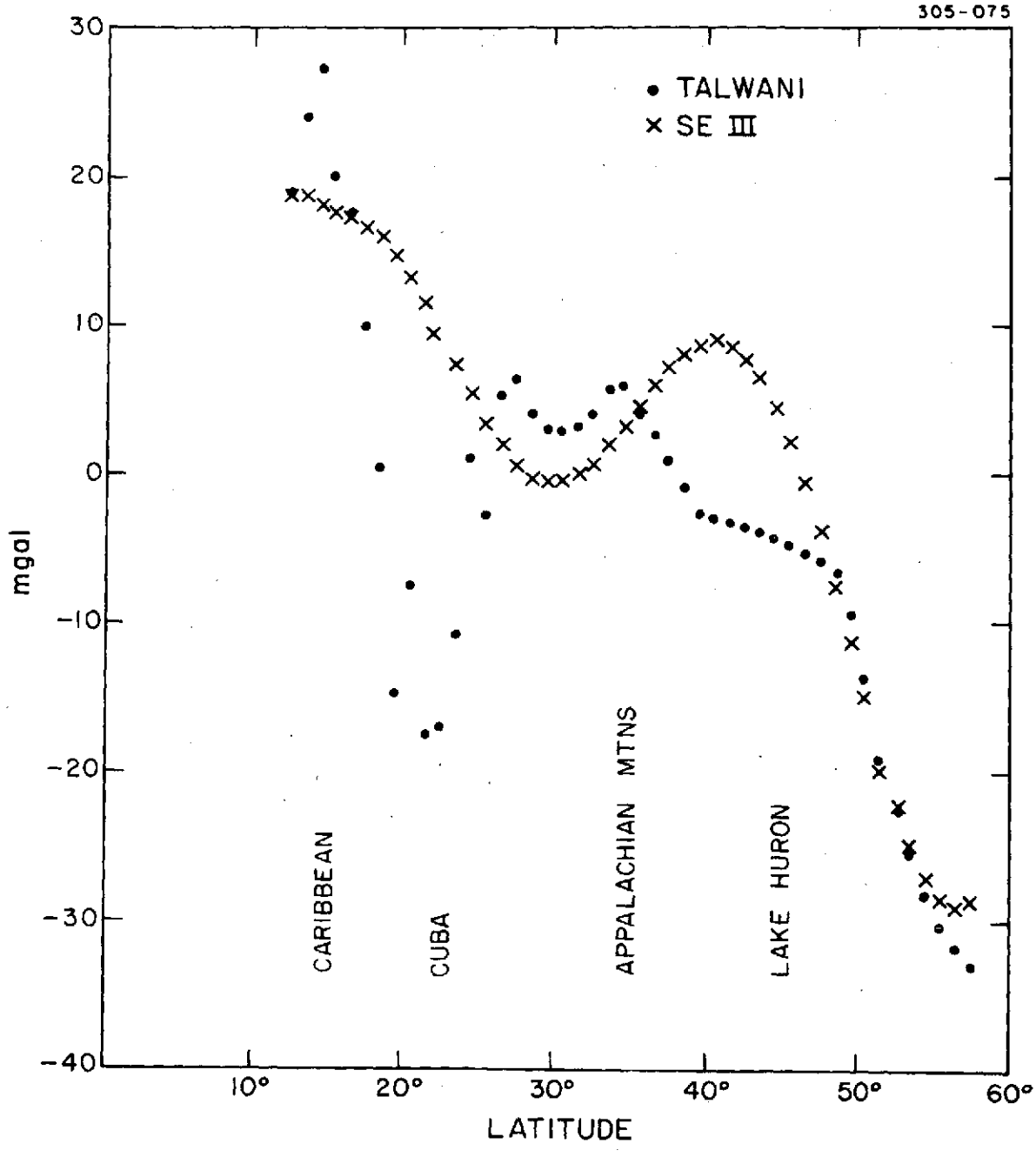

Figure 8. Free-air gravity anomalies for North America at longitude -82.5.

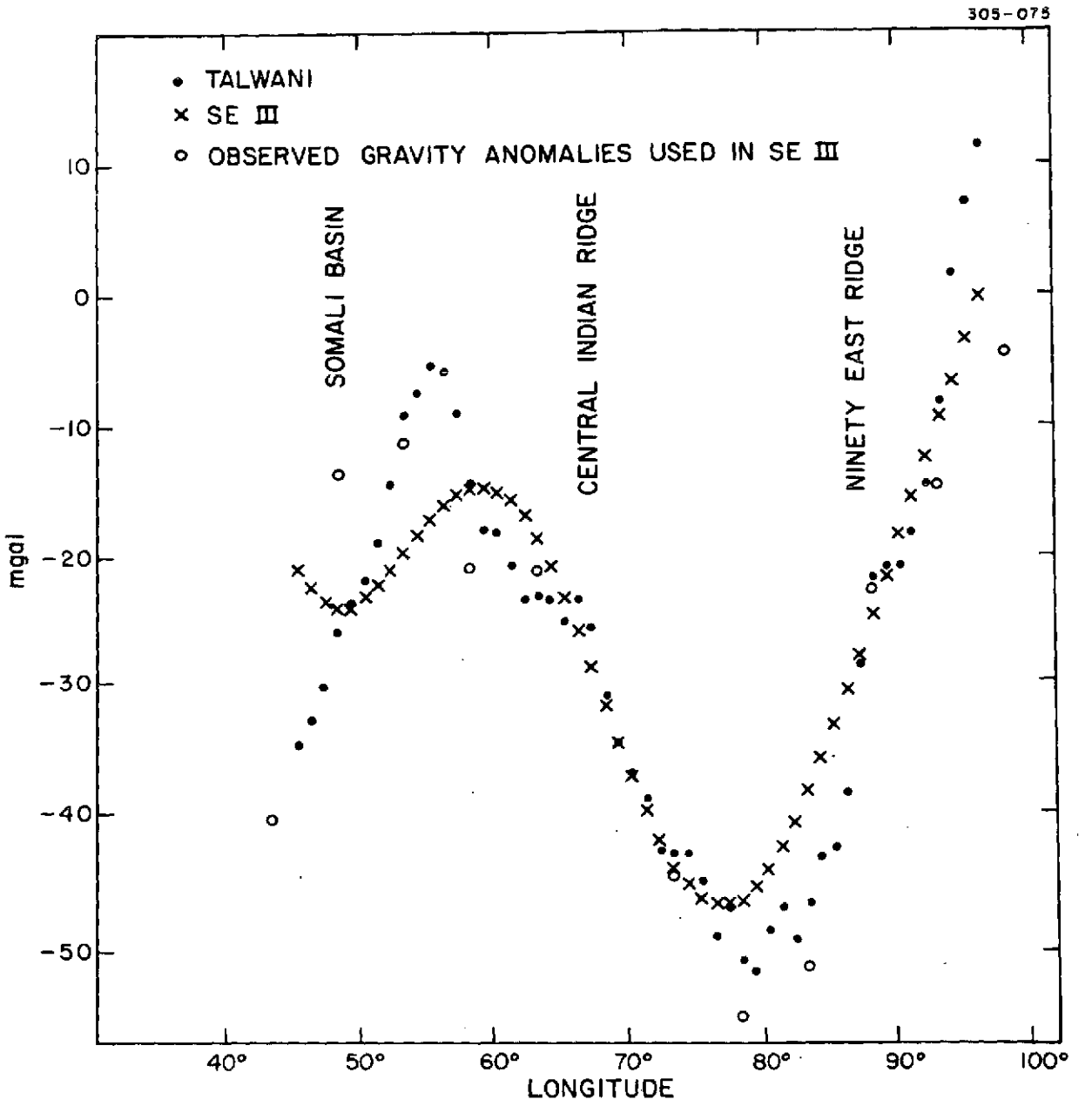

Figure 9. Free-air gravity anomalies for the Indian Ocean at latitude -2°.5.

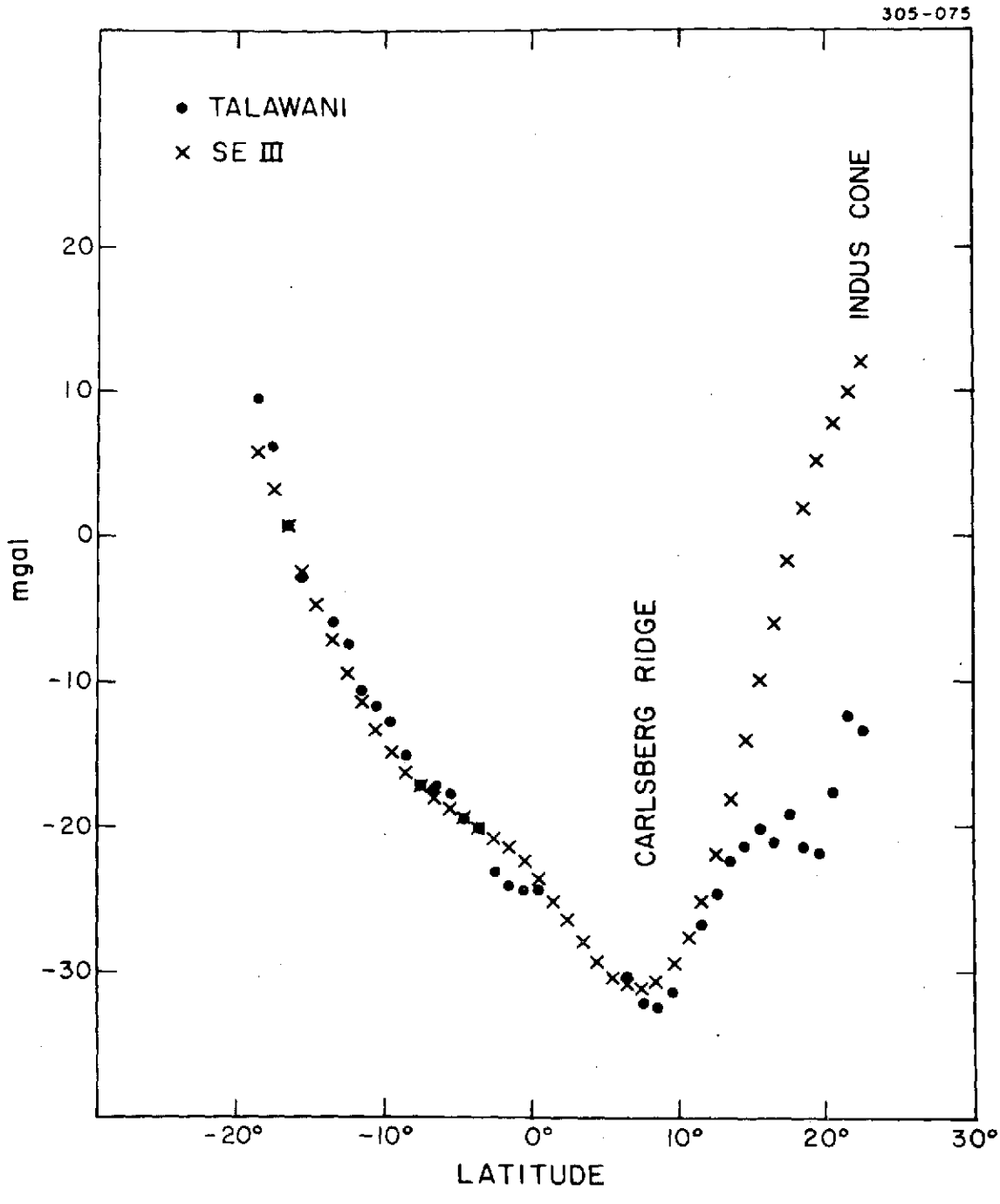

Figure 10. Free-air gravity anomalies for the Indian Ocean at longitude 64°.5.

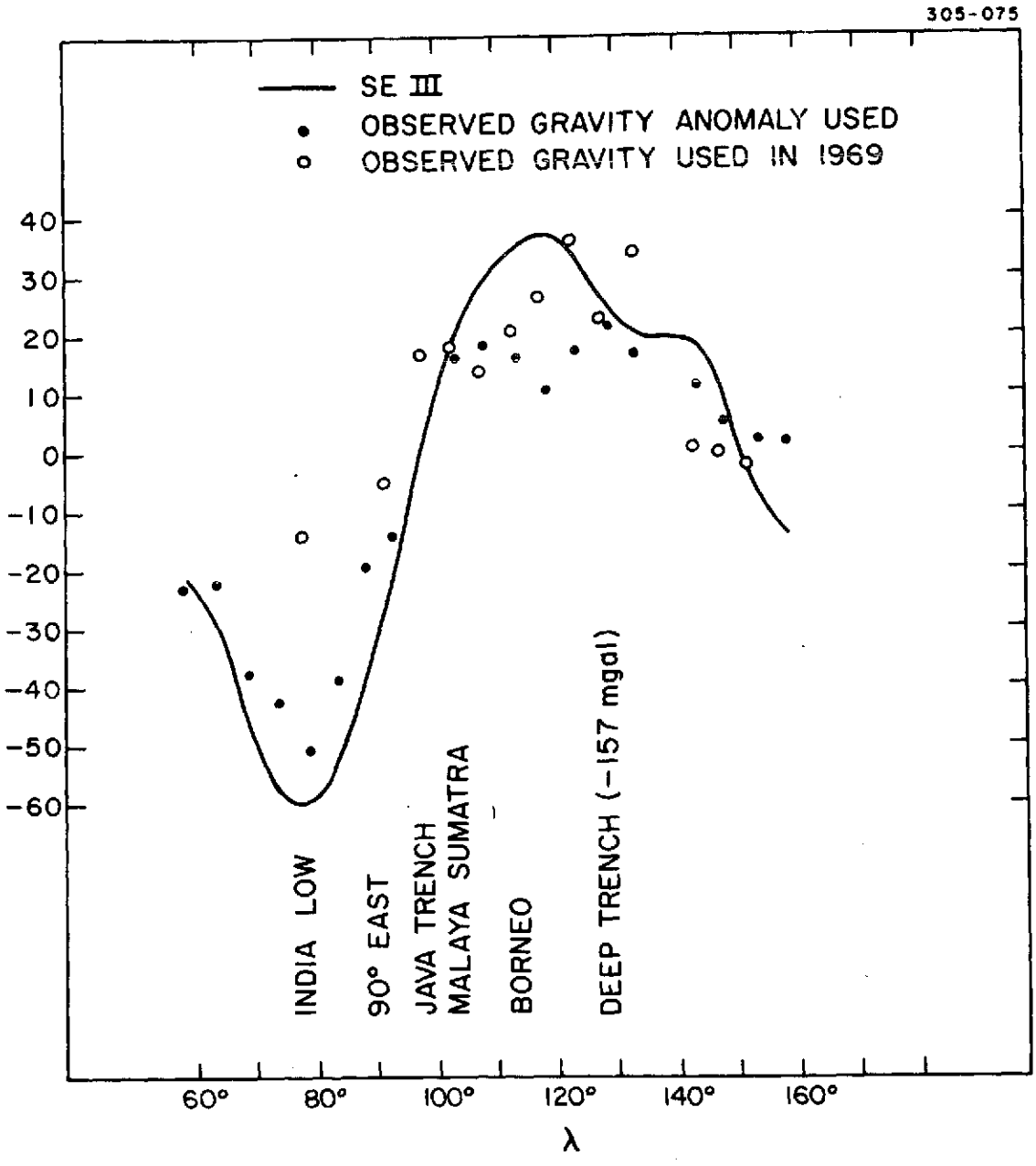

Figure 11. Free-air anomalies; profile at $\phi = 2°.5$.

7. CONCLUSIONS

The results described above, the procedures, the tests and comparisons, and the experience of carrying out the work have led to the following conclusions about the use of artificial satellites for the determination of the geopotential:

A. Satellite-tracking data from 25 satellites have been combined with terrestrial gravity data to determine the spherical-harmonic representation of the geopotential complete through degree and order 18, plus several higher harmonics to which satellite orbits are sensitive.

B. The zonal harmonics are successfully determined from analysis of long-period and secular perturbations, while the tesseral and sectorial harmonics are obtained from short-periodic satellite perturbations and terrestrial gravimetry. Low-degree and low-order $\ell, m \leq 8$ are primarily determined from satellite perturbations, and the short-wavelength $\ell, m \geq 8$, primarily from terrestrial gravity data.

C. The principal improvements over Gaposchkin and Lambeck (1970) are due to 1) the addition of two low-inclination satellites for the determination of the zonal harmonics, 2) the use of a sizable number of precise laser observations, and 3) the use of an improved set of terrestrial gravity anomalies.

D. In the combination of satellite and surface-gravity measurements, some attention must be given to the unobserved areas.

E. The unobserved areas are treated by using anomalies computed from a satellite-determined reference field and by taking the expected value of this residual field as zero, with a large variance.

F. The accuracy of the solution is established by comparison with satellite orbits and with terrestrial gravity data not used in the solution.

G. The lower harmonics have been improved such that the total orbit-computing system has an rms error of between 5 and 10 m for 4-day arcs.

H. The accuracy of the generalized geoid is ≈ 64 mgal^2, or 3 m.

I. The geoid is very similar to that found by Gaposchkin and Lambeck (1970); no new features have been found, and none has disappeared. Therefore, geophysical analyses from these results remain valid (see, e.g., Kaula, 1970, 1972; Gaposchkin, Kaula, and Lambeck, 1970).

PART VI

DETERMINATION OF STATION COORDINATES

ABSTRACT

The analysis of satellite data combined with surface measurements has resulted in the determination of the coordinates of 90 satellite-tracking sites. The tracking data used for determining these station locations come from the following:

SAO camera and laser network,
BC-4 camera network,
Goddard Space Flight Center laser stations,
Centre National d'Etudes Spatiales laser stations,
Jet Propulsion Laboratory Deep Space Net,
Individual cooperating observatories.

The camera systems provided all the simultaneous observations, while both camera and laser stations made routine observations. JPL reduced the DSN tracking data and provided SAO with a solution and its covariance matrix. In some cases, geodetic coordinates were used as observations with a priori variances to relate a set of stations in a local datum.

Combination of these data results in an accuracy of 2 to 4 m for the fundamental laser stations and 5 to 10 m for the fundamental optical network.

RESUME

L'analyse des données du satellite, en conjonction avec les mesures de surface, a permis de déterminer les coordonnées de 90 sites de poursuite de satellites. Les données de poursuite utilisées pour déterminer l'emplacement de ces stations sont d'origine suivante:

Réseau photographique et laser du SAO (Smithsonian Astrophysical Observatory),

Réseau photographique BC-4,

Stations laser du Centre de Vols Spatiaux Goddard,

Stations laser du Centre National d'Etudes Spatiales,

Réseau Spatial Interplanetaire du Laboratoire de Propulsion à Réaction,

Autres observatoires ayant offert leur concours.

Les systèmes photographiques ont fourni toutes les observations simultanées, alors que les stations photographiques et laser ont effectué les observations de routine. Le Laboratoire de Propulsion à Réaction a résumé les données de poursuite du Réseau Interplanétaire et fourni, au SAO, une solution et sa matrice de covariance. Dans certains cas, on a utilisé les coordonnées géodésiques, en guise d'observations, avec des variances a priori, de manière à rattacher un ensemble de stations à une référence locale.

En combiant ces données, on obtient une précision de 2 à 3 m pour les stations laser fondamentales, et de 4 à 8 m pour le réseau optique fondamental.

КОНСПЕКТ

Анализ данных спутников сочетанный с земными измерениями привел к определению координат 90 точек слежения за спутниками. Данные слежения которые использовались для определения местоположений этих станций получались от следующих:

Сети камер и лазера САО (Смитсониан Астрофизической Обсерватории)
Сети камер БС-4
Лазерных станций Центра Космических Полетов Годдард
Лазерных станций Государственного Центра по Исследованию Пространства
Сети Глубокого Пространства Лаборатории Реактивного Движения
Отдельных сотрудничающих обсерваторий

Системы камер обеспечили одновременные наблюдения в то время как обе станции лазера и камер проводили текущие наблюдения. Лаборатория Реактивного Движения обработала данные слежения Сети Глубокого Пространства и снабдила САО решением и ее матрицей ковариации. В некоторых случаях употреблялись геодезические координаты учитывая дисперсию для установления отношения группы станций в местном базисе.

Сочетание этих данных привело к точности от 2 до 3 м для основных лазерных станций и от 4 до 8 м для основной оптической цепи.

PART III

DETERMINATION OF STATION COORDINATES

E. M. Gaposchkin, J. Latimer, and G. Veis

1. INTRODUCTION

The results of the station-coordinate determination of the Smithsonian Standard Earth III (SE III) are given here. The work is a continuation of Standard Earth II (SE II) (Gaposchkin and Lambeck, 1970).

A number of approaches can be used to determine the position of points on the earth's surface. Of these, we have chosen tracking of close-earth satellites, deep-space probes, and surface-triangulation measurements for this analysis. The data and the method of analysis have been selected to optimize the results for a global network of reference points.

The satellite methods separate nicely into two distinct types of analysis: geometrical and dynamical. The former hinges on making simultaneous observations of a satellite from two or more points on the earth's surface. When these are camera observations, the vector connecting the two stations must lie in the plane defined by the two observed directions. A number of independent simultaneous observations will define the direction between the two stations. The Smithsonian Astrophysical Observatory (SAO) has obtained a sufficient number of simultaneous observations to determine a network for the SAO stations. The National Ocean Survey (NOS) of the National Oceanic and Atmospheric Administration has carried out a program of observations with the BC-4 camera to establish a global geometrical network. Figure 1 shows the distribution of observing stations included in SE III.

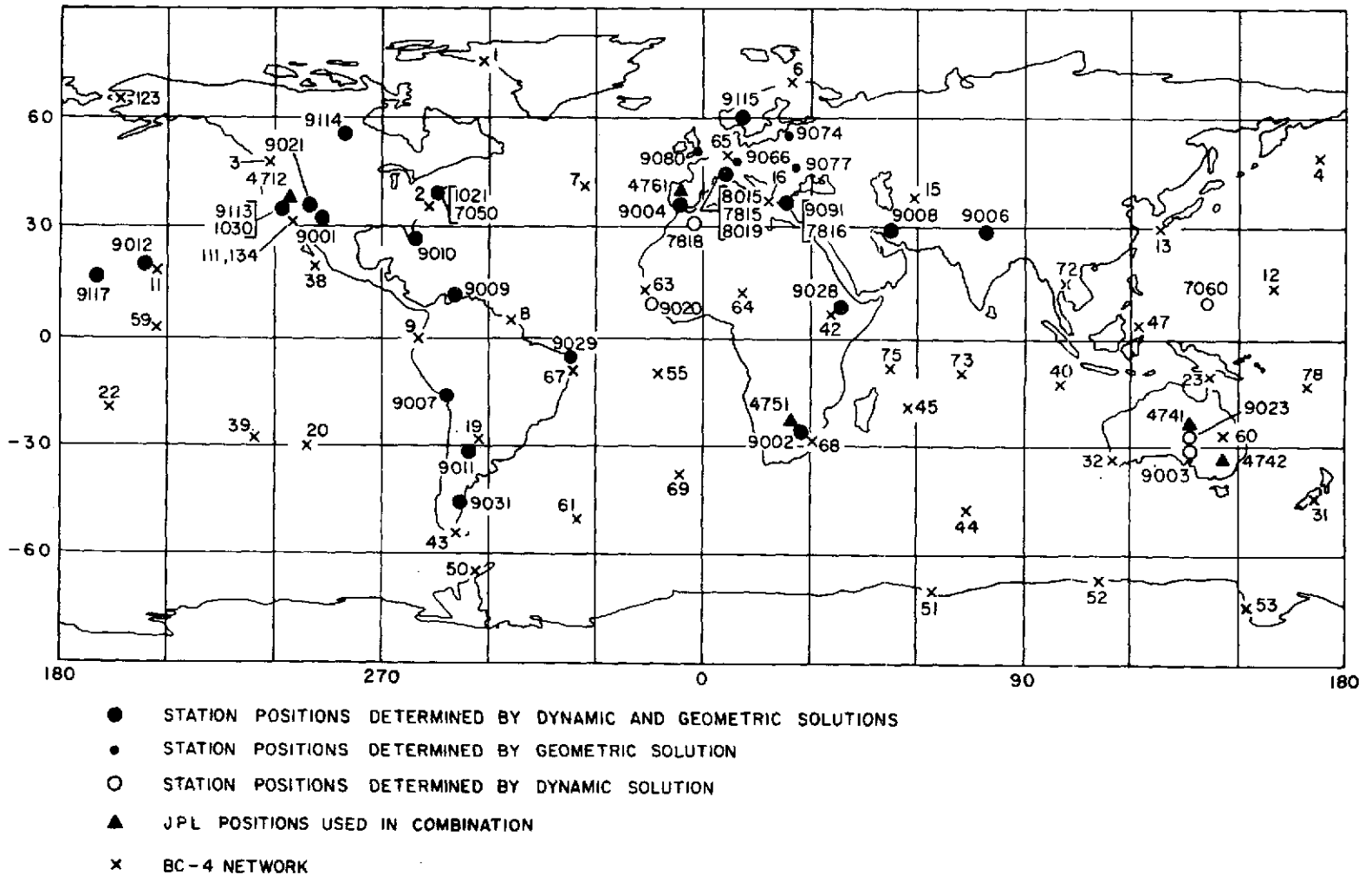

Figure 1. Locations of the observing stations included in SE III.

Alternatively, the dynamical analysis assumes that the satellite's orbit is known, and computes the location of the observing station from individual observations. In practice, the orbit is determined from the same observations. The orbital mode has been used by SAO to analyze tracking data on close-earth satellites and by the Jet Propulsion Laboratory (JPL) to analyze tracking data on deep-space probes.

Surface-triangulation measurements are reduced by organizations such as NOS and the Defense Mapping Agency, who publish coordinates of given points referred to a datum that, in general, has an arbitrary origin, orientation, and scale. The relative positions of stations are determined from these data.

The main objectives of this analysis are the following:

A. To improve the accuracy of the fundamental stations. Heretofore (SE II), the accuracy was estimated as 5 to 10 m.

B. To improve the distribution of reference points or tracking sites. In SE II, coordinates were obtained for 39 independent sites.

C. To use the latest available data. New data include the complete BC-4 network and all the laser tracking data taken during the International Satellite Geodesy Experiment (ISAGEX) program. Surface-triangulation data were used as observations rather than as constraints.

The analysis assumes that the stations form a fixed system (i.e., there is no relative motion), that the pole position and the instantaneous position of the earth are known without error from numerical values published by the International Polar Motion Service (IPMS) and the Bureau International de l'Heure (BIH), that the error in observing time is random, and that atomic time is a satisfactory system for ephemeris calculations.

2. GEOMETRICAL SOLUTION

In deriving a geometrical solution, the objective was to produce a system of normal equations for use in combination with other data. The data consisted of direction observations only, and there is no scale information in the geometric net. Nor is there any information to locate the origin of a geometrical network. Hence, any purely geometrical solution with these data would require an arbitrary scale and origin. The combination of normal systems avoids this problem, as other data sets contain scale and origin information. The result of an unscaled, purely geometrical solution is a set of interstation directions, independent of the arbitrary scale and origin introduced.

The geometrical solution included two networks: 27 stations of the SAO network, including the U.S. Air Force Baker-Nunn cameras and several European stations; and 48 stations of the NOS BC-4 network. Of the SAO group, 21 stations were also included in the dynamical solution. The SAO data block consisted of 5200 pairs of synthetic simultaneous observations, or about 50,000 individual direction observations processed at SAO. The satellites observed were 6102801 (Midas 4), 6303004, 6508901 (Geos 1), 6605601 (Pageos), 6800201 (Geos 2), and 6305501. The BC-4 data consisted of 2157 pairs of simultaneous events of Pageos. Each event generally consisted of seven directions and a covariance matrix from each of two stations. When more than two stations observed the satellite simultaneously, we treated each station pair separately. The BC-4 data were obtained from the National Space Sciences Data Center at the National Aeronautics and Space Administration/Goddard Space Flight Center (NASA/GSFC). The data were acquired, reduced, and processed by the NOS.

In geometric work, SAO observations refer to the equator and equinox of 1950.0. They are corrected for the effects of annual aberration, diurnal aberration, parallactic refraction, and planetary aberration and then converted to the terrestrial system of SAO, which is fundamentally defined by the mean pole of 1900–1905 of the IPMS and by the meridian of the Mean Observatory and UT1 of the BIH. The BC-4 data are in the same reference system.

The computation was divided into two stages. First, all data between pairs of stations were used to determine, by least squares, the interstation direction and its covariance matrix for each pair. The mathematical model for determining this direction uses the condition that the interstation direction (u_3) and the two directions from the stations to the satellite (u_1, u_2) must be coplanar:

$$\hat{u}_1 \cdot \hat{u}_2 \times \hat{u}_3 = 0 \quad . \tag{1}$$

A system of first-order Taylor expansion approximations to equation (1) is solved by least squares to determine u_3 and its 2×2 covariance matrix. In order for truly simultaneous points (u_1, u_2) to be obtained, synthetic observations were computed by interpolation from a series of observations overlapping in time from two stations (Aardoom, Girnius, and Veis, 1966). The synthetic observations (u_1, u_2) are weighted according to the quadratic fit of the individual observations used to determine the synthetic ones. The weight is modified according to SE II (p. 8) to account for the possibility of systematic errors, principally in station timing. Separate synthetic observations are considered to be uncorrelated. For BC-4 data, the NOS has derived seven simultaneous observations from each photographic plate (event) with the associated 14×14 covariance matrix for each set of directions. These are the data provided and used to determine u_3.

The data were then screened. When the adjustments to u_1 and u_2 (corrections to the observations) were judged to be too large with respect to the remaining data for that interstation direction, those points were deleted and the direction redetermined. For the SAO block, 68 directions were determined, and for the BC-4 group, 152.

The second stage consisted of a network adjustment for each data block. The mathematical model for stage two is that of variation of coordinates:

$$\vec{u}_1 - \vec{u}_2 - \vec{u}_3 = 0 \quad ,$$

where $\vec{u}_1$ is the vector from station 1 to the satellite, $\vec{u}_2$ is that from station 2 to the satellite, and $\vec{u}_3$ is the interstation vector. Satellite positions are eliminated, and we

obtain a solution for station coordinates, thus deriving adjusted interstation directions. This is equivalent to adjusting the directions directly by using the coplanarity condition for each triangle formed by observed directions between three stations. The advantage of this normal system is that it refers to coordinates, not directions, and can be readily combined with other normal systems for station coordinates. These directions are given in Table 1.

We have available for comparison the interstation directions and their accuracy estimates σ_1^2 resulting from simultaneous-observation data and also the new directions and accuracy estimates σ_2^2 resulting from the network adjustment. Table 2 gives accuracy estimates for interstation vectors.

We expect that, on the average, for the interstation direction adjustment δ,

$$\delta^2 \leq (\sigma_1^2 + \sigma_2^2)/2 \quad .$$

To satisfy this condition, we must multiply the variance estimates by a factor

$$k^2 = \frac{\delta^2}{(\sigma_1^2 + \sigma_2^2)/2} \quad .$$

From Table 2a, the average value for k^2 is 2.65, and the accuracy estimates for the geometrical solution are scaled by this number. A similar analysis of the BC-4 network (see Table 2b) gives an average value for k^2 of 2.60.

Table 1. Interstation directions resulting from geometrical network adjustment. ψ is in the direction of increasing declination, and μ is in the direction of increasing right ascension. The variances are in units of square microradians.

Interstation direction	Direction cosines x	y	z	σ^2_ψ (μrad)	σ^2_μ (μrad)	$\sigma_{\psi\mu}$ (μrad)	No. obs.
			SAO Network				
8015 8019	.00882676	.99156688	-.12929509	4378.25	3682.33	409.04	29
8015 9004	.40368817	-.77573675	-.48504469	29.21	17.80	7.03	122
8015 9066	-.69623798	.30876457	.64801012	552.99	204.51	-61.20	133
8015 9074	-.72313248	.49965276	.47689259	54.68	21.55	-18.85	25
8015 9080	-.61214261	-.55126892	.56690741	90.07	42.32	18.81	67
8015 9091	.01016606	.95506210	-.29623140	24.96	25.68	.97	30
8019 9004	.37570250	-.81539914	-.44042238	8.99	5.46	2.27	301
8019 9091	.01026610	.95067922	-.31000584	23.46	12.23	-1.87	61
9001 9007	.55330312	-.10133683	-.82679290	7.19	4.91	-1.16	35
9001 9009	.86735366	-.14882984	-.47491821	5.08	6.60	-3.13	183
9001 9010	.96543598	-.16694659	-.20015543	12.00	14.31	-7.74	154
9001 9012	-.79529606	.55903140	-.23449537	9.01	9.63	6.26	187
9001 9113	-.83986557	.49841557	.21495985	119.75	227.49	110.69	20
9001 9114	.10926314	.68566626	.71966892	41.57	18.51	-.64	74
9001 9117	-.71676203	.64999462	-.25250581	8.64	19.81	7.90	16
9002 9008	-.26348098	.26476812	.92761825	23.08	145.74	-37.94	7
9002 9028	-.03862703	.31647694	.94781343	52.37	119.71	21.28	25
9004 9006	-.55902919	.82421914	-.09027272	8.87	8.85	-3.97	14
9004 9008	-.32678915	.93748122	-.11974060	13.50	8.84	-6.96	139
9004 9009	-.44142633	-.81388096	-.37781025	25.76	27.96	20.26	43
9004 9010	-.62748532	-.76680791	-.13515844	26.73	28.14	18.57	41
9004 9028	-.03791383	.84902988	-.52698274	18.85	15.61	-1.99	35
9004 9029	.01497695	-.57362721	-.81897956	68.03	29.79	21.05	42
9004 9051	-.18921279	.98062132	.05079707	2160.68	2169.11	-1375.13	47
9004 9066	-.47967265	.69555278	.53490231	22.93	10.64	-5.24	192
9004 9074	-.60731721	.62469601	.49083673	18.11	7.63	-4.83	65
9004 9080	-.67033878	.23778534	.70292536	29.78	9.92	.41	164
9004 9091	-.19273902	.97976341	.05399383	3.29	3.55	-1.53	442
9004 9115	-.68904482	.39859375	.60526049	74.58	28.34	-8.14	60
9005 9006	.91523602	.38800215	-.10861564	44.80	34.23	32.36	61
9005 9012	-.24735366	-.93945540	-.23714914	106.27	176.50	-114.45	25
9005 9117	-.39077014	-.84919496	-.35519942	182.41	189.44	-154.07	16
9006 9008	.91104375	-.41218149	.01028102	37.46	20.76	16.35	172
9006 9028	.82897555	-.32128702	-.45779273	22.65	23.59	10.19	28
9006 9091	.71232515	-.68338819	.15991701	20.83	36.31	14.13	10
9006 9115	.36069012	-.83668648	.41213877	16.89	16.71	7.12	19
9007 9009	.09844323	-.00408491	.99513428	4.04	9.65	2.17	263
9007 9010	-.20218439	.04240331	.97842906	4.88	5.94	1.92	86
9007 9011	.18500571	.48713975	-.85350322	17.65	9.35	5.14	437
9007 9029	.79974013	.53014621	.28171037	14.15	32.67	2.56	74
9007 9031	-.07668654	.52108904	-.85005022	31.70	22.18	1.86	32
9008 9028	.56732900	-.16303812	-.80719042	69.25	59.45	15.59	25
9008 9051	.44213826	-.85347528	.27585087	7168.06	6510.27	6102.56	13
9008 9080	.10994643	-.91853130	.37975259	38.24	25.92	-8.53	8
9008 9115	-.05681915	-.84719143	.52824073	30.33	16.42	8.31	38
9009 9010	-.63105797	.10662728	.76837260	10.73	18.06	6.43	248
9009 9011	.00603303	.18921650	-.98191686	7.28	2.47	.50	201
9009 9029	.70726024	.52130413	-.47751959	39.98	35.77	2.00	12
9009 9114	-.61426156	.41048104	.67393476	8.47	10.52	3.09	13
9010 9029	.72192397	.33394856	-.60605622	22.19	20.40	2.74	6
9010 9114	-.58073758	.55310520	.59734287	19.62	15.65	5.54	38
9011 9029	.69805266	.30285853	.64884450	52.36	41.72	-13.65	7
9011 9031	-.37633608	.51454022	-.77046707	198.44	140.41	27.09	9
9012 9021	.77402122	-.58631909	.23900017	75.78	18.83	-12.52	29
9012 9113	.75482345	-.55563145	.34859037	23.64	21.19	-16.24	14

Table 1. (Cont.)

Interstation direction		Direction cosines x	y	z	σ^2_ψ (μrad)	σ^2_μ (μrad)	$\sigma_{\psi\mu}$ (μrad)	No. obs.
9012	9114	.80198513	-.20284607	.56184814	22.01	17.31	-.17	24
9012	9117	-.37033001	.88413537	-.28488653	49.17	46.84	27.96	216
9021	9113	-.68537068	.60532001	.40478973	175.96	211.14	9.22	57
9021	9117	-.69236228	.67453906	-.25618651	50.43	26.94	19.65	8
9028	9091	-.08727958	-.54470402	.83407422	105.67	28.64	-3.90	37
9029	9031	-.66437001	-.08721396	-.74229793	23.64	25.10	-2.78	26
9066	9074	-.72259368	.53777749	.43434289	94.27	33.43	-29.12	13
9066	9080	-.45786996	-.78206608	.42276205	120.67	109.92	26.05	27
9074	9077	.77632565	.19416554	-.59968177	453.01	147.30	-165.47	42
9074	9091	.67571606	.29589128	-.67517121	45.42	22.62	6.25	43
9077	9091	.58362963	.37087186	-.72237838	187.65	121.07	-53.33	30
9113	9114	.52234001	.51015375	.68330379	126.10	106.70	38.12	30
9113	9117	-.66910598	.66067102	-.34031014	16.21	29.22	10.95	16
			BC-4 Network					
6001	6002	.14186757	-.83557865	-.53073714	4.88	2.13	.12	
6001	6003	-.68561365	-.61420886	-.39074468	5.55	2.03	.41	
6001	6004	-.90136380	.36609055	-.23134607	7.88	2.47	1.52	
6001	6006	.59118324	.80211453	-.08434841	10.68	2.69	-1.90	
6001	6007	.85315178	-.19274170	-.48475012	6.83	2.27	-.37	
6001	6016	.77326954	.48107640	-.41306140	2.81	.81	-.44	
6001	6065	.80955820	.48808094	-.32617866	3.99	1.22	-1.02	
6001	6123	-.97085420	.23090562	-.06422396	19.08	6.47	-1.12	
6002	6003	-.93493656	.29981654	.18974636	3.10	2.95	1.48	
6002	6007	.79005949	.61300538	-.00551394	7.15	6.25	-1.91	
6002	6008	.58956410	-.09068902	-.80261427	4.37	3.76	-2.32	
6002	6009	.03528776	-.33395182	-.94192938	9.39	4.10	.51	
6002	6038	-.84062618	-.20733306	-.50036051	4.85	4.12	1.11	
6002	6111	-.99243015	.04514765	-.11421070	6.70	6.52	2.33	
6002	6134	-.99242207	.04511901	-.11429219	6.19	5.00	1.27	
6003	6004	-.37965063	.92102495	.08705420	10.44	3.59	.62	
6003	6011	-.76829761	.31794094	-.55554688	4.80	3.85	2.16	
6003	6012	-.54234066	.75307857	-.37247721	3.33	1.88	.59	
6003	6038	-.01032205	-.57810031	-.81590041	5.50	2.64	-.78	
6003	6111	-.22514091	-.61865234	-.75271565	34.64	18.77	12.08	
6003	6123	.07500212	.90641974	.41566566	11.48	8.39	.56	
6003	6134	-.22513146	-.61859094	-.75276894	31.12	17.64	-4.62	
6004	6012	-.54078378	.26896514	-.79700104	18.71	5.13	-2.83	
6004	6013	.06933048	.90307862	-.42384230	9.58	8.25	3.02	
6004	6123	.78613200	-.48239372	.38638423	35.88	8.81	-4.98	
6006	6007	.54457114	-.69857302	-.46415300	7.50	3.40	-.04	
6006	6015	.11508563	.85437921	-.50674595	5.03	3.21	.14	
6006	6016	.78780662	.16766050	-.59266406	4.78	1.88	.10	
6006	6065	.85875769	.04034530	-.51079105	7.60	3.14	.19	
6007	6016	.12797651	.99126729	-.03179892	5.87	4.76	-1.86	
6007	6055	.32513421	.13439975	-.93606862	2.37	2.18	-.80	
6007	6063	.51812769	.14808201	-.84238674	7.86	3.39	-2.96	
6007	6064	.32053602	.78353987	-.53227994	2.68	2.70	-.75	
6007	6065	-.06916360	.97078414	.22977066	13.69	6.15	-.88	
6007	6067	.15402110	-.28354761	-.94650846	3.36	2.86	1.14	
6008	6009	-.88938239	-.39362748	-.23250028	10.72	17.99	8.22	
6008	6019	-.32049121	.07153574	-.94454646	3.83	3.77	-1.25	
6008	6067	.61525290	.61412014	-.49428769	15.83	20.35	1.79	
6009	6019	.26747201	.35752569	-.89478160	6.28	5.31	3.34	
6009	6020	-.72386736	.20465056	-.65888860	10.08	11.65	-1.01	
6009	6038	-.84982114	.15017873	.50522310	7.40	9.49	3.01	

Table 1. (Cont.)

Interstation direction	Direction cosines			σ_{ψ}^2	σ_{μ}^2	$\sigma_{\psi\mu}$
	x	y	z	(μrad)	(μrad)	(μrad)
6009 6043	.01590271	.46305232	-.88618827	4.27	1.63	.70
6011 6012	-.10269751	.99395429	-.03883406	7.10	6.36	2.10
6011 6022	-.15418669	.34223300	-.92687811	2.36	4.39	.66
6011 6038	.71357102	-.69915790	-.04466129	4.93	4.11	-1.83
6011 6059	-.20314666	-.02128930	-.97891685	12.93	3.89	1.67
6011 6111	.75372727	-.56546517	.33487959	8.14	8.17	-2.05
6011 6134	.75372993	-.56550225	.33481098	5.65	5.50	-2.71
6012 6013	.60945015	.72469218	.32154590	13.41	8.85	4.80
6012 6022	-.05510645	-.54597412	-.83598776	2.57	4.53	.36
6012 6023	.21639964	.58647164	-.78052688	4.01	7.30	.90
6012 6059	-.00626811	-.89897636	-.43795229	2.41	3.97	-1.42
6013 6015	.99602691	.05221303	.07214017	3.28	3.62	.01
6013 6040	.48567228	.35602441	-.79835397	2.08	3.88	.87
6013 6047	.07190680	.43904373	-.89558362	8.33	7.00	4.50
6013 6072	.76088082	.53545913	-.36652953	4.36	8.55	1.81
6013 6078	-.37095605	-.44904419	-.81286587	.94	12.01	-3.04
6015 6016	.59083746	-.80632468	.02741557	2.95	2.82	1.04
6015 6040	-.52814299	.27566607	-.80316449	1.65	2.08	-.07
6015 6042	.63085574	-.13074205	-.76480557	2.44	2.82	.60
6015 6045	.10310295	.10012056	-.98961894	1.27	.81	.32
6015 6064	.67671319	-.55938010	-.47869944	1.74	1.85	.53
6015 6065	.39466649	-.88863525	.23359313	5.57	2.35	-.21
6015 6072	-.83996571	.36082497	-.40529367	2.98	4.19	-1.46
6015 6073	-.14328286	.32543415	-.93464573	2.72	1.85	-.69
6015 6075	.22422676	.17832599	-.95808257	2.84	1.86	.81
6016 6042	.00110929	.67608254	-.73682506	4.38	3.04	-.43
6016 6063	.24657417	-.79099005	-.55994279	3.84	2.99	1.33
6016 6064	.40518193	.10848972	-.90777618	5.65	3.07	.89
6016 6065	-.57150716	-.41458906	.70816345	25.62	8.62	1.65
6019 6020	-.98854461	-.10440602	.10899057	8.63	9.11	-4.07
6019 6043	-.39099019	.55892898	-.73124897	6.16	2.42	-.23
6019 6061	.21667072	.81186039	-.54215911	7.88	3.46	.54
6019 6067	.69803894	.30282721	.64887389	3.70	6.55	2.34
6019 6069	.57324908	.81333071	-.09939140	14.67	10.84	5.58
6020 6038	-.05505866	-.05818222	.99678652	9.75	3.90	-1.14
6020 6039	-.88679899	.45092546	.10126101	46.24	84.34	-48.70
6020 6043	.76160348	.40653267	-.50466951	12.13	7.22	2.77
6022 6023	.22939844	.96994665	.08111630	3.97	4.22	.22
6022 6031	.44751200	.47320310	-.75882266	6.38	3.96	-1.71
6022 6039	.55053948	-.79360811	-.25902211	9.48	15.45	6.00
6022 6059	.09273248	-.62694587	.77352412	3.29	6.17	-.26
6022 6060	.31064087	.87304183	-.37589920	4.53	5.01	-.95
6022 6078	.06525885	.98528947	-.15794284	70.31	78.59	53.19
6023 6031	.14030720	-.64535919	-.75088309	1.84	1.15	.56
6023 6032	.73022042	.29245945	-.61745090	4.71	2.62	-.99
6023 6040	.87290005	.48655480	-.03619295	3.22	4.69	-.30
6023 6047	.54413175	.52027613	.65820467	7.08	11.72	1.73
6023 6060	.08857150	-.45655981	-.88527297	2.49	2.26	1.09
6023 6072	.72220386	.38240025	.57636068	2.75	3.73	1.36
6023 6078	-.34421395	-.90126678	-.26312535	38.04	54.65	-32.36
6031 6032	.42101231	.86534395	.27189794	2.21	2.25	-.79
6031 6039	.10377002	-.93588355	.33668052	7.68	9.08	3.79
6031 6051	.94877386	.22348934	-.22333985	3.13	1.18	-.29
6031 6052	.86847044	.38651964	-.31042176	5.11	2.65	-1.05
6031 6053	.86812023	-.16769187	-.46716882	6.20	2.29	.62
6031 6060	-.18248401	.79222053	.58231110	5.04	2.87	-1.64

Table 1. (Cont.)

Interstation direction		Direction cosines			σ_{ψ}^2	σ_{μ}^2	$\sigma_{\psi\mu}$
		x	y	z	(μrad)	(μrad)	(μrad)
6031	6078	-.51978753	.10804239	.84743600	16.60	7.33	1.37
6032	6040	.56273804	.45312081	.69138081	14.56	10.49	-4.02
6032	6044	.85609802	-.29345246	-.42541960	11.72	9.87	-1.56
6032	6045	.97899441	.02969027	.20171374	2.66	3.32	-.96
6032	6047	-.23190326	.11524464	.96588796	2.44	5.19	1.81
6032	6052	.38869791	-.65082451	-.65218202	7.61	2.97	.06
6032	6060	-.75111354	-.65857502	.04590650	3.72	3.86	1.59
6038	6039	-.30533711	.23850297	-.92189239	3.38	10.38	-1.16
6038	6059	-.71196736	.61064824	-.34671488	3.44	3.33	1.84
6038	6134	-.15555027	.52653755	.83580041	7.65	3.15	1.93
6039	6059	-.52378088	.47827300	.70491739	7.29	16.49	-6.47
6040	6045	.94082858	-.27177048	-.20244109	2.41	3.92	-1.07
6040	6047	-.75745932	-.23851117	.60775637	6.92	9.42	-.49
6040	6060	-.71906373	-.60950287	-.33384668	2.87	3.23	.49
6040	6072	-.05889596	-.06586214	.99608908	8.00	9.57	.10
6040	6073	.97900793	-.05862546	.19520896	8.03	11.93	-2.38
6040	6075	.96051205	-.21058346	.18185489	3.21	4.45	-1.29
6042	6045	-.44912782	.28840676	-.84563925	2.23	2.36	.15
6042	6064	.42683435	-.89359514	.13892502	7.17	8.16	-.92
6042	6068	.04651008	-.32793556	-.94355449	2.02	3.55	-.14
6042	6073	-.73989712	.50980226	-.43892358	2.79	3.51	-.32
6042	6075	-.55370869	.54178904	-.63235380	5.24	9.84	1.47
6043	6050	-.13089108	.85241541	-.50621684	39.52	14.49	-6.23
6043	6061	.75855997	.64995905	-.04626024	21.33	11.80	1.07
6044	6045	.55487831	.35538518	.75220438	14.61	15.53	-2.69
6044	6051	.00725312	-.88371318	-.46797266	67.30	23.18	-2.08
6045	6051	-.41189651	-.56088405	-.71815761	4.08	2.14	-.29
6045	6068	.60591270	-.77309759	-.18758976	4.79	5.03	-1.35
6045	6073	-.61337205	.45920180	.64257951	7.17	7.74	2.24
6045	6075	.21941894	.11156529	.96923089	13.52	7.81	-2.45
6047	6072	.86399341	.21477650	.45539701	8.25	9.11	3.04
6050	6053	-.66636022	.73523119	-.12409336	26.19	5.54	3.75
6050	6061	.94337293	.12091400	.30891311	44.80	21.02	-11.51
6051	6052	-.99255605	.11841241	.02847798	20.63	11.42	4.14
6051	6053	-.78860268	-.60492010	-.11035164	7.70	3.72	.10
6051	6061	.39088548	-.90832749	.14882780	12.32	4.36	-.77
6051	6068	.78397660	.09886404	.61286751	3.95	1.37	-.67
6052	6053	-.18777583	-.96511261	-.18247711	12.18	5.73	1.01
6052	6060	-.82424287	.08191608	.56027980	4.14	1.63	.39
6053	6060	-.66129678	.47679155	.57909964	2.98	1.20	-.48
6055	6063	-.09286860	-.11188265	.98937237	6.33	6.52	1.12
6055	6064	-.02445913	.82169272	.56940567	2.34	4.58	.72
6055	6067	-.40655949	-.90836802	.09786177	7.36	8.80	.44
6055	6069	-.35683386	.15178289	-.92175460	32.27	18.85	3.97
6061	6067	.42003359	-.27558772	.86465207	5.97	4.53	1.70
6061	6068	.35779796	.83913675	.40967076	7.54	3.33	.91
6061	6069	.74933462	.42891657	.50450789	53.39	28.14	16.96
6063	6064	.03985527	.99594504	-.08065384	3.07	3.81	-1.04
6063	6067	-.23440311	-.60457106	-.76128116	4.17	7.76	-.64
6064	6068	-.21648233	.24273719	-.94562892	2.77	4.03	1.71
6068	6069	-.02725314	-.96240153	-.27026018	26.89	19.09	-9.25
6068	6075	-.39804164	.68969301	.60488545	5.43	5.59	.88
6072	6073	.70661735	.01609177	-.70741287	4.53	6.29	1.63
6072	6075	.86325760	-.13851763	-.48538560	2.94	3.89	.66
6073	6075	.89481633	-.41852378	.15537564	14.38	17.76	-.98

Table 2a. Accuracy estimates for SAO geometrical network interstation vectors. n is the number of observations; σ_1^2 and σ_2^2 are accuracy estimates before and after network adjustment; δ^2 is the square of the angular difference between the two estimates; and k^2 is the scaling factor.

Line	n	σ_1^2 (μrad)	σ_2^2 (μrad)	δ^2 (μrad)	k^2	Line	n	σ_1^2 (μrad)	σ_2^2 (μrad)	δ^2 (μrad)	k^2
8015–8019	29	1514.4	4031.7	3114.8	1.12	9006–9091	10	30.0	28.6	38.6	1.32
8015–9004	122	7.2	23.4	44.9	2.93	9006–9115	19	5.9	16.8	201.5	17.75
8015–9066	133	79.2	378.5	258.9	1.13	9007–9009	263	1.1	6.9	1.5	0.38
8015–9074	25	37.2	38.1	487.9	12.96	9007–9010	86	2.3	5.5	0.6	0.15
8015–9080	67	20.8	66.2	217.4	5.00	9007–9011	437	1.7	13.5	0.1	0.01
8015–9091	30	10.6	25.3	0.01	0.00	9007–9029	74	1.2	24.1	10.6	0.84
8019–9004	301	0.9	7.2	0.6	0.15	9007–9031	32	3.5	27.0	0.4	0.03
8019–9091	61	4.0	17.9	2.3	0.21	9008–9028	25	16.7	64.3	6.4	0.16
9001–9009	183	1.0	5.8	1.3	0.38	9008–9080	8	233.1	32.1	453.1	3.42
9001–9010	154	2.1	13.1	6.8	0.89	9008–9115	38	6.4	23.3	33.4	2.25
9001–9012	187	1.6	9.4	0.8	0.15	9009–9010	248	2.2	14.4	0.1	0.01
9001–9113	20	32.3	174.1	195.2	1.89	9009–9011	201	1.3	4.9	0.2	0.06
9001–9114	74	5.8	30.0	11.7	0.65	9009–9114	13	21.5	9.5	13.8	0.89
9001–9117	16	11.7	14.4	85.3	6.54	9010–9029	6	59.6	24.9	79.9	1.89
9002–9008	7	19.3	84.3	369.4	7.13	9010–9114	38	7.4	17.6	146.4	11.71
9002–9028	25	11.0	86.0	40.6	0.84	9011–9029	7	734.0	47.9	6252.8	15.99
9004–9006	14	43.2	8.9	44.9	1.72	9011–9031	9	141.1	169.9	78.5	0.50
9004–9008	139	2.8	11.2	20.8	2.97	9012–9021	29	12.5	47.4	10.6	0.35
9004–9009	43	8.0	27.0	0.6	0.03	9012–9113	14	8.2	22.6	8.0	0.52
9004–9010	41	6.9	27.5	1.8	0.10	9012–9114	24	9.8	19.7	31.8	2.16
9004–9028	35	8.2	17.2	83.5	6.57	9012–9117	216	5.8	48.2	3.3	0.12
9004–9029	42	18.0	49.7	0.7	0.02	9021–9113	57	23.1	193.3	4.9	0.05
9004–9066	192	3.3	16.8	24.2	2.41	9021–9117	8	126.0	39.1	800.1	9.69
9004–9074	65	7.3	12.8	90.0	8.96	9028–9091	37	13.3	67.1	290.4	7.22
9004–9080	164	3.4	19.8	7.2	0.62	9029–9031	26	12.6	24.6	2.6	0.14
9004–9091	442	0.6	3.4	0.7	0.35	9066–9074	13	89.9	63.9	461.7	6.00
9004–9115	60	7.7	51.4	21.0	0.71	9066–9080	27	34.1	115.3	68.3	0.91
9005–9006	61	4.8	89.5	0.01	0.00	9074–9077	42	41.0	299.8	15.6	0.09
9005–9012	25	35.0	141.6	98.0	1.11	9074–9091	43	11.7	34.0	204.3	8.94
9005–9117	16	45.5	186.4	108.2	0.93	9077–9091	30	22.6	154.1	11.9	0.13
9006–9008	172	4.2	29.1	0.9	0.05	9113–9114	30	45.0	116.7	424.6	5.25
										k^2 ave =	2.65

Table 2b. Accuracy estimates for BC-4 geometrical network interstation vectors. σ_1^2 and σ_2^2 are accuracy estimates before and after network adjustment; δ^2 is the square of the difference between the estimates; and k^2 is the scaling factor.

Line	σ_1^2 (μrad)	σ_2^2 (μrad)	δ^2 (μrad)	k^2	Line	σ_1^2 (μrad)	σ_2^2 (μrad)	δ^2 (μrad)	k^2
6002–6003	3.0	36.73	26.52	1.34	6011–6059	6.0	8.41	1.17	0.16
6002–6007	14.8	6.70	51.48	4.79	6011–6111	86.6	8.16	8.05	0.17
6002–6008	3.8	4.07	4.03	1.02	6011–6134	9.3	5.57	0.83	0.11
6002–6009	15.4	6.74	7.65	0.69	6012–6013	23.3	5.09	4.10	0.29
6002–6038	12.0	4.48	10.71	1.30	6012–6022	7.1	3.55	9.71	1.82
6002–6111	13.0	6.61	7.63	0.78	6012–6023	8.0	5.66	9.95	1.46
6003–6004	15.1	7.01	112.06	10.14	6012–6059	4.0	3.19	10.43	2.90
6003–6011	6.9	4.33	6.83	1.22	6013–6015	195.8	3.45	174.15	1.75
6003–6012	298.0	2.61	62.48	0.42	6013–6040	17.3	2.98	53.68	5.29
6003–6038	5.3	4.07	7.99	1.71	6013–6047	7.3	7.66	7.18	0.96
6003–6111	17.1	26.70	1.38	0.06	6013–6072	8.0	6.46	2.09	0.29
6003–6123	10.0	9.94	0.45	0.05	6013–6078	25.1	6.48	46.25	2.93
6003–6134	195.7	24.38	232.13	2.11	6015–6016	5.3	2.88	9.40	2.30
6004–6012	31.0	11.92	104.81	4.88	6015–6040	9.8	1.87	3.89	0.67
6004–6013	8.8	8.92	15.37	1.73	6015–6042	2.7	2.63	3.56	1.34
6004–6123	37.9	22.34	88.76	2.95	6015–6045	11.1	1.04	2.47	0.41
6006–6007	27.9	5.45	41.13	2.47	6015–6064	8.9	1.79	49.22	9.21
6006–6015	13.7	4.12	15.36	1.72	6015–6065	6.6	3.96	34.65	6.56
6006–6016	6.4	3.33	52.79	10.85	6015–6072	3.3	3.59	8.29	2.41
6006–6065	4.5	5.37	4.49	0.91	6015–6073	4.3	2.28	2.00	0.61
6007–6016	14.4	5.32	24.89	2.52	6015–6075	7.0	2.35	32.89	7.04
6007–6055	77.9	2.27	21.76	0.54	6016–6042	84.3	3.71	247.16	5.62
6007–6063	5.2	5.62	4.86	0.90	6016–6063	17.2	3.42	90.14	8.74
6007–6064	38.5	2.69	178.65	8.67	6016–6064	3.9	4.36	1.47	0.36
6007–6065	33.2	9.92	31.07	1.44	6016–6065	14.8	17.12	30.86	1.93
6007–6067	17.7	3.11	61.90	5.95	6019–6020	31.4	8.87	159.21	7.91
6008–6009	16.5	14.36	12.03	0.78	6019–6043	2.8	4.29	3.84	1.08
6008–6019	2.7	3.80	4.78	1.47	6019–6061	5.3	5.67	6.77	1.23
6008–6067	21.0	18.09	0.82	0.04	6019–6067	6.8	5.12	13.95	2.34
6009–6019	10.3	5.79	2.96	0.37	6019–6069	82.0	12.76	6.34	0.13
6009–6020	17.3	10.87	32.65	2.32	6020–6038	11.0	6.82	30.71	3.45
6009–6038	16.0	8.45	20.84	1.70	6020–6039	113.8	65.29	11.62	0.13
6009–6043	20.6	2.95	28.89	2.45	6020–6043	11.9	9.68	1.02	0.09
6011–6012	12.5	6.73	54.35	5.66	6022–6023	17.5	4.09	83.06	7.69
6011–6022	165.6	3.38	2.70	0.03	6022–6031	12.5	5.17	18.19	2.06
6011–6038	20.5	4.52	22.72	1.82	6022–6039	29.0	12.46	15.01	0.72

Table 2b. (Cont.)

Line	σ_1^2 (μrad)	σ_2^2 (μrad)	δ^2 (μrad)	k^2	Line	σ_1^2 (μrad)	σ_2^2 (μrad)	δ^2 (μrad)	k^2
6022–6059	3.1	4.73	0.72	0.18	6042–6073	162.0	3.15	720.92	8.73
6022–6060	16.3	4.77	36.84	3.50	6042–6075	15.5	7.54	23.07	2.00
6022–6078	808.0	74.45	2970.60	6.73	6043–6050	19.1	27.00	58.35	2.53
6023–6031	11.1	1.49	11.13	1.77	6043–6061	29.9	16.57	78.65	3.38
6023–6032	4.9	3.66	52.75	12.32	6044–6045	74.5	15.07	19.43	0.43
6023–6040	30.2	3.96	65.25	3.76	6044–6051	38.3	45.24	0.16	0.00
6023–6047	17.8	9.40	63.17	4.64	6045–6051	8.2	3.11	1.14	0.20
6023–6060	1.6	2.38	2.09	1.05	6045–6068	5.0	4.91	0.50	0.10
6023–6072	94.9	3.24	268.78	5.48	6045–6073	6.5	7.46	0.53	0.08
6023–6078	663.6	46.34	1521.11	4.29	6045–6075	7.6	10.67	6.83	0.75
6031–6032	4.2	2.23	4.71	1.47	6047–6072	8.2	8.68	13.27	1.57
6031–6039	122.9	8.38	153.07	2.33	6050–6053	51.3	15.86	512.41	15.26
6031–6051	139.4	2.16	136.70	1.93	6050–6061	32.7	32.91	174.32	5.31
6031–6052	8.9	3.88	4.46	0.70	6051–6052	22.2	16.02	11.87	0.62
6031–6053	4.6	4.25	3.86	0.87	6051–6053	4.8	5.71	6.28	1.20
6031–6060	3.3	3.96	2.36	0.65	6051–6061	20.4	8.34	32.94	2.29
6031–6078	13.3	11.97	0.10	0.01	6051–6068	2.5	2.66	8.36	3.24
6032–6040	31.0	12.53	20.85	0.96	6052–6053	7.1	8.96	1.59	0.20
6032–6044	10.1	10.79	0.52	0.05	6052–6060	6.2	2.88	3.66	0.81
6032–6045	41.3	2.99	233.71	10.55	6053–6060	27.8	2.09	6.33	0.42
6032–6047	7.1	3.81	3.72	0.68	6055–6063	6.0	6.42	2.28	0.37
6032–6052	21.4	5.29	191.15	14.32	6055–6064	4.6	3.46	11.38	2.82
6032–6060	5.6	3.79	9.99	2.13	6055–6067	5.9	8.08	0.71	0.10
6038–6039	9.2	6.88	2.18	0.27	6055–6069	23.5	25.56	4.41	0.18
6038–6059	19.6	3.38	205.25	17.86	6061–6067	238.0	5.25	1099.08	9.04
6038–6134	3.6	5.40	0.82	0.18	6061–6068	29.9	5.44	51.15	2.89
6039–6059	26.4	11.89	4.27	0.22	6061–6069	53.0	40.76	40.50	0.86
6040–6045	3.8	3.16	1.67	0.48	6063–6064	3.3	3.44	1.29	0.38
6040–6047	18.2	8.17	21.08	1.60	6063–6067	10.8	5.97	0.86	0.10
6040–6060	73.6	3.05	12.64	0.33	6064–6068	18.8	3.40	35.10	3.16
6040–6072	21.3	8.79	25.05	1.67	6068–6069	297.5	22.99	27.68	0.17
6040–6073	22.5	9.98	37.66	2.32	6068–6075	128.7	5.51	339.50	5.06
6040–6075	17.6	3.83	31.92	2.98	6072–6073	27.8	5.41	61.70	3.72
6042–6045	2.7	2.30	0.53	0.21	6072–6075	240.5	3.41	397.15	3.26
6042–6064	9.6	7.67	8.74	1.01	6073–6075	31.7	16.07	16.28	0.68
6042–6068	2.8	2.78	1.55	0.56				k^2 ave =	2.60

3. DYNAMICAL SOLUTION

An observation θ of direction (right ascension and declination) or range can be related to the satellite position $\bar{r}(t)$ and to the station position $\bar{X}$ by

$$\theta = [A]\,[\bar{r}(t) - R(\theta, x, y)\,\bar{X}] \quad . \tag{2}$$

In general, A is an easily computed transformation matrix. Further, the orbit $\bar{r}(t)$ depends on the orbital elements, the gravity field, the atmospheric density, solar and lunar gravitational attraction, and radiation pressure. Finally, equation (2) depends on UT1 – i.e., the sidereal angle θ – and on the pole position x and y. None of these quantities is known without error and each, in itself, provides a number of difficult problems. For a certain class of satellites, the earth's gravity field presents the major source of error but is improved as part of the analysis described here.

Two types of data have been used in the dynamical solution. Observations of direction are made by photographing the satellite against a star background. The star positions then define the direction from the observing station to the satellite in the coordinates of right ascension and declination. The star positions are taken from a catalog and refer to its epoch. Precession and nutation are therefore applied to refer the observation to the reference system desired. For reasons related to the orbital theory for r(t), we have chosen to work in the quasi-inertial reference system defined by the equinox of 1950.0 and the equator of date. In addition, UT1 and pole positions are applied to bring the terrestrial reference frame, defined by the Conventional International Origin and the zero meridian of the BIH, into this system. Therefore, orbital elements and station positions are expressed in this quasi-inertial reference system when determined with direction observations. Specifically, the right ascension of the ascending node of the satellite (hereafter called the node) is unambiguously defined.

Observations of range relate the relative position of the satellite to the observer and not to the reference system; i.e., the observation is unchanged if the reference system is transformed by translation or rotation. Specifically, the node is defined only relative to the adopted value of +UT1. Therefore, when only observations of range (and velocity) are used, a correction for the longitude must be allowed for in each orbit. This is accomplished with the following device. In general, the normal system for each orbit has the form

$$\begin{Bmatrix} N & B \\ B^T & C \end{Bmatrix} \begin{Bmatrix} \overline{\Delta X} \\ \overline{\Delta p} \end{Bmatrix} = \begin{Bmatrix} \overline{a} \\ \overline{b} \end{Bmatrix} , \tag{3}$$

where $\overline{\Delta X}$ are the corrections to the station coordinates, and $\overline{\Delta p}$ are the corrections to the orbital elements.

It has been observed that with direction observations, $B \approx 0$, and so the interactions between orbital elements and station coordinates can be ignored. For observations of range, we form the set of reduced normal equations

$$[N - B\,C\,B^T]\ \overline{\Delta X} = \overline{a} - B\,C\,\overline{b} \quad . \tag{4}$$

These equations eliminate the corrections $\overline{\Delta p}$ while preserving the interactions between $\overline{\Delta p}$ and $\overline{\Delta X}$. This set of reduced normal equations can be added to another, and the solution for $\overline{\Delta X}$ can be used to determine $\overline{\Delta p}$ if so desired. The complete set of $\overline{\Delta p}$ was computed and found to be very small. The same device is used in processing simultaneous observations to eliminate the satellite position from each simultaneous observation. In summary, orbits determined by direction observations were processed directly by assuming $B = 0$. Those orbits based primarily on range data were reduced by means of equation (4).

The observations used are from the satellites listed in Table 3. Satellite arcs were chosen from satellites whose orbits were relatively uncorrupted by errors. Specifically, we eliminated satellites with drag model errors (large area-to-mass ratio and low perigee height), particular sensitivity to gravity-field model errors (resonances), or poor orbital distribution (less than six stations observing the satellite).

Table 3. Dynamical data used in SE III.

Satellite Number	Satellite Name	Inclination	Eccentricity	a (km)	Perigee (km)	Laser observations	Station coordinates	Zonal harmonics	Tesseral harmonics	Number of files
7001701	Dial	5°	0.088	7344	301			x		
7010901	Peole	15	0.017	7070	635	x		x	x	4
6001301	Courier 1B 1960 νI	28	0.016	7465	965		x	x	x	7
5900101	Vanguard 2 1959 αl	33	0.165	8300	557		x	x	x	7
5900701	1959 ηl	33	0.188	8483	515		x			18
6100401	1961 δl	39	0.119	7960	700				x	4
6701401	D1D	39	0.053	7337	569	x	x		x	10
6701101	D1C	40	0.052	7336	579	x	x		x	9
6503201	Explorer 24 BE-C	41	0.026	7311	941	x	x		x	13
6202901	Telstar 1 1962 αεl	44	0.241	9672	962			x		4
6000902	1960 ιl2	47	0.011	7971	1512		x	x	x	10
6206001	Anna 1B 1962 βμl	50	0.007	7508	1077		x	x	x	12
6302601	Geophysical Research	50	0.062	7237	424			x		6
6508901	Explorer 29 Geos 1	59	0.073	8074	1121	x	x	x	x	56
6101501	Transit 4A 6101	67	0.008	7318	885			x	x	10
6101502	Injun 1 6102	67	0.008	7316	896				x	9
6506301	Secor 5	69	0.079	8159	1137		x		x	2
6400101		70	0.002	7301	921			x	x	4
6406401	Explorer 22 BE-B	80	0.012	7362	912	x	x	x	x	6
6508101	OGO 2	87	0.075	7344	420			x	x	5
6600501	Oscar 07	89	0.023	7417	868		x		x	1
6304902	5BN-2	90	0.005	7473	1070		x		x	5
6102801	Midas 4 1961 αδl	96	0.013	10005	3503		x	x	x	6
6800201	Explorer 36 Geos 2	106	0.031	7709	1101	x	x		x	13
6507801	OV1-2	144	0.182	8306	416		x		x	4

The data were kept in two parts. Before 1970, most of the observations were directions. A number of laser ranges were made, and where it was possible to do so, they were included in the orbits. In 1971, the cooperative tracking program ISAGEX, with 10 laser stations, provided for the first time relatively complete orbital and geographical coverage with laser data. From these ISAGEX data, 15 orbits were used in the dynamical determination of station coordinates.

Optical data were assigned an assumed accuracy of 4". In these instances in which five or more observations were made within a few minutes – e.g., of Geos flashes – a smoothed or synthetic observation was determined. The same calculation was used to generate simultaneous observations, because one cannot, in general, make exactly simultaneous observations. These synthetic observations were assigned an accuracy determined from the polynomial fit. If the computed uncertainty was less than 2", then 2" was used. In the reduction of optical data, we applied annual aberration, parallactic refraction determined from mean nighttime temperature and pressure for each station, and precession and nutation.

The distance measurement in range data used in this analysis has a precision of 1 to 2 m. The accuracy will not be so good when timing errors are included. In addition, other errors – e.g., those due to the gravity field – are also that large. Therefore, the assumed accuracy of the laser data was taken to be 5 m. Certain laser data taken in 1967 appear to have errors of 1 msec in epoch timing; these data were given an assumed accuracy of 10 m. Some laser systems provide a larger volume of data (e.g., more than 400 points per pass) than is useful here. Therefore, from passes of laser data containing more than 25 points, approximately 25 evenly distributed observations were selected. Numerical experiments indicated no improvement in the results by smoothing the laser points or by calculating synthetic observations.

The laser data were corrected for tropospheric refraction by using observed values of pressure, temperature, and relative humidity. In addition, the laser observations were reduced to the center of mass of the satellite; this correction is relatively small but systematic. The tropospheric correction is 2.1 m at zenith, and the reduction to the center of gravity is 80 cm for Geos 1.

Table 4 gives the number of observations selected both from pre-ISAGEX data and from ISAGEX data. Table 5 summarizes the adopted uncertainties.

Table 4. Observations included in the dynamical solution.

Pre-ISAGEX Data 15 satellites 140 arcs				ISAGEX Data 3 satellites 15 arcs	
Station number	Number of observations	Station number	Number of observations	Station number	Number of observations
7050	274	9011	1637	7050	1425
7818	1223	9012	3088	7060	1514
8015	612	9028	525	7804	625
7815	1970	9029	261	7809	1178
9001	4357	9031	467	7820	296
9002	2120	9021	81	7902	1484
9003	349	9066	809	7907	746
9023	2630	9025	9	7921	225
9004	3343	9080	47	7929	213
9005	945	9091	143	7930	89
9006	3170	7921	9	9030	172
9007	1646	7816	2382	9021	29
9008	2301	7804	200		
9009	1825	7901	761		
9010	2424				

The dynamical solution was based on 140 arcs of 15 satellites from the pre-ISAGEX data taken between 1962 and 1969, and 15 arcs of 3 satellites from the ISAGEX data taken in 1970. These two sources of data were kept separate, and several solutions were made. Since ISAGEX data are of a new type, we examined the origin of the node and the relative weighting in order to find the best treatment. Two iterations were performed as part of the larger computation of station coordinates. The pre-ISAGEX data were in arcs of from 4 to 30 days long, as appropriate, and the ISAGEX data were in 10-day arcs.

Table 5. Assumed accuracy for data used in SE III.

Data	Weight	Remarks
Baker-Nunn	4"	
Smoothed Baker-Nunn	2"	
SAO laser	5 m	Observed before 1970
Centre National d'Etudes Spatiales laser	10 m	Observed before 1970
GSFC laser	5 m	Observed before 1970
ISAGEX laser	5 m	1971 International Campaign

For all practical purposes, the length scale in a dynamical solution is fixed by the value of GM, which directly enters the calculations of the radius vector through

$$r = \left(\frac{GM}{n}\right)^{1/3} (1 + e \cos E)(1 + \text{perturbations}) \quad .$$

With optical directions, no further information in scale is available. With range data, both scale and GM can, in principle, be determined. The unit of distance is then defined by the speed of light and becomes the "light second." In this analysis, GM was assumed to have the value given in Table 6, and our dynamical scale is therefore defined by GM. If this value of GM is far from the exact one, some deterioration of the coordinates will occur. We return to this question in Section 7.

Table 6. Adopted constants.

$GM = 3.986013 \times 10^{20}$ cm^3 sec^{-2}	
$c = 2.997925 \times 10^{10}$ cm sec^{-1}	(velocity of light)
$k_2 = 0.30$	(Love number)

4. INFORMATION FROM DEEP-SPACE PROBES

JPL operates the Deep Space Net (DSN), eight stations for tracking deep-space probes. Data from the DSN have been used to obtain, among other parameters, the longitudes (relative and absolute) of each station and the distance of its antenna to the earth's instantaneous axis of rotation (Vegos and Trask, 1967; Trask and Vegos, 1968). The DSN data are particularly interesting because 1) they constitute a unique, complementary, and independent determination of geocentric locations, and 2) they provide a very strong determination of scale.

Comparisons of the JPL and SAO results were made by Veis (1966a) and Vegos and Trask (1967) from data from the Ranger missions and from SE I (Lundquist and Veis, 1966). More refined JPL solutions were combined with satellite-tracking data in the determination of SE II. The combination was made with Location Set (LS) 25, as determined by Mottinger (1969), by using data from the Mariner 4 and 5 missions. Continued refinement of the DSN data has provided LS 37, which is used in the present analysis (Mottinger, 1973).

Each DSN site is located near other stations whose coordinates were determined in the analysis presented here. Surface-triangulation data, in the form of geodetic coordinates, can be used to relate the DSN coordinates to the SAO coordinates (see Section 5).

The ephemeris r of a deep-space probe is assumed known. For a distant spacecraft, the observed range rate $\dot{\rho}$ can be expressed approximately as

$$\dot{\rho} = \dot{r} + \omega r_s \cos\delta \sin(\alpha_s - \alpha_0) \quad ,$$

where ω is the earth's rotation rate, r_s is the spin-axis distance of the observer, δ and α_0 are the declination and right ascension of the spacecraft, and α_s is the right ascension of the observer. Each station observes a diurnal variation in $\dot{\rho}$, the amplitude and phase depending on r_s and α_s, respectively.

Generally, any data can be analyzed. However, cruise data seem less reliable than close-encounter data for determining a_s (Mottinger, 1973), and they are used only for the determination of r_s. In any case, refraction (tropospheric and ionospheric) and orbit computation must be done with great care, and recent improvements come from refinements in the treatment of refraction. The ephemeris r (δ, a_0) will be determined in the system of the JPL planetary ephemeris. We can expect to find a systematic difference in the definition of longitude between the planetary ephemeris and the astronomical reference system (FK4) used for analysis of close-earth satellites. The DSN data reduction used numerical values for pole position and UT1 from BIH, as was done for the close-earth-satellite analyses.

The data for LS 37 are summarized in Table 7. The main improvements over LS 25 are as follows:

A. Better treatment of refraction, particularly ionospheric.
B. Inclusion of more data because of A.
C. Inclusion of Mariner 6 encounter data.
D. Revision of the planetary ephemeris.
E. Use of BIH polar motion and UT1.

Realistic estimates of accuracy are 2 m for r_s, 4 m for absolute longitude, and 2 m for relative longitude (Mottinger, 1972).

Mottinger (1972) provided a solution and covariance matrix for r_s, λ, in addition to the masses of Venus, Mars, and the moon and the oblateness of Mars. This system was transformed by SAO for corrections in coordinates X, Y of the station. These converted equations were then added to the larger system of normal equations, which included the other stations sought.

The LS 37 coordinates for the DSN stations are given in Table 8. In LS 37, the relative coordinates of 4711, 4712, and 4714 and of 4761 and 4762 were constrained to agree with the survey data.

Table 7. DSN data used in LS 37.

Flight	Tracking time period	δ
Mariner 4 encounter	July 10–21, 1965	-3°
Mariner 5 cruise	July 28–September 16, 1967	-8° to +8°
Mariner 5 encounter	October 14–25, 1967	6°
Mariner 5 post encounter	October 28–November 21, 1967	+2° to -2°
Mariner 6	July 26–31, 1969	-24°

Table 8. LS 37 coordinates, from Mottinger (1973).

Station	r (Mm)	λ	X (Mm)	Y (Mm)
4711	5.2063409	243°15059	-2.3514288	-4.6450800
4712	5.2120525	243.19452	-2.3504424	-4.6519794
4714	5.2039978	243.11047	-2.3536211	-4.6413425
4741	5.4502019	136.88749	-3.9787186	3.7248488
4742	5.2053494	148.98126	-4.4609782	2.6824124
4751	5.7429399	27.68542	5.0854415	2.6682659
4761	4.8626083	355.75097	4.8492431	-0.3602785
4762	4.8608181	355.63217	4.8467007	-0.3701960

5. INFORMATION FROM SURFACE TRIANGULATION

Extensive surface-triangulation data exist that relate station positions. These data are generally given in terms of datum coordinates and occasionally in terms of interstation vectors for collocated stations. We have used this information in four ways:

A. For stations in the same datum, the geodetic coordinates are used as observations relating the positions of the stations in the general combination adjustment.

B. For collocated instruments, these datum coordinates are used as a constraint relating the two sites. These cases could be treated as in A above.

C. The geodetic coordinates are utilized as a check on the accuracy of the final coordinates.

D. The geodetic coordinates are employed to determine the relation of each datum to a geocentric reference system.

Evaluating geodetic coordinates is the most difficult aspect of this analysis. When reliable, they are very accurate; but problems often exist in relating the local survey at the station to the datum.

In A, B, and C above, care must be taken to ensure that datum tilts, distortions, and scale differences do not corrupt the results. For most uses, limiting the application of geodetic coordinates to lengths of 100 km or less is satisfactory. Otherwise, the datum orientation must be determined and applied before the geodetic coordinates can be used with geocentric satellite-based coordinates.

The use of datum coordinates as observations of relative station positions assumes no correlation between X, Y, and Z. If we have datum coordinates for station i, X_i^d, Y_i^d, Z_i^d, and initial values for the geocentric coordinates that are to be corrected, X_i^g, Y_i^g, Z_i^g, we can write observation equations for each component of the vector between two stations:

$$X_i^d - X_j^d = X_i^g - X_j^g + \Delta X_i - \Delta X_j \quad ,$$

with similar expressions for Y and Z. If these are given weights W_{ij}, we can immediately write the normal system as

$$\begin{bmatrix} \sum_i \sigma_{ij} & \cdots & -\sigma_{ij} \\ \vdots & & \vdots \\ -\sigma_{ij} & \cdots & \sum_j \sigma_{ij} \end{bmatrix} \begin{bmatrix} \Delta X_i \\ \vdots \\ \Delta X_j \end{bmatrix} = \begin{matrix} \sum_i \sigma_{ij} \left[\left(X_i^d - X_j^d \right) - \left(X_i^g - X_j^g \right) \right] \\ \\ \sum_j \sigma_{ij} \left[\left(X_j^d - X_i^d \right) - \left(X_j^g - X_i^g \right) \right] \end{matrix} ,$$

where $\sigma_{ij} = (1/W_{ij})^2$. This system can augment a normal system for determining ΔX, ΔY, ΔZ.

The accuracy W_{ij} of the geodetic ties chosen is given in Table 9. Table 10 presents the geodetic coordinates for all the stations used in SE III.

Table 9. The stations related by survey.

Location	Stations pairs	$1/\sigma^2$ (m^{-2})	Location	Station pairs	$1/\sigma^2$ (m^{-2})
Maryland	7050–6002	1.0	California	4714–4712	5.0
Hawaii	9012–6011	1.0		4714–4711	5.0
Argentina	9011–6019	1.0		9113–4714	0.7
Japan	9005–6013	0.1		9113–6111	2.0
Spain	4761–4762	5.0		6111–6134	5.0
	9004–4761	0.20	Ethiopia	9028–6042	2.0
Central Europe	9066–8015	0.25	Australia	6060–4741	1.0
	9066–6065	0.0025		9003–4741	1.0
	7816–9030	0.01		9003–9023	1.0
Brazil	9029–6067	1.0		4741–4742	0.04
			South Africa	9002–6068	1.0
				9002–4751	0.1

Table 10. Geodetic coordinates used in SE III.

AGENCY	STA NO.	LATITUDE (DEG)	LONGITUDE (DEG)	H MSL (M)	H ELL (M)	DATUM	N (M)	NAME	U	V (MEGAMETERS)	W
									A = 6 378 388.0 M	1/F = 297.0000	
JPL	4761	+40 25 47.717	355 45 08.278	788.4	766.4	EU50	-22.0	MADRI1	4.84933201	-.36017192	4.11500579
JPL	4762	+40 27 15.273	355 38 00.572	738.3	716.3	EU50	-22.0	MADRI2	4.84678968	-.37009030	4.11702898
NOAA	6006	+69 39 44.228	018 56 33.868	106.41	119.01	EU50	+12.6	TROMSO	2.10303510	.72178299	5.95830091
NOAA	6012	+19 17 23.227	166 36 39.780	3.5	3.5	ASTR	0.	WAKEIS	-5.85882861	1.39457585	2.09367989
NOAA	6015	+36 14 29.527	059 37 42.729	991.0	959.0	EU50	-32.0	MASMAD	2.60446755	4.44427733	3.75046544
NOAA	6016	+37 26 42.320	015 02 48.376	9.43	-7.17	EU50	-16.6	SICILY	4.89649260	1.31629618	3.85678510
NOAA	6020	-27 10 39.213	250 34 17.495	230.8	230.8	EI67	0.0	EASTER	-1.88879616	-5.35503180	-2.89587721
NOAA	6031	-46 25 03.491	168 19 31.155	0.9	.	NZ49	.	INVERC	-4.31388656	.89137493	-4.59745823
NOAA	6039	-25 04 07.146	229 53 11.882	339.4	339.4	PITC	0.0	PITCAN	-3.72493290	-4.42140620	-2.68614464
NOAA	6043	-52 46 52.468	290 46 29.573	80.7	.	CH63	.	SOMBRO	1.37137597	-3.61494594	-5.05602037
NOAA	6044	-53 01 12.031	073 23 27.415	3.8	3.8	HR69	0.0	HERDIS	1.09907948	3.68466262	-5.07198740
NOAA	6050	-64 46 33.98	295 56 37.04	16.44	.	PLMR	.	PALMER	1.19246038	-2.45102427	-5.74726040
NOAA	6053	-77 50 46.2487	166 38 07.5845	19.0	.	CA62	.	MCMURD	-1.31074080	.31140586	-6.21351412
NOAA	6055	-07 58 16.634	345 35 32.764	70.94	.	AS58	.	ASCENS	6.11856151	-1.57184078	-.87865481
NOAA	6065	+47 48 07.011	011 01 29.378	943.5	942.9	EU50	- 0.6	PEISEN	4.21366502	.82094851	4.70289934
NOAA	6069	-37 03 26.2572	347 40 53.5548	24.8	24.8	TR68	0.0	DACUNA	4.97907544	-1.08729430	-3.82254543
NOAA	6073	-07 20 58.5270	072 28 32.1556	3.9	.	GRAC	.	CHAGOS	1.90493520	6.03272280	-.81050273
NOAA	6078	-17 41 46.956	168 17 57.921	15.2	.	EFAT	.	NWHBRD	-5.95216390	1.23269645	-1.92642529
CNES	7804	+36 27 50.1191	353 47 41.2862	25.40	- 9.6	EU50	-35.0	SFRLAS	5.10570263	-.55512550	3.76976971
CNES	7809	+43 56 00.190	005 42 48.788	657.82	649.4	EU50	-8.4	HTPRVL	4.57843482	.45808230	4.40329178
CNES	7809	+43 56 00.190	005 42 48.788	657.82	647.8	EU50	-10.0	HTPRVL	4.57843596	.45808242	4.40329289
CNES	7815	+43 55 59.183	005 42 48.382	657.83	649.4	EU50	-8.4	HTPRVL	4.57845832	.45807555	4.40327050
CNES	7816	+37 45 17.043	022 49 43.313	803.11	788.7	EU50	-14.4	STPHNL	4.65442139	1.95928240	3.88450187
CNES	7818	+31 43 19.25	357 34 54.06	855.65	813.7	EU50	-42.0	BECHRL	5.42641914	-.22917216	3.33472856
SAO	7930	+38 04 46.147	023 55 59.991	473.02	466.62	EU50	-6.40	DIOSLS	4.59530376	2.03955734	3.91274397
CNES	8015	+43 56 01.142	005 42 49.277	658.85	650.4	EU50	-8.4	HTPROV	4.57841531	.45809132	4.40331474
CNES	8019	+43 43 36.496	007 18 03.309	377.42	369.4	EU50	- 8.	NICEFR	4.57955755	.58672953	4.38653888
SAO	9004	+36 27 51.3666	353 47 42.0891	26.00	- 9.0	EU50	-35.0	S.FERN	5.10568254	-.55510320	3.76980100
SAO	9006	+29 21 38.97	079 27 25.51	1927.	1827.	EU50	-100.	NA.TAL	1.01826970	5.47121880	3.10975910
SAO	9008	+29 38 18.112	052 31 11.445	1597.4	1549.4	EU50	-48.0	SHIRAZ	3.37696353	4.40410229	3.13640545
SAO	9028	+08 44 56.39	038 57 33.61	1925.2	1820.2	EU50	-105.	ETHIOP	4.90385504	3.96530421	.96402118
SAO	9030	+38 04 46.564	023 56 00.130	472.64	466.24	EU50	-6.40	DIOSBN	4.59529486	2.03955710	3.91275385
SAO	9051	+37 58 40.31	023 46 42.89	187.9	180.9	EU50	- 7.0	ATHENG	4.60694919	2.02984975	3.90368223
INT.	9066	+46 52 40.318	007 27 58.238	903.44	900.3	EU50	-3.1	ZIMMWL	4.33139150	.56763749	4.63323685
INT.	9074	+56 56 54.98	024 03 37.81	8.0	2.4	EU50	-5.6	RIGALT	3.18399849	1.42163806	5.32289386
INT.	9077	+48 38 04.56	022 17 57.88	189.0	187.5	EU50	-1.5	UZGROD	3.90749264	1.60253261	4.76403296
INT.	9080	+52 08 39.116	358 01 59.492	113.19	108.6	EU50	-4.6	MALVRN	3.92024942	-.13462434	5.01285024
SAO	9091	+38 04 48.215	023 56 01.587	466.25	460.85	EU50	-6.40	DIONBN	4.59524788	2.03957510	3.91279060
AF	9115	+60 12 40.38	010 45 08.74	575.92	581.7	EU50	+5.8	HAREST	3.12136836	.59274733	5.51282959
AF	9117	+16 44 45.39	190 29 05.59	5.0	5.0	JI61	0.0	JOHNST	-6.00758942	-1.11180181	1.82595115
									A = 6 377 397.2 M	1/F = 299.1528	
NOAA	6013	+31 23 30.1397	130 52 24.8595	65.9	46.9	TKYO	-19.	KANOYA	-3.56571019	4.12020706	3.30274197
SAO	9005	+35 40 11.078	139 32 28.222	59.77	59.8	TKYO	+ 0.0	TOKYOJ	-3.94655504	3.36577471	3.69815201
SAO	9025	+36 00 08.606	139 11 43.159	855.89	855.4	TKYO	-0.5	DODRAJ	-3.91029861	3.37583640	3.72853881

Table 10. (Cont.)

AGENCY	STA NO.	LATITUDE (DEG)	LONGITUDE (DEG)	H MSL (M)	H ELL (M)	DATUM	N (M)	NAME	U	V	W
									(MEGAMETERS)		
									A = 6 378 206.4 M	1/F = 294.9787	
GSFC	1021	+38 25 49.628	282 54 48.225	5.76	6.7	NA27	+ 0.9	IBPOIN	1.11806122	-4.87647215	3.94279354
JPL	4711	+35 23 22.346	243 09 05.262	1036.3	1014.3	NA27	-22.0	GOLDS1	-2.35141501	-4.64522810	3.67358242
JPL	4712	+35 17 59.854	243 11 43.414	988.9	966.9	NA27	-22.0	GOLDS2	-2.35042827	-4.65212755	3.66544706
JPL	4714	+35 25 33.340	243 06 40.850	1031.8	1009.8	NA27	-22.0	GOLDS4	-2.35360704	-4.64149095	3.67687068
NOAA	6001	+76 30 03.4106	291 27 51.8867	206.0	238.	NA27	+32.	THULEG	.54658065	-1.39010720	6.18005957
NOAA	6002	+39 01 39.003	283 10 26.942	44.3	43.9	NA27	- 0.4	BELTVL	1.13079867	-4.83098741	3.99452058
NOAA	6003	+47 11 07.132	240 39 48.118	368.74	356.2	NA27	-12.5	MOSELK	-2.12779649	-3.78601463	4.65584803
NOAA	6004	+52 42 54.89	174 07 37.87	36.8	-9.2	NA27	-46.0	SHEMYA	-3.85174500	.39619209	5.05119936
NOAA	6011	+20 42 38.561	203 44 28.529	3049.27	3041.3	OHAW	- 8.	HAVAII	-5.46606254	-2.40412970	2.24240761
NOAA	6022	-14 20 12.216	189 17 13.242	5.34	5.3	AS62	0.0	PAGOGO	-6.09984241	-.99746771	-1.56900883
NOAA	6038	+18 43 44.93	249 02 39.28	23.2	23.2	ISOC	0.0	GIGEDO	-2.16111455	-5.64291648	2.03486429
NOAA	6047	+06 55 26.132	122 04 04.838	9.39	10.1	LZ11	+ 0.7	ZAMBOA	-3.36182692	5.36586413	.76373596
NOAA	6111	+34 22 54.537	242 19 09.484	2284.41	2258.11	NA27	-26.3	WRWDBA	-2.44881518	-4.66812578	3.58256864
NOAA	6123	+71 18 49.882	203 21 20.720	8.3	- 6.	NA27	-14.	PTBRRW	-1.88175624	-.81258399	6.01940356
NOAA	6134	+34 22 44.444	242 19 09.259	2198.37	2172.07	NA27	-26.3	WRWDBB	-2.44886889	-4.66821579	3.58226330
GSFC	7050	+39 01 13.676	283 10 18.035	54.812	56.1	NA27	+ 1.3	GODLAS	1.13070428	-4.83152429	3.99392150
GSFC	7060	+13 18 28.6136	144 44 05.3744	85.873	85.9	GUAM	0.	GUAMLS	-5.06886706	3.58433433	1.45850959
SAO	7901	+32 25 24.56	253 26 51.17	1651.33	1648.93	NA27	-2.4	ORGN P	-1.53572537	-5.16714655	3.40086741
SAO	7912	+20 42 37.73	203 44 24.03	3034.14	3026.14	OHAW	- 8.	MAUIHL	-5.46611028	-2.40400840	2.24237834
SAO	7921	+31 41 02.87	249 07 21.35	2383.14	2370.4	NA27	-12.7	MHSAOL	-1.93675026	-5.07785596	3.33174402
SAO	9001	+32 25 24.56	253 26 51.17	1651.33	1648.9	NA27	- 2.4	ORGN P	-1.53572537	-5.16714655	3.40086741
SAO	9010	+27 01 12.882	279 53 13.008	15.13	26.5	NA27	+11.4	JUPITE	.97631216	-5.60155092	2.88006423
SAO	9012	+20 42 37.50	203 44 24.08	3034.14	3026.1	OHAW	- 8.	MAUI,H	-5.46611195	-2.40401072	2.24237170
SAO	9021	+31 41 02.67	249 07 21.35	2383.12	2370.4	NA27	-12.7	MTHPBN	-1.93675141	-5.07785898	3.33173878
AF	9113	+34 57 50.742	242 05 11.584	784.231	760.4	NA27	-23.8	ROSMND	-2.44997502	-4.62457236	3.63485119
AF	9114	+54 44 33.858	249 57 26.389	704.6	701.7	NA27	- 2.9	CLALBC	-1.26482581	-3.46704442	5.18527510
									A = 6 378 249.145 M	1/F = 293.465	
JPL	4751	-25 53 21.15	027 41 08.53	1391.0	1399.0	ARCC	+ 8.	JOHANG	5.08558065	2.66837093	-2.76840899
NOAA	6042	+08 46 08.501	038 59 49.164	1886.46	1857.5	ADDN	-29.0	ADDABA	4.90091236	3.96825430	.96611839
NOAA	6063	+14 44 44.228	342 30 55.594	26.3	26.3	YO67	0.	SENGAL	5.88452266	-1.85363929	1.61276005
NOAA	6064	+12 07 51.750	015 02 06.151	295.4	316.4	ADDN	+21.0	FTLAMY	6.02355450	1.61795570	1.33152526
NOAA	6068	-25 52 56.98	027 42 25.17	1523.8	1531.8	ARCC	+ 8.	JOHANS	5.08498216	2.67046691	-2.76779768
NOAA	6075	-04 40 07.23	055 28 50.38	588.98	.	SEIL	.	MAHEIS	3.60287532	5.23842744	-.51567627
CNES	7820	+14 46 04.878	342 35 22.462	28.48	28.5	YO67	0.0	DAKARL	5.88631560	-1.84583600	1.61515750
SAO	7902	-25 57 33.851	028 14 53.909	1543.88	1551.9	ARCC	+ 8.	OLIFTL	5.05626003	2.71663410	-2.77547114
SAO	9002	-25 57 33.85	028 14 53.91	1544.1	1552.1	ARCC	+ 8.	OLFSFT	5.05626019	2.71663422	-2.77547120
CNES	9020	+14 46 05.975	342 35 22.936	24.59	24.6	YO67	0.0	DAKARS	5.88630805	-1.84581878	1.61518911
SAO	9022	-25 57 33.815	028 14 54.351	1543.34	1551.3	ARCC	+ 8.	OLIFTS	5.05625416	2.71664491	-2.77546988
SAO	9028	+08 44 47.23	038 57 30.48	1925.2	1896.2	ADDN	-29.	ETHIOP	4.90390476	3.96522135	.96365606
									A = 6 378 160.0 M	1/F = 298.25	
JPL	4741	-31 22 59.4305	136 53 10.1244	148.28	147.3	AUGD	-1.0	WOOMAU	-3.97856194	3.72489603	-3.30232384

Table 10. (Cont.)

AGENCY	STA NO.	LATITUDE (DEG)	LONGITUDE (DEG)	H MSL (M)	H ELL (M)	DATUM	N (M)	NAME	U	V (MEGAMETERS)	W
JPL	4742	-35 24 08.0381	148 58 48.2057	656.08	664.5	AUGD	+8.4	TIDBIN	-4.46084800	2.68246157	-3.67472947
NOAA	6008	+05 26 55.325	304 47 42.832	18.38	+8.7	SA69	-9.7	SURNAM	3.62333539	-5.21422241	.60159957
NOAA	6009	-00 05 50.468	281 34 49.212	2682.1	2706.7	SA69	+24.6	ECUADR	1.28090438	-6.25097009	-.01076928
NOAA	6019	-31 56 33.9540	294 53 41.3415	608.18	621.2	SA69	+13.0	DLORES	2.28071297	-4.91453950	-3.35538784
NOAA	6023	-10 35 08.0374	142 12 35.4955	60.5	61.7	AUGD	+ 1.2	THURIS	-4.95523608	3.84230946	-1.16399061
NOAA	6032	-31 50 28.992	115 58 26.618	26.30	32.5	AUGD	+6.2	PERTHA	-2.37525720	4.87559999	-3.34553190
NOAA	6060	-30 18 39.4182	149 33 36.8921	211.08	211.8	AUGD	+ 0.7	CULGOR	-4.75150046	2.79212193	-3.20029697
NOAA	6067	-05 55 37.414	324 50 06.200	40.63	66.7	SA69	+26.1	BRAZIL	5.18649484	-3.65391932	-.65424453
SAO	7907	-16 27 55.085	288 30 26.814	2452.274	2486.5	SA69	+34.2	ARQUPL	1.94285944	-5.80408719	-1.79687689
SAO	7929	-05 55 38.616	324 50 08.660	45.6	71.7	SA69	+26.1	NATALL	5.18653940	-3.65385815	-.65428178
SAO	9003	-31 06 07.2608	136 46 58.6988	159.21	158.1	AUGD	- 1.1	WOOMER	-3.98365792	3.74313237	-3.27567647
SAO	9007	-16 27 55.085	288 30 26.814	2451.86	2486.1	SA69	+34.2	AREQUI	1.94285932	-5.80408683	-1.79687677
SAO	9009	+12 05 25.912	291 09 46.078	7.44	-3.4	SA69	-10.8	CURACA	2.25189008	-5.81691837	1.32720069
SAO	9011	-31 56 33.228	294 53 38.949	608.	621.0	SA69	+13.0	V.DLOR	2.28066087	-4.91457654	-3.35536876
SAO	9023	-31 23 30.8163	136 52 39.0156	137.91	136.9	AUGD	- 1.0	LAGOON	-3.97764616	3.72514580	-3.30314365
SAO	9027	-16 27 54.365	288 30 26.578	2450.23	2484.4	SA69	+34.2	AREQU2	1.94285416	-5.80409346	-1.79685506
SAO	9029	-05 55 38.616	324 50 08.660	45.34	71.4	SA69	+26.1	NATLBR	5.18653916	-3.65385798	-.65428174
SAO	9031	-45 53 11.028	292 23 12.215	186.54	172.5	SA69	-14.0	CMDRVD	1.69386960	-4.11233951	-4.55660680
SAO	9039	-05 55 38.616	324 50 09.401	41.6	67.7	SA69	+26.1	NATAL2	5.18654928	-3.65383723	-.65428136
									A = 6 378 140.0 M		1/F = 298.258
NOAA	6007	+38 45 36.725	332 54 21.064	53.3	53.3	GRAC	0.0	AZORES	4.43356344	-2.26819774	3.97162906
NOAA	6040	-12 11 57.91	096 49 47.08	4.4	4.4	ASTR	0.0	COCOIS	-.74146810	6.19080089	-1.33897441
NOAA	6045	-20 13 50.	057 25 15.	149.4	.	NSPC	.	MAURIT	3.22389500	5.04510482	-2.19171644
NOAA	6051	-67 36 03.08	062 52 24.41	11.3	11.3	ASTR	0.0	MAWSON	1.11135985	2.16930795	-5.87428599
NOAA	6052	-66 16 45.12	110 32 04.61	18.0	18.0	ASTR	0.0	WILKES	-.90255177	2.40954573	-5.81656060
NOAA	6059	+02 00 35.622	202 35 21.962	2.75	.	XM67	.	XMASIS	-5.88521981	-2.44850730	.22219823
NOAA	6061	-54 16 39.515	323 30 42.531	4.2	.	SGRG	.	SOGEOR	3.00059110	-2.21936327	-5.15485386
NOAA	6072	+18 46 10.	098 58 15.	319.2	.	NSPC	.	TILAND	-.94203816	5.96745408	2.03930654

6. COMBINATION SOLUTION

The six sources of data to be combined are the following:

SAO dynamical network (pre-ISAGEX),
SAO dynamical network (ISAGEX),
SAO geometrical network,
BC-4 geometrical network,
JPL dynamical network (DSN),
Geodetic coordinates.

As described above, each subset of data was processed individually, with certain internal checks being allowed. Each subset was reduced with its own a priori weighting scheme, which was internally consistent. The greatest difficulty in combining these six sets of data was to establish realistic relative weights for each system. Relative weighting is derived by experiment tempered with some notion of the accuracy and by comparison with datum coordinates and heights (see Section 7). Only the SAO dynamical network and certain geodetic coordinates could not be taken at their given weight.

The geodetic coordinates provided the greatest source of concern and uncertainty in the analysis. Except for the SAO networks, the geodetic coordinates provide the only link between networks, and within networks the link between collocated stations (e.g., 4761–4762, 6111–6134). Geodetic coordinates were used as observations between relatively close stations – i.e., separated by less than 100 km – because the accuracy may not be so good for greater distances and because the use of geodetic coordinates as described above assumes no datum tilt nor scale difference.

Each subset of data was treated to provide a system of normal equations and normal residuals. The systems are combined with their relative weights. In addition, each system may have a different origin, orientation, and scale, but these differences should not occur if each system had been referred to the defined system without error. In the combination, additional parameters as necessary were introduced into the combined normal system to account for possible systematic errors. The SAO dynamical

pre-ISAGEX data were taken as the reference. Since the geometrical networks have no scale, only translation and rotation parameters were introduced. For practical purposes, the SAO geometrical network covers only one hemisphere in an east–west orientation, so only the rotation about the z axis (ϵ_z) may be meaningful. This corresponds to a correction to UT1. The polar orientation for the SAO geometrical network (ϵ_x, ϵ_y) turned out to be smaller than the formal uncertainty. The JPL net had only a scale and ϵ_z parameter as it is not sensitive to ϵ_x, ϵ_y or to the origin. Experiments with determining corrections to the node ($\Delta\Omega$) for each arc of ISAGEX data indicated that 1) the corrections were small, generally less than 1 μrad, and 2) they were satisfactorily included through the reduced normal equations. Therefore, formally, the combination solution contained 14 additional parameters, the final values of which are given in Table 11. The translation of the two geometrical networks is the correction to the station used as the origin. Excellent agreement occurs between these translations and the coordinates determined from an a posteriori geometric adjustment. The formal uncertainty for the translation of the SAO geometrical network is not given, because the origin station 9051 has very few observations and is not determined very well.

Two iterations were completed, the first starting with the coordinates given in Gaposchkin and Lambeck (1970). Examination of the solutions indicated problem stations; in particular, the geodetic coordinates were sometimes seriously in error.

The strategy used to determine the relative weights and the formal uncertainty was based on the geometrical solutions, and all other solutions were referred to them. Geometrical solutions are relatively uncomplicated and free from assumptions. Furthermore, the statistics are straightforward.

The accuracy of each station-to-station direction was computed. This estimate can be verified by comparison with the direction determined in the network adjustment. The adjustment essentially enforces the coplanarity condition for any three directions that connect three stations. By comparing these estimates of the direction, we can compute a scale factor that is a measure of the agreement between the formal statistics of the adjustment and the actual errors. This scale factor turned out to be $k^2 = 2.65$ for the SAO geometrical network and $k^2 = 2.60$ for the BC-4. Since the difference between these estimates of k^2 is not significant, we adopted an overall scale factor of

Table 11. Additional parameters determined.

Relation to the dynamical system	Translation parameters (m)	Rotation parameters about the axis (μrad)	Scale parameter
SAO geometrical	X = - 6.66	ϵ_x = 0.70 ± 1.56	
	Y = -14.88	ϵ_y = 0.84 ± 1.24	
	Z = -9.90	ϵ_z = -0.40 ± 1.43	
BC-4 geometrical	X = -11.25 ± 9.60	ϵ_x = 1.76 ± 0.96	
	Y = -16.63 ± 9.58	ϵ_y = -0.65 ± 0.65	
	Z = - 6.79 ± 13.74	ϵ_z = -2.20 ± 0.82	
JPL		ϵ_z = -3.43 ± 1.02	$0.18 \times 10^{-6} \pm 0.55 \times 10^{-6}$

$k^2 = 2.625$ for the geometrical networks. It is interesting to note that when only the 12 SAO Baker-Nunn cameras are used, the scale factor becomes $k^2 = 1.03$, indicating excellent control of systematic errors.

In the combination of the six types of data, the geometrical networks, the JPL network, and the geodetic survey data were used with a priori variances. The pre-ISAGEX dynamical data were given a weight of 0.25 for the combination of the normal equations, which effectively doubles the assumed accuracy. In addition, the assumed accuracy of the pre-ISAGEX laser data was further multiplied by a factor of $1/\sqrt{10}$, and thus the assumed accuracy of the laser data was multiplied by 6. The ISAGEX data were given an overall weight of 0.0625; i.e., the assumed accuracy was multiplied by 4. Thus, the reference orbits were computed by using the assumed accuracy in Table 5, but the normal system was scaled by these factors. These adjustments were necessary in order to accommodate the enormous volume of data used for the dynamical solutions. Large volumes of well-distributed data lead to cancellation of errors, which is desirable, but give optimistic estimates of variance. The balance of weights presented here leads to an internally consistent solution, which has acceptable agreement with independent data.

Table 12 lists the geocentric coordinates for the stations determined in SE III, together with their uncertainties scaled by $k^2 = 2.625$. Station 7820 (Dakar, Senegal) is not given, the poor agreement and paucity of data precluding reliable results.

Table 12. Geocentric coordinates.

Station	X (Mm)	Y (Mm)	Z (Mm)	σ (m)	Location
7050	1.1306739	-4.8313735	3.9941010	1.81	GREENBELT ,USA
1021	1.1180308	-4.8763213	3.9429730	1.81	BLOSSOM POINT,USA
7060	-5.0689641	3.5841061	1.4587443	2.88	GUAM,USA
7816	4.6543369	1.9591790	3.8843585	2.26	STEPHANION,GREECE
7818	5.4263281	-.2293266	3.3346064	6.07	COLOMB-BECHAR,ALGERIA
8015	4.5783277	.4579748	4.4031797	2.07	HAUTE PROVENCE,FRANCE
7815	4.5783707	.4579591	4.4031355	2.07	HAUTE PROVENCE,FRANCE
7809	4.5783484	.4579659	4.4031579	2.07	HAUTE PROVENCE,FRANCE
9001	-1.5357686	-5.1669890	3.4010425	2.44	ORGAN PASS,USA
7901	-1.5357686	-5.1669890	3.4010425	2.44	ORGAN PASS,USA
9002	5.0561267	2.7165136	-2.7757883	1.79	OLIFANTSFONTEIN,REP.S.AFR.
7902	5.0561265	2.7165135	-2.7757883	1.79	OLIFANTSFONTEIN,REP.S.AFR.
9022	5.0561207	2.7165243	-2.7757870	1.79	OLIFANTSFONTEIN,REP.S.AFR.
9003	-3.9837783	3.7430939	-3.2755610	2.49	WOOMERA,AUSTRALIA
9023	-3.9777668	3.7251061	-3.3030283	2.16	ISLAND LAGOON,AUSTRALIA
9004	5.1055919	-.5552300	3.7696625	3.06	SAN FERNANDO,SPAIN
7804	5.1056120	-.5552523	3.7696312	3.06	SAN FERNANDO,SPAIN
9005	-3.9466906	3.3662957	3.6988334	6.26	TOKYO,JAPAN
9025	-3.9104342	3.3763574	3.7292202	6.26	DODAIRA,JAPAN
9006	1.0182044	5.4711045	3.1096219	2.77	NAINI TAL,INDIA
9007	1.9427769	-5.8040894	-1.7969311	2.11	AREQUIPA,PERU
7907	1.9427770	-5.8040898	-1.7969312	2.11	AREQUIPA,PERU
9027	1.9427718	-5.8040961	-1.7969094	2.11	AREQUIPA,PERU
9008	3.3768929	4.4039823	3.1362578	5.08	SHIRAZ,IRAN
9009	2.2518237	-5.8169157	1.3271635	4.42	CURACAO,ANTILLES
9010	.9762870	-5.6013947	2.8802347	2.86	JUPITER,USA
9011	2.2805913	-4.9145735	-3.3554230	3.19	VILLA DOLORES,ARGENTINA
9012	-5.4660598	-2.4042788	2.2421805	2.72	MAUI,USA
7912	-5.4660630	-2.4042787	2.2421727	2.72	MAUI,USA
9021	-1.9367738	-5.0777083	3.3319024	3.16	MT. HOPKINS,USA
7921	-1.9367727	-5.0777053	3.3319076	3.16	MT. HOPKINS,USA
9028	4.9037652	3.9652160	.9638680	4.85	ADDIS ABABA,ETHIOPIA
9029	5.1864597	-3.6538660	-.6543347	3.86	NATAL,BRAZIL
7929	5.1864599	-3.6538662	-.6543348	3.86	NATAL,BRAZIL
9039	5.1864698	-3.6538452	-.6543344	3.86	NATAL,BRAZIL
9031	1.6938054	-4.1123326	-4.5566531	5.24	COMODORO RIVADAVIA,ARGENTINA
9091	4.5951675	2.0394660	3.9126587	4.11	DIONYSOS,GREECE
7930	4.5952234	2.0394482	3.9126121	4.11	DIONYSOS,GREECE
9030	4.5952145	2.0394480	3.9126220	4.11	DIONYSOS,GREECE
8019	4.5794767	.5866188	4.3864127	10.40	NICE,FRANCE
9066	4.3313047	.5675218	4.6331012	3.67	ZIMMERWALD,SWITZERLAND
9074	3.1838845	1.4214753	5.3228021	20.57	RIGA,LATVIA
9077	3.9074366	1.6024417	4.7638864	83.31	USHGOROD,USSR
9080	3.9201689	-.1347323	5.0127143	13.26	MALVERN,U.K.
9113	-2.4500089	-4.6244149	3.6350288	3.70	ROSAMOND,USA
9114	-1.2648451	-3.4668797	5.1854541	10.87	COLD LAKE,CANADA
9115	3.1212760	.5926423	5.5127109	12.63	HARESTUA,NORWAY
9117	-6.0074079	-1.1118591	1.8257369	7.25	JOHNSTON IS.,USA
4711	-2.3514471	-4.6450706	3.6737600	3.80	CALIFORNIA JPL,USA
4712	-2.3504606	-4.6519699	3.6656247	3.80	CALIFORNIA JPL,USA
4714	-2.3536393	-4.6413332	3.6770483	3.77	CALIFORNIA JPL,USA
4741	-3.9787021	3.7248587	-3.3022081	2.78	AUSTRALIA JPL
4742	-4.4609669	2.6824284	-3.6746138	6.05	AUSTRALIA JPL
4751	5.0854475	2.6682502	-2.7687261	4.73	SO. AFRICA JPL
4761	4.8492411	-.3602972	4.1148673	3.64	SPAIN JPL
4762	4.8466987	-.3702149	4.1168905	3.66	SPAIN JPL
6001	.5465862	-1.3899730	6.1802329	11.15	THULE,GREENLAND
6002	1.1307688	-4.8308360	3.9947002	2.38	BELTSVILLE,USA
6003	-2.1278251	-3.7858474	4.6560279	7.52	MOSES LAKE,USA

Table 12. (Cont.)

Station	X (Mm)	Y (Mm)	Z (Mm)	σ (m)	Location
6004	-3.8517699	.3964305	5.0513354	19.38	SHEMYA,USA
6006	2.1029482	.7216791	5.9581765	13.56	TROMSO,NORWAY
6007	4.4336546	-2.2681407	3.9716410	12.86	AZORES,PORTUGAL
6008	3.6232536	-5.2142311	.6015174	12.95	PARAMARIBO,NETHERLAND
6009	1.2808455	-6.2509435	-.0108277	15.17	QUITO,ECUADOR
6011	-5.4660104	-2.4043979	2.2422163	3.12	MAUI,USA
6012	-5.8585251	1.3945295	2.0937902	13.96	WAKE IS.,USA
6013	-3.5658470	4.1207283	3.3034218	7.56	KANOYA,JAPAN
6015	2.6043786	4.4441667	3.7503171	10.37	MASHHAD,IRAN
6016	4.8964136	1.3161788	3.8566662	10.87	CATANIA,ITALY
6019	2.2806429	-4.9145366	-3.3554419	3.54	VILLA DOLORES,ARGENTINA
6020	-1.8886006	-5.3548647	-2.8957716	19.81	EASTER IS.,CHILE
6022	-6.0999436	-.9973208	-1.5685982	12.65	TUTUILA,AM.SAMOA
6023	-4.9553518	3.8422666	-1.1638598	8.96	THURSDAY IS.,AUSTRALIA
6031	-4.3138010	.8913646	-4.5972827	9.29	INVERCARGILL,NEW ZEALAND
6032	-2.3753707	4.8755672	-3.3454056	10.59	CAVERSHAM,AUSTRALIA
6038	-2.1609779	-5.6426947	2.0353523	8.65	REVILLA GIGEDO,MEXICO
6039	-3.7247525	-4.4211985	-2.6861050	22.12	PITCAIRN IS.,U.K.
6040	-.7419364	6.1908105	-1.3385578	13.24	COCOS IS.,AUSTRALIA
6042	4.9007728	3.9682490	.9663303	4.93	ADDIS ABABA,ETHIOPIA
6043	1.3713935	-3.6147358	-5.0559691	12.76	CERRO SOMBRERO,CHILE
6044	1.0989265	3.6846465	-5.0718835	23.43	HEARD IS.,AUSTRALIA
6045	3.2234594	5.0453453	-2.1918119	9.30	MAURITIUS,U.K.
6047	-3.3619221	5.3658261	.7636214	12.76	ZAMBOANGA,PHILIPPINES
6050	1.1926976	-2.4509877	-5.7470744	19.81	PALMER STA.,ANTARCTIC
6051	1.1113619	2.1692821	-5.8743530	13.95	MAWSON STA.,ANTARCTIC
6052	-.9025718	2.4095500	-5.8165695	13.80	WILKES STA.,ANTARCTIC
6053	-1.3108218	.3112860	-6.2132992	13.45	MCMURDO STA.,ANTARCTIC
6055	6.1183495	-1.5717384	-.8786181	11.14	ASCENSION IS.,U.K.
6059	-5.8853237	-2.4483377	.2216584	10.63	CHRISTMAS IS.,U.K.
6060	-4.7516206	2.7920847	-3.2001812	3.19	CULGOORA,AUSTRALIA
6061	2.9999396	-2.2193526	-5.1552794	15.33	SO. GEORGIA,U.K.
6063	5.8844839	-1.8534891	1.6128432	11.17	DAKAR,SENEGAL
6064	6.0234113	1.6179373	1.3317254	9.89	FORT LAMY,CHAD
6065	4.2135852	.8208359	4.7027662	12.59	HOHENPEISSENBERG,W.GERMANY
6067	5.1864154	-3.6539275	-.6542977	4.13	NATAL,BRAZIL
6068	5.0848489	2.6703463	-2.7681144	2.38	JOHANNESBURG,REP.S.AFR.
6069	4.9784430	-1.0868607	-3.8231816	26.56	TRISTAN DA CUNHA,U.K.
6072	-.9416635	5.9674615	2.0393072	13.65	CHIANG MAI,THAILAND
6073	1.9051653	6.0322878	-.8107365	12.02	CHAGOS,ARCHIPELG
6075	3.6028471	5.2382448	-.5159507	11.39	SEYCHELLES,U.K.
6078	-5.9523041	1.2319412	-1.9259390	22.93	NEW HEBRIDES,U.K.
6111	-2.4488492	-4.6679685	3.5827461	3.83	WRIGHTWOOD,USA
6123	-1.8817815	-.8124227	6.0195886	17.73	POINT BARROW,USA
6134	-2.4489029	-4.6680586	3.5824408	3.89	WRIGHTWOOD,USA

7. COMPARISONS

The combination solution for coordinates scaled by $k^2 = 2.625$ gave estimates of variance of 2 m for the best stations. Since no comparison exists that can verify this accuracy for geocentric coordinates, we are limited to consistency checks. The coordinates should agree with the standard at least as well as the accuracy of the standard. A number of internal checks (e.g., between geometrical and dynamical solutions) can be performed. Comparisons can be made with surface data, but they test only the relative position and not the geocentric position of the coordinates. Nevertheless, these comparisons are instructive and indicate that the computed variances (uncertainties) are realistic estimates. Further, the general agreement internally in the satellite data – and externally with the terrestrial data – indicates that, as a rule, discrepancies are within the expected uncertainties. The large discrepancies are probably due to errors in the survey data, and further analysis is needed.

Comparisons with satellite orbits are inconclusive at best, because of the large number of error sources. In Part V of this Report, numerical results are given for orbit computations with laser data by using the latest gravity field and station coordinates. This comparison indicates that the orbit computing system (data, theory, physical parameters, and station coordinates) has an accuracy of 5 to 10 m, which is not inconsistent with a 2- to 5-m accuracy for the station coordinates.

The typical direction is determined with an accuracy of 5 μrad, equivalent to a relative position of 10 m. For selected sets of stations, Figure 2 compares the determined direction (both before and after the coplanarity condition is applied), the dynamical solution, and the combination solution. In some cases, a direction from the SAO geometrical net and another from the BC-4 geometrical net are available. These comparisons are perhaps unfavorable in that the errors of both stations are reflected in the figures. The error ellipses for all the directions are scaled by the factor

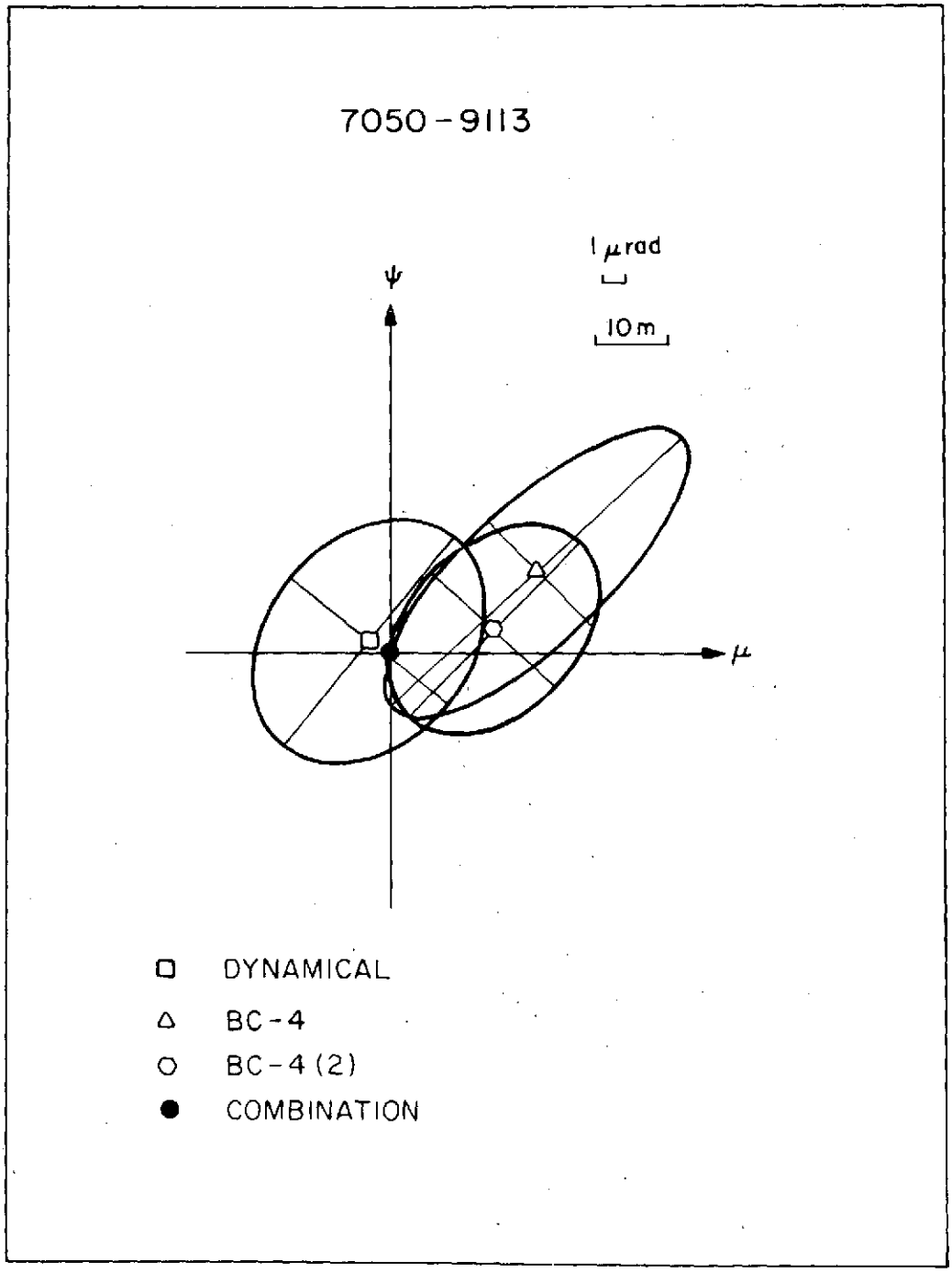

Figure 2. Comparisons of interstation directions from the combination, dynamical, and geometrical solutions. Each of the two geometrical solutions yields two directions. BC-4 (2) and geometrical (2) are the directions obtained from the network adjustment. ψ is in the direction of increasing declination, and μ is in the direction of increasing right ascension.

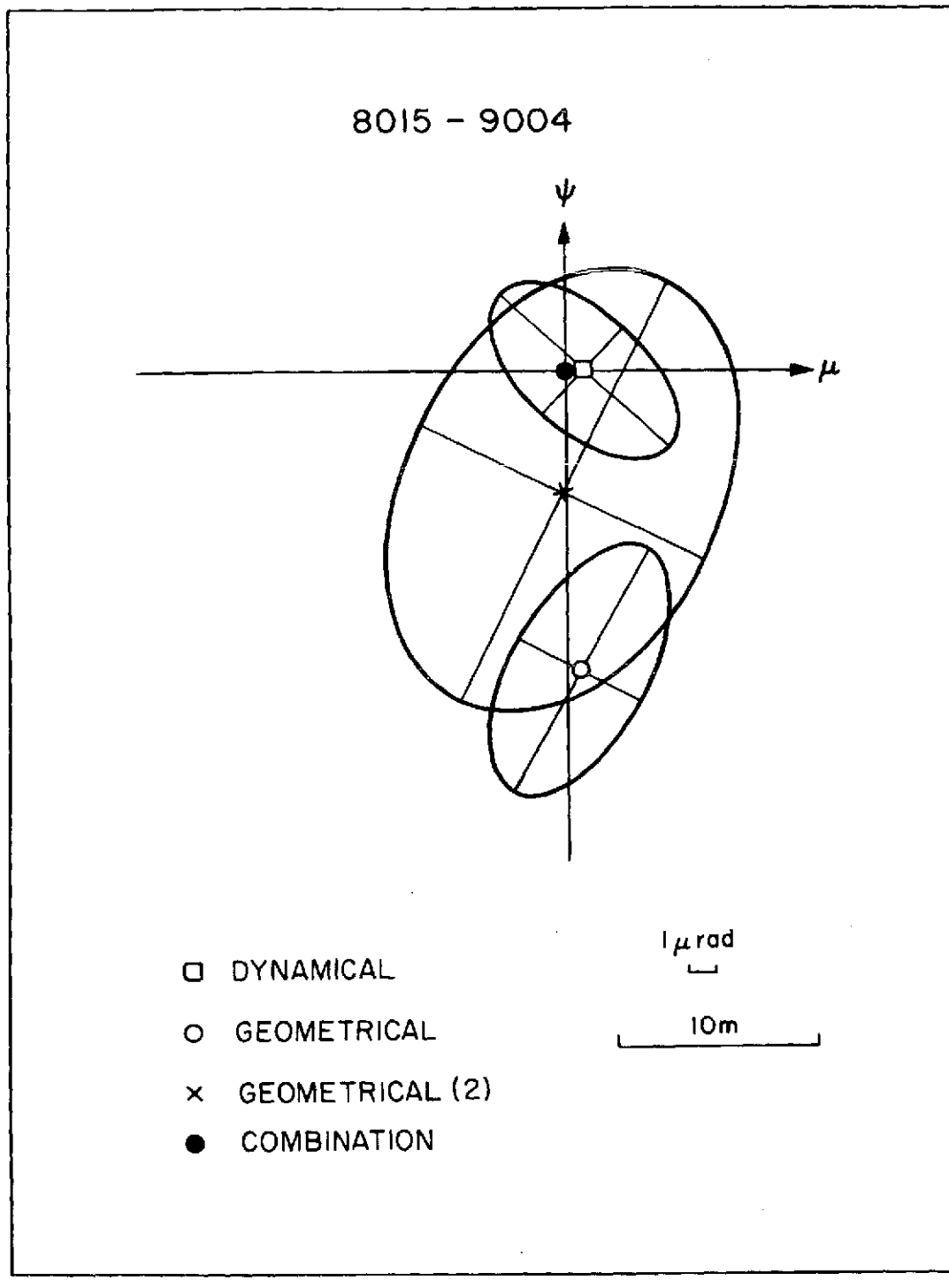

Figure 2. (Cont.)

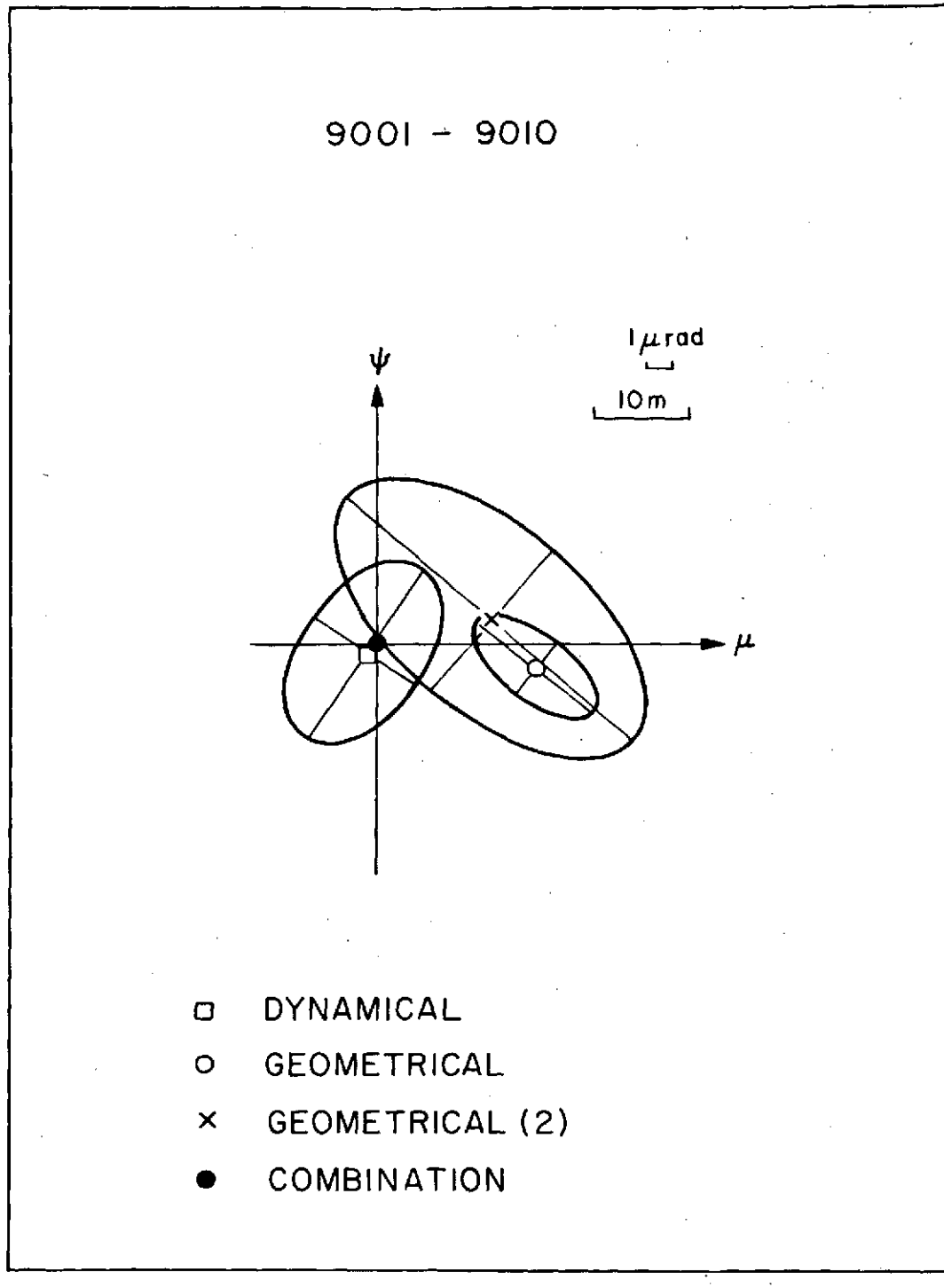

Figure 2. (Cont.)

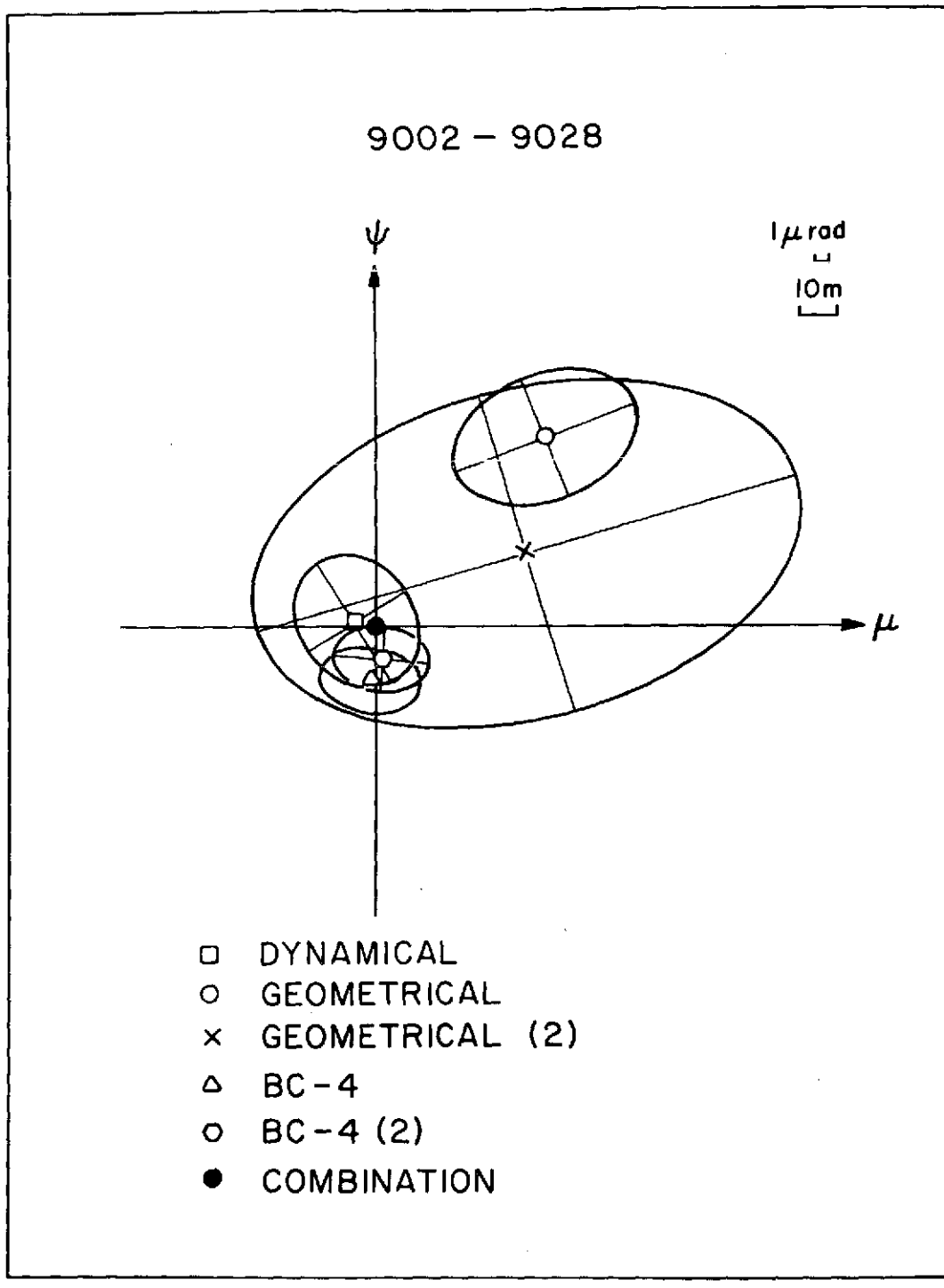

Figure 2. (Cont.)

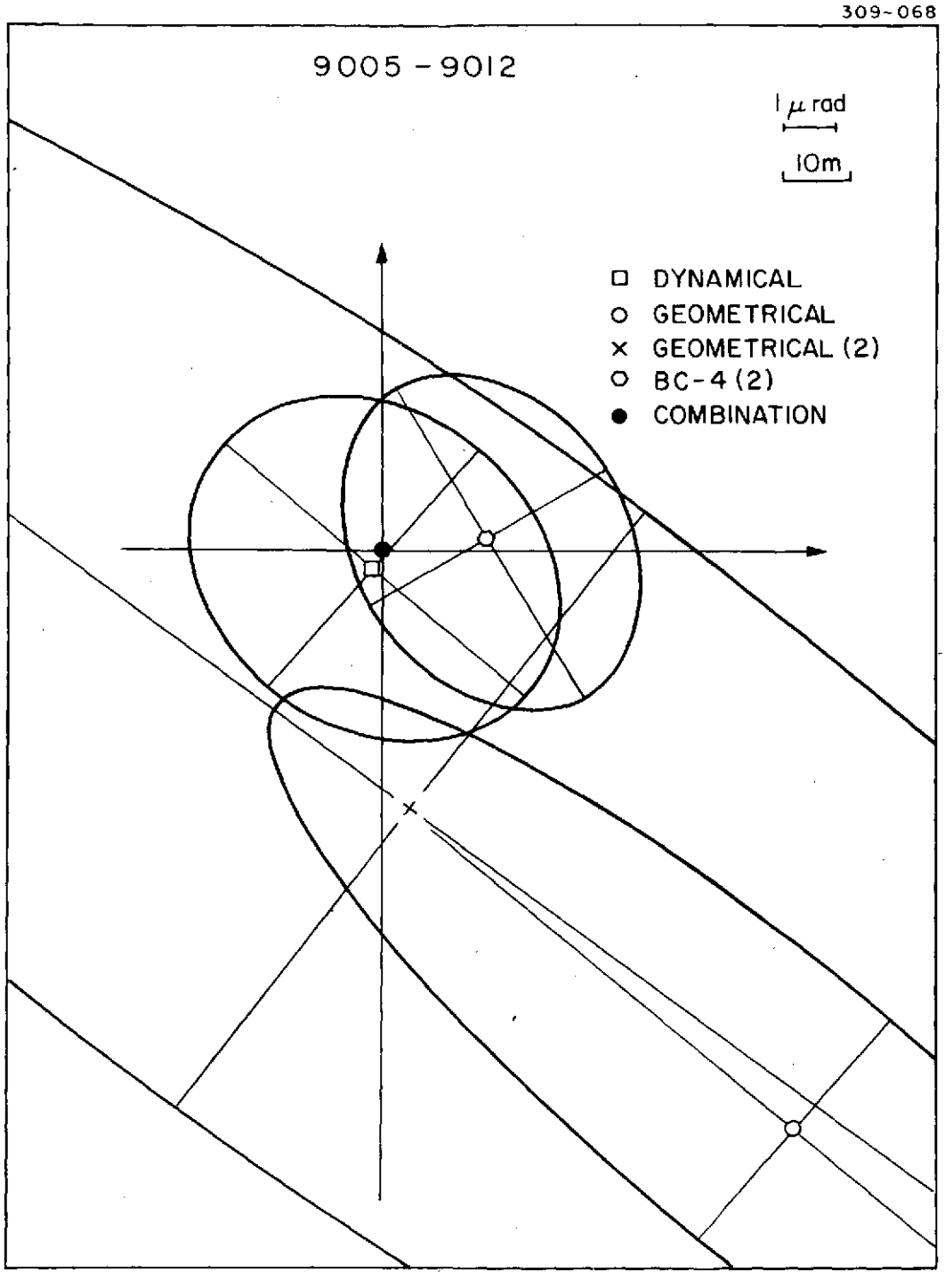

Figure 2. (Cont.)

$k^2 = 2.625$. In order to express all the directions in the same coordinate system, the plotted directions are rotated by the parameters given in Table 11.

When the origin and scale are provided, the BC-4 network of 48 stations gives a geometric solution that can be compared with the combination solution. Table 13 gives the results of such a comparison, with residuals in X, Y, and Z and north, east, and height. The geometrical solution has an average uncertainty of 5 m for each coordinate, while the combined solution has the uncertainty given in Table 12. The adjustment uses a weight computed from the two solutions. The root mean square (rms) of 12 m and the standard error of unit weight $\sigma_0 = 0.8$ indicate the excellent agreement in the coordinates and the estimated uncertainties. A number of individual coordinates are too large. The north–south residual of -25 m for station 6068, which is tied geodetically to 7902 and 4751, is the most troublesome.

The JPL coordinates given by the LS 37 solutions, rotated and scaled by the results in Table 11, are compared in Table 14 with the coordinates determined in the combination solution.

Comparisons within each datum are possible. The four major datums where this was done are as follows:

North American datum (NA27),
South American datum (SA69),
Australian datum (AUGD),
European datum (EU50).

As described earlier, the use of datum coordinates in the combination solution has been restricted to nearby stations, primarily in order to relate different types of observations. Therefore, datum coordinates constitute a relatively independent set of data. However, each datum has an arbitrary origin, orientation, and scale, and the relation between each datum and the geocentric system must be determined. One can therefore determine up to seven parameters, but depending on the size of the datum and the distribution of stations on the datum, some of these transformation parameters may not be significant. The seven transformation parameters are three translations, three rotations, and one scale. We have elected to express the rotations as rotations of the datum origin about the normal to the ellipsoid and around two axes in the tangent plane

Table 13. Comparison of BC-4 geometrical solution with the combination solution (in units of meters). The standard error of unit weight, σ_0, is 0.823.

Station	Weight	Residual ΔX	ΔY	ΔZ	North	East	Height
6001	12.22	0	0	4	0	0	4
6002	5.54	12	-13	9	1	-15	13
6003	9.03	0	- 4	0	- 2	2	2
6004	20.01	2	- 9	1	3	9	0
6006	14.45	- 6	-12	4	11	-10	0
6007	13.80	- 6	- 5	- 1	1	- 7	- 3
6008	13.88	2	- 4	- 4	- 5	0	4
6009	15.97	5	- 5	- 1	- 1	4	6
6011	5.89	15	4	4	9	2	-13
6012	14.83	7	- 2	1	4	0	- 6
6013	9.06	- 1	- 8	12	13	6	1
6015	11.51	- 5	- 9	7	12	0	- 4
6016	11.96	- 5	-11	3	8	-10	- 4
6019	6.13	13	3	- 5	- 3	13	5
6020	20.43	3	5	- 6	- 8	1	- 2
6022	13.60	7	6	- 1	- 3	- 4	- 8
6023	10.26	- 2	3	0	1	- 1	4
6031	10.55	- 2	4	- 9	- 4	- 4	9
6032	11.71	1	7	- 4	0	- 4	6
6038	9.99	4	5	- 1	0	2	- 6
6039	22.68	4	7	- 4	- 7	- 2	- 5
6040	14.15	- 1	0	0	0	1	0
6042	7.02	- 3	- 7	5	6	- 3	- 6
6043	13.70	11	8	- 8	- 8	13	4
6044	23.96	4	7	- 5	3	- 2	10
6045	10.56	- 5	- 1	- 7	- 8	3	- 1
6047	13.70	0	0	5	5	0	1
6050	20.43	10	2	- 6	0	10	6
6051	14.82	5	4	-10	1	- 2	12
6052	14.68	4	5	- 9	0	- 5	10
6053	14.35	3	5	-12	- 5	- 5	11
6055	12.21	- 9	0	11	10	- 1	-11
6059	11.75	9	5	- 2	- 2	- 1	-11
6060	5.93	- 3	3	- 8	- 5	- 1	8
6061	16.12	8	3	- 4	1	8	6
6063	12.24	- 8	- 2	0	2	- 4	- 7
6064	11.08	- 6	-12	5	7	-10	- 7
6065	13.55	- 6	-12	4	9	-11	- 2
6067	6.49	- 5	13	10	9	7	-13
6068	5.54	- 4	- 3	-24	-24	0	5
6069	27.03	- 8	2	5	0	0	-10
6072	14.54	- 3	- 1	9	9	4	1
6073	13.02	- 7	- 2	0	0	6	- 4
6075	12.44	- 4	- 2	1	1	1	- 4
6078	23.47	- 8	3	9	12	- 1	5
6111	6.30	3	2	7	8	2	1
6123	18.42	1	-13	2	- 3	12	3
6134	6.33	4	12	6	12	- 1	- 7
					rms: 7.35	6.33	7.10

Total rms: 12.02

Parameters Determined

	X	Y	Z
Translation (m)	16.32 ± 1.22	23.21 ± 1.22	-4.68 ± 1.22
Rotation	- 0".101 ± 0".050	0".086 ± 0".050	0".388 ± 0".046

Scale (ppm) = 1.17 ± 0.19

oriented north–south and east–west. These rotations have a physical interpretation since they express an error in the azimuth of orientation of the datum and a tilt of the datum ellipsoid. Accordingly, the transformation will be given by

$$\bar{X}_{sat} = \bar{X}_{dat} + \bar{T} + (1 + K)\,\bar{\bar{R}}\,(\bar{X}_{dat} - \bar{X}_0) \quad ,$$

where $\bar{X}_{sat}$ and $\bar{X}_{dat}$ are the coordinates from the satellite solution and the datum, respectively, $\bar{T}$ is the vector of the three translation parameters, K is the scale correction, $\bar{X}_0$ are the coordinates of the datum origin, and $\bar{\bar{R}}$ is a rotation matrix dependent on the three rotational parameters and the latitude and longitude of the datum origin.

Table 14. JPL–SAO residuals.

Rotation: -3.43 ± 1.02 μrad
Scale: $1.8 \times 10^{-7} \pm 5.5 \times 10^{-7}$

Station	R (m)	λ (m)
4711	-0.81	2.69
4712	-0.66	2.63
4714	-0.86	2.57
4741	4.31	-0.21
4742	0.51	1.66
4751	0.96	-3.03
4761	-0.26	2.10
4762	-0.31	2.31

Table 15 gives the translation, rotation, and scale parameters for four major datums as computed from the adjustment of the datum coordinates to the satellite solution. A positive scale here means that the datum scale has to be increased in order to agree with the satellite scale. The table also gives the number of stations used in each datum. In the computation of datum shifts, each station was assigned a weight computed from the standard deviation of the satellite solution and the standard deviation of the datum coordinates, which was taken as $\sigma = 5 \times (S \times 10^{-6})^{2/3}$ (m),

Table 15. Translation, rotation, and scale parameters for the four major datums.

Datum	Number of stations	Translation (m)			Rotation			Scale correction (ppm)	σ_0	σ (m)
		X	Y	Z	Azimuth	E–W	N–S			
NA27	10	- 31.4	154.0	176.3	0!!09	-0!!62	-0!!23	1.78	0.67	8
		± 1.9	± 2.2	± 1.9	±0.24	±0.69	±0.24	±1.13		
EU50	17	- 85.4	-111.1	-131.9	0.56	-0.51	-0.22	2.60	0.59	16
		± 2.0	± 1.9	± 2.0	±0.21	±0.35	±0.22	±0.92		
SA69	8	- 75.3	- 3.3	- 52.2	-0.33	-0.13	-0.33	-1.39	0.61	14
		± 2.5	± 2.6	± 2.5	±0.21	±0.27	±0.33	±0.99		
AUGD	7	-118.2	- 38.6	+119.6	0.23	0.82	-0.22	2.33	0.35	5
		± 1.5	± 1.4	± 1.4	±0.26	±0.41	±0.31	±1.22		

where S is the distance of the station from the datum origin in meters. In all cases, the standard deviation of unit weight σ_0 (given in Table 15) after the adjustment is smaller than 1, which means that the weights are somewhat pessimistic. The root mean squares σ (m) of the final residuals for each datum in Table 15 are between 5 and 16 m. It is apparent that the European and the South American datum coordinates do not agree very well with the satellite solution. The European datum is rather unhomogeneous, and its extension into Africa and Asia – which we used – makes it rather weak.

Further checks with datum information can be obtained with station heights. The height above the reference ellipsoid (h_{ell}) should be equal to the mean height above sea level (h_{msl}), which is approximately the height above the geoid, plus the geoid height N; i.e., the disagreement between these two estimates, Δh, is

$$\Delta h = h_{ell} - h_{msl} - N \quad .$$

If we use the satellite geoid to calculate N, we can make this comparison for all stations but we lose the detailed variation in geoid height. The computation does provide a value for the semimajor axis of the best-fitting ellipsoid used to calculate h_{ell}. We get

$$a_e = 6378140.4 \pm 1.2 \text{ m} \quad .$$

To employ the detailed geoid-height information given for each datum in Table 10, we must refer the coordinates to the datum origin by using the datum shifts in Table 15. Table 16 lists the standard deviations of the heights calculated for each datum. The average of 3.98 m must be considered excellent in view of all the uncertainties in calculating Δh. Figure 3 plots these residual heights as a function of latitude.

The results by Gaposchkin and Lambeck (1970) were derived in the same manner, by combining several types of data, establishing relative weights, and verifying the accuracy by intercomparison. Their accuracy was 7 to 10 m for the fundamental stations. In Table 17, we give the corrections derived in this analysis for selected stations. The overall rms of σ = 10 m and a standard error of unit weight $\sigma_0 = 0.662$ indicate excellent agreement in the derived coordinates and the accuracy estimates; if anything, the accuracy estimates are pessimistic. The very small shift in origin indicates that the whole reference system has not changed.

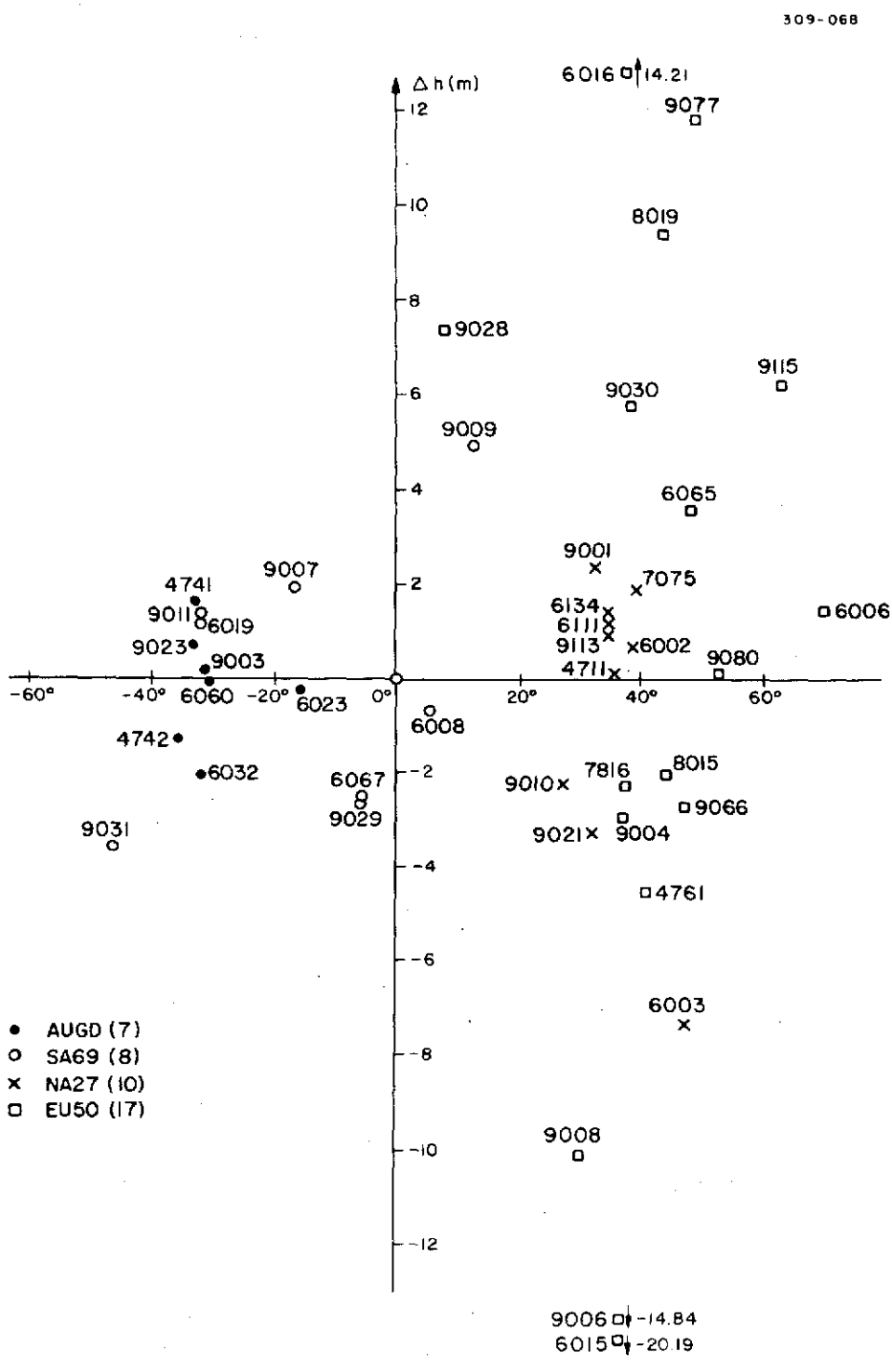

Figure 3. Geoid-height comparison as a function of latitude $\Delta h = h_{ell} - h_{msl} - N_{datum\ geoid} - \bar{h}$ datum mean, where h_{ell} is transformed by the appropriate datum-shift parameters. $\sigma_{\Delta h} = 3.98$ m.

Table 16. Standard deviations of datum-height comparisons.

Datum	σ (m)
NA27	3.07
SA69	2.69
AUGD	1.25
EU50	8.90
Average:	3.98

Williams, Mulholland, and Bender (1972) have determined the spin-axis distance of McDonald Observatory from lunar laser observations. We compare this distance with that deduced by means of the coordinates of station 9001 from survey data in the following. The agreement of -3.51 m must be considered acceptable.

Using SAO station 9001 and geodetic tie	5492412.489 m
Using McDonald lunar laser	5492416.0 ± 3 m
Difference	-3.51 m

The scale of the combination solution is defined by the value of GM adopted in the dynamical solution, given in Table 6. We found a scale difference of 0.18 ± 0.55 ppm between the JPL and the SAO coordinates, the JPL ones being slightly larger. If the discrepancy with the lunar laser is attributed to scale, then the scale difference would be 0.7 ppm. The scale obtained from the four major datums is given in Table 15. It appears from the NA27, EU50, and AUGD datums that the datum scale is smaller than the satellite scale by approximately 2 ± 1 ppm, while from the SA69 datum, it is larger by 1 ± 1 ppm. Since the survey scales are not expected to be established to better than a few ppm, the weighted mean of 1.6 ± 1 ppm is not considered to be significantly different from zero.

Each geometrical network has an arbitrary origin specified by the initial coordinates of one station, a station not explicitly determined in the combination solution. The translation parameters in Table 11 correspond to the correction to the origin of the network, i.e., the correction to the initial coordinates of the reference station.

Table 17. Comparison of coordinates determined in both SE II and SE III. The systematic translation, rotation, and scale differences were removed before the residuals were computed (in units of meters). The standard error of unit weight, σ_0, is 0.662.

Station	Weight	Residual ΔX	ΔY	ΔZ	North	East	Height
7050	7.23	1	- 6	- 9	-12	0	0
8015	5.41	0	7	0	0	7	0
9001	5.58	- 8	4	0	1	- 9	- 1
9002	7.23	1	0	- 3	- 2	- 1	2
9003	6.50	0	0	4	3	0	- 1
9004	5.86	3	- 3	- 4	- 5	- 3	0
9005	11.80	3	- 8	- 1	3	4	- 7
9006	9.42	0	- 2	- 2	- 1	- 1	- 3
9007	7.31	5	-10	3	6	1	10
9008	10.33	- 1	2	6	5	2	4
9009	8.28	- 2	1	4	5	- 1	- 1
9010	5.76	- 1	1	- 4	- 3	- 1	- 3
9011	9.55	5	- 2	5	7	3	1
9012	7.51	- 3	- 1	8	6	0	6
9021	15.33	11	- 6	-13	-13	12	- 5
9023	6.38	1	- 2	5	3	0	- 5
9028	12.94	14	11	- 4	- 6	0	17
9029	12.61	0	-11	- 7	- 7	- 9	7
9031	15.89	5	- 7	- 1	5	2	7
9066	7.90	- 5	8	7	8	9	2
9080	16.03	- 9	4	5	11	3	- 1
9113	7.92	4	3	- 6	- 2	2	- 8
9114	16.19	- 5	2	-13	- 7	- 5	-11
9115	21.18	- 4	- 2	8	8	- 1	5
9117	16.66	- 2	- 4	5	4	4	4
				rms:	6.62	5.02	6.37
				Total rms:	10.47		

	Parameters Determined		
	X	Y	Z
Translation (m)	-1.69 ± 1.19	3.76 ± 1.18	0.04 ± 1.18
Rotation	-0".039 ± 0".047	-0".043 ± 0".049	-0".059 ± 0".044
	Scale (ppm) = -0.26 ± 0.18		

In principle, the orientation of the two geometrical systems and that of the dynamical system should be identical. Orientation parameters ($\epsilon_x, \epsilon_y, \epsilon_z$) are determined to accommodate possible systematic differences in the actual representation of the three systems. Since the SAO geometrical network covers only one hemisphere in an east–west orientation, the orientation of its pole (ϵ_x, ϵ_y) may be poorly determined.

The polar orientation of the BC-4 system with respect to the SAO dynamical system is $1.88 = \sqrt{1.76^2 + 0.65^2} \pm 1.16$ μrad. This systematic difference is obtained by comparing the observed BC-4 directions with directions determined from 11 stations in the combination solution with characteristic interstation distances of 2 to 3 Mm. In metric terms, the orientation difference is $1.88 \times 10^{-6} \times 2 \times 10^6 \approx 4$ m. The accuracy of the mean station for the 11 stations is approximately 4 m. It is assumed that the value of 1.88 μrad results from differences in pole-position data or in processing methods.

The rotation in longitude (ϵ_z) corresponds to a correction in UT1. Figure 4 indicates the relative position of the zero meridian of each system. We note almost the same relation between the SAO and the JPL systems that we found in SE II, which was 4.0 μrad. The difference between the SAO geometrical and the SAO dynamical systems is -0.40 ± 1.43, and that between BC-4 and the SAO dynamical is -2.20 ± 0.82. The relative rotation in longitude between the JPL and the SAO systems is probably due to a difference between the JPL's planetary ephemeris and the FK4 system used by SAO, while that between the geometrical and dynamical nets most likely results from differences in the UT1 data or in the processing methods.

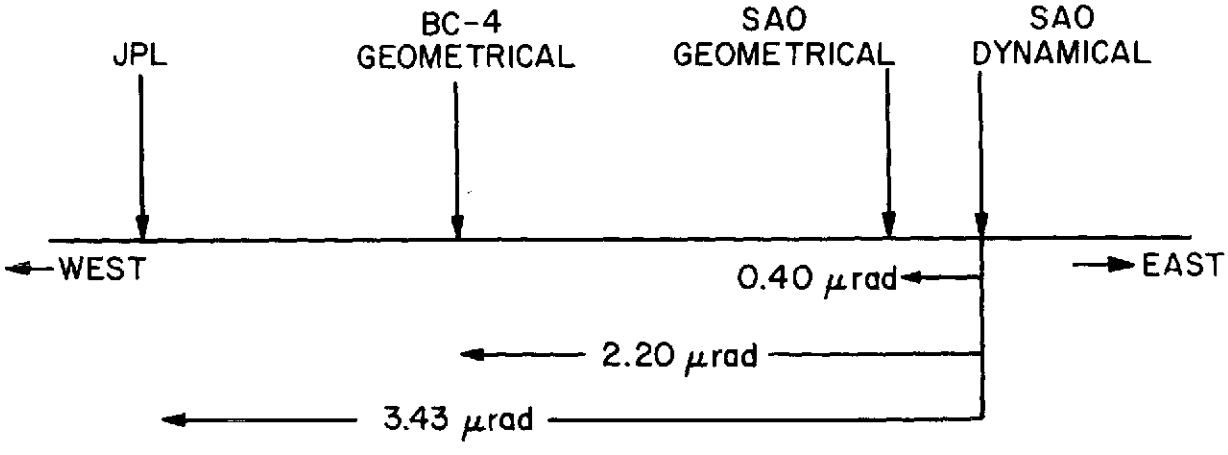

Figure 4. The relative zero meridians of the different systems.

8. CONCLUSIONS

The results described above, the procedures, the tests and comparisons, and the experience of carrying out the work have led to the following conclusions about the use of artificial satellites for the determination of station coordinates:

A. Observations of close-earth satellites have been successfully combined with observations of deep-space probes and surface triangulation, enabling us to determine the coordinates of 90 satellite-tracking sites in a uniform homogeneous system.

B. The combination of these data provides a better solution than we can obtain from each set of data separately, because more complete coverage results and because the combination enables us to overcome weaknesses in each system.

C. The methods of processing each type of data are sufficiently understood to make a rational combination.

D. Successive solutions have resulted in improvements. When compared with the previous solution, each new one has agreed to within the estimated uncertainty, and that uncertainty has steadily decreased from 10 to 20 m in 1966, to 5 to 10 m in 1969, to 2 to 8 m in 1973.

E. Formal statistics are generally optimistic, and therefore the uncertainty in coordinates is established by intercomparison, a method that has proved reliable.

F. A comparison between coordinates indicates an accuracy of 2 to 4 m for fundamental stations and 5 to 10 m for most others.

G. The body of laser data available, though small, has made a significant contribution. The laser data dominate the solution through the relatively great weight assigned and thereby essentially establish the reference frame for the station coordinates.

H. The use of a variety of satellite orbits spanning a considerable period of time is very important. Such data average over error sources with a slow variation such as UT1 or epoch timing and eliminate poor orbital geometry. The laser data suffered from both problems.

I. Geometrical data require a minimum of assumptions, and geometrical solutions have relatively straightforward statistics. Geometrical data are more difficult to obtain owing to the necessity of simultaneous observations. Dynamical data are more plentiful, but their processing requires an elaborate orbit-computation program that may introduce model errors. The well-behaved statistical properties of the geometrical data allowed the use of the geometrical networks to establish the uncertainties.

J. Small but significant systematic differences in scale and orientation are found between satellite coordinate systems. These differences may result from variations in data-processing methods or from fundamental and obscure differences in the definition of reference systems, e.g., the FK4 system and the JPL planetary ephemeris.

K. Satellite determinations of site location are now sufficiently accurate to verify terrestrial survey data. The most troublesome part of the analysis was finding the erroneous survey coordinates. Considerable effort remains in providing global geodetic coordinates with sufficient reliability.

L. Scale obtained for the four major datums is systematically smaller than the satellite results by 1.6 ± 1 ppm. Since survey scales are not expected to be established to better than a few ppm, this result is not considered to be significantly different from zero.

REFERENCES AND BIBLIOGRAPHY

REFERENCES AND BIBLIOGRAPHY

AARDOOM, L., GIRNIUS, A., and VEIS, G.

1966. Geometric methods. In Geodetic Parameters for a 1966 Smithsonian Institution Standard Earth, ed. by C. A. Lundquist and G. Veis, Smithsonian Astrophys. Obs. Spec. Rep. No. 200, vol. 1, pp. 63-75.

1967. Determination of the absolute space directions between Baker-Nunn camera stations. In The Use of Artificial Satellites for Geodesy, ed. by G. Veis, National Tech. Univ., Athens, vol. II, pp. 315-344.

AERONAUTICAL CHART AND INFORMATION CENTER

1971. 1° × 1° Mean Free-Air Gravity Anomalies. ACIC Reference Publ. No. 29, August, 324 pp.

AKSNES, K.

1970. A second-order artificial satellite theory based on an intermediate orbit. Astron. Journ., vol. 75, pp. 1066-1076.

1972. A note on the relationship and agreement between two satellite theories. In SAO ISAGEX Experience. I. Data Acquisition, ed. by E. M. Gaposchkin, Smithsonian Astrophys. Obs., Cambridge, Mass., May, pp. 139-143.

ANDERLE, R. J.

1965a. Geodetic parameter set NWL-5E-6 based on doppler satellite observations. Naval Weapons Lab. Rep. No. NWL-1978, 30 pp.

1965b. Observations of resonance effects on satellite orbits arising from the thirteenth and fourteenth order tesseral gravitational coefficients. Journ. Geophys. Res., vol. 70, pp. 2453-2458.

1966. Computational methods employed with doppler observations and derivation of geodetic results. In Trajectories of Artificial Celestial Bodies, ed. by J. Kovalevsky, Springer-Verlag, Berlin, pp. 178-193.

1967a. Geodetic parameter set NWL-5E-6 based on doppler satellite observations. In The Use of Artificial Satellites for Geodesy, ed. by G. Veis, National Tech. Univ., Athens, vol. II, pp. 197-220.

Pages 365 thru 366 blank

ANDERLE, R. J.

1967b. Determination of the earth's geoid by satellite observations. In Mantles of the Earth and Terrestrial Planets, ed. by S. K. Runcorn, Interscience Publ., London, pp. 150-162.

1974. Transformation of terrestrial survey data to doppler satellite datum. Journ. Geophys. Res., in press.

ANDERLE, R. J., and SMITH, S. J.

1967. NWL-8D geodetic parameters based on doppler satellite observations. Naval Weapons Lab. Tech. Rep. No. 2016, 12 pp.

1968. Observation of twenty-seventh and twenty-eighth order gravity coefficients based on doppler observations. Journ. Astronaut. Sci., vol. 15, pp. 1-4.

ANDERSON, P. H., LEHR, C. G., MAESTRE, L. A., HALSEY, H. W., and SNYDER, G. L.

1966. The two-way transmission of a ruby-laser beam between earth and a retroreflecting satellite. Proc. IEEE, vol. 54, pp. 426-427.

ANDOYER, H.

1903. Contribution à la théorie des petites planètes dont le moyen mouvement est sensiblement double de celui de Jupiter. Bull. Astron., vol. 20, pp. 321-356.

ARLEY, N., and BUCH, K. R.

1950. Introduction to the Theory of Probability and Statistics. John Wiley, New York, 236 pp.

ARNOLD, D. A.

1972. Calculation of retroreflector array transfer functions. Final Report, NASA Grant NGR 09-015-196, Smithsonian Astrophys. Obs., December, 57 pp.

ARNOLD, K.

1965. The orbits of artificial earth satellites as a function of gravity anomalies. Deutsche Akademie der Wissenschaften zu Berlin: Veroffentlichungen des Geodatischen Instituts in Potsdam No. 27, 17 pp.

1966. On the influence of gravity anomalies on satellite orbits. In Gravity Anomalies: Unsurveyed Areas, ed. by H. Orlin, Amer. Geophys. Union Monograph No. 9, pp. 137-142.

ARNOLD, K.

1972. Determination of gravity anomalies by satellite geodesy. In The Use of Artificial Satellites for Geodesy, ed. by S. W. Henriksen, A. Mancini, and B. H. Chovitz, Amer. Geophys. Union Monograph No. 15, pp. 177-179.

BARRAR, R. B.

1970. Convergence of the Von Zeipel procedure. Celestial Mech., vol. 2, pp. 494-504.

BOMFORD, G.

1962. Geodesy. Second ed., Oxford Univ. Press, London, 561 pp.

BRACHET, G.

1970. International Satellite Geodesy Experiment Plan. Prepared by Département Géodésie Spatiale, Division Mathematique et Traitement Centre Spatial de Bretigny, CNES, November, 92 pp.

BROUCKE, R.

1971. Construction of rational and negative powers of a formal series. Commun. Assoc. Comp. Mach., vol. 14, pp. 32-35.

BROUWER, D.

1959. Solution of the problem of artificial satellite theory without drag. Astron. Journ., vol. 64, pp. 378-397.

BROUWER, D., and CLEMENCE, G. M.

1961. Methods of Celestial Mechanics. Academic Press, New York, 598 pp.

CAYLEY, A.

1961. Tables of the developments of functions in the theory of elliptic motion. Mem. Roy. Astron. Soc., vol. 29, pp. 191-306.

CAZENAVE, A., and DARGNIES, O.

1971. Détermination d'une base géodésique à longue distance. In Space Research XI, ed. by K. Ya. Kondratyev, M. J. Rycroft, and C. Sagan, Akademie-Verlag, Berlin, pp. 499-506.

CAZENAVE, A., and FORESTIER, F.

1971. Determination of the equations of condition for the zonal harmonics using the DIAL satellite. In Space Research XI, ed. by K. Ya. Kondratyev, M. J. Rycroft, and C. Sagan, Akademie-Verlag, Berlin, pp. 521-524.

CAZENAVE, A., FORESTIER, F., NOUEL, F., and PIEPLU, J. L.

1971. Improvement of zonal harmonics using observations of low inclination satellites, Dial, SAS and Peole. Presented at the International Association of Geodesy Meeting, Moscow, August.

CHERNIACK, J. R.

1972. Computation of Hansen coefficients. Smithsonian Astrophys. Obs. Spec. Rep. No. 346, 25 pp.

1973. A more general system for Poisson series manipulation. Celestial Mech., vol. 7, pp. 107-121.

CHERNIACK, J. R., and GAPOSCHKIN, E. M.

1963. Smithsonian Astrophysical Observatory program writeup (SCROGE). Smithsonian Astrophys. Obs. Spec. Rep. No. 121, 18 pp.

DOUGLAS, B. C., and MARSH, J. G.

1970. GEOS-II and 13th order terms of the geopotential. Celestial Mech., vol. 1, pp. 479-490.

EICHHORN, H., and GOOGE, W. D.

1968. The improvement of star catalogues by the incorporation of new data. Astron. Nachr., vol. 291, pp. 125-127.

ESAENA

1961. Explanatory Supplement to the Astronomical Ephemeris and the American Ephemeris and Nautical Almanac. Her Majesty's Stationery Office, London.

FAIRMAN, J. B., and VEIS, G.

1958. Charts of predicted satellite positions. Smithsonian Astrophys. Obs. Spec. Rep. No. 11, pp. 24-26.

GAPOSCHKIN, E. M.

1964. Differential orbit improvement (DØI-3). Smithsonian Astrophys. Obs. Spec. Rep. No. 161, 70 pp.

1966. Orbit determination. In Geodetic Parameters for a 1966 Smithsonian Institution Standard Earth, ed. by C. A. Lundquist and G. Veis, Smithsonian Astrophys. Obs. Spec. Rep. No. 200, vol. 1, pp. 77-183.

1967. A dynamical solution for the tesseral harmonics of the geopotential and station coordinates using Baker-Nunn data. In Space Research VII, ed. by R. L. Smith-Rose, S. A. Bowhill, and J. W. King, North-Holland Publ. Co., Amsterdam, pp. 683-693.

GAPOSCHKIN, E. M.

1970a. Improved values for the tesseral harmonics of the geopotential and station coordinates. In Dynamics of Satellites 1969, ed. by B. Morando, Springer-Verlag, Berlin, pp. 109-118.

1970b. Future uses of laser tracking for dynamical satellite geodesy. Presented at the Geos B review meeting, Goddard Space Flight Center, National Aeronautics and Space Administration, May.

1972a. SAO ISAGEX Experience (editor). Smithsonian Astrophys. Obs., internal distribution, May.

1972b. Empirical data and the variance-covariance matrix for the 1969 Smithsonian Standard Earth (II). Smithsonian Astrophys. Obs. Spec. Rep. No. 342, 60 pp.

1973. Smithsonian Standard Earth III (abstract). Trans. Amer. Geophys. Union, vol. 54, p. 229.

GAPOSCHKIN, E. M., CHERNIACK, J. R., BRIGGS, R., and BENIMA, B.

1971. Third-order oblateness perturbations from artificial satellites. Presented at the Third Symposium of Artificial Satellites for Geodesy, Washington, D.C., April.

GAPOSCHKIN, E. M., KAULA, W. M., and LAMBECK, K.

1970. 1969 Smithsonian Standard Earth and global tectonics. In Gravimetric and Geometric Investigations with Geos 1 and Geos 2, vol. I of Proc. Geos Program Review Meeting, ed. by Computer Sciences Corp., NASA, Washington, D.C., pp. 7-59.

GAPOSCHKIN, E. M., and LAMBECK, K.

1970. 1969 Smithsonian Standard Earth (II). Smithsonian Astrophys. Obs. Spec. Rep. No. 315, 93 pp.

1971. The earth's gravity field to sixteenth degree and station coordinates from satellite and terrestrial data. Journ. Geophys. Res., vol. 76, pp. 4855-4883.

GAPOSCHKIN, E. M., LATIMER, J., and VEIS, G.

1973. Smithsonian Institution Standard Earth III. Coordinates. Presented at the First International Symposium on the Use of Artificial Satellites for Geodesy and Geodynamics, Athens, May; also Part VI of this Report.

GAPOSCHKIN, E. M., and VEIS, G.

1968. Comparison of and results obtained from observing systems. In Space Research VIII, ed. by A. P. Mitra, L. G. Jacchia, and W. S. Newman, North-Holland Publ. Co., Amsterdam, pp. 42-51.

GAPOSCHKIN, E. M., VEIS, G., KOZAI, Y., and WEIFFENBACH, G.

1971. Geodetic studies at the Smithsonian Astrophysical Observatory. Presented at the XVth General Assembly of the International Union of Geodesy and Geophysics, Moscow, August.

GARFINKLE, B.

1963. On the critical inclination for satellite orbits of any eccentricity (abstract). In The Use of Artificial Satellites for Geodesy, ed. by G. Veis, North-Holland Publ. Co., Amsterdam, p. 41.

GIACAGLIA, G. E. O.

1973. Lunar perturbations on artificial satellites of the earth. Smithsonian Astrophys. Obs. Spec. Rep. No. 352, 59 pp.; also in Celestial Mech., in press.

GIACAGLIA, G. E. O., and LUNDQUIST, C. A.

1971. Sampling functions as an alternative to spherical harmonics. In Rotation of the Earth, Proc. IAU Symp. No. 48, ed. by S. Yumi, Sasaki Printing and Publ. Co., Sendai, Japan, pp. 149-153.

1972. Sampling functions for geophysics. Smithsonian Astrophys. Obs. Spec. Rep. No. 344, 93 pp.

GOLDSTEIN, H.

1959. Classical Mechanics. Addison-Wesley Publ. Co., Reading, Mass., 399 pp.

GUIER, W. H., and NEWTON, R. R.

1965. The earth's gravity field as deduced from the doppler tracking of five satellites. Journ. Geophys. Res., vol. 70, pp. 4613-4626.

HAEFNER, R. R.

1967. The precise reduction of Baker-Nunn films at the Smithsonian Astrophysical Observatory. In The Use of Artificial Satellites for Geodesy, ed. by G. Veis, National Technical University, Athens, vol. II, pp. 81-94.

HAEFNER, R. R., and MARTIN, R.

1966. Data reduction. In Geodetic Parameters for a 1966 Smithsonian Institution Standard Earth, ed. by C. A. Lundquist and G. Veis, Smithsonian Astrophys. Obs. Spec. Rep. No. 200, vol. 1, pp. 43-62.

HAGIHARA, Y.

1961. The stability of the solar system. In Planets and Satellites, ed. by G. P. Kuiper and B. M. Middlehurst, vol. III of The Solar System, Univ. Chicago Press, Chicago, pp. 95-158.

1970. Celestial Mechanics. Vol. 1: Dynamical Principles and Transformation Theory. The MIT Press, Cambridge, Mass., 689 pp.

1972. Celestial Mechanics. Vol. 2: Perturbation Theory. The MIT Press, Cambridge, Mass., 919 pp.

HAGIHARA, Y., and KOZAI, Y.

1961. The critical inclination case of the satellite motion (abstract). Astron. Journ., vol. 66, p. 45.

HALL, N. M., and CHERNIACK, J. R.

1969. Smithsonian Package for Algebra and Symbolic Mathematics. Smithsonian Astrophys. Obs. Spec. Rep. No. 291, 49 pp.

HARAMUNDANIS, K.

1967. Experience of the Smithsonian Astrophysical Observatory in the construction and use of star catalogues. Astron. Journ., vol. 72, pp. 588-596.

1970. Comparison of the SAO Star Catalog with Cape Catalogues from -64° to -90°. Smithsonian Astrophys. Obs. Spec. Rep. No. 325, 14 pp.

HARAMUNDANIS, K., and VEIS, G.

1971. The SAO Star Catalog. Presented at the XVth General Assembly of the International Union of Geodesy and Geophysics, Moscow, August.

HAYES, E. N.

1968. Trackers of the Skies. Howard A. Doyle Publ. Co., Cambridge, Mass., 169 pp.

HEISKANEN, W. A., and MORITZ, H.

1967. Physical Geodesy. W. H. Freeman and Co., San Francisco, 364 pp.

HEISKANEN, W. A., and VENING-MEINESZ, F. A.

1958. The Earth and Its Gravity Field. McGraw-Hill Book Co., New York, 470 pp.

HENDERSHOTT, M. C.

1972. The effects of solid earth deformation on global ocean tides. Geophys. Journ. Roy. Astron. Soc., vol. 29, pp. 389-403.

1973. Ocean tides. EOS, Trans. Amer. Geophys. Union, vol. 54, pp. 76-86.

HILLER, H., and KING-HELE, D. G.

1972. Equations for 15th-order geopotential coefficients from the orbit of Transit 1B. Planet. Space Sci., vol. 20, pp. 1213-1228.

HOBSON, E. W.

1955. The Theory of Spherical and Ellipsoidal Harmonics. Chelsea Publ. Co., New York, 500 pp.

HOLLAND, B. B.

1973. Uses of geoceiver as a geodetic instrument. In Space Research XIII, ed. by M. J. Rycroft and S. K. Runcorn, Akademie-Verlag, Berlin, pp. 65-72.

HORI, G.

1966. Theory of general perturbations with unspecified canonical variables. Publ. Astron. Soc. Japan, vol. 18, pp. 287-296.

IZSAK, I. G.

1962. Differential orbit improvement with the use of rotated residuals. In Space Age Astronomy, ed. by A. J. Deutsch and W. B. Klemperer, Academic Press, New York, pp. 151-157.

1963a. Tesseral harmonics in the geopotential. Nature, vol. 199, pp. 137-139.

1963b. A second order solution of Vinti's dynamical problem. Smithsonian Contr. Astrophys., vol. 6, pp. 81-107.

1963c. On the critical inclination in satellite theory. In The Use of Artificial Satellites for Geodesy, ed. by G. Veis, North-Holland Publ. Co., Amsterdam, pp. 17-40.

1963d. A note on perturbation theory. Astron. Journ., vol. 68, pp. 559-561.

1964. Tesseral harmonics of the geopotential and corrections to station coordinates. Journ. Geophys. Res., vol. 69, pp. 2621-2630.

1966. A new determination of non-zonal harmonics by satellites. In Trajectories of Artificial Celestial Bodies, ed. by J. Kovalevsky, Springer-Verlag, Berlin, pp. 195-200.

IZSAK, I. G., GERARD, J. M., EFIMBA, R., and BARNETT, M. P.

1964. Construction of Newcomb operators on a digital computer. Smithsonian Astrophys. Obs. Spec. Rep. No. 140, 103 pp.

JACCHIA, L. G.

1960. A variable atmospheric-density model from satellite accelerations. Journ. Geophys. Res., vol. 65, pp. 2775-2782.

1964. Static diffusion models of the upper atmosphere with empirical temperature profiles. Smithsonian Astrophys. Obs. Spec. Rep. No. 170, 53 pp.

JEFFREYS, B. S.

1965. Transformation of tesseral harmonics under rotation. Geophys. Journ., vol. 10, pp. 141-145.

JEFFREYS, H., and JEFFREYS, B. S.

1956. Methods of Mathematical Physics. Third ed., Cambridge Univ. Press, Cambridge, 714 pp.

KAHLE, H. G., and TALWANI, M.

1973. Gravimetric Indian Ocean geoid. Zs. f. Geophys., vol. 39, pp. 167-187.

KAULA, W. M.

1966a. Theory of Satellite Geodesy. Blaisdell Publ. Co., Waltham, Mass., 124 pp.

1966b. Tests and combinations of satellite determinations of the gravity fields with gravimetry. Journ. Geophys. Res., vol. 71, pp. 5303-5314.

1966c. Tesseral harmonics of the earth's gravitational field from camera tracking of satellites. Journ. Geophys. Res., vol. 71, pp. 4377-4388.

1967. Theory of statistical analysis of data distributed over a sphere. Rev. Geophys., vol. 5, pp. 38-107.

1970. Earth's gravity field: Relation to global tectonics. Science, vol. 169, pp. 982-985.

1972. Global gravity and tectonics. In The Nature of the Solid Earth, ed. by E. C. Robinson, J. F. Hays, and L. Knopoff, McGraw-Hill Book Co., New York, pp. 385-405.

KAULA, W. M., and LEE, W.

1967. A spherical harmonic analysis of the earth's topography. Journ. Geophys. Res., vol. 72, pp. 753-758.

KING-HELE, D. G.

1973a. 15th order harmonics in the geopotential, from analysis of decaying satellite orbits. In Space Research XIII, ed. by M. J. Rycroft and S. K. Runcorn, Akademie-Verlag, Berlin, pp. 21-29.

1973b. Resonance effects in decaying satellite orbits, and their use in studies of the geopotential. Presented at the First International Symposium on the Use of Artificial Satellites for Geodesy and Geodynamics, Athens, May.

KING-HELE, D. G., and COOK, G. E.

1973a. Analysis of 24 orbits to determine odd zonal harmonics in the geopotential. Presented at the First International Symposium on the Use of Artificial Satellites for Geodesy and Geodynamics, Athens, May.

1973b. Refining the earth's pear shape – Satellite orbit harmonics. Nature, vol. 246, pp. 86-88.

KING-HELE, D. G., COOK, G. E., and SCOTT, D. W.

1969. Evaluation of odd zonal harmonics in the geopotential, of degree less than 33, from the analysis of 22 satellite orbits. Planet. Space Sci., vol. 17, pp. 629-664.

KOCH, K.

1968. Alternate representation of the earth's gravitational field for satellite geodesy. Boll. Geofis., vol. 10, pp. 318-325.

KOCH, K., and MORRISON, F.

1970. A simple layer model of the geopotential from a combination of satellite and gravity data. Journ. Geophys. Res., vol. 75, pp. 1483-1492.

KOCH, K., and WITTE, B.

1971. Earth's gravity field represented by a simple layer potential from doppler tracking of satellites. Journ. Geophys. Res., vol. 76, pp. 8471-8479.

KÖHNLEIN, W. J.

1965. Determination of station coordinates from optical observations of artificial satellites. Smithsonian Astrophys. Obs. Spec. Rep. No. 189, 25 pp.; also in The Use of Artificial Satellites for Geodesy, ed. by G. Veis, National Tech. Univ., Athens, vol. II, pp. 487-507.

1967. Corrections to station coordinates and to nonzonal harmonics from Baker-Nunn observations. In Space Research VII, ed. by R. L. Smith-Rose, S. A. Bowhill, and J. W. King, North-Holland Publ. Co., Amsterdam, pp. 694-701.

KOZAI, Y.

1959a. The motion of a close earth satellite. Astron. Journ., vol. 64, pp. 367-377.

1959b. The earth's gravitational potential derived from the motion of satellite 1958 Beta Two. Smithsonian Astrophys. Obs. Spec. Rep. No. 22, pp. 1-6.

1959c. On the effects of the sun and moon upon the motion of a close earth satellite. Smithsonian Astrophys. Obs. Spec. Rep. No. 22, pp. 7-10.

1959d. Note on the secular motions of the node and perigee of an artificial satellite. Smithsonian Astrophys. Obs. Spec. Rep. No. 30, pp. 14-15.

1960. Effect of precession and nutation on the orbital elements of a close earth satellite. Astron. Journ., vol. 65, pp. 621-623.

1961a. The gravitational field of the earth derived from motions of three satellites. Astron. Journ., vol. 66, pp. 8-10.

1961b. Comments on the use of osculating ellipse in analysis of near circular orbits. Journ. Amer. Rocket Soc., vol. 31, p. 676.

1961c. Effects of solar radiation pressure on the motion of an artificial satellite. Smithsonian Astrophys. Obs. Spec. Rep. No. 56, pp. 25-33.

1961d. Motion of a particle with a critical inclination in a gravity field of a spheroid. Smithsonian Contr. Astrophys., vol. 5, pp. 53-58.

1961e. Potential field of the earth derived from motions of artificial satellites. In Proceedings of the Symposium of Geodesy in the Space Age, ed. by S. H. Laurila and W. A. Heiskanen, Ohio State Univ. Inst. Geodesy, Photogrammetry and Cartography, Publ. No. 15, pp. 174-176.

1961f. Note on the motion of a close satellite with a small eccentricity. Astron. Journ., vol. 66, pp. 132-133.

1961g. Tesseral harmonics of the gravitational potential of the earth as derived from satellite motions. Astron. Journ., vol. 66, pp. 355-358.

1962a. Second-order solution of artificial satellite theory without air drag. Astron. Journ., vol. 67, pp. 446-461.

1962b. Mean values of cosine functions in an elliptic motion. Astron. Journ., vol. 67, pp. 311-312.

1962c. Numerical results from orbits. Smithsonian Astrophys. Obs. Spec. Rep. No. 101, 21 pp.

KOZAI, Y.

1963a. Numerical results on the gravitational potential of the earth from orbits. In The Use of Artificial Satellites for Geodesy, ed. by G. Veis, North-Holland Publ. Co., Amsterdam, pp. 305-315.

1963b. Potential of the earth derived from satellite motions. In Dynamics of Satellites, ed. by M. Roy, Springer-Verlag, Berlin, pp. 65-73.

1963c. Effects of solar radiation pressure on the motion of an artificial satellite. Smithsonian Contr. Astrophys., vol. 6, pp. 109-112.

1964. New determination of zonal harmonics coefficients of the earth's gravitational potential. Publ. Astron. Soc. Japan, vol. 16, pp. 263-284; also in Smithsonian Astrophys. Obs. Spec. Rep. No. 165, 38 pp.

1966a. Note on expressions for second-order short-periodic perturbations. Smithsonian Astrophys. Obs. Spec. Rep. No. 234, 8 pp.

1966b. The earth's gravitational potential derived from satellite motion. Space Sci. Rev., vol. 5, pp. 818-879.

1966c. Determination of zonal harmonic coefficients. In Geodetic Parameters for a 1966 Smithsonian Institution Standard Earth, ed. by C. A. Lundquist and G. Veis, Smithsonian Astrophys. Obs. Spec. No. 200, vol. 1, pp. 191-194.

1966d. The zonal harmonic coefficients. In Geodetic Parameters for a 1966 Smithsonian Institution Standard Earth, ed. by C. A. Lundquist and G. Veis, Smithsonian Astrophys. Obs. Spec. Rep. No. 200, vol. 2, pp. 67-104.

1966e. Lunisolar perturbations with short periods. Smithsonian Astrophys. Obs. Spec. Rep. No. 235, 26 pp.

1966f. Determination of Love's number from satellite observations. Phil. Trans. Roy. Soc. London, vol. 262, pp. 135-136.

1967a. Summary of numerical results derived from satellite observations. In The Use of Artificial Satellites for Geodesy, ed. by G. Veis, National Tech. Univ., Athens, vol. II, pp. 149-160.

1967b. Long range analysis of satellite observations. In The Use of Artificial Satellites for Geodesy, ed. by G. Veis, National Tech. Univ., Athens, vol. II, pp. 169-178.

KOZAI, Y.

1968. Love's number of the earth derived from satellite observations. Publ. Astron. Soc. Japan, vol. 20, pp. 24-26.

1969. Revised values for coefficients of zonal spherical harmonics in the geopotential. Smithsonian Astrophys. Obs. Spec. Rep. No. 295, 17 pp.

1970. Seasonal variations of the geopotential inferred from satellite observations. Smithsonian Astrophys. Obs. Spec. Rep. No. 312, 6 pp.

1973. A new method to compute lunisolar perturbations in satellite motions. Smithsonian Astrophys. Obs. Spec. Rep. No. 349, 27 pp.

KOZAI, Y., and KINOSHITA, H.

1973. Effects of motion of the equatorial plane on the orbital elements of an earth satellite. Celestial Mech., vol. 7, pp. 356-366.

KOZAI, Y., and WHITNEY, C. A.

1959. Anticipated orbital perturbations of satellite 1959 δ2. Smithsonian Astrophys. Obs. Spec. Rep. No. 30, pp. 1-8.

KRAKIWSKY, E. J., WELLS, D. E., and KIRKHAM, P.

1972. Geodetic control from doppler satellite observations. Canadian Surveyor, vol. 26, pp. 146-162.

LÁLA, P.

1968. Short-periodic perturbations of the satellite orbits caused by solar radiation pressure. Bull. Astron. Czech., vol. 19, pp. 233-239.

1971. Semi-analytical theory of solar pressure perturbations of satellite orbits during short time intervals. Bull. Astron. Czech., vol. 22, pp. 63-72.

LÁLA, P., and SEHNAL, L.

1969. The earth's shadowing effects in the short-periodic perturbations of satellite orbits. Bull. Astron. Czech., vol. 20, pp. 327-329.

LAMBECK, K.

1968a. Comments on the accuracy of Baker-Nunn observations. Presented at the Conference on Photographic Astrometric Techniques, Tampa, Florida, March.

1968b. Effect of random atmospheric refraction on optical satellite observations. Smithsonian Astrophys. Obs. Spec. Rep. No. 269, 27 pp.

1969. A spatial triangulation solution for a global network and the position of the North American Datum within it. Presented at the American Geophysical Union Meeting, Washington, D.C., April.

LAMBECK, K.

1970. Comparisons and combinations of geodetic parameters estimated from dynamic and geometric satellite solutions and from Mariner flights. In Dynamics of Satellites 1969, ed. by B. Morando, Springer-Verlag, Berlin, pp. 170-179.

LANCZOS, C.

1966. The Variational Principles of Mechanics. Third ed., Toronto Univ. Press, Toronto, 375 pp.

LEHR, C.

1972. Atmospheric reduction of laser data. In SAO ISAGEX Experience. I. Data Acquisition, ed. by E. M. Gaposchkin, Smithsonian Astrophys. Obs., Cambridge, Mass., May, p. 31.

LEHR, C. G., MAESTRE, L. A., and DOWNER, R. R.

1968. Laser ranging to satellites: The Smithsonian system on Mt. Hopkins. In Proceedings of the Conference on Refractive Effects in Geodesy and Electronic Distance Measurement, Univ. New South Wales, Kensington, Australia, pp. 123-144.

NNIK, Y. V.

1961. Method of Least Squares and Principles of the Theory of Observations. Translated from the Russian by R. C. Elandt, ed. by N. J. Johnson, Pergamon Press, New York, 360 pp.

LUNDQUIST, C. A.

1966. Satellite geodesy at the Smithsonian Astrophysical Observatory. Presented at the American Congress of Surveying and Mapping and the American Society of Photogrammetry Convention, Washington, D.C., March.

1967. Geodetic Satellite Results During 1967 (editor). Smithsonian Astrophys. Obs. Spec. Rep. No. 264, 344 pp.

LUNDQUIST, C. A., GAY, R. H., and GIACAGLIA, G. E. O.

1972. Spherical sampling functions: Generalizations and applications. Presented at the 9th International Symposium on Geophysical Theory and Computers, Banff, Canada, August.

LUNDQUIST, C. A., and GIACAGLIA, G. E. O.

1969. Possible geopotential improvement from satellite altimetry. Smithsonian Astrophys. Obs. Spec. Rep. No. 294, pp. 1-44.

1972a. A geopotential representation with sampling functions. In The Use of Artificial Satellites for Geodesy, ed. by S. W. Henriksen, A. Mancini, and B. H. Chovitz, Geophys. Mono. 15, Amer. Geophys. Union, Washington, D.C., pp. 125-131.

1972b. Use of altimetry data in a sampling function approach to the geoid. In Sea Surface Topography from Space, vol. 1, ed. by J. R. Apel, NOAA Tech. Rep. ERL 228-AOML 7, U.S. Government Printing Office, Washington, D.C., pp. 4-1 to 4-9.

LUNDQUIST, C. A., GIACAGLIA, G. E. O., and GAY, R. H.

1972. Application of sampling functions to earth gravity models. Presented at the International Symposium on Earth Gravity Models and Related Problems, Amer. Geophys. Union, Washington, D.C., August.

LUNDQUIST, C. A., and VEIS, G.

1966. Geodetic Parameters for a 1966 Smithsonian Institution Standard Earth (editors). Smithsonian Astrophys. Obs. Spec. Rep. No. 200, 3 vols., 686 pp.

MARSH, J. G., DOUGLAS, B. C., and KLOSKO, S. M.

1973. A global station coordinate solution based upon camera and laser data. Presented at the First International Symposium for the Use of Artificial Satellites for Geodesy and Geodynamics, Athens, May.

MARSH, J. G., DOUGLAS, B. C., and MARTIN, C. F.

1971. NASA STADAN and SPEOPT and laser tracking station positions derived from GEOS-1 and 2 observations. In Space Research XI, ed. by K. Ya. Kondratyev, M. J. Rycroft, and C. Sagan, Akademie-Verlag, Berlin, pp. 507-514.

MARTIN, T. V.

1972. GEODYN systems operation description. Wolf Research and Development Corp. Final Report on Contract NAS-5-11736-129, 183 pp.

MATHER, R.

1970. The Australian geodetic datum in earth space. UNISURV Rep. No. 19, Univ. New South Wales, p. 80.

MORSE, P. M., and FESHBACK, H.

1953. Methods of Theoretical Physics. McGraw-Hill Book Co., New York, parts I and II.

MOTTINGER, N.

1969. Status of D.S.F. location solution for deep space probe missions. In Space Programs Summary No. 37-60, Deep Space Network, Jet Propulsion Lab., Pasadena, Calif., vol. II, pp. 77-89.

1972. Letter to E. M. Gaposchkin, May 31.

1973. Jet Propulsion Laboratory's contribution to the National Geodetic Satellite Program Document. Preprint, Jet Propulsion Lab., Pasadena, Calif.

MUELLER, I. I.

1974. Global satellite triangulation and trilateration (solution WN 14). In The National Geodetic Satellite Program, compiled by the Amer. Geophys. Union for the National Aeronautics and Space Administration, chap. 8, in press.

MUNK, W. H., and MacDONALD, G. J. F.

1960. The Rotation of the Earth. Cambridge Univ. Press, Cambridge, 323 pp.

PEKERIS, C. L., and ACCAD, Y.

1969. Solution of Laplace's equation for the M2 tide in the world's oceans. Phil. Trans. Roy. Soc. London, A, vol. 265, pp. 413-436.

PIEPLU, J. L., and LEFEBVRE, M.

1973. Détermination d'equations de conditions entre harmoniques de resonance d'ordre 14 à partir des observations du satellite Eole. In Space Research XIII, ed. by M. J. Rycroft and S. K. Runcorn, Akademie-Verlag, Berlin, pp. 31-33.

PLOTKIN, H. H.

1964. The S-66 laser satellite tracking experiment. In Quantum Electron III, vol. 2, ed. by P. Grivet and N. Bloembergen, Columbia Univ. Press, New York, pp. 1319-1332.

PLUMMER, H. C.

1918. An Introduction Treatise on Dynamical Astronomy. Cambridge Univ. Press, Cambridge, 343 pp.

POINCARÉ, H.

1893. Les Méthodes Nouvelles de la Mécanique Céleste. Gauthier-Villars, Paris, vol. II, 479 pp.

RAPP, R. H.

1968. Gravitational potential of the earth determined from a combination of satellite, observed, and model anomalies. Journ. Geophys. Res., vol. 73, pp. 6555-6562.

1971. The direct combination of satellite and gravimetric data for mean anomaly determination. Ohio State Univ., Dept. Geodetic Sci. Rep. No. 131, 56 pp.

1973. Numerical results from the combination of gravimetric and satellite data using the principles of least squares collocation. Ohio State Univ., Dept. Geodetic Sci. Rep. No. 200, 58 pp.

ROSENBERG, J.

1968. Objectives of the NGSP. In GEOS-I Operations and Plans for GEOS-B, vol. 1 of Proceedings of the Geos 1 Review Meeting, ed. by Communications & Systems, Inc., NASA, Washington, D. C., p. xix.

RYAN, C.

1952. Across the Space Frontier (editor). Viking Press, New York, 147 pp.

SCOTT, F. P.

1964. A method of evaluating the elliptic E terms of the aberration. Astron. Journ., vol. 69, pp. 372-373.

SCOTT, F. P., and SMITH, C. A., Jr.

1967. Comparisons of the SAO and AGK3R star catalogs. In Conference on Photographic Astrometric Technique, ed. by H. Eichhorn, NASA CR-1825, pp. 181-190.

SEHNAL, L., and MILLS, S. B.

1966. The short-period drag perturbations of the orbits of artificial satellites. Smithsonian Astrophys. Obs. Spec. Rep. No. 223, 30 pp.

SLOWEY, J. W.

1973. Earth radiation pressure and the determination of density from atmospheric drag. Presented at the 16th International COSPAR Meeting, Konstanz, Germany, May.

SMART, W. M.

1953. Celestial Mechanics. Longmans Green and Co., London, 381 pp.

SMITH, D. E., KOLENKIEWICZ, R., and DUNN, P. J.

1972. Geodetic studies by laser ranging to satellites. In The Use of Artificial Satellites for Geodesy, ed. by S. W. Henriksen, A. Mancini, and B. H. Chovitz, Amer. Geophys. Union Monograph No. 15, pp. 187-196.

SMITH, D. E., LERCH, F. J., and WAGNER, C. A.

1973. A gravitational field model for the earth. In Space Research XIII, ed. by M. J. Rycroft and S. K. Runcorn, Akademie-Verlag, Berlin, pp. 11-20.

STAFF, SMITHSONIAN ASTROPHYSICAL OBSERVATORY

1966. Smithsonian Astrophysical Observatory Star Catalog. U.S. Government Printing Office, Washington, D.C., 4 vols.

STERNE, T. E.

1959. Effect of the rotation of a planetary atmosphere upon the orbit of a close satellite. Amer. Rocket Soc. Journ., vol. 29, pp. 777-782.

TALWANI, M., POPPE, H. R., and RABINOWITZ, P. D.

1972. Gravimetrically determined geoid in the western North Atlantic. In Sea Surface Topography from Space, vol. II, ed. by J. Apel, NOAA Tech. Rep. ERL 228 - AOML 7-2, pp. 23-1 to 23-33.

TISSERAND, F.

1960. Traité de Mécanique Céleste. Gauthier-Villars, Paris, vols. I and II.

TRASK, D. W., and VEGOS, C. J.

1968. Intercontinental longitude differences of tracking stations as determined from radio tracking data. In Continental Drift, Secular Motion of the Pole, and Rotation of the Earth, Proc. IAU Symp. No. 32, ed. by B. Markowitz and B. Guinot, D. Reidel Publ. Co., Dordrecht-Holland, pp. 91-94.

VEGOS, C. J., and TRASK, D. W.

1967. Tracking station location as determined by radio tracking data. In Space Programs Summary No. 37-43, Deep Space Network, Jet Propulsion Lab., Pasadena, Calif., vol. III, pp. 11-28.

VEIS, G.

1958. Geodetic applications of observations of the moon, artificial satellites, and rockets. Ph.D. Thesis, Ohio State Univ., 165 pp.

1959. The orbit of satellite 1958 Zeta. Smithsonian Astrophys. Obs. Spec. Rep. No. 23, pp. 1-16.

VEIS, G.

1960a. Geodetic uses of artificial satellites. Smithsonian Contr. Astrophys., vol. 3, pp. 95-161.

1960b. SAO D. O. I. improvement program. In Astronautics Information, Seminar Proceedings, Tracking Programs and Orbit Determination, Jet Propulsion Lab., Pasadena, Calif., pp. 165-184.

1961. The positions of the Baker-Nunn camera stations. Smithsonian Astrophys. Obs. Spec. Rep. No. 59, 5 pp.

1963a. Precise aspects of terrestrial and celestial reference frames. Smithsonian Astrophys. Obs. Spec. Rep. No. 123, 16 pp.; also in The Use of Artificial Satellites for Geodesy, ed. by G. Veis, North-Holland Publ. Co., Amsterdam, pp. 201-216.

1963b. Optical tracking of artificial satellites. Space Sci. Rev., vol. 2, pp. 250-296.

1963c. The determination of absolute directions in space with artificial satellites. Smithsonian Astrophys. Obs. Spec. Rep. No. 133, 24 pp.

1964. On the optimum use of satellites for geodesy. COSPAR Information Bull. No. 20, pp. 28-37.

1965. The deflection of the vertical of major geodetic datums and the semimajor axis of the earth's ellipsoid as obtained from satellite observations. In Space Research V, ed. by D. G. King-Hele, P. Muller, and G. Righini, North-Holland Publ. Co., Amsterdam, pp. 849-875.

1966a. Relation with DSIF stations. In Geodetic Parameters for a 1966 Smithsonian Institution Standard Earth, ed. by C. A. Lundquist and G. Veis, Smithsonian Astrophys. Obs. Spec. Rep. No. 200, vol. 3, pp. 115-125.

1966b. The motion of the spin axis and the rotation of the earth. In Scientific Horizons from Satellite Tracking, ed. by C. A. Lundquist and H. D. Friedman, Smithsonian Astrophys. Obs. Spec. Rep. No. 236, pp. 123-142.

1966c. Differential orbit improvement program for lunar orbiters. In Scientific Horizons from Satellite Tracking, ed. by C. A. Lundquist and H. D. Friedman, Smithsonian Astrophys. Obs. Spec. Rep. No. 236, pp. 215-220.

VEIS, G.

1967a. Geodetic interpretation of the results. In Space Research VII, ed. by R. L. Smith-Rose, S. A. Bowhill, and J. W. King, North-Holland Publ. Co., Amsterdam, pp. 776-777.

1967b. Results from geometric methods. In Space Research VII, ed. by R. L. Smith-Rose, S. A. Bowhill, and J. W. King, North-Holland Publ. Co., Amsterdam, pp. 778-782.

1967c. The determination of the radius of the earth and other geodetic parameters as derived from optical satellite data. In Geodetic Satellite Results During 1967, ed. by C. A. Lundquist, Smithsonian Astrophys. Obs. Spec. Rep. No. 264, pp. 73-99.

1968. The determination of the radius of the earth and other geodetic parameters as derived from optical satellite data. Bull. Géod., no. 89, pp. 253-275.

VEIS, G., CRISWELL, S., ROSS, S., and SHAW, J.

1970. The operational aspects of the Smithsonian VLBI program. Presented at the NRAO/URSI Symposium on VLBI, Charlottesville, Va., April.

VEIS, G., and SERVIS, N.

1967. A simple satellite camera for geodetic uses. In The Use of Artificial Satellites for Geodesy, ed. by G. Veis, National Tech. Univ., Athens, vol. II, pp. 29-39.

VEIS, G., and WHIPPLE, F. L.

1961. Experience in precision optical tracking of satellites for geodesy. In Space Research II, ed. by H. C. van de Hulst, C. de Jager, and A. F. Moore, North-Holland Publ. Co., Amsterdam, pp. 17-33.

VEIS, G., and WOLF, M.

1970. A laser satellite ranging system. In Space Research X, ed. by T. M. Donahue, P. A. Smith, and L. Thomas, North-Holland Publ. Co., Amsterdam, pp. 61-66.

VINTI, J. P.

1959. New method of solution for unretarded satellite orbits. Journ. Nat. Bur. Standards, vol. 63B, pp. 105-116.

VON ZEIPEL, H.

1916. Recherches sur le mouvement des petites planètes. Ark. Astron. Mat. Fys., vol. 11, pp. 1-58.

WAGNER, C. A.

1968a. Combined solution for low degree longitude harmonics of gravity from 12- and 24-hour satellites. Journ. Geophys. Res., vol. 73, pp. 7651-7660.

1968b. Determination of low-order resonant gravity harmonics from the drift of two Russian 12-hour satellites. Journ. Geophys. Res., vol. 73, pp. 4661-4674.

WHIPPLE, F. L.

1967. On the satellite geodesy program at the Smithsonian Astrophysical Observatory. In Space Research VII, ed. by R. L. Smith-Rose, S. A. Bowhill, and J. W. King, North-Holland Publ. Co., Amsterdam, pp. 675-683.

WHIPPLE, F. L., and HYNEK, J. A.

1956. A research program based on the optical tracking of artificial earth satellites. Proc. Inst. Radio Engr., vol. 44, pp. 760-764.

1958a. Optical and visual tracking of artificial satellites. In Proceedings of the VIIIth International Astronautical Congress, ed. by F. Hecht, Springer-Verlag, Vienna, pp. 429-435.

1958b. The IGY satellite tracking program as a source of geodetic information. Ann. Géophys., vol. 14, pp. 326-328.

WHIPPLE, F. L., and LUNDQUIST, C. A.

1967. Tracking by the Smithsonian Astrophysical Observatory. Phil. Trans. Roy. Soc. London, A, vol. 262, pp. 14-25.

WHIPPLE, F. L., and VEIS, G.

1965. Erdvermessung mit Satelliten. Bild der Wissenschaft, no. 5, pp. 397-404.

WHITNEY, C. A., and VEIS, G.

1958. A flashing satellite for geodetic studies. Smithsonian Astrophys. Obs. Spec. Rep. No. 19, pp. 9-19.

WHITTAKER, E. T.

1964. Analytical Dynamics of Particles and Rigid Bodies. Cambridge Univ. Press, Cambridge, 456 pp.

WIENER, N.

1966. Extrapolation, Interpolation, and Smoothing of Stationary Time Series with Engineering Applications. The MIT Press, Cambridge, Mass., 160 pp.

WILLIAMS, J. G., MULHOLLAND, J. D., and BENDER, P. L.

1972. Spin-axis distance of the McDonald Observatory. Presented at the fall meeting of the American Geophysical Union, San Francisco, December; abstract in Trans. Amer. Geophys. Union, vol. 53, p. 968.

YIONOULIS, S. M.

1963. Improved coefficients of the thirteenth order harmonics of the geopotential derived from satellite doppler data at three different orbital inclinations. Johns Hopkins Univ. Appl. Phys. Lab. Rep. TG-1003, 8 pp.

YIONOULIS, S. M., HEURING, F. T., and GUIER, W. H.

1972. A geopotential model determined from satellite doppler data at seven inclinations. Journ. Geophys. Res., vol. 77, pp. 3671-3677.

ZADUNAISKY, P.

1960. Shutter corrections in time for Baker-Nunn camera. Smithsonian Astrophys. Obs. Spec. Rep. No. 41, pp. 21-37.

BIOGRAPHICAL NOTES

DAVID A. ARNOLD received his A.B. and A.M. in physics in 1962 and 1969, respectively, from Boston University.

Before coming to Smithsonian Astrophysical Observatory in 1964, he was a physical scientist assistant at the U.S. Army Cold Regions Research and Engineering Laboratory. He has been a senior astrometric computer, a project leader, and a supervisory data analyst in the Data Division at SAO. Since 1972, Mr. Arnold has been a systems analyst in the Experimental Geophysics Department, where he is involved in the calculation of retroreflector-array transfer functions and in the analysis of the performance of laser ranging systems.

E. M. GAPOSCHKIN graduated in electrical engineering from Tufts University in 1957. He received a Degree of Numerical Analysis in 1959 from Cambridge University in England and a Ph.D. in geophysics from Harvard University in 1969.

Dr. Gaposchkin joined the staff at Smithsonian Astrophysical Observatory in 1959, where he has been programer and Division Chief of the Computations Division and mathematician in the Research and Analysis Department. He has helped develop the basic computer program used in all analyses of satellite motion.

Since 1968, Dr. Gaposchkin has been principal scientist of the Analytical Satellite Geophysics Group. His main interests include satellite geodesy and geophysics and applied mathematics. Dr. Gaposchkin spent the last year at Groupe de Recherches de Géodesie Spatiale at the Observatoire de Meudon, Université de Paris.

YOSHIHIDE KOZAI received the M.S. and D.S. degrees from Tokyo University in 1951 and 1958, respectively. He has been associated with the Tokyo Astronomical Observatory since 1952 and has held concurrent positions as staff astronomer with that observatory and consultant to Smithsonian Astrophysical Observatory since 1958.

Dr. Kozai specializes in celestial mechanics, his research at SAO being primarily in the determination of zonal harmonics coefficients in the earth's gravitational potential by use of precisely reduced Baker-Nunn observations. He is also interested in the seasonal variability of the earth's potential. Using satellite-tracking data in studies of the earth's geopotential, he has derived new values for the coefficients of the zonal harmonics of the earth's gravitational field.

JAMES LATIMER graduated from Massachusetts Institute of Technology in 1963 with an S. B. in physics.

Mr. Latimer has been on the Smithsonian Astrophysical Observatory staff since 1963; he served for three years at SAO's observing stations in Argentina and Tokyo before coming to Cambridge. In 1966, he became Operations Officer of STADAD, and from 1967 to 1968, administrative assistant to the manager of the Data-Processing Department. During the next year, he was on the experiment operations staff of Project Celescope, and since that time has been administrative assistant in the Analytical Satellite Geophysics Group.

CARLTON G. LEHR received the S. B. degree in 1943 and the S.M. degree in 1948 from the Massachusetts Institute of Technology.

Mr. Lehr has been a staff engineer at Smithsonian Astrophysical Observatory since 1964 and is currently a senior staff member of the Experimental Geophysics Department. Previously, Mr. Lehr was a principal scientist and manager of the

Microwave Group of Raytheon Company's Research Division. He has also lectured in mathematics at Northeastern University, Graduate Division.

His principal fields of investigation include lasers and optical and electronic methods of tracking satellites.

CHARLES A. LUNDQUIST earned his undergraduate degree in 1949 from South Dakota State College and his doctorate in 1954 from the University of Kansas.

From 1956 to 1960, he was Chief of the Physics and Astrophysics Section, Research Projects Laboratory, Army Ballistic Missile Agency, and from 1960 to 1962, he held concurrent positions as Director of the Supporting Research Office and Chief of the Physics and Astrophysics Branch of the Research Projects Division at Marshall Space Flight Center.

Dr. Lundquist joined the Smithsonian Astrophysical Observatory as Assistant Director for Science in 1962. In this position, he was responsible for organizing and coordinating current research projects, as well as seeking new directions for future research. He resigned in 1973 to become Director of the Space Sciences Laboratory, Marshall Space Flight Center, Huntsville, Alabama.

G. M. MENDES received an A. B. in physics from Northeastern University in 1963 and an M. S. in physics from that same university in 1970.

Since joining Smithsonian Astrophysical Observatory in 1964, she has been a mathematician in the Data Division, responsible for maintaining orbits and predicting satellite positions for SAO's station network. Currently in the Analytical Satellite Geophysics Group, Ms. Mendes has prepared data for studies in polar motion, air drag, and radiation pressure. She has also prepared orbits and selected arcs for use in computing zonal and tesseral harmonics and station coordinates for the Standard Earths (II) and (III).

MICHAEL R. PEARLMAN received his B.S. from the Massachusetts Institute of Technology and his Ph.D. from Tufts University in 1963 and 1968, in physics.

Dr. Pearlman became a scientist on the staff of Smithsonian Astrophysical Observatory in September 1968 in the Satellite Geophysics Group. From February 1971 to July 1972, he was a Visiting Scientist in the Office of Geodetic Satellites at the National Aeronautics and Space Administration Headquarters in Washington, D.C. Since July 1972, Dr. Pearlman has been Chief of the Experimental Geophysics Department in the Observatory's Earth Dynamics Program. He is currently working primarily on laser satellite tracking.

JOHN M. THORP received an A.B. in geology in 1962 from Boston University.

He came to Smithsonian Astrophysical Observatory in 1962, where he has been an astrometric computer in the Photoreduction Department, an observer at the satellite-tracking station in Jupiter, Florida, an administrative officer at SAO in Cambridge, and a station manager in Greece and Spain.

Since 1971, Mr. Thorp has been the Operations Officer for the SAO satellite-tracking network.

CHARLES R. H. TSIANG received a S.B. in electrical engineering in 1966 from the Massachusetts Institute of Technology.

He was an observer at Smithsonian Astrophysical Observatory's station in Argentina from 1966 to 1968, at which time he transferred to Cambridge. From 1968 to 1973, he was an electronics engineer in STADAD, primarily concerned with digital and analog systems and in systems design. He also participated in the magnetosphere and VLBI projects.

Mr. Tsiang resigned in 1973 and is currently attending the Sloan School of Management at MIT.

GEORGE VEIS received his degrees from the National Technical University in Athens, Greece, and Ohio State University in 1951 and 1958, respectively.

Since 1958, Dr. Veis has held concurrent positions as consultant to Smithsonian Astrophysical Observatory and Professor of Land Surveying at the National Technical University. His research at SAO has been concerned with problems of optical satellite tracking for geodetic purposes.

FRED L. WHIPPLE earned his A. B. from the University of California at Los Angeles in 1927 and his Ph. D. from the University of California at Berkeley in 1931.

He has taught at the University of California, Stanford University, and Harvard University and has been Phillips Professor of Astronomy at Harvard since 1968.

Dr. Whipple has been affiliated with Harvard University and Harvard College Observatory since 1931. In 1955, when the Smithsonian Astrophysical Observatory moved to Cambridge, he became Director of that Observatory, a position he held until 1973.

Dr. Whipple's principal fields of investigation have included the study of comets and meteors, of asteroids and planets, and of the interplanetary complex.

M. R. WILLIAMSON graduated in applied mathematics from Brown University in 1963. She received an M. S. in 1965 and a Ph. D. in 1970 in physics from Tufts University.

She has been with the Smithsonian Astrophysical Observatory since 1971 as a mathematician in the Analytical Satellite Geophysics Group. She has developed programs for analyzing surface-gravity data and for studying the effects of solar radiation pressure on satellite motion.

JAKOB WOHN received an A.A.S. degree in electrical engineering from De Vry Institute in 1960 and has attended De Paul University and Illinois Institute of Technology.

Before joining Smithsonian Astrophysical Observatory, Mr. Wohn was an engineer at Webcor and at Northwestern University, working in research and development in electro-optics. From 1963 to 1968, he was an observer at SAO's satellite-tracking stations in Florida, Peru, Iran, Norway, and Spain, and the manager of the SAO site in Villa Dolores, Argentina.

Since 1968, Mr. Wohn has been a laser engineer with the STADAD staff in Cambridge, where he is involved in both laser and optical systems for satellite tracking.

NOTICE

This series of Special Reports was instituted under the supervision of Dr. F. L. Whipple, Director of the Astrophysical Observatory of the Smithsonian Institution, shortly after the launching of the first artificial earth satellite on October 4, 1957. Contributions come from the Staff of the Observatory.

First issued to ensure the immediate dissemination of data for satellite tracking, the reports have continued to provide a rapid distribution of catalogs of satellite observations, orbital information, and preliminary results of data analyses before formal publication in the appropriate journals. The Reports are also used extensively for the rapid publication of preliminary or special results in other fields of astrophysics.

The Reports are regularly distributed to all institutions participating in the U.S. space research program and to individual scientists who request them from the Publications Division, Distribution Section, Smithsonian Astrophysical Observatory, Cambridge, Massachusetts 02138.